

**UNDERSTANDING C-H BOND FUNCTIONALISATION AT
HETEROCYCLES AND BIOMOLECULES: A SYNTHETIC AND
MECHANISTIC STUDY**

Thomas Williams

PhD

**UNIVERSITY OF YORK
CHEMISTRY**

APRIL 2013

Abstract

The Pd-, Cu- and Pd/Cu-mediated direct functionalisation of C2-H bonds at 1,3-X,N-heterocycles (where X = S, O, N) and indole-containing biomolecules has been investigated. Such processes are useful in the synthesis and labeling of complex molecules, and represent an improvement on traditional Pd-mediated cross-coupling.

A study of the mechanism of C2-H bond functionalisation of 1,3-X,N-heterocycles (specifically benzimidazole, benzothiazole and benzoxazole) with Pd/Cu catalyst systems has indicated a key role for Pd⁰ nanoparticles. Nanoparticles have been demonstrated to form *in situ* when molecular Pd^{II} pre-catalysts are employed, and have been characterized by transmission electron microscopy (TEM). The catalytic activity of these nanoparticles has been shown to vary with reaction environment (e.g. the use of different reaction vessels). Pre-synthesised, well-defined Pd⁰ nanoparticles supported on polyvinylpyrrolidone (PVP) are effective catalysts for these processes and increase reaction reliability. It is proposed that Cu *N*-heterocarbene (NHC) intermediates play a key role in these processes. A model system {(1,3-dibenzyl)benzoimidazolylidencopper(I) bromide} has been synthesised using an electrochemical method. The reaction of this model with PhI within and without the presence of Pd^{II} results in arylated product. Whilst conducting these studies, the novel compound bis{(1,3-dibenzyl)benzimidazolium}dicopper(I)tetrabromide was isolated.

The C-H bond functionalisation of benzoxazole with a Pd/(1,10-phenanthroline) catalyst and PhI(OAc)₂ aryl source has been studied in detail. Pd⁰ nanoparticles have been isolated and characterized from this reaction. It has also been demonstrated that PhI(OAc)₂ rapidly degrades to PhI under the reaction conditions.

The indole-based amino acid tryptophan is fluorescent, and modifying this fluorescence is of interest. A mild and selective C2-H bond functionalisation reaction for this amino acid has been developed, both as a single residue and within peptides. NMR spectroscopy, ReactIR® and other techniques have been used to build up a mechanistic picture of this reaction, which is proposed to proceed *via* a Pd^{0/II} manifold.

Contents

Abstract	2
Contents	3
Acknowledgements	6
Author's Declaration	7
Chapter 1: Introduction	8
1.1 Pd-Mediated C-X/C-H Bond Functionalisation	9
1.1.1 Pd-Mediated C-X Bond Functionalisation	9
1.1.2 Pd-Mediated C-H Bond Functionalisation	12
1.1.3 Definition	14
1.2 Aims and Objectives	16
Chapter 2: C-H Bond Functionalisation of Benz(azoles)	17
2.1 Introduction	18
2.1.1 Direct Arylation of Benzazoles	18
2.1.2 Pd-Nanoparticles in Catalysis	28
2.1.3 The Role of <i>N</i> -Heterocyclic Carbenes in Cu-Mediated Catalysis	33
2.1.4 Summary	43
2.2 C-H Functionalisation of Benzoxazoles with Pd ⁰ Nanoparticles	44
2.2.1 Synthesis of Pd-PVP Nanoparticles	44
2.2.2 Role of Pd ⁰ Nanoparticles in Bellina-Rossi Functionalisations	46
2.2.3 Direct C-H Functionalisation of Benzoxazole with PhI(OAc) ₂	54
2.3 Role of Cu-NHC Complexes in Pd/Cu-Mediated Systems	62
2.3.1 Cu(NHC)X Complexes as Model Intermediates	62
2.3.2 Synthesis of Cu-NHC Complexes	64
2.3.3 Application to C-H Bond Functionalisation	76
2.4 Experimental	83

Chapter 3: C-H Bond Functionalisation of Indole Biomolecules	101
3.1 Introduction	102
3.1.1 Arylation of Indoles	102
3.1.2 Pd-Mediated Functionalisation of C-X Bonds in Amino Acids, Peptides and Proteins	110
3.1.3 Pd-Mediated Functionalisation of C-H Bonds in Amino Acids and Peptides	119
3.2 Direct C-H Functionalisation of Tryptophan	124
3.2.1 Initial Method Development	124
3.2.2 Unsymmetric Diaryliodonium Salts	130
3.2.3 Mechanism: Pd ^{0/II} or Pd ^{II/IV} ?	132
3.2.4 Organoboron Reagents	153
3.2.5 Stereochemistry and X-Ray Crystallography	157
3.2.6 UV-Visible and Fluorescence	162
3.2.7 Peptides and Proteins	166
3.3 Experimental	173
Chapter 4: Conclusions and Future Work	203
4.1 Direct C-H Bond Functionalisation of Benzazoles	204
4.1.1 Conclusions	204
4.1.2 Future Work	206
4.2 Direct C-H Bond Functionalisation of Benzazoles	208
4.2.1 Conclusions	208
4.2.2 Future Work	209
List of Abbreviations	212
References	216
Appendix A: Reproduction of NMR Spectroscopic Data (on CD)	
Appendix B: UV-Visible and Fluorescence Spectroscopic Data (on CD)	
Appendix C: CIF Data Files for X-Ray Crystallography (on CD)	

Acknowledgements

I would like to thank my supervisor, Professor Ian J. S. Fairlamb, for all his help, support and patience over the past three and a half years.

I'd also like to thank all members of the Fairlamb Group 2009-2013, but especially Sara, Tom 1.0 and Amanda for their friendship and (foolishly not always taken) advice, and Philippa and Tom 3.0 for their brilliantly pedantic proofreading of this thesis (who knew there were so many different hyphens and dashes?). I have been lucky to assist with the supervision of two excellent final year MChem students: Henry Durant (2010-11) and Tom Herbert (2011-12). Both have contributed to the projects that now form part of this thesis.

I'd like to thank Dr Charlotte Willans and Ben Lake, our collaborators at the University of Leeds, for their expertise and help in the area of NHC-Cu complexes, and allowing us access to their HPLC facilities.

I am grateful for the excellent technical support of Dr Meg Stark (electron microscopy), Dr Adrian Whitwood, Dr Rob Thatcher (X-ray crystallography), Dr Karl Heaton (MS) Fish (NMR spectroscopy) and Dr Charlotte Elkington (general, but essential, technical support). Prof. Peter O'Brien and Dr Christoph Baumann are thanked for the use of various HPLC instruments.

There are a few people away from work who should be thanked for giving me a much-needed break from chemistry once in a while. Thanks to Helen for her genuine kindness and friendship over the last few years. I'd like to thank the City of York Labour Party and its members for much welcome and almost unending entertaining. And thanks to Grace for support, friendship and (occasionally brutal) honesty. The list of things I have to thank my Mum and Dad for is too long to detail here.

Maureen and the rest of the staff at the Alcuin café must be thanked for providing the tea and snacks essential for effective research.

This thesis is dedicated to Colin Williams (1946-2012), Bert Johnson (1924-2010), and Jessie Knott (1926-2013).

Author,s Declaration

I declare that all the work presented in this thesis is my own, and that any material not my own is clearly referenced or acknowledged. The work was conducted between October 2009 and April 2013.

Thomas Williams

April 2013

**CHAPTER 1:
INTRODUCTION**

1.1 Pd-Mediated C-X/C-H Bond Functionalisation

1.1.1 Pd-Mediated C-X Bond Functionalisation

Over the past forty years, Pd-catalysed cross-coupling chemistry has revolutionised the way C-C bonds are formed in the synthesis of complex organic molecules.¹ The first example of Pd cross-coupling, the Mizoroki-Heck reaction, was initially published independently by Mizoroki and Heck in the early 'seventies.^{2,3} Using Pd catalysts, it became possible to cross-couple aryl, benzyl or vinyl halides with a terminal alkene. Since that time, the Stille (coupling organopseudohalides with organotin reagents),^{4,6} Suzuki-Miyaura (coupling organopseudohalides with organoboronic acids),⁷ Sonogashira (coupling organopseudohalides with terminal alkynes),^{8,10} Kumada-Corriu (coupling organopseudohalides with Grignard reagents) and Hiyama (coupling organopseudohalides with organosilanes) reactions have been developed (Figure 1), which take advantage of the unique reactivity of organometallic species.

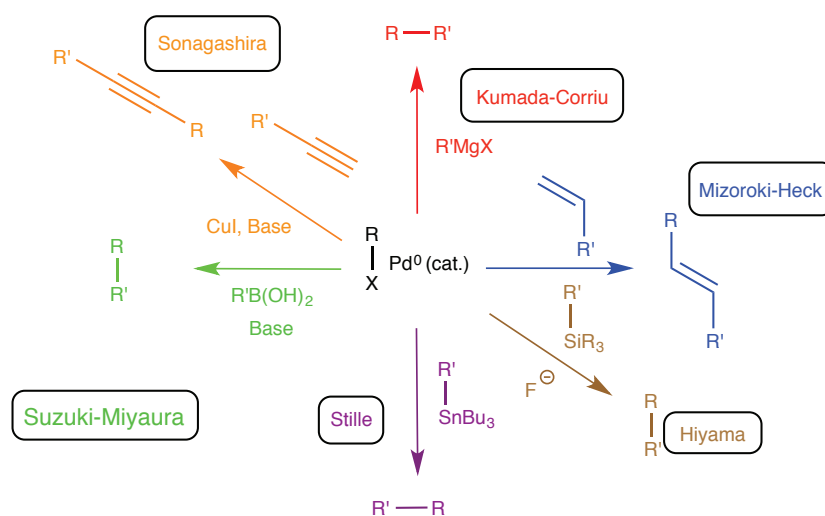
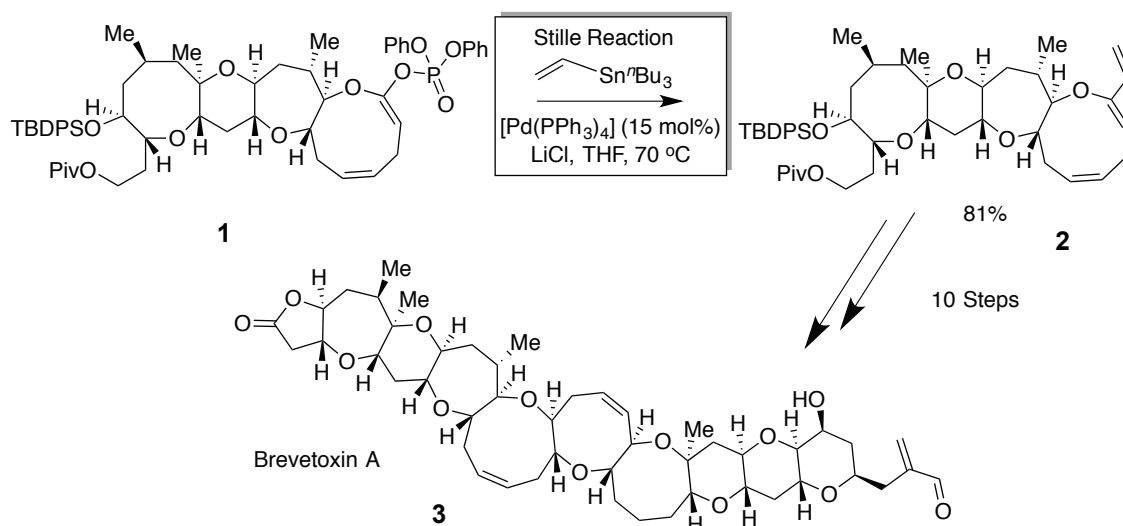


Figure 1: Examples of traditional Pd-catalysed cross-coupling chemistry.

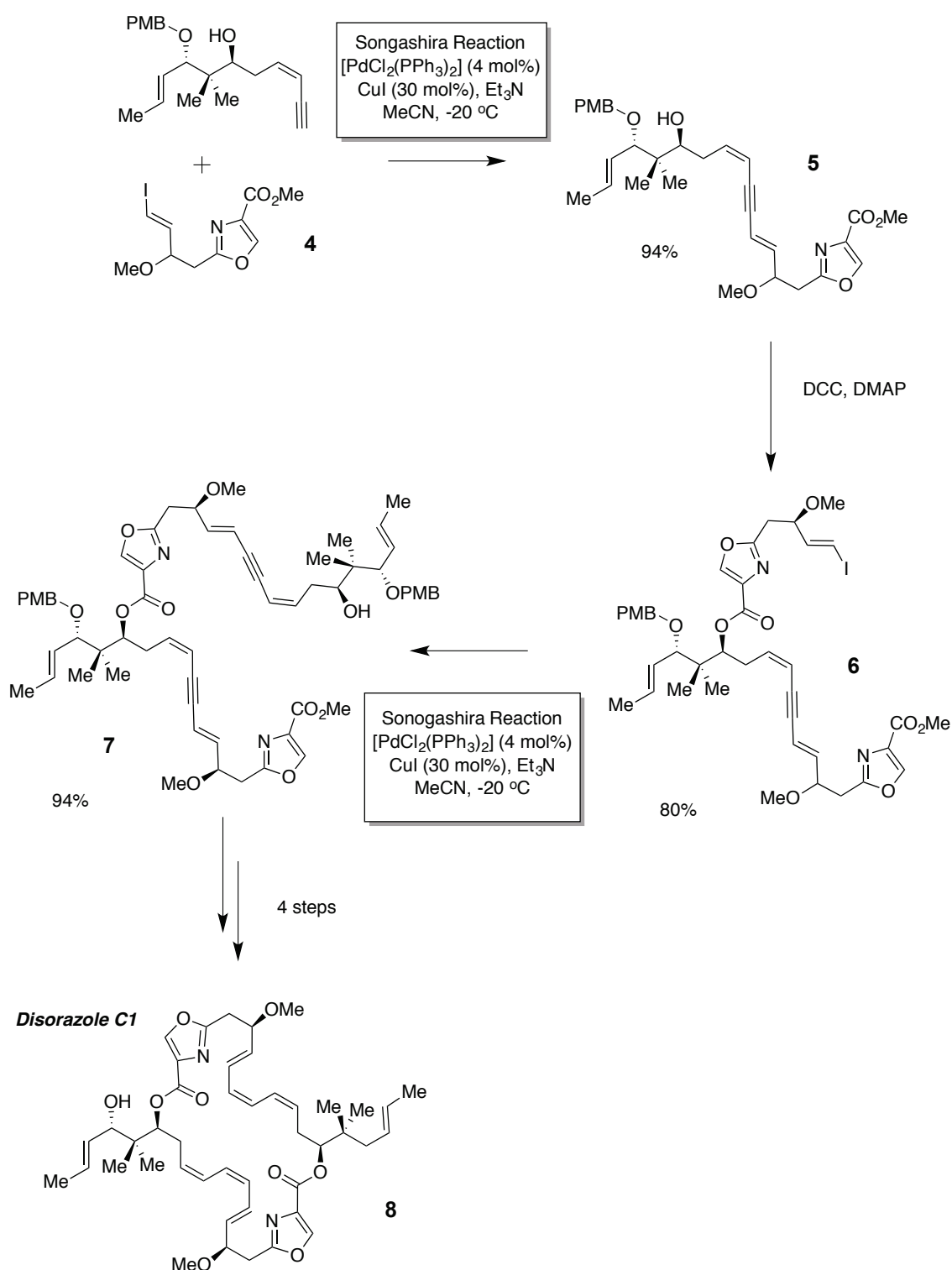
These reactions offer high selectivity and relatively mild conditions which were previously unavailable to synthetic chemists. Indeed, they often become alternatives to alkyl lithium bases (with the exception of the Kumada-Corriu reaction), which can be incompatible with high molecular complexity. Thus they have become an essential part of the organic chemistry tool-kit, and consequently simple cross-coupling partners and catalysts have become commercially available.

The utility of these methodologies can be seen in their application to the synthesis of complex natural products. For example, Nicolaou's 123 step synthesis of Brevetoxin A **3**, a marine algae natural product consisting of ten consecutive fused rings, makes use of a novel ketene acetal phosphate Stille cross-coupling to install a vinyl moiety under relatively mild conditions (Scheme 1).¹¹



Scheme 1: Nicolaou's use of cross-coupling chemistry in the synthesis of Brevetoxin A, **3**.¹¹

Similarly, the Sonagashira reaction has been employed in the syntheses of large macrocyclic natural products, where more conventional organic techniques may have proved less successful. For example, Wipf and Graham's synthesis of disorazole C₁ **8** makes use of two Sonagashira reactions (Scheme 2).¹² Using sub-stoichiometric amounts of copper, it was possible to install two internal alkynes in excellent (94%) yield, which could be later reduced to macrocyclic alkenes.



Scheme 2: Wipf's use of cross-coupling chemistry in the synthesis of Disorazole C1, **8**.¹²

1.1.2 Pd-Mediated C-H Bond Functionalisation

Despite their versatility, traditional cross-coupling methodologies have disadvantages. They require pre-functionalisation of substrates. For example, with an organoboronic acid in the Suzuki-Miyaura reaction or an alkyl tin reagent in a Stille reaction. In cases where these reagents are not commercially available, or prohibitively expensive, this adds an extra reaction step to the pathway and may be a limiting factor. However, such pre-functionalisation is not required in direct C-H bond functionalisation (Figure 2). Broadly, C-H bond functionalisations can be split into those that involve the combination of C-H/C-X (where X is a halide or pseudohalide) or C-H/C-H bond (that is, oxidative couplings). Such transition metal-mediated transformations have employed palladium, rhodium, iron, ruthenium and other metal catalysts.¹³ This results in an enhanced efficiency in synthesis time, atom efficiency and reagent costs over traditional methodologies.

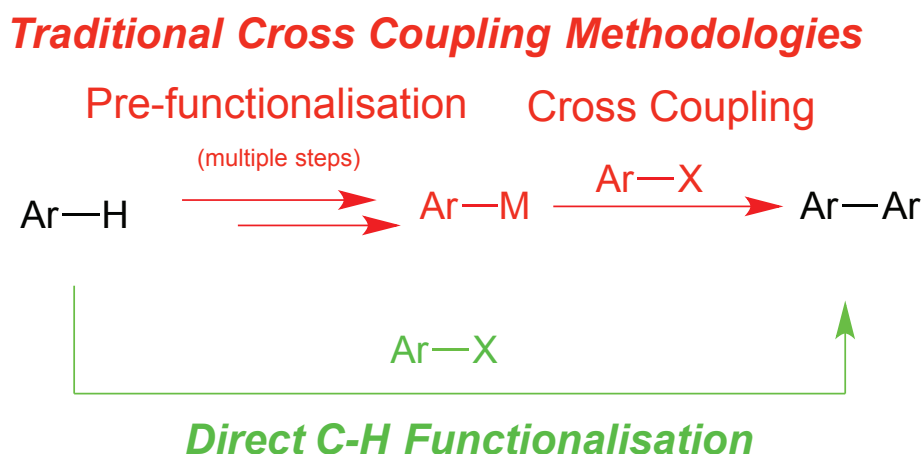
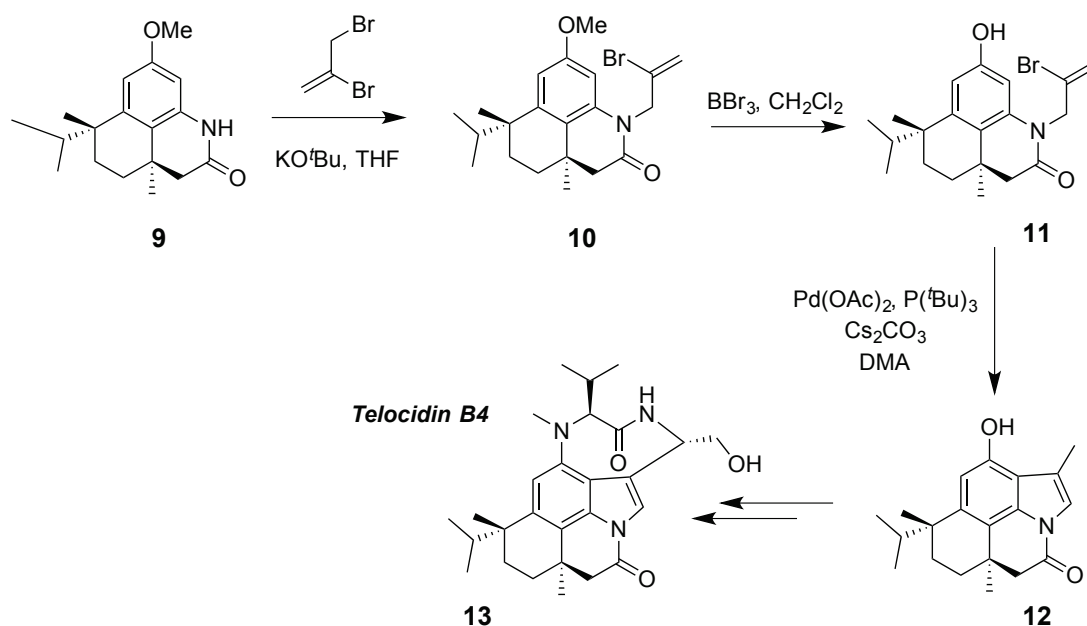


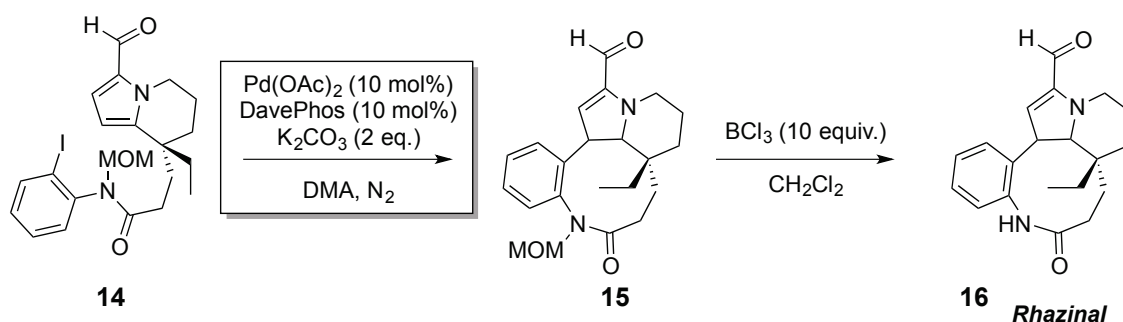
Figure 2: Comparison of direct C-H bond functionalisation and traditional cross-coupling methodologies (X = halide or pseudohalide or boronic acid, M = organometallic reagent).

C-H bond functionalisation remains relatively new, but there are an increasing number of examples of how it might be applied in the literature. For example, Sames and co-workers have published a synthesis of Teleocidin B4 **13** using C-H bond functionalisation in a key step (Scheme 3).¹⁴ Although the yield for the C-H bond functionalisation was moderate, previous methodology would have required pre-functionalisation of the arene ring, increasing the number of steps in the total synthesis. This demonstrates the efficiency of C-H bond functionalisation methodologies as previously discussed.



Scheme 3: Sames and co-workers synthesis of Telocidin B4, **13**.¹⁴

Trauner and co-workers have demonstrated the credibility of C-H bond functionalisations in complex molecules incorporating *N*-containing heterocycles. For example, in their total synthesis of rhazinal **16**, a Pd(OAc)₂/DavePhos-catalyst system is used in a 9-membered macrocyclisation (Scheme 4).¹⁵ The use of C-H bond functionalisation in the synthesis of natural products has recently been extensively reviewed by Chen and Youn.¹⁶



Scheme 4: Trauner and co-workers synthesis of Rhazinal.¹⁵

There has also been early work in the use of C-H bond functionalisation as a methodology for the introduction of labels for biological experiments. The labeling of complicated natural products is often used to deduce mechanistic information in biological processes. For example, the fluorescence of the amino acid tryptophan is

used to determine the surrounding protein environment of the tryptophan, and hence can be used to infer changes in protein conformation.^{17,18} In addition to fluorescence labeling, radio-,¹⁹ spin-,²⁰ electrochemical²¹ and biotin²² labels are also common. Previously labels might have been introduced by, for example, amide formation, or Cu-mediated 'click' cyclisation with azides.²³⁻²⁵ These methods, in general, do not result in the formation of C-C bonds. Although traditional Pd-mediated cross-coupling has also been utilized (*vide infra*), a significant improvement would be to take previously unmodified complex biomolecules and use a C-H bond functionalisation to introduce the label. Fairlamb, Baumann and co-workers have developed a C-H bond functionalisation of purine-based nucleosides which introduces a fluorescent group directly.²⁶⁻²⁸ However, the extension of this and other similar methodologies to more complex systems is limited by the need for exceptionally mild conditions.

This thesis will focus on the direct C-H bond functionalisation of the *N*-containing heterocycles to form C-Ar bonds. Specifically, the arylation of 1,3-azoles (and their benzo-fused analogues, Chapter 2) and indoles (in particular, the amino acid tryptophan, Chapter 3) by Pd, Cu and mixed Pd/Cu catalyst systems will be considered. An in-depth introduction to each area will be given at the start of each relevant chapter.

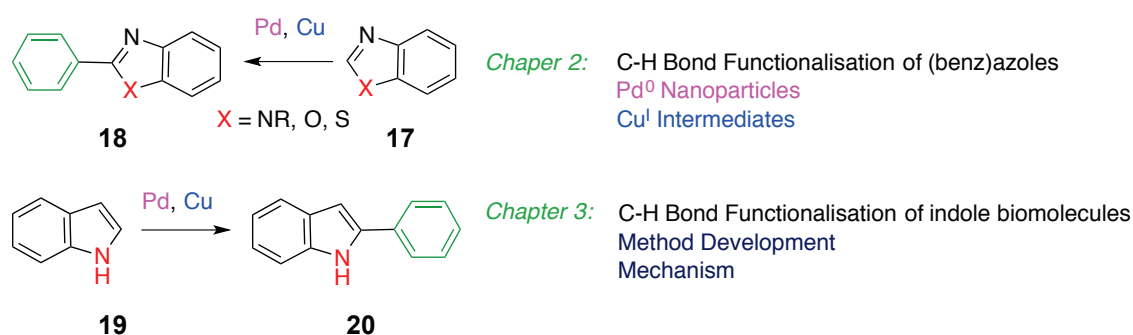


Figure 3: Representation of C-H bond functionalisation of heterocycles in this thesis.

1.1.3 A Definition for Reactions of C-H Bonds

In the chemical literature, reactions in which C-H bonds are modified, either by the formation of C-C or C-X (where X = N, O, S etc) bonds, by transition metal-mediated catalysis are known interchangeably as C-H bond 'functionalisation' or C-H bond

'activation' reactions depending on the author's preference. To further complicate matters, it is also acceptable to refer to metallation processes as 'activation' and the overall process as 'functionalisation'.

Before such reactions became more wide-spread in organic chemistry, the term C-H bond activation was generally used by organometallic chemists to refer to processes in which a metal inserts into a C-H bond, usually in an oxidative process. For example, this term might have been applied to an oxidative addition,²⁹ σ -bond metathesis³⁰ or σ -CAM mechanism.³¹ It would have not been applied to electrophilic or deprotonation/metallation processes, which are the common mechanistic basis for many organic direct C-H bond functionalisations/activations.

For the purposes of this thesis, 'activation' will be avoided. C-H bond functionalisation will refer to the overall process for the modification of a C-H bond in the formation of (unless otherwise stated) C-C bonds.

1.2 Aim of the Project and Objectives

1.1 Aims

- i. To develop new synthetic methods for the direct C-H functionalisation of *N*-containing heterocycles, and related complex biomolecules.
- ii. To increase our mechanistic understanding of catalytic C-H functionalisation processes.

1.2 Objectives

- i. To understand the mechanism of Pd/Cu-mediated direct C-H functionalisation processes for benzoxazoles, benzothiazoles and benzimidazoles, in particular the role of Pd⁰ nanoparticles and Cu-NHC complexes.
- ii. To develop a mild, low-temperature and selective method for the direct C-H functionalisation of the amino acid tryptophan, and to gain a mechanistic understanding of these complicated processes using a variety of techniques, including NMR and ReactIR[®], and to isolate possible Pd^{II} and Pd^{IV} intermediates in these reactions.
- iii. To synthesise a library of C2-aryl labeled tryptophan derivatives
- iv. To apply the methodology developed in (iii) to complex biomolecules, such as short peptides.

**CHAPTER 2:
C-H BOND FUNCTIONALISATION OF BENZAZOLES**

2.1 , Introduction

2.1.1 , Direct Arylation of Benzazoles

Nitrogen-containing heterocycles (azoles) and their benzo-fused analogues are found throughout nature and synthetic chemistry. Imidazole **21** for example, can be found in the proteinogenic amino acid histidine **22**, as well as in synthetic pharmaceuticals such as the antifungal medication clotrimazole **23**. Related heterocycles include oxazoles, thiazoles, xanthines (including caffeine **24**), purines (for example, adenosine) and benzimidazoles **25** (Figure 4).

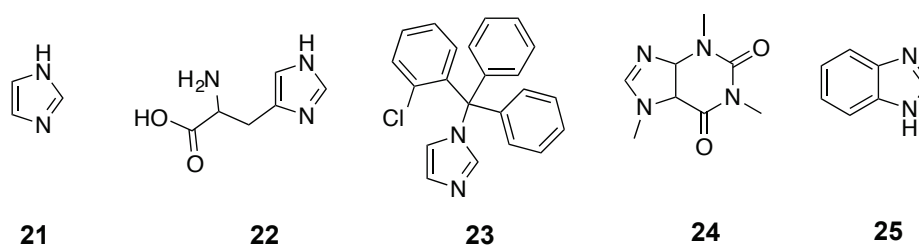
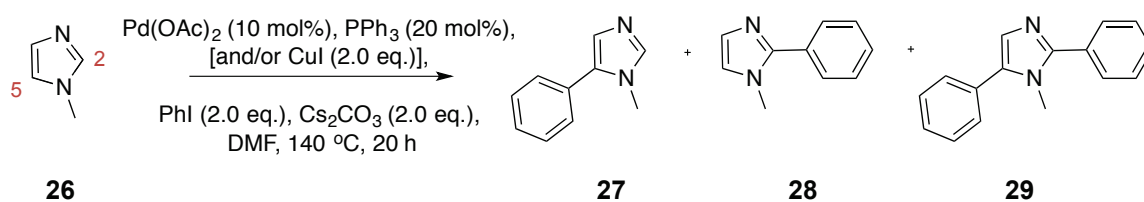


Figure 4: Examples of imidazole-based compounds. (a) *NH*-Imidazole, (b) histidine, (c) clotrimazole, (d) caffeine, and (e) benzimidazole.

The prevalence of these heterocyclic systems has resulted in high levels of interest in the synthesis of functionalised analogues. For many years, organic chemists relied on traditional annulation reactions.³² The advent of Pd-catalysed cross-coupling reactions allowed quick access to scaffolds previously time-consuming to make or entirely unavailable. This methodology also allowed for divergent functionality to be introduced later in synthetic pathways. However, as previously discussed (Chapter 1, Section 1.1.2, page 12), cross-coupling reactions bring their own disadvantages. This, and the relatively high reactivity of *N*-heterocyclic C-H bonds, has led to this class of compounds being fertile ground in the development of transition metal catalysed direct C-H bond functionalisation.

One key area addressed by direct C-H bond functionalisation methodology has been the formation of *N*-heterocycle-arene C-C bonds. Whilst many metals have been used for these transformations, systems mediated by Pd and Cu have proved to be of particular interest.³³ Miura and co-workers pioneered this field in the late nineties with a study of the direct arylation of 1-methylimidazole, **26**, with Pd(OAc)₂ and carbonate bases (Scheme 5).³⁴ By varying the nature of the metal catalyst system, it was found that the regioselectivity of the reaction could be influenced (Figure 5). When catalysed

by Pd alone, the reaction was preferentially selective for the C5 position **27** (although substantial quantities of C2/C5 diarylated product **28** were formed, decreasing the preparative utility of this reaction). However, the addition of stoichiometric quantities of CuI resulted in a switch of selectivity for the C2 position **29**. When the reaction was performed with CuI in the absence of Pd, the reaction was entirely regioselective for the C2 position **29**. However, under these conditions the overall yield was substantially reduced from 77% to 37%.



Scheme 5: Direct C-H bond functionalisation of 1-methylimidazole with Pd, Cu and Pd/Cu catalyst systems, as proposed by Miura and co-workers.³⁴ Results shown in Figure 5.

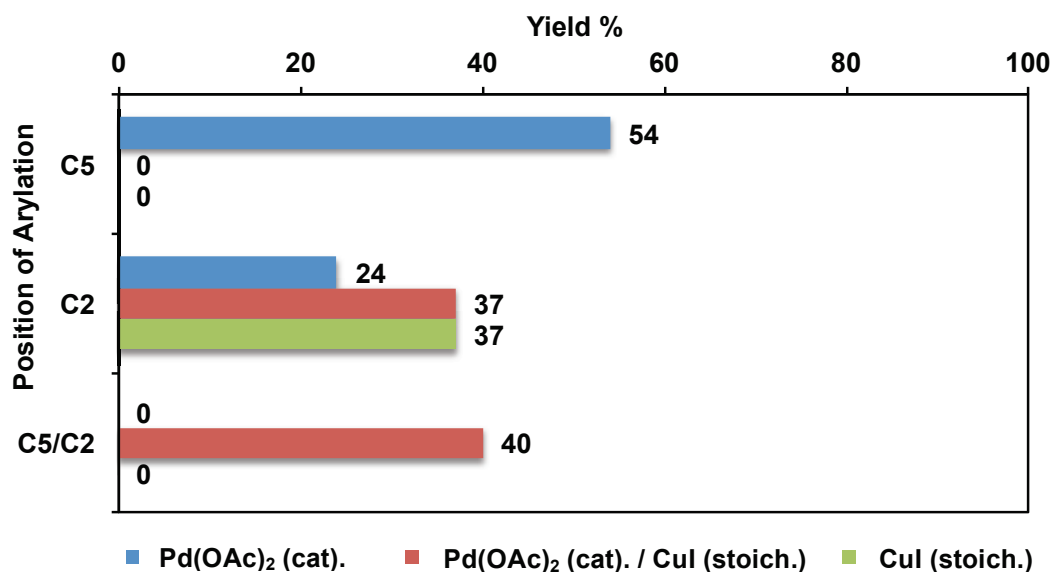
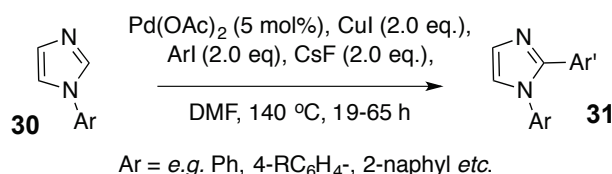


Figure 5: Regioselectivity outcome in the direct C-H bond functionalisation of 1-methylimidazole with Pd, Cu and Pd/Cu catalyst systems displayed graphically, as reported by Miura and co-workers.³⁴

Miura extended this study to other *N*-heterocycles and, whilst this reactivity was mirrored in thiazole analogues, the outcome of the addition of stoichiometric Cu^I salts was found to be substrate dependent. Benzo-fused substrates gave mixed results: the C2 arylation of benzo[*d*]oxazole was optimal in the absence of CuI (95% yield), whilst that of 1-methylbenzo[*d*]imidazole could be performed with CuI in the absence of Pd

(89% yield). Uniquely, diarylation of benzo[*d*]thiazole was most efficient with a substoichiometric quantity of CuI (2 eq.).

In an in-depth study by Bellina, Rossi and co-workers in 2005, the regioselectivity observed by Miura in the C-H bond functionalisation of imidazoles was corroborated.³⁵ Optimised, 'ligandless'^{*} conditions for this chemistry were later developed, with CsF emerging as a more suitable base than Cs₂CO₃ (Scheme 6).³⁶ It is hypothesised by Bellina that the greater efficacy of CsF results from greater solubility in DMF, increasing the homogeneity of the reaction mixture. However, CsF is a significantly harder base than its carbonate analogue (driven by the formation of the HF₂⁻ anion), and this may account for the difference in reactivity. A range of 2-arylated imidazoles were synthesised by this route in reasonable yields (38 – 79%), and little diarylated product was observed (<20%).

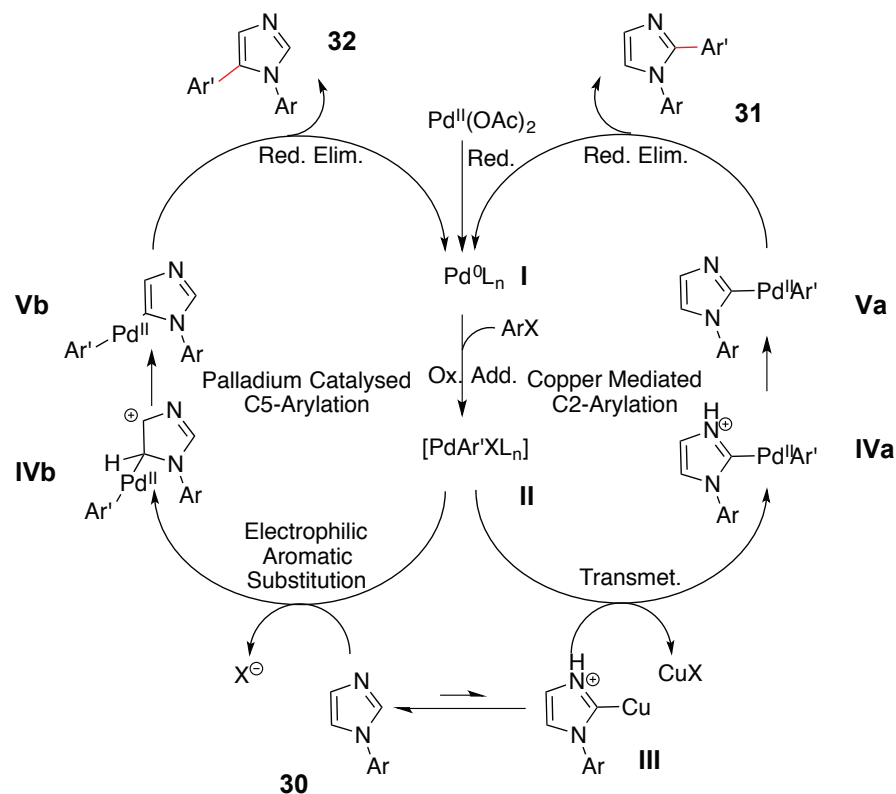


Scheme 6: Direct C-H bond functionalisation of 1-arylimidazoles using Pd/Cu catalyst systems and CsF base, as proposed by Bellina, Rossi and co-workers.³⁶

Bellina proposed that different catalytic manifolds are operative which gives rise to the different regioselectivity (Scheme 7). C5 arylation was proposed to result from oxidative addition of the aryl iodide to Pd⁰, followed by electrophilic aromatic substitution of the C5-H. The product is then reductively eliminated. Conversely, C2 arylation results from what can be described as a more traditional cross-coupling reaction mechanism. CuI was proposed to coordinate with the substrate, with this complex existing in equilibrium with an organocuprate **III**. This can be thought of as analogous to the Sonagashira reaction.¹⁰ Transmetalation with Pd^{II} can then occur with loss of CuX. The C2-arylated product is reductively eliminated. This mechanism was well supported by experimental evidence. Electron-donating substituents, such as phenylmethylsulfinate, were found to be rate enhancing. Bellina proposed that the substituents altered the acidity of the C2-H and, therefore, the rate of cupration.

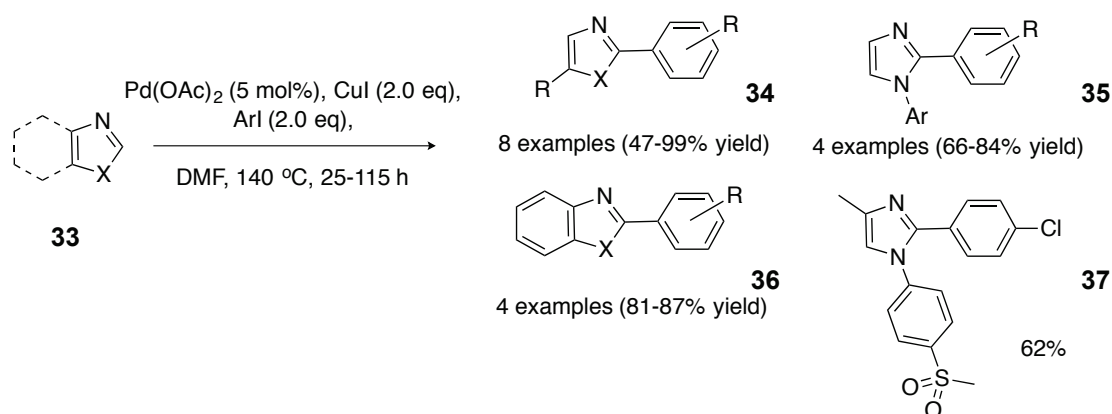
* 'Ligandless' refers, in this context, to the absence of deliberately added 2-electron

Further, decreased selectivity with increased Pd-loading supported the existence of a rate-limiting cupration.



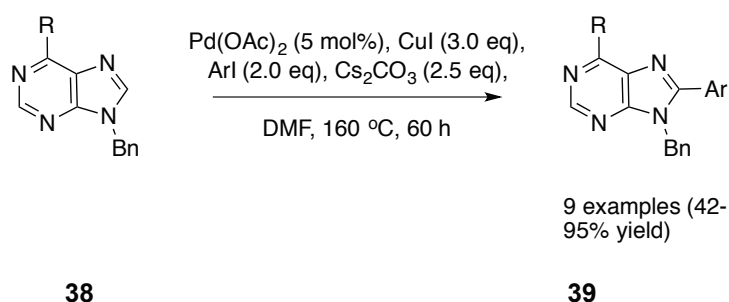
Scheme 7: Mechanism for the direct C-H bond functionalisation of imidazoles using Pd/Cu catalyst systems, demonstrating the reason for the effect of Cu^I stoichiometry on reaction regiochemistry.³⁶

However, this mechanism is not a complete description. Indeed, it suggests that the reaction should be catalytic in Cu^I , but when the stoichiometry of CuI was reduced the selectivity switched back to C5. To explain this, Bellina proposed that the equilibrium between the organocuprate and CuI lies towards the imidazole starting material. By using excess CuI , this equilibrium can be pushed towards the organocuprate.



Scheme 8: 'Base-free' conditions using Pd/Cu catalyst systems for the C-H bond functionalisation of (benz)azole heterocycles, proposed by Bellina and Rossi.^{37,38}

Bellina and Rossi later published 'base-free' conditions for the same reaction (Scheme 8).^{37,38} These reactions are performed at high temperatures in DMF. At these temperatures, DMF has been demonstrated to degrade to the dimethylamine.³⁹ As such, these reactions are free of carbonate base, but not strictly 'base-free' as described. These conditions were found to be applicable to a wide variety of 1,3-*N,X*-heterocycles including 1-substituted imidazoles (66–99% yield), thiazole (84% yield), oxazole (23% yield), and imidazole (47–89% yield with various aryl iodides). *NH*-indole was also successfully functionalised (35% yield). Piguel and co-workers applied these conditions to the C2-arylation of oxazoles using aryl bromides with microwave irradiation.⁴⁰

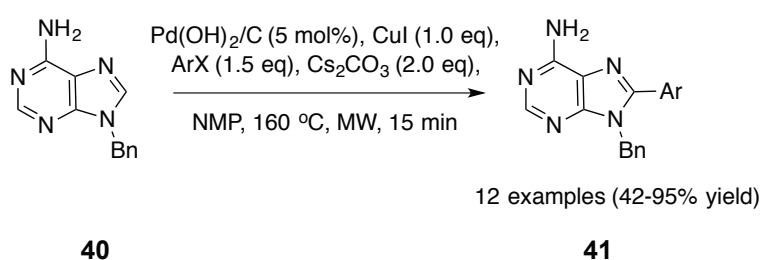


Scheme 9: The direct C-H bond functionalisation of benzyl-protected purines, as proposed by Hocek and co-workers.⁴¹

Hocek and co-workers demonstrated that similar conditions could be applied to benzyl protected purine heterocycles **38**, functionalising at the C8 position **39** (Scheme 9).⁴¹ In this case, Cs_2CO_3 was found to be the optimal base. Depending on reaction conditions,

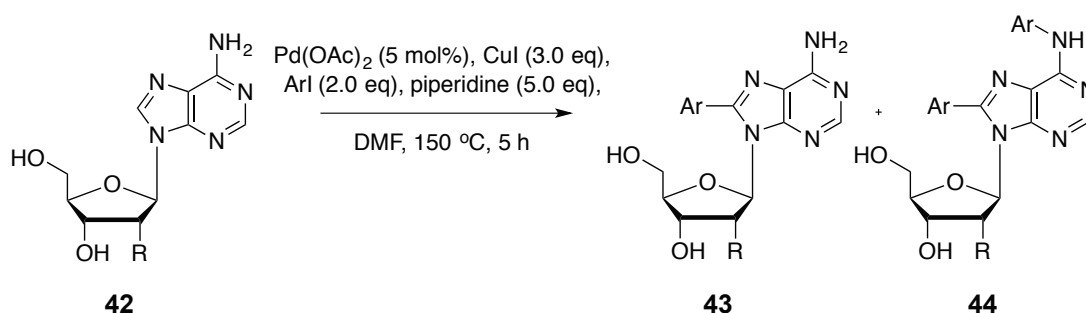
The direct C-H functionalisation of indoles will be discussed further in Chapter 4.

dipurinyl homocoupling and other by-products were also observed. The use of aryl iodides gave good yields (85-95%), whilst aryl bromides were less efficacious (62% yield for 1-bromo-2-methylbenzene, compared with 95% yield for the iodide analogue). The scope of these conditions with different substituents was explored in-depth.⁴² The use of 9-aryladenines was, although moderately successful, plagued by poor selectivity (with functionalisation proceeding at the N^6 position resulting from a competing Cu-catalysed Ullman-type reaction). This remained a problem even at lower temperatures and decreased reaction times (120 °C, 48 h).



Scheme 10: An improved direct C-H bond functionalisation of benzyl-protected purine using microwave irradiation, as proposed by Alami and co-workers.⁴³

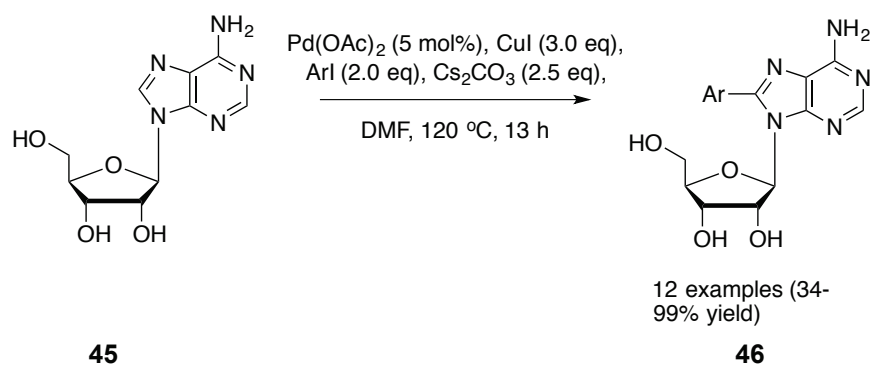
Alami and co-workers significantly improved upon Hocek's functionalisation of free-NH₂ adenines, using Pd(OH)₂/C, NMP solvent and microwave irradiation (Scheme 10).⁴³ A variety of aryl halides (iodides, bromides and chlorides) were found to give good yields (42-95% yield). Interestingly, 8-vinylation was also demonstrated to be possible with β -*E*-bromostyrene (55% yield).



Scheme 11: Direct C-H bond functionalisation of adenosine using Pd/Cu catalyst systems, at high temperature, as proposed by Hocek and co-workers.⁴⁴

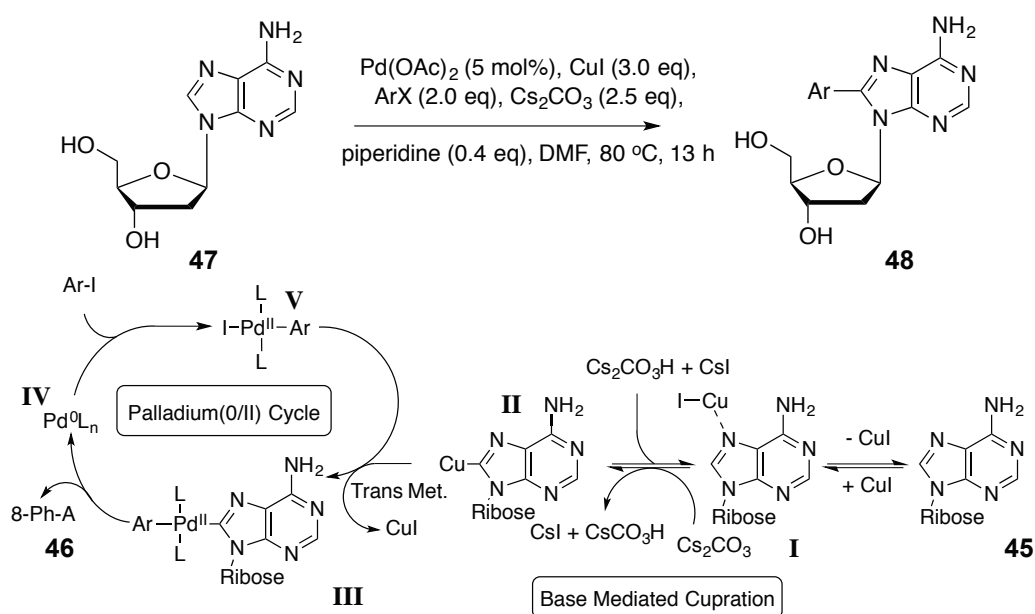
The high temperatures employed for these reactions made them unsuitable for application to natural purines, including nucleosides (Scheme 11). Hocek was able to functionalise adenosine **42**, using 4-iodotoluene at 150 °C using piperidine as a base (68% yield, with 18% of 8, N^6 -diarylated product **44**). A reduced yield was observed at

125 °C, with an increased proportion of diarylation. 2'-Deoxyadenosine was found to be too sensitive for these conditions.



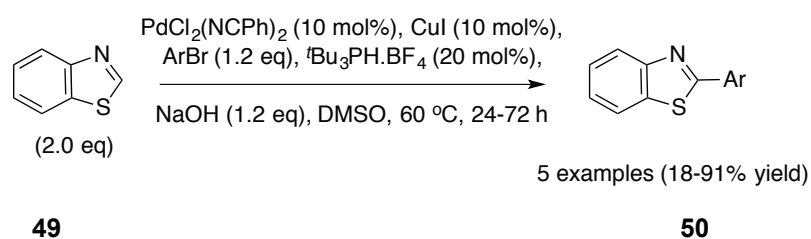
Scheme 12: An improved direct C-H bond functionalisation of adenosine using Pd/Cu catalyst systems, as proposed by Fairlamb and co-workers.²⁶

Fairlamb and co-workers simultaneously developed similar conditions with significantly better yields for the arylation of nucleosides (Scheme 12).²⁶ Reaction temperature and time were both reduced (120 °C, 13 h), and Cs₂CO₃ used as base. Application of these conditions to adenosine **45**, proved successful (34-99% yields). In general, electron-withdrawing *ortho*-substituted aryl iodides proved to be problematic, as is preceded in the literature for other Pd-catalysed reactions. For 2'-deoxyadenosine **47**, the temperature was lowered to 80 °C (84% yield was recorded using PhI). However, yields for the deoxyadenosine were not repeatable and found to be dependent on the solvent batch. The presence of trace dimethylamine, from the degradation of DMF, was found to reduce the Pd(OAc)₂ precatalyst to the active Pd⁰ species.³⁹ The addition of piperidine (0.4 eq.) was shown to give reliably high yields (Scheme 13).²⁷



Scheme 13: The direct C-H bond functionalisation of adenosine and deoxyadenosine at much reduced temperature, and reaction mechanism, as proposed by Fairlamb and co-workers.²⁷

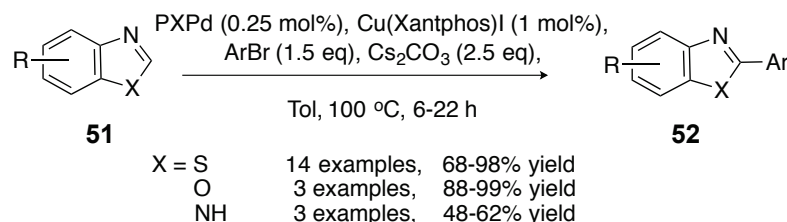
Fairlamb proposed a reaction mechanism similar to that of Bellina and Rossi (Scheme 13).³⁶ A recurring theme of these reactions is the necessity for stoichiometric quantities of CuI despite the proposed mechanisms suggesting a catalytic amount should function just as well.



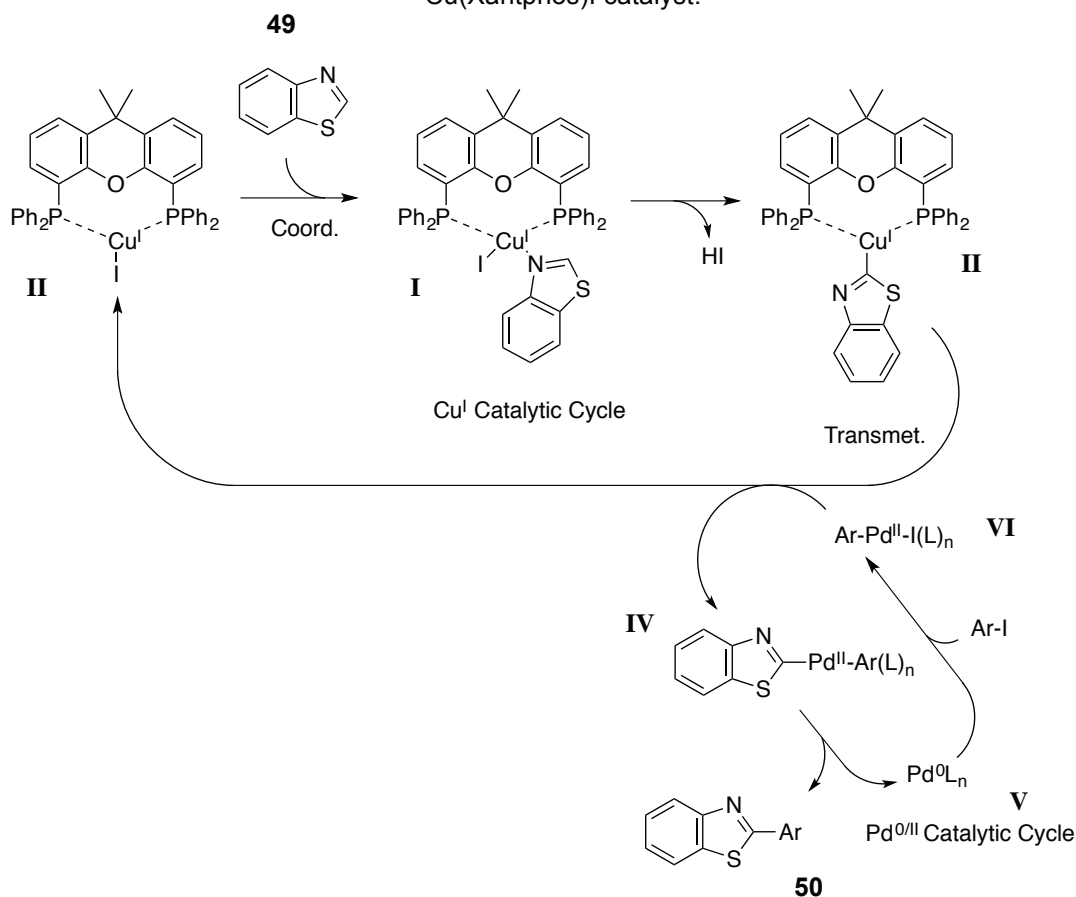
Scheme 14: The direct C-H bond functionalisation of benzothiazole, using a Pd/Cu catalyst system, as proposed by Mori and co-workers.^{45,46} Note the stoichiometry of the Cu.

Mori and co-workers have developed a mild process for the C2-arylation of benzothiazole **49**, using Pd and Cu in sub-stoichiometric quantities, with TBAF used as an 'activator' (its exact role is not commented on, however it is possible that degradation to tributylamine occurs *via* a Hoffmann elimination)⁴⁷ at 60 °C in DMSO (Scheme 14).^{45,46} This methodology was applied, with a sequential Pd-catalysed C5-arylation, to the synthesis of diarylthiazoles for liquid crystal applications. Mori later adapted these conditions for benzo[d]thiazole by substituting expensive TBAF with

solid NaOH and tri-*tert*-butylphosphine•HBF₄.⁴⁸ Although these adapted conditions could be used for thiazoles, some diarylation was observed.



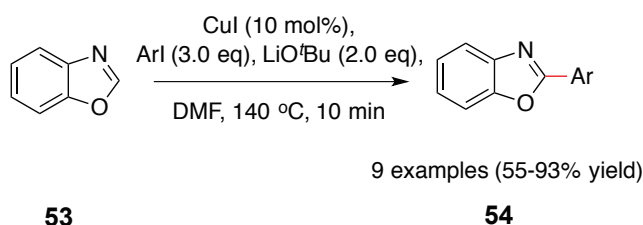
Scheme 15: The direct C-H bond functionalisation of benzazoles, using Pd and a Cu(Xantphos)I catalyst.⁴⁹



Scheme 16: Mechanism proposed by Huang and co-workers.⁴⁹

Interestingly, Huang and co-workers have proposed similar conditions to Miura, Bellina, Hocek and Fairlamb that are catalytic in CuI (Schemes 15 and 16).⁴⁹ A catalytic system comprising of Cu(Xantphos)I (1 mol% loading) **III** and PXPd (0.25 mol%) gave high yields with benzo[*d*]oxazole **53** and benzo[*d*]thiazole **49** but more moderate yields with benzo[*d*]imidazoles (benzimidazoles are generally more resistant to functionalisation than their sulfur or oxygen analogues due to increased *p*K_a).

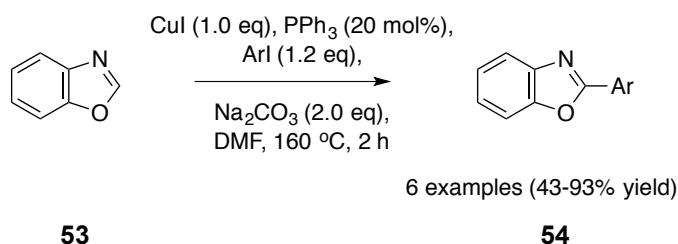
Miura's pioneering results demonstrated that it was possible to arylate with a CuI-only system. In 2007, Daugulis and co-workers reported conditions for the arylation of benzo[d]oxazole **53** using a substoichiometric quantity of copper with butoxide bases (Scheme 17).⁵⁰ Daugulis' conditions benefited from both short reaction times and high yields: after a reaction time of only 10 minutes, 91% yield was obtained with PhI. All aryl iodides assessed achieved yields of greater than 85% except 2-iodomesitylene (55% yield). However, high temperatures were required. Other fused heterocycles, including benzo[d]thiazole **49**, benzo[d]imidazoles and caffeine also gave high yields. However, under these conditions non-fused systems lacked the selectivity demonstrated by Miura.³⁴



Scheme 17: Cu-only mediated direct C-H bond functionalisation of benzoxazole, as proposed by Daugulis and co-workers.⁵⁰

Mechanistic investigations on these reactions indicated that base played a key role. KO^tBu, when used with iodobenzene-*d*₅ resulted in ¹H-incorporation at the *ortho* position of the arene. The authors explain that this suggests a benzyne mechanism. No such incorporation is observed when LiO^tBu is used. This suggests a deprotonation/Li-Cu transmetalation followed by the reaction of the organocuprate species with the aryl iodide.

Do and Daugulis later developed these conditions into a 'general method' for the arylation of arenes and heteroarenes.⁵¹ 1,10-Phenanthroline had been employed by Daugulis in the C-H functionalisation of fluoroarenes with Cu^I,⁵² and previously by Buchwald^{53,54} and Venkataraman⁵⁵ in the formation of C-N and C-O bonds. When applied to the C-H arylation of heterocycles, it allowed substrates previously requiring KO^tBu {which proceeds *via* a benzyne mechanism, making it incompatible with substituted aryl iodides (*vide supra*)} to be functionalised with weaker bases. For most acidic heterocycles (such as thiazole), K₃PO₄ was found to be effective. For others, including caffeine, LiO^tBu was used.⁵⁶



Scheme 18: Direct C-H bond functionalisation of benzoxazole using a stoichiometric quantity of Cu, and a substoichiometric quantity of PPh₃, as proposed by Miura and co-workers.⁵⁷ This methodology allows for a reduced stoichiometry of ArI.

The work of Daugulis and co-workers required a significant excess of aryl iodide (3 equivalents). Miura has demonstrated that by using a stoichiometric quantity of Cu^I and phosphine (20 mol%), a reduction in the stoichiometry of aryl iodide could be achieved in the C-H arylation of benzo[*d*]oxazole **53**.⁵⁷ This system also allowed for the use of weaker bases. These conditions were extended to 1-methylbenzo[*d*]imidazole, oxazole,⁵⁸ oxadiazoles, and triazoles.⁵⁹ When a sub-stoichiometric quantity of Cu^I was used, ring-opening (to *ortho*-(diphenyl)aminophenol) was observed. This side product was suppressed by increasing the stoichiometry of the aryl iodide, supporting Daugulis' findings.

2.1.2 , Pd Nanoparticles in Catalysis

Heterogeneous catalysis is defined as a process in which the catalyst is in a different phase from the reagents. Often, it involves metal species held on a support (e.g. silica, alumina or carbon). This allows for the easy separation of catalyst from reaction mixture during work-up and purification, which represents a significant advantage over homogeneous catalysis (that is, when the catalyst is in the same phase as the reagents).⁶⁰

Transition metal (including Pt, Pd and Re supported on alumina, silica and zeolites) nanoparticles have been used in catalysis since ca. 1950.⁶¹ Generally, this has been in large-scale gaseous processes, particularly in the petrochemical industry, and hydrogenation.⁶² Pt nanoparticles have also been utilised in catalytic converters.⁶³ Lewis and co-workers first identified the use of Pt nanoparticles in a solution system for hydrosilylation reactions.⁶⁴ Over this period there has been an increase in research interest, as can be shown by Figure 6.

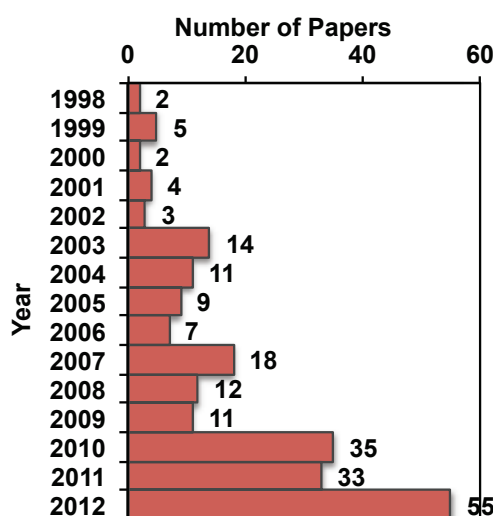
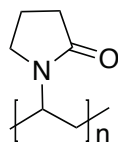


Figure 6: The number of papers matching the Web of Science® search phrase ‘nanoparticles AND catalysis’ on 17th April 2013.

The first use in a Pd-mediated cross-coupling reaction was in a Mizoroki-Heck reaction, reported by Beller, Herrmann and co-workers.⁶⁵ Pd colloid was derived from PdCl₂, N(*n*-oct)₄Br and sodium triethyl boronate (using the method of Bonnemann and co-workers).⁶⁶ Blackmond and co-workers have developed Pd nanoparticles supported on polymer (specifically polyvinylpyrrolidone, PVP **55** and applied these as catalysts in the Mizoroki-Heck reaction.⁶⁷ The nanoparticles were easily accessible from the hydrogenation of Pd₂(dba)₃.dba in the presence of the polymer. By varying the pressure of H₂, the size (as measured by transmission electron microscopy) of the nanoparticles could be controlled: higher pressures result in smaller nanoparticles, possibly due to forcing conditions resulting in rapid nucleation. From the micrographs, it could be seen that these nanoparticles were equidimensional polyhedra, allowing the authors to characterize them by applying statistics relevant to face-centred cubic cuboctahedra, also called truncated polyhedra (Figure 8).⁶⁸



55

Figure 7: Structure of polyvinylpyrrolidone (PVP).

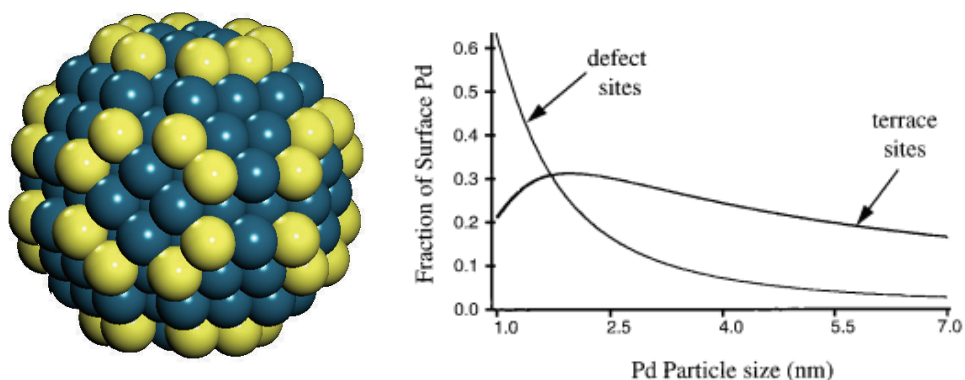


Figure 8: (a) A truncated icosohedral nanoparticle, showing terrace (blue) and defect (yellow) sites, and (b) graph showing the ratio of defect to terrace sites with the increase in particle size (nm).⁶⁹ (Nanoparticle image prepared by Prof. I. J. S. Fairlamb and Prof. A. F. Lee)
Adapted with permission from *Langmuir* 1999, 15, 7621.
Copyright 1999 American Chemical Society

On the surface of these polyhedral nanoparticles are two different Pd sites: terrace (high valent) and defect (low valent). Blackmond calculated how the ratio of terrace to defect sites varies with particle size (Figure 8). Nanoparticles of various sizes were then applied to a cross-coupling reaction. Exceptionally high yields (99%), TON ($100,000 \text{ h}^{-1}$) and TOF ($80,000 \text{ h}^{-1}$) could be obtained. Initial rates were measured for nanoparticles of each size, and normalized per surface Pd atom. If all nanoparticles were equally reactive, there should be no variation in initial rate with particle size. However, it was shown that smaller nanoparticles (*i.e.* those with a greater proportion of defect sites) had a higher initial rate. When the initial rate was normalized per *defect* Pd atom, there is no variation in the initial rate with particle size. This confirms that the defect site is the active site (whether active to surface chemistry or to leaching, *vide infra*). Further work on the Mizoroki-Heck reaction has been reported by Antonietti and co-workers (catalyzing with Pd colloids stabilized by block co-polymer micelles), and Ding and co-workers (liquid crystal polymer templates).^{70,71}

Reetz and co-workers reported a Suzuki-Miyaura reaction catalysed by Pd/Ni nanoparticles (prepared electrochemically, and redispersed in DMA).⁷² El-Sayed and co-workers developed a Suzuki-Miyaura cross-coupling reaction catalysed by nanoparticles (diameter *ca.* 3.6 nm) similar to those of Blackmond and co-workers, stabilized by PVP.⁷³ However, El-Sayed's nanoparticles were generated in aqueous EtOH solution from H_2PdCl_4 , using the methodology of Miyake and co-workers.⁷⁴ Using this methodology, nanoparticle size can be varied by changing the concentration of PVP, and type/concentration of alcohol in solution. El-Sayed used these

nanoparticles, in 40% EtOH at reflux, to synthesise a variety of biaryl products. Pd nanoparticles stabilised by PVP can also be generated by the reduction of Na_2PdCl_4 by H_2 in sodium polyphosphate, or from $\text{Pd}(\text{PPh}_3)_4$.⁷⁵

Despite these findings, the activation of C-X or C-H bonds in Pd-mediated catalysis had generally been considered to be an exclusively homogeneous process. Indeed, significant progress has been made in the elucidation of mechanisms for homogeneous cross-coupling reactions.^{76,78} However, some processes have displayed heterogeneous characteristics, including the observation of Pd^0 nanoparticles following the degradation of pre-catalysts (including palladacycles),⁷⁹ as well as kinetic profiles that cannot be explained by exclusively homogeneous mechanisms.⁸⁰ Some workers have attempted to explain such findings with Pd^0 nanoparticles acting as a 'reservoir' of molecular Pd^0 which is the active catalytic species in the homogeneous phase.^{81,82}

The catalytic activity of nanoparticle surfaces have been assessed in several ways. Single Pd crystals have been used as model systems in a clean environment using ultra high vacuum techniques. However, although evidence is available in the literature for the binding of sulphate anions and acetic acid,⁶⁹ little is known with regard to the activity of the organoboronic acids.

Rothanberg and co-workers have shown that Mizoroki-Heck and Sonagashira couplings can be catalysed by Pd clusters of < 5 nm in diameter. That is, using a nanoporous alumina membrane to separate other reagents from Pd nanoparticles of 15 nm in diameter (stabilized by $\text{N}(n\text{-oct})_4\text{Br}$, and too large to pass through the membrane) reaction would still occur. Rothanberg described this as being indicative of molecular Pd leaching. However, since Blackmond and co-workers' most active PVP stabilized Pd nanoparticles are <5 nm, this is inconclusive. Davis and co-workers have reported studies in which an atomic force microscopy (AFM) probe was coated with Pd nanoparticles.⁸³ This probe was then used to initiate spatially-controlled coupling of surface-tethered aryl halides with phenylboronic acid. Such a reaction would be unlikely to occur if the reaction was mediated by Pd species in solution.

Fairlamb, Lee and co-workers have used *in operando* (*i.e.* under working conditions) X-ray absorbance spectroscopy (XAS) to study PVP stabilized Pd nanoparticles in Suzuki-Miyaura cross-coupling reactions.^{84,85} The XAS studies yielded TOF, which can be expressed with respect to nanoparticle size. When the TOF was normalized per

surface Pd atom, an inverse relationship with nanoparticle size was observed. When normalized per defect site, no variation with nanoparticle was observed. This supports the findings of Blackmond and co-workers. However, it has been suggested that this correlation may result from the greater propensity of lower coordinate Pd to solubilize (*i.e.* leach). XAS was further used to study leaching from the nanoparticle leaching sites – the co-ordination number of the defect sites did not change throughout the reaction (Figure 9). This data was confirmed by monitoring of EXAFS fine structure (Figure 9 inset), which remained constant throughout the reaction.

Fairlamb and co-workers also conducted leaching/spiking experiments on this system. The reaction was run under normal working conditions, and conversion monitored. At $t = 18$ min, the theoretical amount of leached Pd was added in the form of Pd(OAc)₂. No change in conversion was observed as compared to normal working conditions. The Hg drop-test has been shown to inhibit surface reactions.^{86,87} When Hg was added to the reaction at $t = 8$ min, there was a significant reduction in conversion (note: the Hg-coated Pd nanoparticles were characterised by XPS, which revealed the formation of Pd core, Hg-shell nanoparticles). Conversion did not recover on the addition of Pd(OAc)₂ at $t = 18$ min (the amount added mirrored the theoretical amount of Pd that would be leached from a nanoparticle surface).

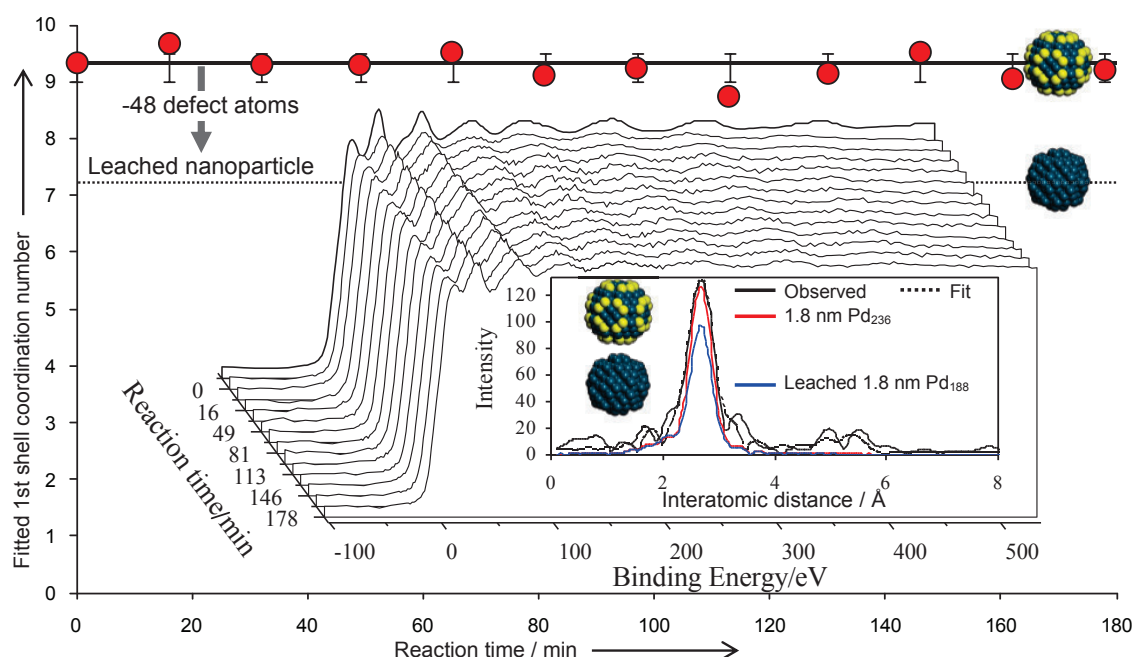
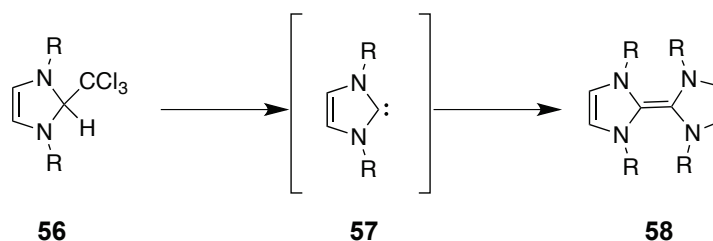


Figure 9: XAS study demonstrating lack of leaching from Pd-PVP nanoparticles.^{85,88}
Adapted with permission from *Angew. Chem, Int. Ed.* 2010, 49, 1820.
Copyright 2010 Wiley®

Evidence for nanoparticles being involved in direct C-H bond functionalisation reactions remains scarce. Fairlamb and co-workers have demonstrated that Pd nanoparticles do form in the C-H bond functionalisation nucleosides (*vide supra*), and these nanoparticles have been characterized by TEM.^{26,27}

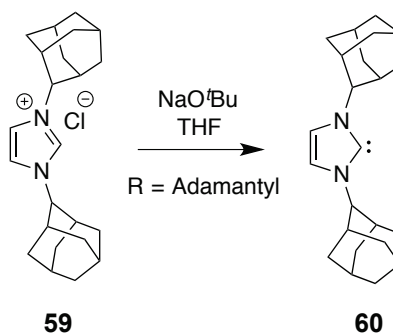
2.1.3 , The Role of *N*-Heterocyclic Carbenes in Cu-Catalysis

The existence of *N*-heterocyclic carbene (NHC) species was first hypothesised by Wanzlick and co-workers (Figure 19).⁸⁹ Although only a dimer (the Wanzlick dimer **58**) was isolated from this reaction, it was conjectured that an intermediate carbene was generated from the elimination of chloroform.



Scheme 19: Synthesis of the Wanzlick dimer.⁸⁹

Wanzlick dedicated much of his career to the isolation of a stable *N*-heterocyclic carbene but never succeeded. It was not until the 1990s that Arduengo and co-workers published their isolation of 1,3-diadamantylimidazol-2-ylidene **60**. This carbene (IAd) ' accessed from the deprotonation of the parent imidazolium salt **59** (Scheme 20) ' has been shown to be kinetically and thermodynamically stable. Indeed, Arduengo has retained a solution of IAd in THF-*d*₈ (under an atmosphere of CO) for over seven years without observing decomposition or other reaction. The lack of reactivity when stored in this manner is unexpected, as other carbenes have been shown to generate ketenes under CO atmospheres.⁹⁰



Scheme 20: Synthesis of IAd, as proposed by Arduengo.⁸⁹

A crystal structure of IAd **60** obtained by Arduengo demonstrated that the valence angle (102°) was consistent with calculated angles for singlet carbenes. Arduengo later isolated a variety of analogues, including *p*-tolyl **62** (ITol), mesityl **63** (IMes), and methyl **66** (IMe) (Figure 10).

The isolation of IAd resulted in significant interest in the synthesis of similar stable nucleophilic carbenes, including other imidazole heterocycles and structures based on triazole backbones. Germanylenes⁹¹ and silylenes⁹² have also been isolated and characterised

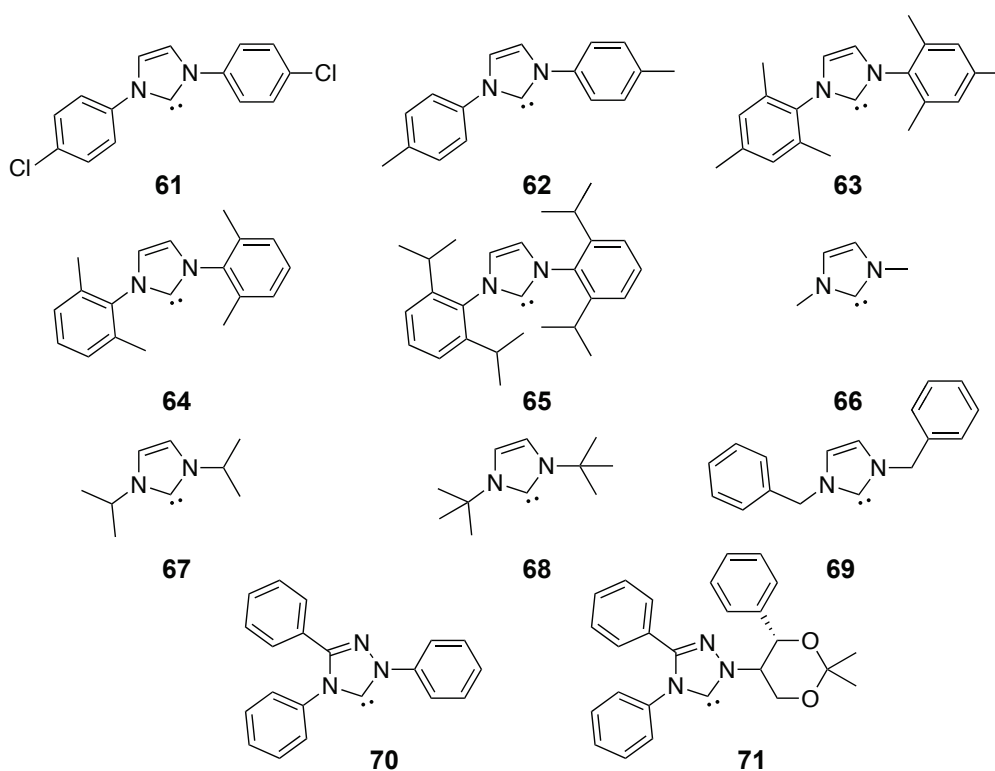
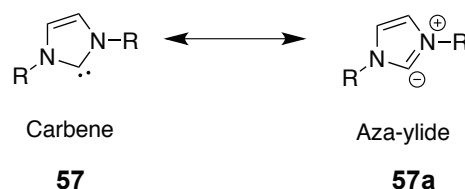


Figure 10: Examples of unsaturated *N*-heterocyclic carbenes.

Arduengo and co-workers turned to the isolation of saturated variants of these compounds. Calculations and electron density studies indicated that, although, delocalization of electrons did play a part in the stability of unsaturated NHC species, there was little evidence of a highly delocalized π -system. In fact, compared to their parent imidazolium salts they appeared to show a substantial decrease in delocalization. 1,3-Dimesitylimidazolin-2-ylidene (SIMes) was the first of these carbenes to be isolated, again from the deprotonation of parent imidazolium salts. This discovery led to, as with their unsaturated counterparts, the synthesis of a

significant library of analogues. Shortly after, Alder and co-workers published the isolation of an acyclic diaminocarbene (bis(diisopropylamino)carbene).⁹³

In the literature, there has been some discussion as to the electronic nature of *N*-heterocyclic carbenes. A true carbene is defined as a compound containing a two-coordinate carbon, in oxidation state II, which has two non-bonding electrons and no formal charge. In *N*-heterocyclic carbenes ‘a subset of the Fischer carbene class’ the divalent carbon centre is stabilized by a ‘push-pull’ effect: electron density is withdrawn by the nitrogen atoms through the σ -bond network, whereas the nitrogen lone pairs donate electron density into the empty p-orbital. As such, these species can be seen as either truly carbenoid **57** in character or as diamino ylides **57a** (Scheme 21).



Scheme 21: Resonance structures of *N*-heterocyclic carbenes. There is debate as to whether these are most appropriately described as *N*-heterocyclic carbenes or amino ylides.

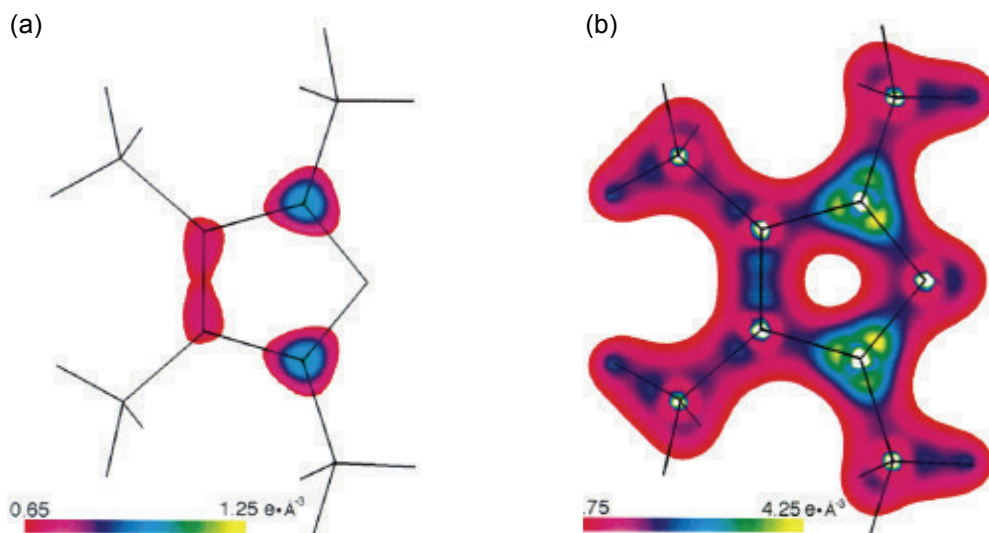


Figure 11: Diagrammatic representation of calculations showing the electron density of a model *N*-heterocyclic carbene (a) in the molecular plane, and (b) 70 pm above the molecular plane.⁸⁹

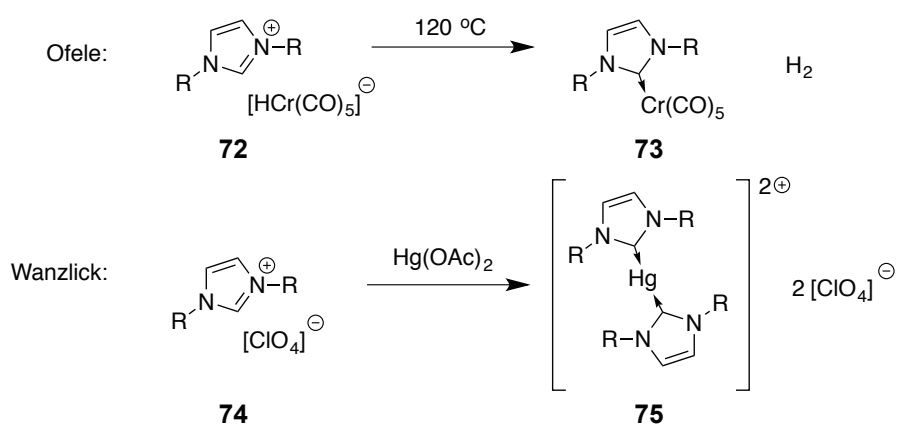
Adapted with permission from *Acc. Chem. Res.*, 1999, 32, 913.

Copyright 1999 American Chemical Society.

Neutron diffraction, X-ray diffraction, DFT calculations and solid-state ^{13}C NMR spectroscopic data published by Arduengo have pointed to a true carbene character.^{94,95} In the molecular plane, electron density is highest at the C2 position, *i.e.* a σ lone-pair as would be expected in a singlet carbene. At 70 pm above the molecular plane, the π -bond of the C4-C5 bond is clearly visible, as are the nitrogen lone-pairs (Figure 11). However, little delocalization of these lone pairs into the empty p-orbital at C2 can be seen. This hypothesis has been supported by various *ab initio* studies.

In-depth work by Schwarz and co-workers has indicated that there is a role for aromatic stabilization in unsaturated *N*-heterocyclic carbenes (that is, an ylide model), but noted that different theoretical approaches lead to different conclusions. Schwarz provides, in this paper, a comparison of different work on the subject and the conclusions reached. Studies by Sauers indicate that the extent of aromatic stabilisation is dependent on the carbene studied, and that in some there is theoretically some build-up of negative charge on the C2 position, as one might expect in an ylide model.

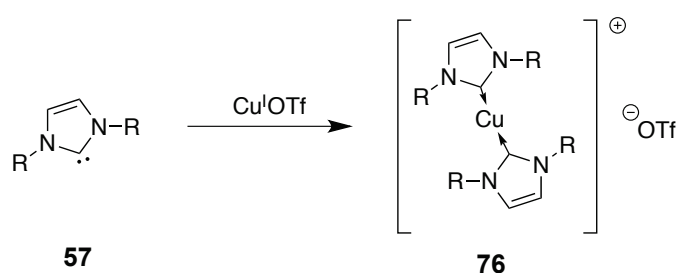
NHC species have shown to be of interest to the organocatalytic community, but have found a key role in organo-transition metal chemistry, in particular transition-metal mediated catalysis. The first NHC-metal complex was reported by Ofele in the mid-'sixties, long before the isolation of stable free carbenes.⁹⁶ Simultaneously, Wanzlick published a synthesis of NHC-Hg compounds (Scheme 22).



Scheme 22: Early organometallic complexes containing *N*-heterocyclic carbenes.^{96,97}

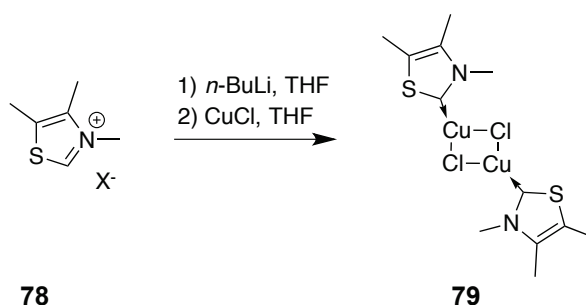
Note: the use of perchlorate salts (ClO_4^-) should be carried out with extreme caution, as they are potentially explosive.

NHC-Cu^I complexes have been shown to have important roles in catalysis,^{98, 101} and demonstrated cytotoxic activity.¹⁰² The first NHC-Cu^I complex was isolated by Arduengo and co-workers from Cu^IOTf (Scheme 22). Nolan and co-workers have used similar homoleptic complexes, with PF₆ or BF₄ counter anions, as efficient pre-catalysts for the hydrosilylation of carbonyl compounds.¹⁰³ These catalysts mediated these reactions with good yields and selectivity with short reaction times.



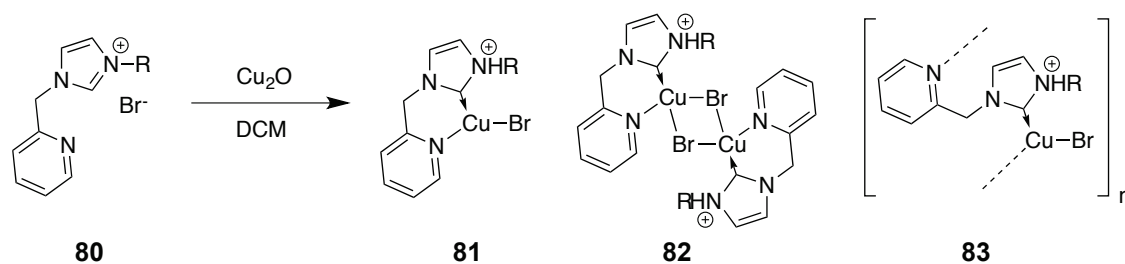
Scheme 23: Synthesis of the first Cu-NHC complex, as proposed by Arduengo and co-workers.¹⁰⁴

However, the first monocarbene complex was characterised by Raubenheimer and co-workers (Scheme 24). These complexes using thiazole-derived carbenes existed as chloride dimers in the solid-state. This methodology was extended to a greater variety of thiazolylidene and *N*-methylimidazolylidene scaffolds.¹⁰⁵



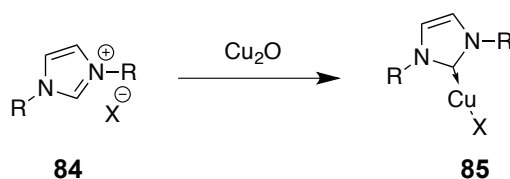
Scheme 24: Initial monocarbene Cu-NHC complex, as proposed by Raubenheimer and co-workers.¹⁰⁵

NHC-Cu complexes remained relatively rare in comparison to other group 11 transition metals. This was despite calculations by Boehme and Frenking reporting that the C-Cu dissociation energy would be 61 kcal mol⁻¹ higher than their Ag congeners. Danopoulos and co-workers synthesised pyridine-*N*-functionalised Cu^I complexes from imidazolium bromides and Cu₂O (Scheme 25).¹⁰⁶ Dependent on substituents and recrystallisation conditions, these complexes existed as monomers, dimers and polymers.



Scheme 25: Synthesis of Cu-NHC complexes with Cu_2O , as proposed by Danopoulos and co-workers.¹⁰⁶

Douthwaite and co-workers used this method in the synthesis of carbene-phenoximine complexes.¹⁰⁷ Cazin and co-workers demonstrated that this 'green' approach (the only by-product being water) to $\text{Cu}(\text{NHC})\text{X}$ **85** formation could be applied to a variety of well used NHC.HX **84** salts, including (S)IMes, (S)IPr, and (S)ICy in different solvents (Scheme 26, Figure 12).¹⁰⁸



Scheme 26: Synthesis of $\text{Cu}(\text{NHC})\text{X}$ complexes using the Danopoulos method, in different solvents, as proposed by Cazin and co-workers.¹⁰⁹

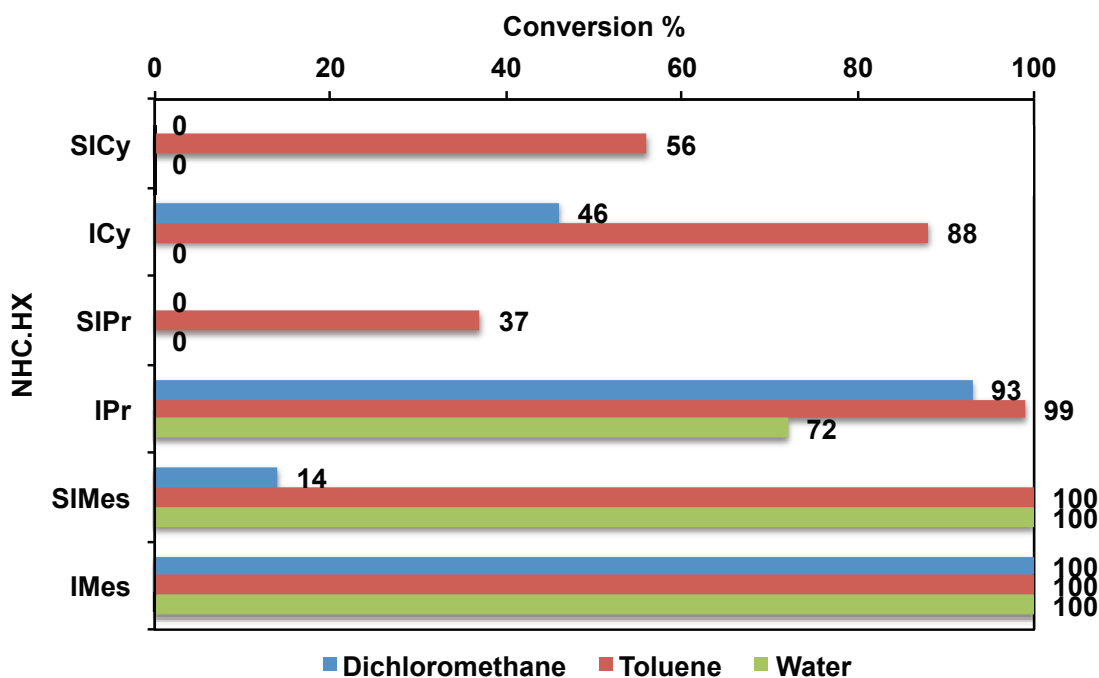
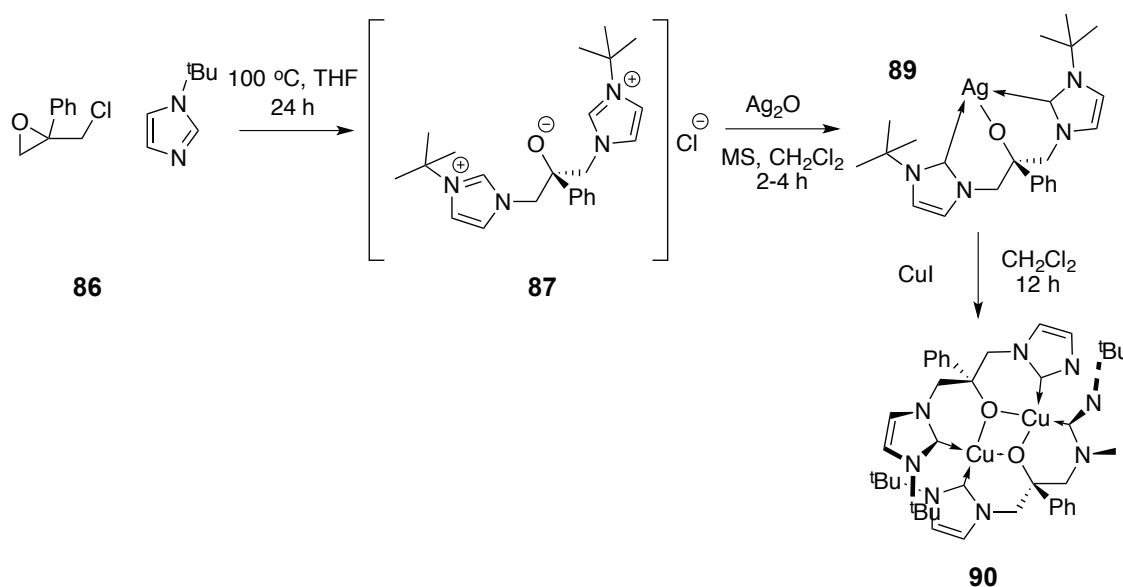


Figure 12: Results for the synthesis of Cu(NHC)X complexes using the Danopoulous method, in different solvents, as proposed by Cazin and co-workers.¹⁰⁸

In water, when ICy or SICy are used, formation of imidazolid-2-one is observed, confirming findings by Albrecht (*vide infra*).¹¹⁰

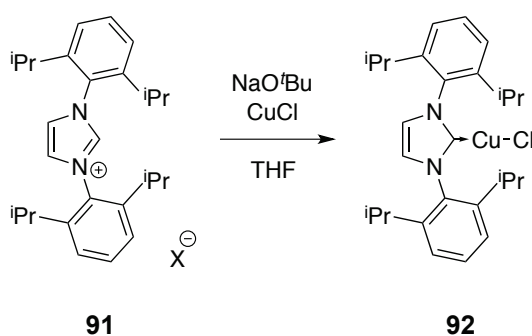
Arnold and co-workers reported the first use of a NHC-chelate ligand in Cu^I complexes (Scheme 27).¹¹¹ The proligand (*i.e.* the imidazolium salt) is synthesised in one step with epichlorohydrin and 1-*tert*-butylimidazole. The ligand is then treated with Ag₂O, followed by Cu^I, to yield **90** (85% yield).



Scheme 27: First synthesis of a NHC-chelate ligand, proposed by Arnold and co-workers.¹¹¹

Other bidentate NHC-CuI complexes have been synthesised by Bellemin-Laponnaz and Gade.¹¹²

Buchwald and co-workers synthesised the first NHC-Cu complex of the form (NHC)CuX, where X is a halide, *via* the simple reaction of free carbene with Cu^ICl (Scheme 28).⁵³ The resulting complex was found to be air and moisture stable, and demonstrated to be useful as a catalyst in the conjugative reduction of α,β -unsaturated carbonyl compounds.

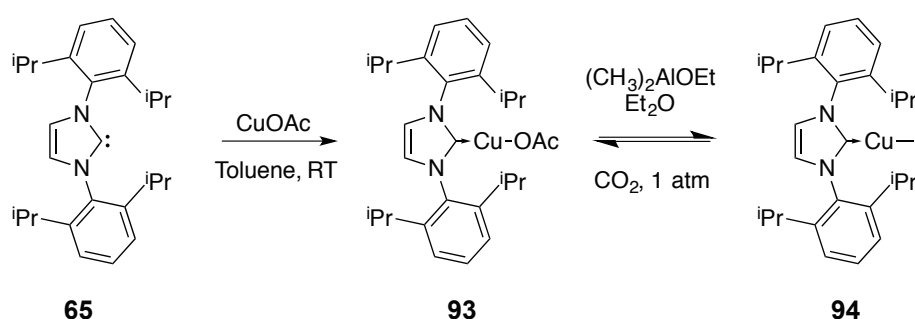


Scheme 28: Synthesis of monocarbene Cu-NHC complexes, as proposed by Buchwald and co-workers.⁵³

In similar work by Nolan and co-workers, the reduction of carbonyls was performed by (NHC)CuCl complexes formed *in situ* from the parent imidazolium salt.¹¹³ The reaction was found to be as efficacious when a pre-synthesised (using a method identical to that used by Buchwald), well-defined (NHC)CuCl complex was used. Lebel has utilized Nolan's catalysts in the synthesis of styrenes and aliphatic alkenes from carbonyls.¹¹⁴

Nolan later demonstrated the utility of Cu(NHC)X complexes in the hydrosilylation of ketones and 'click' chemistry,¹¹⁵ and to the direct C-H bond carboxylation of arenes.¹⁰⁹

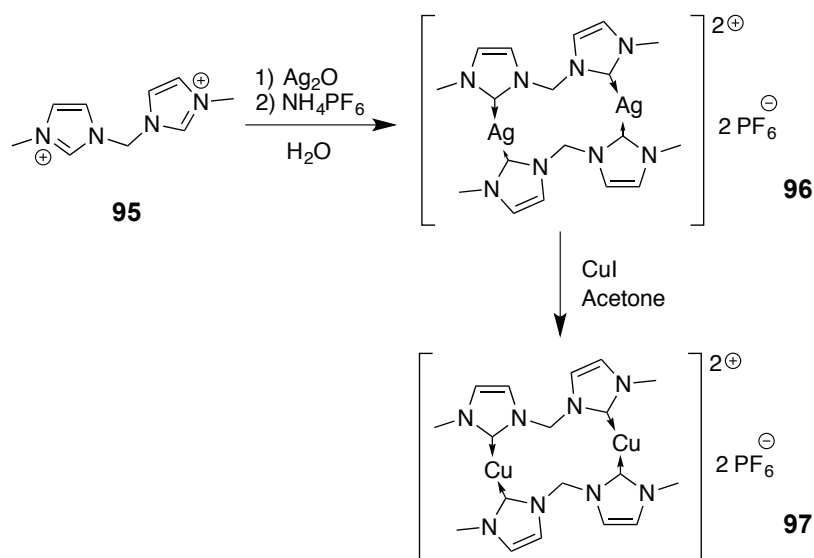
Sadighi and co-workers have successfully synthesised a (NHC)CuMe complex **94**, via a novel (NHC)CuOAc complex **93** (Scheme 29).¹¹⁶ This complex reacts cleanly with CO₂ to reform the acetate complex in near-quantitative yield, which suggests these species could be utilised in Cu^I-catalysed carboxylation reactions. Sadighi later published syntheses of (NHC)CuO^tBu, (NHC)CuH and (NHC)Cu(alkenyl) complexes. Wang and co-workers have successfully synthesised (NHC)Cu^ICp complexes.¹¹⁷



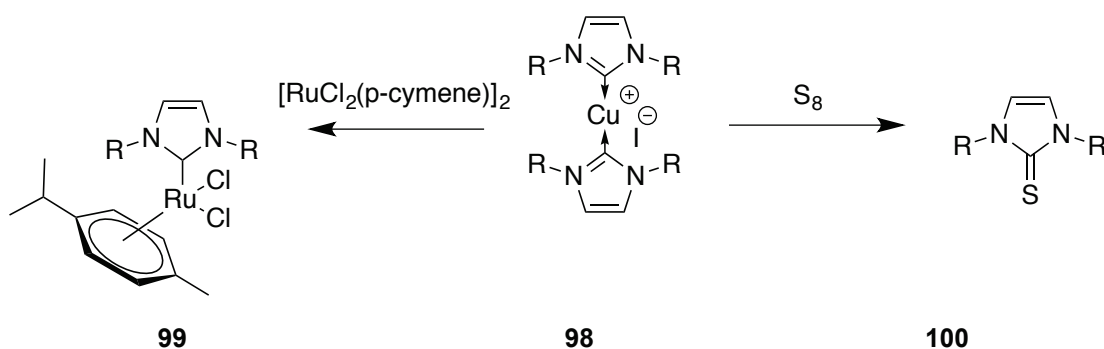
Scheme 29: Synthesis of a (NHC)CuMe complex, proposed by Sadighi and co-workers.¹¹⁶

Tsubomura and co-workers have synthesised a bi-metallic NHC-Cu^I complex **97** (Scheme 30).¹¹⁸ In doing so, they also demonstrated these complexes could be produced *via* transmetalation from Ag^I. These complexes were considered for applications as luminescent materials in light emitting diodes. Similar bi-metallic complexes 'with only one carbene per metal' were reported by Hoffman and co-workers.¹¹⁹

Albrecht and co-workers, after a study of a comprehensive library of *bis*-NHC-Cu^I complexes, demonstrated that substituents play an important role in stability.¹¹⁰ Their complexes, synthesised either by the Buchwald/Nolan method or from the reaction of free carbene with [Cu(NCMe)₄]PF₆, demonstrated that aryl (e.g. IMes or IDipp) produced the most stable Cu^I complexes, whilst alkyl substituents (including seemingly more hindered NHCs such as IPr) induced rapid demetallation in the presence of water. Albrecht used these complexes in a novel ligand transfer to Ru (Scheme 31). Furst and Cazin demonstrated that Cu(NHC)X complexes could also be used as carbene transfer reagents to Au^I and Pd^{II}.¹²⁰



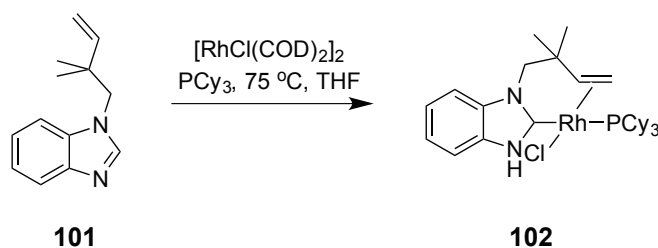
Scheme 30: Synthesis of bimetallic Cu(NHC) complexes, proposed by Tsubomura and co-workers.¹¹⁸



Scheme 31: Cu(NHC) complexes as a carbene transfer agent to S and to other transition metals, as proposed by Albrect and co-workers.

Metal-carbene complexes as intermediates in catalysis are well known, and have been particularly well studied in cross-metathesis reactions. CuI carbene complexes have been implicated in the Cu-catalysed cyclopropanation of alkenes.^{121, 123} However, in general these intermediates have been traditional Fischer or Schrock carbenes, rather than NHCs.

Bergman and Ellman have shown the intermediacy of NHCs in the C-H bond functionalisation of benzimidazoles with Rh (Scheme 32).¹²⁴ Using calculations and stoichiometric studies, it was demonstrated that this intermediate is a catalytic resting state, and the insertion into the Rh-carbene bond is the rate-limiting step of this reaction.



Scheme 32: Bergman and Ellman's synthesis of proposed Rh(NHC) intermediates for C-H bond functionalisation reactions.¹²⁴

NHCs have most usually been synthesised *via* the deprotonation of their onium salts, as demonstrated by Arduengo's initial synthesis of IAd.¹²⁵ However, the generation of carbene by this method can prove problematic, especially in the presence of other acidic protons (benzylic positions, for example). A relatively underused method, developed by Hedrick and Waymouth, uses pentafluorophenyl in place of a chloroform adduct.¹²⁶ These have been shown, on heating, to release free carbene and C₆F₅H, and have been used as organocatalysts in polymerisation chemistry. They are also useful synthons for generating the free carbene for use in organometallic chemistry.

2.1.4 Summary

As detailed above, direct C-H bond functionalisation with Pd, Cu and Pd/Cu systems has become an important and highly productive area of research. However, the mechanism of these reactions – in particular the role of Cu^I salts – is poorly understood. Further, although the catalytic phase of traditional Pd-mediated cross-coupling reactions has been probed in depth, the possibility of heterogeneous or hybrid-phase catalysis in direct C-H bond functionalisation chemistry remains relatively underexplored.

In this chapter are detailed studies into the role played by Pd⁰ nanoparticles in the C-H bond functionalisation of benzoxazoles and benzothiazoles using pre-synthesised Pd⁰ nanoparticles, trapping of nanoparticles formed *in situ*, and their analysis by transmission electron microscopy. The role of Cu^I in direct C-H bond functionalisation chemistry (specifically that developed by Miura, Bellina and Rossi) is probed using model (1,3-dibenzylbenzimidazolidene)copper(I) halide complexes in stoichiometric reactions.

2.2 C-H bond Functionalisation of Benzazoles with Pd⁰ Nanoparticles

2.2.1 Synthesis of Pd-PVP Nanoparticles

Pd⁰ nanoparticles supported on PVP (molecular weight ca. 29,000) were synthesised by reduction in the presence of polymer, using the method of Fairlamb and co-workers.^{60,84} The particles produced were a black, glass-like solid which were ground to a black powder for use in reaction mixtures using a pestle and mortar.

The particles were suspended in EtOH, applied to transmission electron microscopy slides, and micrographs of the sample recorded (Figure 13). These experiments were performed with the assistance of Thomas Herbert MChem (project student).

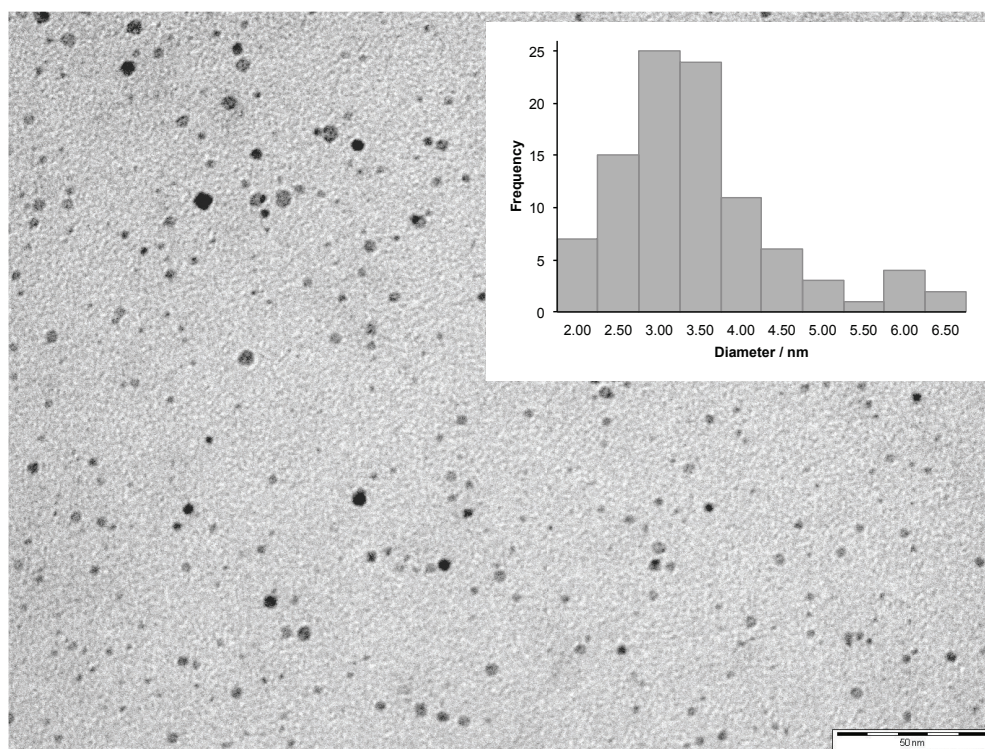


Figure 13: Example electron micrograph of sample of pre-synthesised PVP (MW = 29,000) stabilised Pd nanoparticles. Inset shows histogram of particle diameter (nm) across a sample of nanoparticles ($n = 98$).

A random sample of nanoparticles was chosen ($n = 98$) and their diameter measured manually. Statistical data is shown in Table 1. This data can also be represented as a histogram (inset, Figure 13).

Table 1: Table showing simple statistical measurement for Pd-PVP particles (MW = 29000). SD = Standard Deviation, IQR = Interquartile Range, IQM = Interquartile Mean

	Mean	SD	Median	Mode	IQR	IQM
Pd-PVP	3.20	1.01	3.09	3.34	1.17	3.04

This data shows that the particles are within the 2-5 nm size regime and, within error, are consistent with previously reported data.⁸⁴

X-ray photoelectron spectroscopy (XPS) on this sample provided information on particle surface oxidation state, and was performed by Dr K. Wilson (Cardiff Catalysis Institute, University of Cardiff). The Pd 3d XP spectrum for the sample is shown in Figure 14. It indicates the presence of Pd⁰ and a small amount of Pd^{II}. The higher oxidation state is probably the result of minor oxidation of surface Pd. This is consistent with previously recorded data.⁸⁵

The nanoparticles also exhibit a strong NR₃ bonding mode in the N 1s XP spectrum (Figure 15). This is consistent with the structure of the tertiary amide present in the polymer subunit. Further, this is evidence that polymeric degradation has not occurred under the reaction conditions.

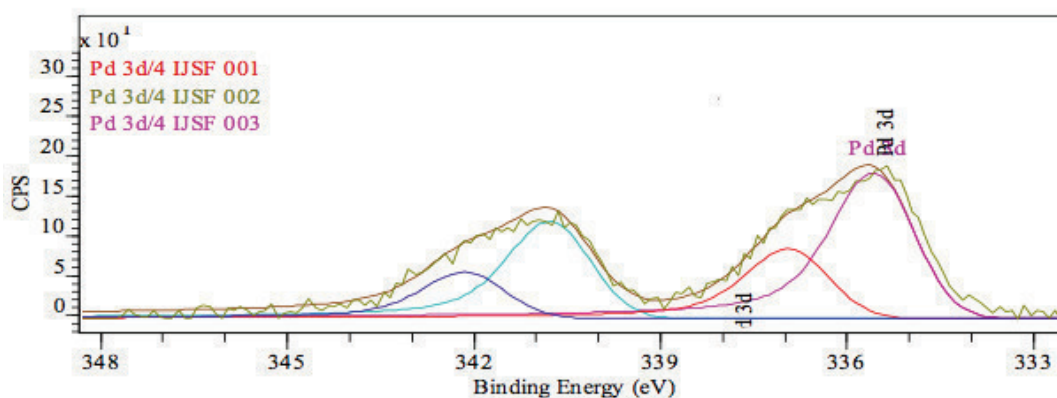


Figure 14: Pd 3d XP spectral data showing the presence of Pd⁰, and a small quantity of Pd^{II}. Analysis performed by Dr K. Wilson, University of Cardiff.

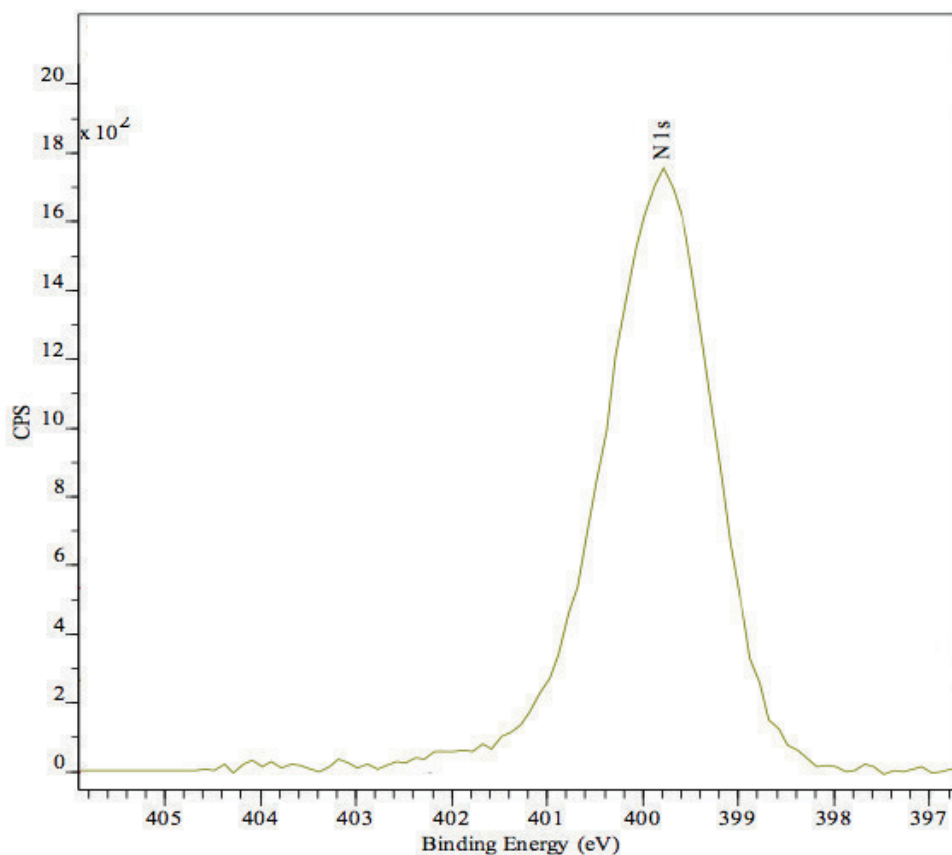


Figure 15: N 1s XP spectral data showing the NR₃ bonding mode. Analysis performed by Dr. K. Wilson, University of Cardiff.

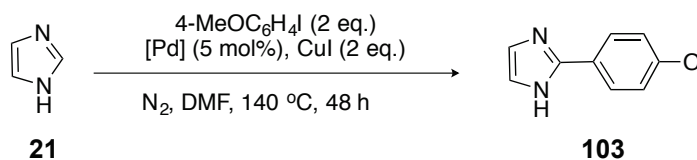
2.2.2 Role of Pd⁰ Nanoparticles in Bellina-Rossi Functionalisations

Bellina and Rossi have published base- and ligand-free C-H bond functionalisation of 1*H*-imidazole **21** (*vide supra*) which have previously been studied within the Fairlamb group by Dr Jonathan P. Reed (Scheme 33).^{37,38,127} It was noted that in different vessels (Radley's® carousel tube and Schlenk tube, Figure 16), using otherwise identical conditions starkly different results were obtained (Table 2, Entries 1-2). When the reaction was performed using Pd(OAc)₂ as a pre-catalyst in the Radley's® carousel tube, 57% yield was obtained. However only trace product was observed in the Schlenk tube. It is proposed in this, and similar systems, that the Pd(OAc)₂ is reduced *in situ* to Pd⁰. Nanoparticles (Pd black) are clearly present in the reaction mixture. It was thought that the presence of these nanoparticles could explain the difference in reactivity.

The Radley's® carousel system is generally thought to exclude air and water less vigorously than traditional Schlenk techniques. This suggests that trace quantities of air and water could be necessary for the reaction to proceed. However, intentional addition of air and water to the reaction mixture in the Schlenk tube had no effect (entries 4-6).



Figure 16: Radley's® Carousel Tube (left) and traditional Schlenk tube.



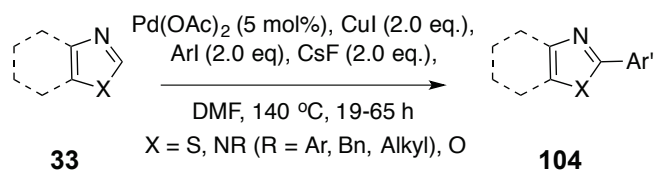
Scheme 33: Direct C-H bond functionalisation of 1*H*-imidazole using Pd/Cu system, and no base.¹²⁷

Similarly, when the reaction was performed in an open system (that is, with a constant flow of N₂ exiting through a bubbler) or with a balloon, no increase in yield was observed (entries 9, 10). Other Pd^{II} and Pd⁰ palladium sources (entries 3, 11) gave only trace yields. Unsurprisingly, the use of Pd₂(OMe-dba)₃·(OMe-dba) as a catalyst in a Radley's® carousel tube resulted in some conversion to product (35% yield). However, this did confirm that Pd⁰ could be the active catalyst. The successful reactions with both Pd^{II} and Pd⁰ precatalysts could be visibly observed to form Pd⁰ nanoparticles during the course of the reaction. In light of the group's experience with Pd⁰ nanoparticles in the Suzuki-Miyaura reaction,^{84,85} it was decided to test some pre-synthesised nanoparticles to assess their efficacy as catalysts for this process. Excitingly, the use of Pd-PVP nanoparticles in the reaction gave a higher yield than

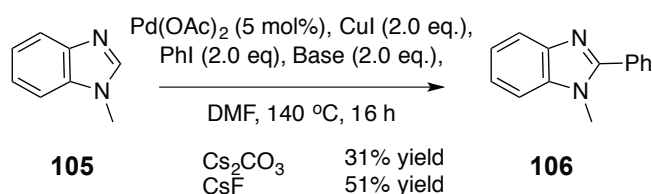
Pd(OAc)₂ in the Radley's® tube. We were keen to examine whether nanoparticles could catalyse C-H bond functionalisation in other reactions and on other heterocycles.

Table 2: Results for the direct C-H bond functionalisation of 1*H*-imidazole using Pd/Cu system, and no base.¹²⁷ These reactions were performed in a traditional Schlenk tube unless otherwise stated

Entry	Pd Source	Conditions	Yield %
1	Pd(OAc) ₂	Radley's® Carousel	57
2	Pd(OAc) ₂		Trace
3	[Pd(mal) ₂ (MeCN) ₂]		Trace
4	Pd(OAc) ₂	30 mL air	0
5	Pd(OAc) ₂	Trace Air	Trace
6	Pd(OAc) ₂	H ₂ O	Trace
7	Pd(OAc) ₂	NMP solvent	Trace
8	Pd(OAc) ₂	Cu(OAc) ₂	0
9	Pd(OAc) ₂	Balloon	Trace
10	Pd(OAc) ₂	Bubbler	7
11	[Pd ₂ (OMe-dba) ₃ .(OMe-dba)]		Trace
12	[Pd ₂ (OMe-dba) ₃ .(OMe-dba)]	Radley's® Carousel	35
13	Pd-PVP	Radley's® Carousel	67



Scheme 34: Direct C-H bond functionalisation of benzo(azoles) using Pd/Cu catalyst systems.



Scheme 35: Direct C-H bond functionalisation of benzimidazole using Pd/Cu catalyst systems, demonstrating that CsF is a more effective base for these transformations than Cs₂CO₃.

The direct C-H bond functionalisation reactions published by Bellina and Rossi¹²⁸ that are not 'base-free' (specifically, utilising Cs₂CO₃ or CsF, Scheme 34) were investigated in a similar fashion to above. First, the efficacy of each base was assessed on 1-methylbenzimidazole **105** (Scheme 35). CsF was found to be a more effective base in line with the findings of Bellina and Rossi. As such, this was selected as a base for this study. Benzoxazole **53** and benzothiazole **49** were used as substrates. The reaction time in Bellina and Rossi's published work varies on substrate between 19 and 40 h. It was considered that for comparison of catalyst efficiency, a uniform reaction time was required. A time of 16 h was chosen because it was felt it would give conversion reflective of reaction efficacy within a reasonable (*i.e.* preparatively useful) timeframe. Therefore, the yields presented below cannot be compared directly with those in Bellina and Rossi's papers. Indeed, they all represent a significant reduction in reaction time.

When Pd(OAc)₂ was used as a pre-catalyst, yields were found in both substrates to be lower in the carousel tube than the Schlenk tube (Table 3). This is the opposite effect to that observed by J. P. Reeds above, where the reaction performed in a carousel tube was found to be more effective.

For benzothiazole **49**, the use of Pd-PVP nanoparticles increased yields in both reaction vessels (an increase of 8% in the Schlenk tube, 36% in the carousel tube). This is consistent with the previous results. Indeed, it makes the yields in both vessels almost identical. It is therefore proposed, for benzothiazole **49**, the exact nature of the Pd⁰ nanoparticles is key to ensuring catalytic efficacy. The nanoparticles formed *in situ* in the Schlenk tube are more effective catalysts than those formed in the carousel tube. When the nature of the particles is fixed by using pre-synthesised Pd-PVP catalyst, there is less difference in reactivity between the two systems.

The situation with benzoxazole **53** does differ. For Pd(OAc)₂, again we see reduced yield in the carousel tube as compared to the Schlenk tube. However, whilst the reaction in the carousel tube experiences a significantly increased yield (difference 52%) with Pd-PVP nanoparticles, in the Schlenk tube the opposite is true (the yield is reduced by 31%). The reason for this is unclear. However, on both substrates it would seem that the Pd-PVP in a carousel tube is an effective reaction system.

Table 3: Table showing the results for the direct C-H bond functionalisation of benzoxazole and benzothiazole in different reaction vessels with molecular and nanoparticle catalysts.

Entry	Heterocycle	Schlenk Tube		Carousel Tube	
		Pd(OAc) ₂	Pd-PVP	Pd(OAc) ₂	Pd-PVP
1	Benzothiazole 49	53	61	23	59
2	Benzoxazole 53	71	40	27	79

It was thought that the reactivity difference with Pd(OAc)₂ pre-catalyst could result from the nature of the Pd⁰ nanoparticles formed. It is possible that the difference in H₂O/O₂ concentration, or the reaction stirring (the dynamics of which would differ based on reaction vessel), could result in nanoparticles of different size, shape or composition. It was hypothesised that the particles generated *in situ* with the Schlenk tube might mimic the pre-synthesised Pd-PVP nanoparticles, hence explaining the increase in reactivity when the pre-synthesised particles are used.

It is worth noting that for the C-H bond functionalisation of benzoxazole **53**, Miura and co-workers had previously recorded a yield of 88% over a period of 9 h using Pd(OAc)₂ for a similar reaction (PPh₃ was also added). However, this reaction was run at 140 °C. The work presented here demonstrates that similarly high yields can be obtained at lower temperatures with Pd-PVP nanoparticles.

Previously, the Fairlamb group has developed a method for the trapping of Pd⁰ nanoparticles that have been generated *in situ*.²⁷ This involves the addition of an extragenous polymer, which acts as a stabiliser. PVP is usually employed for this purpose. This polymer encapsulates the nanoparticles, and improves the reliability of size distribution analysis without changes in solvent concentration *in vacuo* promoting metal aggregation.

Two samples were taken from the direct C-H bond functionalisation reaction of benzothiazole **49** with Pd(OAc)₂ in the Schlenk and carousel tube. To a reaction sample was added PVP (10 eq. per theoretical quantity of Pd, assuming a fully homogenous mixture in the reaction, thus in reality a large excess). The solvent was removed from the samples under reduced pressure, heating at ca. 50 °C. Transmission electron micrographs were recorded for each of these samples (Figure 17, 18). In the samples containing polymer, Pd⁰ nanoparticles were clearly observed. The samples without polymers were unclear, and could not be analysed (indeed one, shown in Figure 19, showed large needle-shaped crystals believed to be CsF).

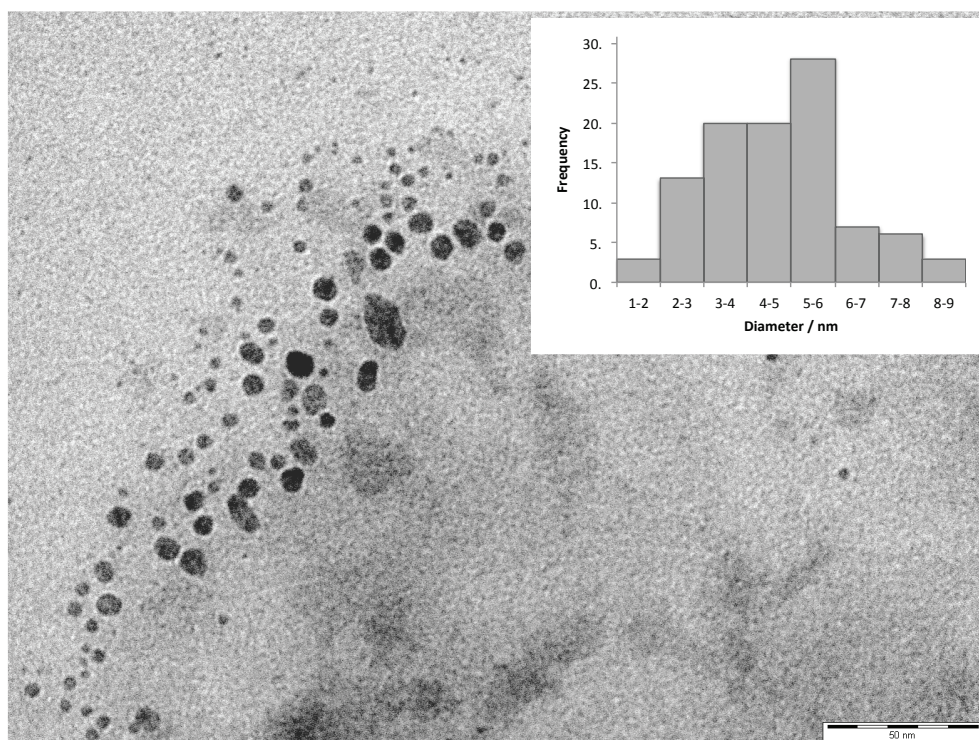


Figure 17: Example electron micrograph of sample taken from the direct C-H bond functionalisation of benzothiazole **49** performed in a Carousel tube after 2 h, with PVP (10 eq. per Pd) added before solvent removal. Inset shows histogram of particle diameter (nm) across a sample of nanoparticles ($n = 100$).

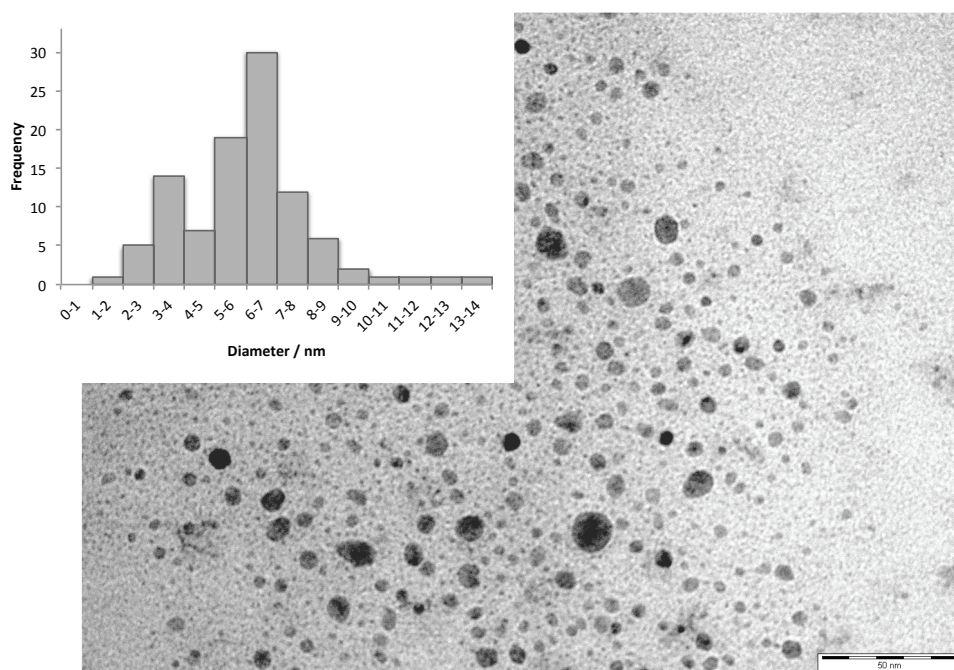


Figure 18: Example electron micrograph of sample taken from the direct C-H bond functionalisation of benzothiazole **49** performed in a Schlenk tube after 2 h, with PVP (10 eq. per Pd) added before solvent removal. Inset shows histogram of particle diameter (nm) across a sample of nanoparticles ($n = 100$).

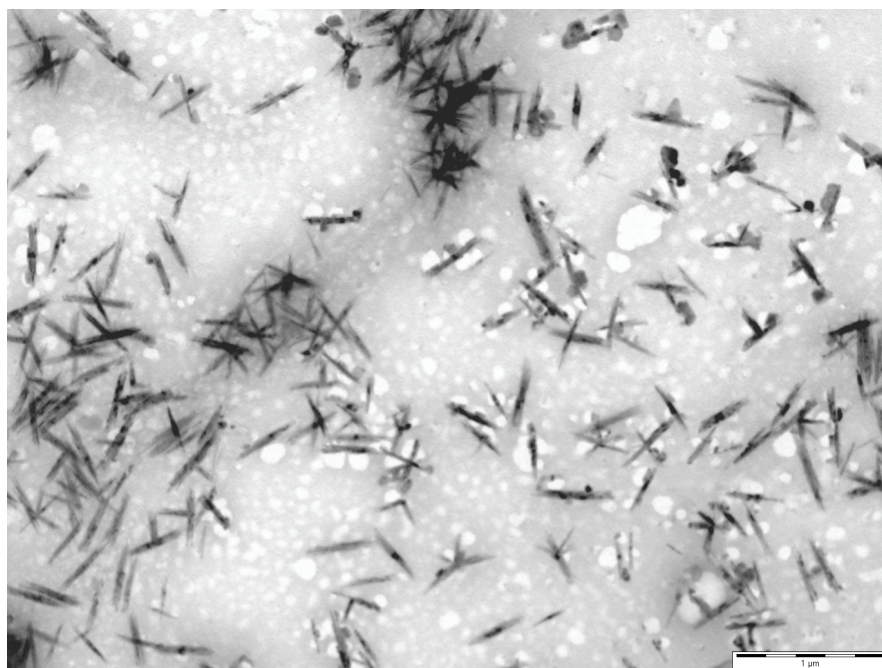


Figure 19: Example electron micrograph of sample taken from the direct C-H bond functionalisation of benzothiazole **49** performed in a Schlenk tube after 2 h followed by solvent removal. There is a significant quantity of large needle-shaped crystals, hypothesized to be CsF. Note the scale is significantly larger than Figures 17-18.

A random sample of nanoparticles was chosen ($n = 100$) from each sample and measured manually. Statistical data is shown in Table 4. This data can also be represented in a histogram (insets, Figures 17, 18).

Table 4: Table showing simple statistical measures for nanoparticles isolated from the direct C-H bond functionalisation of benzothiazole **49** with Pd(OAc)₂/CuI catalyst systems. SD = Standard Deviation, IQR = Interquartile Range, IQM = Interquartile Mean

	Mean	SD	Median	Mode	IQR	IQM
Carousel	4.64	1.62	3.39	3.39	2.54	4.52
Schlenk	6.07	2.25	6.68	6.03	1.72	5.98

The average size of the nanoparticles generated in both the Carousel and Schlenk vessels are slightly larger than the pre-synthesised nanoparticles and, indeed, other *in situ* generated nanoparticles found elsewhere in this thesis (*vide infra*). The nanoparticles generated in the reaction in the Schlenk tube are larger than those taken from the Carousel tube (difference in mean size 1.43 nm). This size difference is not within the estimated error. The Schlenk tube sample exhibits a larger range of particle

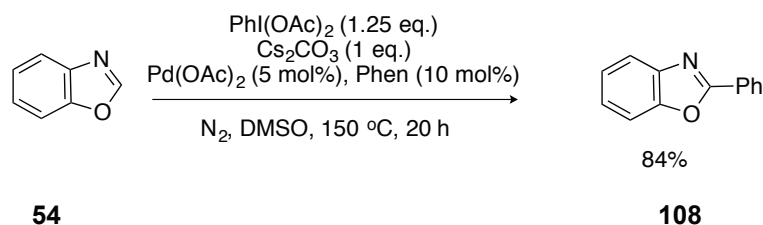
sizes, as shown by the greater standard deviation and interquartile range. Further, visual inspection of the histograms (Figures 18-18, insets) reveals a greater number of outlying sizes (at sizes > 10 nm).

This result was unexpected. The more active (Schlenk) *in situ* generated nanoparticles were larger than both those generated in the carousel and the Pd-PVP nanoparticles. As previously stated, it is generally assumed that the carousel tube excludes O₂ and H₂O less vigorously than the Schlenk. Generally, their presence results in the growth of larger nanoparticles.¹²⁹ Therefore, the slight difference in particle size is surprising. It cannot be said that mimicking the Pd-PVP particle size can explain their reactivity.

2.2.3 Direct C-H bond Functionalisation of Benzoxazole with PhI(OAc)₂

This section resulted in the following publication: Williams, T. J.; Fairlamb, I. J. S. A key role for iodobenzene in the direct C-H bond functionalisation of benzoxazoles using PhI(OAc)₂ mediated by a Pd(OAc)₂/1,10-phenanthroline catalyst system: *in situ* formation of well-defined Pd nanoparticles. *Tetrahedron Letters* (in press).

In 2012, Chen, Cheng and co-workers published a methodology for the direct C-H functionalisation of benzoxazole **53** mediated by Pd(OAc)₂ to give 2-phenylbenzoxazole **14**.¹³⁰ This work differed from conditions for this transformation previously published, in that PhI(OAc)₂ **107** was utilized as an aryl source (Scheme 36). Although hypervalent iodine compounds are found as aryl sources in the direct C-H bond functionalisation of indoles (*vide supra*), PhI(OAc)₂ **107** had not previously been used for this purpose.^{131,132} By comparison with other functionalisations using hypervalent iodine salts, and considering the strong oxidizing nature of the reagent, the authors proposed that this reaction proceeded *via* a Pd^{III/IV} manifold (the intermediacy of Pd^{IV} complexes is discussed in more detail in Chapter 3).¹³³



Scheme 36: Direct C-H bond functionalisation of benzoxazoles with PhI(OAc)₂.

This reaction is performed at high temperature (150 °C) in polar solvent (DMSO), with carbonate base (Cs₂CO₃). These conditions are similar to those previously reported for the functionalisation of benzazoles with aryl iodide. For example, studies by Murai and co-workers use near-identical conditions with PhI, and DMA as opposed to DMSO.¹³⁴ Chen and Cheng, however, report that the reaction with PhI does not proceed.

When this work was repeated using PhI(OAc)₂ **107**, a 69% yield was obtained (84% reported). Almost immediately on addition of solvent to the reaction mixture, a colour change from orange to dark brown was observed, which indicates the presence of Pd⁰ colloidal nanoparticles (Figure 20). The reaction appeared similar to the Bellina-Rossi arylations previously discussed. Consequently, two separate aliquots of the reaction mixture were taken (after 2 h heating). To one of these samples, PVP (10 eq. per

theoretical amount of Pd, assuming the reaction was a homogenous mixture) was added. Solvent was removed from both samples under reduced pressure, heating at 50 °C. Transmission electron micrographs were recorded for each of these samples (Figure 21). In both samples, Pd⁰ nanoparticles were clearly observable.



Figure 20: Reaction using ‘Chen-Cheng’ conditions for the direct C-H bond functionalisation of benzazole – taken immediately after the addition of dry solvent, under N₂.¹³⁰

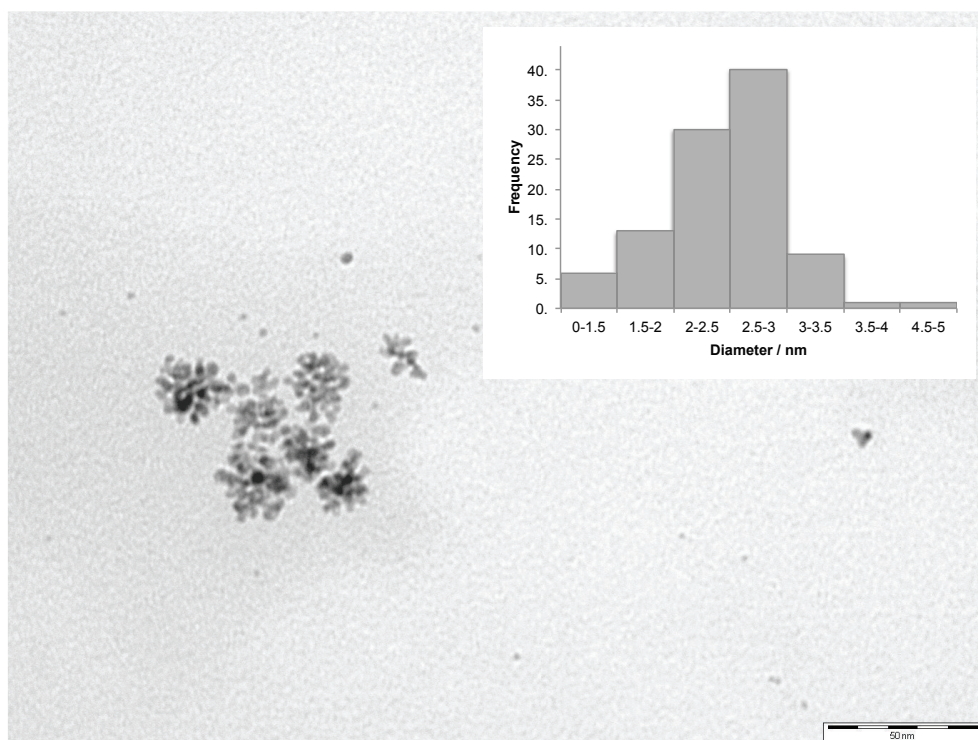


Figure 21: Example electron micrograph of sample taken from ‘Chen-Cheng’ reaction after 2 h, with PVP (10 eq. per Pd) added before solvent removal. Inset shows histogram of particle diameter (nm) across a sample of nanoparticles ($n = 100$).

A random sample of nanoparticles was chosen ($n = 100$) from each sample and measured manually. Statistical data is shown in Table 5. This data can also be represented in a histogram (inset, Figure 21).

Table 5: Statistical analyses for nanoparticles produced in Chen-Cheng reaction.

	Mean	SD	Median	Mode	IQR	IQM
With PVP	2.44	0.58	2.13	2.55	0.638	2.43
Without PVP	2.11	0.46	1.69	1.69	0.636	2.07

Nanoparticles in both samples are generally < 5 nm, similar to pre-synthesised nanoparticles supported on PVP. There is a small difference between the two samples, which is within error (mean difference 0.3 nm).

The stability of $\text{PhI}(\text{OAc})_2$ **107**, under the reaction conditions was assessed. The reagent was purchased from Sigma-Aldrich®, and purity established by comparison to literature ^1H NMR spectra in CDCl_3 . It has previously been reported that (dicarboxy)iiodoarenes are susceptible to degradation *via* thermal and radical

mechanisms.^{135,136} PhI(OAc)₂ **107** was fully dissolved in DMSO-*d*₆ at ambient temperature (Figure 22). A ¹H NMR spectrum recorded *ca.* 5 min after dissolution indicated the presence of one major species. After *ca.* 30 min, several species are observable in solution, including PhI (identified by comparison with an authentic sample). These species continue to grow over time. The presence of AcOH in solution can also be observed.

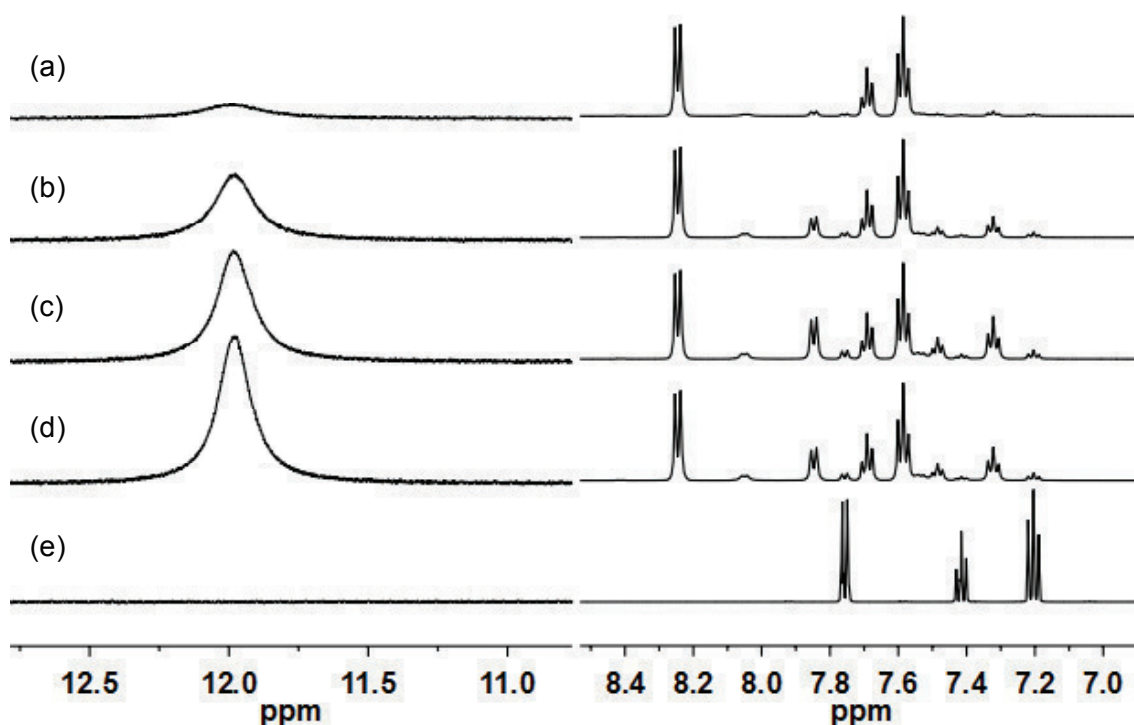


Figure 22: ¹H NMR spectra for the degradation of PhI(OAc)₂ **107** at ambient temperature (500 MHz, DMSO-*d*₆); (a) *t* = 5 min, (b) *t* = 30 min, (c) *t* = 40 min, (d) *t* = 50 min, (e) PhI (commercial sample, Sigma-Aldrich®). Note: the stacked spectra on the left hand side show the appearance of an acetic acid proton.

The progress of this reaction has been monitored by ¹H NMR spectroscopy over 16 h, integrating a resonance for each species with respect to residual deuterated solvent (Figure 23). Rapid formation of intermediate was observed over the initial 30 min. After this time, loss of intermediate was observed concomitant with the increased formation of PhI. An apparent slight recovery of PhI(OAc)₂ **107** concentration is also observed, however ¹H-¹³C HSQC has indicated that this is the result of a fourth uncharacterised species which is co-incident with the proton resonances of PhI(OAc)₂ **107**. This experiment indicates that this reaction does not proceed to completion at ambient temperature.

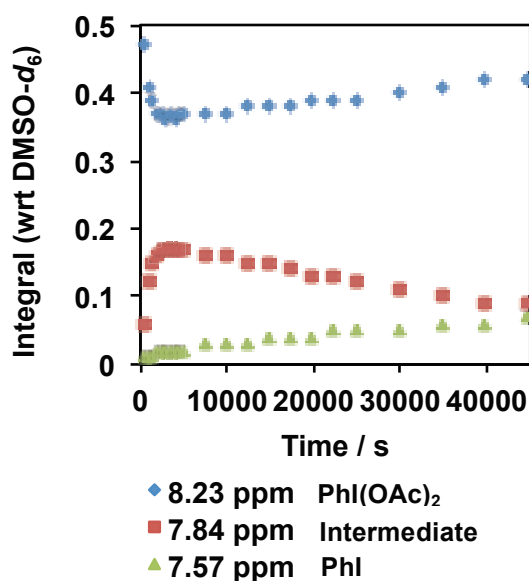


Figure 23: Kinetic curves (^1H NMR spectroscopy, 500 MHz, $\text{DMSO-}d_6$) showing relative integrations of PhI(OAc)_2 , intermediate and PhI with respect to residual undeuterated solvent.

This reaction was repeated in the presence of Cs_2CO_3 (0.8 eq., as per the reaction stoichiometry). Cs_2CO_3 does not fully dissolve in $\text{DMSO-}d_6$. A ^1H NMR spectrum was recorded at $t = 5$ min, and shows an identical but accelerated reaction. Further spectra were recorded at $t = 10, 30$ and 60 min intervals (Figure 24). The AcOH resonance is not observed, and is presumably being sequestered by the base.

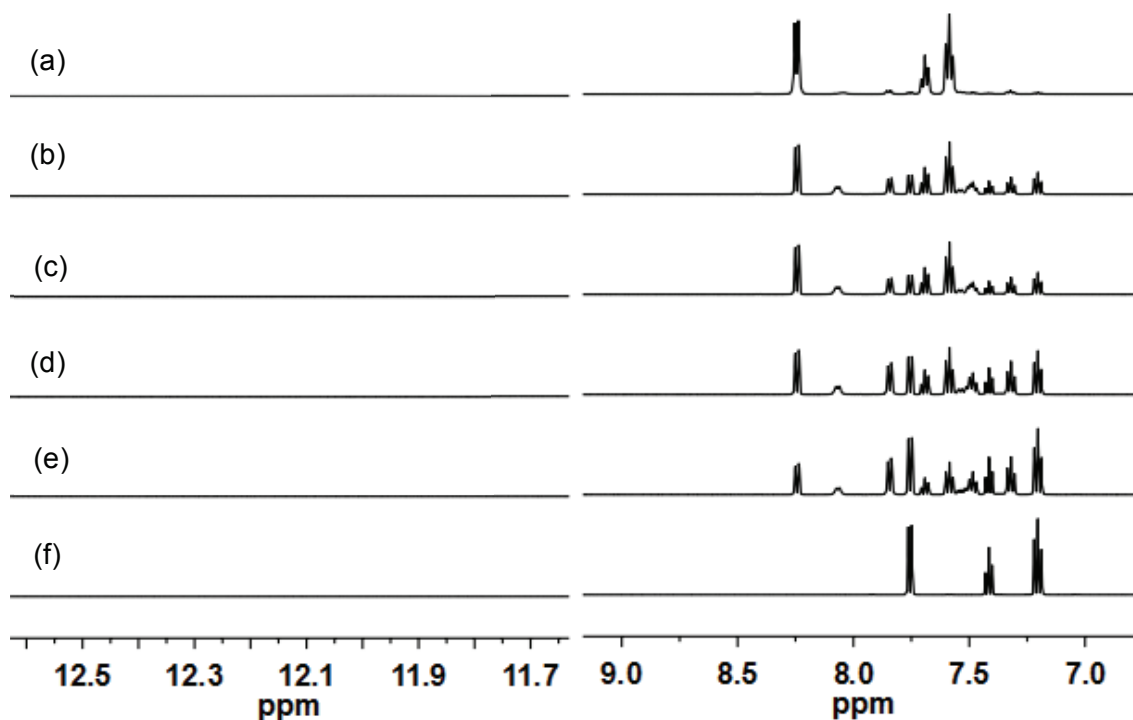


Figure 24: ^1H NMR spectra for the degradation of $\text{PhI}(\text{OAc})_2$ and Cs_2CO_3 at ambient temperature (500 MHz, $\text{DMSO-}d_6$); (a) $\text{PhI}(\text{OAc})_2$ without Cs_2CO_3 ($t = 5$ min after dissolution) (b) $\text{PhI}(\text{OAc})_2$ and Cs_2CO_3 , $t = 5$ min, (c) $\text{PhI}(\text{OAc})_2$ and Cs_2CO_3 , $t = 10$ min, (d) $\text{PhI}(\text{OAc})_2$ and Cs_2CO_3 , $t = 30$ min, (e) $\text{PhI}(\text{OAc})_2$ and Cs_2CO_3 , $t = 60$ min, (f) PhI (commercial sample, Sigma-Aldrich®). Note: the stacked spectra on the left hand side show the acetic acid proton does not appear.

A freshly prepared sample of $\text{PhI}(\text{OAc})_2$ in $\text{DMSO-}d_6$ was heated to $150\text{ }^\circ\text{C}$ for 10 min (Figure 25). A ^1H NMR spectrum was then recorded, which indicated complete conversion to PhI . Therefore, under the reaction conditions, $\text{PhI}(\text{OAc})_2$ rapidly degrades to PhI . The intermediate species observed at room temperature is most likely the product of solvolysis, consistent with the formation of AcOH . This reaction was repeated with Cs_2CO_3 (0.8 eq., reaction stoichiometry), and an identical result recorded. It can be assumed that, as at room temperature, the reaction is accelerated but this cannot be observed due to the rapid nature of the reaction.

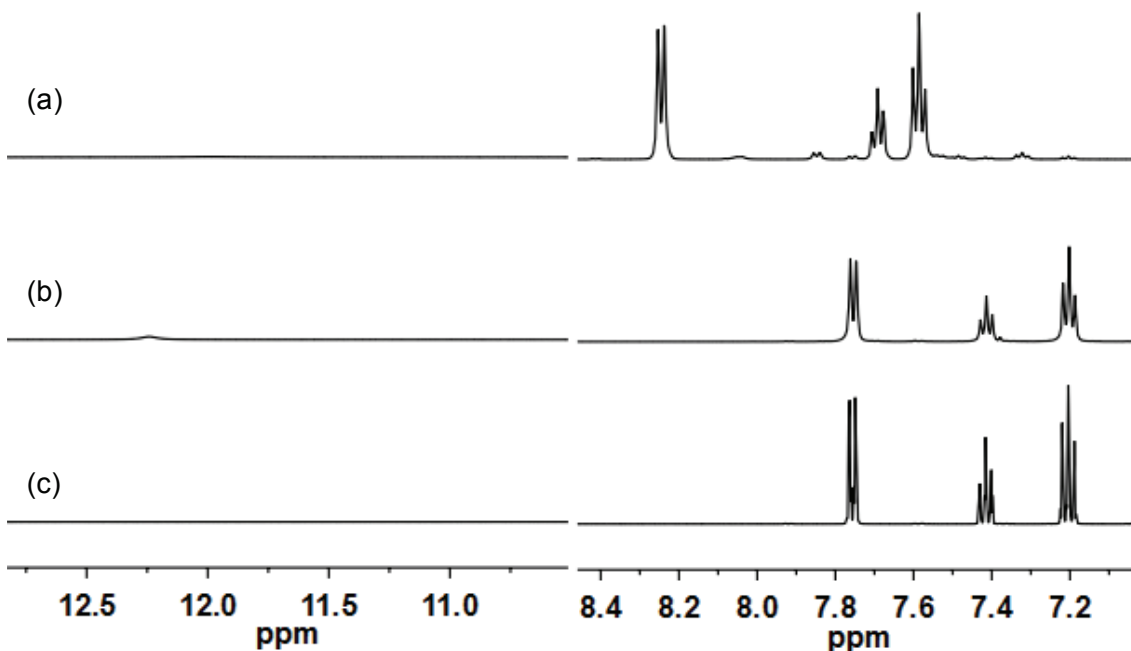
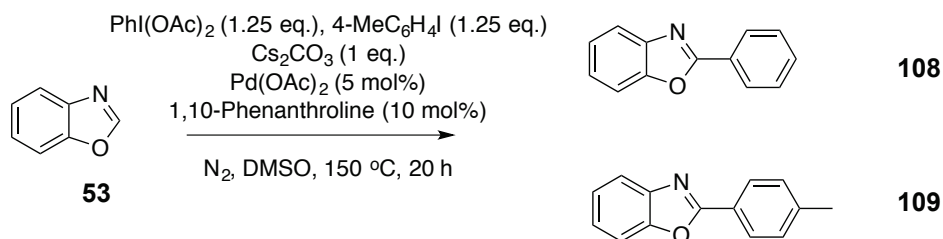


Figure 25: ^1H NMR spectra for the degradation of $\text{PhI}(\text{OAc})_2$ at $150\text{ }^\circ\text{C}$ in a sealed Young's Tap tube (500 MHz, $\text{DMSO-}d_6$); (a) before heating, ca. 5 min after dissolution (b) $t = 10$ min (c) PhI (commercial sample, Sigma-Aldrich®). Note: the stacked spectra on the left hand side show the appearance of acetic acid proton [in (b)].

When the reaction was performed using PhI , an 84% yield was obtained. Chen, Cheng and co-workers had previously reported that PhI as an aryl source gave only trace product. To understand this, it was found that when the reaction was conducted in the presence of air, a lower yield (45%) was recorded.



Ratio of **108:109** by ^1H NMR spectroscopy: 1:1.5

Scheme 37: Competition experiment between $\text{PhI}(\text{OAc})_2$ and 1-iodo-4-methylbenzene.

A competition experiment was run between $\text{PhI}(\text{OAc})_2$ **107** and 1-iodo-4-methylbenzene with benzoxazole (Scheme 37). Two products, **108** and **109**, were formed in this reaction, in a ratio of 1.5:1 (as determined by ^1H NMR spectroscopy,

Figure 26). The observation demonstrates that both aryl sources are viable cross-coupling partners. The reactivity difference between iodobenzene generated *in situ* and 1-iodo-4-methylbenzene is as expected for a Pd⁰/Pd^{II} type catalytic process, as demonstrated by Jutand and co-workers.^{137–139}

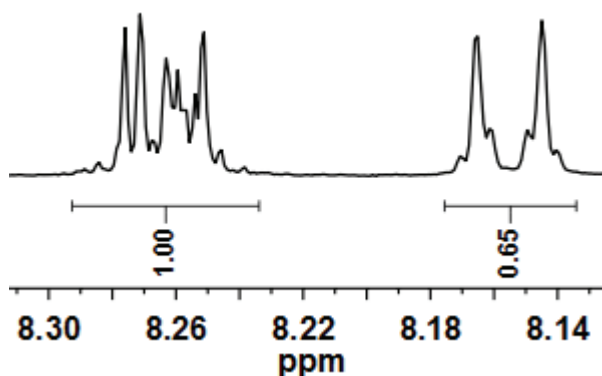


Figure 26: ¹H NMR spectrum (selected region) of the crude mixture from the competition experiment using PhI(OAc)₂ and 4-MeC₆H₄I. Resonances shown have been identified as 2-(4-methylphenyl)benzoxazole (8.18 ppm – 2H, d) and 2-phenylbenzoxazole (8.26 ppm – 2H, m) by comparison with literature data.

Therefore, it seems most likely that PhI(OAc)₂ **107** is not the aryl source in this reaction. Rather, it is proposed that PhI is formed *in situ*. In light of the presence of Pd⁰ nanoparticles, which have now been characterized, the PhI will functionalise benzoxazole in an electrophilic aromatic substitution mechanism consistent with that proposed in Scheme 7. That is, one mediated by a Pd^{0/II} manifold as opposed to the Pd^{II/IV} process postulated by Chen, Chang and co-workers (with little evidence).¹⁴⁰

2.3 Role for Cu-NHC Complexes in Pd/Cu-Mediated Systems

2.3.1 Cu(NHC)X Complexes as Model Intermediates

Elements of this section resulted in the following publications: Lake, B. R. M.; Bullough, E. K.; Williams, T. J.; Whitwood, A. C.; Little, M. A.; Willans, C. E. Simple and versatile selective synthesis of neutral and cationic copper(I) *N*-heterocyclic carbene complexes using an electrochemical procedure. *Chem Commun.* **2012**, *48*, 4887-4889; Williams, T. J.; Lake, B. R. M.; Whitwood, A. C.; Willans, C. E.; Fairlamb, I. J. S. Arylation and decomposition of copper(I) *N*-heterocyclic carbenes of relevance in C-H bond functionalisation (*submitted*).

Bellina, Rossi and co-workers and Fairlamb and co-workers have proposed similar mechanisms for the C-H bond functionalisation of *N*-heterocycles using Pd and Cu catalysts.^{26-28,35-37} A combined mechanism is shown in Figure 27. Complex **I** is proposed as an intermediate formed from the cupration of imidazole. They propose that the equilibrium for the deprotonation/cupration lies significantly towards the starting material. Therefore, they propose that an excess of CuI is required to push the equilibrium towards the intermediate. Complex **I** is a tautomer of intermediate **II**, an *N*-heterocyclic carbene copper(I) complex. Daugulis has proposed similar intermediates for sub-stoichiometric Cu-only C-H bond functionalisations.¹⁴¹

As discussed, Cu(NHC)X complexes are well known in the literature. Cu(NHC) complexes with sterically unhindered *N*-substituents are unstable and susceptible to oxidation. Therefore, the proposed intermediate **II** would be highly sensitive and it would be impractical to detect *in situ* or isolate from a stoichiometric study.

It was thought that 1,3-disubstituted imidazolyidene complexes could be used as model systems to test whether these complexes could be intermediates in C-H bond functionalisation reactions. It was decided that (1,3-dibenzylbenzimidazolydene)copper(I) bromide **110** might be an effective model. 1-benzylimidazole is a common substrate in direct C-H bond functionalisation, and the second benzyl group could mimic the proton in intermediate **II**. The use of a benzo-fused system avoids complications with activation at the C4 and C5 positions, which might occur with the imidazolium analogues.

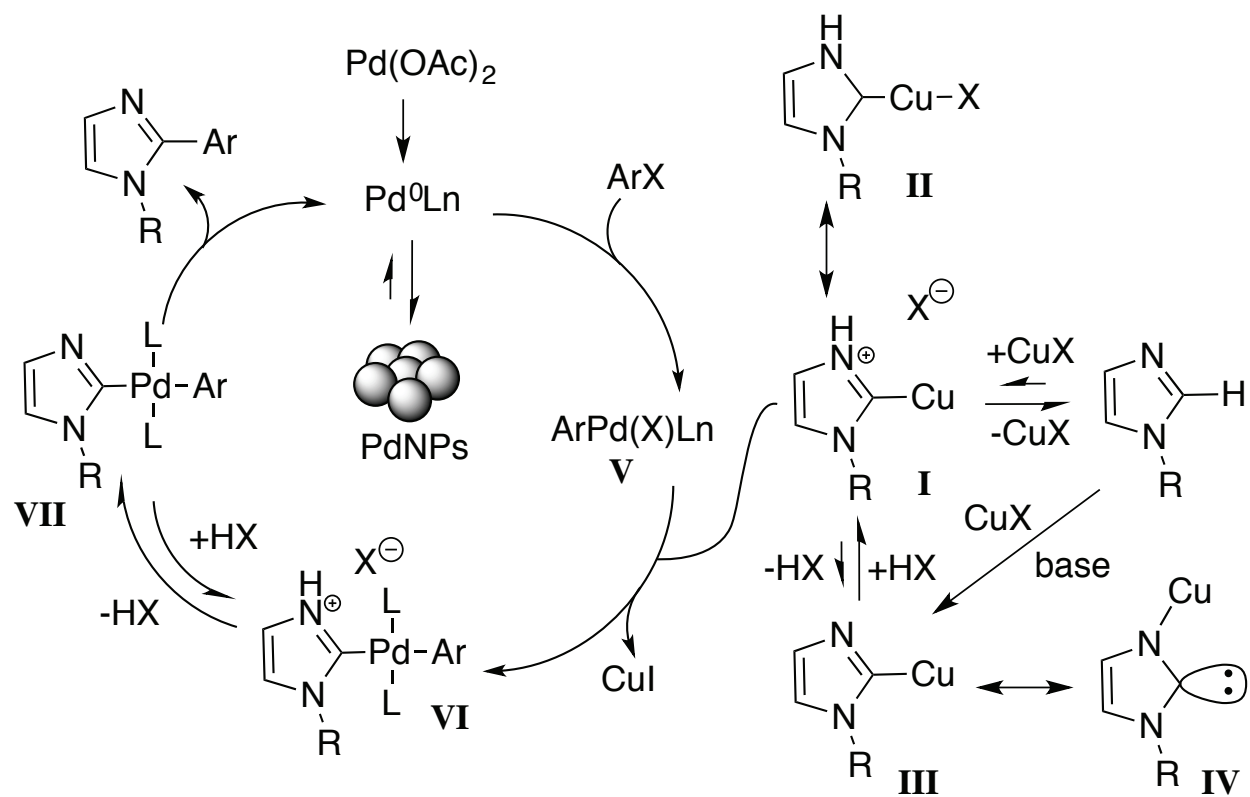


Figure 27: Mechanism for the direct C-H bond functionalisation of imidazoles and related purines, as proposed by Bellina, Rossi and Fairlamb.^{26,27,142}

2.2.2 Synthesis of Cu-NHC Complexes

As discussed, Cu-NHC complexes can be synthesised by a variety of different methods. 1,3-Dibenzylbenzoimidazolium bromide **113** (Figure 28 shows single crystal X-ray diffraction structure) is a sensitive substrate due to the relatively high acidity of the benzylic position. Of particular interest was the method of Cazin and co-workers,¹⁰⁸ which allows access to a variety of different NHC complexes whilst avoiding *tert*-butoxide or lithium amide/alkyl bases.

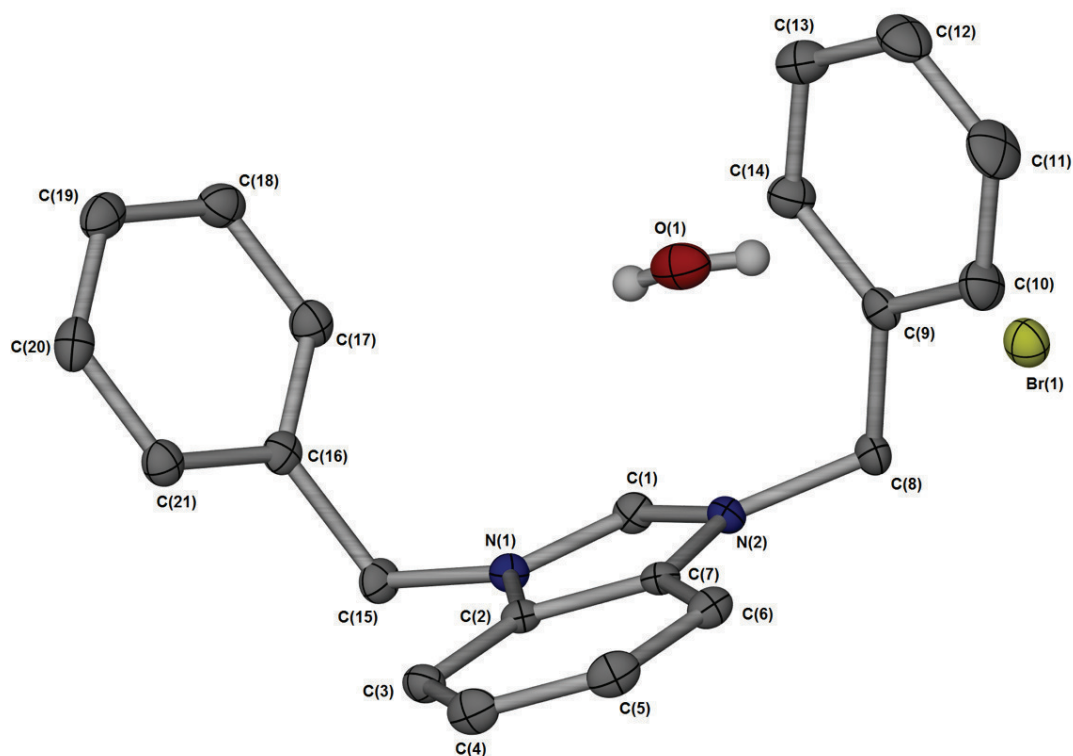


Figure 28: Single crystal X-ray diffraction structure of 1,3-dibenzylbenzoimidazolium bromide **113** (the bromide anion and H₂O not bonded to the benzimidazolium). Hydrogen atoms have been removed for clarity. Thermal ellipsoids shown at 50%. Selected bond lengths (Å), bond angles and torsion angles (°): N(2)-C(8) = 1.476(2), C(15), N(1)-C(15) = 1.481(2), N(2)-C(8)-C(9) = 112.20(16), C(7)-N(2)-C(8)-C(9) = 76.2(2).

When 1,3-dibenzylimidazolium bromide was subjected to these reaction conditions, Cu(NHC)X product was not observed. Instead, brown needle crystals were isolated from recrystallization of the reaction mixture from CDCl₃.

Single crystal X-ray diffraction studies were initially inconclusive. The 1,3-dibenzylimidoloylidene was present, and an intriguing $^{\circ}\text{CuBr}_2^{\circ}$ cluster. However, initial structural solutions also indicated the presence of Li (a Q peak with ca. 3 electrons) interacting with the carbene. This seemed an unlikely solution, given that no Li was present in the reaction mixture. It was possible that Li could be a contaminant in the Cu_2O from the manufacturing process (although Sigma-Aldrich® consider their process to be commercially sensitive), XPS analysis of a sample by Dr. K. Wilson at the University of Cardiff showed no Li present (although it did contain ca. 0.6% Pb). A sample of the Cu_2O was also analyzed by solid-state ^7Li NMR (Solid-State NMR Service, Durham University), but again no Li was detected.

The brown crystals were dissolved in $\text{DMSO-}d_6$ and the ^1H NMR spectrum compared to that of (1,3-dibenzyl)benzimidazolium bromide **113** starting material (Figure 29). A small change in resonance chemical shifts can be observed. Crucially, a resonance characteristic of an imidazolium C2-H is present. This has shifted upfield in comparison with the starting material, becoming more shielded and less acidic.

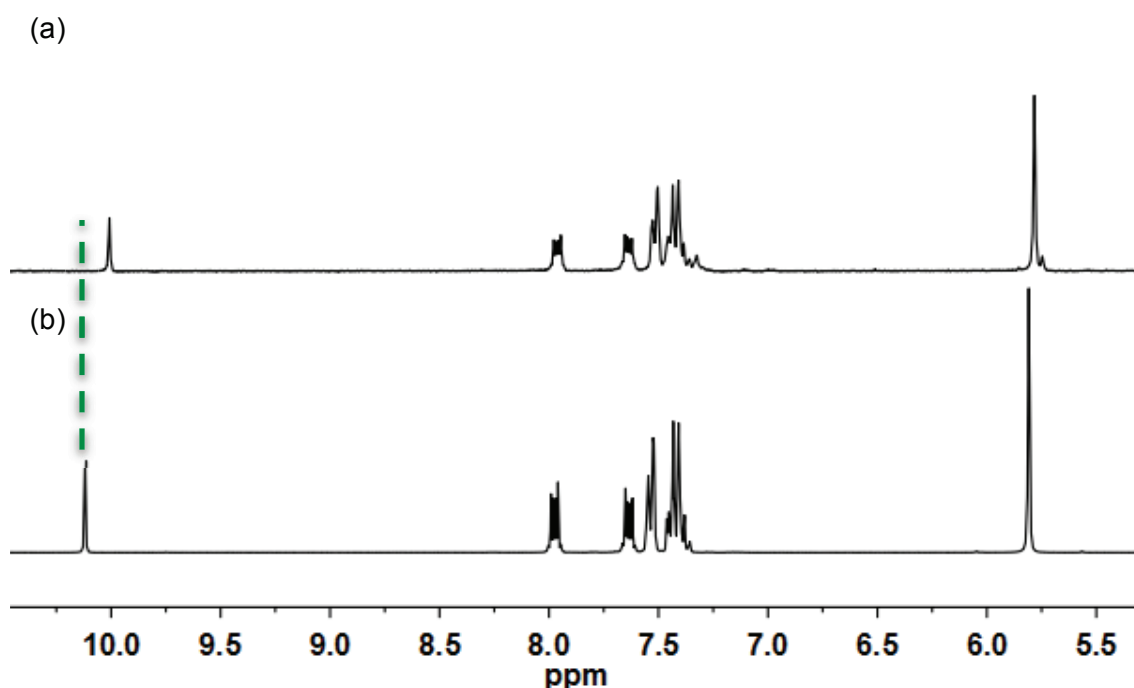


Figure 29: ^1H NMR (300 MHz) spectra of (a) product of the reaction of (1,3-dibenzyl)benzimidazolium bromide and Cu_2O , recrystallized from CDCl_3 , in $\text{DMSO-}d_6$ and (b) (1,3-dibenzyl)benzimidazolium bromide in $\text{DMSO-}d_6$.

A ^1H NMR spectrum was recorded in various solvents ($\text{DMSO-}d_6$, CD_2Cl_2 and $\text{MeCN-}d_3$, Figure 30). The complex was stable in both $\text{DMSO-}d_6$ and $\text{MeCN-}d_3$, but degraded

in CD_2Cl_2 . A similar degradation occurred over time in $\text{MeCN-}d_3$ (four weeks, Figure 31).

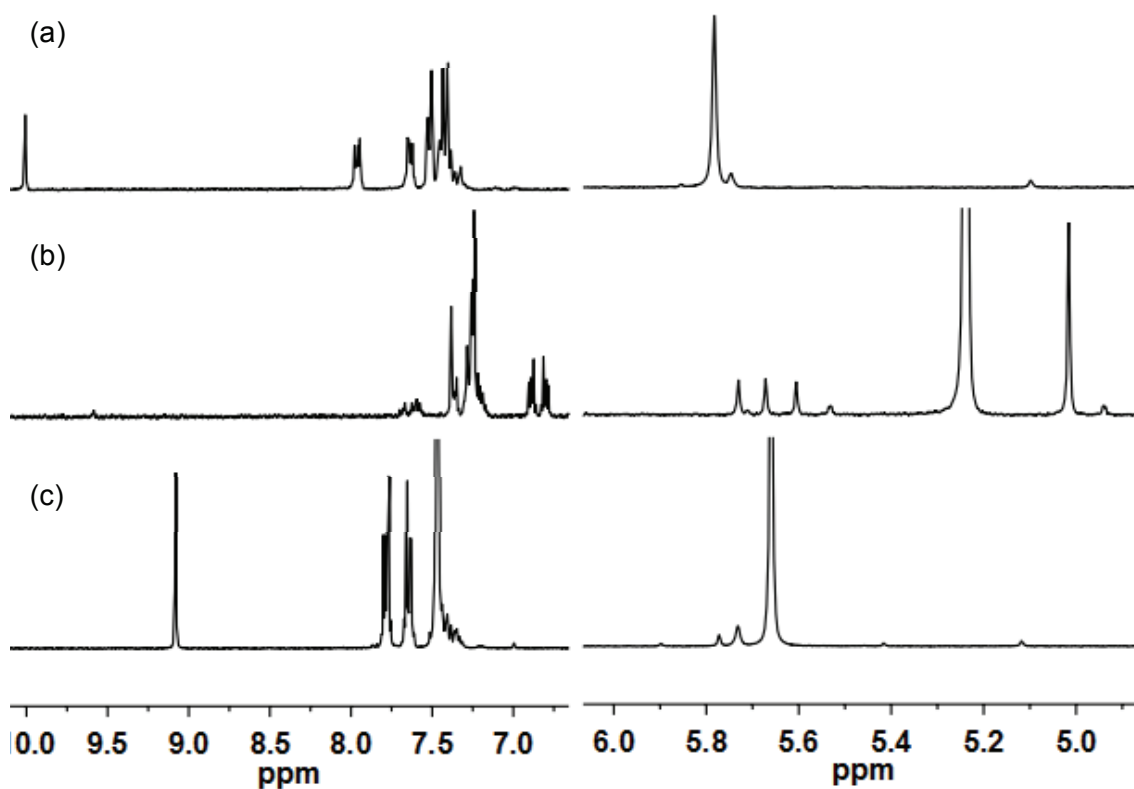


Figure 30: ^1H NMR spectrum of unknown complex in various solvents, showing aromatic and benzylic ^1H environments; (a) $\text{DMSO-}d_6$, (b) CD_2Cl_2 , (c) $\text{MeCN-}d_3$.

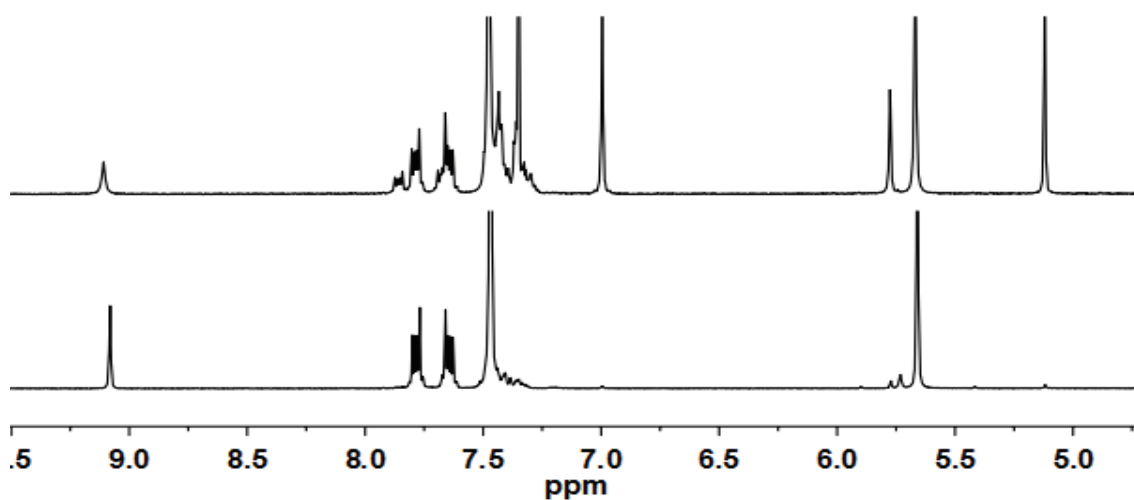


Figure 31: ^1H NMR of unknown complex in $\text{MeCN-}d_3$, showing degradation of the sample after 4 weeks (upper).

The presence of C2-H in the ^1H NMR spectra suggests that a carbene had not been formed. Rather, it is proposed that the imidazolium C2-H is in place, and interacting with a $[\text{Cu}_2\text{Br}_4]$ counterionic cluster **114** (Figure 32). Complexes where imidazolium cations can act as hydrogen bond donors (or carbenes as hydrogen bond acceptors, depending on C-H and H-X distances involved) in the form NHC-H-X are well known.^{143,144} Generally, X is a halide or oxygen. Indeed, in 1,3-(2,4,6-trimethylphenyl)imidazolium chloride there is an identified hydrogen bond interaction between the C2-H and the chloride anion. The distance between C2-H and the chloride anion is 3.3 Å.¹⁴⁵ It is worth noting that the comparable distance in 1,3-dibenzylbenzoimidazolium bromide is 4.604(2) Å, and therefore out of the range normally associated with hydrogen bonding. 'Exotic' examples of NHC-H-X interactions with arene π -systems are known. Typically, such complexes have donor-acceptor distances of ca. 3 Å. Complexes containing hydrogen bonds of the form Y-H-M (where $\text{Y} = \text{N}, \text{O}, \text{C}$ and $\text{M} = \text{transition metal}$) are known, but those where $\text{Y} = \text{C}$ are rare. Indeed, to our knowledge, this complex would be the only example of such an interaction with a (benz)imidazolium C2-H participating.

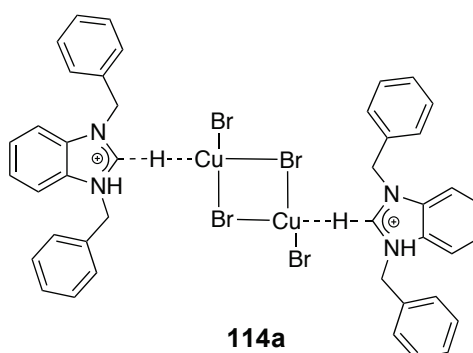


Figure 32: The chemical structure of 114a.

Calculations (by Dr. A. C. Whitwood, Small Molecule X-Ray Crystallographic Service, University of York) showed that these complexes had co-crystallised with 10% and 8% of the initially desired $\text{Cu}(\text{NHC})\text{Br}$ **110**. This results in the unusual electron density observed experimentally. The single X-ray diffraction structure is shown in Figure 33 ° it should be noted that the C2-H cannot be located definitively by this technique (in that case neutron diffraction would be required), but is shown here to give structural clarity.

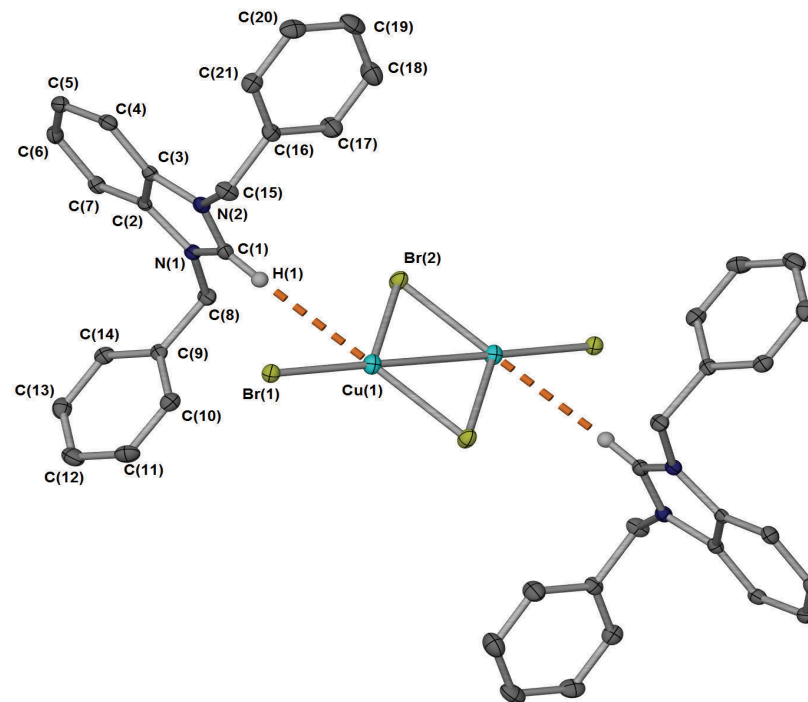


Figure 33: Single crystal X-ray diffraction structure of 1,3-dibenzylbenzoimidazolium copper dibromide complex **114a**. Hydrogen atoms have been removed, with the exception of C2-H, for clarity. Thermal ellipsoids shown at 50%. Selected bond lengths (Å), bond angles (°): C(1)-Cu(1) = 3.8293(1), Cu(1)-Cu(1) = 2.8093(4), Cu(1)-Br(1) = 2.3201(3), Cu(1)-Br(2) = 2.4164(3), Br(1)-Cu(1)-Br(2) = 125.812(11), Cu(1)-Br(2)-Cu(1) = 71.099(10). Two molecules of CHCl₃ omitted.

In separate reactions, a polymorph of this complex has been isolated where, as opposed to being a stoichiometrically defined cluster, $\mu\text{Cu}_x\text{Br}_y\mu$ exists as an infinite anionic polymer **114b** (Figure 34)

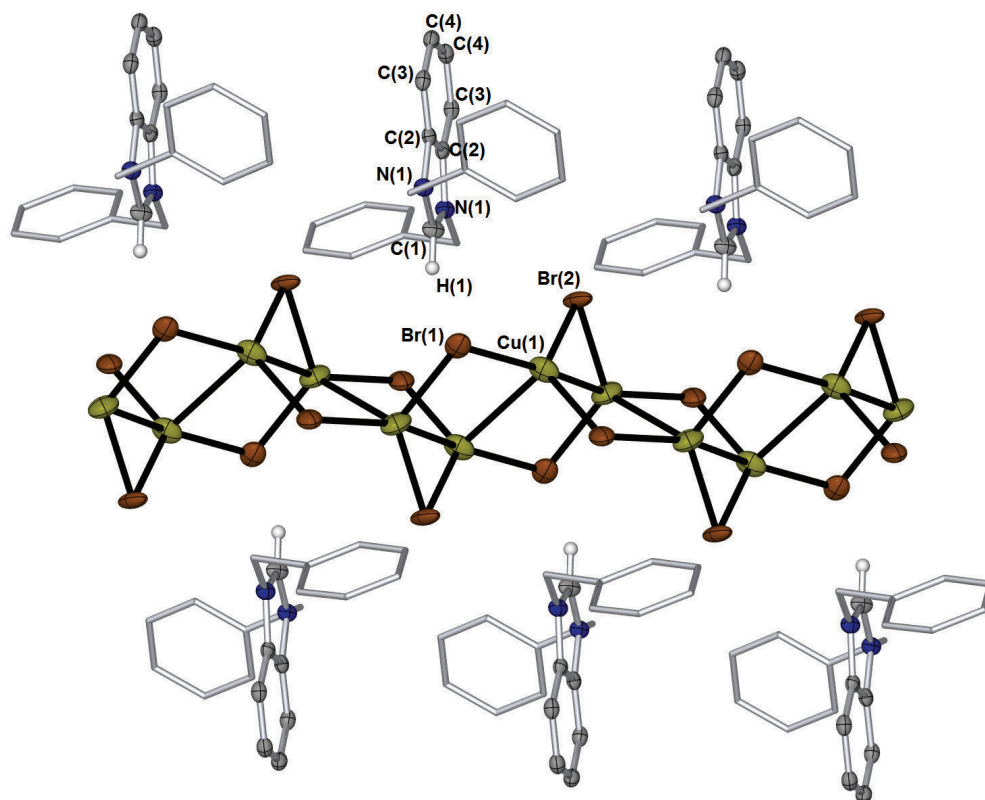


Figure 34: Single crystal X-ray diffraction structure of 1,3-dibenzylbenzoimidazolium copper dibromide complex **114b**, where the cluster exists as an infinite anion polymer. Benzyl groups are shown in stick-form.

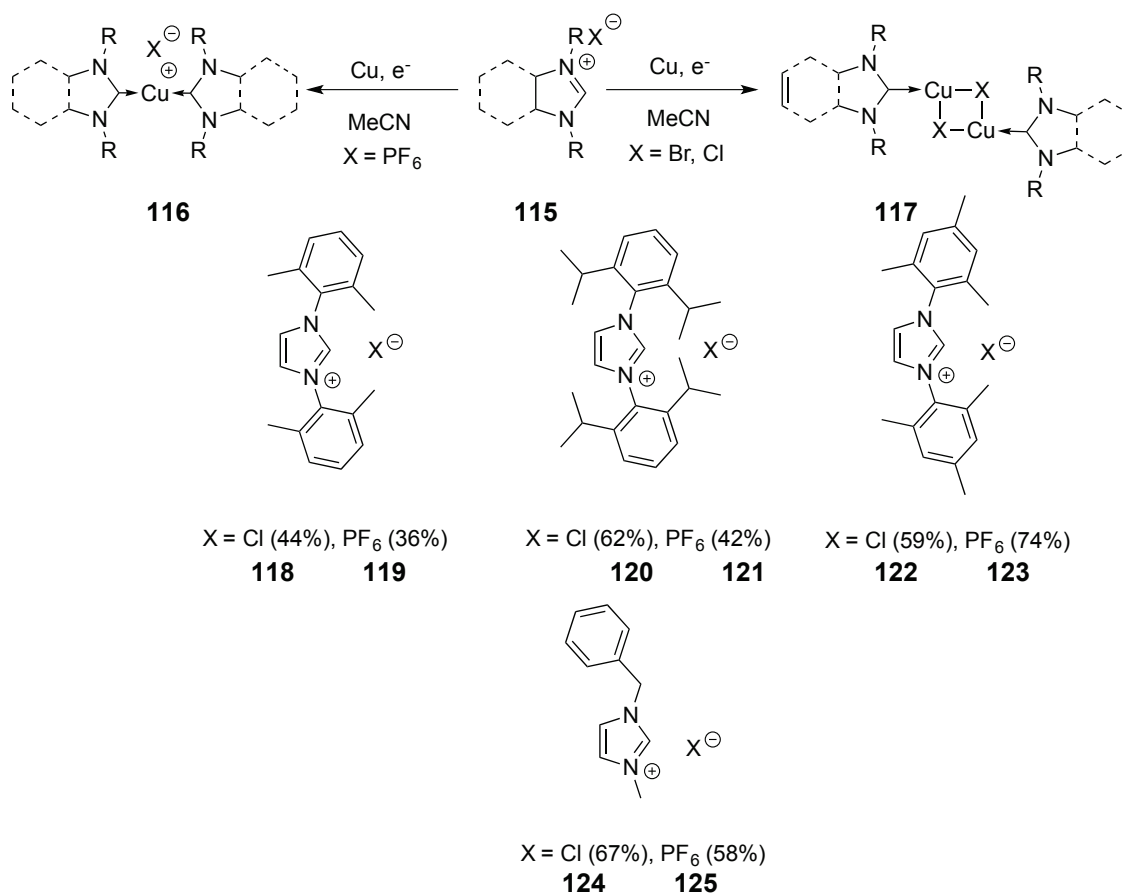
The distance between C(1) and Cu(1) is 3.83 Å. As previously discussed, typical donor-acceptor distances for similar complexes are ca. 3 Å. As such, this interaction is considerably weaker. Jeffrey has described hydrogen bonds with a distance of 2.2-2.5 Å as to be considered to mostly covalent, 2.5-2.3 Å as mostly electrostatic, and 3.2-4.0 Å is considered to be entirely electrostatic.^{146,147} As such, the interaction is here entirely electrostatic, and the bond energy to be $<4 \text{ kcal mol}^{-1}$. Given the marginal nature of this length, there is some ambiguity as to whether this really constitutes a weak hydrogen bond or a van der Waals-type interaction. However, hydrogen bonds express a preference of linearity that is generally not observed in van der Waals interactions.

Bond angle C(1)-H(1)-Cu(1) is 177° , and such linearity would suggest a hydrogen bond interaction. However, linearity could be considered to be induced by packing.

Cu^I complexes are known to form close Cu-Cu interactions. This phenomenon is known as cuprophilicity, and is usually defined as twice the van der Waals of Cu (*ca.* 2.8 Å).^{148,151} The nature of these interactions is controversial, and they may or not be considered bonds. Cu^I is d^{10} , and therefore repulsion should be generally expected between metal centres. However, it has been shown theoretically that van der Waals-type forces (attractive dispersion) can overcome this repulsion, resulting in interactions of approximately the same strength as a hydrogen bond.¹⁵² Further, often it is unclear whether or not the Cu atoms are fixed in position by the ligands. A similar observation has been made in binuclear Au complexes (aurophilicity), and this interaction is better characterized and stronger due to relativistic effects.^{153,154} In this complex, the Cu(1)-Cu(1) distance is 2.8093(4) Å, this is on the outer limit of the accepted cuprophilic distance. Generally Cu-Cu distances for the $[\text{Cu}_2\text{Br}_4]^{2-}$ counter-anion fall in the range of 2.6-2.9 Å,^{155,159} although there are outliers > 3 Å.¹⁶⁰ The only example of an imidazolium salt (in this case, 3-allyl-1-(4-cyanobenzyl)-2-methylbenzimidazolium), has a Cu-Cu distance of 2.8874(15) Å.¹⁶¹ The literature has not discussed whether or not this cluster exhibits a Cu-Cu interaction, and the experimental data here is fundamentally inconclusive.

It was found that $\text{Cu}(\text{NHC})\text{Br}$ **110** could be prepared using this method when both the reaction and the work-up were performed under anaerobic conditions. Decreasing reaction concentration and increased reaction time increased yield of **110**. However, an amount of **114** was always present.

Willans and co-workers have developed an electrochemical method for the synthesis of $\text{Cu}(\text{NHC})\text{X}$ **117** and $\text{Cu}(\text{NHC})_2\text{X}$ **116** (Scheme 38). Cu metal plates are used as sacrificial electrodes. The electrolyte is imidazolium salt dissolved in MeCN (Cl/Br salts resulted in monocarbene complexes, whereas PF_6 salts gave the homoleptic cationic complex). At the anode, Cu^0 is oxidized to Cu^I , whilst at the cathode imidazolium is reduced to imidazolyidene. As can be seen, this methodology is effective for both hindered and unhindered NHCs.



Scheme 38: Electrochemical synthesis of Cu(NHC) complexes from benzimidazolium salts and Cu^0 , as proposed by Willans and co-workers.¹⁶²

Using this method, Mr B. R. M. Lake and Dr C. E. Willans at the University of Leeds were able to provide (1,3-dibenzylbenzimidazolydene)copper(I) bromide **110** in 68% yield. This was recrystallized by vapour diffusion of pentane into a solution of CH_2Cl_2 containing the complex. Single crystal X-ray diffraction (Figure 35) shows that the complex exists in the solid-state as a bromide-bridged dimer. The geometry at Cu is distorted trigonal planar. The C-Cu bond is 1.914(3) Å, which is average for complexes of this type. The Cu-Cu distance is 3.1589(5) Å, and therefore we can assume that there is no cuprophilic interaction in this complex.

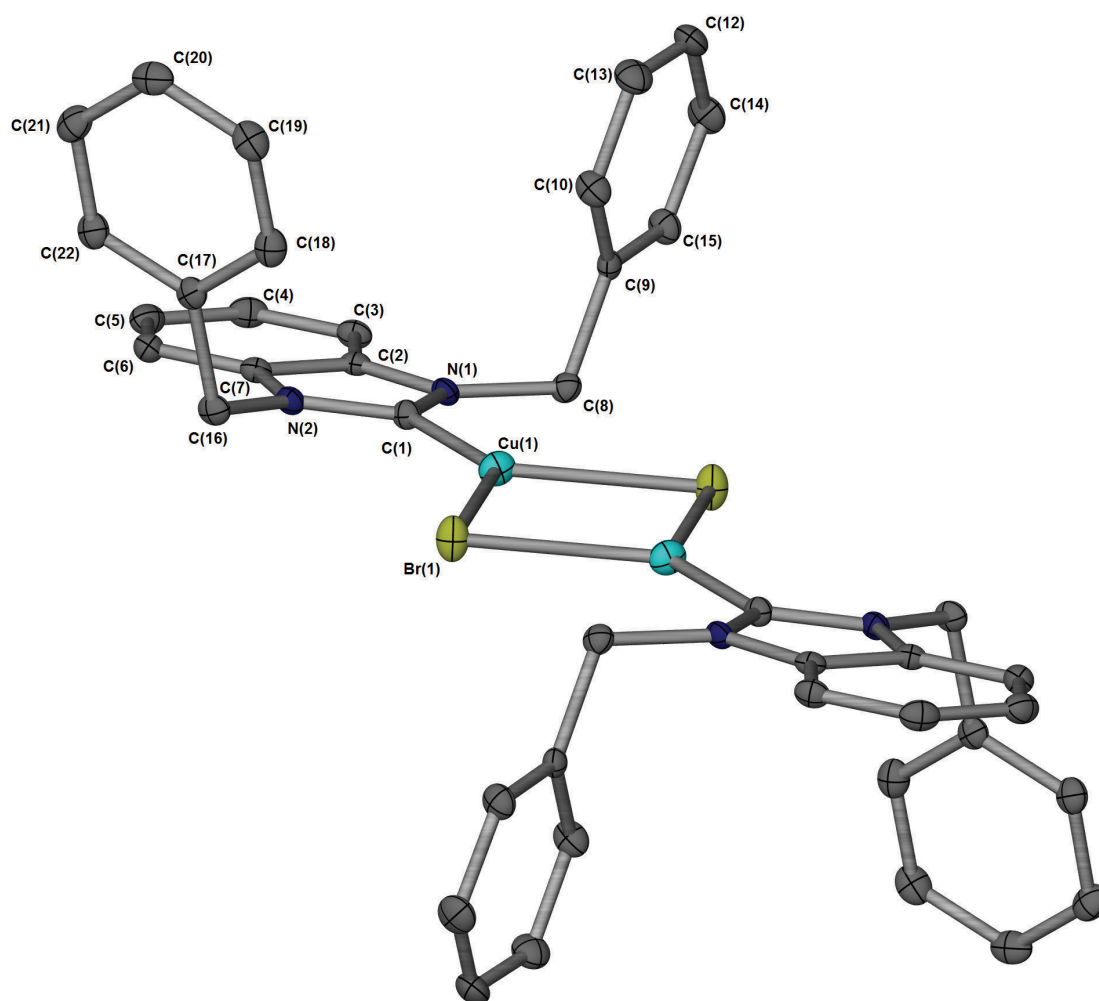
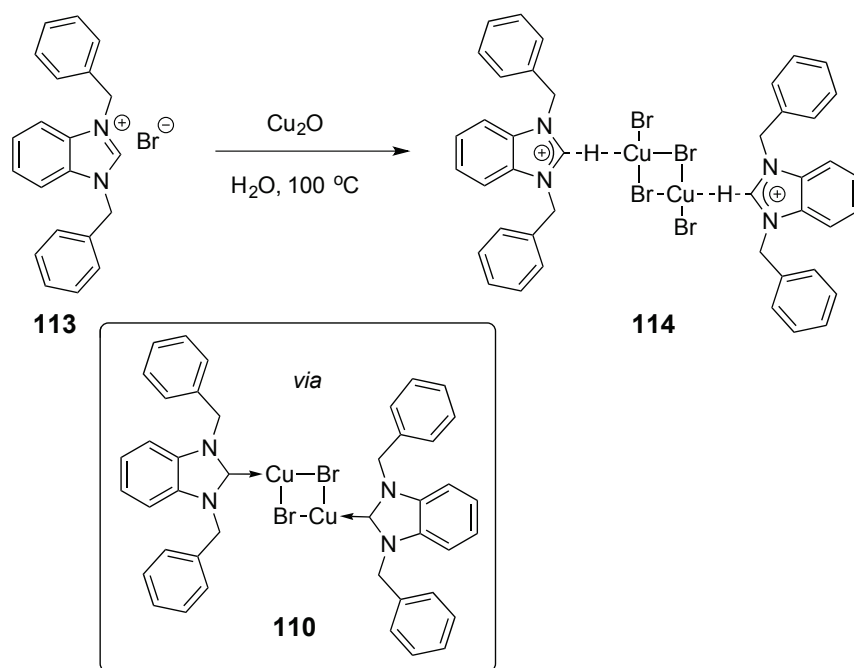


Figure 35: Single crystal X-ray diffraction structure of (1,3-dibenzylbenzoimidazolylidene)copper(I) bromide complex **110**, which exists as a bromide-bridged dimer in the solid-state. Hydrogen atoms have been removed for clarity. Thermal ellipsoids shown at 50%. Selected bond lengths (Å), bond angles (°): C(1)-Cu(1) = 1.914(3), Cu(1)-Br(1) = 2.5073(5), Cu(1)-Cu(1) = 3.1589(5), N(2)-C(1) = 1.365(3), N(1)-C(1) = 1.369(3), C(1)-Cu(1)-Br(1) = 134.16(8), N(1)-C(1)-N(2) = 104.9(2).

When complex **110** was dissolved in H₂O, and heated at 100 °C for 16 h under N₂, recrystallization of the reaction mixture from CDCl₃ results in the formation of complex **113**. It is therefore proposed that in the reaction of 1,3-dibenzylbenzimidazolium bromide **113** and Cu₂O, the NHC complex is formed. However, the relative lack of fixed steric bulk (compared to the substituents on IMes, IPr, or I^tBu, the benzyl groups are highly flexible) the NHC exposes the carbene to electrophilic attack by water. This results in the formation of **113**. Gunnoe and co-workers have shown that when ((1,3-bis(2,6-diisopropylphenyl)imidazol-2-ylidene)copper(I) chloride complex (IPrCuCl) is exposed to water, no reaction occurs. However, addition of strong acid decomposes this complex to [IPrH][CuCl₂] in a similar fashion. IPr is considerably more hindered than the benzylic ligand presented in this thesis.¹⁶³



Scheme 39: Synthesis of complex **114** from the (1,3-dibenzyl)benzimidazolium bromide from Cu₂O.

The stability of **110** was assessed. A sample was dissolved in dry, degassed MeCN-*d*₃. Under these anhydrous conditions, the complex was found to be stable. On the addition of 40 µl of degassed H₂O, a shift in the benzylic ¹H chemical shift was observed from δ 5.69 to δ 5.63 ppm (Figure 36, spectrum c). After 31 h, a minor new species evolves on the right shoulder of this signal. This new signal can be identified as **114**, by comparison to an authentic sample. Simultaneously, multiplet ¹H signals are

observed at δ 7.74 μ 7.59 ppm. When this sample is exposed to air,^u the formation of complex **17** accelerates. At 69 h, a 1:1 ratio of **110**:**114** is observed.

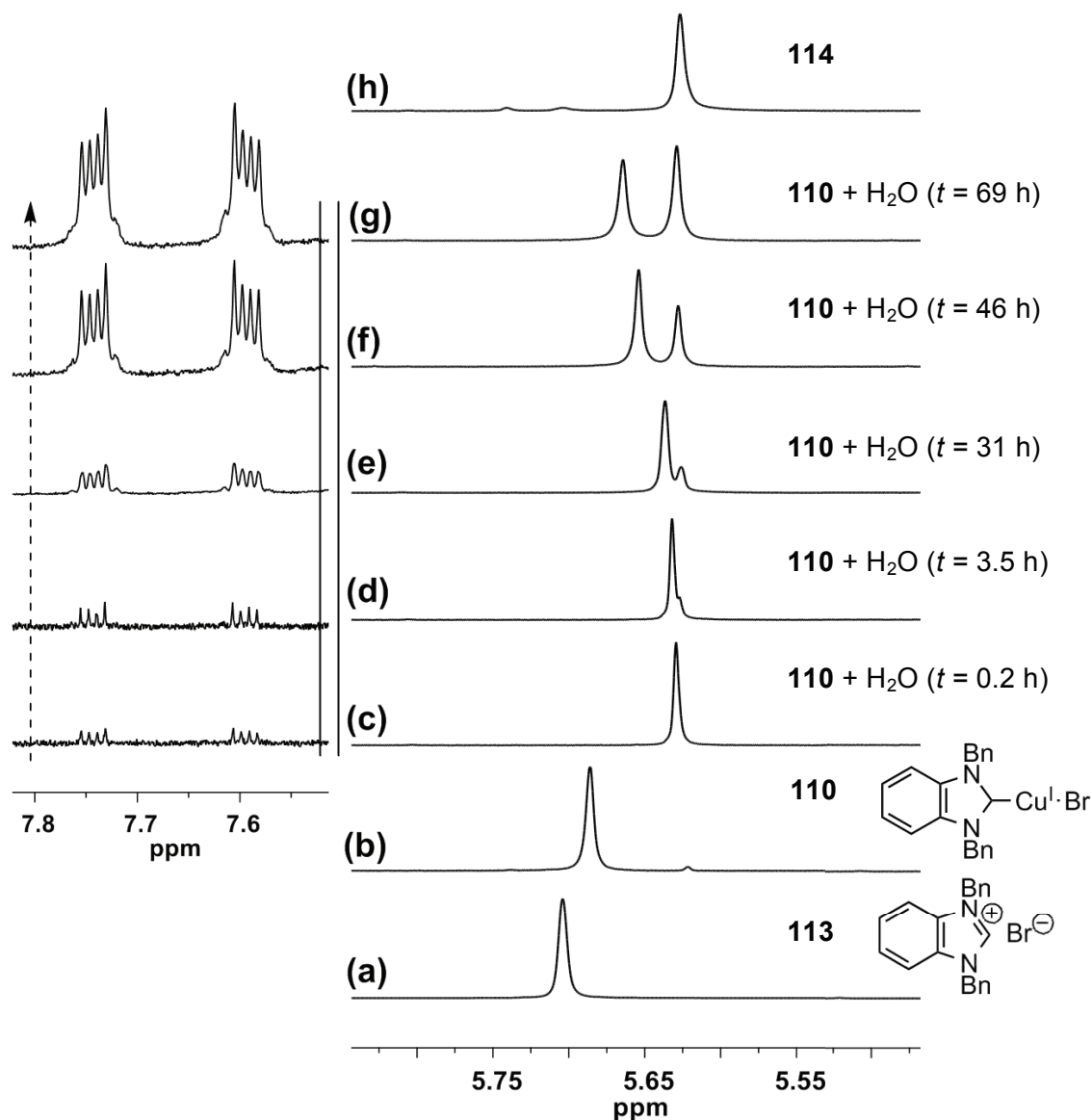


Figure 36: Stability of complex **110** (in anhydrous CD_3CN , under N_2 and in a Younglings NMR tube) monitored by ^1H NMR spectroscopic analysis and its decomposition on exposure to H_2O and air. (a) authentic sample of **113** (b) authentic sample of **110**, (c) addition of degassed H_2O (40 mL) to (b) under N_2 , (d) after 3.5 h, (e) after 31 h, (f) at 45 h, the Younglings tube was exposed to air for 1 min, then sealed and shaken (x3), (g) after 55 h, (h) authentic sample complex **114**.

The expanded section on the left shows the benzo-protons which are observed on formation complex **114**.

Note: experiment carried out with the assistance of Dr C. E. Willans and Prof. I. J. S. Fairlamb.

^u Although $\text{Cu}(\text{NHC})\text{Br}$ complex **110** has low solubility in CD_3CN , the degradation products are soluble.

After 9 days (Figure 37), a ratio of 5:1 was observed for **114**:**110**. A minor species is observed resonating at δ 5.09 and δ 6.97 ppm. A sample was taken of the reaction mixture and analysed by HPLC-MS (Figure 38), and this species has been identified 1,3-dibenzyl-2-benzimidazolone **126**. This was confirmed by removing solvent from the HPLC-MS, dissolving the residue in CDCl_3 and comparing to literature values.¹⁶⁴

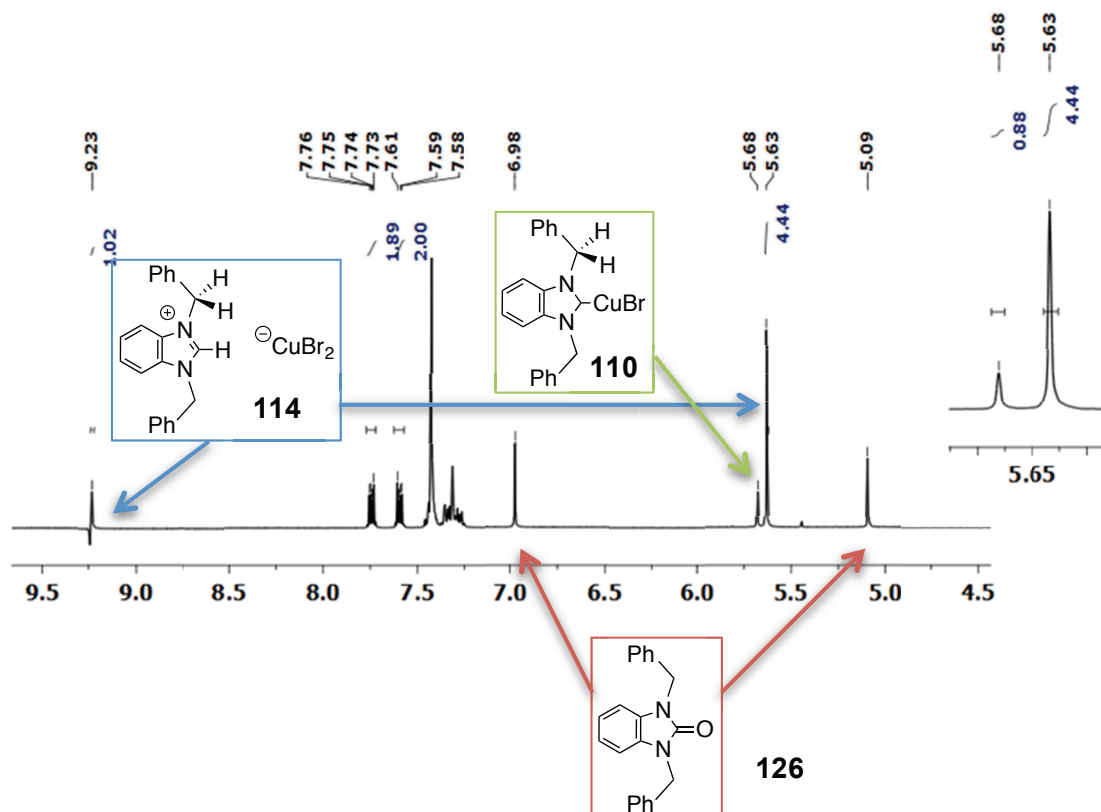


Figure 37: ^1H NMR spectrum (400 MHz, $\text{MeCN-}d_3$) of the decomposition of **110** after 9 d μ products **114** and **126** are observed (labelled).

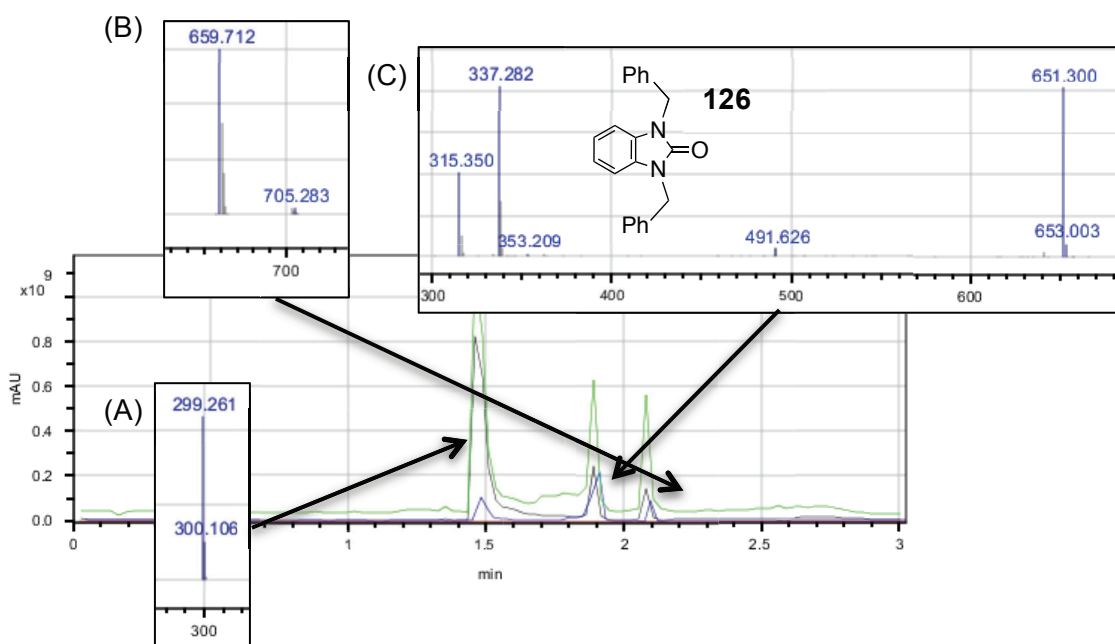
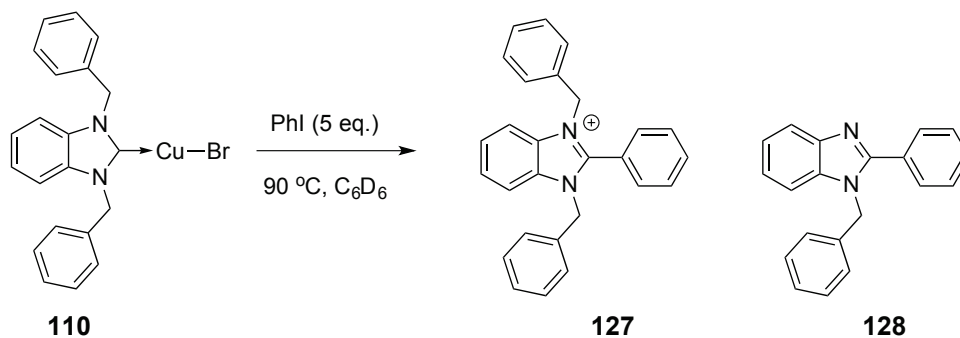


Figure 38: HPLC-MS data indicating the presence of (a) **11** (derived fragment $[\text{NHC}\cdot\text{H}]^+$, m/z 299), (b) **110** (derived fragment $[\text{Cu}(\text{NHC})_2]^+$, m/z 659), (c) 1,3-dibenzyl-2-benzimidazolone **129** (molecular ion $[\text{C}_{21}\text{H}_{19}\text{N}_2\text{O}]^+$, m/z 215, Na dimer $[\text{C}_{42}\text{H}_{36}\text{N}_4\text{NaO}_2]^+$, m/z 651).

In C-H bond functionalisations with Pd and Cu, both O_2 and H_2O have been found to negatively affect reaction efficacy. These findings reflect this.

2.3.3 Application to C-H Bond Functionalisation

A reliable method for the synthesis of **110** had been established. To test the viability of such intermediates in C-H bond functionalisation reactions, a set of model reaction conditions had to be developed. C_6D_6 was selected as a reaction solvent. In addition to ease of availability, aromatic hydrocarbon solvents (e.g. xylene and mesitylene) are used in the arylations developed by Daugulis and co-workers.¹⁴¹



Scheme 40: Proposed reaction of **110** with PhI.

Several products might be expected from this process: the direct C-H bond arylation product (1,3-dibenzyl-2-phenylbenzimidazolium bromide **127**), an arylation/debenzylation product (1-benzyl-2-phenylbenzimidazole **128** μ loss of H^+ from arylated cuprate was hypothesised by Bellina and Rossi,¹⁴² which is being modelled by a benzyl group in this system), and a protodecuprated product (1,3-dibenzylimidazolium bromide **113**). Authentic samples of these compounds were synthesised.

An initial reaction of complex **110** and PhI (2 eq.) was performed (Scheme 40, Figure 39) μ this reaction was performed on a small scale (ca. 10 mg) in a NMR tube equipped with a Youngs μ Tap. The reaction was monitored by observing the resonance associated with the benzylic position (4H, δ 4.93 ppm, s). Complex **110** is partially soluble in C_6D_6 (spectrum A). After the addition of PhI, no reaction was observed (spectrum B). The reaction mixture was then heated to 90 °C. After 2 h, the starting material had been entirely consumed. Two singlets could be observed at 5.10 (broad) and 4.81 ppm. After 24 h heating, the singlet at 4.80 had grown. The second singlet had shifted slightly to 5.14 ppm, and had significantly broadened.

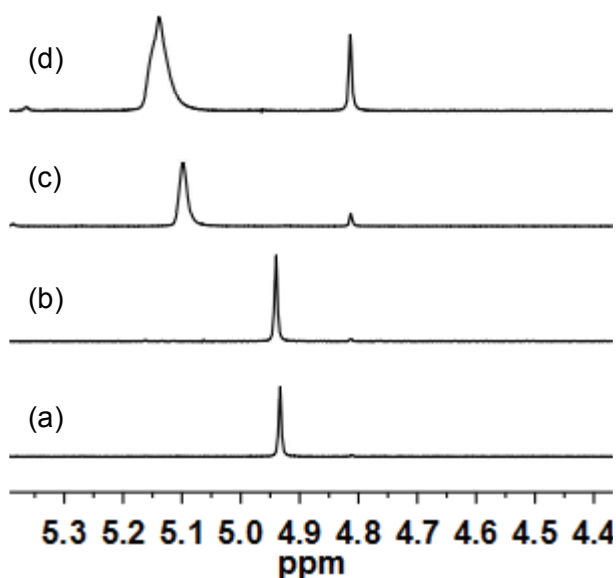


Figure 39: ¹H NMR spectra for the reaction of PhI and complex **110** in C_6D_6 (a) complex **110** immediately after addition, (b) complex **110** and PhI, (c) complex **110** and PhI, after heating at 90 °C for 2 h, (d) complex **110** and PhI, after heating at 90 °C for 24 h.

The solubility of authentic samples of possible products in C_6D_6 was low (the counterion may have an effect on solubility). As such it was not possible to identify these resonances as products. The solvent was thus removed under reduced pressure, and redissolved in $MeCN-d_3$ (Figure 40).

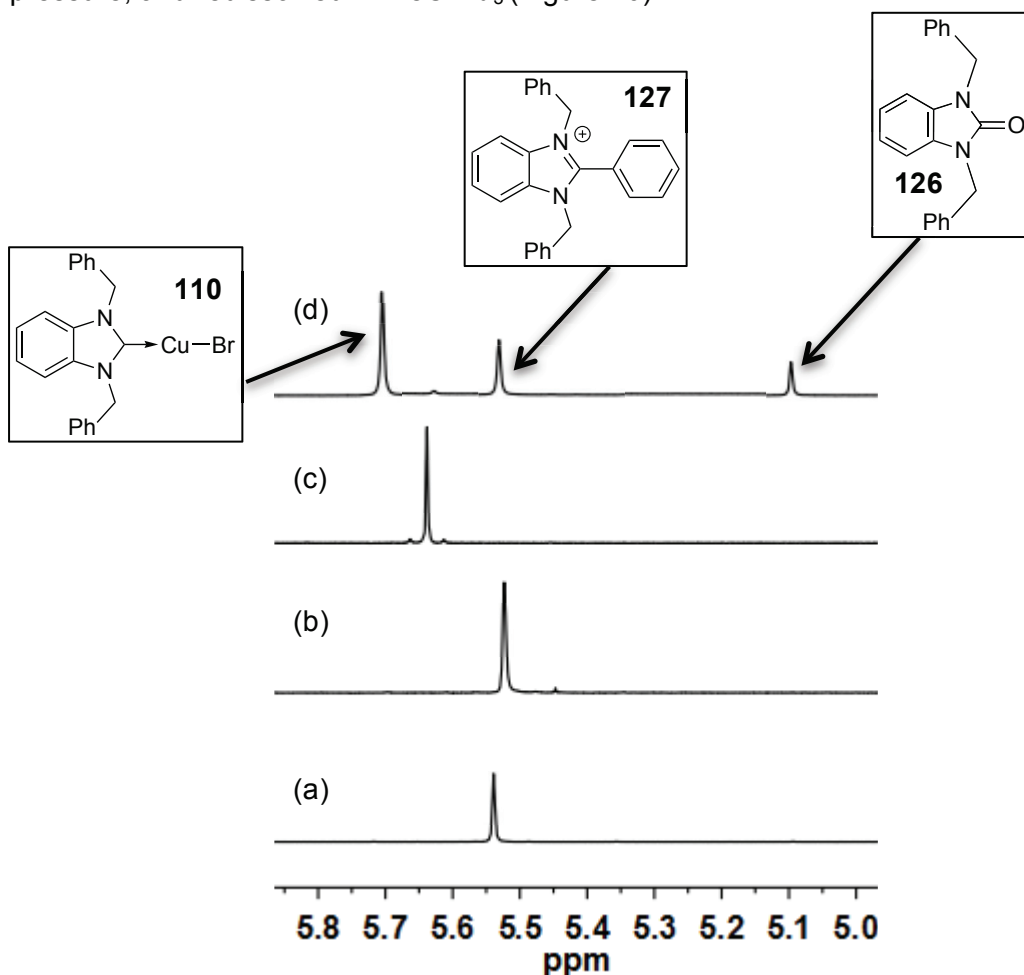


Figure 40: 1H NMR spectra for the work up of reaction of complex **110** and PhI in $MeCN-d_3$ (a) authentic sample of 1,3-dibenzyl-2-phenylbenzimidazolium bromide **127**, (b) authentic sample of 1-benzyl-2-phenylbenzimidazole **128**, (c) authentic sample of 1,3-dibenzylimidazolium bromide **113** (d) work-up of reaction mixture.

In $MeCN-d_3$, three major benzyl species are observed in the 1H NMR spectrum: δ 5.71 ppm (s), δ 5.53 ppm (s), δ 5.09 ppm (s). This was compared to spectra of authentic samples of possible products (spectra a-c). The resonance at 5.53 ppm was ambiguous μ both arylated and arylated/debenzylated products were possible. ESI-MS (Figure 41) revealed the presence of arylated product (m/z 375) and not arylated/bebenzylated product. Therefore, it is proposed that the peak at 5.53 ppm is **127**.

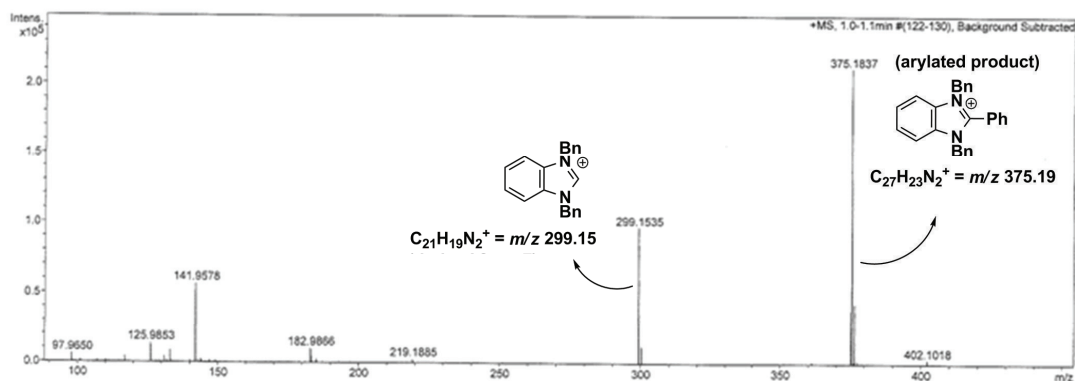
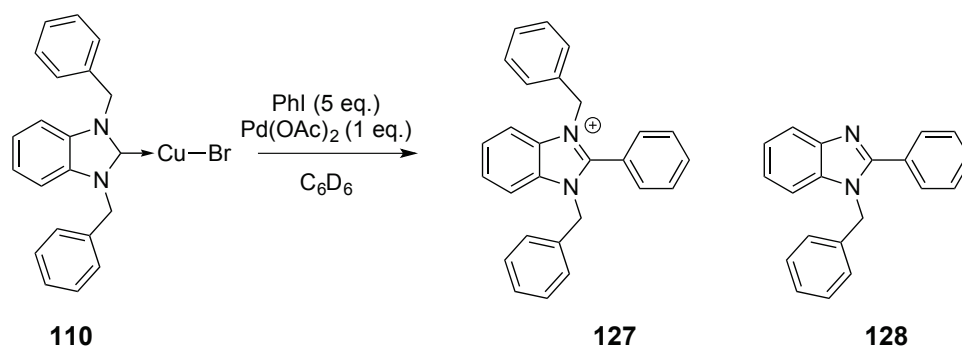


Figure 41: ESI-MS of the reaction of complex **18** and PhI at 24 h.

The resonance at δ 5.81 ppm has been identified as **110** complex by comparison to the starting material. The resonance at δ 5.09 ppm has previously been identified as (1,3-dibenzyl-2-benzimidazolone **126**. Therefore, the complex **110** has been arylated under these reaction conditions, but the reaction has not proceeded to full conversion.



Scheme 41: Reaction of **110** with PhI in the presence of Pd(OAc)₂.

The reaction was then performed in the presence of Pd(OAc)₂ (1 eq. with respect to complex **110**, Scheme 41). Again, this reaction was performed on a small scale (ca. 10 mg) in a NMR tube equipped with a Youngsµ Tap (under N₂). On the addition of Pd(OAc)₂ (Figure 42, spectrum c), the resonance at 4.98 ppm was no longer present. A new resonance at δ 6.07 ppm appears. HPLC-MS (Figure 43) has indicated that this compound is [PdBr(Bn₂-bimy)₂]⁺ (*m/z* 783). Cu(NHC)X complexes have been demonstrated to act as carbene transfer reagents to Pd by Cazin and co-workers.¹²⁰ The reaction mixture was heated at 90 °C. Reduction to Pd⁰ was observed immediately. After 2 h, no benzylic resonances are visible in the ¹H NMR spectrum (spectrum d). No further change occurred after 24 h heating.¹²⁰

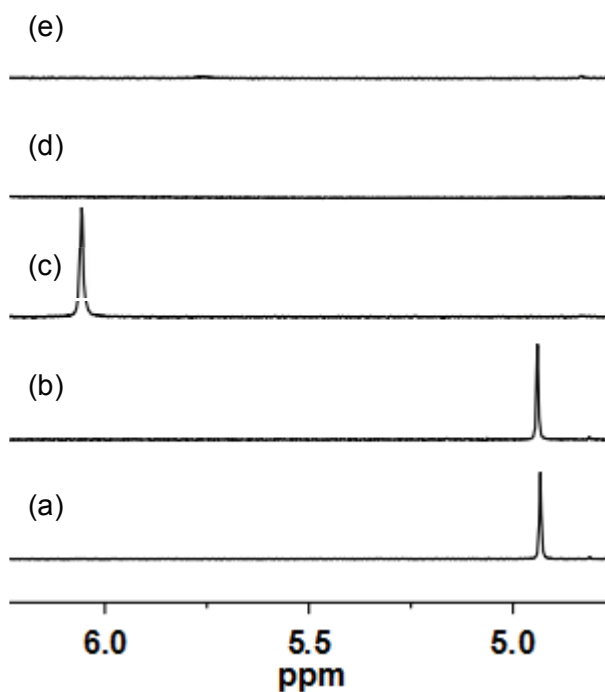


Figure 42: ^1H NMR spectra for the reaction of complex **110** and PhI in the presence of $\text{Pd}(\text{OAc})_2$ in C_6D_6 (a) complex **110** immediately after addition, (b) complex **110** and PhI, (c) complex **110**, PhI and $\text{Pd}(\text{OAc})_2$ (identified as $[\text{PdBr}(\text{Bn}_2\text{-bimy})_2]^+$), (d) complex **110**, PhI and $\text{Pd}(\text{OAc})_2$, after heating at $90\text{ }^\circ\text{C}$ for 2 h, (e) complex **110**, PhI and $\text{Pd}(\text{OAc})_2$, after heating at $90\text{ }^\circ\text{C}$ for 24 h.

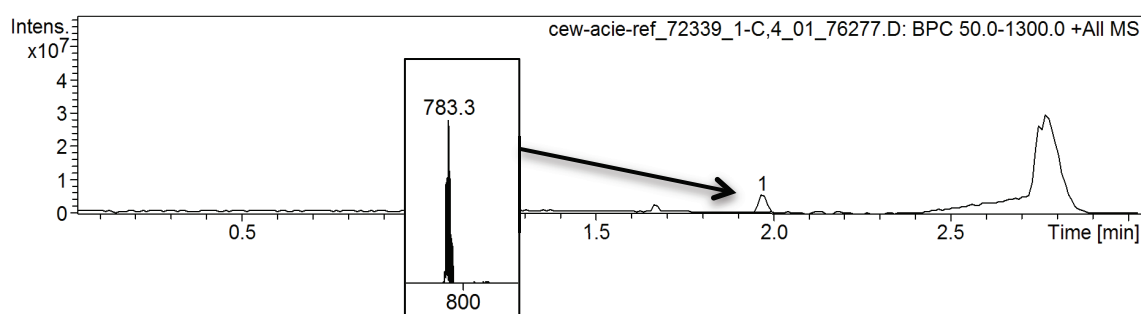


Figure 43: HPLC-MS data identifying the resonance at δ 6.07 ppm as Pd transmetalation product $[\text{PdBr}(\text{Bn}_2\text{-bimy})_2]^+$ (m/z 783).

Identical reactions were stopped at 2 h and 24 h, respectively. Solvent was removed under reduced pressure, and $\text{MeCN-}d_3$ added. In both cases, only one major benzylic resonance was observed (Figure 44, spectra d and e). By comparison to an authentic

sample, this was identified as 1,3-dibenzyl-2-phenylbenzimidazolium salt **113**. In ESI-MS, only this product was observed (Figure 45). No Cu(NHC)Br complex **110** was observed.

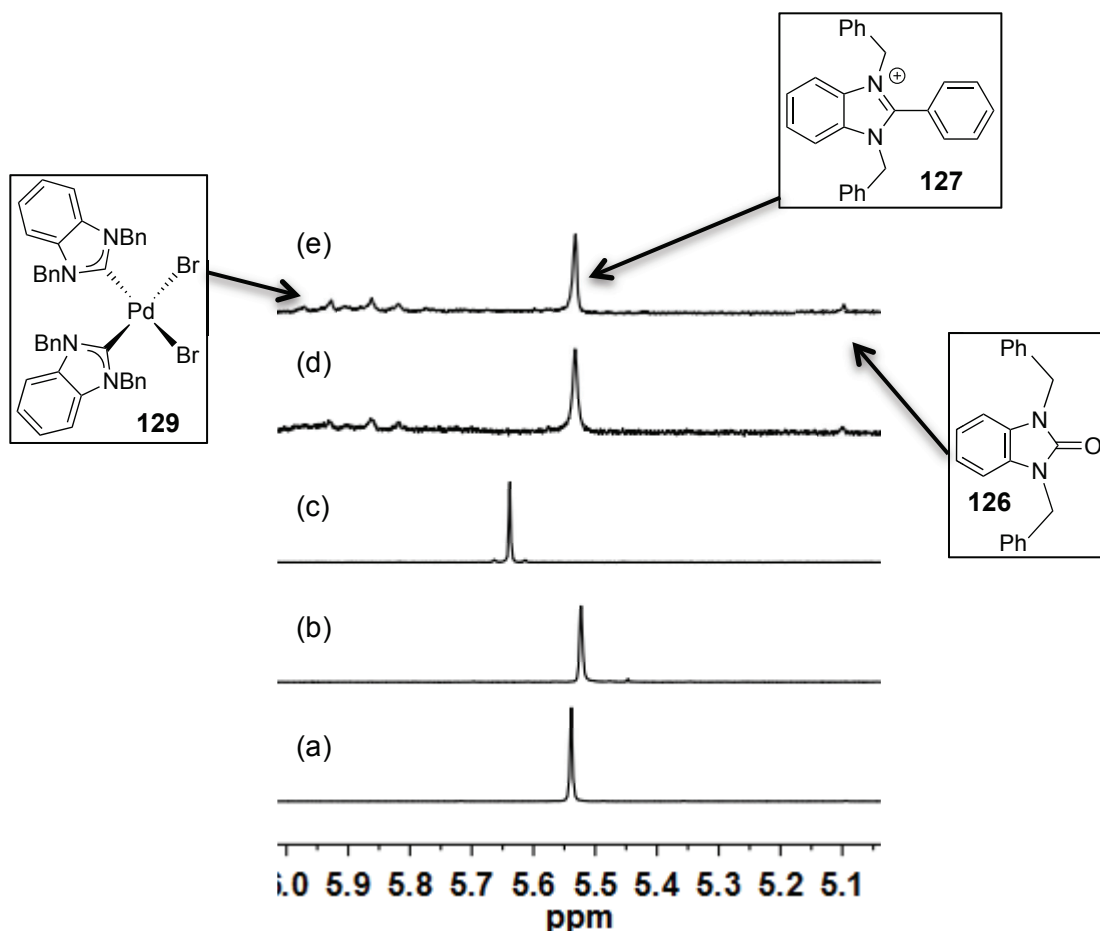


Figure 44: ^1H NMR spectra for the work up of reaction of complex **110** and PhI in the presence of $\text{Pd}(\text{OAc})_2$ in $\text{MeCN-}d_3$. (a) authentic sample of 1-benzyl-2-phenylbenzimidazole **128**, (b) authentic sample of 1,3-dibenzyl-2-phenylbenzimidazolium bromide **127**, (c) authentic sample of 1,3-dibenzylimidazolium bromide **113**, (d) work-up of reaction mixture at 2h, (e) work-up of reaction mixture at 24 h.

Minor resonances can be observed at δ 5.09 ppm (1,3-dibenzyl-2-benzimidazolone) and an AB quartet centred at 5.9 ppm ($^2J_{\text{HH}}$ ca. 17 Hz). This AB quartet is identified as *cis*- $[\text{PdBr}_2(\text{Bn}_2\text{-bimy})_2]$ **129**.¹⁶⁵ The diastereotopy is determined by the molecular symmetry.¹⁶⁵ A trace amount of 1,3-dibenzylbenzimidazolone **129** is also observed.

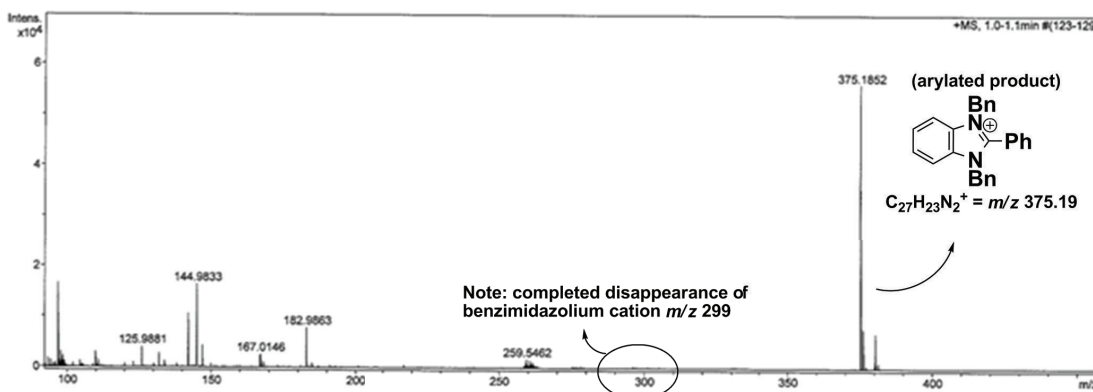
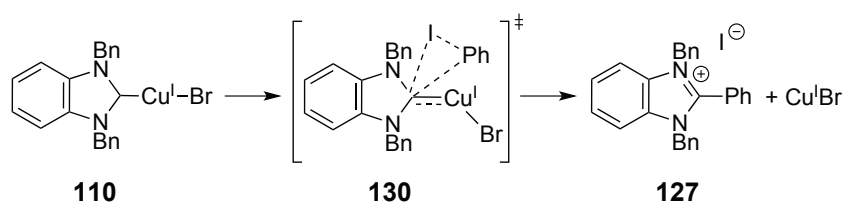


Figure 45: ESI-MS of the reaction of complex **110**, Pd(OAc)₂ and PhI at 24 h.

In the presence of Pd, arylation is cleaner and considerably faster μ rather than multiple products, only one (the desired product) is observed. Transmetalation appears to be rapid. It is proposed, therefore, that the subsequent reductive elimination from Pd is faster than the electrophilic aromatic substitution proposed to occur in the Cu-only systems.

The mechanism for these processes requires further study. However, it seems possible that a carbene insertion mechanism (as reported by Perez and co-workers)¹⁶⁶ could be in operation (Scheme 42). Alternatively, a Cu^{I/III} manifold could be operative.



Scheme 42: Possible mechanism of arylation.

2.4 Experimental

2.4.1 General Experimental Details

Reagents were purchased from Sigma-Aldrich®, Alfa Aesar® or Fluorochem® and used as received unless otherwise stated. Dry THF, CH₂Cl₂, hexane, toluene and acetonitrile were obtained from a Pure Solv MD-7 solvent system and stored under nitrogen. Dry methanol was obtained by drying over 3 Å molecular sieves. Dry DMF was obtained from Acros® and degassed by N₂ bubbling with sonication. Dry deuterated solvents were distilled (under static vacuum) from Na. Petroleum ether refers to the fraction of petroleum that is collected at 40 μ 60 °C. Air sensitive procedures were performed using standard Schlenk techniques. Nitrogen gas was oxygen free and dried immediately prior to use by passing through a column of sodium hydroxide pellets and silica. Where indicated, a Braun® Unilab glove (dry) box used (<0.5 ppm O₂). Filtration was performed under gravity through fluted filter paper unless otherwise stated.

TLC analysis was carried out using Merck 5554 aluminium backed silica plates, and visualised using UV light (254 nm) or an iodine tank. All column chromatography was performed using silica gel 60 and a solvent system as stated in the text.

¹H, ¹³C, ¹⁹F and ³¹P NMR spectra were recorded on a Jeol ECS/ECX400 (400, 100, 376 and 162 MHz respectively). Alternatively and where specified, ¹H, ¹³C and ³¹P NMR spectra were recorded on a Bruker AV500 (500, 126 and 202 MHz respectively) spectrometer. Chemical shifts are reported in parts per million and were referenced to residual undeuterated solvent. Coupling constants have been quoted to ±0.2 Hz. ¹H NMR chemical shift are given to 2 decimal places; ¹³C NMR chemical shift are given to 1 decimal place. Spectra were typically recorded at 298 K. ¹³C, ³¹P, and ¹⁹F spectra were obtained with ¹H decoupling. ¹⁹F and ³¹P spectra were externally referenced to CFC₃ and H₃PO₄ respectively. Spectra were processed using MestreNova®. Some images were produced as .png, .bmp or .jpeg files and copied into ChemDraw, then structures added. Finally, the file was saved as an appropriate image file.

IR spectroscopy was performed using a Perkin Elemer Spectrum 2 or a Unicam Research Series FTIR, both using an ATR attachment. Where indicated, reactions were monitored *in situ* using a Mettler Toledo ReactIRμ ic10 with K6 conduit SiComp

(silicon) probe and MCT detector. Resolution 4 cm^{-1} , range $4000\text{-}650\text{ cm}^{-1}$ and gain adjustment at 1x.

UV-Visible spectroscopy was performed on a Jasco® V-560 spectrometer. A baseline in the appropriate solvent was obtained prior to recording spectra.

Mass spectrometry was performed using a Bruker daltronics micrOTOF spectrometer, an Agilent series 1200 LC, or a Thermo LCQ using electrospray ionization (ESI), with less than 5 ppm error for all HRMS. Liquid induction field desorption ionization (LIFDI) mass spectrometry was performed using a Wasters GCT Premier mass spectrometer.

Chiral stationary phase HPLC was performed with a multiple wavelength, UV-vis diode array detector; integration was performed at 210, 230, and 250 nm. Optical rotations were recorded at $20\text{ }^{\circ}\text{C}$ (using the sodium D line; 259 nm), and $[\alpha]_{\text{D}}$ values are given in units of $10^{-1}\text{ deg cm}^3\text{ g}^{-1}$. Melting points were recorded using a Stuart digital SMP3 machine.

Transmission electron microscopy was performed at the University of York Department of Biology Technology Facility using a Technai 12 BioTWIN microscope, operated at 120 kV. The images were enlarged, and particle sizes measured manually. Statistical analyses were performed and histograms drawn using Microsoft Excel:mac 2010 with AnalystSoft StatPlus:mac LE.2009 (build 5.8.0.0).

Diffraction data were collected at 110 K on an Oxford Diffraction SuperNova diffractometer with Mo-K $_{\alpha}$ radiation ($\lambda = 0.71073\text{ \AA}$) using a EOS CCD camera. The crystal was cooled with an Oxford Instruments Cryojet. Diffractometer control, data collection, initial unit cell determination, frame integration and unit-cell refinement was carried out with $\mu\text{Crysalis}\mu$ ¹⁶⁷. Face-indexed absorption corrections were applied using spherical harmonics, implemented in SCALE3 ABSPACK scaling algorithm. OLEX2¹⁶⁸ was used for overall structure solution, refinement and preparation of computer graphics and publication data. Within OLEX2, the algorithms used for structure solution were direct methods.¹⁶⁹ Refinement by full-matrix least-squares used the SHELXL-97¹⁷⁰ algorithm within OLEX2. All non-hydrogen atoms were refined anisotropically. Hydrogen atoms were placed using a riding model and included in the refinement at calculated positions.

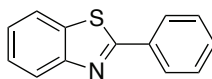
Pd-PVP Nanoparticles

To a three-necked round-bottomed flask fitted with a mechanical stirrer and reflux condenser was added PdCl₂ (255 mg, 1.44 mmol), HCl (aq., 0.2 M, 14.4 mL), and water (706 mL). The reaction mixture was stirred for 1 h, after which time PdCl₂ had dissolved to give an orange solution. PVP (3.2 g), water (672 mL) and EtOH (1000 mL) were added and the reaction heated to reflux with stirring for 4.5 h. The mixture was cooled to room temperature, and the solvent removed under reduced pressure to give 3.367 g of black solid.

Ca. 1 mg of material was suspended in EtOH (with vigorous shaking), applied to a TEM slide, and the solvent evaporated. They were then analyzed by transmission electron microscopy. This data is shown on page 45.

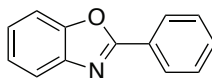
General Procedure for the Bellina-Rossi Direct Arylation Reaction

To an oven-dried Schlenk or carousel tube was added CsF (2.5 eq.), Pd catalyst, and CuI (2 eq.). The reaction vessel was evacuated under high vacuum with stirring and refilled with N₂. This process was repeated twice. To this was added heterocycle (1 eq.), iodobenzene (2 eq.) and DMF (5 mL). The reaction mixture was then heated to 120 °C with stirring for 24 h. To the reaction mixture was added sat. aq. NH₄Cl (20 mL) and the mixture stirred in air for 1 h to give a homogeneous blue solution. If the mixture remained heterogeneous, pyridine (100 µl) was added. The mixture was then extracted into EtOAc (3 x 40mL). The organic layers were combined, dried over MgSO₄, filtered and the solvent removed under reduced pressure. The resulting brown residue was dry-loaded onto silica gel, and purified by flash chromatography eluting with EtOAc in petroleum ether solvent systems to give product.

2-Phenylbenzo[*d*]thiazole, **131**

Eluted from silica gel column using 4% EtOAc in petroleum ether.

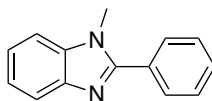
R_F 0.88 (20% EtOAc/PE); MP 114 μ 116 °C (lit. 111 μ 112 °C)⁴⁹; ^1H NMR (400 MHz, CDCl_3) δ 8.11 μ 8.05 (m, 3H), 7.92 μ 7.89 (m, 1H), 7.53 μ 7.45 (m, 4H), 7.38 (ddd, J = 8.2, 7.4, 1.1 Hz, 1H); ^{13}C NMR (101 MHz, CDCl_3) δ 168.2, 154.2, 135.2, 133.7, 131.1, 129.1, 127.7, 126.4, 125.3, 123.3, 121.7; ESI-MS m/z 212 [M+H]; ESI-HRMS m/z 212.0532 [M+H] (calc. for $\text{C}_{13}\text{H}_{10}\text{NS}$ 212.0528); IR (solid-state ATR, cm^{-1}) 1509, 1477, 1454, 1432, 1313, 1257, 1225, 1159, 1088, 1070, 1012, 962, 797, 758, 729, 684.

2-Phenylbenzo[*d*]oxazole, **108**

Eluted from silica gel column using 4% EtOAc in petroleum ether.

R_F 0.79 (20% EtOAc/PE); MP 103 μ 106 (lit. 102.8 °C)⁴⁹; ^1H NMR (400 MHz, CDCl_3) δ 8.31 μ 8.20 (m, 2H), 7.83 μ 7.72 (m, 1H), 7.63 μ 7.55 (m, 1H), 7.55 μ 7.48 (m, 3H), 7.37 μ 7.31 (m, 2H); ^{13}C NMR (101 MHz, CDCl_3) δ 163.2, 150.9, 142.2, 131.7, 129.1, 127.8, 127.3, 125.3, 124.7, 120.2, 110.8; ESI-MS m/z 196 [M+H]; ESI-HRMS m/z 196.0855 [M+H] (calc. for $\text{C}_{13}\text{H}_{10}\text{NO}$ 196.0757); IR (solid-state ATR, cm^{-1}) 1617, 1552, 1446, 1258, 1241, 1021, 923, 806, 780, 758.

1-Methyl-2-phenylbenzo[d]imidazole, **106**¹⁷¹



Eluted from silica gel column using 20-26% EtOAc in petroleum ether.

R_F 0.23 (20% EtOAc/PE); ^1H NMR (400 MHz, CDCl_3) δ 7.86 μ 7.79 (m, 3H), 7.57 μ 7.46 (m, 3H), 7.36 μ 7.27 (m, 3H), 3.85 (s, 3H); ^{13}C NMR (101 MHz, CDCl_3) 153.9, 143.0, 136.4, 130.3, 129.9, 129.5, 128.8, 122.9, 122.6, 119.9, 109.7, 31.8; ESI-MS m/z 209 [M+H]; ESI-HRMS m/z 209.1076 [M+H] (calc. for $\text{C}_{14}\text{H}_{13}\text{N}_2$ 209.1073, error 1.7 ppm); IR (solid-state ATR, cm^{-1}) 1468, 1440, 1377, 1328, 1277, 1243, 1197, 1177, 1151, 1128, 1099, 1075, 1052, 1020, 1006, 925, 849, 819, 774, 764.

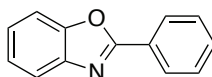
Analysis of Nanoparticles from the Bellina-Rossi Direct Arylation Reaction

Two reactions were prepared, using the general procedure with benzothiazole: one in a Schlenk tube and the second in a Radleys® carousel tube. The reactions were heated to 120 °C for 2 h.

Each sample was suspended in EtOH, applied to a TEM slide, and the solvent evaporated. They were then analyzed by transmission electron microscopy. Representative images are shown in Figures 17 and 18 (page 51). Two aliquots (1 mL) were removed from each reaction mixture *via* syringe. To one aliquot per reaction, PVP (22 mg, 10 eq. per theoretical amount of Pd) was added. The solvent of all aliquots was removed under reduced pressure.

2.4.3 Direct C-H Bond Functionalisation of Benzoxazole with $\text{PhI}(\text{OAc})_2$

*General Procedure for the 'Chen-Cheng' Direct Arylation of Benzoxazole, 108*¹³⁰



To a Schlenk tube was added benzoxazole (119 mg, 1 mmol, 1 eq.), $\text{PhI}(\text{OAc})_2$ (415 mg, 1.25 mmol, 1.25 eq.), Cs_2CO_3 (326 mg, 1 mmol, 1 eq.), 1,10-phenanthroline (18.0 mg, 0.1 mmol, 0.1 eq.) and $\text{Pd}(\text{OAc})_2$ (11.1 mg, 0.05 mmol, 0.05 eq.). The reaction vessel was then placed under vacuum and refilled with N_2 . This process was repeated twice. DMSO (5 mL) was added *via* syringe, and the reaction heated to 150 °C for 20 h. The reaction mixture was then exposed to air, diluted with EtOAc (15 mL) and washed with water (3 x 20 mL). The organic layer was dried over MgSO_4 , filtered, and the solvent removed under reduced pressure to give a residue. This residue was dry loaded onto silica gel, and purified by flash chromatography (4% EtOAc in petroleum ether 40-60 °C) to give product as a white solid (135 mg, 69% yield).

Analytical data identical to that reported above.

Degradation of $\text{PhI}(\text{OAc})_2$ at Room Temperature

To a NMR tube was added $\text{PhI}(\text{OAc})_2$ (15 mg) which was then dissolved in $\text{DMSO}-d_6$ (0.7 mL). ^1H NMR spectra were recorded at *ca.* $t = 5, 30, 40$ and 50 min intervals.

Spectra shown in Figure 22 (page 57).

Degradation of $\text{PhI}(\text{OAc})_2$ at 150 °C

To a Younglin Tap NMR tube was added $\text{PhI}(\text{OAc})_2$ (15 mg) which was then dissolved in $\text{DMSO}-d_6$ (0.7 mL). A ^1H NMR spectrum was recorded. The reaction mixture was heated to 150 °C for 10 min, and a ^1H NMR spectrum recorded.

Spectra shown in Figure 25 (page 60).

Analysis of Nanoparticles from the Direct C-H Bond Functionalisation with PhI(OAc)₂

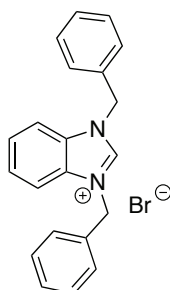
To a Schlenk tube was added benzoxazole (119 mg, 1 mmol, 1 eq.), PhI(OAc)₂ (415 mg, 1.25 mmol, 1.25 eq.), Cs₂CO₃ (326 mg, 1 mmol, 1 eq.), 1,10-phenanthroline (18 mg, 0.1 mmol, 0.1 eq.) and Pd(OAc)₂ (11.1 mg, 0.05 mmol, 0.05 eq.). The reaction vessel was then placed under vacuum and refilled with N₂. This process was repeated twice. DMSO (5 mL) was added via syringe, and the reaction heated to 150 °C for 2 h. Two aliquots (1 mL) were removed *via* syringe from the reaction mixture. To one aliquot, PVP (22 mg, 10 eq. per theoretical amount of Pd) was added. The solvent of both aliquots was removed under reduced pressure.

Each sample was suspended in EtOH, applied to a TEM slide, and the solvent evaporated. They were then analyzed by transmission electron microscopy. Representative images are shown in Figure 21 (page 56).

Particle size was measured according to the method outlined in general experimental procedure.

2.4.4 Role for Cu-NHC Complexes in Pd/Cu-Mediated Systems

*Dibenzylbenzo[d]imidazolium bromide, 113*¹⁷²



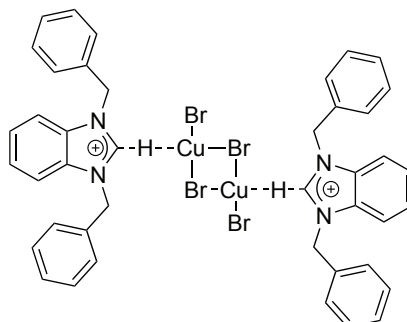
To a round-bottom flask was added benzimidazole (10 g, 84.7 mmol, 1 eq.), benzyl bromide (29 g, 169.5 mmol, 20 mL, 2 eq.), K₂CO₃ (17.527 g, 127 mmol, 1.6 eq.) and acetonitrile (200 mL). This mixture was stirred for 3 d at ambient temperature. Solvent was removed under reduced pressure. Water (200 mL) was added, and the mixture stirred. The reaction mixture was filtered to give product as a white solid (31.873 g, 99% yield).

MP 228 μ 229 °C (lit. 210-212 °C); ¹H NMR (400 MHz, (CD₃)₂SO) δ 9.98 (s, 1H), 7.96 μ 7.90 (m, 2H), 7.64 μ 7.57 (m, 2H), 7.50 μ 7.46 (m, 4H), 7.43 μ 7.33 (m, 6H), 5.75 (s, 4H); ¹³C NMR (101 MHz, (CD₃)₂SO) 134.0, 131.1, 129.0, 128.8, 128.3, 126.8, 114.0, 50.0 (note: C2 not observed); ESI-MS *m/z* 299 [M-Br]; ESI-HRMS *m/z* 299.1539 [M-Br] (calc. for C₂₁H₁₉N₂ 229.1543).

Crystals suitable for X-ray diffraction were grown from CHCl₃ solution in air at ambient temperature. .

Summary of X-ray data for 113

Chemical formula	Br ₁ C ₂₁ H ₁₉ N ₂ H ₂ O
Formula Mass	397.31
Crystal system	Triclinic
<i>a</i> /Å	9.3864(4)
<i>b</i> /Å	9.9323(4)
<i>c</i> /Å	11.3331(6)
<i>α</i> /°	69.308(4)
<i>β</i> /°	80.860(4)
<i>γ</i> /°	69.207(4)
Unit cell volume/Å ³	923.36(7)
Temperature/K	110(2)
Space group	<i>P</i> $\bar{1}$
No. of formula units per unit cell, Z	2
No. of reflections measured	8860
No. of independent reflections	5751
<i>R</i> _{int}	0.0204
Final <i>R</i> ₁ values (<i>I</i> > 2σ(<i>I</i>))	0.0392
Final <i>wR</i> (<i>F</i> ²) values (<i>I</i> > 2σ(<i>I</i>))	0.0929
Final <i>R</i> ₁ values (all data)	0.0482
Final <i>wR</i> (<i>F</i> ²) values (all data)	0.0978

Bis{1,3-dibenzylbenzo[d]imidazolium} dicopper(I)tetrabromide, 114a

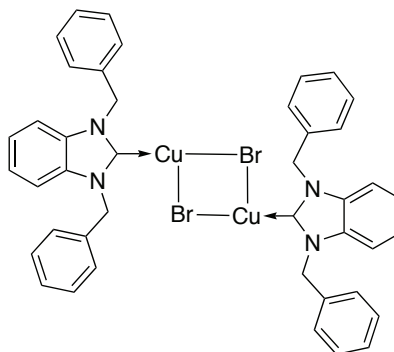
To a Schlenk tube was added 1,3-dibenzylbenzo[d]imidazolium bromide (500 mg, 1.318 mmol, 1 eq.) and Cu_2O (71 mg, 0.657 mmol). The reaction vessel was placed under vacuum and back-filled with N_2 (3 cycles). Water (5 mL, degassed) was added, and the reaction heated at 100 °C for 16 h. The solvent was removed *in vacuo*, and the resulting solid dissolved in laboratory grade (*i.e.* wet) CH_2Cl_2 (20 mL). This was filtered, and the solvent removed under reduced pressure. The resulting solid was recrystallised from laboratory grade CHCl_3 to give product as brown crystals (60.4 mg, 8.3% yield).

From separate reactions were obtained different polymorphs in which Cu_xBr_y exists as an infinite anionic polymer, as opposed to a stoichiometrically defined cluster.

X-Ray crystallographic data for each observed structure shown on the following page.

Compound reference	ijsf1222 (CuBr ₂)	ijsf1221 (Cu _x Br _y)	ijsf1103 (Cu _x Br _y)
Chemical formula	0.5(Br ₄ Cu ₂)AC ₂₁ H ₁₉ N ₂ ACHCl ₃	C ₂₁ H _{18.91} Br ₃ Cu _{2.09} N ₂	0.5(C ₄₂ H _{37.84} Br ₆ Cu _{4.1} N ₄)
Formula Mass	642.11	672.10	671.29
Crystal system	Triclinic	Orthorhombic	Orthorhombic
<i>a</i> /Å	9.5428(3)	20.7826(7)	20.6640(18)
<i>b</i> /Å	11.1470(4)	14.9253(4)	14.8519(12)
<i>c</i> /Å	11.8115(4)	6.9568(2)	6.9524(7)
<i>α</i> °	74.193(3)	90.00	90.00
<i>β</i> °	89.234(3)	90.00	90.00
<i>γ</i> °	83.652(3)	90.00	90.00
Unit cell volume/Å ³	1201.32(7)	2157.90(12)	2133.7(3)
Temperature/K	110.00(10)	110.00(10)	110.0
Space group	<i>P</i> $\bar{1}$	<i>Pbcn</i>	<i>Pbcn</i>
No. of formula units per unit cell, Z	2	4	4
No. of reflections measured	19512	6663	5150
No. of independent reflections	7072	2979	2208
<i>R</i> _{int}	0.0246	0.0240	0.0283
Final <i>R</i> ₁ values (<i>I</i> > 2σ(<i>I</i>))	0.0250	0.0457	0.0509
Final <i>wR</i> (<i>F</i> ²) values (<i>I</i> > 2σ(<i>I</i>))	0.0529	0.0854	0.0888
Final <i>R</i> ₁ values (all data)	0.0314	0.0624	0.0645
Final <i>wR</i> (<i>F</i> ²) values (all data)	0.0553	0.0927	0.0938

(1,3-dibenzylbenzo[d]imidazolin-2-ylidene) copper(I) bromide, **110**¹⁶²



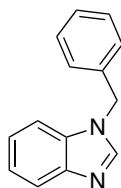
To a three-necked round-bottom flask was added 1,3-dibenzylbenzo[d]imidazolium bromide (389 mg, 1 mmol, 1 eq.) and MeCN (15 mL, dry) to form a suspension. Cu electrodes (1 x 3 cm³) were inserted into the reaction mixture, and 50 mA current passed through solution for 45 min. The reaction mixture was then filtered, and the solvent removed under reduced pressure to give an off-white solid. This was washed with MeOH, dissolved in CH₂Cl₂ and filtered. The solvent was removed under reduced pressure to give an off-white solid. This was dissolved in CH₂Cl₂, and layered with Et₂O. This resulted in the formation of crystals, which were collected by filtration to give product as a white solid (300 mg, 68% yield).

MP 211 – 213 °C; ¹H NMR (500 MHz, CD₂Cl₂) δ 7.40 – 7.32 (m, 12H), 7.30 – 7.27 (m, 2H), 5.69 (s, 4H); ¹³C NMR (126 MHz, CD₂Cl₂) δ 135.9, 129.6, 129.0, 128.0, 124.7, 112.5, 53.4 (only 7 of 9 resonances observed); LIFDI-MS *m/z* (%) 440 (67) [⁶³Cu⁷⁹BrM], 441 (12) [⁶³Cu⁷⁹Br¹³CM], 442 (100) [⁶³Cu⁸¹BrM and ⁶⁵Cu⁷⁹BrM], 442 (22) [⁶³Cu⁸¹Br¹³CM or ⁶⁵Cu⁷⁹Br¹³CM], 443 (28) [⁶⁵Cu⁸¹BrM] (observed as monomer only); Anal. calc. for C₂₁H₁₈BrCuN₂ C 57.09, H 4.11, N 6.34, observed C 56.90, H 4.05, N 6.15.

Crystals suitable for X-ray diffraction were grown by vapour diffusion of pentane into a CH₂Cl₂ solution under N₂.

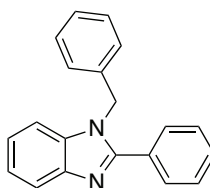
Summary of X-ray data for 110

Chemical formula	C ₄₂ H ₃₆ Br ₂ Cu ₂ N ₄
Formula Mass	883.65
Crystal system	Orthorhombic
<i>a</i> /Å	9.4581(6)
<i>b</i> /Å	9.5482(7)
<i>c</i> /Å	11.2949(10)
α /°	69.206(7)
β /°	82.837(6)
γ /°	69.262(6)
Unit cell volume/Å ³	891.80(12)
Temperature/K	110.00(10)
Space group	<i>P</i> $\bar{1}$
No. of formula units per unit cell, Z	1
No. of reflections measured	8485
No. of independent reflections	5176
<i>R</i> _{int}	0.0285
Final <i>R</i> ₁ values (<i>I</i> > 2σ(<i>I</i>))	0.0406
Final <i>wR</i> (<i>F</i> ²) values (<i>I</i> > 2σ(<i>I</i>))	0.0877
Final <i>R</i> ₁ values (all data)	0.0539
Final <i>wR</i> (<i>F</i> ²) values (all data)	0.0953

*1-Benzylbenzo[d]imidazole, 132*¹⁷³

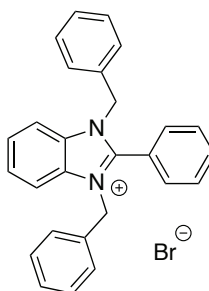
To a round-bottomed flask was added ground KOH (950 mg, 16.94 mmol) and DMSO (13.5 mL). The reaction mixture was stirred vigorously for 5 min at ambient temperature. Benzo[d]imidazole (1 g, 8.47 mmol) was added to give a pale yellow solution which was stirred for 45 min. Benzylbromide (1.21 mL, 1.740 g, 10.2 mmol) was added drop-wise and the reaction mixture stirred for 2 h. The reaction mixture was then added to water (50 mL) and extracted into Et₂O (3 x 50 mL). The organic layers were combined, dried over MgSO₄, filtered and the solvent removed under reduced pressure to give a yellow solid. This was dry-loaded onto silica gel and purified by column chromatography, eluting with 50-100% EtOAc in petroleum ether to give product as a white solid (778 mg, 3.7 mmol, 44%).

MP 119.8 – 121.1 °C (lit. 119 – 120 °C); ¹H NMR (400 MHz, (CD₃)₂SO) δ 8.37 (s, 1H), 7.66 – 7.58 (m, 1H), 7.51 – 7.43 (m, 1H), 7.33 – 7.21 (m, 5H), 7.20 – 7.11 (m, 2H), 5.46 (s, 2H); ¹³C NMR (101 MHz, (CD₃)₂SO) δ 144.3, 143.6, 133.7, 137.5, 129.2, 128.3, 128.0, 122.9, 122.1, 120.0, 111.2, 48.14; ESI-MS *m/z* 209 [M+H].

*1-Benzyl-2-phenylbenzo[d]imidazole, 128*¹⁷⁴

To a sealed tube was added 1-benzylbenzimidazole (60 mg, 0.288 mmol, 1 eq.), CuI (26 mg, 0.136 mmol, 0.47 eq.), LiO^tBu (216 mg, 2.04 mmol, 7 eq.) and *p*-xylene (3.4 mL). PhI (278 mg, 1.364 mmol, 152 μ l, 4.7 eq.) was added *via* syringe. The reaction mixture was heated to 160 °C for 16 h. The reaction mixture was added to water (10 mL), and extracted into CH₂Cl₂ (3 x 20 mL). The organic layers were combined, dried over MgSO₄, filtered and the solvent removed under reduced pressure to give a yellow solid. This was dry-loaded onto silica gel and purified by flash chromatography eluting with 20% EtOAc in petroleum ether to give product as a white solid (22 mg, 23% yield).

MP 142 μ 144 °C; ¹H NMR (400 MHz, CD₃CN) δ 7.76 μ 7.79 (m, 3H), 7.56 μ 7.46 (m, 3H), 7.35 μ 7.21 (m, 6H), 7.05 μ 7.00 (m, 2H), 5.54 (s, 2H); ¹³C NMR (101 MHz, CD₃CN) δ 154.0, 143.3, 137.1, 136.2, 130.7, 129.9, 129.3, 128.9, 128.8, 127.6, 126.2, 110.9, 48.0 (only 13 of 16 resonances observed); ESI-MS *m/z* 285 [M+H]; ESI-HRMS *m/z* 285.1382 (calc. for C₂₀H₁₇N₂ 285.1385); IR (solid-state ATR, cm⁻¹) 3060, 1924, 1495, 1460, 1452, 1443, 1377, 1354, 1330, 1250, 1074, 1028, 777, 764, 743, 729, 696.

(1,3-Dibenzyl)-2-phenylbenzo[d]imidazolium bromide, 127

To a sealed tube was added 1,3-dibenzylbenzimidazole **113** (100 mg, 0.263 mmol, 1 eq.), CuI (13 mg, 0.067 mmol, 0.25 eq.), LiO^tBu (106 mg, 1.00 mmol, 4 eq.) and *p*-xylene (3.4 mL). PhI (278 mg, 0.668 mmol, 75 μ l, 4.7 eq.) was added *via* syringe. The reaction mixture was heated to 160 °C for 16 h. The reaction mixture was added to water (10 mL), and extracted into CH₂Cl₂ (3 x 20 mL). The organic layers were combined, dried over MgSO₄, filtered and the solvent removed under reduced pressure to give a yellow solid. This was dry-loaded onto silica gel and purified by flash chromatography eluting with MeOH:CH₂Cl₂ (4:96) to give product as a white solid (25 mg, 19% yield).

MP 101 μ 103 °C (decomp.); ¹H NMR (400 MHz, CD₃CN) δ 7.85 μ 7.74 (m, 3H), 7.71 μ 7.61 (m, 6H), 7.38 μ 7.29 (m, 6H), 7.18 μ 7.09 (m, 4H), 5.54 (s, 4H); ¹³C NMR (101 MHz, CD₃CN) 134.5, 134.40, 132.6, 131.2, 130.9, 130.0, 129.6, 128.4, 128.1, 121.7, 115.0, 50.9 (note: C2 not observed); ESI-MS *m/z* 374 [M+H]; ESI-HRMS *m/z* 375.1854 (calc. for C₂₇H₂₃N₂ 375.1856); IR (solid-state ATR, cm⁻¹) 3036, 2190, 1501, 1478, 1466, 1453, 1432, 1018, 917, 727, 697.

NMR Study into the Decomposition of (1,3-dibenzylbenzo[d]imidazolin-2-ylidene) copper(I) bromide

To a Younglin Tap NMR tube in the glovebox a saturated anhydrous CD₃CN solution of (1,3-dibenzylbenzo[d]imidazolin-2-ylidene) copper(I) bromide (ca. 1.5 mg) was made, and ¹H NMR spectrum recorded. No change was observed over a period of 24 h by ¹H NMR spectroscopy. Degassed water (40 µl) was added to the sample under N₂ and Younglin Tap NMR tube resealed. ¹H NMR spectra were recorded at regular intervals to (see page 74). After 31 h, the tube was exposed to air for 1 min and shaken (3 times). Regular ¹H NMR spectra were then taken up to 9 days. The last sample indicated that the ratio of 7:9 was 1:5 at this time. LC-MS analysis of this mixture revealed three major components (characterised). The acetonitrile was removed from the LC-MS analysis sample, dissolved in CDCl₃ and a ¹H NMR spectrum recorded.

Spectra shown in Figure 36, page 74.

NMR Study of the Arylation of (1,3-dibenzylbenzo[d]imidazolin-2-ylidene)copper(I) bromide

To a Younglin Tap NMR tube in the glovebox was added (1,3-dibenzylbenzo[d]imidazolin-2-ylidene) copper(I) bromide (6 mg, 0.0145 mmol, 1 eq.) and dissolved in C₆D₆. A ¹H NMR spectrum (400 MHz) was recorded. In the glovebox, PhI (14.7 mg, 0.0724 mmol, 8 µl, 5 eq.) was added. A ¹H NMR spectrum was recorded. The sample was then heated to 90 °C, and ¹H NMR spectra recorded at regular intervals to monitor any change (over 24 h). Spectra shown in Figure 39, page 77.

The solvent was removed under reduced pressure, to give a brown solid (no mass was lost). A sample of this solid was analysed by ESI-MS. Under air, MeCN-*d*₃ was added to the mixture. A ¹H NMR spectrum was recorded. Spectra shown in Figure 40, page 78.

NMR Study of the Arylation of (1,3-dibenzylbenzo[d]imidazolin-2-ylidene) copper(I) bromide with Pd(OAc)₂

To a Young's Tap NMR tube in the glovebox was added (1,3-dibenzylbenzo[d]imidazolin-2-ylidene) copper(I) bromide (6 mg, 0.0145 mmol, 1 eq.) and Pd(OAc)₂ (3 mg, 0.0146 mmol, 1 eq.) and dissolved in C₆D₆. A ¹H NMR spectrum (400 MHz) was recorded. In the glovebox, PhI (14.7 mg, 0.0724 mmol, 8 ul, 5 eq.) was added. A ¹H NMR spectrum was recorded. In a glovebox, Pd(OAc)₂ was added. A ¹H NMR spectrum was recorded. The sample was then heated to 90 °C, and ¹H NMR spectra recorded at regular intervals to monitor any change (over 24 h). Immediately on heating, Pd black was observed to form. Spectra shown in Figure 42, page 80.

The solvent was removed under reduced pressure, to give a brown solid (no mass was lost). A sample of this solid was analysed by ESI-MS. Under air, MeCN-*d*₃ was added to the mixture. A ¹H NMR spectrum was recorded. Spectra shown in Figure 44, page 81.

**CHAPTER 3:
C-H BOND FUNCTIONALISATION OF INDOLE BIOMOLECULES**

3.1 Introduction

3.1.1 Arylation of Indoles

Indoles are a key sub-class of benzo-fused *N*-heterocycles. The indole moiety is found embedded in important biomolecules, including the proteinogenic amino acid tryptophan **132** and the metabolite serotonin, other natural products (for example, meridianins A-E **134**)¹⁷⁵ and synthetic pharmaceuticals (for example, the migraine drug sumatriptan **133**).¹⁷⁶

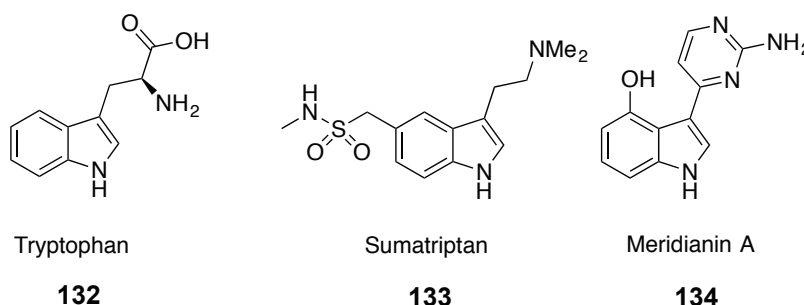
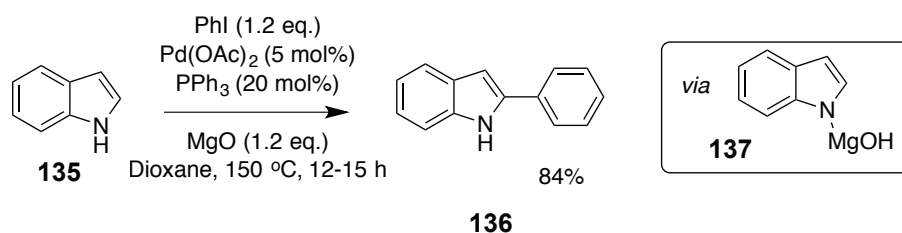


Figure 46: Examples of natural products and pharmaceuticals containing indole functionality.

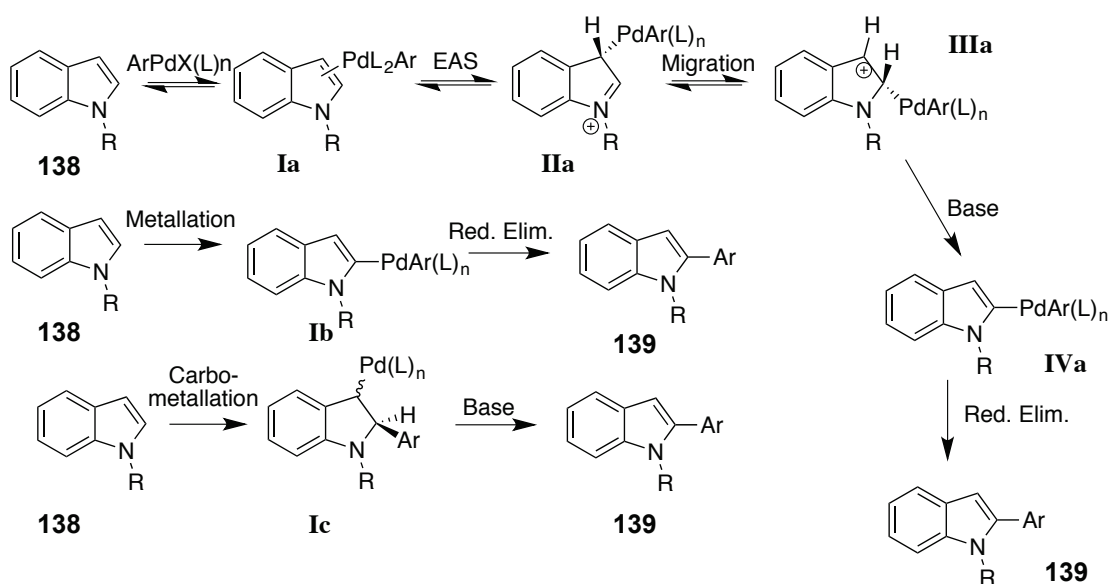
Arylated indoles can be difficult to access *via* traditional methods (for example, the Fisher indole synthesis)¹⁷⁷ and have typically required the use of Pd-catalysed cross-coupling methodologies such as the Suzuki-Miyaura reaction.¹⁷⁸ There are limited examples of Pd-catalysed cross-couplings performed at the C2 and C3 position of indole. As such, the ability to selectively functionalise indole C-H bonds under mild conditions is of considerable interest. This would not only be useful in the synthesis of new natural products and pharmaceutical candidates, but also in fluorescence labelling similar to work on purines reported by Fairlamb and co-workers.^{26–28,179,180}

As with the direct C-H bond functionalisation of imidazoles, Pd is commonly used as the metal catalyst, although Rh,¹⁸¹ Ir,¹⁸² and Ni¹⁸³ have also been applied. The use of catalytic Pd for arylation at the C2 of indole **135** with aryl iodides was developed by Sames and co-workers, utilising catalytic amounts of Pd(OAc)₂ and PPh₃, with a stoichiometric quantity of MgO (acting as the base) (Scheme 43). The reaction proceeds *via* a *N*-Mg^{II}OH intermediate **137**, which consequently makes it highly sensitive to air and moisture.



Scheme 43: Pd-mediated direct C-H bond functionalisation of NH-indole with PhI, as proposed by Sames, proceeding *via* a *N*-Mg intermediate.¹⁸⁴

When indole was substituted with 1-methylindole, it was found that these conditions were no longer effective. However, CsOAc was found to be an effective alternative base. This supported the hypothesis that MgO played a key role in the arylation of the NH-indole. Larger *N*-alkyl substituents were tolerated, as were *N*-aryl substituents. Electron-withdrawing groups, such as Ac, were not.

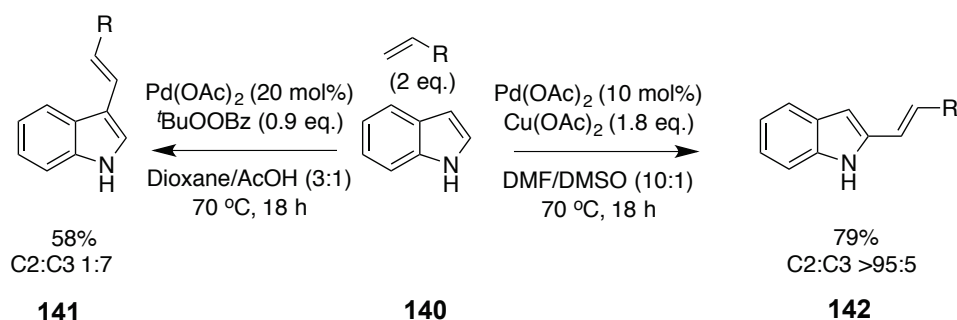


Scheme 44: Possible mechanisms for the direct C-H of indole, as proposed by Sames.^{33,184}

Kinetic studies indicated that this reaction was zero order with respect to iodobenzene, suggesting that the rate-determining step occurred after oxidative addition (it would normally be first order). Sames proposed three possible reaction pathways (Scheme 44): electrophilic metallation migration (a 1,2-migration of Pd must be included in this pathway, as electrophilic substitution on indoles is known to occur preferentially at the C3-position), non-electrophilic metallation (σ -bond metathesis) and carbometallation (*i.e.* a “Heck-type” reaction).¹⁸⁵ Kinetic isotope effect (KIE) studies suggested that electrophilic metallation-migration was most likely.

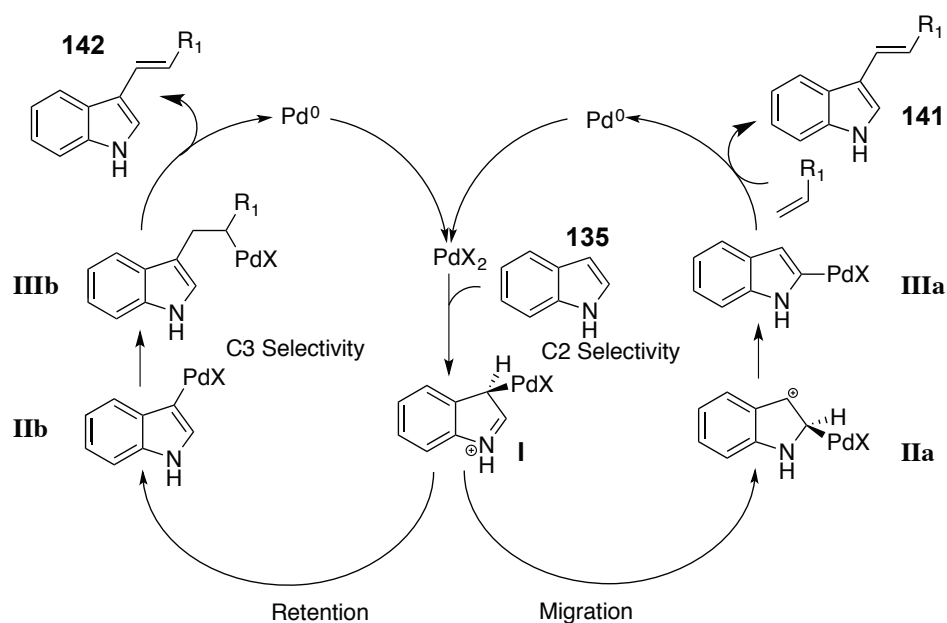
Using this mechanistic interpretation, it was possible for the investigators to develop a C3-selective methodology. Increased steric bulk on both the indole and Pd-catalyst disfavoured the 1,2-migration. When MgCl/TMEDA or Mg(HMDS)₂ were used, a C3:C2 selectivity of 14:1 and 26:1 were obtained, respectively. Furthermore, by employing IMes in place of PPh₃, a selectivity of 98.5:1.5 was recorded.

The functionalisation of indoles with alkenes in a Fujiwara-Moritani oxidative Heck-type fashion has been pioneered by Gaunt and co-workers (Scheme 45).^{186,187} By variation of solvent and additives, it has proved possible to control the regioselectivity of the process. Utilising Cu(OAc)₂ in DMF/DMSO (10:1, v/v), it was possible to achieve an impressive C3:C2 ratio of >95:5, with a 79% combined yield. These results are particularly interesting as they occur under milder conditions (70 °C).



Scheme 45: Pd-mediated direct C-H bond functionalisation via an oxidative Fujiwara-Moritani oxidative Heck-type process, showing that careful selection of reagents can influence regiochemistry.¹⁸⁶

Gaunt proposes a mechanism (Scheme 46) which bears some similarities to that offered by Sames, with both suggesting an electrophilic substitution occurring at the C3-position. Solvent-controlled palladation results either in the retention of C3 regiochemistry, or a 1,2-migration into the C2 position.

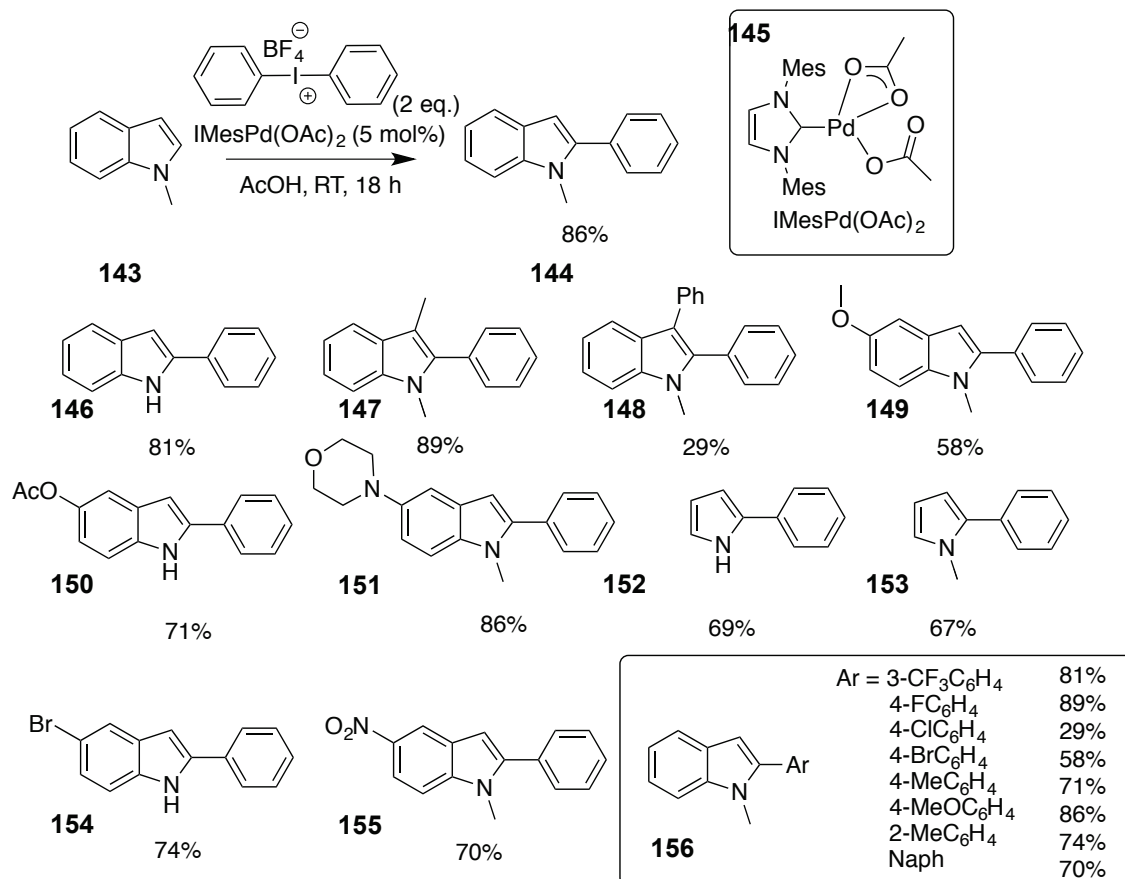


Scheme 46: Mechanistic basis of regioselectivity in oxidative Fujiwara-Moritani oxidative Heck-type direct C-H bond functionalisation process, as proposed by Gaunt and co-workers.¹⁸⁶

An active area of research in modern organometallic chemistry has been the use of proposed $\text{Pd}^{\text{II/IV}}$ manifolds in catalysis.¹³³ Although the first organopalladium(IV) complex was identified in 1975 by Uson and co-workers (Nyholm had previously claimed such a synthesis by the reaction of $\text{BrTI}(\text{C}_6\text{F}_5)_2$ and $\text{Cl}_2\text{Pd}(\text{PPh}_3)_2$,¹⁸⁸ but it was later shown that this in fact led to a mixture of bi- and mononuclear Pd^{II} complexes¹⁸⁹), it has been in the past five-to-ten years that such intermediates have been significantly implicated to have a role in various reactions catalysed by Pd.^{188–190} Molecules accessible from these new methods include the synthesis of conjugated dienes.^{191,192} Cross-coupling and C-H bond functionalisation processes were also possible.^{193,194}

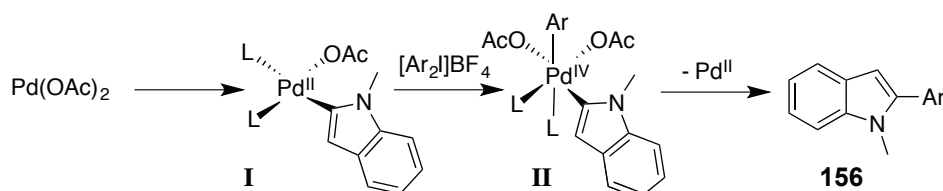
In 2006, Sanford and co-workers published a method using such chemistry to selectively arylate the C2-position of *N*-methylated **143** and free 1*H*-indole **135** (and analogues, Scheme 47) using aryl iodonium salts.¹³¹ Initial work on this methodology utilised $\text{Pd}(\text{OAc})_2$, giving moderate yields; after five minutes' reaction time, only 49% yield was obtained. However, leaving the reaction for a greater period of time did not increase the yield, suggesting catalyst deactivation was occurring. Following a catalyst screen, $\text{IMesPd}(\text{OAc})_2$ **145** was found to be the most suitable for this system. This reaction has a high selectivity for the C2 position, with a C3:C2 ratio of 1:20. High yields were obtained at ambient temperature on a variety of substituted indoles and pyrroles (Scheme), both with *N*-H and *N*-Me derivatives. Where the C2 position was

blocked, a low yield of C3 functionalised product was obtained. Substituted symmetrical diaryliodonium salts were found to be well tolerated.



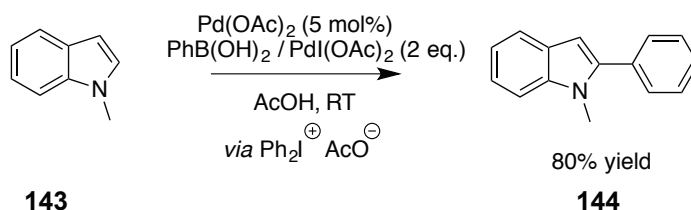
Scheme 47: Pd-mediated direct C-H bond functionalisation of *N*-Me indole with diaryliodonium salts, as proposed by Sanford and co-workers.¹³¹

The proposed mechanism (Scheme 48) for this reaction involves palladation at the indole C2 position, followed by oxidative addition of the aryl iodonium salt to give a Pd^{IV} octahedral intermediate. The product is then reductively eliminated.



Scheme 48: Pd^{II/IV}-mediated mechanism for the direct C-H bond functionalisation of indole using diaryliodonium salts, as proposed by Sanford and co-workers.¹³¹

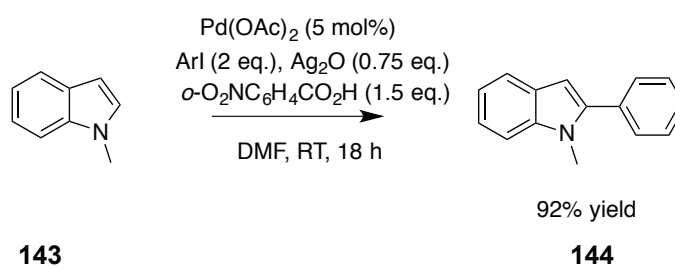
This work was further developed to allow for the *in situ* formation of aryl iodonium salts from diacetoxyiodobenzene and phenylboronic acid. With these conditions, it was found that Pd(OAc)₂ performed better than the IMePd(OAc)₂ catalyst.



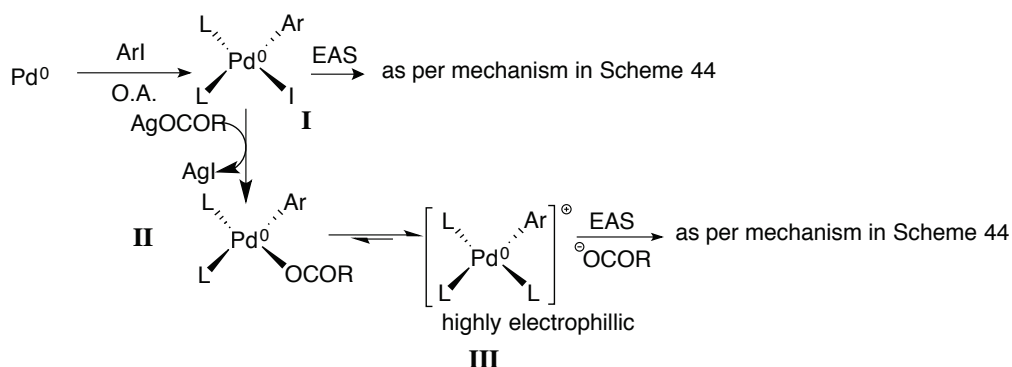
Scheme 49: Pd-mediated direct C-H bond functionalisation of *N*-Me indole with diaryliodonium salts formed *in situ*, as proposed by Sanford and co-workers.

It should be noted that, through the work of Ritter and co-workers, some processes previously proposed to proceed *via* Pd^{IV} intermediates are thought by some (including Sanford) to be Pd^{III}-mediated.^{195–198}

Larossa has developed a room temperature C2 arylation of indole utilising substoichiometric amounts of Ag₂O (Scheme 50).¹⁹⁹ Since it is believed that the rate-limiting step of indole C-H bond functionalisation is electrophilic palladation, Larossa reasoned that the use of Ag^I salts would increase rate by abstraction of a halide anion from the Pd^{II} oxidative addition product (Scheme 51).



Scheme 50: Pd-mediated direct C-H bond functionalisation of indole using Ag₂O, as proposed by Larossa and co-workers.¹⁹⁹

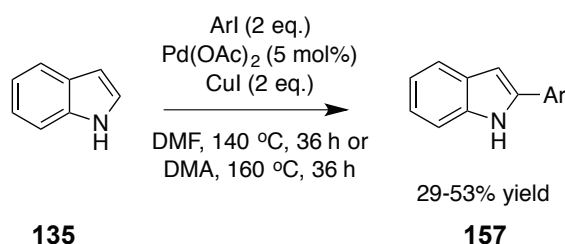


Scheme 51: Mechanism for the direct C-H bond functionalisation of indole with Ag_2O , as proposed by Larossa and co-workers.¹⁹⁹

These conditions were found to be tolerant of functional groups on both the aryl iodide and the indole. Changing the *N*-protecting group from Me to Bn was also tolerated. However, free *NH*-indoles gave only moderate yields, despite an increase in catalyst loading to 10 mol% and temperature to 50 °C.

Other room temperature conditions in acidic media have recently been developed, including arylation with arylsiloxanes.²⁰⁰

Bellina and Rossi have developed anazole C-H bond functionalisation methodology for azoles (Scheme 52) using what they describe as ligand- and base-free conditions (*vide supra*).^{37,38} These conditions were applied to free *NH*-indole **135** and gave moderate results (29 – 53% yield), and negligible yields for substituted analogues.

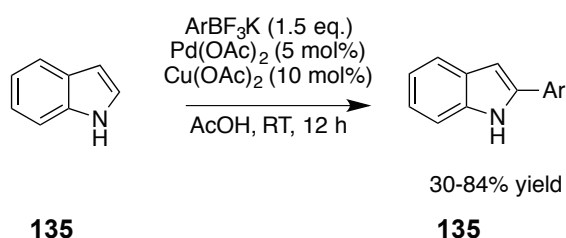


Scheme 52: Pd-mediated direct C-H bond functionalisation of indole using stoichiometric quantities of CuI, as proposed by Bellina, Rossi and co-workers.³⁵

Bellina and Rossi have since developed a further 'ligandless' set of conditions specifically for the arylation of indoles with aryl bromides.³⁵ An extensive screen of bases, ligands, aryl bromides and solvents indicated that there was no beneficial role for the ligand in this reaction. However, the addition of substoichiometric amounts of a lipophilic quaternary ammonium salt, such as BnEt_3NCl or BnBu_3NCl , substantially increased yield. It is known that these lipophilic salts stabilise Pd clusters, slowing their

deactivation by conversion to Pd black.²⁰¹ Similar to previous conditions, *N*-substituted indoles proved unsuitable for arylation.

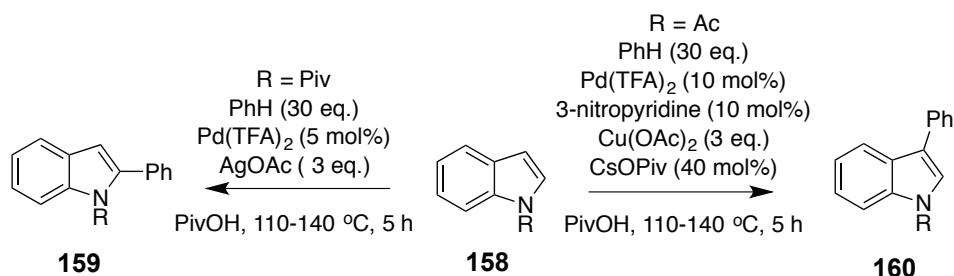
Although most indole C-H arylations are performed using aryl halides, other reagents have been used in their place. Zhang and co-workers have published conditions (Scheme 53) utilising potassium aryl trifluoroborates (reagents which have become popular as alternatives to aryl boronic acids in the Suzuki-Miyaura reaction for their supposed resistance to homocoupling)^{202,203} with a Pd(OAc)₂/Cu(OAc)₂ co-catalyst system.²⁰⁴ These conditions are air and moisture stable, where O₂ acts as a terminal oxidant.



Scheme 53: Pd-mediated direct C-H bond functionalisation of indole using potassium aryltrifluoroborates.

Fagnou and co-workers published an oxidative cross-coupling (Scheme 54), described as ‘double C-H activation’ between *N*-acetate protected indole and benzene.²⁰⁵ Pd(TFA)₂ was used as catalyst, with substoichiometric amounts of Cu(OAc)₂. The arene was required to be in large excess (30 eq.).

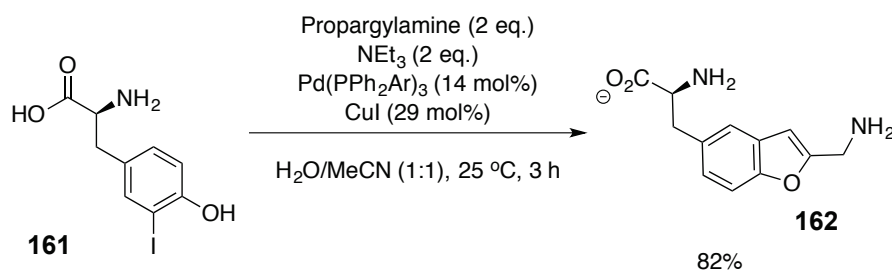
Fagnou expanded this work to allow for regiocontrol based on oxidant and protecting group. By substituting AgOAc for Cu(OAc)₂, and pivaloate for acetate (pivaloate has a greater degree of steric bulk than acetate), it was possible to switch preferential regioselectivity from C3 to C2 (C3:C2 ratio of 1:25).



Scheme 54: Pd-mediated oxidative direct C-H bond functionalisation of indole using benzene, showing that careful choice of reagents can affect the regiochemistry.

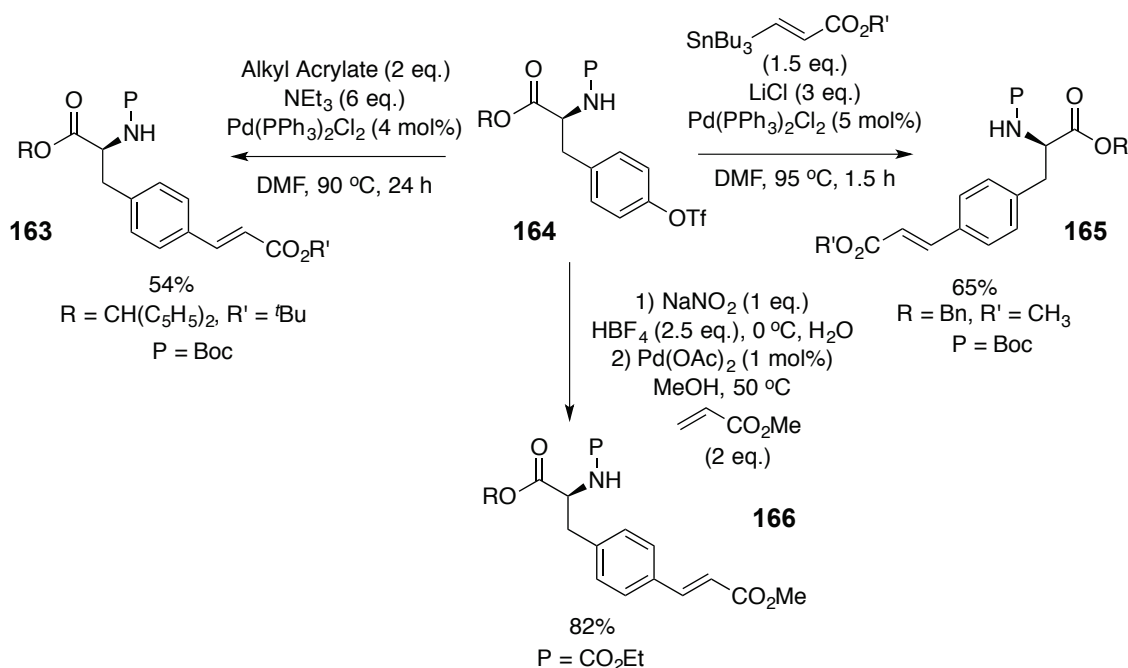
3.1.2 Pd-Mediated Functionalisation of C-X Bonds in Amino Acids, Peptides and Proteins

The modification of amino acids by the metal-catalysed formation of C-C bonds was pioneered by Casalnuovo and co-workers in their paper on cross-coupling in aqueous media.²⁰⁶ In the paper's single example of an amino acid, it was demonstrated that the Sonogashira reaction [mediated by Pd(*tppms*)₃] could functionalise 4-iodotyrosine **161** (Scheme 55). The cross-coupled product cyclised *in situ* to form a benzofuran, a process common in *ortho*-OH phenylalkynes.²⁰⁷ Crisp and co-workers also developed a set of conditions for low temperature Sonogashira reactions for the labelling of amino acids with a variety of commercially available fluorescent tags. However, these conditions required highly undesirable solvents (DMF, DMSO and piperidine).²⁰⁸



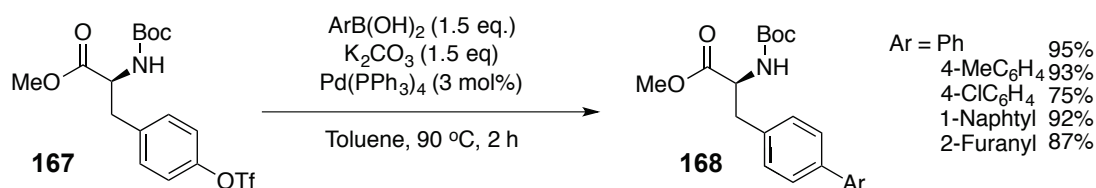
Scheme 55: The functionalisation of iodotyrosine using the Sonogashira reaction, as proposed by Casalnuovo and co-workers.²⁰⁶

Tilley and co-workers first developed the use of Mizoroki-Heck and Stille cross-coupling reactions on amino acids (Scheme 56): tyrosine *p*-triflate **164** (triflates had been demonstrated as suitable cross-coupling partners in the literature, and were found in this case to be more accessible than organohalides)²⁰⁹ was cross-coupled with stannyl (65% yield after 1.5 h) and *tert*-butyl acrylates (54% after 24 h).²¹⁰ Sengupta and co-workers have published a one-pot Heck-Matsuda reaction.²¹¹



Scheme 56: Functionalisation of tryosine *p*-triflate using Stille, Mizoroki-Heck and Heck-Matsuda reactions.²¹⁰

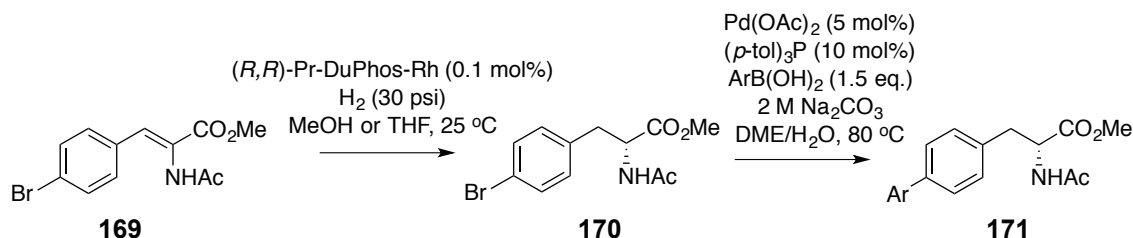
Although these are important proofs-of-concept, the use of Sn and diazo- reagents remains undesirable. The Suzuki-Miyaura reaction was applied to similar substrates by Shieh and co-workers (Scheme 57).²¹² Initial conditions (Pd(PPh₃)₄, K₂CO₃ in DMF at 90 °C) afforded high yields, but suffered from erosion of enantiomeric purity. Extensive optimisation (which considered, amongst other bases, TIOH)²¹³ led to a solvent switch to toluene, which resulted in both high yield and high retention of enantiomeric purity (93% yield, >99% ee by chiral HPLC).



Scheme 57: Functionalisation of tryosine *p*-triflate using the Suzuki-Miyaura reaction.²¹²

The first amino acid Suzuki-Miyaura reaction on a halide substrate was developed by Burk and co-workers (Scheme 58).²¹⁴ Using DuPHOS-Rh catalyst, they successfully synthesised 2-, 3- and 4-bromophenylalanine. Cross-coupling was performed using Pd(OAc)₂, 2 M Na₂CO₃ and P(*p*-tol)₃ in DME at 80 °C, and excellent yields (75-99%)

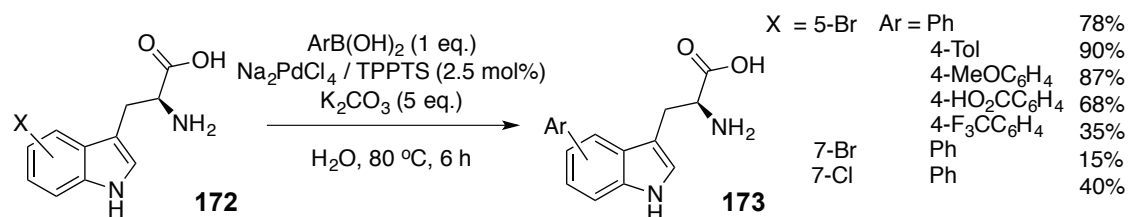
were observed without loss of enantiomeric purity and with good tolerance to substitution on the boronic acid. The conditions were applied to a tri-peptide substrate, and product was isolated in excellent yield (71%).



Scheme 58: Synthesis of Ar-functionalised tryosine from vinyl substrates, using Ru- and Pd-mediated catalysis.

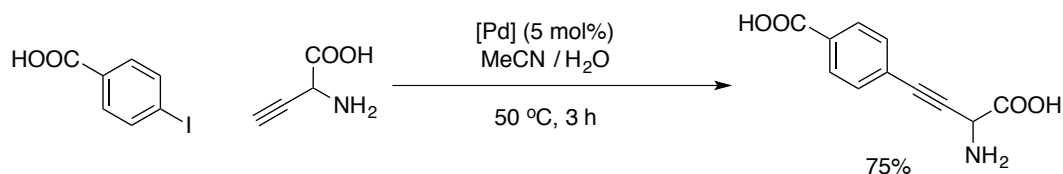
Sato and co-workers have developed Suzuki-Miyaura methodology where the organoboron cross-coupling partner rather than the pseudo(halide) is incorporated within the amino acid.^{215,216} It was found that (4-pinacolyborono)phenylalanine ethyl ester was successfully coupled with aryl halides using Pd and Ni catalysts in NMP/dioxane.

These methodologies have generally moved away from the aqueous conditions first developed by Casalnuovo.²⁰⁶ The use of non-polar organic solvents (e.g. benzene and toluene) makes conditions unsuitable for the modification of unprotected amino acids, or peptides and proteins. DMF can result in mechanistic complications, toxicity and occasional irreproducibility.³⁹ Goss, Wagner and co-workers have developed conditions (Scheme 59) for aqueous media Suzuki-Miyaura reactions on halotryptophans (available *via* an enzymatic route).^{217,218} Utilising Na₂PdCl₄ with TPPTS, 5-bromo- and 5-chlorotryptophan were both functionalised with organoboronic acids in reasonable yield. 7-Bromotryptophan was also functionalised, but in poor yield. By substituting TPPTS with TXPTS, a reduction in temperature to 40 from 80 °C proved possible. Application to a dipeptide gave good yield (62% by HPLC), although some methyl ester deprotection was also observed.

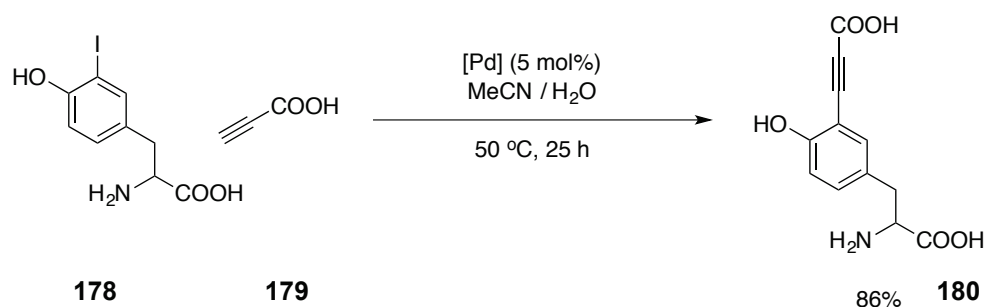


Scheme 59: Functionalisation of halotryptophan using the Suzuki-Miyaura reaction, as proposed by Wagner, Goss and co-workers.²¹⁷

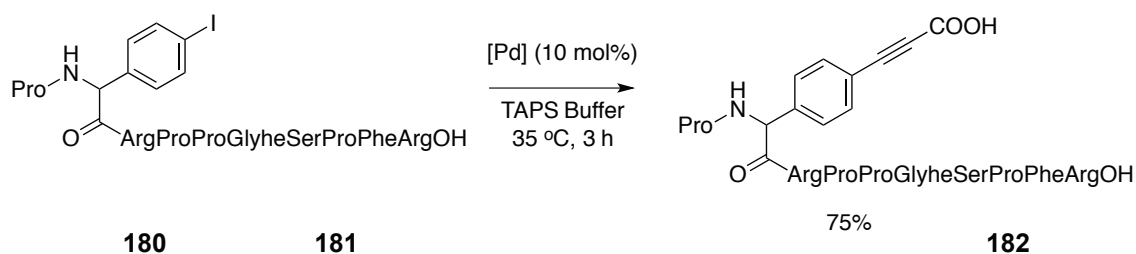
Cross-coupling on peptides was pioneered by Schmittchen and co-workers.²¹⁹ Schmittchen suggested that, as under the basic conditions of cross-coupling reactions peptides would carry an overall negative charge, the sulfonate-containing water soluble phosphines developed by Casalnuovo would have an electrostatic barrier compared to cross-coupling on uncharged substrates (although, this had not been found to be a problem on nucleotides).²⁰⁶ Peptides were encoded with haloaryl and propargyl modified amino acids. To solve this supposed problem, positively charged analogues were developed, e.g. guanadinophosphines.^{220,221} The catalyst was prepared by mixing Pd(OAc)₂, guanadinophosphine ligand and CuI (1:5:10) in acetonitrile, and allowing the solution to 'condition' over five days under an N₂ atmosphere at 4 °C. Initially, the Sonogashira reaction was performed on 4-iodobenzoate **174** and propargyl glycine **175** in water/acetonitrile (7:3), from which a good yield (71%) was obtained (Scheme 60), with no evidence of homocoupled products.²²² When these conditions were applied to the cross-coupling of 3-iodotyrosine **178** with propiolic acid **179** (Scheme 61), 86% yield was obtained after a 25 h reaction time (longer reaction times, or exposure to acidic conditions, resulted in rearrangements). The reaction was found to be as effective in buffered solution (3-[tri(hydroxymethyl)methylamino]-1-propanesulfonic acid, TAPS, pH 8). Application to multi-functional peptide **181** (Scheme 62) resulted in an excellent 75% yield, and it was demonstrated to be possible to functionalise using a alkynylated biotin derivative (commonly used in biological chemistry, Scheme 63).²²³



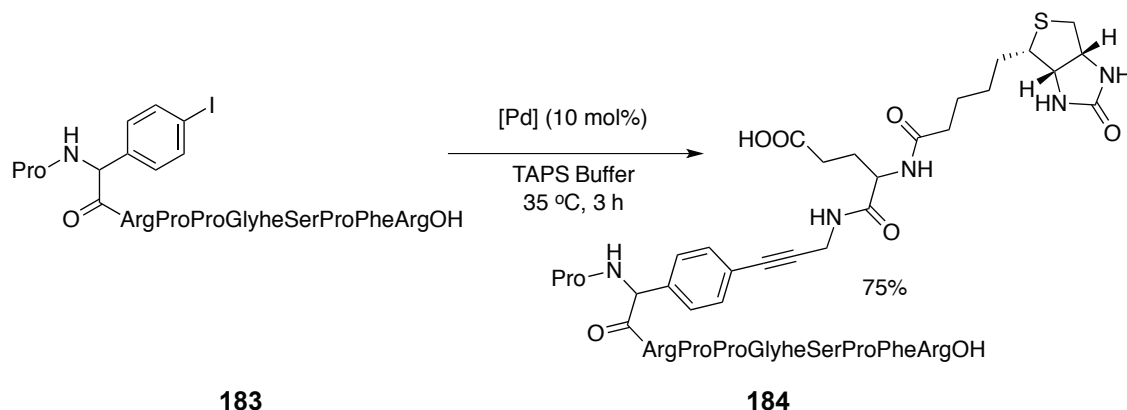
Scheme 60: The functionalisation of 4-iodobenzoic acid using the Sonogashira reaction. [Pd] is a solution of Pd(OAc)₂, guanadinophosphate and CuI (1:5:10) in MeCN which has been 'conditioned' for 5 d at 4 °C under N₂. No stereochemistry given.²²⁰



Scheme 61: The functionalisation of 3-iodotyrosine using the Sonogashira reaction. [Pd] is a solution of Pd(OAc)₂, guanidinophosphine and CuI (1:5:10) in MeCN which has been 'conditioned' for 5 d at 4 °C under N₂. No stereochemistry given.



Scheme 62: The functionalisation of a peptide using the Sonogashira reaction. [Pd] is a solution of Pd(OAc)₂, guanidinophosphine and CuI (1:5:10) in MeCN which has been 'conditioned' for 5 d at 4 °C under N₂. No stereochemistry given.



Scheme 63: The functionalisation of a peptide using the Sonogashira reaction. [Pd] is a solution of Pd(OAc)₂, guanidinophosphine and CuI (1:5:10) in MeCN which has been 'conditioned' for 5 d at 4 °C under N₂. No stereochemistry given.

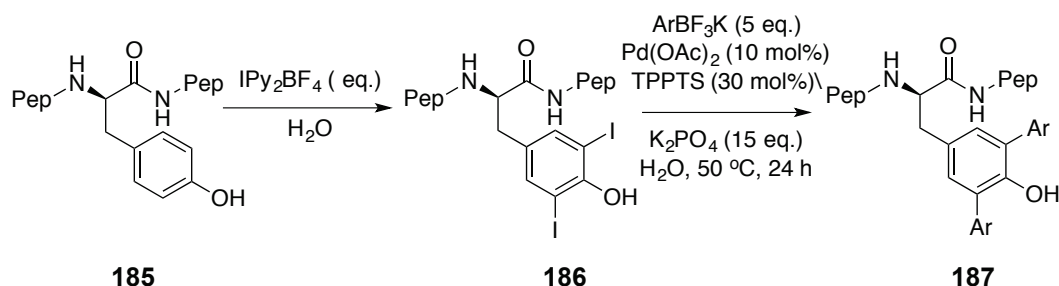
Ghadiri and co-workers, contrary to Schmittchen's hypothesis that negatively charged phosphine ligands would be inappropriate for the functionalisation of peptides, have shown that quantitative yields can be achieved in such Sonogashira reactions.²²⁴ This work also indicated that the presence of thiol, thioether or bipyridyl functionality in the peptide was not tolerated by the reaction, presumably due to competitive ligation to

Pd and Cu. This is surprising, as Schmittchen had demonstrated that when biotin, a cyclic thioether, was included in the alkynyl coupling partner, a reaction could occur. In addition, biotin is generally tolerated in cross-coupling on small molecules.²²⁵

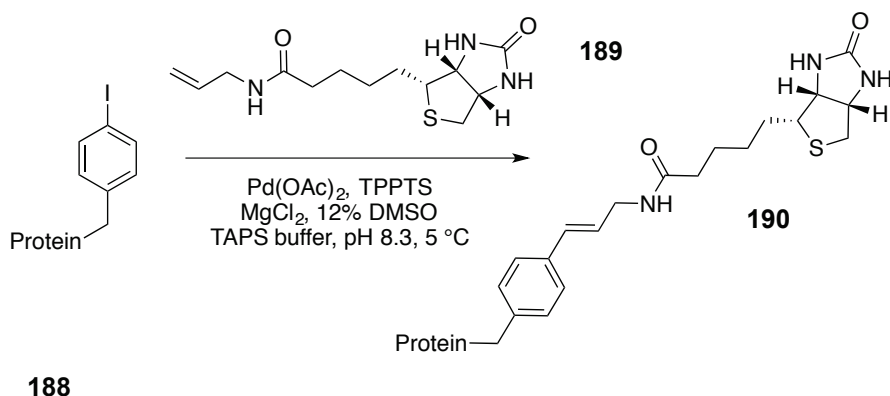
The use of the Suzuki-Miyaura cross-coupling reaction on peptides was first developed by Kotha and co-workers.²²⁶ In a biphasic (THF/toluene/water) system, good yields were generally obtained. Hamachi and co-workers have shown that a 33-residue peptide (WW domain, Pin1 protein) could be functionalised by the Suzuki-Miyaura reaction.²²⁷ Using Na_2PdCl_4 (10 mol% with respect to boronic acid) as catalyst, moderate yields were obtained (40%). Higher temperatures increased yield, and the addition of substoichiometric quantities of glycerol (10-50 mol%) resulted in significant improvements (54-90% yield, depending on substrate). Glycerol likely increased peptide solubility, but it does have a demonstrated role in the stabilisation of Pd-nanoparticles.²²⁸

Fournier and co-workers have shown that it is possible to use the Suzuki-Miyaura reaction to functionalise peptides whilst they are tethered to solid-phase resin as used in peptide synthesis.²²⁹ Higher temperatures in DMF, with $\text{Pd}(\text{PPh}_3)_4$, were found to be optimal.

Work by Valencia, Barluenga and co-workers (Scheme 64) has combined, in a one-pot process, aqueous iodination of tyrosine and phenylalanine residues in peptides with a Suzuki-Miyaura reaction.²³⁰ The cross-coupling conditions differ from Casalnuovo's conditions only by the use of potassium aryltrifluoroborates (which are only partially soluble in water),²⁰² and Barluenga had previously reported the iodination of biomolecules.²³¹ However, this paper represents the first entirely post-synthetic modification of peptides by Pd-catalysed cross-coupling chemistry.

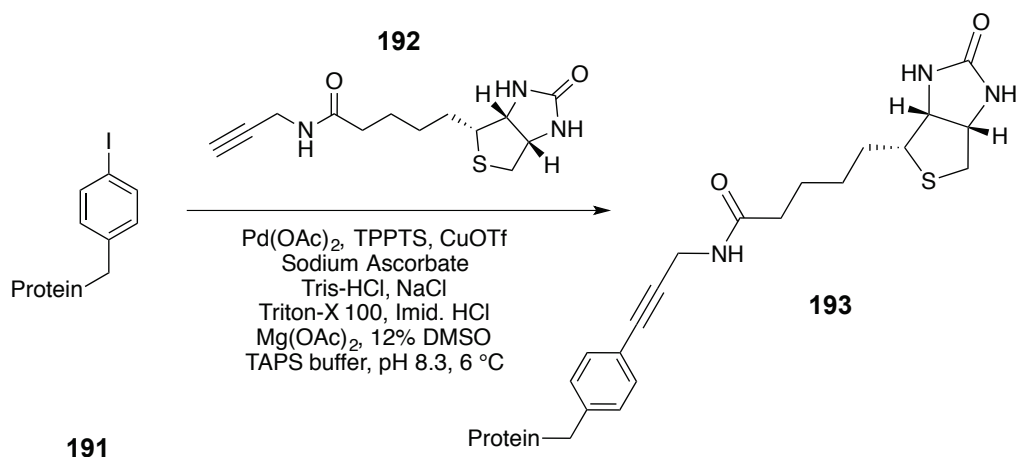


Scheme 64: Post-synthetic modification of a peptide using iodination and Suzuki-Miyaura cross-coupling chemistry.²³⁰



Scheme 65: Mizoroki-Heck reaction performed on a peptide, as proposed by Tachibana and co-workers.²³²

The first cross-coupling reaction performed on a protein was developed by Tachibana and co-workers (Scheme 65).²³² iF32-Ras-His **188** was functionalised using a Mizoroki-Heck reaction with vinylated biotin **189**, $\text{Pd}(\text{OAc})_2$, TPPTS, 12% DMSO and MgCl_2 (to suppress biotinylation at cysteine by S-coordination) in TAPS buffer (pH 8.3). The reaction occurred at 5 °C, although a 50 h reaction time was needed. An estimated 2% yield was observed, with significant amounts of dehalogenation of the protein (28%). Mg and Pd were removed by the addition of sodium stearate in reaction work-up, and the authors performed experiments that indicated that the use of transition metals did not affect the biological assays.



Scheme 66: Sonogashira reaction performed on a peptide, as proposed by Tachibana and co-workers.²³³

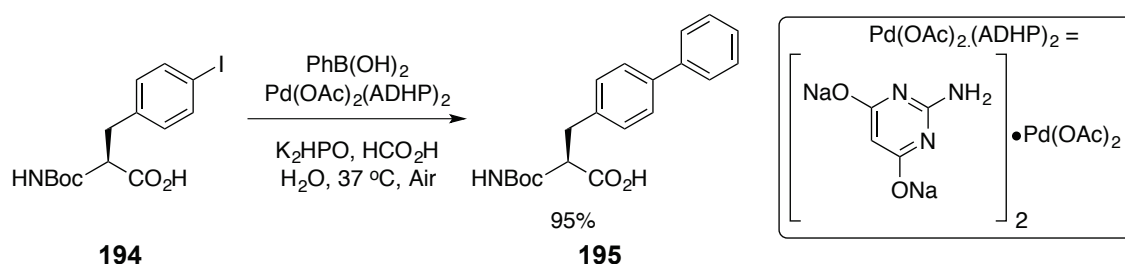
Tachibana and co-workers performed further investigations into these conditions using a model peptide substrate.²³³ Optimisation gave conditions which resulted in quantitative conversion to product by HPLC. This optimisation screen considered

concentration, reaction time, temperature, and the presence of additives. The optimal conditions were peptide, vinylated biotin, decyl- β -D-glucopyranoside and Pd-TPPTS (1:7.14:1.45:1:43) at 22 °C, giving 26% isolated yield.

This methodology was extended to the Sonogashira (Scheme 66) and Suzuki-Miyaura cross-coupling. The Sonogashira reaction was significantly faster than the Suzuki-Miyaura, and finished typically after 4 h. The conditions were applied to Ras protein containing a 4-iodophenylalanine residue, and a 25% yield was obtained (yields were calculated by HPLC, SDS-PAGE or Western Blot).

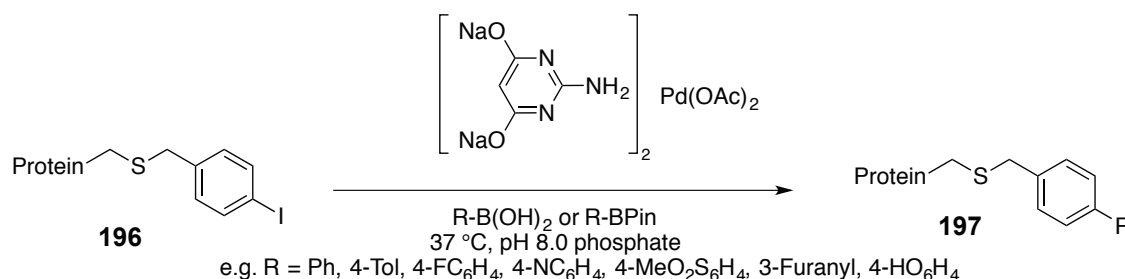
Conversely, Schultz and co-workers have developed a method for encoding boronate-containing amino acid residues into proteins.²³⁴ The Suzuki-Miyaura reaction was applied to these modified proteins, coupling with an iodinated bodipy 'reporter' molecule. The solvent for these reactions was EPPS aqueous buffer (3-[4-(2-hydroxyethyl)-1-piperazinyl]propanesulfonic acid, pH 8.5), using Pd₂(dba)₃.dba as the Pd source.²³⁵ This is unusual for aqueous cross-coupling methodologies, although a substituted water-soluble dba has been reported, but not used for this type of chemistry.²³⁶

Davis and co-workers have developed ground-breaking conditions which begin to address some of the problems associated with preceding methodologies (Scheme 67).²³⁷ They considered phosphines to be too sensitive to oxidation for the everyday functionalisation of proteins. Hence, the sodium salt of 2-amino-4,6-dihydropyridine was used as an alternative. These ligands had previously been used in Mizoroki-Heck alkynylation reactions in organic solvents.²³⁸ Near quantitative yields were obtained for cross-coupling reactions on model amino acids and short-chain peptides. The conditions were effective for aryl bromides and iodides, but not for aryl chlorides. Terminal cysteine and cysteine-derived residues inhibited catalysis, but internal S-containing *p*-iodobenzyl cysteine (Pic) residues gave cross-coupled products in excellent yield.



Scheme 67: Functionalisation of *p*-iodobenzyl cysteine using the Suzuki-Miyaura reaction, as proposed by Davis and co-workers.²³⁷

Pic was chemically incorporated into the serine protease subtilisin *Bacillus lentus* (SBL) mutant S156C. Davis applied these conditions to this protein, using phenylboronic acid as a cross-coupling partner. After 30 min, conversions to product exceeded 95% (by HPLC-MS). Similar excellent yields were obtained with a variety of aryl and vinylboronic acids. This work was later extended to cross-coupling on genetically encoded phenylalanine-derived aryl iodides.²³⁹ Maltose binding protein (MBP) was chosen for stability and solubility.^{240,241} Problems with non-specific metal binding initially resulted in signal suppression in mass spectral measurements.²³ EDTA, DTT, and cysteine were tested as Pd scavengers.²⁴² However, 3-mercaptopropionic acid was found to be effective in low concentrations ($4.4 \mu\text{mol mL}^{-1}$, or 3 eq. with respect to Pd).

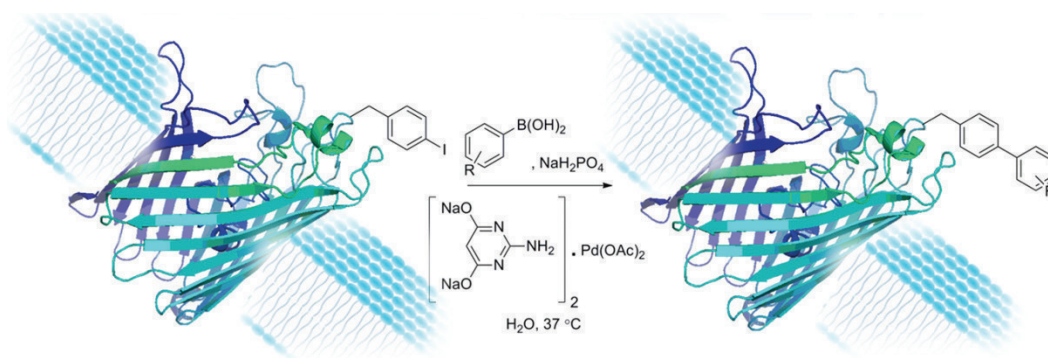


Scheme 68: Functionalisation of *p*-iodobenzyl cysteine residues in peptides using the Suzuki-Miyaura reaction, as proposed by Davis and co-workers.²³⁷

With the reaction-monitoring problem solved, the cross-coupling reaction was found to be effective with *ca.* 680 eq. of furan-3-boronic acid. Full conversion was observed after 37 °C. The catalyst was loaded at 50 eq. with respect to protein. Control reactions without Pd or organoboronic acid were performed, confirming that this reaction is Pd-mediated.

Davis later demonstrated that it was possible to perform cross-coupling reactions on proteins residing within cell membranes (Scheme 69).²⁴³ *Escherichia coli* strains were

grown containing outer member OmpC proteins modified with *p*-iodophenylalanine residues incorporated at different positions.²⁴⁴ These cells ($OD_{600} = 0.2$) were treated with a fluorescein-derived organoboronic acid and $Pd(OAc)_2(ADHP)_2$ in phosphate buffer at 37 °C. The labelling was visible (exciting at 488 nm, emitting at 500-640 nm) after 1 h. At lower temperatures, labelling was decreased even with high Pd loadings. Control experiments were performed, again demonstrating a need for both Pd and organoboronic acid. The reaction remained effective even in the presence of reducing sugars.



Scheme 69: Functionalisation of *p*-iodobenzyl cysteine residues in proteins in the cell wall of cells using the Suzuki-Miyaura reaction, as proposed by Davis and co-workers. Reprinted and adapted with permission from C. D. Spicer, T. Triemer, and B. G. Davies, *J. Am. Chem. Soc.* 2012, 800-803. © American Chemical Society.

It is difficult to compare μ cell surface reactions with the stoichiometry of traditional small molecule cross-coupling reactions. Optimal organoboronic acid concentration is achieved at *ca.* 7.5 eq. relative to Pd. No cross-coupling is observed at Pd concentrations lower than 330 μ M, at which a critical point is reached. No further benefit to increased Pd loading is observed after 450 μ M. Many metal-catalysed synthetic modifications in biology, for example Cu-catalysed μ click chemistry, suffer from toxicity problems.²⁴⁵ Davis and co-workers demonstrated that at optimal Pd concentration, cell death was identical to control (<3%).

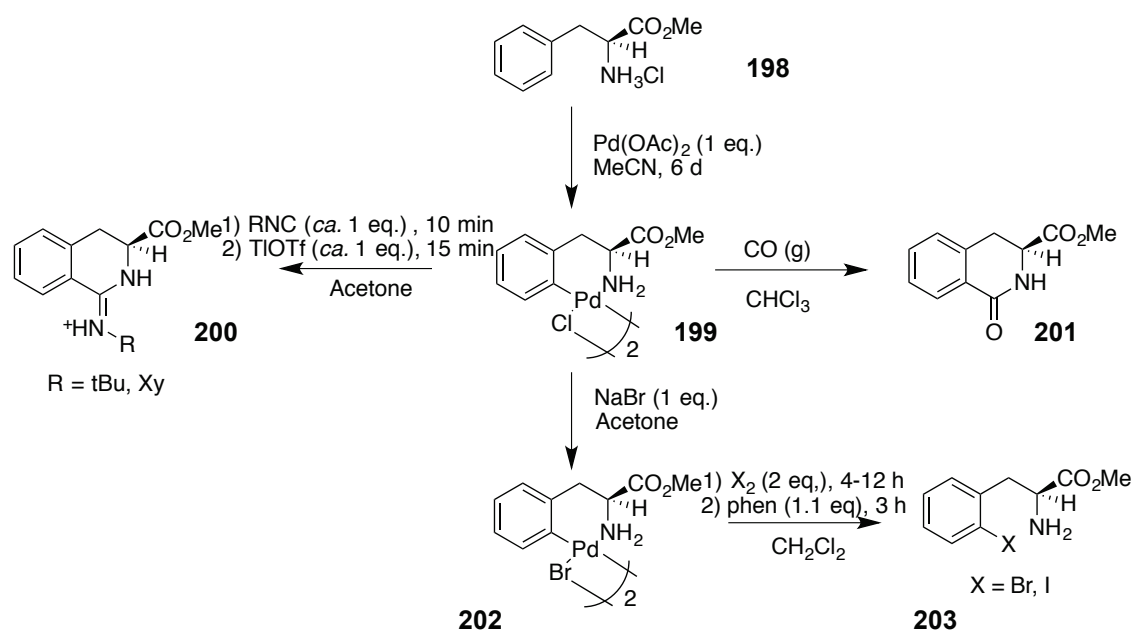
3.1.3 Pd-Mediated Functionalisation of C-H Bonds in Amino Acids and Peptides

Over the years Grignard, Mannich or enolate chemistries have been used for the C-C bond formation by functionalisation of C-H bonds in amino acids. For example, the Mannich reaction was used by Li and co-workers to form a C-C bond at the α -position

of protected glycine.²⁴⁶ Other examples include the reaction of Li-enolates quenched with alkylstannanes,¹⁰⁷ or low-temperature Grignard chemistry.²⁴⁷

Examples of Pd-catalysed direct C-H bond functionalisation reactions on amino acids, however, are limited. In the literature, there are a number of examples of the synthesis of *ortho*-palladacycle complexes of amino acids, including phenylglycine and phenylalanine.^{248–253} Pd^{II} metalocycles are of interest as pre-catalysts for cross-coupling reactions,⁷⁹ as well as for their cytotoxicity.^{254–256} Vicente and Urriolabeitia have demonstrated how *ortho*-palladacycle amino acid complexes can be used in organic synthesis.

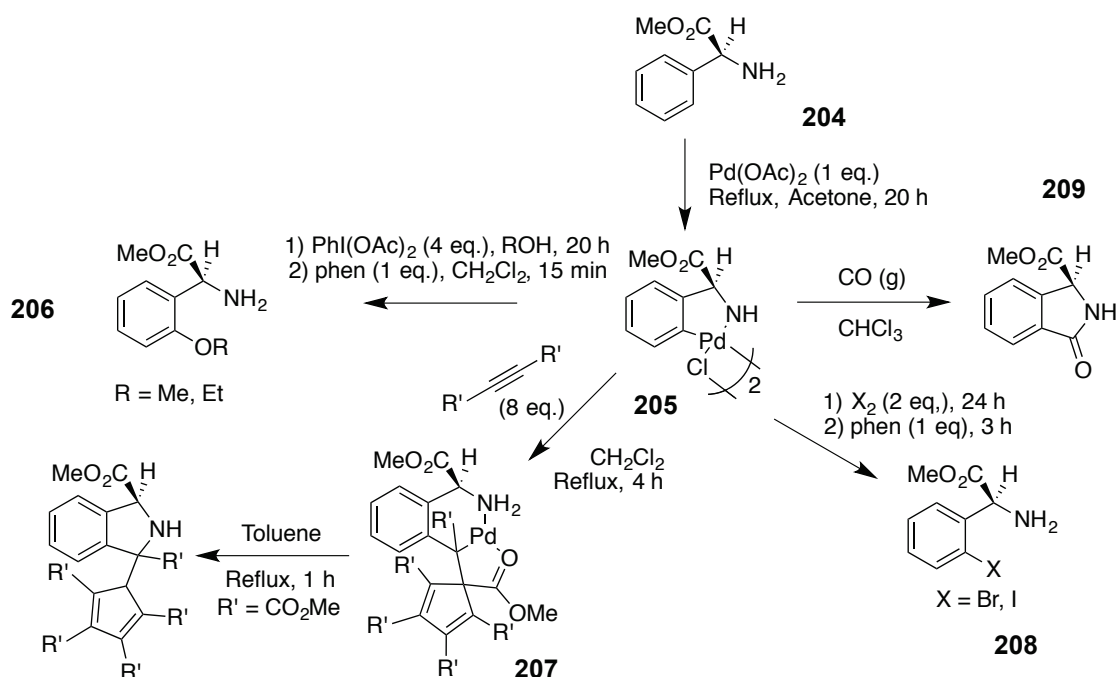
Vicente and co-workers synthesised a phenylalanine palladacycle complex by reacting methyl protected phenylalanine with Pd(OAc)₂ in MeCN (Scheme 70).²⁴⁸ Using this compound it was possible to carbonylate to form tetrahydroisoquinoline heterocycles **201**, and react with isocyanide to form isoquinolinium salts **200**. Swapping to a bromide bridged complex facilitated halogenation to **203** via a proposed Pd^{IV} intermediate **202**. However, no evidence for this high valence Pd species was proposed in the paper.¹³³ 1,10-Phenanthroline was then used to promote de-coordination of the organic product from the complex.



Scheme 70: Stoichiometric Pd-mediated direct C-H bond functionalisation of phenylalanine.²⁴⁸

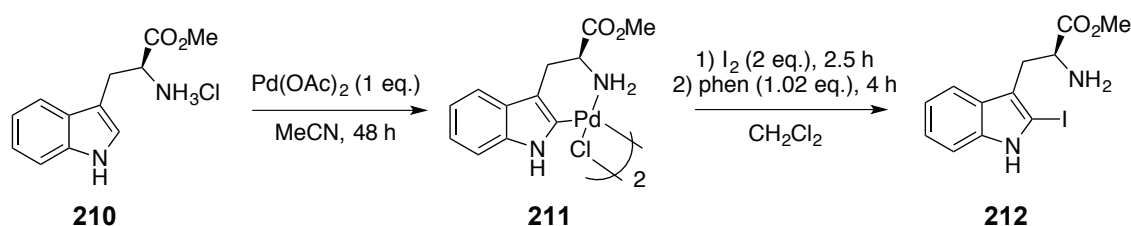
Urriolabeitia and co-workers, in similar studies, have shown that a cyclopalladated phenylglycine can be functionalised in a similar way (Scheme 71).^{250,253} Halogenation

proceeds from the chloride dimer (as opposed to the bromide dimer, as required in the work of Vicente). An alternate mechanism is also proposed, although still *via* a Pd^{IV} pathway. Measurement of enantiomeric purity by the Mosher amide approach^{257,258} showed there to be some racemisation (ee 82% and 87% for bromo- and iodo-products respectively). Carboxylation results in an isoindole, although complete racemisation was noted. Isocyanides are unreactive, forming only co-ordination complexes.



Scheme 71: Stoichiometric Pd-mediated direct C-H bond functionalisation of phenylglycine.²⁵³

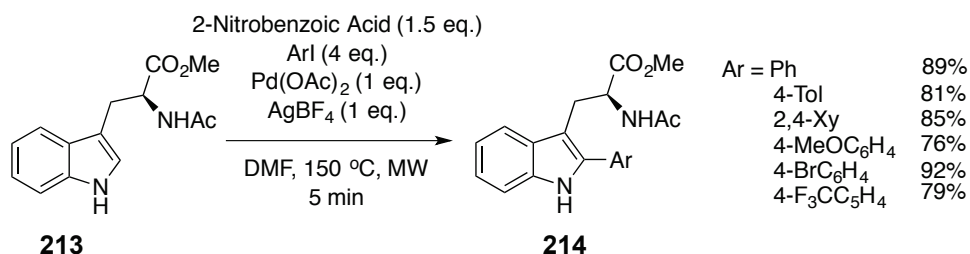
Iodine(III) reagents^{259,260} are often used to access Pd^{IV}/Pt^{IV} species. In the presence of PhI(OAc)₂ and a large excess of alcohol, the palladacycle can be etherified. Significant amounts of racemisation do occur in this process (ee 20% for MeOH and 50% for EtOH), but could be a useful method for accessing these modified amino acids which has previously been unavailable. When the cyclopalladated phenylglycine reacts with dimethyl acetylenedicarboxylate (DMAD), C-C bond formation occurs simultaneously with the generation of spiro-palladacycles. Reductive elimination of the isolated intermediate resulted in C-N bond formation. Cyclopalladated complexes of *N*-dimethylphenylglycine are also accessible.²⁶¹ When this complex is carbonylated in the presence of a nucleophile such as an alcohol or an amine, esters and amides are obtained respectively.



Scheme 72: Stoichiometric Pd-mediated direct C-H bond functionalisation of tryptophan with I_2 .²⁶²

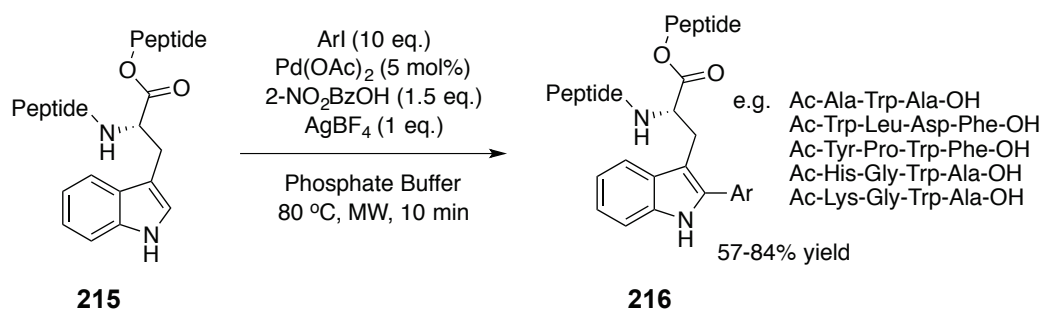
A tryptophan palladacycle complex **211** has been synthesised by Vicente and co-workers (Scheme 72).²⁶² With I_2 , this complex reacts to give iodination at the C2-position of the indole (to give **212**).

Lavilla and co-workers have demonstrated C2-position selective arylation of tryptophan using a Pd-mediated system similar to that initially developed by Larrosa (Scheme 73).^{199,263} Very good yields were obtained with a protected amino acid, with retention of enantiomeric purity. However, a significantly higher temperature was required as compared to Larrosa's methodology for indoles, which would make it incompatible with protein functionalisation.



Scheme 73: Arylation of tryptophan as proposed by Lavilla and co-workers.²⁶³

Lavilla adapted this methodology to the C-H bond functionalisation of peptides (Scheme 74) in phosphate buffer, lowering the temperature to 80 °C. Peptides with S-containing residues were not tolerated by these conditions, due to selective hydrolysis of the peptide bond. These conditions still suffer from high temperatures, so application to proteins remains limited. The stereochemical integrity of the peptides was preserved, and assessed by chiral HPLC.

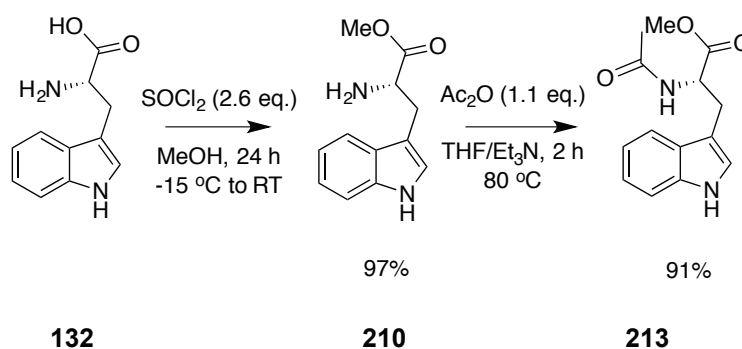


Scheme 74: Arylation of tryptophan residues in peptides as proposed by Lavilla and co-workers.²⁶³

3.2 Direct C-H bond Functionalisation of Tryptophan

3.2.1 Initial Method Development

It was initially decided to consider the C-H bond functionalisation of tryptophan protected at both the *N* and *O* positions. Whilst this would simplify method development and mechanistic interpretation, selection of appropriate protecting groups could provide an accurate model for internal tryptophan residues in peptides. As such, *N*-acetyl-*O*-methyl tryptophan **213** was synthesised in excellent yield over two well-precedented steps using the method of Taylor and co-workers.²⁶⁴ The resulting product was demonstrated to have high enantiomeric purity by chiral HPLC (Figure 47).



Scheme 75: Synthesis of *N*-Ac, *O*-Me protected tryptophan, **213**, over two steps (overall yield 94%) using the method established by Taylor and co-workers.²⁶⁴

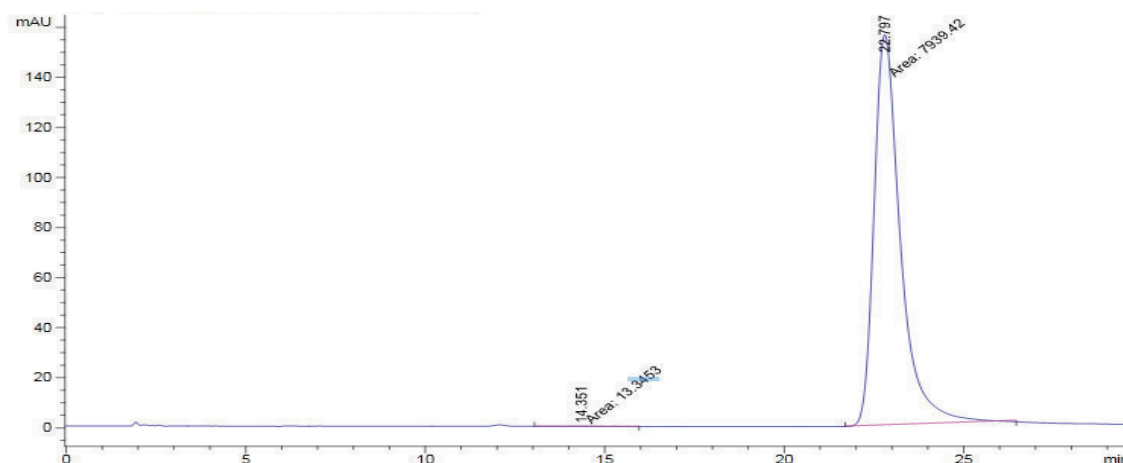
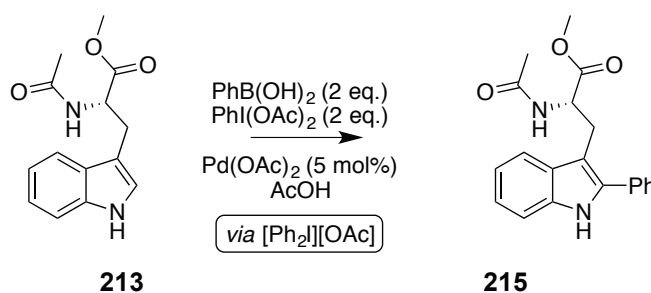


Figure 47: Chromatogram showing enantiomeric purity of protected tryptophan **213**, recorded on chiral stationary phase HPLC[§] monitoring at multiple wavelengths.

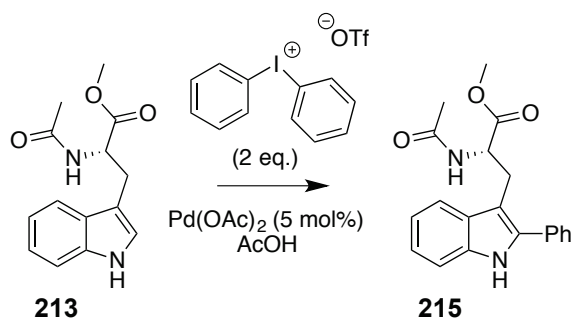
[§] Chiralcel OD column, eluting with 99.5:0.5 hexane:*i*-propanol at 1 mL min⁻¹.

Although there is an extensive variety of possible conditions available in the literature for the direct C-H bond functionalisation of indoles (*vide supra*) only a few are appropriate for this type of transformation. Mild and selective reactions were required, especially if the methodology was to be extended to more complicated and sensitive substrates at a later stage. As such, the work of Shi, Larossa and Sanford was carefully considered. Sanford's direct C-H bond functionalisation of indole¹³¹ with hypervalent iodine reagents (formed *in situ* from organoboronic acid and diacetoxyiodobenzene, or pre-prepared) seemed especially favourable, due to low reaction temperature and high efficacy. The wide availability and stability of organoboronic acids (as of 18/03/13, Sigma-Aldrich listed 1165 products in the category 'boronic acids') could allow for significant freedom in the synthesis of analogues. Additional to this, it was felt that the unique properties of tryptophan might allow the proposed Pd^{IV}-mediated mechanism to be probed in more detail.

As discussed, the Sanford indole functionalisation can be conducted using either phenylboronic acid and diacetoxyiodobenzene (*Method A*, Scheme 76) or using a pre-prepared diaryl iodonium salt (*Method B*, Scheme 77). Initial results for both methods were encouraging (Table 6) with 22% and 35% yields obtained, respectively. Raising the temperature to 40 °C increased yields to 57% and 51% respectively.



Scheme 76: Direct C-H bond functionalisation of tryptophan with PhI(OAc)₂/PhB(OH)₂ (Method A).



Scheme 77: Direct C-H bond functionalisation of tryptophan with $[Ar_2I][OTf]$ (Method B).

Table 6: Initial results for the direct C-H bond functionalisation of tryptophan.

Entry	Method	Temperature / °C	Yield / %
1	A	Ambient ^{**}	22
2	B	Ambient ^{**}	35
3	A	40	57
4	B	40	51

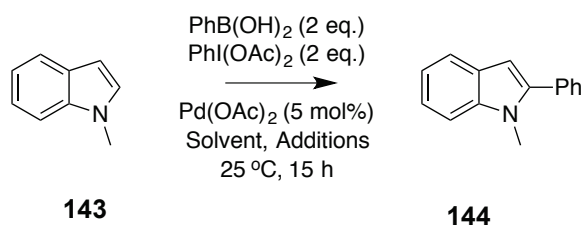
It was thought that glacial AcOH could possibly be an unsuitable solvent for highly sensitive substrates. However, an attempt to develop a non-acidic or diluted AcOH medium for Method A proved fruitless. Acetic acid/sodium acetate buffer solution (pH 5.6) gave no conversion to product, either with $Pd(OAc)_2$ or with water-soluble Na_2PdCl_4 . The use of THF/AcOH solvent mixtures in varying ratios resulted in dramatic drops in yields. Addition of sodium dodecyl sulphate (SDS) to the increase mixture resulted in slightly depressed yield (40%). It had been previously shown that this additive could increase the stability of proteins in acidic solution.

Table 7: Variation of solvent and additives for the C-H bond functionalisation of tryptophan.
^a Na_2PdCl_4 catalyst used.

Entry	Solvent	Yield / %
1	AcOH/NaOAc Buffer	0
2	AcOH/NaOAc Buffer ^a	0
3	4:1 AcOH/THF	28
4	3:2 AcOH/THF	21
5	AcOH (with SDS)	40

^{**} Ambient temperature ranged from 6 – 15 °C.

This mirrored similar observations in 1-methylindole, although in a more pronounced fashion (Table 8). A variety of solvents (including THF and toluene) and additives (including the well-precedented oxidant *p*-benzoquinone) were used, but none gave the same efficacy as glacial AcOH. Use of stoichiometric and substoichiometric quantities of AcOH also failed. TFA and pivalic acid additives were similarly unsuccessful – Fagnou and co-workers had previously used these in CMD/AMLA-6-mediated C-H functionalisations.²⁶⁵



Scheme 78: The C-H bond functionalisation of *N*-methylindole.

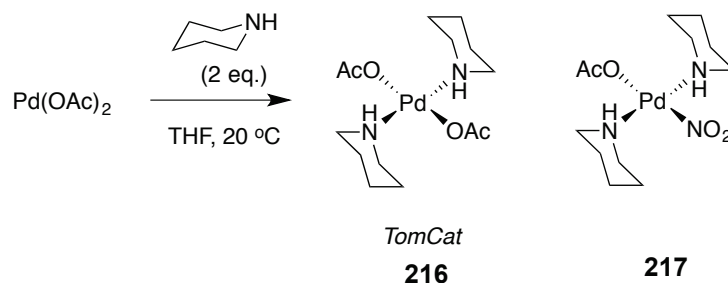
Table 8: Variation of solvent and additives for the C-H bond functionalisation of *N*-methylindole.

Entry	Solvent	Additive	Yield [†] / %
1	AcOH	-	84
3	THF	-	0
4	THF	NaOAc (3 eq.)	0
5	THF	<i>p</i> -Benzoquinone (2 eq.)	0
6	THF	<i>p</i> -Benzoquinone (2 eq.)	Trace
7	THF / AcOH (1:1)	NaOAc (3 eq.)	72
8	THF	AcOH (2 eq.) / NaOAc (2 eq.)	14
9	THF	AcOH (10 mol%)	Trace
10	THF	TFA (2 eq.)	Trace
11	THF	PivOH (2 eq.)	Trace
12*	AcOH	-	58
13	Tol.	-	0
14	Tol. / AcOH (1:1)	-	64
15	AcOH	-	0

* using Pd₂(dba)₃ instead of Pd(OAc)₂, † Yield after flash chromatography.

Pd(OAc)₂(pip)₂ (*TomCat* **216**), has been found to be an excellent pre-catalyst for the direct C-H bond functionalisation of nucleosides with Pd/Cu-mediate systems.²⁷ The complex is synthesised from Pd(OAc)₂ (Scheme 79). However, the reaction mixture

contained a 2.1:1 mixture of $\text{Pd}(\text{OAc})_2(\text{pip})_2$ and, unexpectedly, $\text{Pd}(\text{OAc})(\text{NO}_2)(\text{pip})_2$.²⁶⁶ The source of nitrate contamination was traced to commercial $\text{Pd}(\text{OAc})_2$.



Scheme 79: Synthesis of *TomCat* **216** and the discovery of impurities in $\text{Pd}(\text{OAc})_2$.

Cotton had noted non-trivial behaviour of $\text{Pd}(\text{OAc})_2$, which exists as a trinuclear complex $\text{Pd}_3(\text{OAc})_6$ with D_{3h} symmetry.²⁶⁷ With trace water, an acetate bridge is disrupted to form $\text{Pd}_3(\text{OAc})_6(\text{OH}_2)$ – this results in desymmetrisation of the ^1H NMR spectrum. $\text{Pd}_3(\text{OAc})_6$ is synthesised from metallic Pd^0 by oxidation with HNO_3/AcOH mixture. A strong flow of N_2 should remove the $\text{NO}_{2(\text{g})}$ evolved by this process. However, a poor flow will result in the formation of the nitrate complex $\text{Pd}_3(\text{OAc})_5(\text{NO}_2)$. Recrystallisation of $\text{Pd}(\text{OAc})_2$, followed by manual separation and characterisation (by elemental analysis, ^1H NMR and IR spectroscopy) confirmed complex was the contaminant. In a study of commercial $\text{Pd}(\text{OAc})_2$ sources from various research groups at the University of York showed that 80% of the samples tested were contaminated with nitrate (Figure 48).

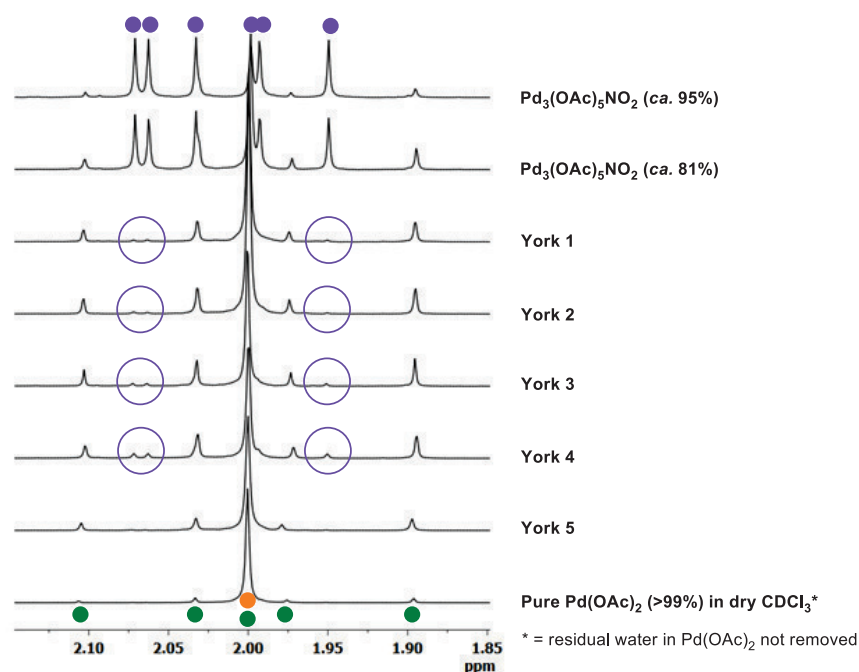
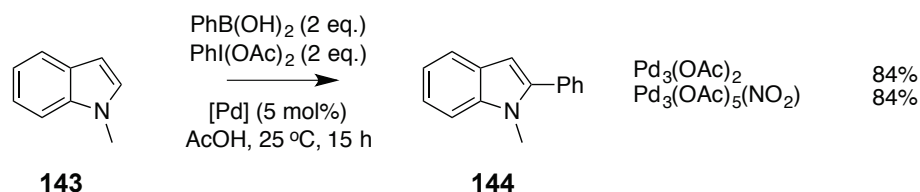


Figure 48: ^1H NMR spectra showing 'pure' $\text{Pd}(\text{OAc})_2$ (>99%, orange) compared to a variety of commercial samples collected at the Department of Chemistry, University of York. All these samples show the presence of $\text{Pd}_3(\text{OAc})_5\text{NO}_2$ impurity (purple). Green indicates $\text{Pd}_3(\text{OAc})_6(\text{OH}_2)$. (Figure prepared by Prof. I. J. S. Fairlamb).

The presence of nitrate impurity can have a profound effect in Pd co-ordination chemistry, and should be a significant cause for concern for those working in that field. In addition to **216**, Fairlamb and co-workers have shown that nitrate has a non-innocent role in the synthesis of papavarine palladacycles.^{268,269} Nonoyama and co-workers had suggested the unexpected synthesis of nitrate complexes arises from oxidation of acetonitrile. This was shown not to be the case, with the nitrate thought most likely to have been from a significantly contaminated batch of $\text{Pd}(\text{OAc})_2$.

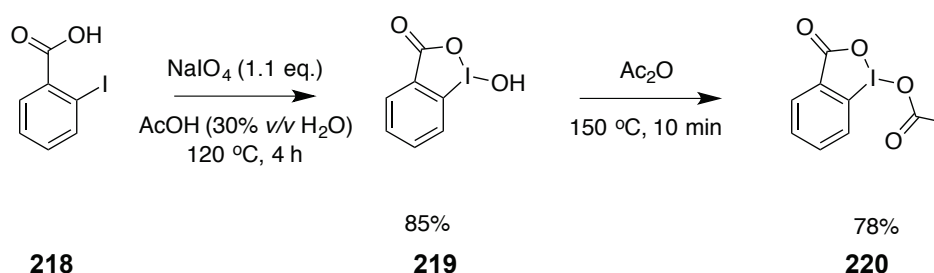
$\text{Pd}(\text{OAc})_2$ is often found as a pre-catalyst in Pd-mediated cross-coupling reactions. Given the lack of literature comment, and the apparent ubiquity of the contaminant, it seems reasonable to conclude that in such processes there is no difference in catalytic activity between $\text{Pd}_3(\text{OAc})_6$ and $\text{Pd}_3(\text{OAc})_5(\text{NO}_2)$ complexes in orthodox $\text{Pd}^{\text{0/III}}$ systems. However, in the $\text{Pd}^{\text{III/IV}}$ manifold proposed for Sanford's indole C-H functionalisation, it was hypothesised that the nitrate complex could help to stabilise Pd^{IV} intermediates. The direct C-H bond functionalisation of *N*-methylindole was performed using pure samples of $\text{Pd}_3(\text{OAc})_6$ and $\text{Pd}_3(\text{OAc})_5(\text{NO}_2)$. Both catalysts gave identical yields (84%). This does not preclude differences in other catalytic systems.



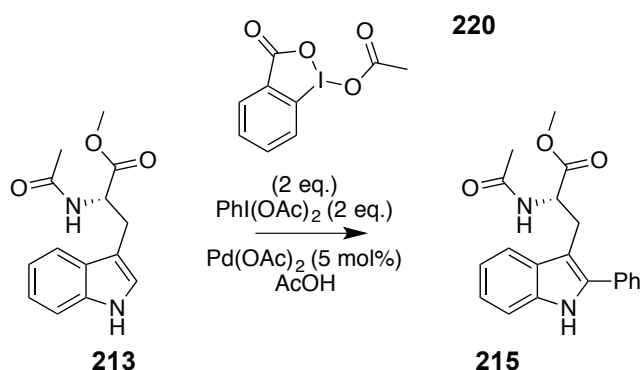
Scheme 80: Direct C-H bond functionalisation of 1-methylindole using pure $\text{Pd}_3(\text{OAc})_6$ and that contaminated with $\text{Pd}_3(\text{OAc})_5(\text{NO}_2)$.

3.2.2 Unsymmetrical Diaryliodonium Salts

Work by Gaunt and co-workers on the selective functionalisation of aryl *meta* C-H bonds had indicated that the use of asymmetric diaryl iodonium salts in which one aryl ring is highly substituted results only in the transfer of the less sterically hindered aryl.¹³² Rather than synthesising a number of such diaryliodonium salts, it was thought that it might be possible to introduce different substituents to the tryptophan using a constant, sterically hindered hypervalent iodine compound and varying aryl boronic acid, forming the diaryl iodonium salt *in situ*. Attempts to synthesise bis(acetyloxy)(2,4,6-trimethylphenyl)- λ^3 -iodane, however, proved to be unsuccessful. (3-Oxo-1- λ^3 -2-benziodoxol-1(3H)-yl)methyl acetate **220** is a by-product of Dess-Martin periodinane (DMP) oxidation.²⁷⁰ The I^{III} in this compound is in a similar environment to diacetyloxyiodobenzene, and it was proposed that this hypervalent iodine compound could be used as a non-transferring half of a diaryl iodonium salt. It can be easily synthesised in two steps in excellent overall yield (Scheme 81): 2-iodobenzoic acid is oxidised to I^{III} using NaIO_4 , followed by a rapid (10 min) acylation with neat Ac_2O .



Scheme 81: Synthesis of iodine(III) compound **220**.



Scheme 82: Direct C-H functionalisation of tryptophan using iodine(-III) compound **220**.

When applied to the direct C-H functionalisation no reaction was observed. The employment of unsymmetrical arylmesityliodonium salts have been previously used by Gaunt and Greaney.^{132,271,272} These reagents are available from aryl iodide and mesitylene, oxidised to iodine(III) by *m*-CPBA. Triflate is commonly used as the counter-ion. Generally, the yields of these salts range from moderate to poor. Application of these reagents proved to be disappointing. Although yields were maintained with the 4-tolylmesityliodonium triflate (Table 9, entry 1), CF₃-substituents resulted in poor yield (entries 2-3).

Table 9: The direct C-H bond functionalisation of tryptophan using [(Mes)I(Ar)][OTf].

Entry	Compound	Ar	Yield [†] / %
1	221		52
2	222		28
3	223		21

[†] Yield after flash chromatography.

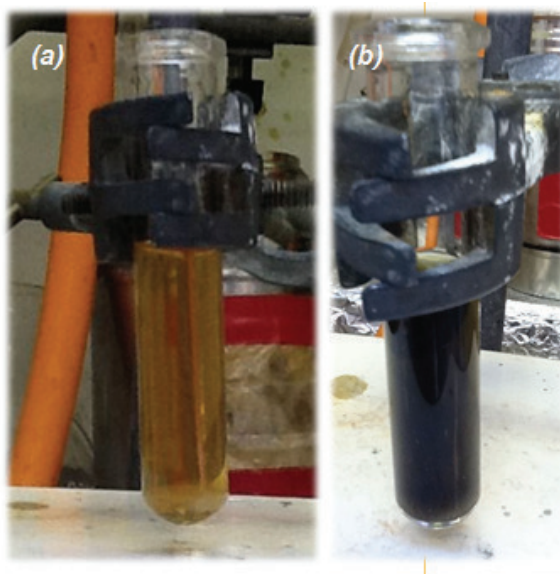
3.2.3 Mechanism: Pd^{0/II} or Pd^{II/IV}?

Figure 49: Direct C-H bond functionalisation reaction of indole. (a) Solution of PhI(OAc)₂/PhB(OH)₂ and Pd(OAc)₂ in AcOH (b) Immediately (ca. 15 s) after the addition of 1-methylindole.

These reactions were notable for their rapid (sometimes immediate) formation of Pd⁰ (Figure 49), which appear as nanoparticulate species (most likely colloidal in nature). To analyse these Pd nanoparticles, two samples of reaction mixture after heating for 1 h were collected. To one of these samples, PVP (10 eq. per theoretical amount of Pd, assuming the reaction was a homogenous mixture) was added. Solvent was removed from both samples under reduced pressure, heating at 40 °C. Transmission electron micrographs were recorded for each of these samples (Figures 50 and 51). As with the direct C-H bond functionalisation of benzazoles discussed in Chapter 2, Pd⁰ nanoparticles were clearly visible.

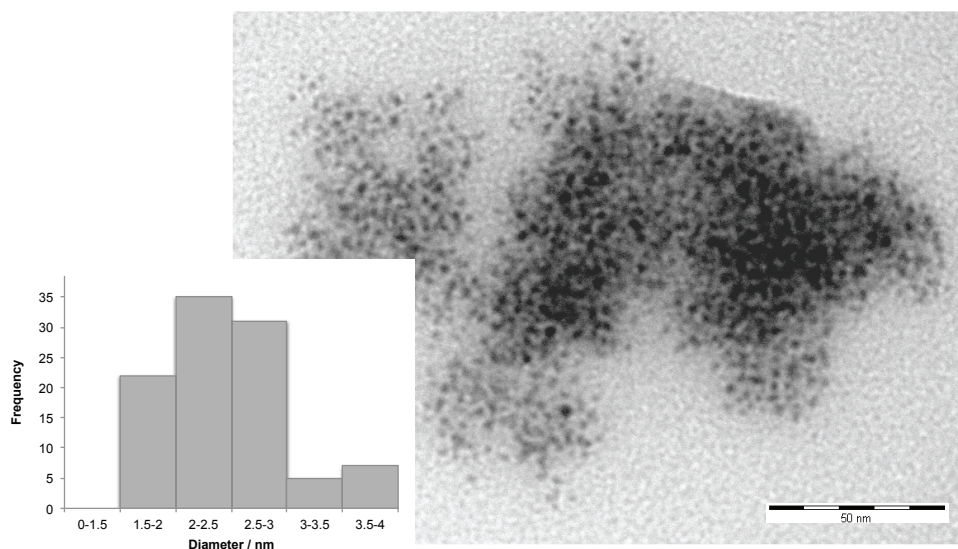


Figure 50: TEM image of Pd⁰ nanoparticles isolated from the direct C-H bond functionalisation of tryptophan using PhI(OAc)₂/PhB(OH)₂, trapped with PVP. Inset: histogram showing the distribution of particles by size, $n = 100$.

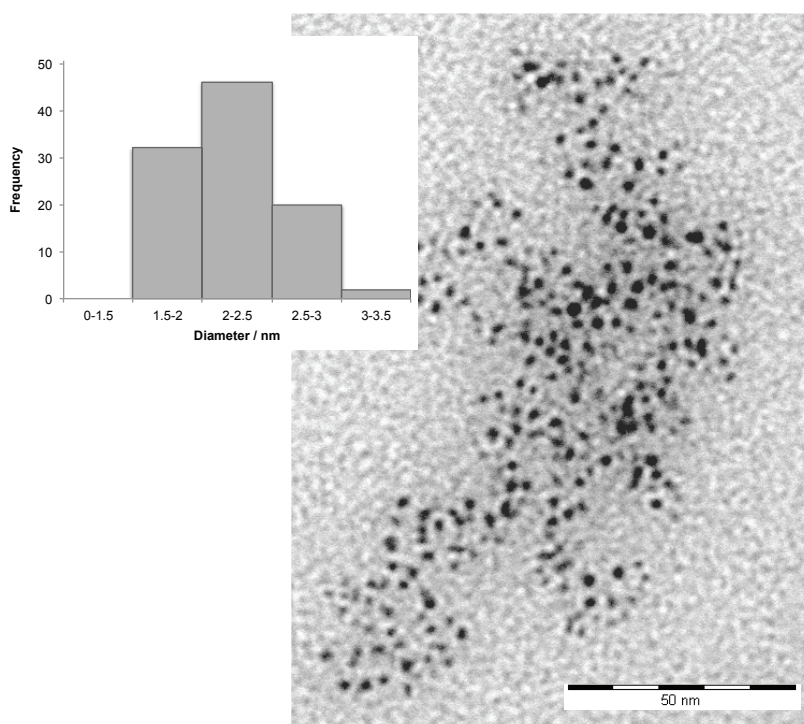
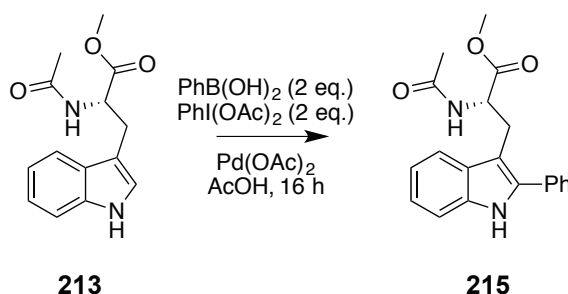


Figure 51: TEM image of Pd⁰ nanoparticles isolated from the direct C-H bond functionalisation of tryptophan using PhI(OAc)₂/PhB(OH)₂, without PVP. Inset: histogram showing the distribution of particles by size, $n = 100$.

Table 10: Simple statistical analyses of the Pd nanoparticles isolated from the direct C-H bond functionalisation of tryptophan using $\text{PhI}(\text{OAc})_2/\text{PhB}(\text{OH})_2$ (see Figures 50 and 51)

	Mean	SD	Median	Mode	IQR	IQM
With PVP	2.52	0.52	2.20	2.40	0.680	2.46
Without PVP	2.22	0.32	3.05	2.17	0.435	2.20

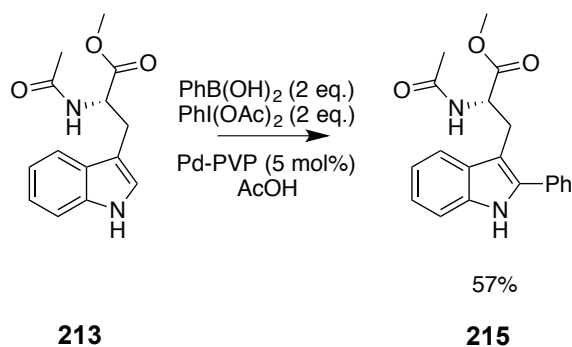
These nanoparticles are small (in the 2-5 nm size regime) and well defined (as demonstrated by small standard deviation). No significant difference was noted between the samples (the mean difference, 0.3 nm, is within the estimated error).

**Scheme 83:** See Table 11.**Table 11:** Variation of catalyst loading for the direct C-H bond functionalisation of tryptophan.
^a Reaction time 69 h.

Entry	Catalyst Loading	Yield / %	TON
1	100	79	0.79
2	10	66	6.60
3	5	57	11.4
5	2.5	44	17.6
6	1	15	15.0
7 ^a	1	44	44.0

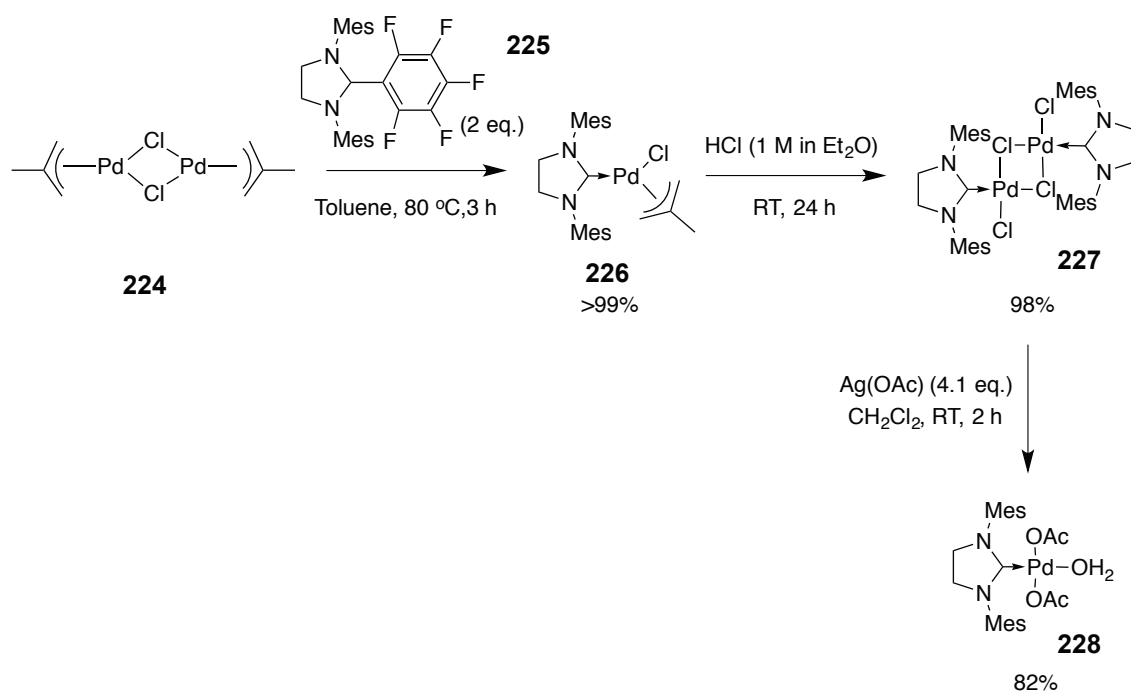
Sanford, in the original publication, noted the formation of nanoparticles and suggested it was the result of catalyst poisoning (*i.e.* that active Pd^{II} is reduced to Pd^0 , effectively removing it from the catalytic cycle). If this hypothesis was correct, then avoiding colloid formation could increase reaction yield. Reduction in catalyst loading did prevent visible Pd colloid formation, and there was a significant increase in turnover number. This could suggest the active phase of the reaction is in solution. However, low yields were observed (Table 11). At lower loadings, the catalyst remained active for

longer periods: when the reaction with 1 mol% Pd(OAc)₂ was left for 69 h, an increased yield was observed over that reacted for 16 h. This observation was not repeated at higher loadings. Negligible change in yield was observed when the reaction was performed under inert conditions. This would suggest that Ostwald ripening (that is, aggregation resulting from interaction of the Pd nanoparticles with O₂, potentially seeding growth) was not an issue in aggregation.¹²⁹



Scheme 84: Direct C-H bond functionalisation of tryptophan using Pd-PVP nanoparticles.

It was found that intentionally synthesised Pd-PVP nanoparticles (*ca.* 3 nm) gave a comparable yield to the Pd(OAc)₂-catalysed reactions (Scheme 84). Since this reaction – both on simple indole and tryptophan substrates – had been proposed to proceed *via* a Pd^{II/IV}-mediated manifold, this result was surprising. This suggests that either this reaction proceeds *via* a traditional Pd^{0/II} manifold or that atoms of Pd are labilised from the polymer support and oxidised to Pd^{II} by solvent, reagents or air. Although by no means conclusive, infrared spectroscopic analysis under working conditions did not show the appearance of Pd(OAc)₂ (by ReactIR®) when Pd-PVP nanoparticles were suspended in acetic acid.



Scheme 85: Synthesis of complex Pd(SIMes)(OAc)₂(H₂O), via Pd-allyl complexes x to y.

The amino acid tryptophan had been C-H bond functionalised in moderate yield, and Pd⁰ nanoparticles had been identified in the reaction mixture. Further, pre-synthesised nanoparticles had been shown to be catalytically active. In Sanford's direct C-H bond functionalisation of indoles, it was noted that *N*-heterocyclic carbene Pd^{II} complexes were highly efficacious for this reaction, particularly when used with pre-synthesised diaryliodonium salts. It is thought that such complexes are particularly stable at Pd^{II}. Novel SIMes complex **228** was synthesised in three steps (Scheme 85) with excellent overall yield (93%). 2-Methylallyl complex **224** was heated under reflux in air with 1,3-di(2,4,6-trimethylphenyl)-2-(pentafluorophenyl)-2,4,5-trihydroimidazole, allowing novel complex **228** to be collected in quantitative yield.¹²⁶ When treated with ethereal HCl, **226** dimerises with loss of 2-methylpropene to give known **227**. Treatment with AgOAc yields the desired catalyst [1,3-di(2,4,6-trimethylphenyl)-4,5-dihydroimidazolyliidene]diacetateaquopalladium(II) **228**. Novel complexes **226** and **228** have been thoroughly characterised by NMR spectroscopy.

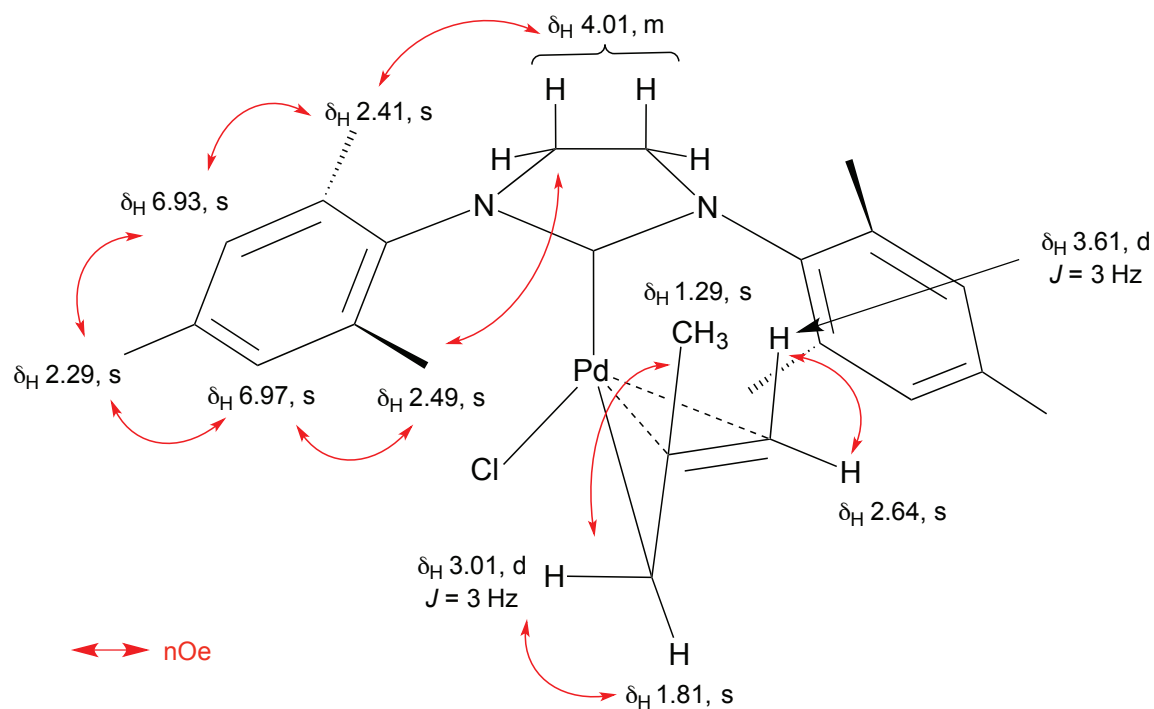


Figure 52: ^1H NMR assignments for complex **226**.

For **226** (Figure 52), ^1H NMR spectroscopy (Figure 53) revealed a simple aromatic region consisting of two equally integrating singlets (δ 6.97, 6.93 ppm). These were integrated as 2H each, and correspond to the ArH in the mesityl groups. Three singlets (δ 2.49, 2.41, 2.29 ppm), each integrating to 6H, were observed and assigned as the mesityl CH_3 groups. ^1H - ^1H NOESY experiments (Figure 55) indicated interaction between the singlet at δ 2.29 ppm and both ArH environments – this indicated that this methyl group is situated in the *para* position. nOe interactions for δ 2.49/6.97 and δ 2.41/6.93 were both observed, suggesting they are adjacent to each other.

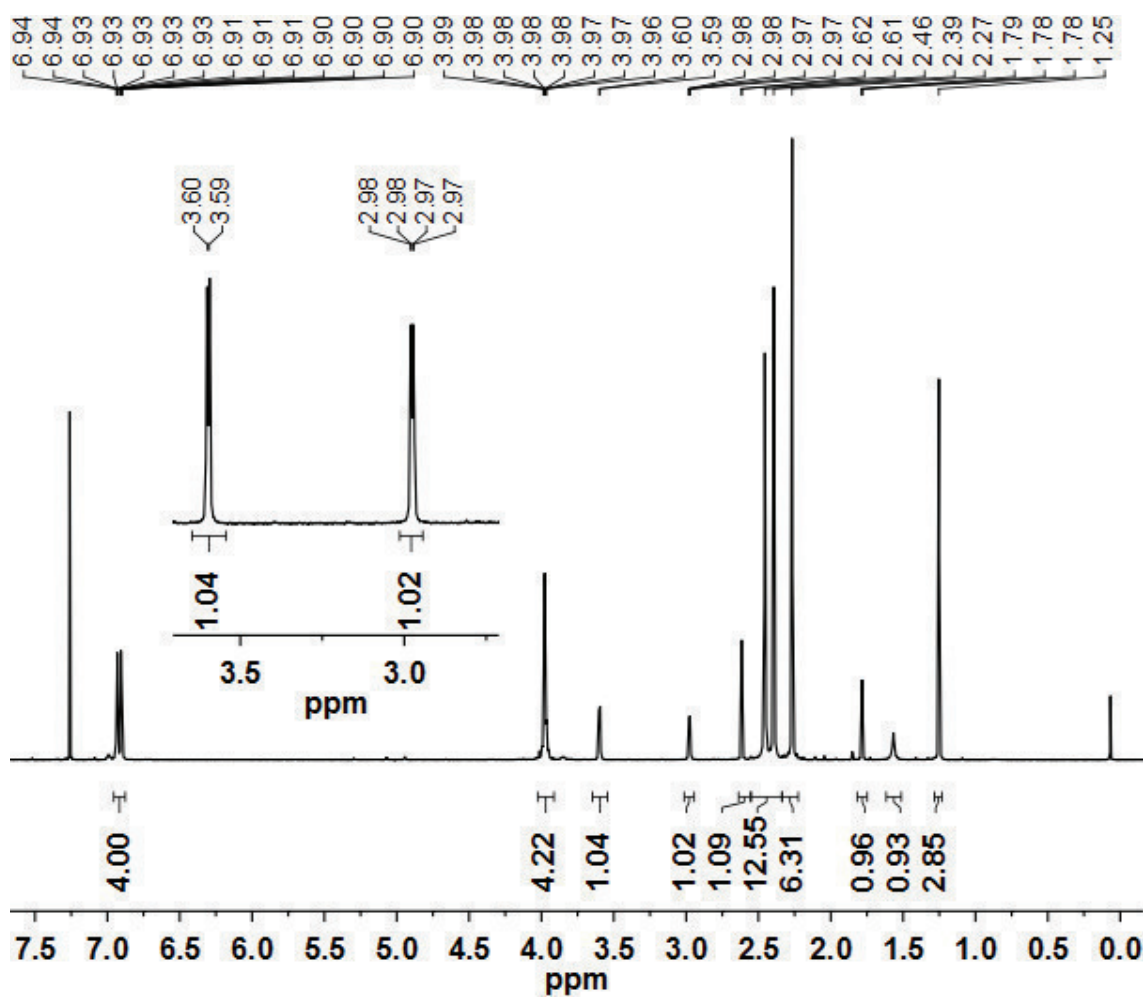


Figure 53: ^1H NMR (400 MHz, CDCl_3) spectrum of complex 226.

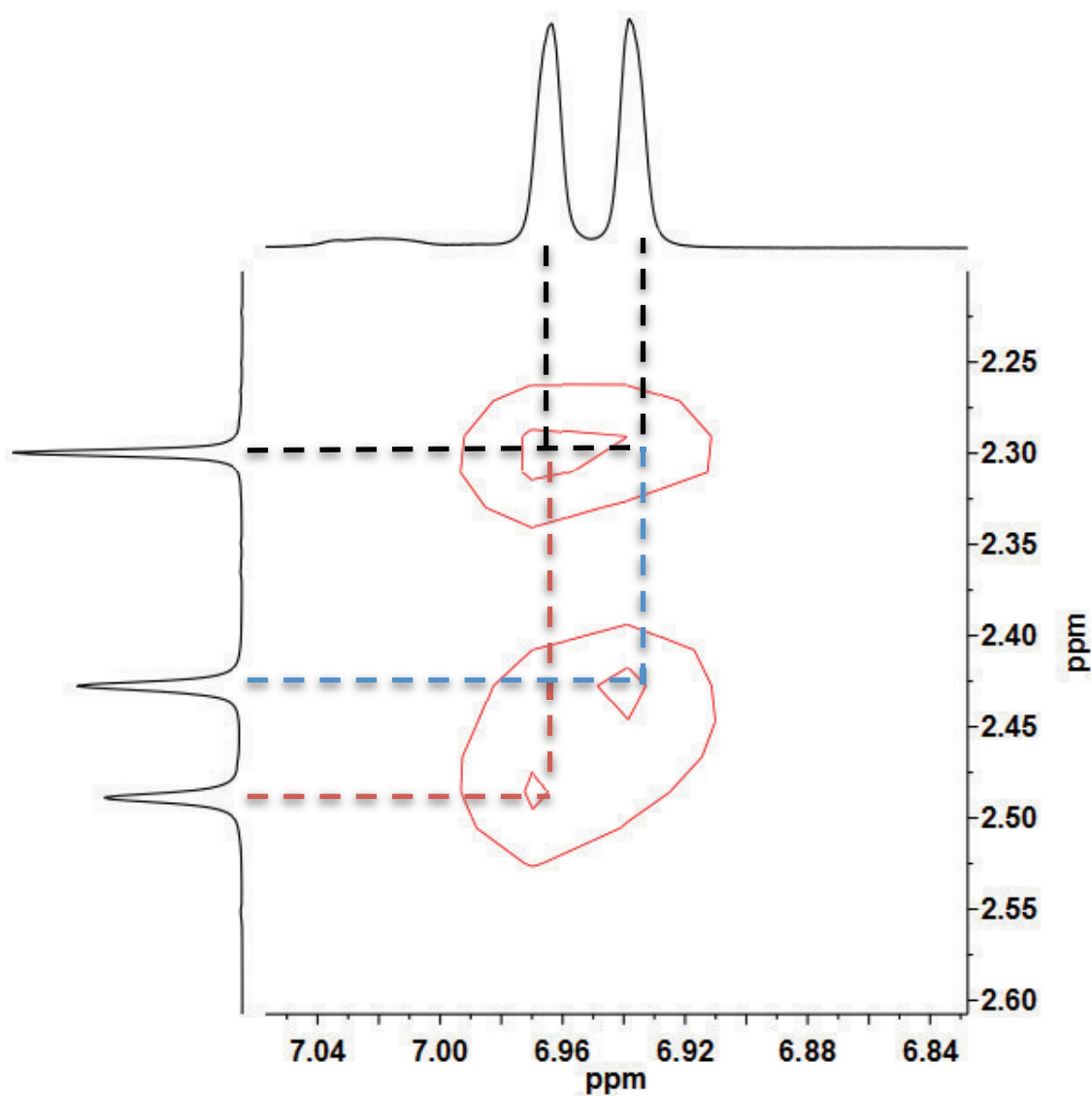


Figure 54: ^1H - ^1H COSY NMR (500 MHz, CDCl_3) spectrum of **226**. Coloured lines connect resonances for which cross-peaks are observed.

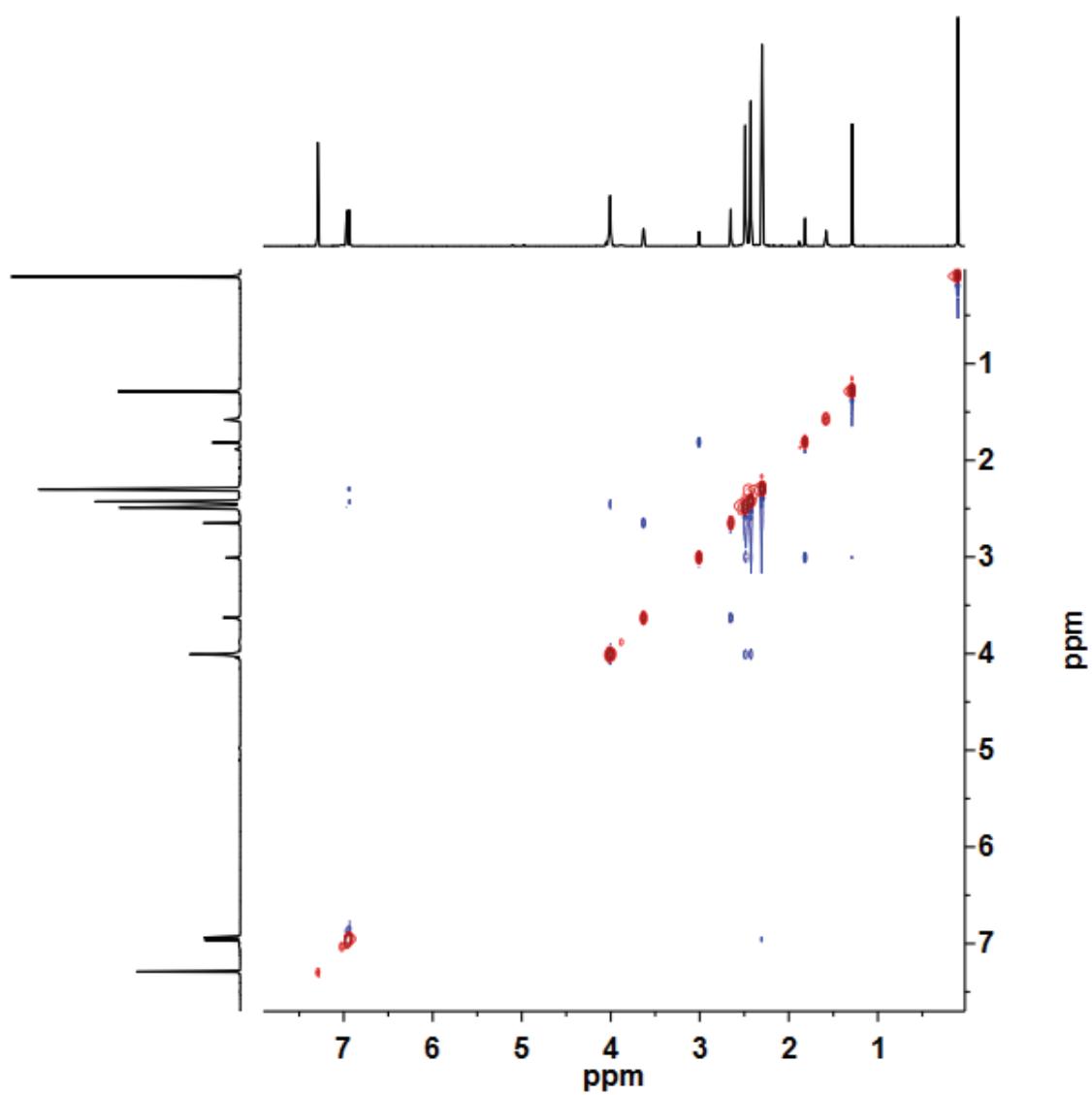


Figure 55: ^1H - ^1H NOESY NMR of **226** (500 MHz, CDCl_3) spectrum.

The singlets at δ 2.49 and δ 2.41 ppm also exhibit nOe interactions with a 4H multiplet at 4.01. This signal is assigned as the C3-H₂ and C4-H₂ of the dihydroimidazolyl moiety.

The 2-methyl allyl ligand is represented by two 1H doublets, two 1H singlets, and a 3H singlet (assigned as the methyl group). A significant difference in chemical shifts between the signals suggests an asymmetric or 'slipped' allyl complex – the highest field signals are the 'end' of the allyl with the most double-bonded character. The doublets have a coupling constant of δ 3.01 Hz – this indicates an allyl W-coupling.²⁷³ Each doublet exhibits an nOe interaction with one singlet, suggesting they are on the same C atom. This is confirmed by HSQC (Figure 58). The doublet proton signals also exhibit nOe interactions with the methyl group, suggesting they are on the same side of the allyl.

nOe interactions are observed between the singlet at δ 2.49 ppm and the double bond character end of the allyl, suggesting that this end is closer in space to the mesityl moiety, and that both the allyl and mesityls are locked in space.

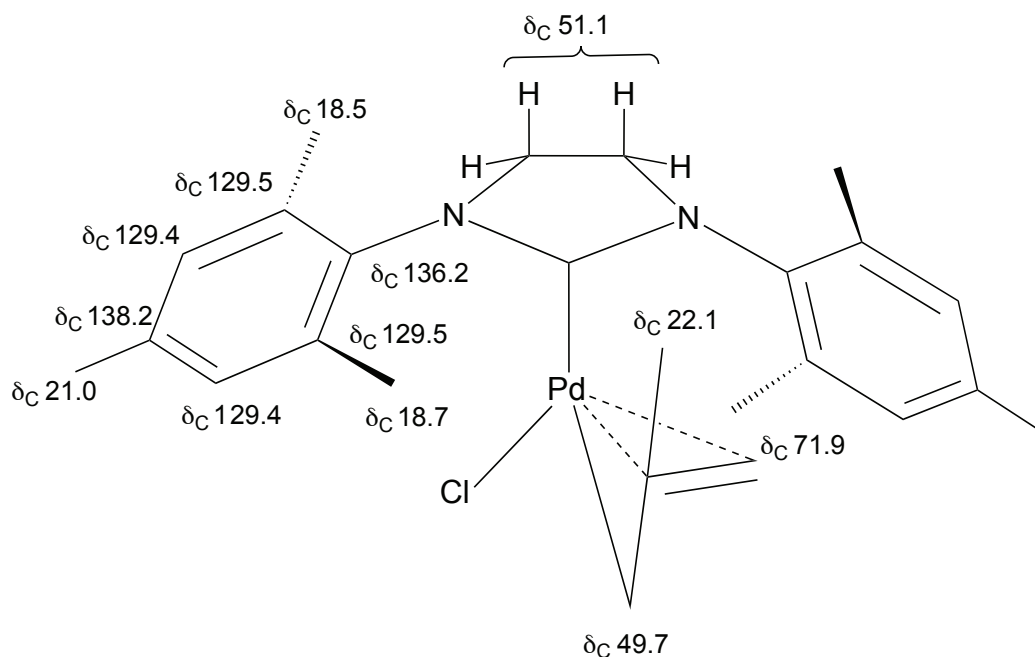


Figure 56: ¹³C NMR assignments for complex **226**.

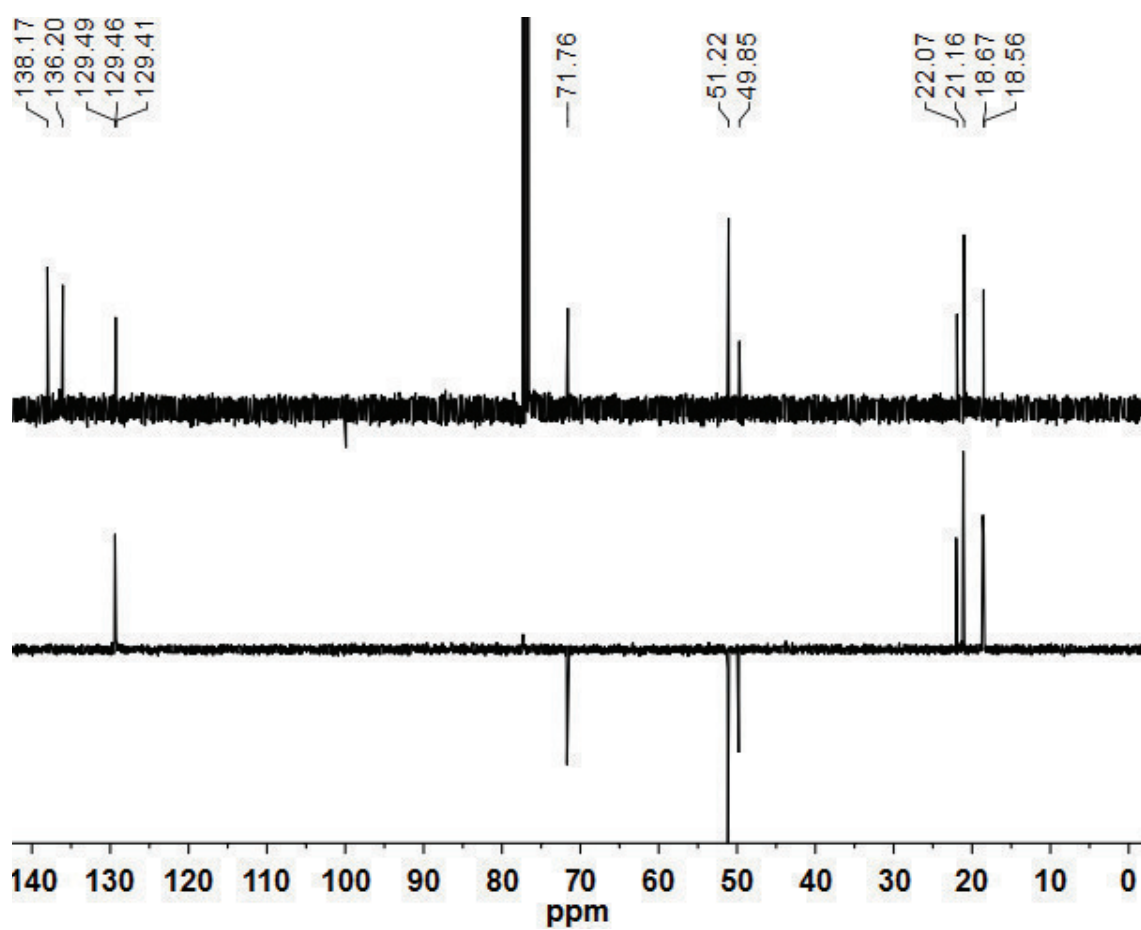


Figure 57: ^{13}C and ^{13}C DEPT 135 NMR spectra for **226** (101 MHz, CDCl_3).

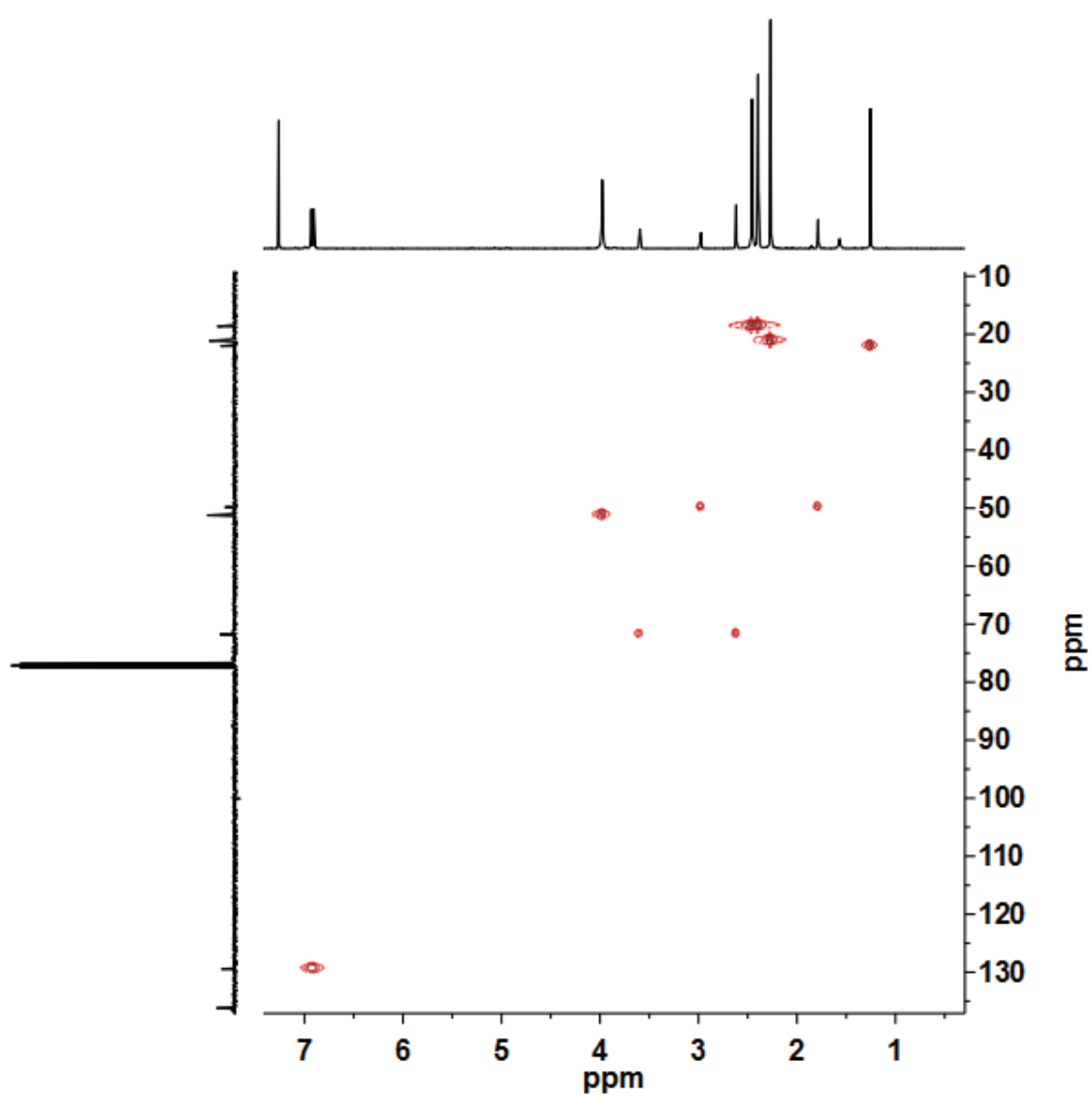


Figure 58: ^1H - ^{13}C HSQC NMR (400, 101 MHz, CDCl_3) spectrum of **226**.

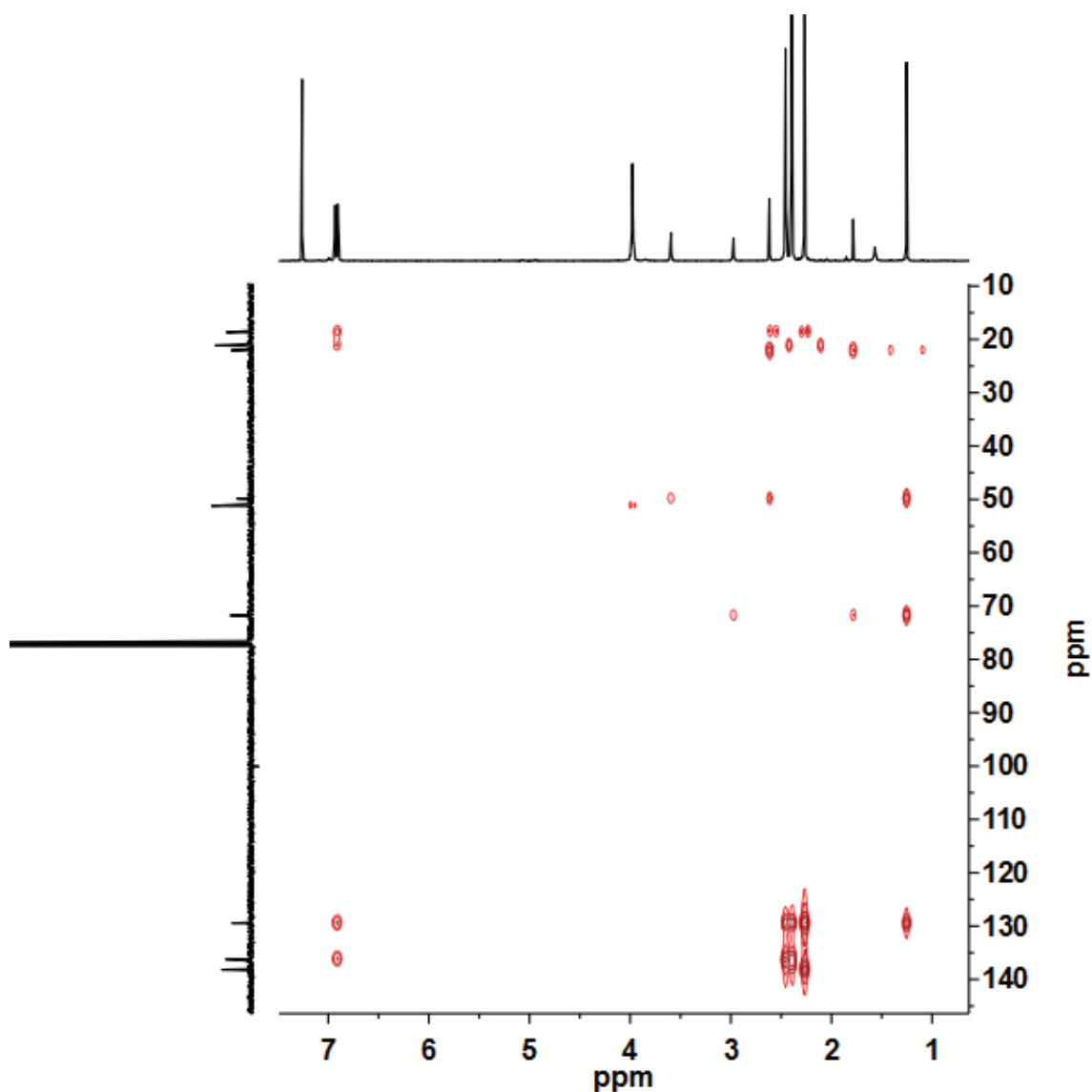


Figure 59: ^1H - ^{13}C HMBC NMR (400, 101 MHz, CDCl_3) spectrum of **226**.

^{13}C resonances were assigned by comparison with HSQC (Figure 58) and HMBC (Figure 59). Allyl C2 carbon and the dihydroimidazolyl C1 have not been observed.

Complex **228** was similarly characterised, and the ^1H and ^{13}C resonances are shown in Figures 60 and 61. Similarly, the dihydroimidazolyl C1 have not been observed.

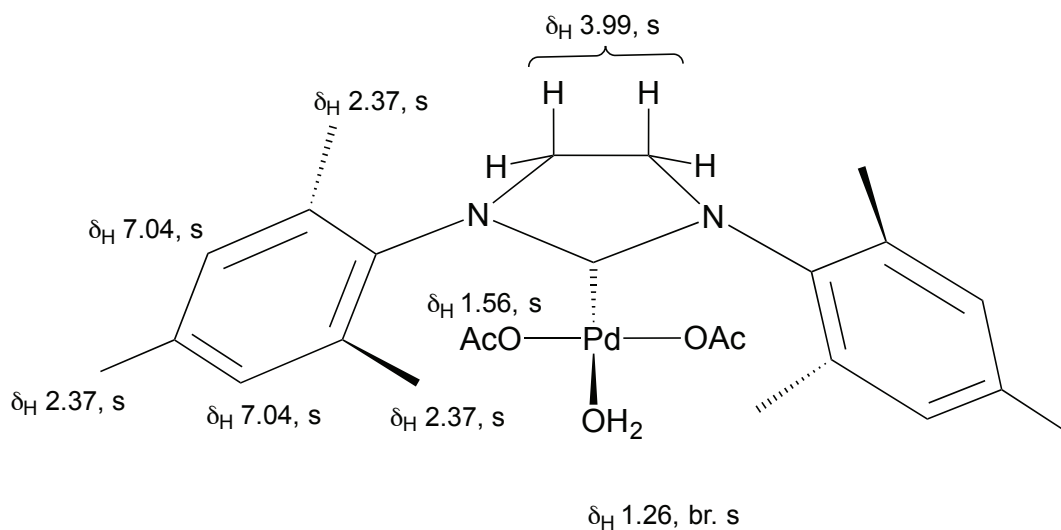


Figure 60: ^1H NMR assignments for **228**.

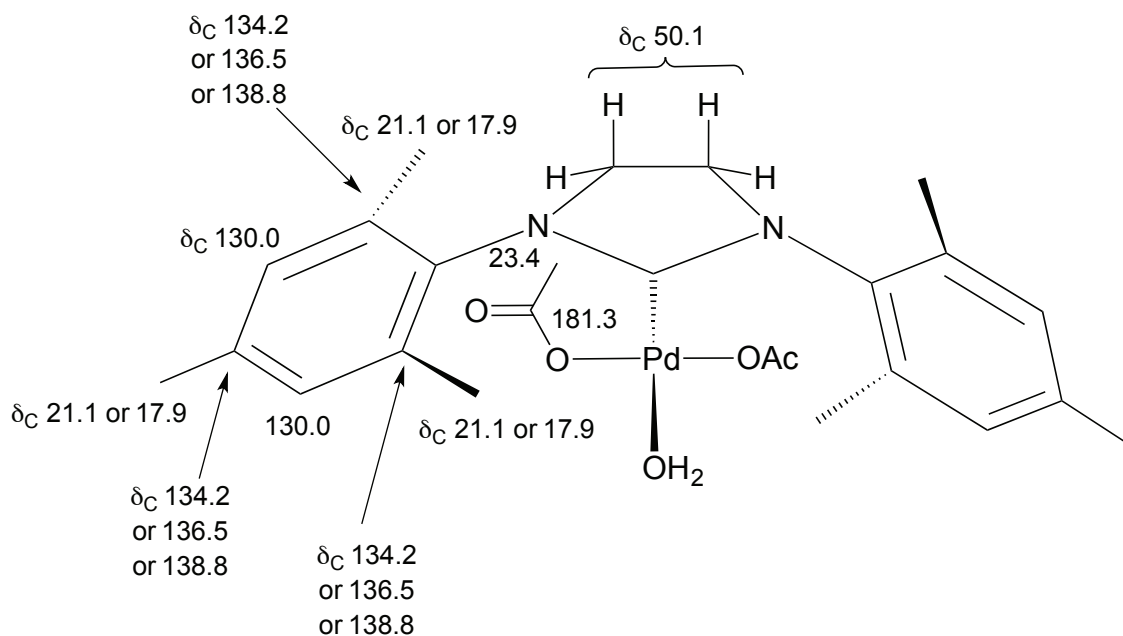
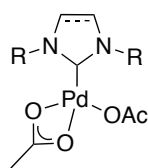
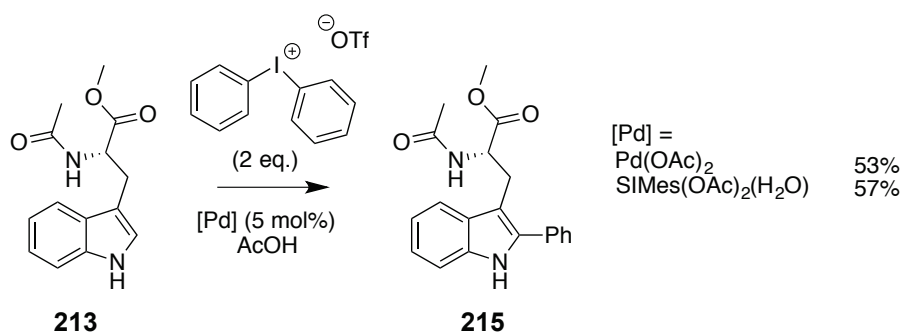


Figure 61: ^{13}C NMR assignments for complex **228**.

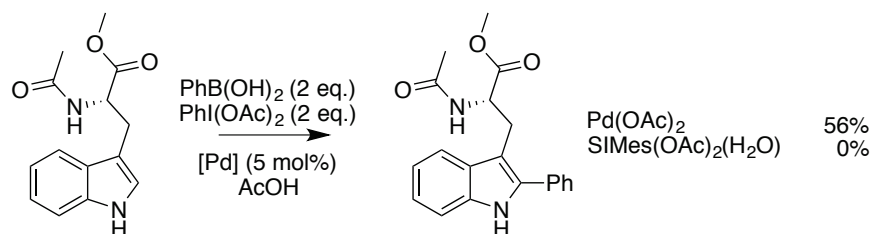
Nolan and co-workers have synthesised similar complexes (of 1,3-di(2,4,6-trimethylphenyl)-4,5-imidazolyliene) from free carbene and recrystallized $\text{Pd}(\text{OAc})_2$, in which one acetate adopts a $\kappa^2\text{O},\text{O}$ configuration (Figure 62).²⁷⁴ However, in complex **228** only one acetate environment is observed by ^1H NMR spectroscopic analysis. Furthermore, a broad ligated H_2O signal is also present.

**228b****Figure 62:** Possible $\kappa^2\text{O},\text{O}$ configuration of **228**.

In the C-H bond functionalisation of tryptophan **213** using a pre-synthesised diphenyliodonium triflate salt (*Method B*), a slight increase in yield is obtained for **228** over $\text{Pd}(\text{OAc})_2$ (Scheme 86).

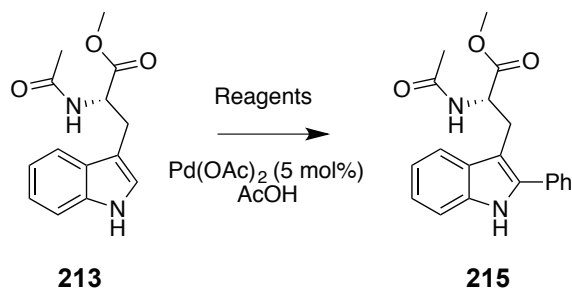
**Scheme 86:** The direct C-H bond functionalisation of tryptophan using *Method B*, catalysed by **228** and $\text{Pd}(\text{OAc})_2$.

However, a significant difference in reactivity is observed for C-H bond functionalisation with phenylboronic acid and diacetoxyiodobenzene (Scheme 87). The reaction with $\text{SIMes}(\text{OAc})_2(\text{H}_2\text{O})$ does not proceed at all. This gives the first indication that there could be a different mechanism operating under the two reaction conditions (*i.e.* the different methods).

**Scheme 87:** The direct C-H bond functionalisation of tryptophan using *Method A*, catalysed by **228** and $\text{Pd}(\text{OAc})_2$.

The roles of reagents in *Method A* were scrutinised. Reagent elimination studies on *Method A* (Scheme 88, Table 12) indicated that, as expected, the reaction did not

proceed in the absence of Pd. Also, in the absence of PhB(OH)₂, the reaction did not proceed. This was consistent with the proposed *in situ* formation of diaryliodonium salt. However, when PhI(OAc)₂ was omitted, the yield increased to 93%. Without PhI(OAc)₂, the diaryliodonium salt cannot be forming.

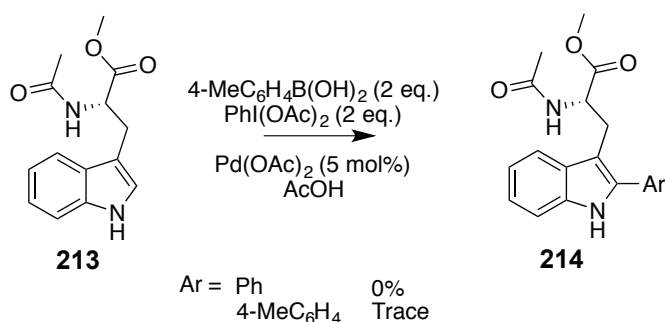


Scheme 88: Component elimination studies in the direct C-H bond functionalisation of tryptophan using Method B, catalysed by **228** and Pd(OAc)₂.

Table 12: Component elimination studies for the direct C-H bond functionalisation of tryptophan, **213**.

Entry	Reagents	Omitted Component	Yield / %
1	PhI(OAc) ₂ (2 eq.) PhB(OH) ₂ (2 eq.)	None	56
2	PhI(OAc) ₂ (2 eq.) PhB(OH) ₂ (2 eq.)	Pd(OAc) ₂	0
3	PhI(OAc) ₂ (5 mol%)	PhB(OH) ₂	0
4	PhB(OH) ₂ (2 eq.)	PhI(OAc) ₂	93

This reactivity was further probed using PhI(OAc)₂ and 4-MeC₆H₄B(OH)₂ in the reaction. If the diaryliodonium salt was formed, as proposed, then we should expect an equal mixture of tryptophan functionalised with Ph- and 4-MeC₆H₄- groups. However, by ESI-MS only trace quantities of 4-MeC₆H₄-modified tryptophan were observed by ESI-MS and ¹H NMR spectroscopy and no Ph-modified tryptophan.

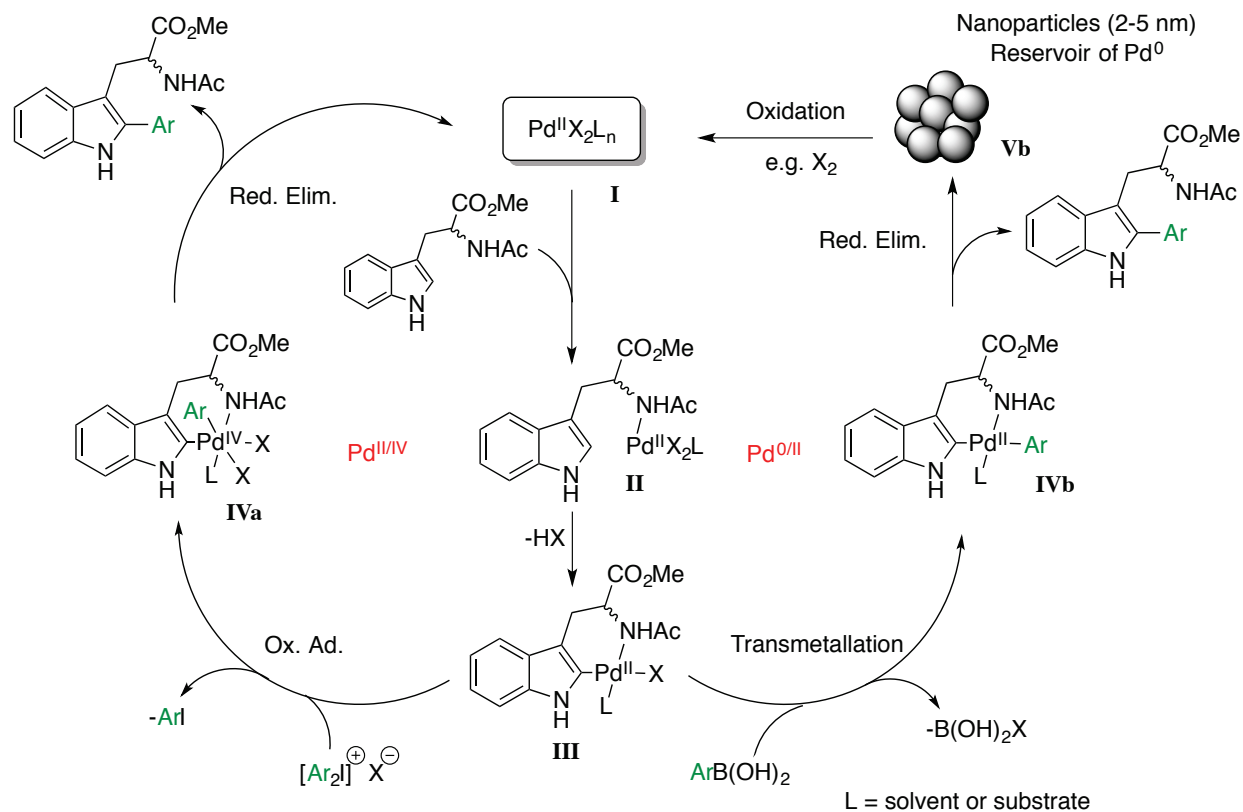


Scheme 89: The direct C-H bond functionalisation of tryptophan using PhI(OAc)_2 and 4- $\text{MeC}_6\text{H}_4\text{B(OH)}_2$, catalysed by Pd(OAc)_2 .

These results suggest that the diaryliodonium salt is not being formed *in situ* in the C-H bond functionalisation of tryptophan using ArB(OH)_2 and PhI(OAc)_2 . As a consequence, it seems unlikely that this reaction is proceeding *via* the same $\text{Pd}^{\text{III/IV}}$ mediated mechanism as Method B. The presence and catalytic activity of Pd^0 nanoparticles suggest that a $\text{Pd}^{\text{0/II}}$ catalytic manifold is operative.

The proposed mechanisms for both methods are shown in Scheme 90. Both mechanisms involve coordination of tryptophan *via* the amide nitrogen (intermediate **II**). Cyclopalladation can then occur (intermediate **III**). Presumably, this occurs initially at the C3-position, followed by a rapid 3,2-migration as proposed by Sames. After this point, the two mechanisms diverge. For Method B, diaryliodonium oxidatively adds, resulting in Pd^{IV} intermediate **IVa**. Reductive elimination of product can then occur, feeding Pd^{II} back into the catalytic cycle.

For Method A, transmetalation occurs with aryl boronic acid to give Pd^{II} intermediate **IVb**. Reductive elimination of the product regenerates Pd^0 . It is proposed that this is in equilibrium with Pd^0 nanoparticles – that is, that the nanoparticles are acting as a resting state or reservoir. The Pd^0 **IVb** can be returned by Pd^{II} using a sacrificial oxidant (possibly due to oxidation from the surface of the particle). PhI(OAc)_2 was acting in this fashion. It has been shown this can also act as an oxidant in the boronic acid homocoupling process – a process that can outcompete with C-H bond functionalisation, consuming the boronic acid (dependent on the structure of the boronic acid) and reducing the reaction yield. With PhI(OAc)_2 removed, O_2 in the air can act as the oxidant. Homocoupling can still occur, but at a reduced rate.



Scheme 90: Proposed catalytic cycles for Pd^{0/II} and Pd^{III/IV} mediated direct C-H bond functionalisation of tryptophan **213**. It is thought that Pd⁰ colloidal nanoparticles may act as a reservoir for molecular Pd

The formation of intermediate **II** was also observed by *in situ* monitoring by ReactIR®. Tryptophan **213** was dissolved in THF, and Pd(OAc)₂ added. The reaction was monitored at 1616 cm⁻¹ (Figures 63-64) This is a carbonyl stretching band associated with Pd(OAc)₂ {e.g. Pd₃(OAc)₆}.²⁶⁷ Within 45 minutes of addition, the starting material had been entirely consumed. A new band at 1586 cm⁻¹ concurrently increased in intensity. It is proposed that this infrared band is associated with intermediate **II**.

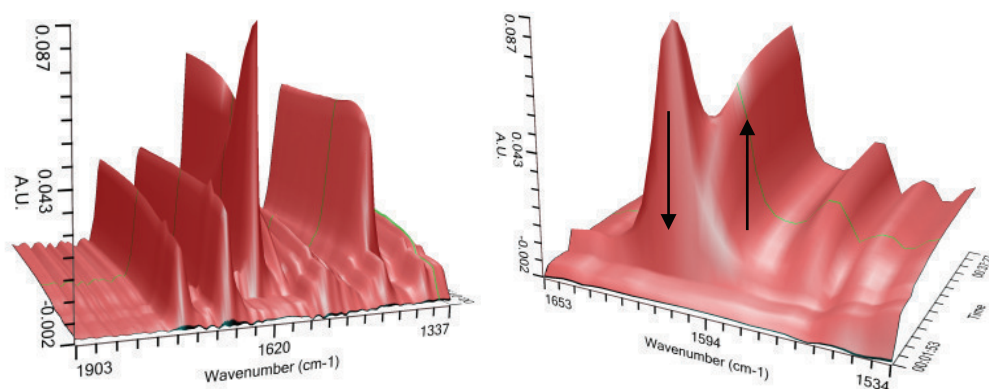


Figure 63: 3D plots on data acquired on ReactIR® for the formation of intermediate **II** (Scheme 90).

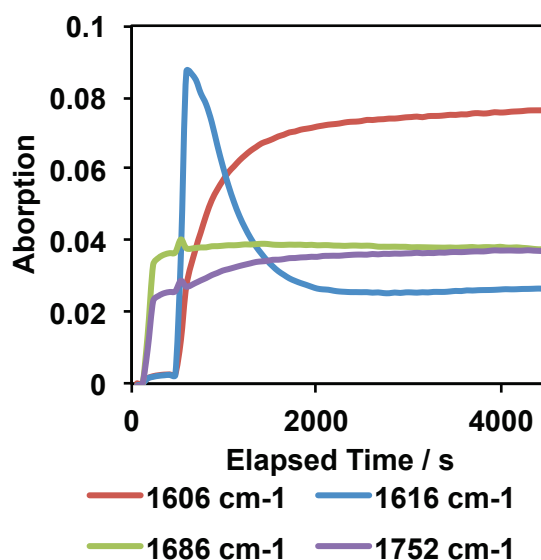


Figure 64: Kinetic curves for the reaction of tryptophan and Pd(OAc)₂, monitored by ReactIR®

Intermediate **II** proved to be unstable in solution for extended periods. Attempts to recrystallise the proposed intermediate, or obtain LIFDI-MS evidence, resulted in

formation of insoluble Pd^0 precipitate. It is thought that this arises from the rapid reductive elimination of AcOH . It was considered that the trifluoroacetate analogue might exhibit increased stability. The complexation of $\text{Pd}(\text{F}_3\text{CCOO})_2$ and tryptophan **213** was monitored by ^{19}F NMR spectroscopy. Immediate formation of a single new species was observed. However, this complex suffered from the same stability issues as **II**, and no further evidence was obtained. Complex **213** did not react with $\text{Pd}(\text{acac})_2$.

Attempts to isolate intermediate **III** proved inconclusive. **213** was dissolved in $\text{AcOH-}d_4$, and a ^1H NMR spectrum recorded. $\text{C}2\text{-}^1\text{H}$ is observed as a singlet at δ 7.08 ppm, coincident with an indole aromatic multiplet (2H). Overall, this multiplet was integrated as 3H with respect to an indole ^1H resonating at δ 7.34 ppm. It was thought that, on the addition of $\text{Pd}(\text{OAc})_2$, the cyclopalladated intermediate could be observed. However, a ^1H NMR spectrum recorded immediately after addition showed no change (Figure 65).

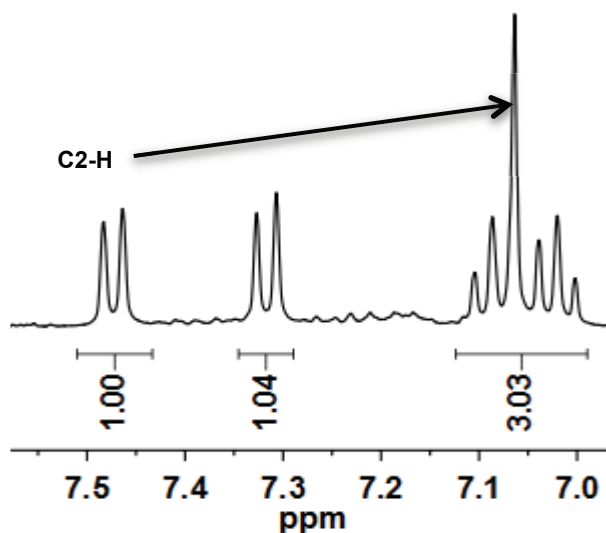
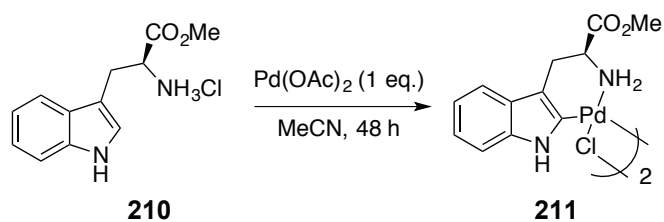


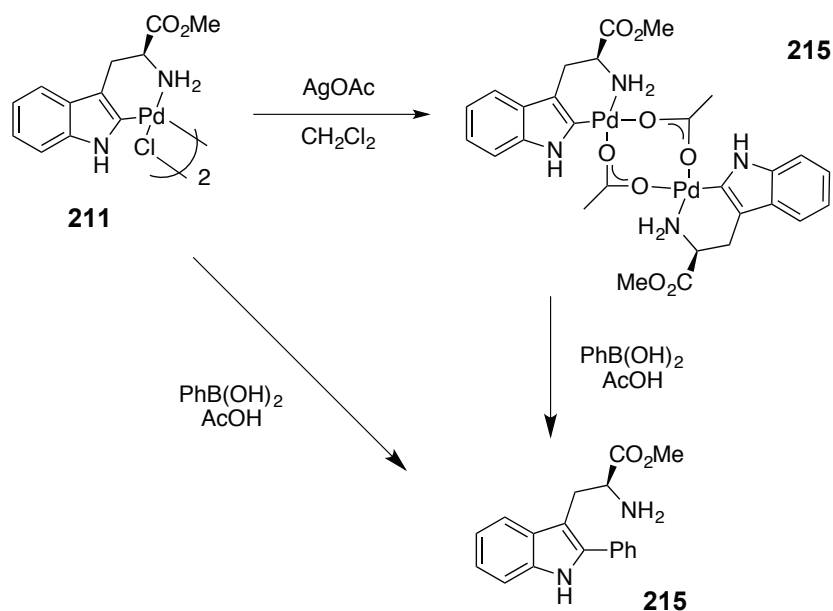
Figure 65: ^1H NMR (400 MHz, CD_3COOD) spectrum of tryptophan **213**, following the addition of $\text{Pd}(\text{OAc})_2$. Integration indicates no metallation has occurred at C2.

Since intermediate **III** could not be observed directly, it was proposed that it may be accessible using the methodology developed by Vicente and co-workers (*vide supra*) in stoichiometric cyclopalladations.²⁶² It was proposed that tryptophan **213** could be exposed to these conditions and, in the absence of a chloride anions, would form the acetate bridge complex. Unfortunately, only insoluble Pd^0 precipitate was obtained from this reaction.



Scheme 91: Synthesis of chloride-bridge complex **211**.

It was found that Vicente's cyclopalladated complex could be successfully synthesised in good yield (Scheme 91). It was anticipated that treatment of **211** with AgOAc would exchange the bridging chloride ligands for acetate groups, giving intermediate **III**. With this in hand, the reaction of this complex with $\text{PhB}(\text{OH})_2$ could then be studied.



Scheme 92: Proposed stoichiometric studies for the direct C-H bond functionalisation of tryptophan from chloride- and acetate-bridged complexes.

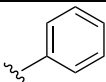
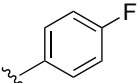
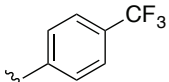
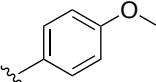
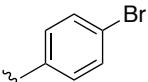
However, the ligand exchange did not proceed to give the desired product. Instead, a significant amount of Pd^0 precipitate was observed both under air and in an inert atmosphere. Therefore, as a model system complex **211** was subjected to $\text{PhB}(\text{OH})_2$ (10 eq.) for 16 h. After approximately 20 minutes, Pd^0 precipitate was observed in the reaction mixture. Crude ESI-MS indicated the starting material had been consumed and arylated product had been formed.

The reaction was found to be unreliable when performed under air μ different rates of stirring and changing the reaction vessel were found to have an effect on reaction efficacy. This was not observed when the reaction was performed under O_2 (1 atm). However, the addition of a substoichiometric quantity (10 mol%) of $Cu(OAc)_2$ increased the reliability of this reaction (with a 94% yield obtained of product **215**). Cu^{II} simply catalyses the oxidation process μ O_2 remains the terminal oxidant. Indeed, when the reaction is performed under an inert atmosphere (Ar), only 11% yield is obtained, which is equal to one turnover of Cu^{II} .

3.2.4 Organoboron Reagents

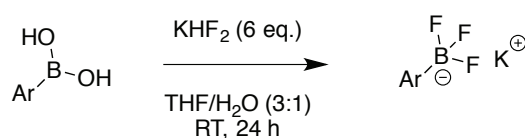
Mechanistic studies have, therefore, demonstrated that Method A for the direct C-H bond functionalisation of tryptophan may be mediated by a $Pd^{0/II}$ manifold rather than by $Pd^{III/IV}$. With this enhanced mechanistic knowledge, hypervalent iodide reagents could be removed from the method, and a 94% yield obtained for the reaction with $PhB(OH)_2$. Method development was then extended to variation of substituents on the phenyl group of the organoboronic acid. With the exception of **230** (entry 2), yields were poor (Table 13), and it appeared that substitution on the arylboronic acid was not tolerated by the current conditions. Performing the reaction under O_2 (1 atm) had no effect.

Table 13: Direct C-H bond functionalisation of tryptophan using $ArB(OH)_2$ (2 eq.) under air.

Entry	Compound	Ar	Yield / %
1	215		94
2	230		66
3	222		7 ^a
4	231		23 ^a
5	232		0

It was thought that C-H bond functionalisation could be competing with homocoupling of the aryl boronic acid. This process, oxidised by O₂, is a common side reaction in the Suzuki-Miyaura cross-coupling reaction, and has been extensively studied.^{275,280} This oxidation has been shown to be catalysed by Cu^{II} complexes, similar to the conditions proposed here.²⁸¹ Molander and co-workers have proposed aryltrifluoroborate potassium salts can be used as substitutes for traditional arylboronic acids in the Suzuki-Miyaura reaction, and do not suffer from many of the problems supposedly associated with arylboronic acids, including homocoupling.^{202,282,284} However, this is disputed by Lloyd-Jones and co-workers, who showed after significant mechanistic investigation that these compounds hydrolyse to give the boronic acid.²⁰³ The rate of this hydrolysis determines the amount of homocoupling that occurs. Nonetheless, these reagents have become popular and it was thought that they may be useful reagents for this direct C-H bond functionalisation.

A variety of aryltrifluoroborate potassium salts were synthesised using the method developed by Vedejs and co-workers (Scheme 93) in excellent yields (Table 14).²⁸⁵ It should be noted that since these compounds were prepared, Lloyd-Jones and co-workers have developed a much improved and milder methodology for the synthesis of these salts which does not involve the generation of HF.²⁸⁶ PhBF₃K was obtained commercially.



Scheme 93: Synthesis of potassium aryltrifluoroborate salts.

Table 14: Synthesis of potassium aryltrifluoroborates using the method of Vedejs.

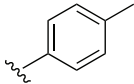
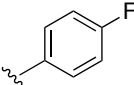
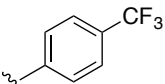
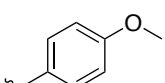
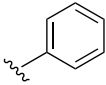
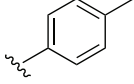
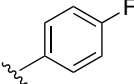
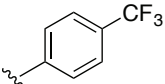
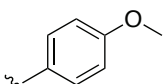
Entry	Compound	Ar	Yield / %
1	233		97
2	234		>99
3	235		93
4	236		75

Table 15: Direct C-H bond functionalisation of tryptophan using potassium aryltrifluoroborates. Trace is < 5% conversion observed by ¹H NMR spectroscopy.

Entry	Compound	Ar	Yield / %
1	215		60
2	221		56
3	230		21
4	222		Trace
5	231		Trace

Boronic *neo*-pentyl esters have been used in the Suzuki-Miyaura reaction, either as a protecting group (for selective functionalisation) or to inhibit homocoupling reactions. Boronic ester **237** was synthesised in excellent yield (94%). When applied to the C-H bond functionalisation reaction only 20% conversion was observed by ¹H NMR

spectroscopic analysis. Although low, this was better than the trace yield obtained using the analogous aryltrifluoroborate.

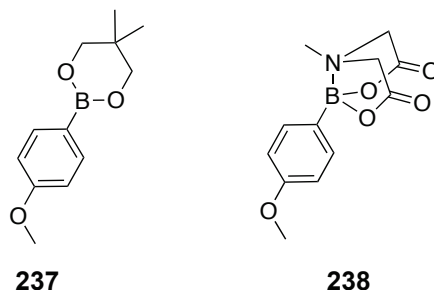


Figure 66: 4-Methoxyphenylboronic *neo*-pentyl ester and 4-methoxyphenylboronic boronic MIDA ester.

MIDA boronic esters, such as commercially available compound **238**, are used in a similar way. These organoboron reagents are highly resistant to homocoupling. However, this has a consequential impact on their reactivity. When applied to the C-H bond functionalisation reaction, no conversion to product was observed.

Varying the nature of the organoboron reagent had not increased product yield. Using reagents that inhibited homocoupling generally led to inhibited transmetalation with intermediate **II** (Scheme 90). Since it was hypothesised that non-productive consumption of boronic acid was depressing yield, increasing the stoichiometry of the boronic acid could lead to increased yields. With five equivalents of $\text{ArB}(\text{OH})_2$, generally good yields were obtained (Table 16).

Table 16: Direct C-H bond functionalisation of tryptophan using ArB(OH)_2 (5 eq.).

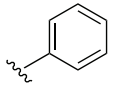
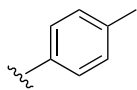
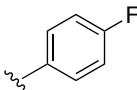
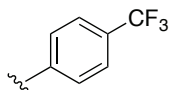
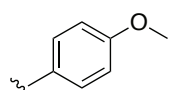
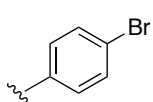
Entry	Compound	Ar	Yield %
1	215		93
2	221		88
3	230		79
4	222		58
5	231		28
6	239		0

Table 17: Direct C-H bond functionalisation of tryptophan using ArB(OH)_2 (5 eq.).

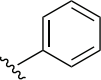
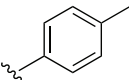
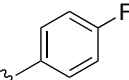
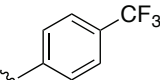
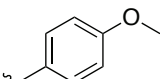
The reduced yields of the electron rich aryl boronic acid could be due to their increased propensity to form homocoupled products, which have been observed by HPLC (*vide infra*). The lack of reactivity of the 4-bromophenylboronic acid is likely due to poor solubility in AcOH.

3.2.5 Stereochemistry and X-Ray Crystallography

The stereochemistry of amino acids is important, particularly as residues in larger systems such as peptides (where molecular shape can affect biological functionality, with respect to enzymes and proteins) or, more fundamentally, proteins (where stereochemistry helps define secondary, tertiary and quaternary structure). Therefore, it is essential that any modification strategy must result not in racemisation.

To assess this for the C-H bond functionalisation reaction, $[\alpha]_D$ measurements were recorded for the synthesised analogues. They were found to be non-zero, and in agreement with the literature values (Table 18).

Table 18: $[\alpha]_D$ values for tryptophan analogues, as compared to literature values.

Entry	Ar	Found $[\alpha]_D^\circ$ (conc)	Lit. $[\alpha]_D^\circ$ (conc)
1		47.3 (0.11)	48.3 (0.13) ²⁶³
2		54.4 (0.10)	47.6 (0.15) ²⁶³
3		59.1 (0.10)	38.2 (0.65) ²⁸⁷
4		62.0 (0.13)	47.2 (0.13) ²⁶³
5		34.9 (0.10)	37.5 (0.16) ²⁶³

Racemic protected starting material was synthesised from DL-tryptophan in excellent overall yield. Using chiral HPLC, it was determined that the racemate had an enantiomeric ratio of 52.1:47.9 (the error in the measurement is therefore *ca.* 5%). Both the racemate and an enantiopure sample (er 99.9:0.1 by HPLC) were functionalised, and the products analysed by chiral HPLC (Figure 67). No racemisation was found to occur μ the product obtained from enantiopure starting material had an enantiomeric ratio of 99.9:0.1.

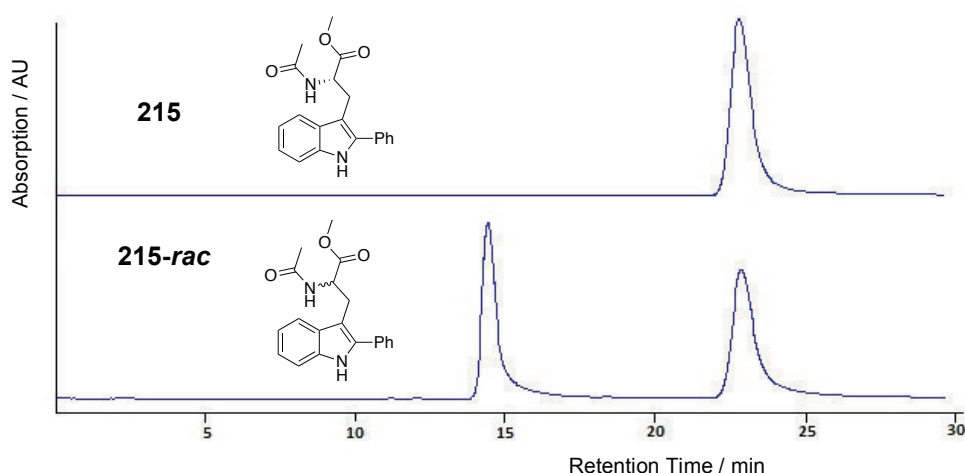
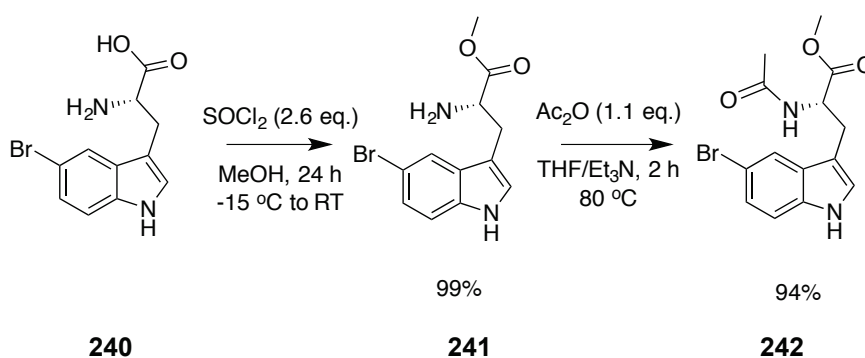


Figure 67: Chiral HPLC traces of product as compared to known racemate.

X-ray crystal structures have been obtained for 4- $\text{CF}_3\text{C}_6\text{H}_4$ - and 4- FC_6H_4 - analogues (Figures 68-69). However, absolute configuration of stereochemistry could not be obtained from these two structures as they lack a heavy atom, such as Br. Attempts to introduce a Br proved unsuccessful. Functionalisation with 4- $\text{BrC}_6\text{H}_4\text{B}(\text{OH})_2$ had failed due to lack of solubility in AcOH. Increasing to ten equivalents of the aryl boronic acid had no effect. 5-Bromotryptophan was obtained from Dr. Rebecca Goss (University of East Anglia, now St. Andrews), and protected (Scheme 94) in excellent overall yield (98%). However, only trace product was obtained when the C-H bond functionalisation conditions applied. Running the reaction under O_2 (1 atm) had no effect.



Scheme 94: Protection of 5-bromotryptophan.

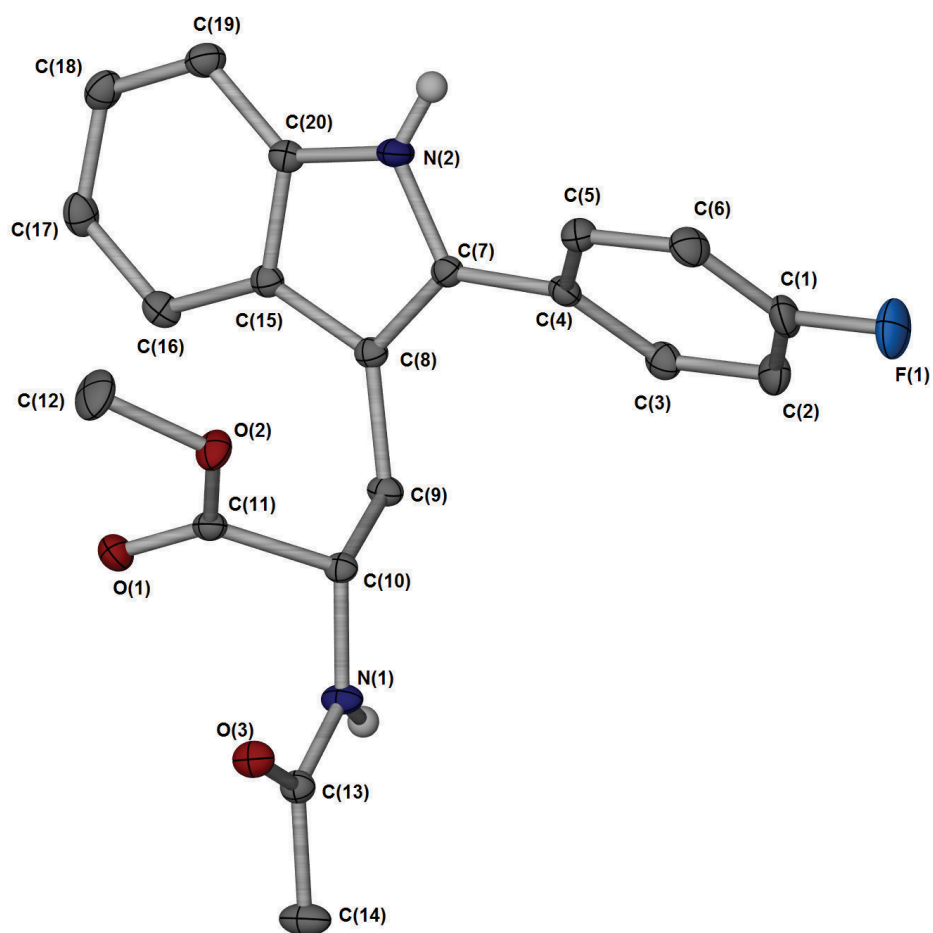


Figure 68: 4-FC₆H₄-functionalised analogue of tryptophan, **230**. Hydrogen atoms have been removed for clarity. Thermal ellipsoids shown at 50%. Selected bond lengths (Å) and torsion angles (°): (F(1)-C(1) = 1.3600(18), N(2)-C(7)-C(4)-C(3) = 135.53(15).

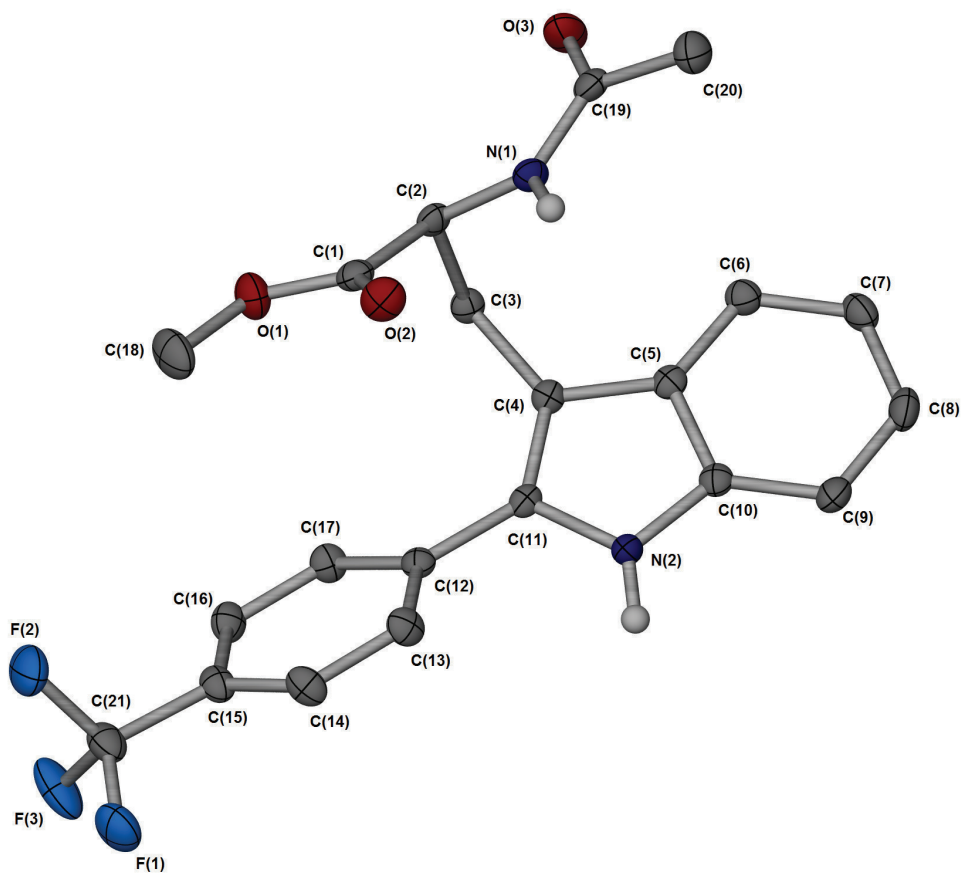


Figure 69: 4-F₃CC₆H₄-functionalised analogue of tryptophan, **222**. Hydrogen atoms have been removed for clarity. Thermal ellipsoids shown at 50%. Selected bond lengths (Å) and torsion angles (°): F(1)-C(21) 1.340(3), N(2)-C(11)-C(12)-C(17) 142.1(2)..

3.2.5 UV-Visible and Fluorescence of 2-Aryltryptophan Analogues

UV-Vis spectra were recorded for the unsubstituted tryptophan starting material and each of the synthesised analogues. Overlaid examples of spectra are shown in Figure 70 (complete spectra available in Appendix B). The λ_{\max} of the analogues are shifted with respect to the unsubstituted starting material. All of the analogues have points at which they absorb where the unsubstituted tryptophan does not μ this is encouraging for the intended use, as it is important to be able to selectively excite the analogues without exciting unlabelled tryptophan residues.

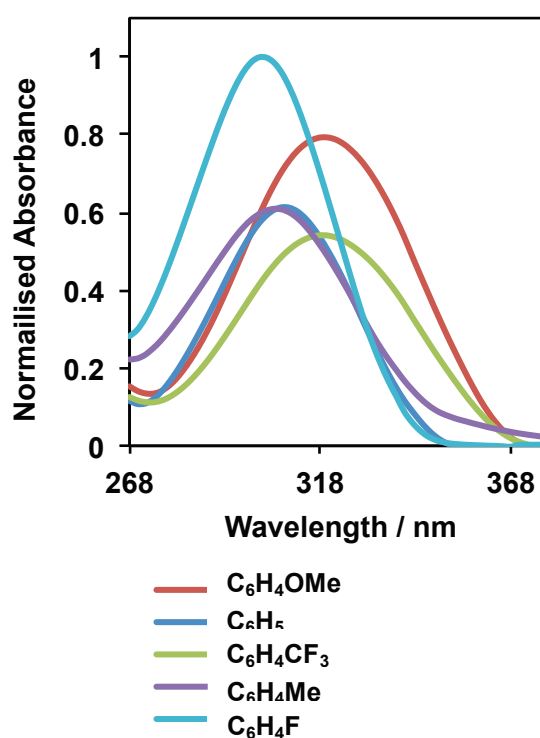
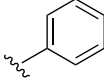
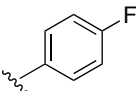
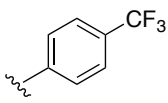
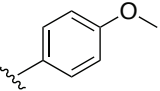
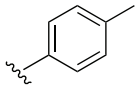
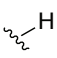


Figure 70: Comparative UV-Visible λ_{\max} , normalised with respect to C_6H_4F - analogue.

The absorbance of a compound is related to its concentration by the Beer-Lambert Law.²⁸⁸ Using this law, the molar absorption coefficients can be calculated for each analogue (Table 19). All the analogues have molar absorption coefficients of similar magnitude. All are higher than that recorded for the unsubstituted tryptophan, and the C_6H_4F analogue has the highest. This suggests it absorbs most strongly of these analogues.

Table 19: Molar absorption coefficients for tryptophan analogues, as compared to unsubstituted tryptophan starting material. ϵ given at λ_{\max} .

Entry	Compound	Ar	λ_{\max} / nm	ϵ / $\text{cm}^{-1} \text{mol}^{-1} \text{dm}^{-3}$
1	215		308	9120
2	230		306	14684
3	222		318	10297
4	231		320	11644
5	221		310	8893
6	213		282	5804

The λ_{\max} of the analogues were plotted against their σ_p Hammett parameters (Figure 71). The analogues were bathochromically (red) shifted with respect to the unsubstituted tryptophan (as indicated by the red dashed line). The most electronically extreme analogues (both electron-withdrawing and electron-donating) have the most shifted absorptions, generating a characteristic V-shape. This pattern has been observed by Marder and co-workers in 1,4-bis(*p*-R-phenylethynyl)benzenes and 2,5-bis(phenylethynyl) thiophenes.^{289,290} It was proposed by Marder that electron-donating substituents increase HOMO energy further with respect to LUMO. Conversely, electron-withdrawing substitutes decrease LUMO energy further with respect to the HOMO. Both these processes result in a lower HOMO-LUMO energy gap, and a bathochromically shifted absorption.

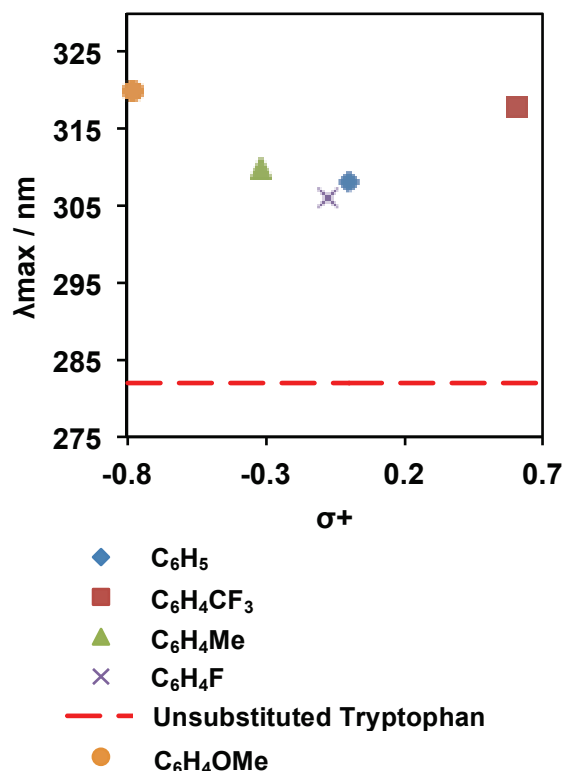


Figure 71: Absorption maxima (nm) of tryptophan analogues plotted against Hammett parameters (σ^+), and compared to the unsubstituted tryptophan.

Fluorescence spectra were similarly recorded (Figure 72). Fluorescence typically occurs when an excited state (S_1) returns to the ground state (S_0) by the emission of a photon. In DMSO solution, the substituted tryptophan compounds were excited by irradiation with light at the UV-Visible maximum. The emission maxima are bathchromically shifted from the parent tryptophan, unsubstituted compound. This was typically a shift of *ca.* 30 nm. However, unexpectedly the $\text{C}_6\text{H}_4\text{F}$ substituted tryptophan recorded an emission maximum of 416 nm.

The Stokes shift is defined as the difference in wavelength between the excitation maximum (*i.e.* the absorption maximum) and the emission maximum. This can be plotted against the Hammett parameters (Figure 73). $\text{C}_6\text{H}_4\text{F}$ is clearly shown to be a furthest shifted with respect to the other analogues.

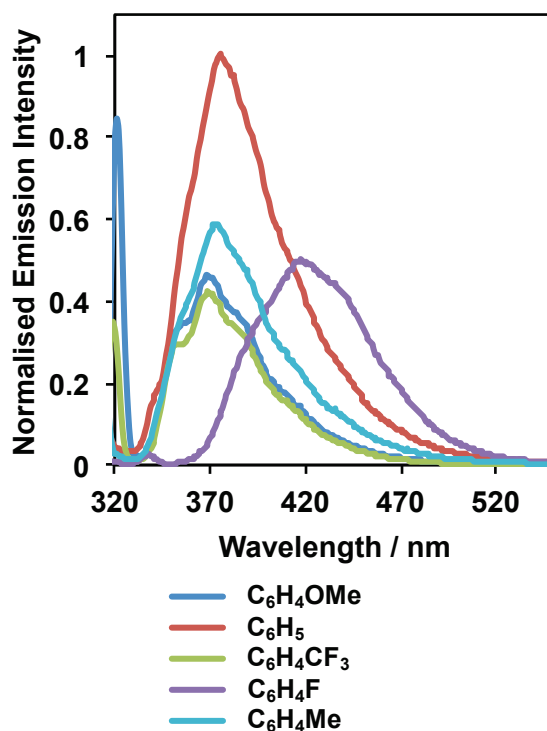


Figure 72: Comparative fluorescence λ_{\max} , normalised with respect to C₆H₅- analogue.

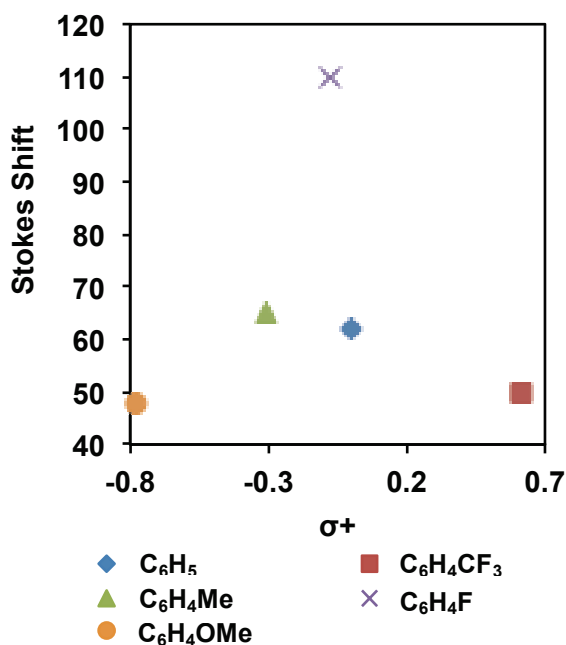


Figure 73: Stokes shift of tryptophan analogues plotted against Hammett parameters (σ^+), and compared to the unsubstituted tryptophan.

The relative intensity of emission maxima were recorded on the same instrument at different concentrations for each compound. Since this instrument was not appropriately calibrated, this can not be used as a general method to quantify emissivity (which would be most accurately done by recording quantum yields μ see Future Work section, Chapter 4, Section 4.2.2), however it allows us to directly compare these analogues. Linear regression was used to calculate a gradient coefficient, which was used to normalise the emission maxima with respect to the most emissive compound (set at 1 arbitrary unit). This is shown in Figure 72. The substituted compounds are greater than 10 times more emissive than tryptophan itself.

When these normalised intensities are plotted against σ_P Hammett parameters (Figure 74), The Ph analogue is considerably more emissive than the 4-substituted aromatic analogues.

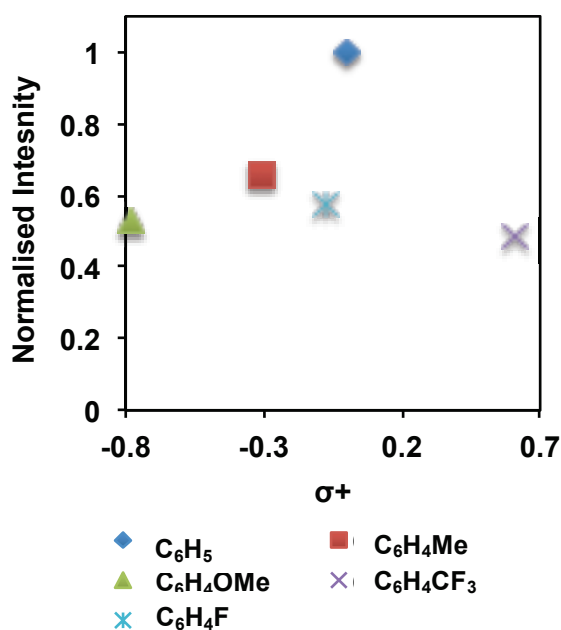
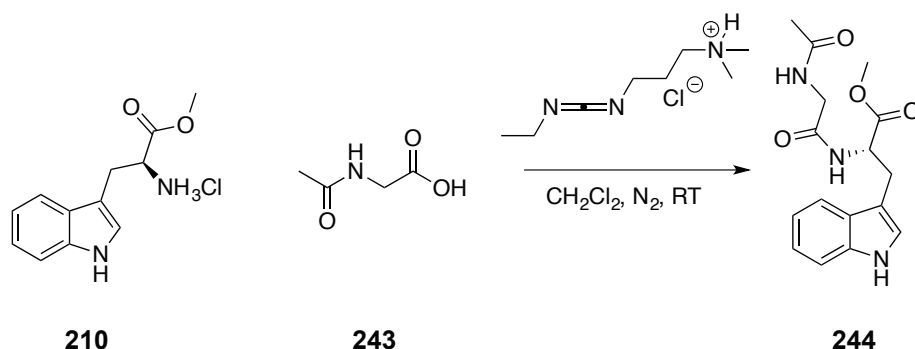


Figure 74: Relative intensity of emission maxima (nm) of tryptophan analogues plotted against Hammett parameters (σ^+).

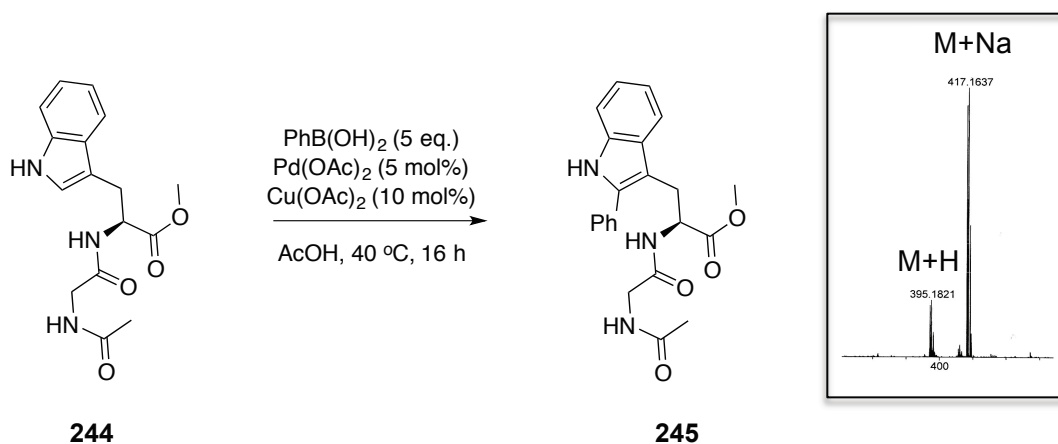
3.2.6 Peptides

Designed as a simple extension of the protected tryptophan used above, compound **240** was synthesised by a traditional carbodiimide-mediated solution-phase peptide

coupling methodology (Scheme 95). Glycine **243** was chosen as a second amino acid as, although it would increase the molecular weight of the system (and hence the possibility of non-specific peptide binding to the metal catalysts), it did not introduce significantly different, and complicating, chemical functionality.



Scheme 95: Synthesis of **244** using EDC.HCl (WSC).



Scheme 96: Direct C-H bond functionalisation of **244**. Inset: ESI-MS signals of product.

The dipeptide was subjected to the C-H bond functionalisation conditions. ESI-MS indicated the presence of product (Scheme 96, inset). Analysis of the reaction mixture by HPLC showed complete conversion of starting material to product (Figure 75). Also present in the reaction mixture (as identified by comparison to an authentic sample) was biphenyl.

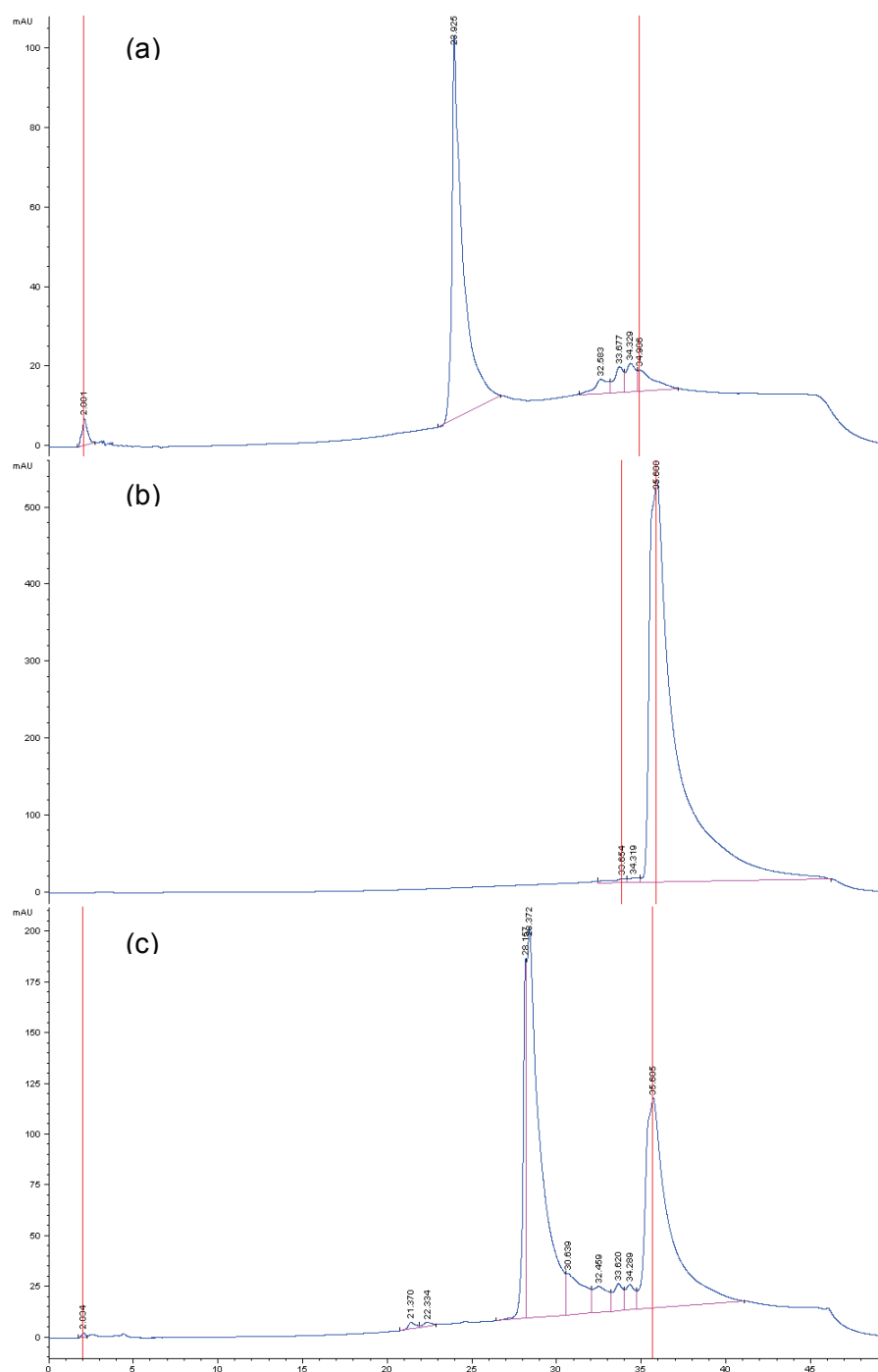
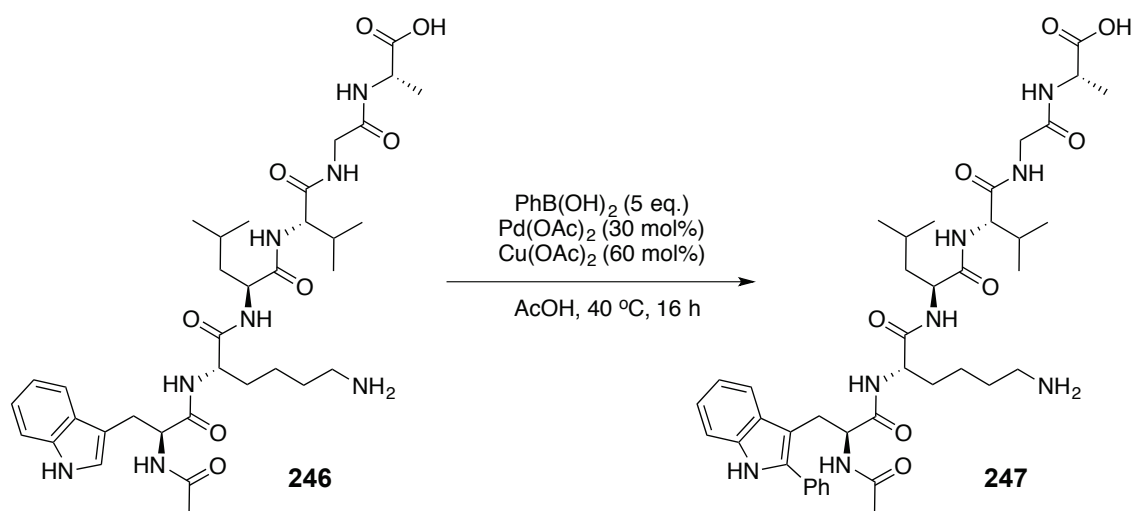


Figure 75: Stacked HPLC data for the C-H bond functionalisation of dipeptide **244**; (a) dipeptide **244**, (b) biphenyl (Sigma-Aldrich®), (c) reaction mixture of C-H bond functionalisation reaction.



Scheme 97: Direct C-H bond functionalisation of peptide **246**.

Longer chained peptides were obtained commercially from GeneCust Europe (Laboratoire de Biotechnologie du Luxembourg S.A.). Peptide **246** was subjected to the C-H bond functionalisation condition (Scheme 97). Higher loadings of Pd(OAc)_2 and Cu(OAc)_2 (to 30 mol% and 60 mol%, respectively) were required to obtain functionalisation. It was proposed that this resulted from the non-specific binding of Pd and Cu by the peptide. The reaction mixture was analysed by HPLC-MS (Figure 76). A conversion to product of 86% was observed (starting material, 14%).

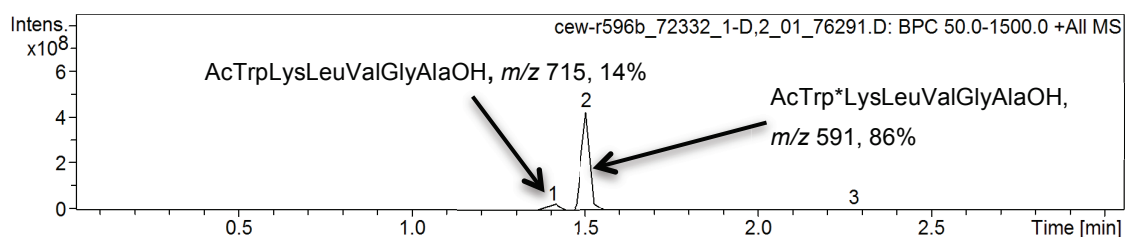


Figure 76: HPLC-MS BPC of the direct C-H bond functionalisation of peptide **246**.

ESI-MS-MS was used to demonstrate that functionalisation had occurred on the tryptophan (spectrum shown in Figure 78). The molecular ion (m/z 791.8) was selected. Ions from fragmentations at amide bonds were identified, the structural evidence for which are shown in Figure 77. Fragment m/z 305 was identified as the phenylated tryptophan residue.

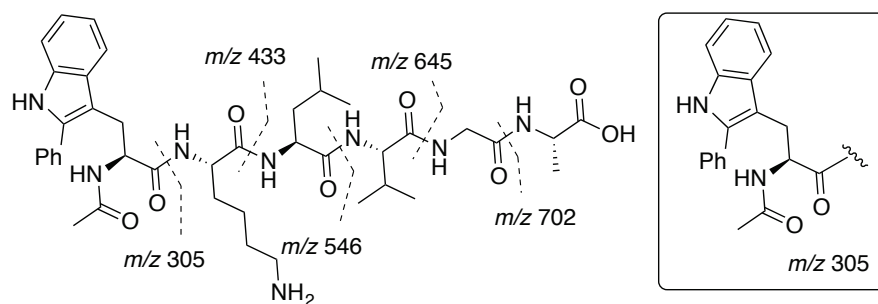


Figure 77: Direct C-H bond functionalisation of peptide **246**.

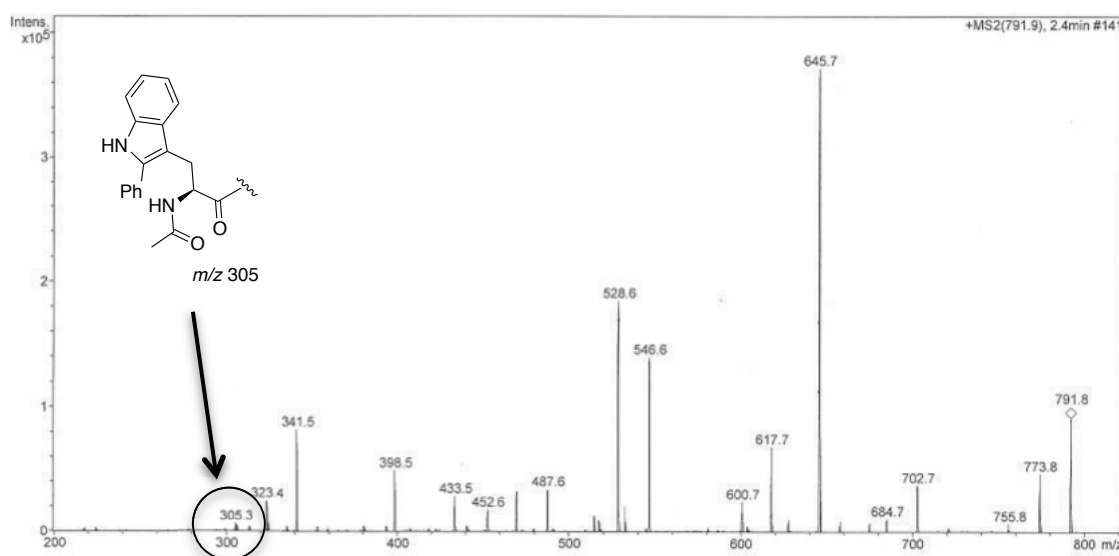
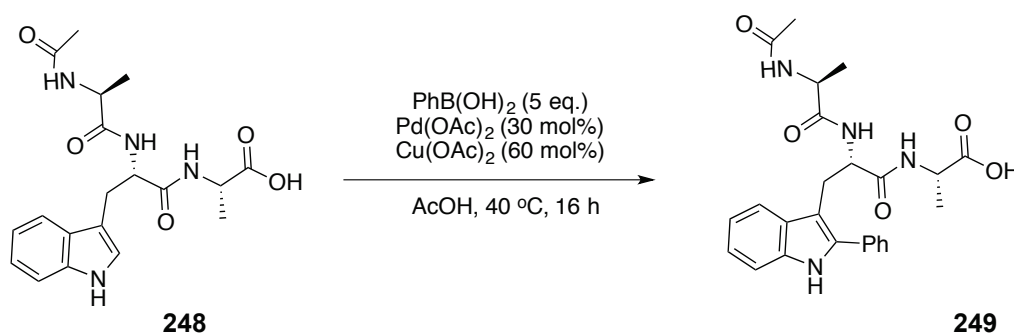


Figure 78: ESI-MS-MS spectrum of the reaction mixture of the C-H bond functionalisation of peptide **246**, selected for m/z 791 ($[M+H]^+$ ion). Ion arising from phenyltryptophan residue is highlighted.



Scheme 98: Direct C-H bond functionalisation of peptide **248**.

When tripeptide **248** was subjected to the same conditions (Scheme 98), complete consumption of starting material was observed. By HPLC-MS (Figure 80), there was a

54% conversion to arylated product. Also observed was a peak with m/z corresponding to a diarylation product (this is the first time such a product has been observed). Two other products with identical masses were also identified as dihydroxylation products μ the position of the hydroxyls in each product is currently unknown, although purification and high field NMR studies are being carried out by another member of the Fairlamb research group. It is most likely that the phenyl group has been oxidised, and 3- and 4-hydroxylated products are tentatively proposed. Cu^{I} and Cu^{II} complexes play an important role in many oxidation processes, including as enzymatic co-factors.^{291,292} Extensive work by Karlin and co-workers has shown that $\text{Cu}^{\text{II}}\text{-O-O-Cu}^{\text{II}}$ species can oxidise C-H bonds.²⁹² Furthermore, it is clear that Cu^{II} can bond *via* the terminal oxygen of a carboxylic acid terminated peptide sequence. For example, Costa-Filho and co-workers have demonstrated that TrpGly Cu^{II} complexes can be synthesised and isolated. X-ray diffraction studies indicate that the Cu^{II} centre can be brought in close proximity to an adjacent tryptophan residue (Figure 79).²⁹³ It is notable that peptides which exhibit the dihydroxylation products in this thesis (*vide infra*) contain a tryptophan adjacent to the terminal residue whilst these products are not observed in other positions.

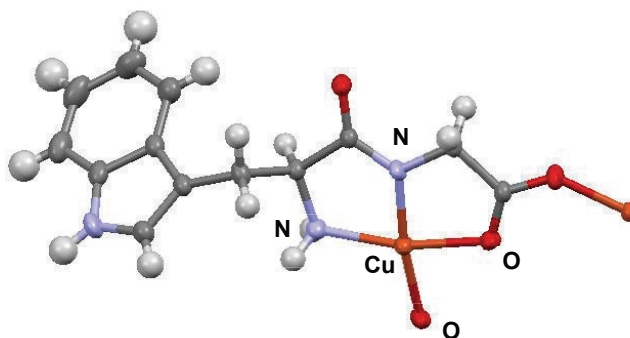


Figure 79: TryGlyOH Cu^{II} complex (coordination polymer), isolated by Costa-Filho and co-workers.²⁹³

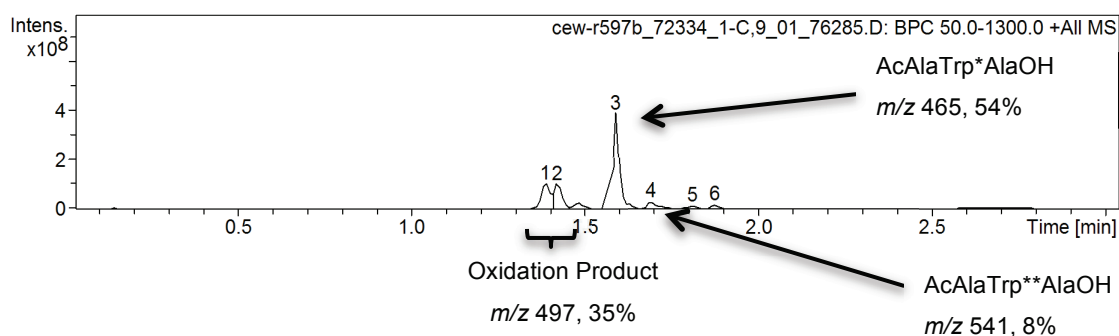
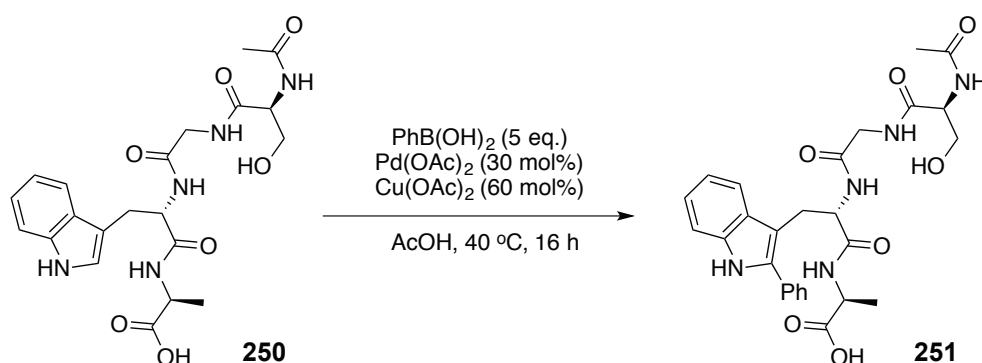


Figure 80: HPLC-MS BPC of the direct C-H bond functionalisation of peptide **248**.



Scheme 99: Direct C-H bond functionalisation of peptide **250**.

Similar results were observed with peptide **250** (Scheme 99). The starting material was completely consumed. Arylated product was observed in 42% conversion (Figure 81). No diarylation product was observed, although large quantities of dioxidation products were observed.

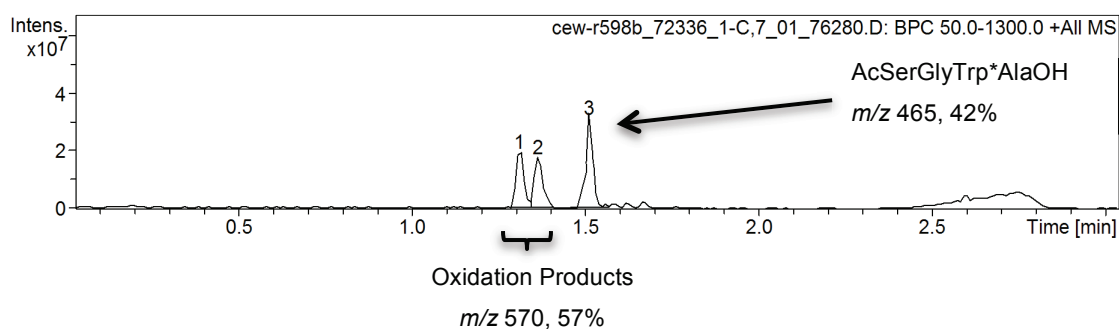


Figure 81: HPLC-MS BPC of the direct C-H bond functionalisation of peptide **250**.

3.3 Experimental

3.3.1 General Information

General information as detailed in Chapter 2, page 83.

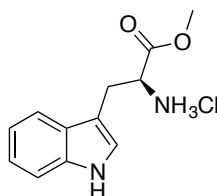
Where indicated, reactions were monitored *in situ* using a Mettler Toledo ReactIR μ ic10 with K6 conduit SiComp (silicon) probe and MCT detector. Resolution 4 cm^{-1} , range 4000-650 cm^{-1} and gain adjustment at 1x.

Peptide HPLC-MS was performed on a Bruker® HCTultra at the University of Leeds.

Chiral stationary phase HPLC was performed with a multiple wavelength, UV-vis diode array detector; integration was performed at 210, 230, and 250 nm. Optical rotations were recorded at 20 °C (using the sodium D line; 259 nm), and $[\alpha]_{\text{D}}$ values are given in units of $10^{-1} \text{ deg cm}^3 \text{ g}^{-1}$.

3.3.2 Synthesis of Protected Amino Acid Residues

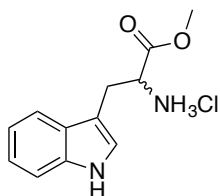
Methyl (2R)-2-amino-3-(1H-indol-3-yl)propionate, 210



To a Schlenk tube under N_2 was added dry MeOH (50 mL). Thionyl chloride (7.04g, 59 mmol, 4.3 mL, 2.4 eq.) was added dropwise at $-15\text{ }^\circ\text{C}$. Tryptophan (5 g, 24.5 mmol, 1 eq.) was then added in three portions, resulting in a white suspension. The reaction mixture was warmed to ambient temperature and stirred for 24 h. During this time, an orange solution was formed. Water (5 mL) was added to the reaction mixture, and the solvent removed under reduced pressure to give product as an off-white solid (2.027 g, 97%).

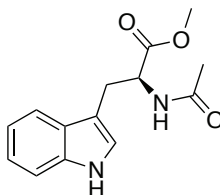
MP $211\text{ }^\circ\text{C}$ (lit. $214\text{ }^\circ\text{C}$, decomp.)²⁹⁴; ^1H NMR (400 MHz, $(\text{CD}_3)_2\text{SO}$) δ 11.11 (s, 1H), 8.55 (s, 3H), 7.50 (d, $J = 8.0$ Hz, 1H), 7.37 (dt, $J = 8.0, 1.0$ Hz, 1H), 7.24 (d, $J = 2.5$ Hz, 1H), 7.09 (ddd, $J = 8.0, 7.0, 1.0$ Hz, 1H), 7.01 (ddd, $J = 8.0, 7.0, 1.0$ Hz, 1H), 4.28 μ 4.17(m, 1H), 3.66 (s, 3H), 3.33 μ 3.26 (m, 2H); ^{13}C NMR (101 MHz, $(\text{CD}_3)_2\text{SO}$) δ 170.0, 136.2, 126.9, 125.0, 121.2, 118.6, 118.0, 111.6, 106.5, 52.8, 52.6, 26.3; ESI-MS m/z 219 [M+H], 241 [M+K]; ESI-HRMS m/z 219.1136 [M+H] (calc. for $\text{C}_{12}\text{H}_{14}\text{N}_2\text{O}_2$ 219.1128); IR (solid-state ATR, cm^{-1}) 1747, 1549, 1501, 1437, 1284, 1229, 1210, 1108, 1074, 1007, 730.0.

Methyl (2RS)-2-amino-3-(1H-indol-3-yl)propionate, 210-rac



The racemate was prepared from DL-tryptophan using the method outlined for **210**. Product was obtained as a white solid (5.72 g, 92%).

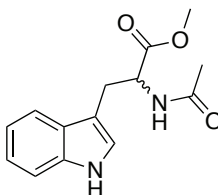
The analytical data was identical to that reported for **210**.

Methyl (2R)-2-acetylamino-3-(1H-indol-3-yl)propionate, 213

To a three-necked round-bottomed flask fitted with a reflux condenser and purged with N_2 , was added methyl (2*R*)-2-amino-3-(1*H*-indol-3-yl)propanoate (300 mg, 1.38 mmol, 1 eq.). To this was added dry THF (15 mL) and triethylamine (0.2 mL). The mixture was stirred to give a white suspension. The mixture was cooled to 0 °C, and acetic anhydride (143 μ l, 154 mg, 1.51 mmol, 1.1 eq.) added in one portion. The reaction was then stirred for 2 h at 80 °C to give a white suspension. This was added to water (40 mL) and extracted into EtOAc (3 x 50 mL). The organic layers were combined and washed sequentially with 1 M aq. HCl (1 x 40 mL), sat. aq. $NaHCO_3$ (40 mL) and brine (1 x 40 mL). The organic layer was collected and dried over $MgSO_4$, filtered and the solvent removed under reduced pressure to give colourless oil. Trituration with Et_2O resulted in product as an off-white solid (327 mg, 91%, *er* 99.9:1 by HPLC).

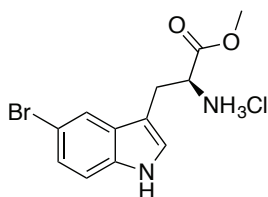
$[\alpha]_D = +52.5$ (*c* 0.11, $CHCl_3$); MP 156 μ 157 °C (lit. 155 μ 156 °C)²⁶⁴; 1H NMR (400 MHz, $CDCl_3$) δ 8.07 (s, 1H), 7.52 (dq, *J* = 8.0, 1.0 Hz, 1H), 7.36 (dt, *J* = 8.0, 1.0 Hz, 1H), 7.19 (ddd, 8.2, 7.0, 1.0 Hz, 1H), 7.11 (ddd, *J* = 8.2, 7.0, 1.0 Hz, 1H), 6.97 (d, *J* = 2.4 Hz, 1H), 5.96 (d, *J* = 8.0 Hz, 1H), 4.95 (dt, *J* = 8.0, 5.2 Hz, 1H), 3.69 (s, 3H), 3.35 (ddd, *J* = 15.0, 5.2 Hz, 0.8, 1H), 3.29 (ddd, *J* = 15.0, 5.2, 0.8 Hz, 1H), 1.95 (s, 3H); ^{13}C NMR (101 MHz, $CDCl_3$) δ 172.5, 169.8, 136.3, 127.8, 122.7, 122.4, 119.7, 118.7, 111.4, 110.2, 53.1, 52.5, 27.7, 23.4; ESI-MS *m/z* 261 [M+H], 283 [M+K]; ESI-HRMS *m/z* 261.1234 [M+H] (calc. for $C_{14}H_{17}N_2O_3$ 261.1234); IR (solid-state ATR, cm^{-1}) 3404, 3317, 1732, 1660, 1521, 1434, 1434, 1221, 848, 747; UV-Vis (DMSO, nm) λ_{max} 282 (ϵ = 5804 mol dm^{-3} cm^{-1}).

Methyl (2RS)-2-acetylamino-3-(1H-indol-3-yl)propionate, 213-rac



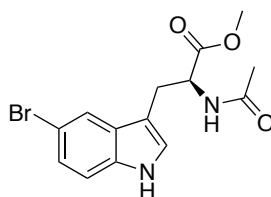
The racemate was prepared from methyl (2*RS*)-2-amino-3-(1*H*-indol-3-yl)propionate using the method outlined for **213**. Product was obtained as a white solid (6.3 g, 83%, *er* 52.1:47.9 by HPLC).

$[\alpha]_D = +0.353$ (*c* 0.11, CHCl₃). The remaining data analytical data was identical to that reported for **213**.

Methyl (2R)-2-amino-3-(1H-5-bromoindol-3-yl)propionate, 241

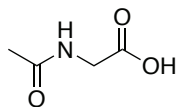
To a Schlenk tube under N₂ was added dry MeOH (2 mL). Thionyl chloride (93 mg, 0.785 mmol, 57 μl) was added dropwise at -15 °C. 5-Bromotryptophan (52 mg, 0.166 mmol) was then added in three equal portions, resulting in a white suspension. The reaction mixture was warmed to ambient temperature and stirred for 24 h. During this time, a red solution was formed. Water (5 mL) was added to the reaction mixture, and the solvent removed under reduced pressure to give product as a pink solid (55 mg, 99%).

¹H NMR (400 MHz, CD₃OD) δ 10.85 (s, 1H), 7.66 (d, *J* = 1.8 Hz, 1H), 7.30 (d, *J* = 8.6 Hz, 1H), 7.23 μ 7.18 (m, 2H), 4.30 (t, *J* = 6.4 Hz, 1H), 3.78 (s, 3H), 3.38 (dd, *J* = 18.0, 6.4 Hz, 2H); ¹³C NMR (101 MHz, CD₃OD) δ 169.4, 135.7, 128.7, 126.0, 124.3, 120.3, 113.1, 112.2, 106.0, 53.2, 52.4, 25.9; ESI-MS *m/z* (%) 297 (99) [⁷⁹BrM-Cl], 399 (100) [⁸¹BrM-Cl]; ESI-HRMS *m/z* 297.0243 [⁷⁹BrM-Cl] (calc. for C₁₂H₁₄BrN₂O₂ 297.0243).

Methyl (2R)-2-acetylamino-3-(1H-5-bromoindol-3-yl)propionate, 242

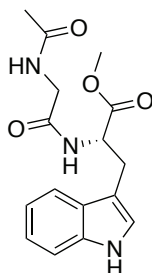
To a three-necked round-bottomed flask fitted with a reflux condenser, purged with N₂, was added methyl (2*R*)-2-amino-3-(1*H*-5-bromoindol-3-yl)propanoate (55 mg, 0.166 mmol). To this was added dry THF (10 mL) and triethylamine (0.125 mL). The mixture was stirred to give a pink suspension. The mixture was cooled to 0 °C, and acetic anhydride (19 mg, 0.183 mmol, 17.2 μl) added in one portion. The reaction was then stirred for 2 h at 80 °C to give a yellow solution. This was added to water (20 mL) and extracted into EtOAc (3 x 20 mL). The organic layers were combined and washed sequentially with 1 M aq. HCl (10 mL), sat. aq. NaHCO₃ (10 mL) and brine (10 mL). The organic layer was collected and dried over MgSO₄, filtered and the solvent removed under reduced pressure to give product as brown oil (52.9 mg, 94%).

¹H NMR (400 MHz, CDCl₃) δ 8.63 (s, 1H), 7.62 (d, *J* = 1.8 Hz, 1H), 7.24 (dd, *J* = 8.6, 1.8 Hz, 1H), 7.20 (d, *J* = 8.6 Hz, 1H), 6.95 (d, *J* = 2.2 Hz, 1H), 6.15 (d, *J* = 7.8 Hz, 1H), 4.91 (dt, *J* = 7.8, 5.2 Hz, 1H), 3.70 (s, 3H), 3.29 (dd, *J* = 14.8, 5.2 Hz, 1H), 3.22 (dd, *J* = 14.8, 5.2 Hz, 1H), 1.98 (s, 3H); ¹³C NMR (101 MHz, CDCl₃) δ 170.0, 134.9, 129.5, 125.1, 125.0, 124.2, 121.3, 113.0, 109.7, 53.1, 52.6, 27.6, 23.3, 23.3; ESI-MS *m/z* (%) 339 (13) [⁷⁹BrM+H], 361 (100) [⁸¹BrM+H], [⁷⁹BrM+Na], 363 (88) [⁸¹BrM+Na]; ESI-HRMS *m/z* 339.0356 [⁷⁹BrM+H] (calc. for C₁₄H₁₆BrN₂O₃ 339.0339).

N-Acetylglycine, 243

To a round-bottomed flask was added glycine (5 g, 66.6 mmol, 1 eq.) and water (150 mL). To this, acetic anhydride (20.4 g, 200 mmol, 18.9 mL, 3 eq.) was added dropwise and the reaction mixture was stirred at ambient temperature for 1 h. The mixture was then cooled to 4 °C for 16 h, and the resulting precipitate collected by filtration through a sintered funnel to give product as a white solid (4.46 g, 57%).

MP 207 μ 208 °C (decomp., lit. 206 μ 208 °C)²⁹⁵; ¹H NMR (400 MHz, (CD₃)₂SO) δ 12.51 (s, 1H), 8.18 (s, 1H), 3.71 (d, *J* = 6.0 Hz, 2H), 1.84 (s, 3H); ¹³C NMR (101 MHz, (CD₃)₂SO) δ 171.5, 169.6, 40.6, 22.3; ESI-MS *m/z* 118 [M+H], 140 [M+Na]; ESI-HRMS *m/z* 118.0501 [M+H] (calc. for C₄H₈NO₃ 118.0499); IR (solid-state ATR, cm⁻¹) 3350, 1944, 1897, 1717, 1580, 1547, 1439, 1379, 1351, 1276, 1227, 1137, 993, 902. 682.

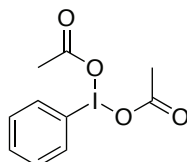
AcNGlyTrpOMe, 240

To a Schlenk tube was added methyl (2*R*)-2-amino-3-(1*H*-indol-3-yl)propionate (190 mg, 0.872 mmol, 1 eq.), *N*-acetylglycine (102 mg, 0.872 mmol, 1 eq.) and 1-ethyl-3-(3-dimethylaminopropyl)carbodiimide hydrochloride (167 mg, 0.872 mmol, 1 eq.). The reaction mixture was placed under vacuum and refilled with N₂, and this process repeated twice. Dry CH₂Cl₂ (5 mL) was added, and the mixture stirred for 16 h at ambient temperature. The solvent was removed under reduced pressure. The resulting residue was dissolved in EtOAc (15 mL) and washed with 1 M aq. HCl (20 mL), sat. aq. NaHCO₃ (40 mL) and brine (1 x 40 mL). The organic layer was collected and dried over MgSO₄, filtered and the solvent removed under reduced pressure to give product as a white solid (96 mg, 35%).

MP 98 μ 102 °C; ¹H NMR (400 MHz, CD₃OD) δ 7.48 (dt, *J* = 8.0, 1.0 Hz, 1H), 7.31 (dt, *J* = 8.0, 1.0 Hz, 1H), 7.10 μ 7.04 (m, 3H), 7.00 (ddd, *J* = 8.0, 7.0, 1.0 Hz, 1H), 4.73 (dd, *J* = 7.0, 5.8 Hz, 1H), 3.83 (d, *J* = 16.6, 1H), 3.78 (d, *J* = 16.6 Hz, 1H), 3.64 (s, 3H), 3.27 (ddd, *J* = 14.6, 7.2, 0.6 Hz, 1H), 3.19 (ddd, *J* = 14.6, 7.2, 0.6 Hz, 1H), 1.92 (s, 3H); ¹³C NMR (101 MHz, CD₃OD) δ 173.9, 173.7, 171.4, 138.0, 128.7, 124.6, 122.5, 119.9, 119.1, 112.3, 110.3, 54.8, 52.7, 49.0, 43.4, 28.4; ESI-MS *m/z* 318 [M+H], 340 [M+Na]; ESI-HRMS *m/z* 318.1433 [M+H] (calc. for C₁₆H₂₀N₃O₄ 318.1448); IR (solid-state ATR, cm⁻¹) 3286, 2947, 1737, 1655, 1610, 1508, 1460, 1439, 1372, 1285, 1248, 1215, 1177, 1030.

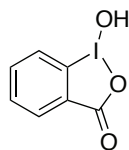
3.3.3 Synthesis of Hypervalent Iodine Compounds

Bis(acetyloxy)phenyl- λ^3 -iodane (Diacetoxiodobenzene/DIB), 107^{259,296}



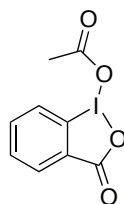
To a three-necked round-bottomed flask fitted with a reflux condenser was added acetic anhydride (6 mL) and hydrogen peroxide (30% in water, 2 mL). The reaction mixture was heated to 40 °C with stirring for 4 h. Iodobenzene (1 g, 4.9 mmol, 546 μ l) was added, and heating continued for 1.5 h. The mixture was left to stir at ambient temperature for 15 h. Water (50 mL) was added. The resulting white precipitate was collected by filtration through a sintered funnel and washed with cold water (2 x 10 mL) to give product as a white solid (1.275 g, 80%).

MP 163 μ 167 °C (lit. 164 °C)¹⁴⁰; ¹H NMR (400 MHz, CDCl₃) δ 8.07 (ddd, J = 4.5, 2.2, 1.1 Hz, 2H), 7.61 μ 7.56 (m, 1H), 7.48 (m, 2H), 1.99 (s, 6H); ¹³C NMR (101 MHz, CDCl₃) δ 176.4, 135.0, 131.8, 131.0, 121.7, 20.4; LIFDI-MS m/z 321.97 [M+H]; IR (solid-state ATR, cm⁻¹) 1737, 1642, 1626, 1365, 1290, 1270, 1012, 924.

1-Hydroxy-1H-1λ³-benzo[d][1,2]iodoxol-3-one, 219

To a round-bottomed flask fitted with a reflux condenser was added NaIO_4 (950 mg, 4.43 mmol, 1.1. eq.) and 4-iodobenzoic acid (1 g, 4.03 mmol, 1 eq.) The apparatus was purged with N_2 . AcOH (10 mL, 30% v/v in water) was added to give a white suspension. The reaction mixture was heated to reflux with stirring for 4 h. The reaction mixture was then diluted with cold water, and left to cool to ambient temperature. The resulting precipitate was collected by filtration and washed with cold water and acetone. This was dried under reduced pressure to give product as a white solid (9.7 mg, 85%).

MP 225 μ 227 °C (lit. 223 μ 225 °C, decomp.)²⁹⁷; ^1H NMR (400 MHz, $(\text{CD}_3)_2\text{SO}$) δ 8.00 (s, 1H), 7.97 (dd, $J = 7.6, 1.4$ Hz, 1H), 7.92 (ddd, $J = 8.6, 7.2, 1.6$ Hz, 1H), 7.80 (d, $J = 8.0, 1.0$ Hz, 1H), 7.67 (app. td, $J = 7.4, 1.0$ Hz, 1H); ^{13}C NMR (101 MHz, $(\text{CD}_3)_2\text{SO}$) δ 167.7, 134.4, 131.5, 131.1, 130.4, 126.3, 120.4; ESI-MS m/z 264 [M+H]; ESI-HRMS m/z 264.9430 [M+H] (calc. for $\text{C}_7\text{H}_6\text{IO}_3$ 264.9356, error 31.1 ppm); IR (solid-state ATR, cm^{-1}) 2390, 1598, 1553, 1441, 1338, 1301, 1148, 1018, 835, 809.

1-Acetyl-1H-1λ³-benzo[d][1,2]iodoxol-3-one, 220

To a round-bottomed flask fitted with a reflux condenser was added 1-hydroxy-1*H*-1λ³-benzo[d][1,2]iodoxol-3-one (850 mg, 3.22 mmol) and acetic anhydride (5 mL). The reaction mixture was heated to reflux with stirring for 10 min, and then left to cool to ambient temperature to give a white precipitation. The resulting precipitate was collected by filtration and dried under reduced pressure to give product as a white solid (765 mg, 78%).

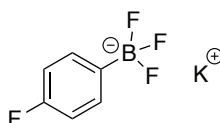
MP 175 μ 177 °C (lit. 165 μ 167 °C, decomp.)²⁹⁸; ¹H NMR (400 MHz, CDCl₃) δ 8.25 (dd, *J* = 7.5, 1.6 Hz, 1H), 7.99 (d, *J* = 7.7 Hz, 1H), 7.91 (ddd, *J* = 8.4, 7.3, 1.5 Hz, 1H), 7.74 μ 7.68 (m, 1H), 2.24 (s, 3H); ¹³C NMR (101 MHz, CDCl₃) δ 176.4, 168.2, 136.2, 133.2, 131.3, 129.4, 129.1, 118.4, 20.4; ESI-MS *m/z* 279 [M-Ac+MeOH], 301 [M-Ac+MeOH+Na]; ESI-HRMS *m/z* 278.9519 [M-Ac+MeOH] (calc. for C₈H₈IO₃ 279.9518); IR (solid-state ATR, cm⁻¹) 3071, 1652, 1586, 1568, 1447, 1366, 1249, 1260, 1240, 1126, 1025, 1013, 921, 807, 824, 754, 674.

3.3.4 Synthesis of Potassium Aryltrifluoroborates

General Procedure

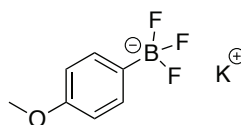
In a round-bottomed flask, boronic acid (1 eq.) was dissolved in THF (40 mL). To this was slowly added a suspension of potassium hydrogen bifluoride (6 eq.) in water (12.5 mL). The reaction mixture was stirred at ambient temperature for 24 h. The solvent was removed under reduced pressure. The resulting white solid was suspended in acetone and filtered through a glass sinter. The precipitate was washed with hot acetone, and the combined filtrate collected. The solvent was removed under reduced pressure to give potassium aryltrifluoroborate as a white solid.

Potassium 4-fluorophenylborontrifluoride, **234**



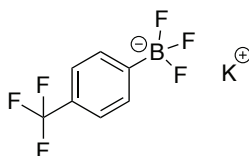
Obtained according to the general procedure as a white solid (1.046 g, 100%).

MP 290 °C (lit. 297 °C, decomp.)²⁰²; ¹H NMR (400 MHz, (CD₃)₂CO) δ 7.45 (app. t, *J* = 7.3 Hz, 2H), 6.81 (br t, 2H); ¹³C NMR (101 MHz, (CD₃)₂CO) δ 162.6 (d, *J*_{CF} = 242.4 Hz), 134.0 (dq, *J*_{CB} = 6.9, 1.9 Hz), 113.4 (d, *J* = 18.7 Hz) (three of four resonances observed μ ¹³C *ipso* to B substituent not observed)²⁸⁴; ¹¹B NMR (128 MHz, (CD₃)₂CO) δ 2.63 (q, *J* = 48.2 Hz); ¹⁹F NMR (376 MHz, (CD₃)₂CO) δ -120.58 (m), -142.42 (dd, *J* = 99.6, 46.5 Hz); ESI-MS *m/z* (%) 185 (12) [¹¹BM-H], 184 (3) [¹⁰BM-H], 163 (100) [¹¹BM-K], 162 (26) [¹⁰BM-K]; ESI-HRMS *m/z* 163.0352 [¹¹BM-K] (calc. for C₇H₄BF₄ 163.0349); IR (solid-state ATR, cm⁻¹) 1607, 1512, 1224, 1209, 986, 969, 952, 917, 831.

Potassium 4-methoxyphenylborontrifluoride, 236

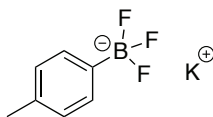
Obtained according to the general procedure as a white solid (1.046 g, 74%).

MP 259 μ 261 °C (lit. 250 °C, decomp.)²⁰²; ¹H NMR (400 MHz, (CD₃)₂CO) δ 7.38 (d, *J* = 8.5 Hz, 2H), 6.67 (br d, *J* = 8.5 Hz, 2H), 3.70 (s, 3H); ¹³C NMR (101 MHz, (CD₃)₂CO) δ 158.7, 133.4 (q, *J* = 1.9 Hz), 112.6, 55.0 (four of five resonances observed)²⁸⁴; ¹⁹F NMR (376 MHz, (CD₃)₂CO) δ -62.26; ¹¹B NMR (128 MHz, (CD₃)₂CO) δ 3.74 μ 0.99 (m); ESI-MS *m/z* (%) 197 (100) [¹¹BM-H], 196 (21) [¹⁰BM-H], 175 (65) [¹¹BM-K], 174 (14) [¹⁰BM-K]; ESI-HRMS *m/z* 175.0554 [¹¹BM-K] (calc. for C₇H₇BF₃O 175.0549); IR (solid-state ATR, cm⁻¹) 1604, 1568, 1513, 1463, 1443, 1404, 1281, 1213, 1175, 1032, 985, 968, 910, 828, 730. 644.

Potassium 4-(trifluoromethyl)phenylborontrifluoride, 235

Obtained according to the general procedure as a white solid (1.236 g, 93%).

MP 298 °C (lit. >300 °C, decomp.)²⁰²; ¹H NMR (400 MHz, (CD₃)₂CO) δ 7.65 (d, *J* = 7.6 Hz, 2H), 7.40 (d, *J* = 7.6 Hz, 2H); ¹³C NMR (126 MHz, (CD₃)₂CO) δ 156.2 (br), 132.8, 127.5 (q, *J* = 34.0 Hz), 126.5 (q, *J* = 270 Hz), 123.5; ¹¹B NMR (128 MHz, (CD₃)₂CO) δ 2.10 (q, *J* = 52.1, 50.9 Hz); ¹⁹F NMR (376 MHz, (CD₃)₂CO) δ -138.59, -143.64 (m); ESI-MS *m/z* (%) 235 (100) [¹¹BM-H], 234 (21) [¹⁰BM-H], 213 (30) [¹¹BM-K], 212 (6) [¹⁰BM-K]; ESI-HRMS *m/z* 213.0320 [¹¹BM-K] (calc. for C₇H₄BF₆ 213.0320); IR (solid-state ATR, cm⁻¹) 1397, 1328, 1206, 11521108, 1061, 1020, 957, 941, 853, 825, 773, 744, 701.

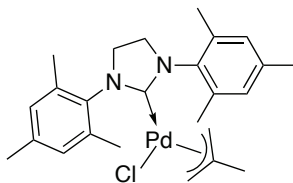
Potassium 4-methylphenylborontrifluoride, 233

Obtained according to the general procedure as a white solid (1.452 g, 97%).

MP 294 μ 295 °C (lit. 293 μ 294 °C, decomp.)²⁰²; ¹H NMR (400 MHz, (CD₃)₂CO) δ 7.36 (d, J = 7.6 Hz, 2H), 6.92 (d, J = 7.6 Hz, 2H), 2.22 (s, 3H); ¹³C NMR (101 MHz, (CD₃)₂CO) δ 134.3, 132.6 (q, J = 1.9 Hz), 127.8, 21.5 (four of five resonances observed)²⁸⁴; ¹¹B NMR (128 MHz, (CD₃)₂CO) δ 2.67 (q, J = 55.8 Hz); ¹⁹F NMR (376 MHz, (CD₃)₂CO) δ -142.26 (m); ESI-MS m/z (%) 181 (100) [¹¹BM-H], 180 (23) [¹⁰BM-H], 159 (88) [¹¹BM-K], 158 (16) [¹⁰BM-K]; ESI-HRMS m/z 159.0608 [¹¹BM-K] (calc. for C₇H₇BF₃ 159.0600); IR (solid-state ATR, cm⁻¹) 1242, 1231, 1198, 1023, 968, 918, 807.

3.3.5 Synthesis of Palladium Catalysts

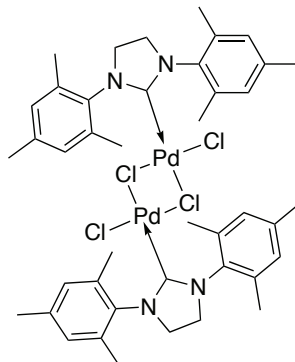
1,3-[di(2,4,6-trimethylphenyl)-4,5-dihydroimidazolyliidene](η^3 -2-methylpropenyl)chloropalladium(II), **226**²⁹⁹



To a round-bottomed flask containing 1,3-di(2,4,6-trimethylphenyl)-2-(pentafluorophenyl)-2,4,5-trihydroimidazole (200 mg, 0.421 mmol, 2 eq.) and di- μ -chlorobis(η^3 -2-methylpropenyl)dipalladium(II) (82.7 mg, 0.211 mmol) was added toluene (5 mL). The reaction mixture was stirred at 80 °C for 3 h. Solvent was removed under reduced pressure to give product as a white solid (211 mg, 100%).

MP 135 μ 136 °C; ¹H NMR (400 MHz, CDCl₃) δ 6.92 (d, J = 10.0 Hz, 4H), 4.02 μ 3.91 (m, 4H), 3.60 (d, J = 3.1 Hz, 1H), 2.98 (d, J = 2.4 Hz, 1H), 2.62 (s, 1H), 2.46 (s, 6H), 2.39 (s, 6H), 2.27 (s, 6H), 1.79 (s, 1H), 1.25 (s, 3H); ¹³C (101 MHz, CDCl₃) δ 138.2, 136.2, 129.5, 129.4, 71.8, 51.1, 49.7, 22.1, 21.0, 18.7, 18.6 (allyl C2 carbon has not observed); IR (solid-state ATR, cm⁻¹) 3651, 3238, 2912, 1734, 1656, 1607, 1488, 1434, 1403, 1376, 1298, 1265, 1232, 1184, 1098, 1061, 860, 850, 837, 738, 696.

Trans-di-μ-chlorobis{[1,3-di(2,4,6-trimethylphenyl)-4,5-dihydroimidazolylidene]chloropalladium(II)}, **227**

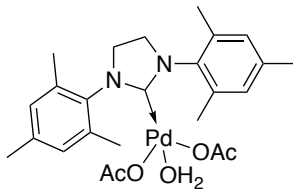


To a round-bottomed flask containing 1,3-[di(2,4,6-trimethylphenyl)-4,5-dihydroimidazolylidene](η^3 -2-methylpropenyl)chloropalladium(II) (150 mg, 0.297 mmol) was added hydrogen chloride (6 mL, 1 M in diethyl ether). The reaction was stirred at ambient temperature for 24 h. The solvent was removed under reduced pressure to give product as an orange solid (146 mg, 98%).

MP >260 °C (lit. >239 °C)¹²⁰; ¹H NMR (400 MHz, CDCl₃) δ 6.99 (s, 4H), 3.85 (s, 4H), 2.49 μ 2.18 (m, 18H); ¹³C (101 MHz, CDCl₃) δ 177.8, 138.4, 134.4, 129.7, 122.8, 51.3, 21.3, 19.1; IR (solid-state ATR, cm⁻¹) 3650, 2967, 1607, 1489, 1452, 1404, 1377, 1265, 11847, 1099, 1029.

This compound was not observed by ESI-MS or LIFDI-MS.

[1,3-Di(2,4,6-trimethylphenyl)-4,5-dihydroimidazolyli-dene]diacetateaquopalladium(II),
228³⁰⁰

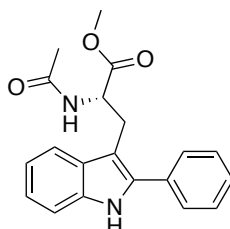


To a round-bottomed flask containing *trans*-di- μ -chlorobis{[1,3-di(2,4,6-trimethylphenyl)-4,5-dihydroimidazolyli-dene]chloropalladium(II)} (120 mg, 0.124 mmol, 1 eq.) and CH₂Cl₂ (6 mL) was added silver acetate (167 mg, 0.510 mmol, 4.1 eq.). The reaction mixture was stirred at ambient temperature for 2 h. The reaction mixture was filtered through Celite® to give a yellow solution. Solvent was removed under reduced pressure to give product as a yellow solid (112 mg, 82%).

MP 259 μ 261 °C (decomp.); ¹H NMR (400 MHz, CDCl₃) δ 7.04 (s, 4H), 4.00 (d, *J* = 5.6 Hz, 4H), 2.37 (s, 18H), 1.75 (s, 6H); ¹³C NMR (101 MHz, CDCl₃) δ 181.5, 181.3, 139.1, 136.6, 134.4, 129.8, 50.6, 23.7, 21.3, 17.9; ESI-MS *m/z* 307 [M-Pd-2OAc-H₂O]; IR (solid-state ATR, cm⁻¹) 3438, 3415, 3229, 3310, 3229, 1723, 1444, 1406, 1331, 1276, 1237, 1119, 1104, 1068, 1008, 918, 738, 651, 638, 506.

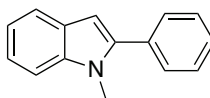
3.3.6 Direct C-H bond functionalisation of Tryptophan with Boronic Acids/DIB

Methyl (2S)-2-acetyl-3-(2-phenyl-1H-indol-3-yl)propanoate, **215**



To a microwave tube was added phenylboronic acid (47 mg, 0.384 mmol, 2 eq.), bis(acetyloxy)phenyl- λ^3 -iodane (123 mg, 0.384 mmol, 2 eq.), Pd(OAc)₂ (2 mg, 9.6 μ mol, 5 mol%) and acetic acid (5 mL). The reaction mixture was stirred at 40 °C for 10 min. To the resulting orange-brown solution was added methyl (2*R*)-2-acetyl-3-(1*H*-indol-3-yl)propionate (50 mg, 0.192 mmol, 1 eq.). The reaction was stirred at 40 °C for 16 h. The resulting black reaction mixture was filtered through Celite®, and the solvent removed under reduced pressure to give a brown solid. This was dissolved in EtOAc (10 mL) and washed with sat. aq. NaHCO₃. The organic layer was collected and dried over MgSO₄, filtered and the solvent removed under reduced pressure to give a brown solid. This was dry-loaded onto silica gel and purified by flash chromatography eluting with ethyl acetate:petroleum ether (1:1) to give product as a white solid (36 mg, 56%).

MP 83 μ 84 °C; ¹H NMR (400 MHz, CDCl₃) δ 8.20 (s, 1H), 7.63 μ 7.54 (m, 3H), 7.51 μ 7.45 (m, 2H), 7.44 μ 7.33 (m, 2H), 7.21 (ddd, *J* = 8.0, 7.0, 8.0 Hz, 1H), 7.15 (ddd, *J* = 8.0, 7.0, 8.0 Hz, 1H), 5.77 (d, *J* = 8.0 Hz, 1H), 4.84 (dt, *J* = 8.0, 5.5 Hz, 1H), 3.56 (dd, *J* = 15.0, 5.5 Hz, 1H), 3.53 (dd, *J* = 15.0, 5.5 Hz, 1H), 3.30 (s, 3H), 1.67 (s, 3H); ¹³C NMR (101 MHz, CDCl₃) δ 172.6, 170.0 136.4, 136.1, 133.6, 129.9, 129.6, 128.7, 128.6, 123.0, 120.5, 119.4, 111.4, 107.2, 53.2, 52.5 27.0, 23.4.; ESI-MS *m/z* 337 [M+H], 359 [M+Na], 395 [M+K]; ESI-HRMS *m/z* 337.1539 [M+H] (calc. for C₂₀H₂₀N₂O₃ 337.1547); IR (solid-state ATR, cm⁻¹) 3284, 2961, 1735, 1654, 1525, 1434, 1259, 1094, 1013, 795, 741, 697.

*1-Methyl-2-phenylindole, 144*¹³¹

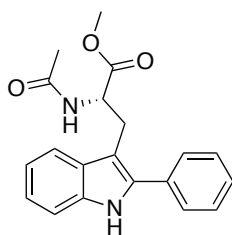
To a microwave tube was added phenylboronic acid (93 mg, 0.763 mmol, 2 eq.), bis(acetyloxy)phenyl- λ^3 -iodane (246 mg, 0.763 mmol, 2 eq.) and Pd(OAc)₂ (4 mg, 19.1 μ mol, 5 mol%) and acetic acid (5 mL). The reaction mixture was stirred at 40 °C for 10 min. To the resulting orange-brown solution was added 1-methylindole (50 mg, 0.381 mmol, 48 μ l, 1 eq.). The reaction was stirred at 40 °C for 16 h. The resulting black reaction mixture was filtered through Celite®, and the solvent removed under reduced pressure to give a brown solid. This was dissolved in EtOAc (10 mL) and washed with sat. aq. NaHCO₃. The organic layer was collected and dried over MgSO₄, filtered and the solvent removed under reduced pressure to give a solid. This was dry-loaded onto silica gel and purified by flash chromatography eluting with ethyl acetate:petroleum ether (1:24) to give product as a white solid (66 mg, 84%).

MP 101.1 μ 102.9 °C (lit. 99 μ 102 °C); ¹H NMR (500 MHz, CDCl₃) δ 7.65 (dt, *J* = 8.1, 1.0 Hz, 1H), 7.55 μ 7.51 (m, 2H), 7.48 (t, *J* = 7.5 Hz, 2H), 7.43 μ 7.39 (m, 1H), 7.38 (dd, *J* = 8.1, 1.0 Hz, 1H), 7.26 (ddd, *J* = 8.1, 7.0, 1.0 Hz, 1H), 7.16 (ddd, *J* = 8.1, 7.0, 1.0 Hz, 1H), 6.58 (s, 1H), 3.76 (s, 3H); ¹³C NMR (126 MHz, CDCl₃) δ 141.68, 138.47, 132.97, 129.49, 128.59, 128.09, 127.95, 121.77, 120.58, 119.96, 109.70, 101.77, 31.26; ESI-MS *m/z* 208 ([M+H]⁺); ESI-HRMS *m/z* 208.1120 [M+H] (calc. for C₁₅H₁₄N 208.1121); IR (CDCl₃ solution, cm⁻¹) ν 3061, 2948, 2365, 2338, 2245, 1470; UV-Vis³⁰¹ (cyclohexane, nm) λ_{maxima} 206 (26304), 222 (ϵ = 27028 mol dm⁻³ cm⁻¹), 298 (ϵ = 15334 mol dm⁻³ cm⁻¹).

Using the same procedure, the reaction was performed using Pd(OAc)₂ contaminated with palladium nitro complex²⁶⁶ (4 mg) to give the title compound as a white solid (67 mg, 84%).

3.3.7 Direct C-H bond functionalisation of Tryptophan with Diaryliodonium Trifluoromethanesulfonates

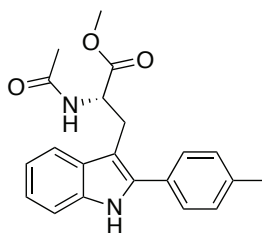
Methyl (2S)-2-amino-3-(2-phenyl-1H-indol-3-yl)propanoate



215

To a microwave tube was added methyl (2*R*)-2-acetylamino-3-(1*H*-indol-3-yl)propanoate (50 mg, 0.192 mmol, 1 eq.), Pd(OAc)₂ (2 mg, 9.6 μmol, 5 mol%) and acetic acid (5 mL). The reaction mixture was stirred at 40 °C for 10 min. To the resulting orange-brown solution was added diphenyliodonium trifluoromethanesulfonate (159 mg, 0.384 mmol, 2 eq.). The reaction was stirred at 40 °C for 16 h. The resulting black reaction mixture was filtered through Celite®, and the solvent removed under reduced pressure to give a brown solid. This was dissolved in EtOAc (10 mL) and washed with sat. aq. NaHCO₃. The organic layer was collected and dried over MgSO₄, filtered and the solvent removed under reduced pressure to give a brown solid. This was dry-loaded onto silica gel and purified by flash chromatography eluting with ethyl acetate:petroleum ether (1:1) to give product as a white solid (34 mg, 51%).

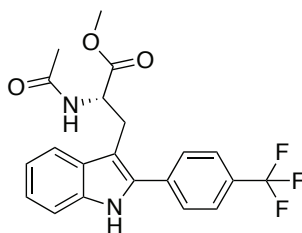
Analytical data identical to that reported above, on page 191.

Methyl (2S)-2-amino-3-[2-(4-methylphenyl)-1H-indol-3-yl]propanoate, 221

To a conical flask was added methyl (2*R*)-2-acetylamino-3-(1*H*-indol-3-yl)propionate (50 mg, 0.192 mmol, 1 eq.), Pd(OAc)₂ (0.0096 mmol, 2 mg, 5 mol%) and acetic acid (5 mL). The reaction mixture was stirred for 10 min at 40 °C. 4-methylphenyl(mesityl)iodonium trifluoromethanesulfonate (187 mg, 0.384 mmol, 2 eq.) was added in one portion, and the reaction mixture stirred 16 h at 40 °C. The resulting black suspension was filtered through Celite®, and the filter cake and reaction vessel were washed with toluene and acetic acid. The solvent was removed under reduced pressure. The resulting brown solid was dissolved in EtOAc (20 mL) and washed with sat. aq. NaHCO₃ (20 mL). The organic layer was dried over MgSO₄, filtered and the solvent removed under reduced pressure to give a yellow oil. This was dry-loaded onto silica gel and purified by flash chromatography eluting with 50% EtOAc in petroleum ether to give product yellow solid (36 mg, 53 %).

R_F 0.32 (50% EtOAc/PE); MP 97 μ 99 °C; ¹H NMR (400 MHz, CDCl₃) δ 8.09 (s, 1H), 7.56 (d, *J* = 7.8 Hz, 1H), 7.48 μ 7.44 (m, 2H), 7.36 (d, *J* = 7.8 Hz, 1H), 7.30 (d, *J* = 7.8 Hz, 2H), 7.19 (ddd, *J* = 8.0, 7.0, 1.0 Hz, 1H), 7.13 (ddd, *J* = 8.0, 7.0, 1.0 Hz, 1H), 5.77 (d, *J* = 8.0 Hz, 1H), 4.82 (dt, *J* = 7.8, 5.4 Hz, 1H), 3.53 (d, *J* = 5.4 Hz, 1H), 3.52 (d, *J* = 5.5 Hz, 1H), 3.33 (s, 3H), 2.41 (s, 3H), 1.66 (s, 3H); ¹³C NMR (126 MHz, CDCl₃): δ 172.3, 169.9, 136.1, 134.4, 134.2, 131.8, 129.9, 129.5, 123.3, 120.5, 119.4, 111.3, 108.2, 52.9, 52.2, 31.8, 29.8, 26.9, 23.0; ESI-HRMS *m/z* 391.0166 [M+H] (calc. for C₁₆H₁₅F₃I 391.1065); IR (solid-state ATR, cm⁻¹) 3331, 2951, 1731, 1657, 1506, 1372, 1305, 1215, 1010, 822, 742.

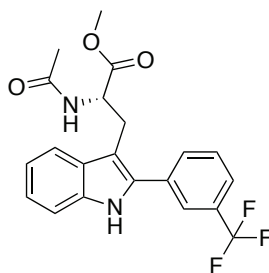
Methyl (2S)-2-amino-3-{2-[4-(trifluoromethyl)phenyl]-1H-indol-3-yl}propanoate, 222



Obtained according to the procedure for **221** as an off-white solid (22 mg, 28%).

R_F 0.34 (50% EtOAc/PE); MP 202 μ 206 °C; ^1H NMR (400 MHz, CDCl_3) δ 8.41 (s, 1H), 7.72 μ 7.63 (m, 4H), 7.58 (d, $J = 8.0$ Hz, 1H), 7.35 (d, $J = 8.0$ Hz, 1H), 7.22 (ddd, $J = 8.2, 7.0, 1.2$ Hz, 1H), 7.15 (ddd, $J = 8.2, 7.0, 1.2$ Hz, 1H), 5.87 (d, $J = 8.0$ Hz, 1H), 4.84 (dt, $J = 8.0, 5.2$ Hz, 1H), 3.59 μ 3.48 (m, 2H), 3.29 (s, 3H), 1.67 (s, 3H); ^{13}C NMR (101 MHz, CDCl_3) δ 172.2, 169.9, 136.9, 136.1, 134.3, 129.9 (q, $J = 31.8$ Hz), 129.5, 128.5, 126.1 (q, $J = 3.8$ Hz), 124.1 (q, $J = 247$ Hz), 123.3, 120.4, 119.2, 111.4, 108.2, 53.0, 52.2, 27.0, 23.0; ESI-MS m/z 405 [M+H], 427 [M+Na]; ESI-HRMS m/z 405.1410 [M+H] (calc. for $\text{C}_{21}\text{H}_{20}\text{F}_3\text{N}_2\text{O}_3$ 405.1421); IR (solid-state ATR, cm^{-1}) 3288, 2925, 2860, 1730, 1651, 1505, 1438, 1285, 1245, 1215, 1027, 835, 743.

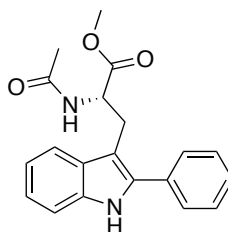
Methyl (2S)-2-amino-3-{2-[3-(trifluoromethyl)phenyl]-1H-indol-3-yl}propanoate, 223



Obtained according to the procedure for **221** as an orange solid (16 mg, 21%).

^1H NMR (400 MHz, CDCl_3) δ 8.15 (s, 1H), 7.80 (m, 2H), 7.65 (s, 1H), 7.62 (s, 1H) 7.61 (m, 1H), 7.39 (dd, $J = 8.0, 1.0$ Hz, 1H), 7.24 (dd, $J = 8.0, 1.0$ Hz, 1H), 7.17 (dd, $J = 8.0, 1.0$ Hz, 1H), 5.81 (s, 1H), 4.86 (dt, $J = 8.0, 5.4$ Hz, 1H), 3.54 (t, $J = 5.4$ Hz, 2H), 3.30 (s, 3H), 1.71 (s, 3H); ^{13}C NMR (126 MHz, CDCl_3): δ 231.5, 172.4, 169.9, 151.0, 138.1, 136.3, 135.7, 130.3, 129.9, 129.6, 128.3, 122.5, 120.1, 118.9, 111.0, 106.5, 53.0, 52.2, 38.6, 31.1, 29.8; ESI μ HRMS m/z 405.1422 [M+H] (calc. for $\text{C}_{21}\text{H}_{19}\text{F}_3\text{N}_2\text{O}_3$ 405.1421).

3.3.8 Direct C-H bond Functionalisation of Tryptophan with Boronic Acids

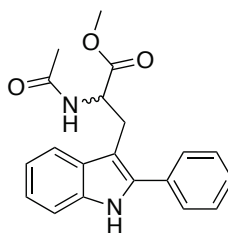
Methyl (2S)-2-amino-3-(2-phenyl-1H-indol-3-yl)propanoate 215

To a microwave tube was added phenylboronic acid (47 mg, 0.384 mmol, 2 eq.), methyl (2*R*)-2-acetylamino-3-(1*H*-indol-3-yl)propionate (50 mg, 0.192 mmol, 1 eq.) and Pd(OAc)₂ (2 mg, 9.6 μmol, 5 mol%) and acetic acid (5 mL). The reaction mixture was stirred at 40 °C for 16 h. The resulting black reaction mixture was filtered through Celite®, and the solvent removed under reduced pressure to give a brown solid. This was dissolved in EtOAc (10 mL) and washed with sat. aq. NaHCO₃. The organic layer was collected and dried over MgSO₄, filtered and the solvent removed under reduced pressure to give a brown solid. This was dry-loaded onto silica gel and purified by flash chromatography eluting with ethyl acetate:petroleum ether (1:1) to give product as a white solid (60 mg, 93%, *er* 99.9:1).

[α]_D = +47.3 (*c* 0.11, CHCl₃); UV-Vis (DMSO, nm) λ_{maxima} 308 (ε = 9120 mol dm⁻³ cm⁻¹).

Other analytical data identical to that reported above.

Methyl (2RS)-2-amino-3-(2-phenyl-1H-indol-3-yl)propanoate, 215-rac

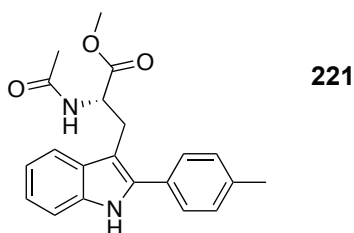


Obtained according to the method outlined above to give product as a white solid (59 mg, 91%, *er* 50.9:49.1).

$[\alpha]_D = +0.0353$ (*c* 0.11, CHCl₃).

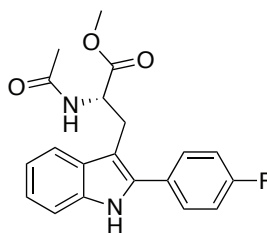
Other analytical data identical to that reported above.

Methyl (2S)-2-amino-3-[2-(4-methylphenyl)-1H-indol-3-yl]propanoate



$[\alpha]_D = +51.9$ (*c* 0.10, CHCl₃); UV-Vis (DMSO, nm) λ_{maxima} 310 ($\epsilon = 8893 \text{ mol dm}^{-3} \text{ cm}^{-1}$).

Other analytical data identical to that reported above.

Methyl (2S)-2-amino-3-[2-(4-fluorophenyl)-1H-indol-3-yl]propanoate, 230

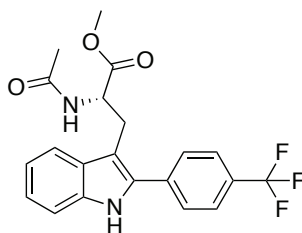
R_F 0.57 (50% EtOAc/PE); $[\alpha]_D = +54.4$ (c 0.10, CHCl_3); MP 213 μ 216 °C (decomp.); ^1H NMR (400 MHz, CDCl_3) δ 8.26 (s, 1H), 7.55 (d, $J = 8.0$ Hz, 1H), 7.53 μ 7.46 (m, 2H), 7.34 (d, $J = 8.0$ Hz, 1H), 7.23 μ 7.10 (m, 4H), 5.83 (d, $J = 8.1$ Hz, 1H), 4.82 (dt, $J = 8.0$, 5.4 Hz, 1H), 3.50 (dd, $J = 15.0$, 5.5 Hz, 1H), 3.46 (dd, $J = 15.0$, 5.5 Hz, 1H), 3.32 (s, 3H), 1.70 (s, 3H); ^{13}C (101 MHz, CDCl_3) 172.3, 169.7, 163.6, 160.9, 135.8, 135.1, 130.2 (d, $J_{CF} = 8.1$), 129.4, 129.3 (d, $J_{CF} = 3.5$ Hz), 121.6 (d, $J_{CF} = 253.0$ Hz), 119.5, 116.1, 116.2, 111.1, 106.9, 52.9, 52.2, 26.8, 23.0; ^{19}F NMR (376 MHz, CDCl_3) δ -112.83 (m); ESI-MS m/z 355 $[\text{M}+\text{H}]$, 377 $[\text{M}+\text{Na}]$; ESI-HRMS m/z 355.1443 $[\text{M}+\text{H}]$ (calc. for $\text{C}_{20}\text{H}_{20}\text{FN}_2\text{O}_3$ 355.1452); IR (solid-state ATR, cm^{-1}) 3332, 2960, 1729, 1659, 1541, 1505, 1444, 1219, 848, 749; UV-Vis λ_{maxima} 306 ($\epsilon = 14684$ $\text{mol dm}^{-3} \text{cm}^{-1}$).

Crystals suitable for X-ray diffraction were grown from CDCl_3 .

Summary of X-ray data

Compound reference	ijsf1202
Chemical formula	$\text{C}_{20}\text{H}_{19}\text{F}_1\text{N}_2\text{O}_3$
Formula mass	345.37
Crystal system	Trigonal
$a/\text{\AA}$	21.0404(11)
$b/\text{\AA}$	21.0404(11)
$c/\text{\AA}$	10.4652(7)
$\alpha/\text{\AA}$	90.00
$\beta/\text{\AA}$	90.00
$\gamma/\text{\AA}$	120.00
Unit cell volume/ \AA^3	4012.2(6)
Temperature/K	110.00(10)
Space group	R3
No. of formula units per unit cell, Z	9
No. of reflections measured	9531
No. of independent reflections	5613
R_{int}	0.0271
Final R_1 values ($I > 2\sigma(I)$)	0.0424
Final $wR(F^2)$ values ($I > 2\sigma(I)$)	0.0946
Final R_1 values (all data)	0.0479
Final $wR(F^2)$ values (all data)	0.0995

Methyl (2S)-2-amino-3-{2-[4-(trifluoromethyl)phenyl]-1H-indol-3-yl}propanoate, 222



$[\alpha]_D = +62.0$ (c 0.13, CHCl_3); UV-Vis (DMSO, nm) λ_{max} 318 ($\epsilon = 10297 \text{ mol dm}^{-3} \text{ cm}^{-1}$).

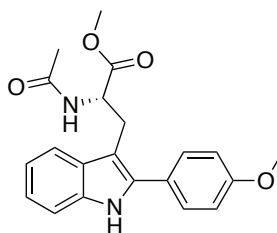
Other analytical data identical to that reported above.

Crystals suitable for X-ray diffraction were grown from CDCl_3 .

Summary of X-ray data

Compound reference	ijsf1201
Chemical formula	$\text{C}_{21}\text{H}_{19}\text{F}_3\text{N}_2\text{O}_3$
Formula mass	404.38
Crystal system	Monoclinic
$a/\text{\AA}$	8.7492(3)
$b/\text{\AA}$	9.0043(3)
$c/\text{\AA}$	24.1842(7)
$\alpha/\text{\AA}$	90.00
$\beta/\text{\AA}$	98.900(3)
$\gamma/\text{\AA}$	90.00
Unit cell volume/ \AA^3	1882.30(10)
Temperature/K	110.00(10)
Space group	$P2_1$
No. of formula units per unit cell, Z	4
No. of reflections measured	14377
No. of independent reflections	8188
R_{int}	0.0306
Final R_1 values ($I > 2\sigma(I)$)	0.0480
Final $wR(F^2)$ values ($I > 2\sigma(I)$)	0.1077
Final R_1 values (all data)	0.0572
Final $wR(F^2)$ values (all data)	0.1135

Methyl (2S)-2-amino-3-[2-(4-methoxyphenyl)-1H-indol-3-yl]propanoate, 213



R_F 0.12 (50% EtOAc/PE); $[\alpha]_D = +34.9$ (c 0.10, CHCl_3); MP 202 μ 205 $^\circ\text{C}$; ^1H NMR (400 MHz, CDCl_3) δ 8.07 (s, 1H), 7.56 (d, $J = 7.5$ Hz, 1H), 7.53 μ 7.45 (m, 2H), 7.35 (d, $J = 7.5$ Hz, 1H), 7.19 (ddd, $J = 8.0, 7.0, 1.5$ Hz, 1H), 7.13 (ddd, $J = 8.0, 7.0, 1.5$ Hz, 1H), 7.02 (d, $J = 9.0$ Hz, 2H), 5.78 (d, $J = 8.0$ Hz, 1H), 4.83 (dt, $J = 8.0, 5.5$ Hz, 1H), 3.87 (s, 3H), 3.48 (m, 2H), 3.35 (s, 3H), 1.70 (s, 3H); ^{13}C NMR (101 MHz, CDCl_3) δ 172.4, 169.7 159.6, 136.1, 135.6, 129.7, 129.6, 125.6, 122.4, 120.1, 118.8, 114.7, 111.0, 106.3, 55.6, 53.0, 52.2, 26.8, 23.1; ESI-MS m/z 367 $[\text{M}+\text{H}]$, 389 $[\text{M}+\text{Na}]$; ESI-HRMS m/z 367.1644 $[\text{M}+\text{H}]$ (calc. for $\text{C}_{21}\text{H}_{23}\text{N}_2\text{O}_4$ 367.1652); IR (solid-state ATR, cm^{-1}) 3333, 2954, 1728, 1656, 1505, 1458, 1439, 1246, 1216, 1177, 1027, 836, 747; UV-Vis (DMSO, nm) λ_{max} 320 ($\epsilon = 11644$ mol dm^{-3} cm^{-1}).

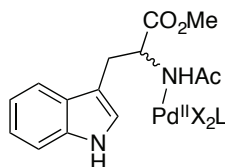
3.3.9 Peptide Arylations

All peptides were functionalised using a general experimental procedure:

Peptide (10 mg), $\text{PhB}(\text{OH})_2$ (5 eq.), $\text{Pd}(\text{OAc})_2$ (30 mol%) and $\text{Cu}(\text{OAc})_2$ (60 mol%) were dissolved in AcOH (0.5 mL) at 40 $^\circ\text{C}$. The reaction mixture was stirred for 16 h. The solvent was removed under reduced pressure (at a temperature that did not exceed 40 $^\circ\text{C}$) to give a brown residue. This was analysed by HPLC-ESI-MS.

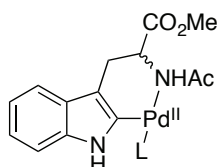
3.3.10 Mechanistic Experiments

Detection of Mechanistic Intermediate II (Scheme) by ReactIR®



To a three-necked round-bottomed flask fitted with a nitrogen inlet and ReactIR® probe was added THF (3 mL). The reaction was monitored by IR at 1616 and 1606 cm⁻¹. To this was added methyl (2*R*)-2-acetylamino-3-(1*H*-indol-3-yl)propionate (45 mg, 0.173 mmol, 1 eq.). Once this was observed to be fully dissolved, Pd(OAc)₂ (39 mg, 0.173 mmol, 1 eq.) was added. The reaction was monitored for ca. 1.5 h (page 150).

Detection of Mechanistic Intermediate III (Scheme) by NMR Spectroscopy



To a NMR tube in air was added methyl (2*R*)-2-acetylamino-3-(1*H*-indol-3-yl)propionate (10 mg, 38.4 μmol, 1 eq.), Pd(OAc)₂ (8.6 mg, 38.4 μmol, 1 eq.) and CD₃COOD (0.7 mL). ¹H NMR spectrum was immediately recorded (page 151).

**CHAPTER 4:
CONCLUSIONS AND FUTURE WORK**

4.1 – Direct C-H Bond Functionalisation of Benzoxazole

4.1.1 – Conclusions

Pd⁰ nanoparticles have previously been implicated in traditional Pd cross-coupling reactions, and extensive studies have demonstrated the viability of heterogeneous and hybrid-phase reactions in these systems (*vide supra*).^{60,84,85} However, their activity has remained underexplored in the field of direct C-H bond functionalisation reactions, beyond acknowledgement of their presence.²⁶ In this thesis has been presented compelling evidence for the presence and activity of such nanoparticles in these reactions. Nanoparticles have been shown to play a role in both µredox-neutralµC-H bond functionalisations (formal loss of HX) and oxidative coupling processes, at both high and ambient temperatures, and across a variety of electronically diverse heterocycles.

The difficult reproducibility of C-H bond functionalisations catalysed by Pd (cat.) and Cu (stoich.) µbase-freeµ systems, as developed by Bellina, Rossi and co-workers had previously been noted by J. P. Reeds, who also noted that PVP stabilised Pd⁰ nanoparticles could act as efficient catalysts.¹²⁷ Here, Bellina and Rossiµ C-H bond functionalisations of benzoxazole and benzothiazole in the presence of base (specifically, CsF) was studied in a similar way. Varying results were observed in different vessels. With Pd(OAc)₂ precatalysts (observed to reduce under the reaction conditions), isolated yields were higher in the Schlenk tube than the Radleys® carousel tube. With Pd-PVP nanoparticles, the yields with benzothiazole increased in both the Schlenk tube and (considerably) in the carousel. For benzoxazole **53**, the yield increased in the carousel, but decreased in the Schlenk tube.

It was proposed that, with Pd(OAc)₂, different sizes of nanoparticles were being formed in in the different vessels. This could result from differences in stirring, in water/air infiltration, or from Pd-PVP. Using benzothiazole **49**, nanoparticles (which were trapped using the method of Fairlamb and co-workers using PVP) were isolated and characterized by TEM. There was a difference in particle size, with larger particles (by 1.43 nm) being observed in the Schlenk tube. This was unexpected, as in previous work it has been suggested that smaller particles have increased activity (due to a greater proportion of active defect sites). It was proposed initially that by pre-

synthesising Pd-PVP, and controlling the size and composition of the nanoparticles, greater reproducibility across reaction vessels could be obtained. However, this increase was not observed in the benzoxazole C-H bond functionalisations. These are complicated, multicomponent systems, and it seems likely that other factors may play a role. Importantly, it suggests that the benz(azole) heterocycles display reactivity differences.

Chen and Cheng have published a direct C-H functionalisation of benzoxazole using $\text{PhI}(\text{OAc})_2$ **107** catalysed by $\text{Pd}(\text{OAc})_2$.¹³⁰ They have proposed this to proceed *via* a $\text{Pd}^{\text{III/IV}}$ manifold. $\text{PhI}(\text{OAc})_2$ is a commonly used oxidant in organic chemistry. It has been demonstrated here that this species, in DMSO solution, will degrade *via* multiple uncharacterised intermediates to PhI. This process is observable on the NMR spectroscopic timescale at room temperature. At elevated temperatures, this process is rapid. Full conversion is observed after only 10 minutes heating at 150 °C. When the Chen-Cheng arylation was attempted, it was found that PhI was an efficacious aryl source. Therefore, it is proposed that $\text{PhI}(\text{OAc})_2$ is degrading rapidly under reaction conditions to give PhI.

Aryl iodides are rarely implicated in Pd^{II} to Pd^{IV} oxidative addition processes. Whilst performing these reactions, Pd^0 nanoparticles were observed. These were isolated and characterised by TEM. This evidence suggests that this process does not proceed *via* Pd^{IV} intermediates. Rather, a traditional $\text{Pd}^{\text{0/II}}$ cycle is proposed, with the nanoparticles acting as a reservoir for Pd^0 . Further evidence was obtained with a competition experiment between $\text{PhI}(\text{OAc})_2$ and 1-iodo-4-methylbenzene, which gave results consistent with oxidative addition to Pd^0 .

$\text{Cu}(\text{NHC})\text{X}$ (X = halide) complexes have been proposed as intermediates in the direct C-H bond functionalisation of imidazoles catalysed by Pd/Cu and Cu-only systems. A model complex (1,3-dibenzylbenzimidazolilydenecopper(I) bromide) **110** has been synthesised, and it has been demonstrated that this complex undergoes a direct reaction with PhI, in the presence and absence of $\text{Pd}(\text{OAc})_2$. The reaction is less effective in the absence of $\text{Pd}(\text{OAc})_2$. This is consistent with previous methodological studies which have shown that Cu only C-H functionalisations require higher temperatures.

The decomposition of 1,3-dibenzylbenzimidazolilydenecopper(I) bromide is observed in the presence of H₂O and air (accelerated by the latter). The novel bis(1,3-dibenzylbenzimidazolium) dicoppertetrabromide **114a** is observed as a decomposition product, and has been characterized by NMR spectroscopy and single crystal X-ray diffraction. This can exist as different polymorphs, including where dicopper tetrabromide is not a definitive stoichiometric cluster, but rather an infinite anionic polymer in the form Cu_xBr_{2y} **114b**. This decomposition provides the first clear explanation for the requirement for stoichiometric Cu^I in several C-H bond functionalization reactions.

4.1.2 – Future Work

Although the presence and catalytic relevance of Pd⁰ nanoparticles has been established in various systems for the C-H bond functionalisation of benz(azoles), the exact nature of their role remains undetermined. For example, it remains unclear whether catalysis occurs on the surface of the observed particles or whether they are merely acting as a reservoir for Pd⁰, leaching molecular Pd (*i.e.* complexes of Pd⁰ or Pd^{II} that contain only one metal centre) or smaller clusters of Pd⁰.

A kinetic study of the C-H bond functionalisation of benz(azoles) with Pd(OAc)₂ and Pd-PVP (monitoring, for example, by GC) is key to understanding the role of nanoparticles further. If the formation of nanoparticles is required before catalysis can occur, we should expect an induction period with Pd(OAc)₂ and not in the Pd-PVP nanoparticles. An induction period observed with Pd-PVP nanoparticles might suggest leaching, aggregation or disaggregation to smaller particles. The use of extended X-ray absorption fine structure (EXAFS) to study the particles *in operando* would provide complementary information.

The Hg drop test has previously been used to assess the catalytic relevance of Pd nanoparticles. However, on its own it can lack reliability. Using a methodology developed to study nanoparticles in the Suzuki-Miyaura reaction,⁸⁴ a more adequate picture might be obtained. Conversion as a function of time is monitored in the presence and absence of Hg. For catalytically active nanoparticles (both as heterogeneous catalysts or a reservoir for homogeneous Pd), we should observe reaction cessation. Molecular Pd (in the form of Pd(OAc)₂), equal to the amount that

can theoretically be leached from particles of that size, is added to the reaction. If the reaction resumes, then it is likely that leaching is important in that process. This study would not only provide information on the role of nanoparticles in the C-H functionalisation of benz(azoles), but also in arylation of tryptophan discussed elsewhere in this thesis.

Further studies are required on the degradation of $\text{PhI}(\text{OAc})_2$ to PhI in DMSO solution. The intermediate has not been identified. An in-depth kinetic study may provide more information. If such a study could identify a period where the populations of different species in solution are stable, detailed NMR spectroscopic experiments (for example, ^1H DOSY experiments) might give more insight into the nature of the observed species. Synthesis of possible hypervalent iodine intermediates (such as iodosylbenzene, PhIO) could also provide useful information.

A role for *N*-heterocyclic carbene complexes in C-H bond functionalisation has been established, although some factors are still unknown. The mode of transmetalation to Pd has not been explored. This could happen at both Pd^{II} (post-oxidative addition of ArI) and Pd^0 (before oxidative addition of ArI). This could be tested by the synthesis of Pd^0 and Pd^{II} *N*-heterocyclic carbenes analogous to the Cu complexes described in this thesis. DFT calculations would also provide valuable information into these processes.

The requirement for stoichiometric quantities of Cu^{I} in Bellina-Rossi and Fairlamb C-H bond functionalisations is still not completely understood. Although the stability of the $\text{Cu}(\text{NHC})$ complexes could play a decisive role, this has not been established. There is further evidence that Cs_2CO_3 reactions with CuI to give Cu_2CO_3 , and eventually Cu_2O and CO_2 .³⁰² A kinetic study of these reactions to ascertain the reaction order with respect to Cu, Pd and substrates is required.

4.2 – Direct C-H Bond Functionalisation of Indole Biomolecules

4.2.1 – Conclusions

A key objective of this work was the development of a mild and selective C-H bond functionalisation for the amino acid tryptophan **213**. In initial experiments, $\text{PhI}(\text{OAc})_2$ (2 eq.), $\text{ArB}(\text{OH})_2$ (2 eq.) and $\text{Pd}(\text{OAc})_2$ (5 mol%) were used in AcOH. This methodology was adapted from that developed by Sanford and co-workers.¹³¹ Moderate yields were obtained (maximum 56%). It had previously been proposed that this system resulted in the *in situ* formation of diaryliodonium salts, which acted as the aryl source. However, reagent elimination studies indicated that the process performed better in the absence of $\text{PhI}(\text{OAc})_2$ with trace air acting as the oxidant. When *p*-TolB(OH)₂ and $\text{PhI}(\text{OAc})_2$ were used in conjunction, only the incorporation of *p*-TolB(OH)₂ into the tryptophan was observed. If an unsymmetrical diaryliodonium ($[\text{Ar}^{\text{I}}\text{Ar}^{\text{II}}][\text{OAc}]$) salt had been formed, a mixture of products would be expected. Therefore, it is proposed that the diaryliodonium salts are not forming *in situ*, under the reaction conditions tested.

Similarly, this methodology had previously been proposed to proceed *via* a $\text{Pd}^{\text{III/IV}}$ manifold. However, Pd^0 nanoparticles were observed to form in the reaction mixture. These well-defined particles have been characterized by TEM, and were found to have a mean diameter of 2.5 nm. When pre-synthesised Pd nanoparticles supported on polymer (PVP) were used instead of $\text{Pd}(\text{OAc})_2$, similar yields were obtained (57%).

Therefore, it is proposed this reaction proceeds *via* a traditional $\text{Pd}^{\text{0/II}}$ mechanism. $\text{ArB}(\text{OH})_2$ acts as an aryl source, transmetallating to Pd^{II} . Product is reductively eliminated to leave Pd^0 . It is proposed that this exists in equilibrium with Pd^0 nanoparticles, which acts as a reservoir. The Pd^0 is then oxidized to Pd^{II} . This occurs in the initial methodology with $\text{PhI}(\text{OAc})_2$. Without the $\text{PhI}(\text{OAc})_2$ present, O_2 acts as a terminal oxidant. It was found that this reaction was more reliable in the presence of a substoichiometric quantity of $\text{Cu}(\text{OAc})_2$ (10 mol%). This is a known catalyst for oxidation processes. In the absence of air, only one turnover of $\text{Cu}(\text{OAc})_2$ is observed.

Therefore, a mild, low-temperature and selective method for the direct C-H bond functionalisation of the amino acid tryptophan **213** has been developed. A small library of analogues was synthesised. With substituted organoboronic acids, an increase in

stoichiometry was required to give good yields. It is proposed organoboronic acid is consumed competitively by Pd⁰ catalyst homocoupling. These were screened for their fluorescence properties (UV-Vis absorption maxima and emission spectra). It was important that these properties were sufficiently removed from those of unsubstituted tryptophan. It was found that those with the most extreme electronic properties (-C₆H₄OMe, -C₆H₄CF₃) were most effective for absorption (with the most shift absorption maxima of the analogues). The -C₆H₅ and -C₆H₄F had favourable fluorescence data, showing a significant shift from starting material was observed for the latter, whereas the -C₆H₅ analogue was especially emissive.

The optimized methodology was then applied to simple peptides. The dipeptide AcGlyTrpOMe showed full conversion to arylated product. Also observed in this reaction mixture was biphenyl, confirming the operation of an organoboronic acid Pd⁰-catalysed homocoupling pathway.

These conditions were applied to more complicated peptides, including tri-, tetra and hexapeptides. Arylated product was detected in all systems, in 46-86% yields. Small quantities of dioxidised product were observed in some peptides (specifically, where Trp is adjacent to a terminal Ala residue possessing a carboxylic acid end group), although the position of oxidation has not been determined.

4.2.2 – Future Work

The fluorescent analogues of tryptophan described in this thesis must be assessed for their use in biological experiments. It is proposed they might be of particular use when probing protein-peptide interactions. In order to be effective, they would have to be shown to be distinct from background fluorescence (for example, from unlabeled tryptophan-containing compounds, protein backbone, and DNA/RNA). It has already been demonstrated they are distinct from native tryptophan absorption and fluorescence. This work would have to be undertaken with the assistance of collaborators in biology. If these labels prove unsuitable, work should be undertaken to attempt to incorporate more traditional fluorescent labels such as fluorescein **250** or *N*-hydroxysuccinimide esters **251** (Figure 83).³⁰³

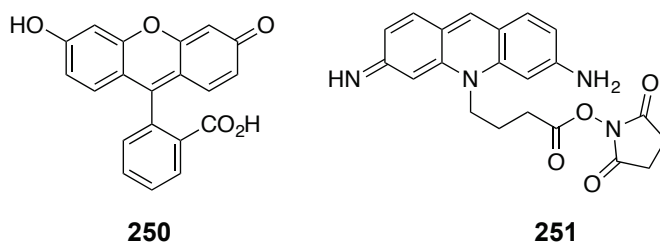


Figure 82: Fluorescein and Atto 465 NHS Ester.

There is an overwhelming number of peptides known, and an almost infinite number of possible permutations (e.g. for di- to decapeptides alone, there are 44,352,143 possible permutations using the 21 eukaryotic proteinogenic amino acids). Although only a small percentage of these are known natural peptides, a significant amount of work is required to assess the application of the C-H bond functionalisation conditions in different peptidic environments. Of particular interest will be peptides that contain cysteine residues (which has an S-functionalised side chain). Sulfur ligands have been implicated in the poisoning of Pd catalysts in cross-coupling reactions, and Davies and co-workers used a sulfur-ligand (3-mercaptopropionic acid) as a scavenger for Pd in their cross-coupling on the surface of proteins.^{239,304} These conditions may require further optimization to overcome these possible problems. The functionalized peptides are to be purified by preparative HPLC-MS, and the products analysed by NMR spectroscopy (using a 700 MHz instrument). Their UV-visible and fluorescent spectroscopic data will also be analysed.

The fluorescent properties of the analogues must be characterized further. Quantum yields and fluorescent lifetimes will give further details on the effectiveness of these compounds as photochemical probes. This work is to be done in collaboration with Prof. Andy Beeby at the University of Durham.

Pd⁰ nanoparticles have been characterised in this reaction. Studies similar to those outlined in 4.2.1 (kinetics, XPS, Hg drop tests and EXAFS) would provide more information on their exact nature and role.

The ultimate goal in the development of this methodology is the C-H bond functionalisation of tryptophan residues in proteins. The challenges associated with long chain peptides (multiple sites of functionalisation, non-specific binding of metal catalysts *etc.*) are relevant to proteins, but interruption of tertiary and quaternary

structure (unfolding) and loss of co-factors (e.g. heme) are also key problems to be solved. An initial way forward would be to select a simple well-characterized protein for early method development. It is proposed that equine apomyoglobin might be a suitable substrate, as it contains only one tryptophan residue. Further, it does not incorporate any co-factors or have a quaternary structure. An important and challenging area of study would be the detection of products, and possible methods include ESI-MS or MALDI-MS, fluorescence spectroscopy, and circular dichroism (CD).

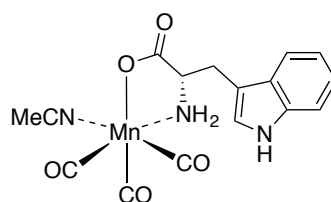


Figure 83: CO-RM JW-3.

The Fairlamb group has developed a light-activated CO releasing molecule (CO-RM)³⁰⁵³¹³ based on tryptophan. In the future, the tryptophan analogues described in this thesis could be used to modify the UV-Visible and fluorescence properties of these compounds.

ABBREVIATIONS

Ac	Acetyl
OAc	Acetate
AFM	Atomic force microscopy
aq.	Aqueous
Ar	Aryl
Bn	Benzyl
^t Bu	<i>tert</i> -Butyl
cat.	Catalytic
Coord.	Coordination
<i>m</i> -CPBA	2-Chloroperoxybenzoic acid
δ	Chemical shift downfield from tetramethylsilane
d (NMR)	Doublet
Deprot.	Deprotonation
DMA	<i>N,N'</i> -Dimethylacetamide
DMF	<i>N,N'</i> -Dimethylformamide
DMSO	Dimethylsulfoxide
EAS	Electrophilic aromatic substitution
Et	Ethyl
eq.	Equivalents
ESI	Electrospray ionisation
g	gram(s)
h	hour(s)
Het	Heteroarene
HRMS	High-resolution mass spectrometry
Hz	Hertz
IR	Infrared
<i>J</i>	Spin-spin coupling constant
L	Ligand
LIFDI	Liquid introduction field desorption ionisation
lit.	Literature value
μ	Micro
M (concentration)	mol dm ⁻³
m	Milli
m (NMR)	Multiplet
Me	Methyl
Mes	Mesityl
MP	Melting point
MW	Microwave

<i>m/z</i>	Mass-to-charge ratio
NHC	<i>N</i> -Heterocyclic carbene
NMP	1-Methyl-2-pyrrolidinone
NMR	Nuclear magnetic resonance
ⁿ Oct	<i>n</i> -Octyl
OMe-dba	4,4'-dimethoxydibenzylideneacetone
Ox. Add.	Oxidative addition
Ph	Phenyl
Phen	1,10-Phenanthroline
Pic	<i>p</i> -Iodobenzyl cysteine
ppm	Part(s) per million
ⁱ Pr	<i>iso</i> -Propyl
PXPd	Dichlorobis(chlorodi- <i>tert</i> butylphosphine)palladium(II)
PVP	Polyvinylpyrrolidone
Pd-PVP	PVP stabilised Pd ⁰ nanoparticles
Py	Pyridine
q (NMR)	Quarter
R	Substituent
Red.	Reduction
Red. Elim.	Reductive elimination
R _f	Retention factor
s	Second(s)
s (NMR)	Singlet
Stoich.	Stoichiometric
t (NMR)	Triplet
<i>t</i>	Time
TEM	Transmission electron microscopy
Tf	Trifluoromethylsulfonyl (triflyl)
TLC	Thin layer chromatography
THF	Tetrahydrofuran
TMS	Trimethylsilane
TOF	Time-of-flight
Tol	Toluene
<i>p</i> -Tol	4-Methylphenyl
Trans. Met.	Transmetallation
UV	Ultra-violet
Vis	Visible
X	(Pseudo)halide

Xantphos	4,5-Bis(diphenylphosphino)-9,9-dimethylxanthene
EXAFS	Extended X-ray fine structure spectroscopy
XAS	X-Ray absorption spectroscopy
XPS	X-ray photoelectron spectroscopy

REFERENCES

- (1) Nicolaou, K. C.; Bulger, P. G.; Sarlah, D. *Angew. Chem., Int. Ed.* **2005**, *44*, 4442-4489.
- (2) Mizoroki, T.; Mori, K.; Ozaki, A. *Bull. Chem. Soc. Jpn.* **1971**, *44*, 581-586.
- (3) Heck, R. F.; Nolley, J. P. *J. Org. Chem.* **1972**, *37*, 2320-2328.
- (4) Milstein, D.; Stille, J. K. *J. Am. Chem. Soc.* **1978**, *100*, 3636-3638.
- (5) Milstein, D.; Stille, J. K. *J. Am. Chem. Soc.* **1979**, *101*, 4992-4998.
- (6) Farina, V.; Kapadia, S.; Krishnan, B.; Wang, C. J.; Liebeskind, L. S. *J. Org. Chem.* **1994**, *59*, 5905-5911.
- (7) Miyaura, N.; Yamada, K.; Suzuki, A. *Tetrahedron Lett.* **1979**, *20*, 3437-3440.
- (8) Sonogashira, K.; Tohda, Y.; Hagihara, N. *Tetrahedron Lett.* **1975**, 4467-4470.
- (9) Sonogashira, K. *J. Organomet. Chem.* **2002**, *653*, 46-49.
- (10) Chinchilla, R.; Najera, C. *Chem. Rev.* **2007**, *107*, 874-922.
- (11) Nicolaou, K. C.; Yang, Z.; Shi, G. Q.; Gunzner, J. L.; Agrios, K. A.; Gartner, P. *Nature* **1998**, *392*, 264-269.
- (12) Wipf, P.; Graham, T. H. *J. Am. Chem. Soc.* **2004**, *126*, 15346-15347.
- (13) Ackermann, L.; Vicente, R.; Kapdi, A. R. *Angew. Chem., Int. Ed.* **2009**, *48*, 9792-9826.
- (14) Dangel, B. D.; Godula, K.; Youn, S. W.; Sezen, B.; Sames, D. *J. Am. Chem. Soc.* **2002**, *124*, 11856-11857.
- (15) Bowie Jr., A. L.; Trauner, D. *J. Org. Chem.* **2009**, *74*, 1581-1586.
- (16) Chen, D. Y. K.; Youn, S. W. *Chem. Eur. J.* **2012**, *18*, 9452-9474.
- (17) Vivian, J. T.; Callis, P. R. *Biophys. J.* **2001**, *80*, 2093-2109.
- (18) Callis, P. R.; Burgess, B. K. *J. Phys. Chem. B* **1997**, *101*, 9429-9432.
- (19) Boutureira, O.; Bernardes, Goncalo, J. L.; D'Hongre, F.; Davis, B. G. *Chem. Commun.* **2011**, *47*, 10010-10012.
- (20) Constantine, K. L. *Biophys. J.* **2001**, *81*, 1275-1284.
- (21) Yang, X. Q.; Guo, L. H. *Anal. Chim. Acta.* **2009**, *632*, 15-20.
- (22) Hermanson, G. T. *Bioconjugate Techniques*; Academic Press: St. Louis, MO., 1996.

-
- (23) Antos, J. M.; Francis, M. B. *Curr. Opin. Chem. Biol.* **2006**, *10*, 253μ262.
- (24) Foley, T. L.; Burkart, M. D. *Curr. Opin. Chem. Biol.* **2007**, *11*, 12μ19.
- (25) Chalker, J. M.; Davis, B. G. *Curr. Opin. Chem. Biol.* **2010**, *14*, 781μ789.
- (26) Storr, T. E.; Firth, A. G.; Wilson, K.; Darley, K.; Baumann, C. G.; Fairlamb, I. J. S. *Tetrahedron* **2008**, *64*, 6125μ6137.
- (27) Storr, T. E.; Baumann, C. G.; Thatcher, R. J.; De Ornellas, S.; Whitwood, A. C.; Fairlamb, I. J. S. *J. Org. Chem.* **2009**, *74*, 5810μ5821.
- (28) Storr, T. E.; Strohmeier, J. A.; Baumann, C. G.; Fairlamb, I. J. S. *Chem. Commun.* **2010**, *46*, 6470μ6472.
- (29) Janowicz, A. H.; Bergman, R. G. *J. Am. Chem. Soc.* **1982**, *104*, 352μ354.
- (30) Dawoodi, Z.; Green, M. L. H.; Mtetwa, V. S. . B.; Prout, K. *J. Chem. Soc., Chem. Commun.* **1982**, 802μ803.
- (31) Perutz, Robin N., Sabo-Etienne, S. *Angew. Chem., Int. Ed.* **2007**, *46*, 2578μ2592.
- (32) Grimmett, M. R. In *Comprehensive Heterocyclic Chemistry, Volume 5*; Katritzky, A. R.; Rees, C. W., Eds.; Pergamon Press: Oxford, UK, 1984; pp. 345μ498.
- (33) De Ornellas, S.; Storr, T. E.; Williams, T. J.; Baumann, C. G.; Fairlamb, I. J. S. *Curr. Org. Synth.* **2011**, *8*, 79μ101.
- (34) Pivsa-Art, S.; Satoh, T.; Kawamura, Y.; Miura, M.; Nomura, M. *Bull. Chem. Soc. Jpn.* **1998**, *71*, 467μ473.
- (35) Bellina, F.; Cauteruccio, S.; Mannina, L.; Rossi, R.; Viel, S. *J. Org. Chem.* **2005**, *70*, 3997μ4005.
- (36) Bellina, F.; Cauteruccio, S.; Mannina, L.; Rossi, R.; Viel, S. *Eur. J. Org. Chem.* **2006**, 693μ703.
- (37) Bellina, F.; Cauteruccio, S.; Rossi, R. *Eur. J. Org. Chem.* **2006**, 1379μ1382.
- (38) Bellina, F.; Calandri, C.; Cauteruccio, S.; Rossi, R. *Tetrahedron* **2007**, *63*, 1970μ1980.
- (39) Muzart, J. *Tetrahedron* **2009**, *65*, 8313μ8323.
- (40) Besselievre, F.; Mahuteau-Betzer, F.; Grierson, D. S.; Piguel, S. *J. Org. Chem.* **2008**, *73*, 3278μ3280.
- (41) Cerna, I.; Pohl, R.; Klepetarova, B.; Hocek, M. *Org. Lett.* **2006**, *8*, 5389μ5392.

-
- (42) Cerna, I.; Pohl, R.; Klepetarova, B.; Hocek, M. *J. Org. Chem.* **2008**, *73*, 9048μ9054.
- (43) Sahnoun, S.; Messaoudi, S.; Peyrat, J. F.; Brion, J. D.; Alami, M. *Tetrahedron Lett.* **2008**, *49*, 7279μ7283.
- (44) Vrabel, M.; Pohl, R.; Votruba, I.; Sajadi, M.; Kovalenko, S. A.; Ernsting, N. P.; Hocek, M. *Org. Biomol. Chem.* **2008**, *6*, 2852μ2860.
- (45) Mori, A.; Sekiguchi, A.; Masui, K.; Shimada, T.; Horie, M.; Osakada, K.; Kawamoto, M.; Ikeda, T. *J. Am. Chem. Soc.* **2003**, *125*, 1700μ1701.
- (46) Masui, K.; Mori, A.; Okano, K.; Takamura, K.; Kinoshita, M.; Ikeda, T. *Org. Lett.* **2004**, *6*, 2011μ2014.
- (47) Sun, H. R.; DiMagno, S. G. *J. Am. Chem. Soc.* **2005**, *127*, 2050μ2051.
- (48) Miyaoku, T.; Mori, A. *Heterocycles* **2009**, *77*, 151μ155.
- (49) Huang, J. K.; Chan, J.; Chen, Y.; Borths, C. J.; Baucom, K. D.; Larsen, R. D.; Faul, M. M. *J. Am. Chem. Soc.* **2010**, *132*, 3674μ3675.
- (50) Do, H. Q.; Daugulis, O. *J. Am. Chem. Soc.* **2007**, *129*, 12404μ12405.
- (51) Do, H. O.; Khan, R. M. K.; Daugulis, O. *J. Am. Chem. Soc.* **2008**, *130*, 15185μ15192.
- (52) Do, H. Q.; Daugulis, O. *J. Am. Chem. Soc.* **2008**, *130*, 1128μ1129.
- (53) Wolter, M.; Nordmann, G.; Job, G. E.; Buchwald, S. L. *Org. Lett.* **2002**, *4*, 973μ976.
- (54) Altman, R. A.; Shafir, A.; Choi, A.; Lichtor, P. A.; Buchwald, S. L. *J. Org. Chem.* **2008**, *73*, 284μ286.
- (55) Gujadhur, R. K.; Bates, C. G.; Venkataraman, D. *Org. Lett.* **2001**, *3*, 4315μ4317.
- (56) Shen, K.; Fu, Y.; Li, J. N.; Liu, L.; Guo, Q. X. *Tetrahedron* **2007**, *63*, 1568μ1576.
- (57) Yoshizumi, T.; Tsurugi, H.; Satoh, T.; Miura, M. *Tetrahedron Lett.* **2008**, *49*, 1598μ1600.
- (58) Yoshizumi, T.; Satoh, T.; Hirano, K.; Matsuo, D.; Orita, A.; Otera, J.; Miura, M. *Tetrahedron Lett.* **2009**, *50*, 3273μ3276.
- (59) Kawano, T.; Yoshizumi, T.; Hirano, K.; Satoh, T.; Miura, M. *Org. Lett.* **2009**, *11*, 3072μ3075.
- (60) Ellis, P. J. *Mechanistic Studies of Cross-Coupling Reactions Using Palladium Nanoparticles*, University of York, 2009.

-
- (61) Bell, A. T. *Science* **2003**, *14*, 1688.
- (62) Haensel, V.; Bloch, H. S. *Platinum Met. Rev.* **1964**, *8*, 2.
- (63) Tollefson, J. *Nature* **2007**, *450*, 334.
- (64) Lewis, L. N.; Lewis, N. *J. Am. Chem. Soc.* **1986**, *108*, 7228μ7231.
- (65) Beller, M.; Fischer, H.; Kuhlein, K.; Reisinger, C. P.; Herrmann, W. A. *J. Organomet. Chem.* **1996**, *520*, 257μ259.
- (66) Bonnemann, H.; Brijoux, W.; Brinkmann, E.; Dinjus, R.; Fretzen, T.; Joußen, T.; Korall, B. *Angew. Chem., Int. Ed.* **1991**, *30*, 1312.
- (67) Le Bars, J.; Specht, U.; Bradley, J. S.; Blackmond, D. G. *Langmuir* **1999**, *15*.
- (68) Van Hardelveld, R. Hartog, F. *Surface Sci.* **1969**, *15*, 189μ230.
- (69) Davis, J. L.; Barteau, M. A. *Langmuir* **2002**, *5*, 1299μ1309.
- (70) Ding, J. H.; Gin, D. L. *Chem. Mater.* **2000**, *12*, 22μ24.
- (71) Klingelhofer, S.; Heitz, W.; Greiner, A.; Oestreich, S.; Forster, S.; Antonietti, M. *J. Am. Chem. Soc.* **1997**, *119*, 10116μ10120.
- (72) Reetz, M. T.; Breinbauer, R.; Wanninger, K. *Tetrahedron Lett.* **1996**, *37*.
- (73) Li, Y.; Hong, X. M.; Collard, D. M.; El-Sayed, M. A. *Org. Lett.* **2002**, *2*, 2385μ2388.
- (74) Teranishi, T.; Miyake, M. *Chem. Mater.* **1998**, *10*, 594μ600.
- (75) Tang, T.; Metanawin, T.; Hebden, A.; McGowan, P.; Wang, X. S. *Chem. Commun.* **2010**, *46*, 6663μ6665.
- (76) Hartwig, J. *Organotransition Metal Chemistry: From Bonding to Catalysis*; University Science Books: South Orange, NJ, 2010.
- (77) Carrow, B. P.; Hartwig, J. F. *J. Am. Chem. Soc.* **2011**, *133*, 2116μ2119.
- (78) Amatore, C.; Jutand, A.; Le Duc, G. *Chem. Eur. J.* **2011**, *17*, 2492μ2503.
- (79) Luis Serrano, J.; Garcia, L.; Perez, J.; Perez, E.; Garcia, J.; Sanchez, G.; Sehnal, P.; De Ornellas, S.; Williams, T. J.; Fairlamb, I. J. S.; Serrano, J. L. *Organometallics* **2011**, *30*, 5095μ5109.
- (80) Consorti, C. S.; Flores, F. R.; Dupont, J. *J. Am. Chem. Soc.* **2005**, *127*, 12054μ12065.

-
- (81) Phan, N. T. S.; Van der Sluys, M.; Jones, C. W. *Adv. Synth. Catal.* **2006**, *348*, 609μ679.
- (82) Cassol, C. C.; Umpierre, A. P.; Machado, G.; Wolke, S. I.; Dupont, J. J. *Am. Chem. Soc.* **2005**, *127*, 3298μ3299.
- (83) Davis, J. J.; Coleman, K. S.; Busuttill, K. L.; Bagshaw, C. B. *J. Am. Chem. Soc.* **2005**, *127*, 13082μ13083.
- (84) Ellis, P. J.; Fairlamb, I. J. S.; Hackett, S. F. J.; Wilson, K.; Lee, A. F. *Angew. Chem., Int. Ed.* **2010**, *49*, 1820μ1824.
- (85) Lee, A. F.; Ellis, P. J.; Fairlamb, I. J. S.; Wilson, K. *Dalton Trans.* **2010**, *39*, 10473μ10482.
- (86) Widegren, J. A.; Bennett, M. A.; Finke, R. G. *J. Am. Chem. Soc.* **2003**, *125*, 10301μ10310.
- (87) Widegren, J. A.; Finke, R. G. *J. Mol. Catal. A: Chem.* **2003**, *198*, 317μ341.
- (88) Lee, A. F.; Ellis, P. J.; Fairlamb, I. J. S.; Wilson, K. *Abstracts of Papers of the American Chemical Society* **2010**, *240*.
- (89) Arduengo, A. J. *Acc. Chem. Res.* **1999**, *32*, 913μ921.
- (90) Goedecke, C.; Leibold, M.; Siemeling, U.; Frenking, G. *J. Am. Chem. Soc.* **2011**, *133*, 3557μ3569.
- (91) Herrmann, W. A.; Denk, M.; Behm, J.; Scherer, W.; Klingan, F. R.; Bock, H.; Solouki, B.; Wagner, M. *Angew. Chem., Int. Ed.* **1992**, *31*, 1485μ1488.
- (92) Denk, M.; Lennon, R.; Hayashi, R.; West, R.; Belyakov, A. V.; Verne, H. P.; Haaland, A.; Wagner, M.; Metzler, N. *J. Am. Chem. Soc.* **1994**, *116*, 2691μ2692.
- (93) Alder, R. W.; Allen, P. R.; Murray, M.; Orpen, A. G. *Angew. Chem., Int. Ed.* **1996**, *35*, 1121μ1123.
- (94) Arduengo, A. J.; Bock, H.; Chen, H.; Denk, M.; Dixon, D. A.; Green, J. C.; Herrmann, W. A.; Jones, N. L.; Wagner, M.; West, R. *J. Am. Chem. Soc.* **1994**, *116*, 6641μ6649.
- (95) Arduengo, A. J.; Dias, H. V. R.; Dixon, D. A.; Harlow, R. L.; Klooster, W. T.; Koetzle, T. F. *J. Am. Chem. Soc.* **1994**, *116*, 6812μ6822.
- (96) Ofele, K. *J. Organomet. Chem.* **1968**, *12*, P42μP43.
- (97) Wanzlick, H. W.; Schonher, H. *Angew. Chem., Int. Ed.* **1968**, *7*, 141μ&.
- (98) Diez-Gonzalez, S.; Nolan, S. P. *Synlett* **2007**, 2158.

-
- (99) Diez-Gonzalez, S.; Nolan, S. P. *Acc. Chem. Res.* **2008**, *41*.
- (100) Munro-Leighton, M.; Delp, S. A.; Blue, E. D.; Gunnoe, T. B. *Organometallics* **2007**, *26*, 1483.
- (101) Munro-Leighton, M.; Delp, S. A.; Alsop, N. M.; Blue, E. D.; Gunnoe, T. B. *Chem. Commun.* **2008**, 111.
- (102) Teyssot, M. L.; Jarrousse, A. S.; Manin, M.; Chevry, A.; Roche, S.; Norre, F.; Deaudoin, C.; Morel, L.; Boyer, D.; Mahiou, R.; Gautier, A. *Dalton Trans.* **2009**, 6894.
- (103) Diez-Gonzalez, S.; Scott, N. M.; Nolan, S. P. *Organometallics* **2006**, *25*, 2355μ2358.
- (104) Arduengo, A. J.; Dias, H. V. R.; Calabrese, J. C.; Davidson, F. *Organometallics* **1993**, *12*, 3405μ3409.
- (105) Raubenheimer, H. G.; Cronje, S.; Olivier, P. J. *J. Chem. Soc., Dalton Trans.* **1995**, 313μ316.
- (106) Tulloch, A. A. D.; Danopoulos, A. A.; Kleinhenz, S.; Light, M. E.; Hursthouse, M. B.; Eastham, G. *Organometallics* **2001**, *20*, 2027μ2031.
- (107) Simonovic, S.; Whitwood, A. C.; Clegg, W.; Harrington, R. W.; Hursthouse, M. B.; Male, L.; Douthwaite, R. E. *Eur. J. Inorg. Chem.* **2009**, 1786μ1795.
- (108) Citadelle, C. A.; Le Nouy, E.; Bisaro, F.; Slawin, A. M. Z.; Cazin, C. S. J. *Dalton Trans.* **2010**, *39*, 4489μ4491.
- (109) Boogaerts, I. I. F.; Fortman, G. C.; Furst, M. R. L.; Cazin, C. S. J.; Nolan, S. P. *Angew. Chem., Int. Ed.* **2010**, *49*, 8674μ8677.
- (110) Venkatachalam, G.; Heekenroth, M.; Neels, A.; Albrecht, M. *Helv. Chim. Acta.* **2009**, *92*, 1034μ1045.
- (111) Arnold, P. L.; Scarisbrick, A. C.; Blake, A. J.; Wilson, C. *Chem. Commun.* **2001**, 2340μ2341.
- (112) Schneider, N.; Cesar, V.; Bellemin-Lapponnaz, S.; Gade, L. H. *J. Organomet. Chem.* **2005**, *690*, 5556μ5561.
- (113) Kaur, H.; Zinn, F. K.; Stevens, E. D.; Nolan, S. P. *Organometallics* **2004**, *23*, 1157μ1160.
- (114) Lebel, H.; Davi, M.; Diez-Gonzalez, S.; Nolan, S. P. *J. Organomet. Chem.* **2007**, *72*, 144μ149.
- (115) Diez-Gonzalez, S.; Escudero-Adan, E. C.; Benet-Buchholz, J.; Stevens, E. D.; Slawin, A. M. Z.; Nolan, S. P. *Dalton Trans.* **2010**, *39*, 7595μ7606.

-
- (116) Mankad, N. P.; Gray, T. G.; Laitar, D. S.; Sadighi, J. P. *Organometallics* **2004**, *23*, 1191μ1193.
- (117) Ren, H.; Zhao, X.; Xu, S.; Song, H.; Wang, B. *J. Organomet. Chem.* **2006**, *691*, 4109μ4113.
- (118) Matsumoto, K.; Matsumoto, N.; Ishii, A.; Tsukuda, T.; Hasegawa, M.; Tsubomura, T. *Dalton Trans.* **2009**, 6795μ6801.
- (119) Shishkov, I. V.; Rominger, F.; Hofmann, P. *Dalton Trans.* **2009**, 1428μ1435.
- (120) Furst, M. R. L.; Cazin, C. S. J. *Chem. Commun.* **2010**, *46*, 6924μ6925.
- (121) Doyle, M. P.; Forbes, D. C. *Chem. Rev.* **1998**, *98*, 911μ935.
- (122) Buhl, M.; Terstegen, F.; Loffler, F.; Meynhardt, B.; Kierse, S.; Muller, M.; Nather, C.; Luning, U. *Eur. J. Org. Chem.* **2001**, 2151μ2160.
- (123) Straub, B. F.; Hofmann, P. *Angew. Chem., Int. Ed.* **2001**, *40*, 1288μ+.
- (124) Tan, K. L.; Bergman, R. G.; Ellman, J. A. *J. Am. Chem. Soc.* **2002**, *124*, 3202μ3203.
- (125) Benhamou, L.; Chardon, E.; Lavigne, G.; Bellemin-Lapponnaz, S.; Cesar, V. *Chem. Rev.* **2011**, *111*, 2705μ2733.
- (126) Nyce, G. W.; Csihony, S.; Waymouth, R. M.; Hedrick, J. L. *Chem. Eur. J.* **2004**, *10*, 4073μ4079.
- (127) Reeds, J. P.; Fairlamb, I. J. S. Exploiting imidate ligand effects in transition metal-mediated C-C bond forming processes, University of York, 2011, Vol. PhD.
- (128) Bellina, F.; Cauteruccio, S.; Rossi, R. *Curr. Org. Chem.* **2008**, *12*, 774μ790.
- (129) Zou, J.; Stewart, S. G.; Raston, C. L.; Iyer, K. S. *Chem. Commun.* **2011**, *47*, 1803μ1805.
- (130) Yu, P.; Zhang, G.; Chen, F.; Cheng, J. *Tetrahedron Lett.* **2012**, *53*, 4588μ4590.
- (131) Deprez, N. R.; Kalyani, D.; Krause, A.; Sanford, M. S. *J. Am. Chem. Soc.* **2006**, *128*, 4972μ4973.
- (132) Phipps, R. J.; Gaunt, M. J. *Science* **2009**, *323*, 1593μ1597.
- (133) Sehnal, P.; Taylor, R. J. K.; Fairlamb, I. J. S. *Chem. Rev.* **2010**, *110*, 824μ889.
- (134) Shibahara, F.; Yamaguchi, E.; Murai, T. *Chem. Commun.* **2010**, *46*, 2471μ2473.
- (135) Lynch, B. M. Pausacker, K. H. *Aust. J. Chem.* **1957**, *10*, 329μ333.

-
- (136) Leffler, J. E.; Ward, D. C.; Burduroglu, A. *J. Am. Chem. Soc.* **1972**, *94*, 5339-5341.
- (137) Amatore, C.; Jutand, A.; Khalil, F.; M'Barki, M. A.; Mottier, L. *Organometallics* **1993**, *12*, 3168-3178.
- (138) Amatore, C.; Fuxa, A.; Jutand, A. *Chem. Eur. J.* **2000**, *6*, 1474-1482.
- (139) Alami, M.; Amatore, C.; Bensalem, S.; Choukchou-Brahim, A.; Jutand, A. *Eur. J. Inorg. Chem.* **2001**, 2675-2681.
- (140) Jia, X. F.; Yang, D. P.; Wang, W. H.; Luo, F.; Cheng, J. *J. Org. Chem.* **2009**, *74*, 9470-9474.
- (141) Daugulis, O.; Do, H. Q.; Shabashov, D. *Acc. Chem. Res.* **2009**, *42*, 1074-1086.
- (142) Bellina, F.; Rossi, R. *Adv. Synth. Catal.* **2010**, *352*, 1223-1276.
- (143) Chui, J. K. W.; Ramnial, T.; Clyburne, J. A. C. *Comm. Inorg. Chem.* **2003**, *24*, 165-187.
- (144) Cowan, J. A.; Clyburne, J. A. C.; Davidson, M. G.; Harris, R. L. W.; Howard, J. A. K.; Kupper, P.; Leech, M. A.; Richards, S. P. *Angew. Chem., Int. Ed.* **2002**, *41*, 1432-1434.
- (145) Arduengo, A. J.; Gamper, S. F.; Tamm, M.; Calabrese, J. C.; Davidson, F.; Craig, H. A. *J. Am. Chem. Soc.* **1995**, *117*, 572.
- (146) Jeffrey, G. A. *An Introduction to Hydrogen Bonding*; Oxford University Press: Oxford, UK, 1997.
- (147) Steiner, T. *Angew. Chem., Int. Ed.* **2002**, *41*, 48-76.
- (148) Merz Jr, K. M.; Hoffman, R. *Inorg. Chem.* **1988**, *27*, 2120-2127.
- (149) Kolmel, C.; Ahlrichs, R. *J. Phys. Chem.* **1990**, *94*, 5536-5542.
- (150) Abraham, S. P.; Samuelson, A. G.; Chandrasekhar, J. *Inorg. Chem.* **1993**, *32*, 6107-6111.
- (151) Poblet, J. M.; Bernard, M. *Chem. Commun.* **1998**, 1179-1180.
- (152) Pyykko, P. *Chem. Rev.* **1997**, *97*.
- (153) Schmidbaur, H.; Grad, W.; Muller, G. *Angew. Chem., Int. Ed.* **1988**, *27*, 417-419.
- (154) Schmidbaur, H. *Chem. Soc. Rev.* **1995**, 391-400.

-
- (155) Kanehama, R.; Umemiya, M.; Iwahori, F.; Miyakaska, H.; Sugiura, K.; Yamashita, M.; Yokochi, Y.; Ito, H.; Kuroda, S.; Kishida, H.; Okamoto, H. *Inorg. Chem.* **2003**, *42*, 7173μ7181.
- (156) Asplund, M.; Jagner, S. *Acta Chem. Scan.* **1984**, *38A*, 135μ139.
- (157) Andersson, S.; Jagner, S. *Acta Chem. Scan.* **1987**, *41A*, 230μ236.
- (158) Lu, W.; Zhu, Q. Y.; Zhang, Y.; Lin, X. M.; Dai, J. *Acta. Cryst. C.* **2007**, *63*, M496μM498.
- (159) Huang, X. F.; Song, Y. M.; Wang, X. S.; Pang, J.; Zuo, J. L.; Ziong, R. G. *J. Organomet. Chem.* **2006**, *691*, 1065μ1074.
- (160) Swank, D. D.; Willett, R. D. *Inorg. Chem.* **1980**, 2321μ2323.
- (161) Xu, G. H.; Wang, W. *Acta. Cryst. E.* **2008**, *64*, M1198.
- (162) Lake, B. R. M.; Bullough, E. K.; Williams, T. J.; Whitwood, A. C.; Little, M. A.; Willans, C. E. *Chem. Commun.* **2012**, *48*, 4887μ4889.
- (163) Blue, E. D.; Gunnoe, T. B.; Petersen, P. D.; Boyle, P. D. *J. Organomet. Chem.* **2006**, *691*, 5988μ5993.
- (164) Li, Y.; Deng, W.-P.; Du, W. *Tetrahedron* **2012**, *68*, 3611μ3615.
- (165) Huynh, H. V.; Jothibas, L. L.; Koh, L. L. *Organometallics* **2007**, *26*, 6852μ6856.
- (166) Caballero, A.; Despagnet-Ayoub, E.; Diaz-Requejo, M. M.; Diaz-Rodriguez, A.; Gonzalez-Nunez, M. E.; Mello, R.; Muoz, B. K.; Ojo, W. S.; Asensio, G.; Etienne, M.; Perez, P. J. *Science* **2012**, *332*, 835μ838.
- (167) CrysAlisPro.
- (168) Dolomanov, O. V.; Bourhis, L. J.; Gildea, R. J.; Howard, J. A. K.; Puschmann, H. *J. Appl. Cryst.* **2009**, *42*, 339μ341.
- (169) Sheldrick, G. M. SHELXS-97 **1997**.
- (170) Sheldrick, G. M. SHELXL-97 **1997**.
- (171) Turner, G. L.; Morris, J. A.; Greaney, M. F. *Angew. Chem., Int. Ed.* **2007**, *46*, 7996μ8000.
- (172) Patil, S.; Claffey, J.; Dealley, A.; Hogan, M.; Gleeson, B.; Mendez, L. M. M. ; Muller-Bunz, H.; Paradisi, F.; Tckle, M. *Eur. J. Inorg. Chem.* **2010**, 1020μ1031.
- (173) Lee, H.-G.; Won, J.-E.; Kim, M.-J.; Park, S.-E.; Jung, K.-J.; Bo, R. K.; Lee, S.-G. *J. Org. Chem.* **2009**, *74*, 5675μ5678.

-
- (174) Zhong-Hua, M.; Lin, S.; Nie, J. *Synth. Comm.* **2012**, *42*.
- (175) Franco, L. H.; Joffe, E. B. D.; Puricelli, L.; Tatian, M.; Seldes, A. M.; Palermo, J. *A. J. Nat. Prod.* **1998**, *61*, 1130µ1132.
- (176) Evans, B.; Oxford, A. W.; Butain, D. *Indole Derivatives* **1985**.
- (177) Humphrey, G. R.; Kuethe, J. T. *Chem. Rev.* **2006**, *106*, 2875µ2911.
- (178) Billingsley, K. L.; Anderson, K. W.; Buchwald, S. L. *Angew. Chem., Int. Ed.* **2006**, *45*, 3484µ3488.
- (179) Firth, A. G.; Fairlamb, I. J. S.; Darley, K.; Baumann, C. G. *Tetrahedron Lett.* **2006**, *47*, 3529µ3533.
- (180) Firth, A. G.; Wilson, K.; Baumann, C. G.; Fairlamb, I. J. S. *Nucleosides, Nucleotides Nucleic Acids* **2011**, *30*, 168µ184.
- (181) Lewis, J. C.; Bergman, R. G.; Ellman, J. A. *Acc. Chem. Res.* **2008**, *41*, 1013µ1025.
- (182) Fujita, K.; Nonogawa, M.; Yamaguchi, R. *Chem. Commun.* **2004**, 1926µ1927.
- (183) Canivet, J.; Yamaguchi, J.; Ban, I.; Itami, K. *Org. Lett.* **2009**, *11*, 1733µ1736.
- (184) Wang, X.; Gribkov, D. V.; Sames, D. *J. Org. Chem.* **2007**, *72*, 1476µ1479.
- (185) Jackson, A. H.; Lynch, P. P. *J. Chem. Soc., Perkin Trans. 2* **1987**, 1215µ1219.
- (186) Grimster, N. P.; Gauntlett, C.; Godfrey, C. R. A.; Gaunt, M. J. *Angew. Chem., Int. Ed.* **2005**, *44*, 3125µ3129.
- (187) Moritani, I.; Fujiwara, Y. *Tetrahedron Lett.* **1967**, *8*, 1119µ1122.
- (188) Nyholm, R. S.; Royo, P. *J. Chem. Soc., D: Chem. Commun.* **1969**, 421.
- (189) Uson, R.; Royo, P.; Fornies, J.; Martinez, F. *J. Organomet. Chem.* **1975**, *90*, 367µ374.
- (190) Uson, R.; Fornies, J.; Navarro, R. *J. Organomet. Chem.* **1975**, *96*, 307.
- (191) VanBelzen, R.; Hoffman, H.; Elsevier, C. J. *Angew. Chem., Int. Ed.* **1997**, *36*, 1743.
- (192) VanBelzen, R.; Elsevier, C. J.; Dedieu, A.; Veldman, N.; Spek, A. L. *Organometallics* **2003**, *22*, 722.
- (193) Guo, R. Y.; Portscheller, J. L.; Day, V. W.; Malinakova, H. C. *Organometallics* **2007**, *26*, 3874.

-
- (194) Tremont, S. J.; Rahman, H. U. *J. Am. Chem. Soc.* **1984**, *106*, 5759.
- (195) Powers, D. C.; Ritter, T. *Nature Chem.* **2009**, *1*, 302μ309.
- (196) Powers, D. C.; Ritter, T. *Top. Organomet. Chem.* **2001**, *35*, 129μ156.
- (197) Powers, D. C.; Lee, E.; Ariafard, A.; Sanford, M. S.; Yates, B. F.; Canty, A. J.; Ritter, T. *J. Am. Chem. Soc.* **2012**, *134*, 12002μ12009.
- (198) Ariafard, A.; Hyland, C. J. T.; Canty, A. J.; Sharma, M.; Brookes, N. J.; Yates, B. F. *Inorg. Chem.* **2010**, *49*, 11249μ11253.
- (199) Lebrasseur, N.; Larrosa, I. *J. Am. Chem. Soc.* **2008**, *130*, 2926μ2927.
- (200) Liang, Z.; Yao, B.; Zhang, Y. *Org. Lett.* **2010**, *12*, 3185μ3187.
- (201) De Vries, A. H. M.; Mulders, J.; Mommers, J. H. M.; Henderickx, H. J. W.; De Vries, J. G. *Org. Lett.* **2003**, *5*, 3285μ3288.
- (202) Molander, G. A.; Biolatto, B. *Org. Lett.* **2002**, *4*, 1867μ1870.
- (203) Butters, M.; Harvey, J. N.; Jover, J.; Lennox, A. J. J.; Lloyd-Jones, G. C.; Murray, P. M. *Angew. Chem., Int. Ed.* **2010**, *49*, 5156μ5160.
- (204) Zhao, J.; Zhang, Y.; Cheng, K. *J. Org. Chem.* **2008**, *73*, 7428μ7431.
- (205) Stuart, D. R.; Fagnou, K. *Science* **2007**, *316*, 1172μ1175.
- (206) Casalnuovo, A. L.; Calabrese, J. C. *J. Am. Chem. Soc.* **1990**, *112*, 4324μ4330.
- (207) Kundu, N. G.; Pal, M.; Mahanty, J. S.; Dasgupta, S. K. *J. Chem. Soc., Chem. Commun.* **1992**, 41μ42.
- (208) Crisp, G. T.; Gore, J. *Tetrahedron* **1997**, *53*, 1523μ1544.
- (209) Echavarren, A. M.; Stille, J. K. *J. Am. Chem. Soc.* **1987**, *109*, 5478μ5486.
- (210) Tilley, J. W.; Sarabu, R.; Wagner, R.; Mulkerins, K. *J. Org. Chem.* **1990**, *55*, 906μ910.
- (211) Sengupta, S.; Bhattacharyya, S. *Tetrahedron Lett.* **1995**, *36*, 4475μ4478.
- (212) Shieh, W. C.; Carlson, J. A. *J. Org. Chem.* **1992**, *57*, 379μ381.
- (213) Uenishi, J.; Beau, J. M.; Armstrong, R. W.; Kishi, Y. *J. Am. Chem. Soc.* **1987**, *109*, 4756μ4758.
- (214) Burk, M. J.; Lee, J. R.; Martinez, J. P. *J. Am. Chem. Soc.* **1994**, *116*, 10847μ10848.

-
- (215) Firooznia, F.; Gude, C.; Chan, K.; Satoh, Y. *Tetrahedron Lett.* **1998**, *39*, 3985μ3988.
- (216) Satoh, Y.; Gude, C.; Chan, K.; Firooznia, F. *Tetrahedron Lett.* **1997**, *38*, 7645μ7648.
- (217) Roy, A. D.; Goss, R. J. M.; Wagner, G. K.; Winn, M. *Chem. Commun.* **2008**, 4831μ4833.
- (218) Goss, R. J. M.; Newill, P. L. A. *Chem. Commun.* **2006**, 4924μ4925.
- (219) Dibowski, H.; Schmidtchen, F. P. *Angew. Chem., Int. Ed.* **1998**, *37*, 476μ478.
- (220) Hessler, A.; Stelzer, O.; Dibowski, H.; Worm, K.; Schmidtchen, F. P. *J. Org. Chem.* **1997**, *62*, 2362μ2369.
- (221) Dibowski, H.; Schmidtchen, F. P. *Tetrahedron* **1995**, *51*, 2325μ2330.
- (222) Batsanov, A. S.; Collings, J. C.; Fairlamb, I. J. S.; Holland, J. P.; Howard, J. A. K.; Lin, Z. Y.; Marder, T. B.; Parsons, A. C.; Ward, R. M.; Zhu, J. *J. Org. Chem.* **2005**, *70*, 703μ706.
- (223) Bayer, E. A.; Wilchek, M. *Methods Enzymol.* **1990**, *184*, 138μ160.
- (224) Bong, D. T.; Ghadiri, M. R. *Org. Lett.* **2001**, *3*, 2509μ2511.
- (225) Corona, C.; Bryant, B. K.; Arterburn, J. B. *Org. Lett.* **2006**, *8*, 1883μ1886.
- (226) Kotha, S.; Lahin, K. *Biopolymers* **2003**, *69*, 517μ528.
- (227) Ojida, A.; Tsutsumi, H.; Kasagi, N.; Hamachi, I. *Tetrahedron Lett.* **2005**, *46*, 3301μ3305.
- (228) Lee, Y. W.; Han, S. B.; Ko, A. R.; Kim, H. S.; Park, K. W. *Catal. Commun.* **2011**, *15*, 137μ140.
- (229) Doan, N. D.; Bourgault, S.; Letourneau, M.; Fournier, A. *J. Comb. Chem.* **2008**, *10*, 44μ51.
- (230) Vilaro, M.; Arsequell, G.; Valencia, G.; Ballesteros, A.; Barluenga, J. *Org. Lett.* **2008**, *10*, 3243μ3245.
- (231) Espuna, G.; Andreu, D.; Barluenga, J.; Perez, X.; Planas, A.; Arsequell, G.; Valencia, G. *Biochemistry* **2006**, *45*, 5957μ5963.
- (232) Kodama, K.; Fukuzawa, S.; Nakayama, H.; Kigawa, T.; Sakamoto, K.; Yabuki, T.; Matsuda, N.; Shirouzu, M.; Takio, K.; Tachibana, K.; Yokoyama, S. *ChemBioChem* **2006**, *7*, 134μ139.

- (233) Kodama, K.; Fukuzawa, S.; Nakayama, H.; Sakamoto, K.; Kigawa, T.; Yabuki, T.; Matsuda, N.; Shirouzu, M.; Takio, K.; Yokoyama, S.; Tachibana, K. *ChemBioChem* **2007**, *8*, 232μ238.
- (234) Brustad, E.; Bushey, M. L.; Lee, J. W.; Groff, D.; Liu, W.; Schultz, P. G. *Angew. Chem., Int. Ed.* **2008**, *47*, 8220μ8223.
- (235) Jarvis, A. G.; Fairlamb, I. J. S. *Curr. Org. Chem.* **2011**, *15*, 3175μ3196.
- (236) Adams, B. K.; Ferstl, E. M.; Davis, M. C.; Herold, M.; Kurtkaya, S.; Camalier, R. F.; Hollingshead, M. G.; Kaur, G.; Sausville, E. A.; Rickes, F. R.; Snyder, J. P.; Liotta, D. C.; Shoji, M. *Bioorg. Med. Chem.* **2006**, *12*, 3871μ3883.
- (237) Chalker, J. M.; Wood, C. S. C.; Davis, B. G. *J. Am. Chem. Soc.* **2009**, *131*, 16346μ16347.
- (238) Li, J. H.; Zhang, X. D.; Xie, Y. X. *Eur. J. Org. Chem.* **2005**, 4256μ4259.
- (239) Spicer, C. D.; Davis, B. G. *Chem. Commun.* **2011**, *47*, 1698μ1700.
- (240) Zwick, M. B.; Bonnycastle, I. L. C.; Noren, K. A.; Venturini, S.; Barbas, C. F.; Noren, C. J.; Scott, J. K. *Anal. Biochem.* **1998**, *264*, 87μ97.
- (241) Fox, J. D.; Kapust, R. B.; Waugh, D. S. *Protein Sci.* **2001**, *10*, 622μ630.
- (242) Rossi, L. M.; Vono, L. L. R.; Silva, F. P.; Kiyohara, P. K.; Duarte, E. L.; Matos, J. R. *Appl. Catal., A.* **2007**, *330*, 139μ144.
- (243) Spicer, C. D.; Triemer, T.; Davis, B. G. *J. Am. Chem. Soc.* **2012**, *134*, 800μ803.
- (244) Liu, D. R.; Magliery, T. J.; Pasternak, M.; Schultz, P. G. *Proc. Nat. Acad. Sci.* **1997**, *94*, 10092μ10097.
- (245) Hong, V.; Steinmetz, N. F.; Manchester, M.; Finn, M. G. *Bioconjugate Chem.* **2010**, *21*, 1912μ1916.
- (246) Zhao, L.; Li, C. J. *Angew. Chem., Int. Ed.* **2008**, *47*, 7075μ7078.
- (247) Castelhana, A. L.; Horne, S.; Taylor, G. J.; Billedeau, R.; Krantz, A. *Tetrahedron* **1988**, *44*, 5451μ5466.
- (248) Vicente, J.; Saura-Llamas, I.; Antonio Garcia-Lopez, J.; Calmuschi-Cula, B.; Bautista, D. *Organometallics* **2007**, *26*, 2768μ2776.
- (249) Albert, J.; Cadena, J. M.; Granell, J. *Tetrahedron: Asymmetry* **1997**, *8*, 991μ994.
- (250) Fuchita, Y.; Yoshinaga, K.; Ikeda, Y.; Kinoshita-Kawashima, J. *J. Chem. Soc., Dalton Trans.* **1997**, 2495μ2499.
- (251) Albert, J.; Granell, J.; Muller, G. *J. Organomet. Chem.* **2006**, *691*, 2101μ2106.

-
- (252) Hajipour, A. R.; Karami, K.; Pirisedigh, A.; Ruoho, A. E. *Amino Acids* **2009**, *37*, 537μ541.
- (253) Nieto, S.; Arnau, P.; Serrano, E.; Navarro, R.; Soler, T.; Cativiela, C.; Urriolabeitia, E. P. *Inorg. Chem.* **2009**, *48*, 11963μ11975.
- (254) Navarroranninger, C.; Lopezsolera, I.; Perez, J. M.; Rodriguez, J.; Garciaruano, J. L.; Raithby, P. R.; Masaguer, J. R.; Alonso, C. *J. Med. Chem.* **1993**, *36*, 3795μ3801.
- (255) Navarroranninger, C.; Lopezsolera, I.; Gonzalez, V. M.; Perez, J. M.; Alvarezvaldes, A.; Martin, A.; Raithby, P. R.; Masaguer, J. R.; Alonso, C. *Inorg. Chem.* **1996**, *35*, 5181μ5187.
- (256) Zamora, F.; Gonzalez, V. M.; Perez, J. M.; Masaguer, J. R.; Alonso, C.; Navarroranninger, C. *Appl. Organomet. Chem.* **1997**, *11*, 659μ666.
- (257) Dale, J. A.; Dull, D. L.; Mosher, H. S. *J. Org. Chem.* **1969**, *34*, 2543μ2549.
- (258) Seco, J. M.; Quinoa, E.; Riguera, R. *Chem. Rev.* **2004**, *104*, 17μ117.
- (259) Varvoglis, A. *Hypervalent Iodine in Organic Synthesis*; Academic Press: London, 1997.
- (260) Stang, P. J.; Zhdankin, V. V. *Chem. Rev.* **1996**, *96*, 1123μ1178.
- (261) Urriolabeitia, E. P.; Laga, E.; Cativiela, C. *Belstein. J. Org. Chem.* **2012**, *8*, 1569μ1575.
- (262) Vicente, J.; Saura-Llamas, I.; Bautista, D. *Organometallics* **2005**, *24*, 6001μ6004.
- (263) Ruiz-Rodriguez, J.; Albericio, F.; Lavilla, R. *Chem. Eur. J.* **2010**, *16*, 1124μ1127.
- (264) Evans, E. F.; Lewis, N. J.; Kapfer, I.; Macdonald, G.; Taylor, R. J. K. *Synth. Comm.* **1997**, *27*, 1819μ1825.
- (265) Gorelsky, S. I.; Lapointe, D.; Fagnou, K. *J. Am. Chem. Soc.* **2008**, *130*, 10848μ10849.
- (266) Bajwa, S. E.; Storr, T. E.; Hatcher, L. E.; Williams, T. J.; Baumann, C. G.; Whitwood, A. C.; Allan, D. R.; Teat, S. J.; Raithby, P. R.; Fairlamb, I. J. S. *Chem. Sci.* **2012**, *3*, 1656μ1661.
- (267) Bakhmutov, V. I.; Berry, J. F.; Cotton, F. A.; Ibragimov, S.; Murillo, C. A. *Dalton Trans.* **2005**, 1989μ1992.
- (268) Nonoyama, M.; Nakajima, K. *Polyhedron* **1998**, *18*, 1601μ1605.
- (269) Nonoyama, M. *Synth. React. Inorg. Met. Org. Chem.* **1999**, *29*, 119μ124.

-
- (270) Dess, D. B.; Martin, J. C. *J. Org. Chem.* **1983**, *48*, 4155-4156.
- (271) Bielawski, M.; Olofsson, B. *Chem. Commun.* **2007**, 2521-2523.
- (272) Suarez, L. L.; Greaney, M. F. *Chem. Commun.* **2011**, *47*, 7992-7994.
- (273) Williams, D.; Fleming, I. *Spectroscopic Methods in Organic Chemistry*; 6th ed.; McGraw-Hill: Maidenhead, UK, 2008.
- (274) Singh, R.; Viciu, M. S.; Kramareva, N.; Navarro, O.; Nolan, S. P. *Org. Lett.* **2005**, *7*, 1829-1832.
- (275) Davidson, J. M.; Triggs, C. *J. Chem. Soc. (A)* **1968**, 1324-1330.
- (276) Campi, E. M.; Jackson, W. R.; Marcuccio, S. M.; Naeslund, C. G. M. *J. Chem. Soc., Chem. Commun.* **1994**, 2395.
- (277) Gillmann, T.; Weeber, T. *Synlett* **1994**, 649-651.
- (278) Song, Z. Z.; Wong, H. N. C. *J. Org. Chem.* **1994**, *59*, 33-41.
- (279) Adamo, C.; Amatore, C.; Ciofini, I.; Jutand, A.; Lakmini, H. *J. Am. Chem. Soc.* **2006**, *128*, 6898-6836.
- (280) Moreno-Manas, M.; Perez, M.; Pleixats, R. *J. Org. Chem.* **1996**, *61*, 2346-2351.
- (281) Koza, D. J.; Carita, E. *Synthesis* **2002**, 2183-2186.
- (282) Molander, G. A.; Bernardi, C. R. *J. Org. Chem.* **2002**, *67*, 8424-8429.
- (283) Molander, G. A.; Biolatto, B. *J. Org. Chem.* **2003**, *68*, 4302-4314.
- (284) Oliveira, R. A.; Silva, R. O.; Molander, G. A.; Menezes, P. H. *Magn. Reson. Chem.* **2009**, *47*, 873-878.
- (285) Vedejs, E.; Chapman, R. W.; Fields, S. C.; Lin, S.; Schrimpf, M. R. *J. Org. Chem.* **1995**, *60*, 3020-3027.
- (286) Lennox, A. J. J.; Lloyd-Jones, G. C. *Angew. Chem., Int. Ed.* **2012**, *51*, 9385-9388.
- (287) Kieffer, M. E.; Repka, L. M.; Reisman, S. E. *J. Am. Chem. Soc.* **2012**, *134*, 5131-5137.
- (288) McNaught, A. D.; Wilkinson, A.; Nic, M.; Jirat, J.; Kosata, B.; A., J. In *IUPAC Compendium of Chemical Terminology ('The Gold Book') 2nd Edition*; 2006.
- (289) Nguyen, P.; Zheng, Y. A.; Agocs, L.; Lesley, G.; Marder, T. B. *Inorg. Chim. Acta.* **1994**, *220*, 289-296.

- (290) Siddle, J. S.; Ward, R. M.; Collings, J. C.; Rutter, S. R.; Porres, L.; Applegarth, L.; Beeby, A.; Batsanov, A. S.; Thompson, A. L.; Howard, J. A. K.; Boucekkine, A.; Costuas, K.; Halet, J. F.; Marder, T. B. *New J. Chem.* **2007**, *31*, 841μ851.
- (291) Kaim, W.; Rall, J. *Angew. Chem., Int. Ed.* **1996**, *35*, 2541μ2562.
- (292) Fykuzimi, S.; Karlin, K. D. *Cood. Chem. Rev.* **2013**, *257*, 187μ195.
- (293) Nascimento, O. R.; Costa-Filho, A. J.; De Moraes, D. I.; Ellena, J.; Delboni, L. F. *Inorg. Chim. Acta.* **2001**, *312*, 133μ138.
- (294) Appleton, D. R.; Babcock, R. C.; Copp, B. R. *Tetrahedron* **2001**, *57*, 10181μ10190.
- (295) Holla, B. S.; Malini, K. V.; Sarojini, B. K.; Poojary, B. *Synth. Comm.* **2005**, *35*, 333μ340.
- (296) Yusubov, M. S.; Zholobova, G. A.; Filimonova, I. L.; Chi, K. W. *Russ. Chem. Bull* **2004**, *53*, 1735μ1742.
- (297) Gonzalez, D. F.; Brand, J. P.; Waser, J. *Chem. Eur. J.* **2010**, *16*, 9457μ9461.
- (298) Leslie, D. R. *Aust. J. Chem.* **1989**, *42*, 2119μ2126.
- (299) Fevre, M.; Pinaud, J.; Leteneur, A.; Gnanou, Y.; Vignolle, J.; Taton, D. *J. Am. Chem. Soc.* **2012**, *134*, 6776μ6784.
- (300) Jensen, D. R.; Sigman, M. S. *Org. Lett.* **2003**, *5*, 63μ65.
- (301) Catalan, J.; Mena, E.; Fabero, F.; Amatguerri, F. *J. Chem. Phys.* **1992**, *96*, 2005μ2016.
- (302) De Ornellas, S. PhD Thesis, University of York, 2012.
- (303) Ueno, Y.; Jiao, G.-S.; Burgess, K. *Synthesis* **2004**, *15*, 2591μ2593.
- (304) Ogawa, A.; Ikeda, T.; Kimura, K.; Hirao, T. *J. Am. Chem. Soc.* **1999**, *121*, 5108μ5114.
- (305) Fairlamb, I. J. S.; Lynam, J. M.; Taylor, I. E.; Whitwood, A. C. *Organometallics* **2004**, *23*, 4964μ4969.
- (306) Fairlamb, I. J. S.; Duhme-Klair, A. K.; Lynam, J. M.; Moulton, B. E.; O'Brien, C. T.; Sawle, P.; Hammad, J.; Motterlini, R. *Bioorg. Med. Chem. Lett.* **2006**, *16*, 995μ998.
- (307) Atkin, A. J.; Lynam, J. M.; Moulton, B. E.; Sawle, P.; Motterlini, R.; Boyle, N. M.; Pryce, M. T.; Fairlamb, I. J. S. *Dalton Trans.* **2011**, *40*, 5755μ5761.

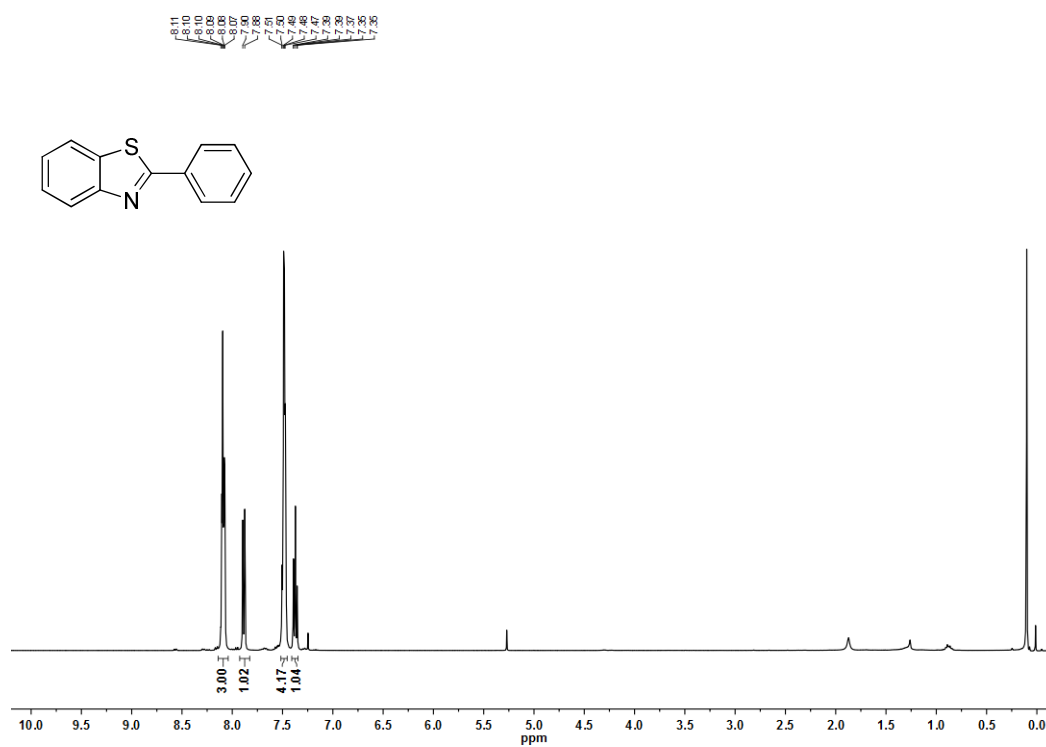
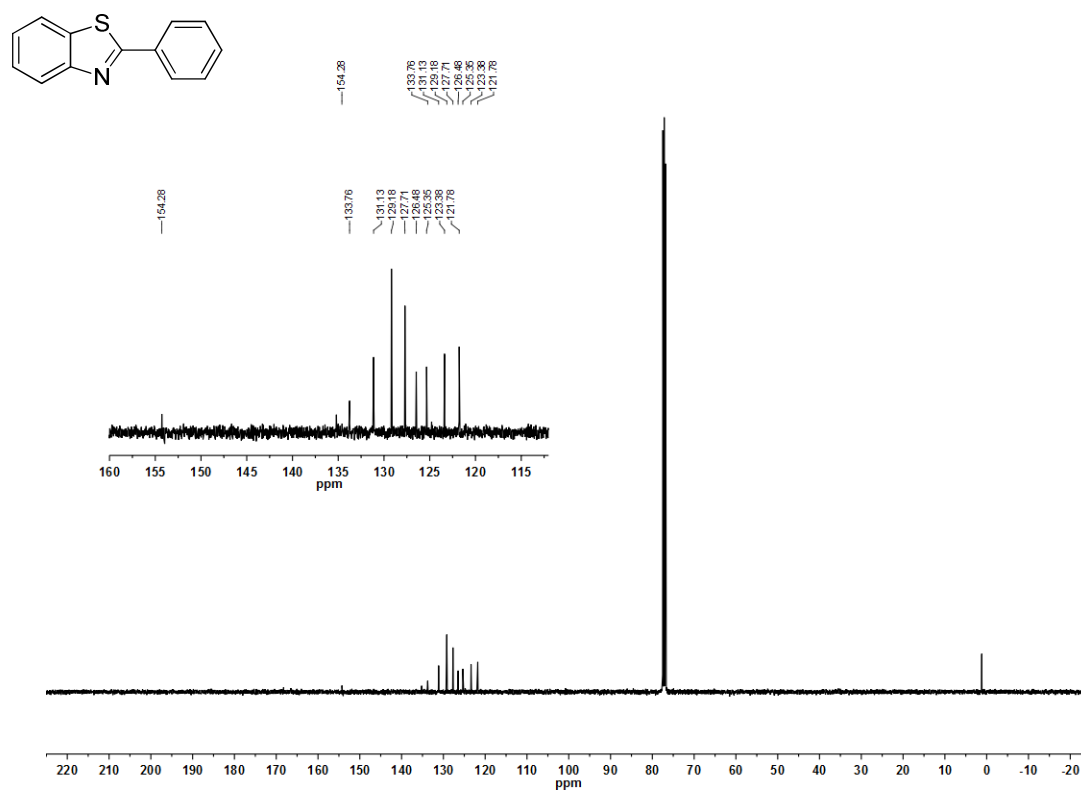
-
- (308) Atkin, A. J.; Williams, S.; Sawle, P.; Motterlini, R.; Lynam, J. M.; Fairlamb, I. J. S. *Dalton Trans.* **2009**, 3653μ3656.
- (309) Fairlamb, I. J. S.; Lynam, J. M.; Moulton, B. E.; Taylor, I. E.; Duhme-Klair, A. K.; Sawle, P.; Motterlini, R. *Dalton Trans.* **2007**, 3603μ3605.
- (310) Sawle, P.; Hammad, J.; Fairlamb, I. J. S.; Moulton, B.; O'Brien, C. T.; Lynam, J. M.; Duhme-Klair, A. K.; Foresti, R.; Motterlini, R. *J. Pharmacol. Exp. Therap.* **2006**, 318, 403μ410.
- (311) Moulton, B. E.; Duhme-Klair, A. K.; Fairlamb, I. J. S.; Lynam, J. M.; Whitwood, A. C. *Organometallics* **2007**, 26, 6354μ6365.
- (312) Zhang, W.-Q.; Whitwood, A. C.; Fairlamb, I. J. S.; Lynam, J. M. *Inorganic Chemistry* **2010**, 49, 8941μ8952.
- (313) Zhang, W.-Q.; Atkin, A. J.; Thatcher, R. J.; Whitwood, A. C.; Fairlamb, I. J. S.; Lynam, J. M. *Dalton Trans.* **2009**, 4351μ4358.

**APPENDIX A:
NMR SPECTROSCOPIC DATA**

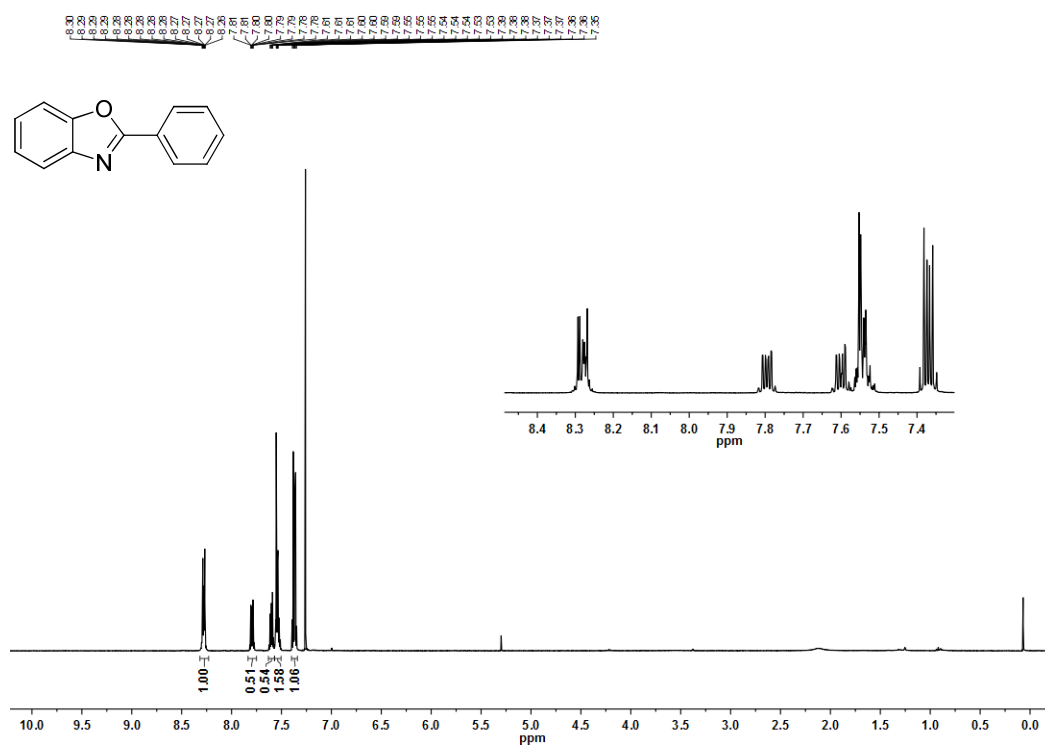
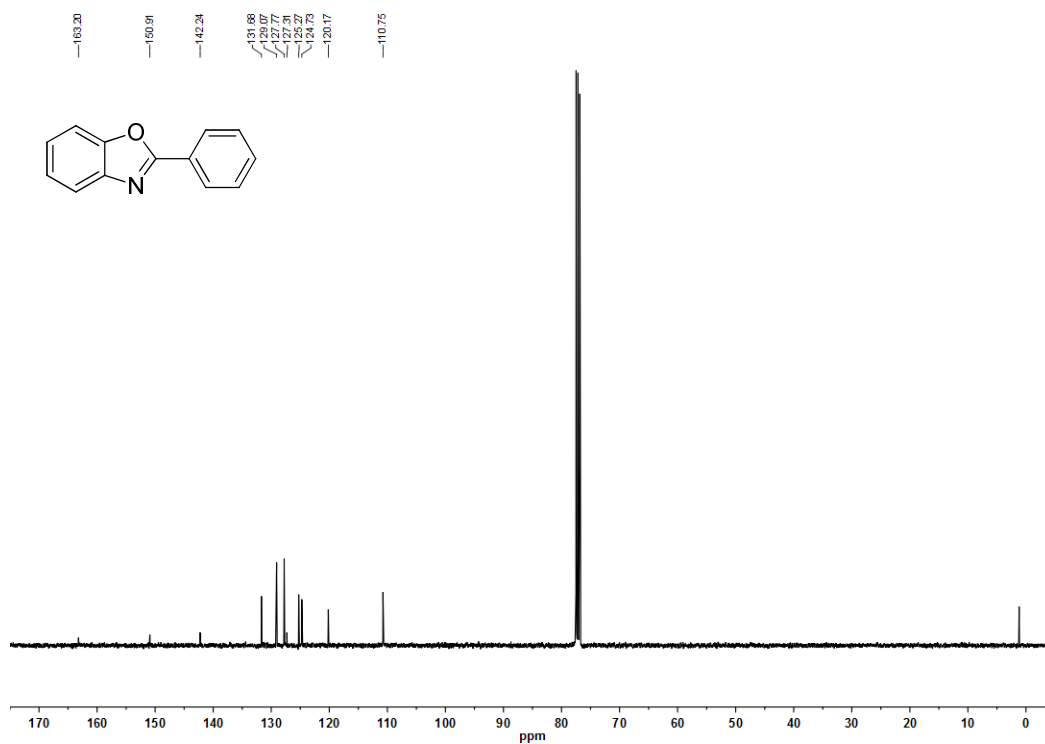
2-Phenylbenzo[<i>d</i>]thiazole	A4
2-Phenylbenzo[<i>d</i>]benzoxazole	A5
1-Methyl-2-phenylbenzo[<i>d</i>]imidazole	A6
1,3-Dibenzylbenzo[<i>d</i>]imidazolium bromide	A7
(1,3-Dibenzylbenzo[<i>d</i>]imidazolin-2-ylidene)copper(I) bromide	A8
1-Benzylbenzo[<i>d</i>]imidazole	A9
1-Benzyl-2-phenylbenzo[<i>d</i>]imidazole	A10
(1,3-Dibenzyl)-2-phenylbenzo[<i>d</i>]imidazolium bromide	A11
Methyl (2 <i>R</i>)-2-amino-3-(1 <i>H</i> -indol-3-yl)propionate hydrochloride	A12
Methyl (2 <i>R</i>)-2-acetylamino-3-(1 <i>H</i> -indol-3-yl)propionate	A13
Methyl (2 <i>R</i>)-2-benzylamino-3-(1 <i>H</i> -indol-3-yl)propionate	A14
Methyl (2 <i>R</i>)-2-(trifluoroacetyl)-3-(1 <i>H</i> -indol-3-yl)propionate	A15
Methyl (2 <i>R</i>)-2-amino-3-(1 <i>H</i> -5-bromoindol-3-yl)propionate	A16
Methyl (2 <i>R</i>)-2-acetyl-3-(1 <i>H</i> -5-bromoindol-3-yl)propionate	A17
<i>N</i> -Acetylglycine	A18
AcNGlyTrpOMe	A19
Bis(acetyloxy)phenyl- λ^3 -iodane	A20
1-Hydroxy-1 <i>H</i> -1 λ^3 -benzo[<i>d</i>][1,2]iodoxol-3-one	A21
1-Acetyl-1 <i>H</i> -1 λ^3 -benzo[<i>d</i>][1,2]iodoxol-3-one	A22

Potassium 4-fluorophenylborontrifluoride	A23
Potassium 4-methoxyphenylborontrifluoride	A25
Potassium 4-(trifluoromethyl)phenylborontrifluoride	A27
1,3-[di(2,4,6-trimethylphenyl)-4,5-dihydroimidazolylidene](η^3 -2-methylpropenyl)chloropalladium(II)	A29
Trans-di- μ -chlorobis{[1,3-di(2,4,6-trimethylphenyl)-4,5-dihydroimidazolylidene]chloropalladium(II)}	A32
[1,3-di(2,4,6-trimethylphenyl)-4,5-dihydroimidazolylidene]diacetateaquopalladium(II)	A33
1-Methyl-2-phenylindole	A36
Methyl (2S)-2-acetyl-3-[2-phenyl-1H-indol-3-yl]propanoate	A37
Methyl (2S)-2-acetyl-3-[2-(4-methylphenyl)-1H-indol-3-yl]propanoate	A40
Methyl (2S)-2-amino-3-{2-[3-(trifluoromethyl)phenyl]-1H-indol-3-yl}propanoate	A41
Methyl (2S)-2-amino-3-[2-(4-fluorophenyl)-1H-indol-3-yl]propanoate	A42
Methyl (2S)-2-amino-3-[2-(4-methoxyphenyl)-1H-indol-3-yl]propanoate	A43

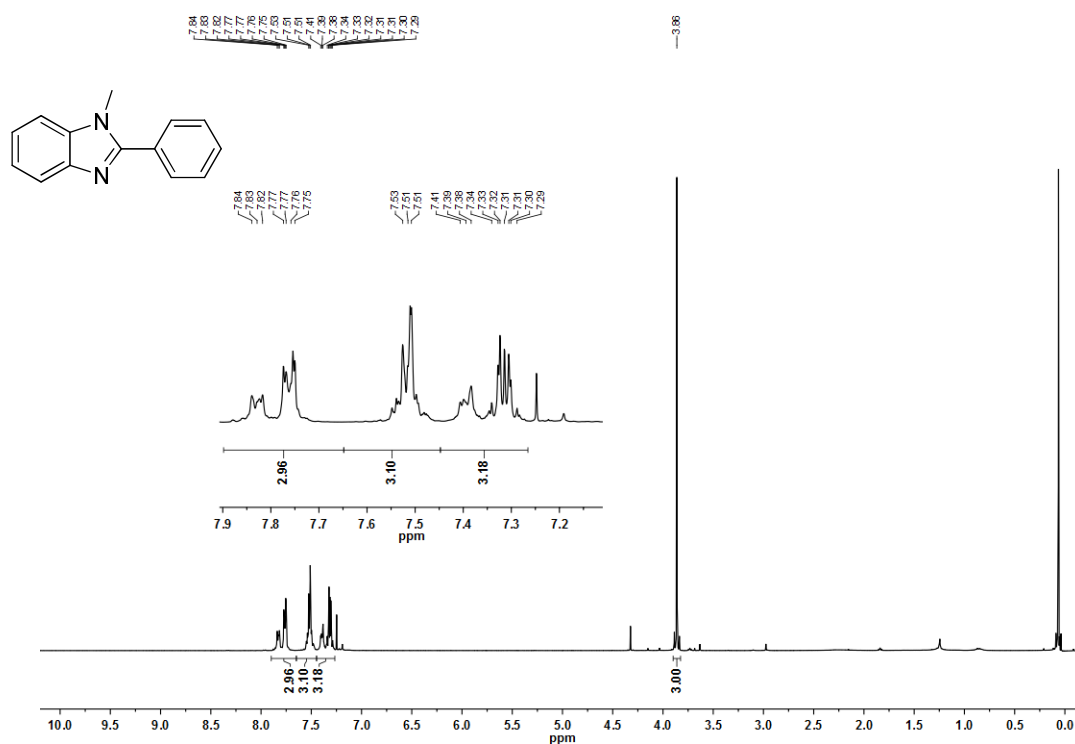
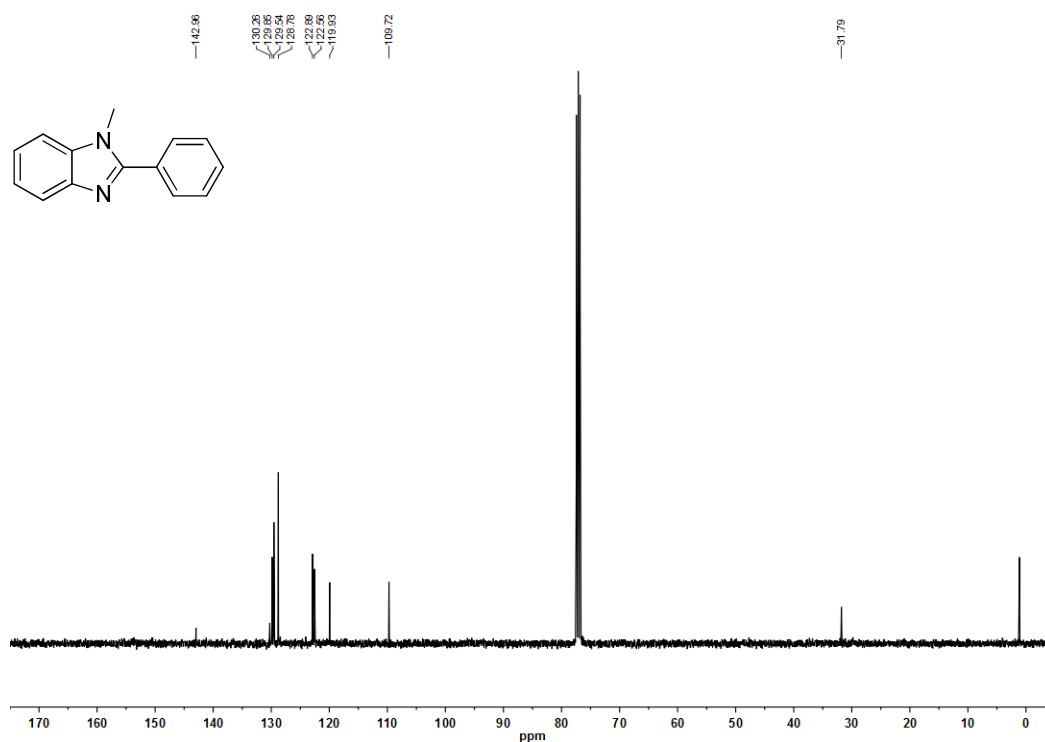
2-Phenylbenzo[d]thiazole

Figure 1: ¹H NMR spectrum (400 MHz, CDCl₃).Figure 2: ¹³C NMR spectrum (101 MHz, CDCl₃).

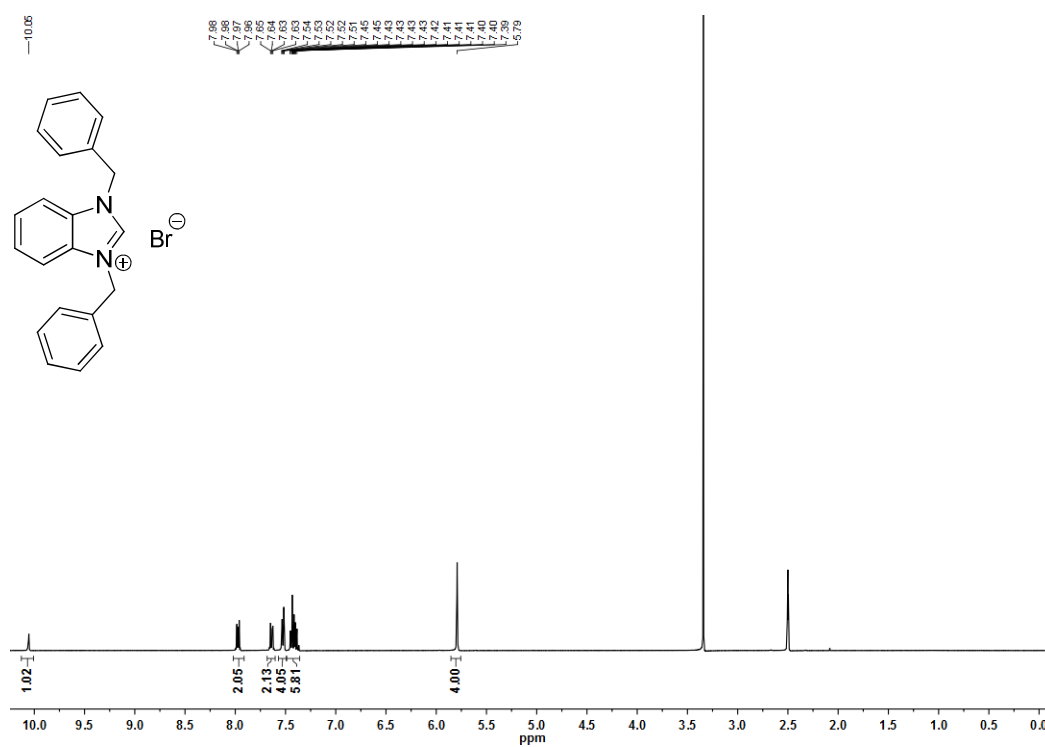
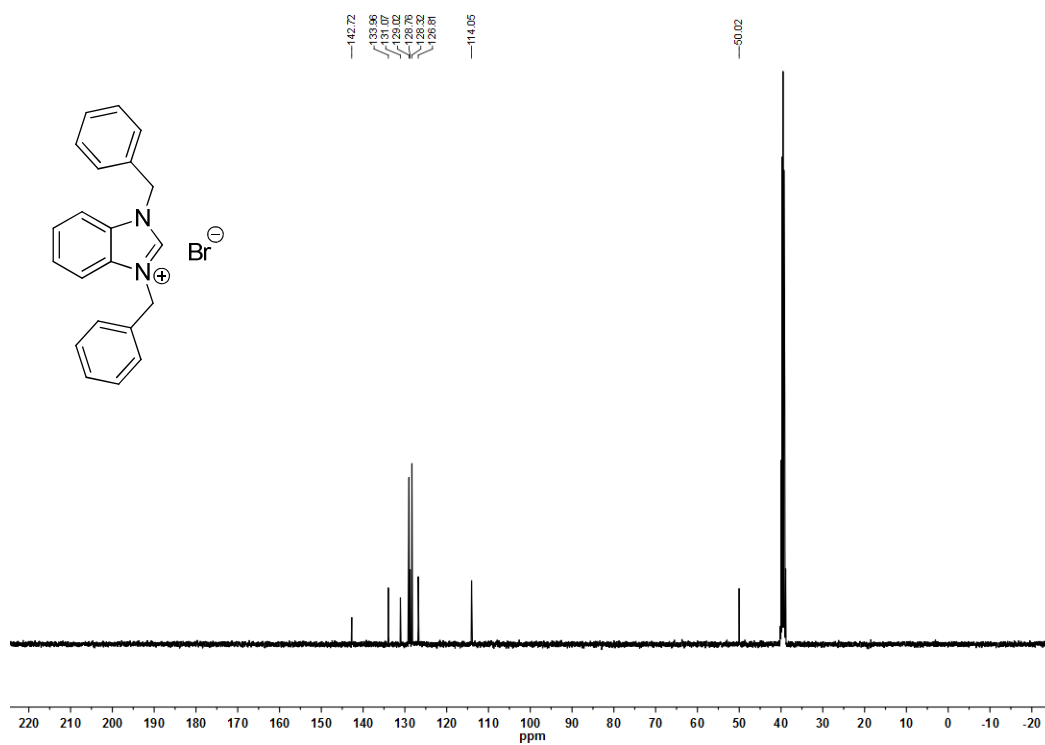
2-phenylbenzo[d]oxazole

Figure 3: ^1H NMR spectrum (400 MHz, CDCl_3).Figure 4: ^{13}C NMR spectrum (101 MHz, CDCl_3).

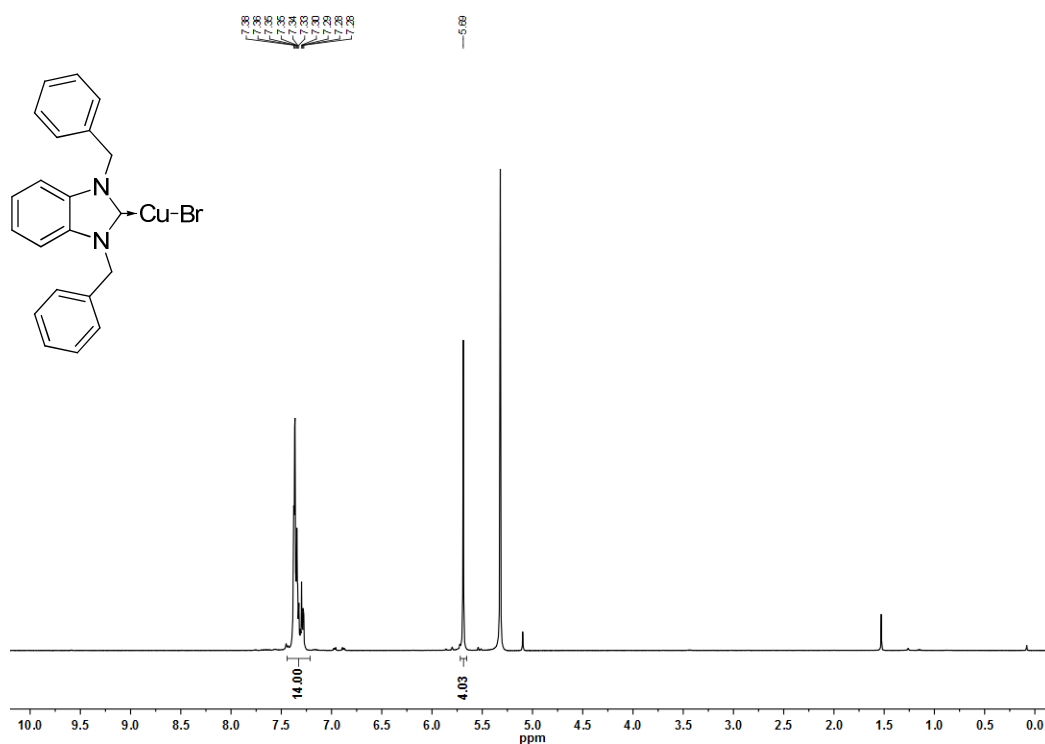
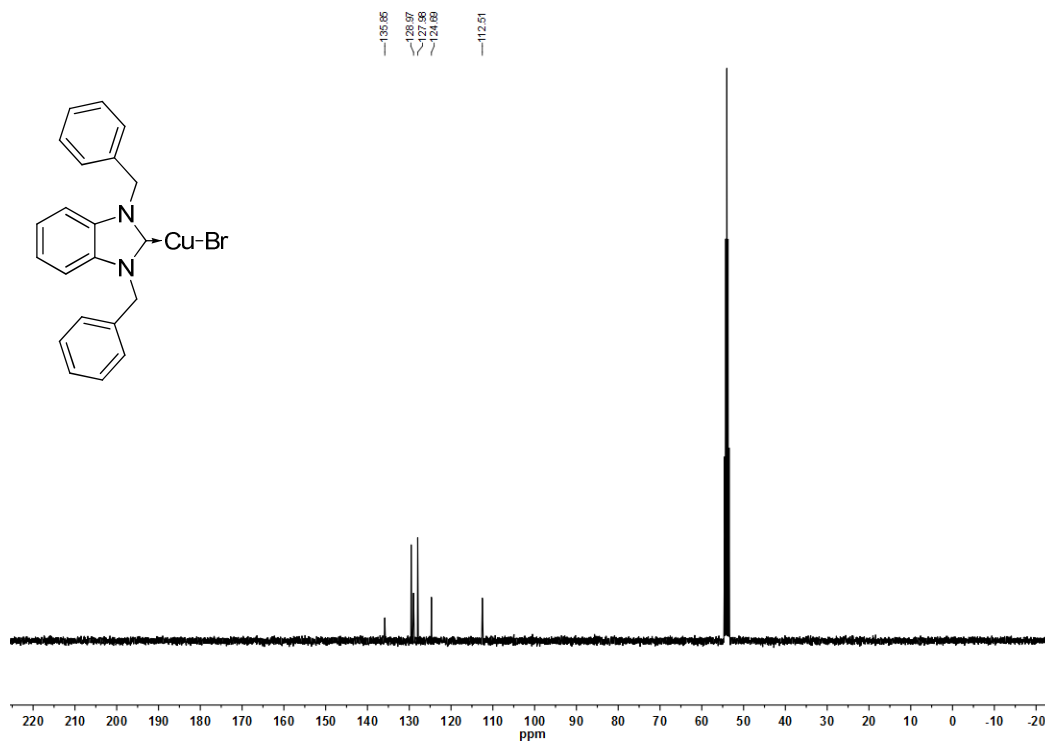
1-Methyl-2-phenylbenzo[d]imidazole

Figure 5: ¹H NMR spectrum (400 MHz, CDCl₃).Figure 6: ¹³C NMR spectrum (101 MHz, CDCl₃).

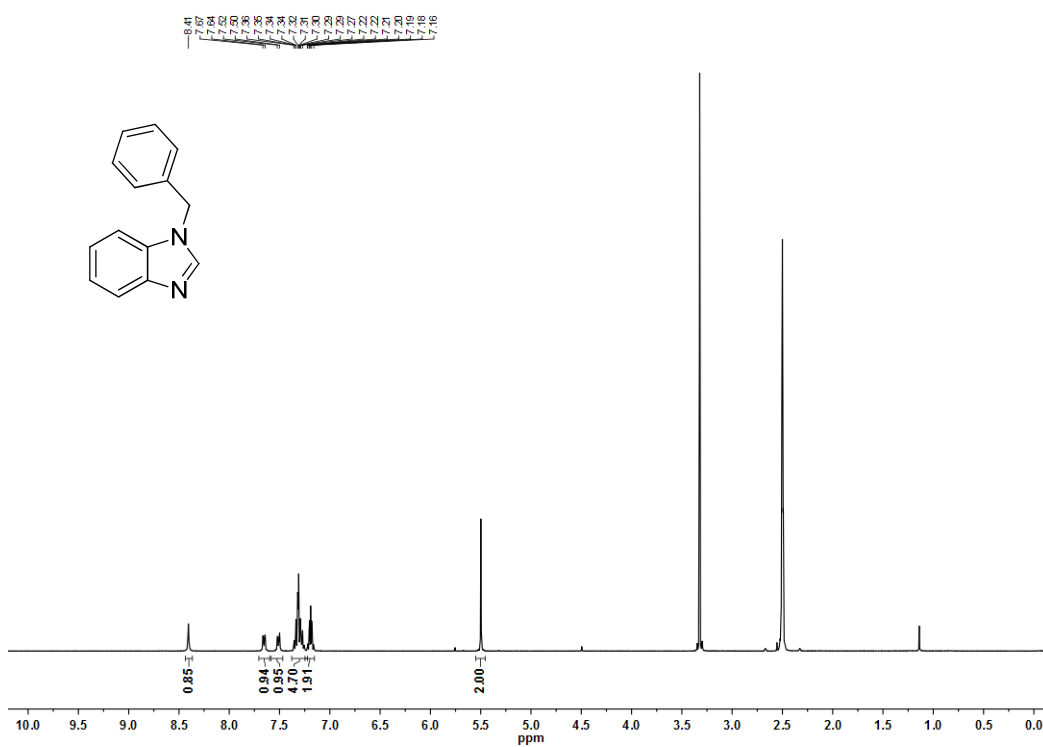
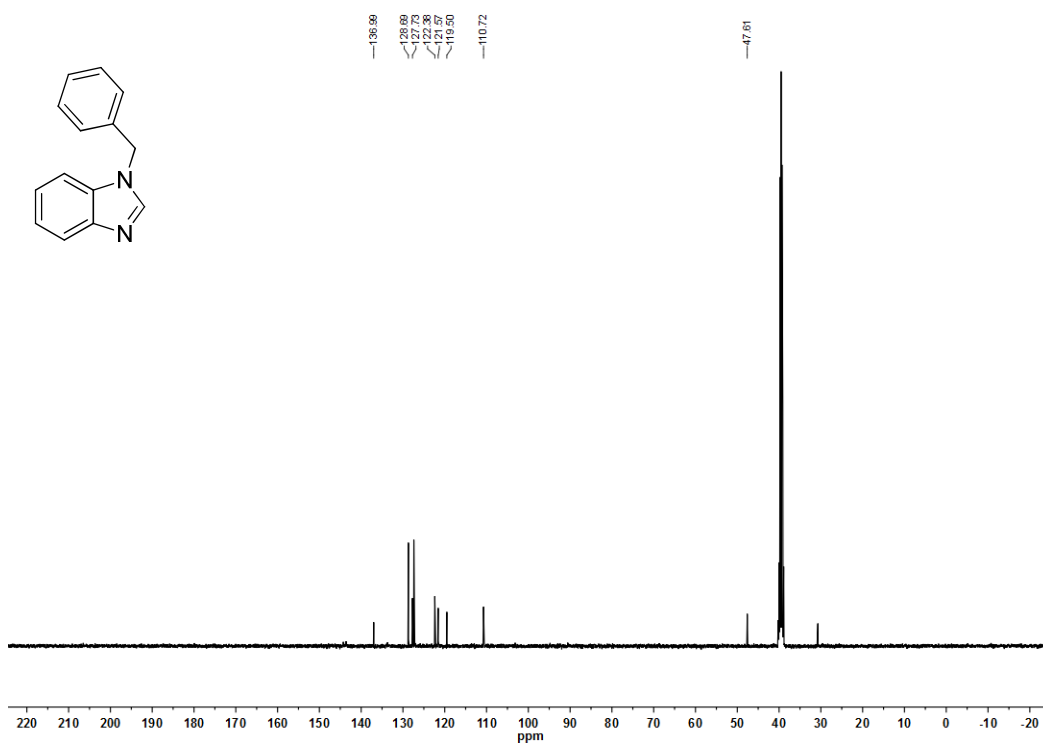
1,3-Dibenzylbenzo[d]imidazolium bromide

Figure 7: ¹H NMR spectrum (400 MHz, (CD₃)₂SO).Figure 8: ¹³C NMR spectrum (101 MHz, (CD₃)₂SO).

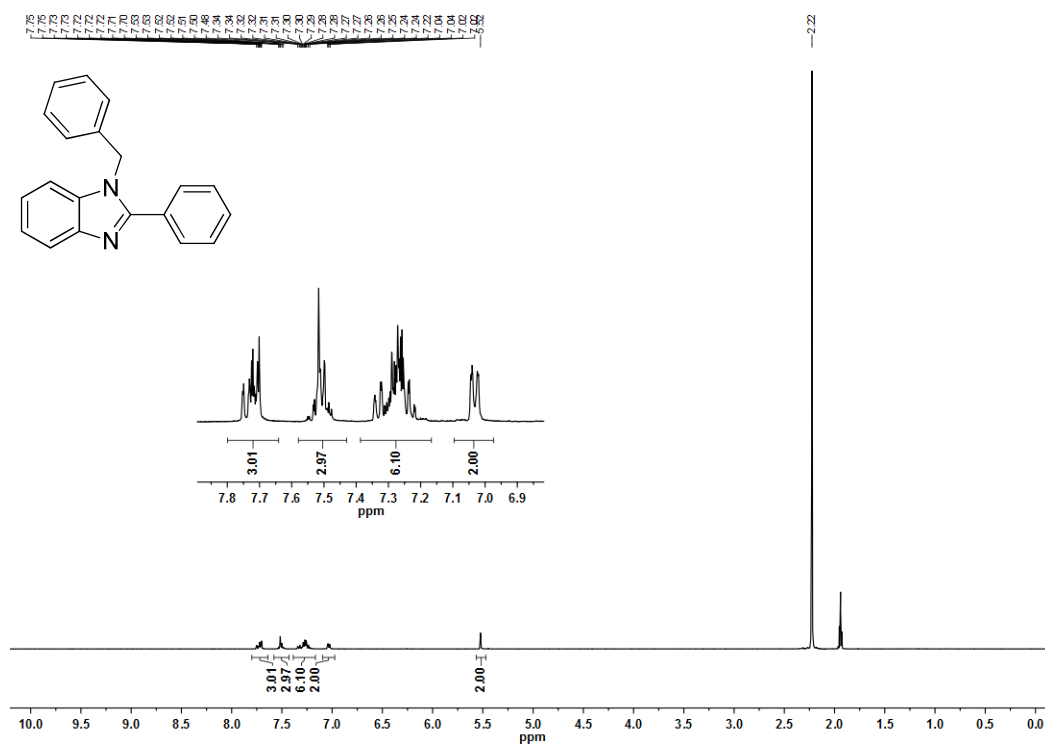
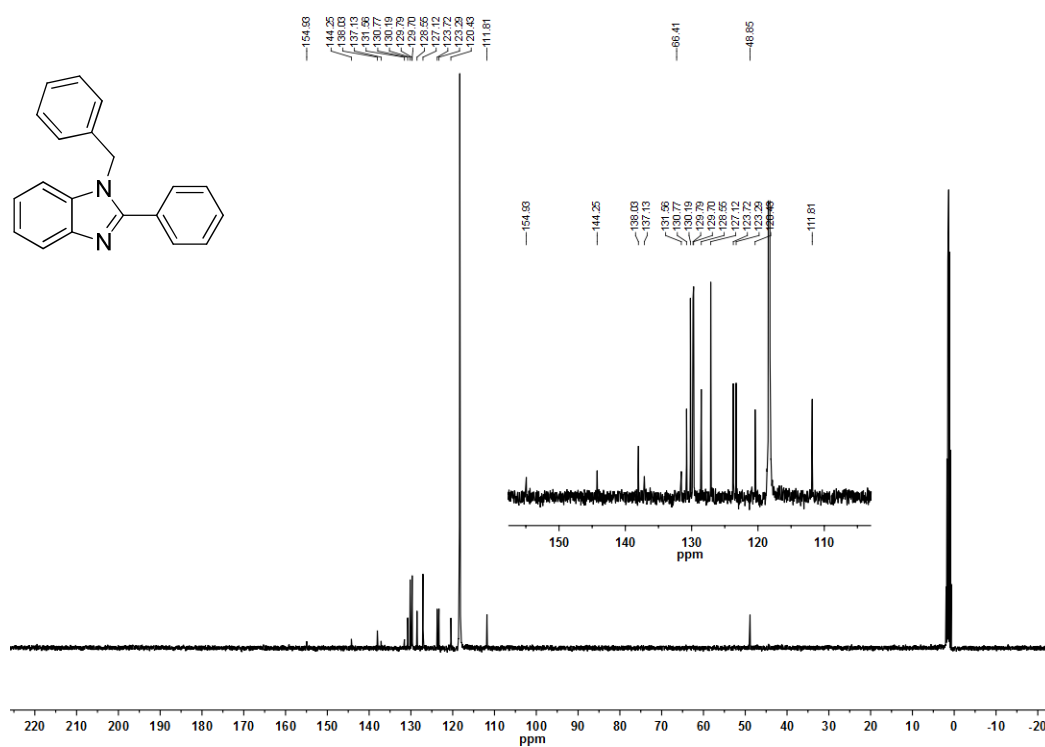
(1,3-Dibenzylbenzo[d]imidazolin-2-ylidene)copper(I) bromide

Figure 9: ^1H NMR spectrum (400 MHz, CD_2Cl_2).Figure 10: ^{13}C NMR spectrum (101 MHz, CD_2Cl_2).

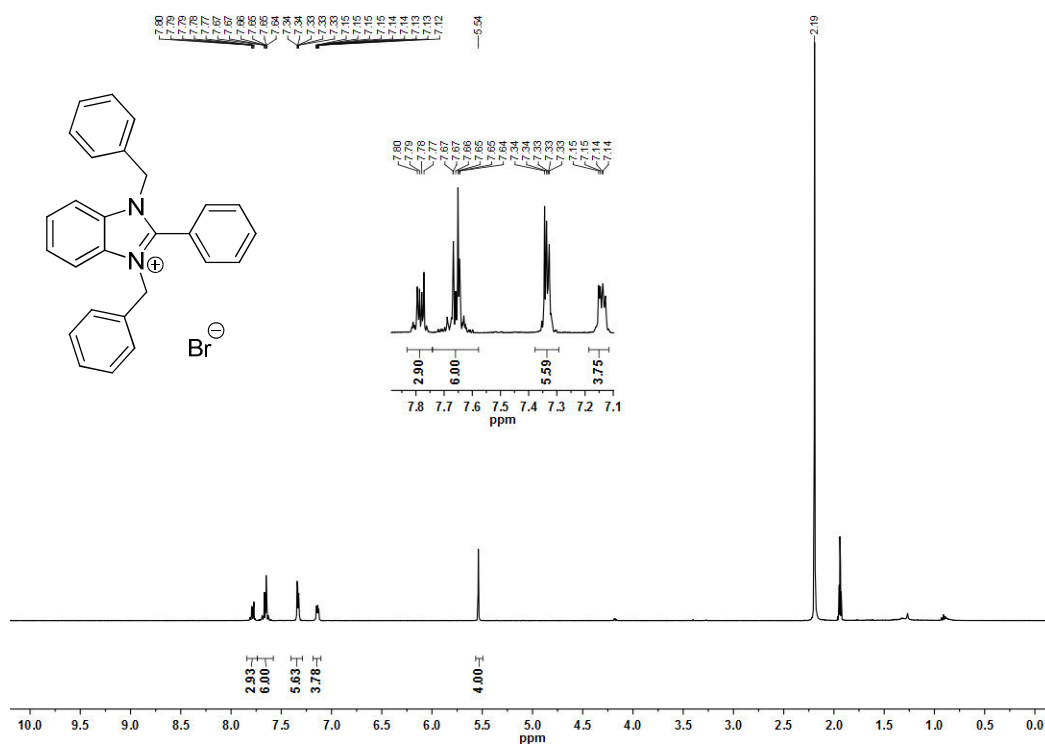
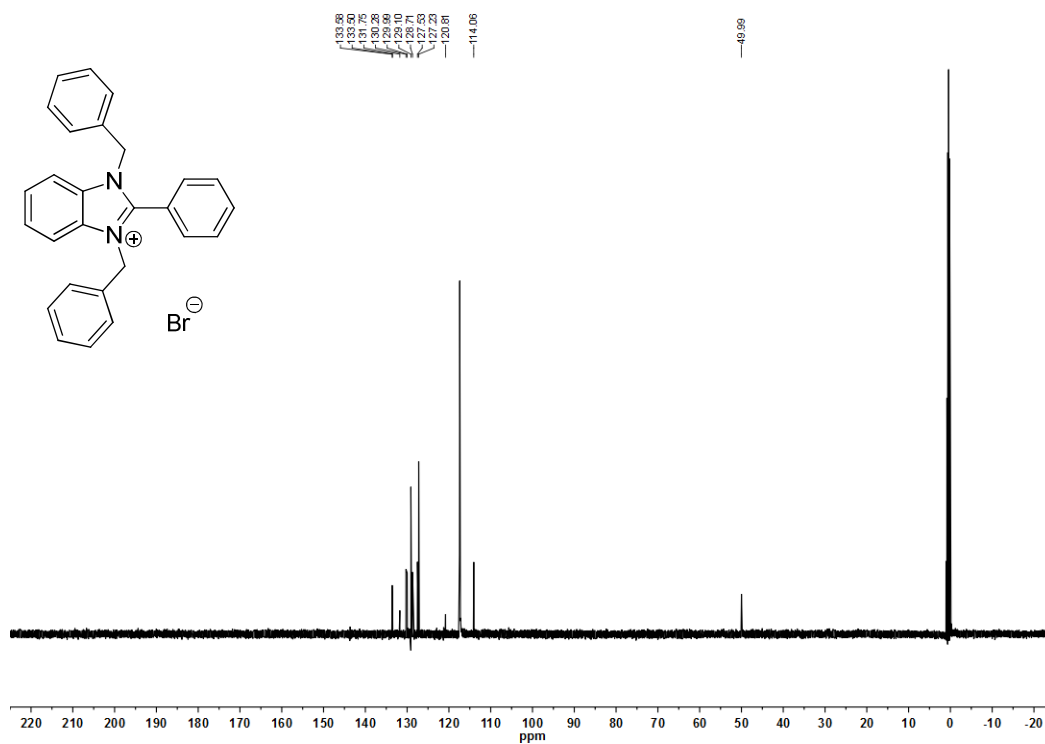
1-Benzylbenzo[d]imidazole

Figure 11: ¹H NMR spectrum (400 MHz, (CD₃)₂SO).Figure 12: ¹³C NMR spectrum (101 MHz, (CD₃)₂SO).

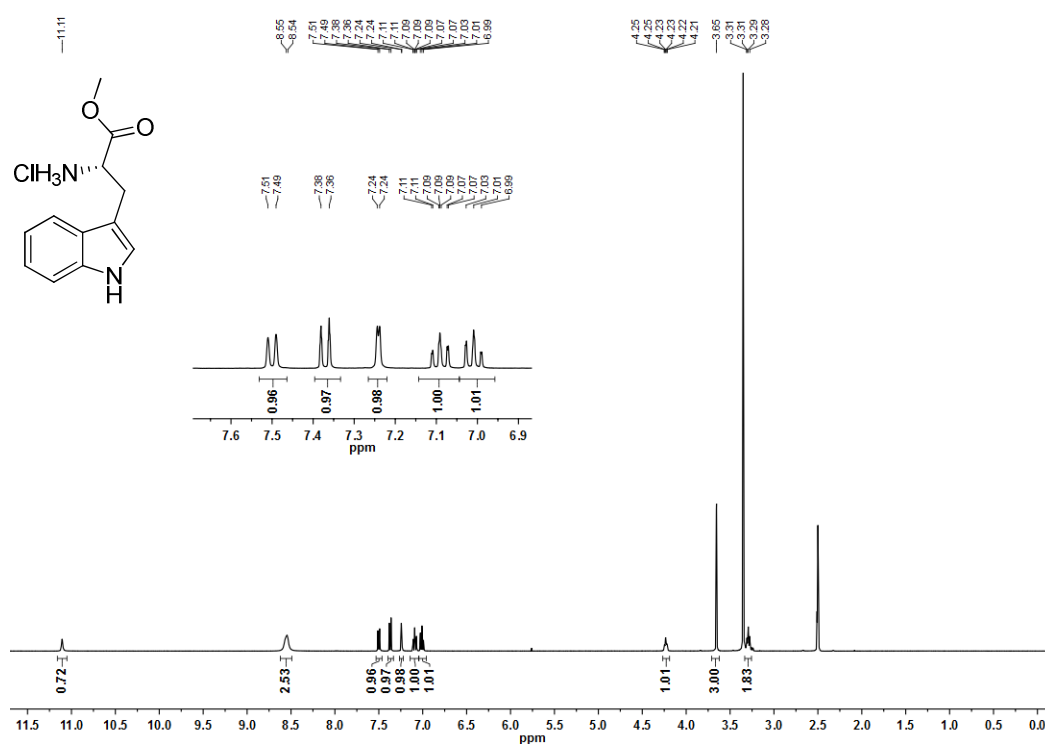
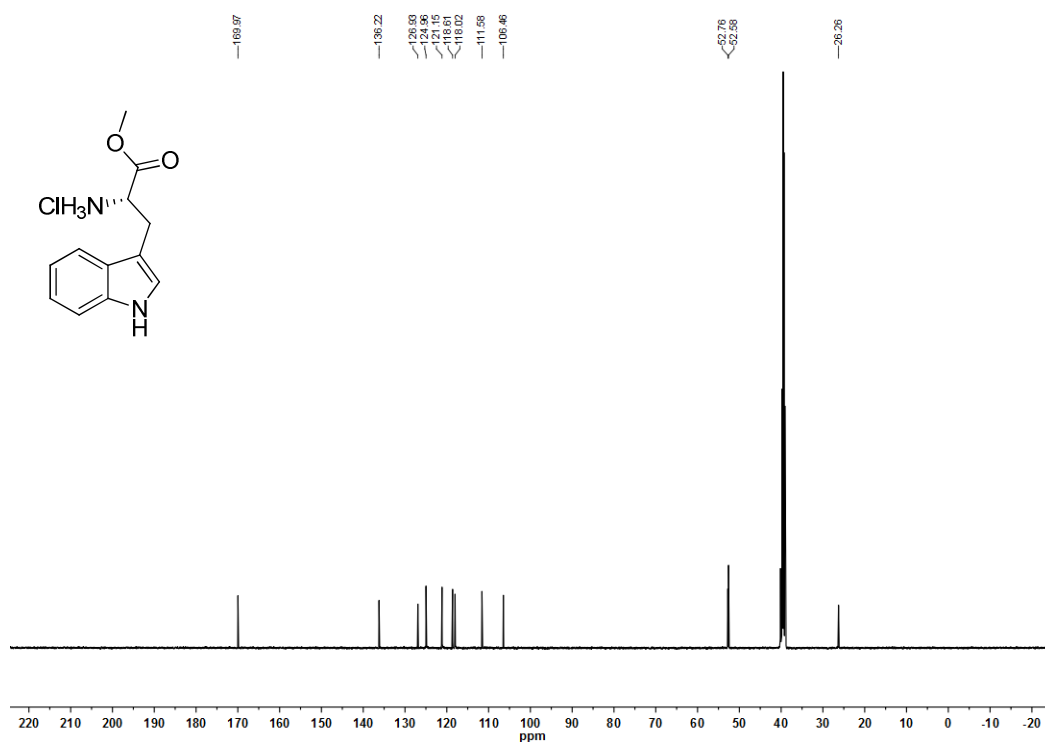
1-Benzyl-2-phenylbenzo[d]imidazole

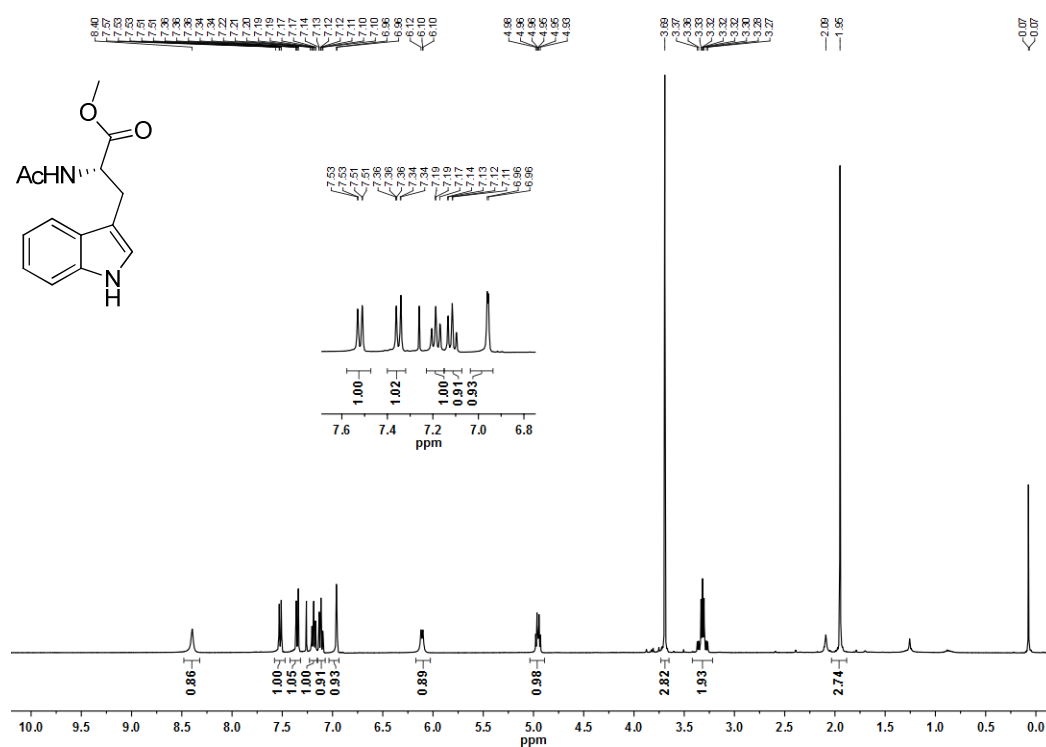
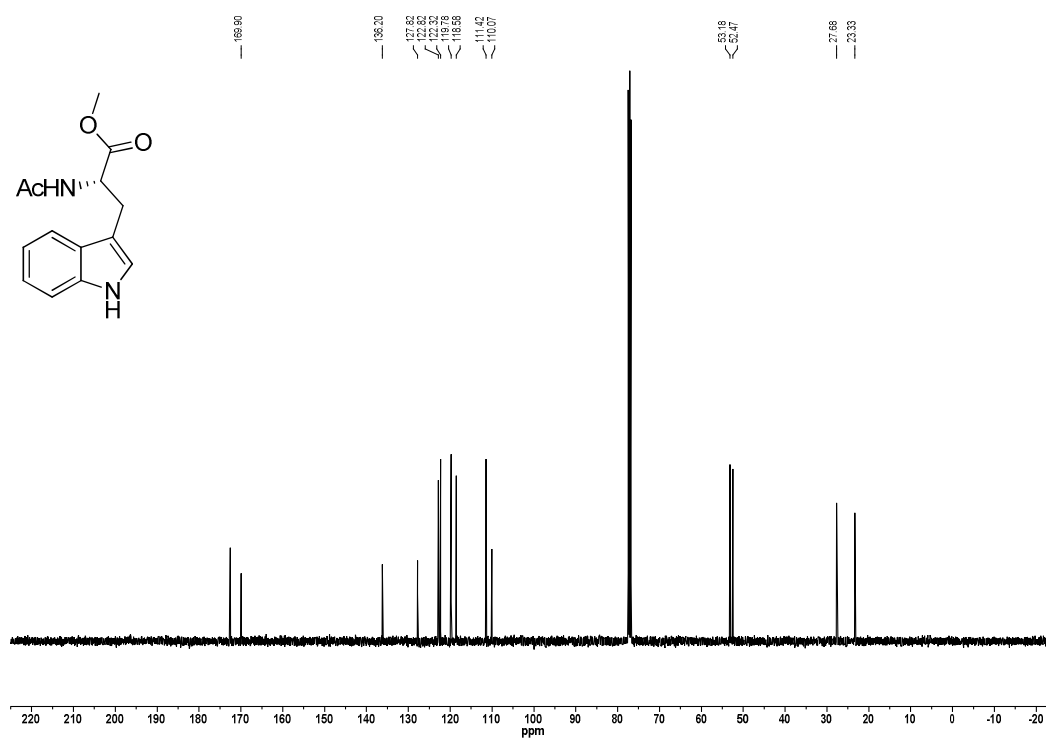
Figure 13: ¹H NMR spectrum (400 MHz, CD₃CN).Figure 14: ¹³C NMR spectrum (101 MHz, CD₃CN).

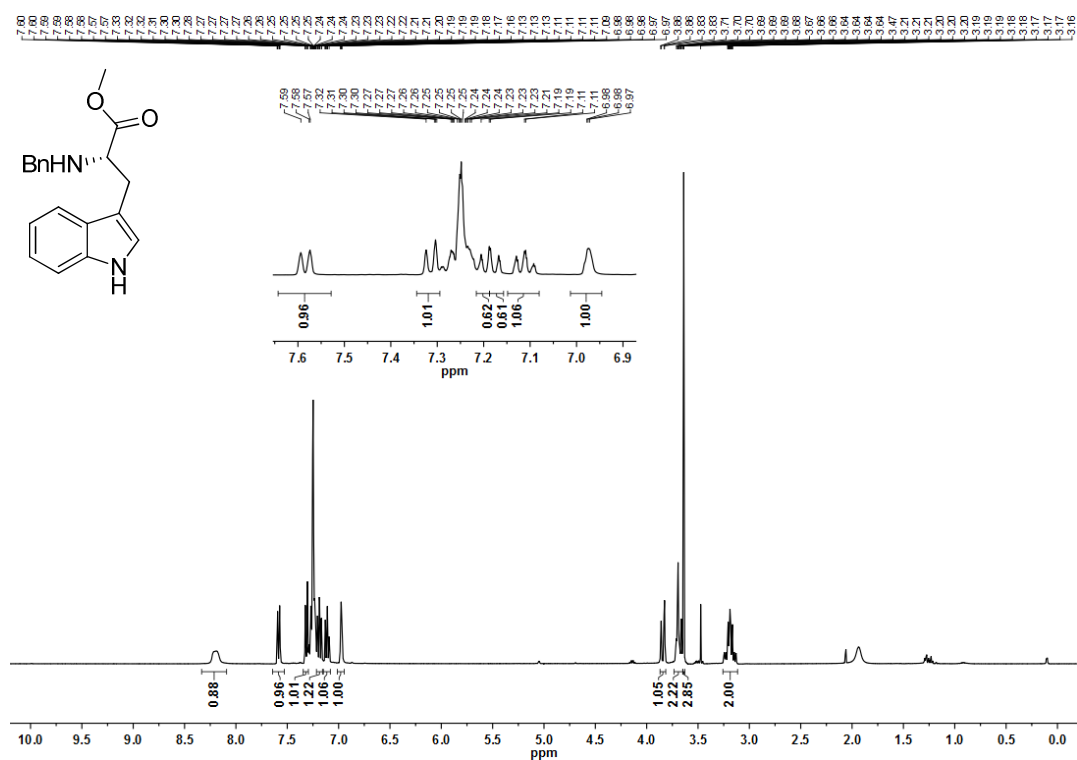
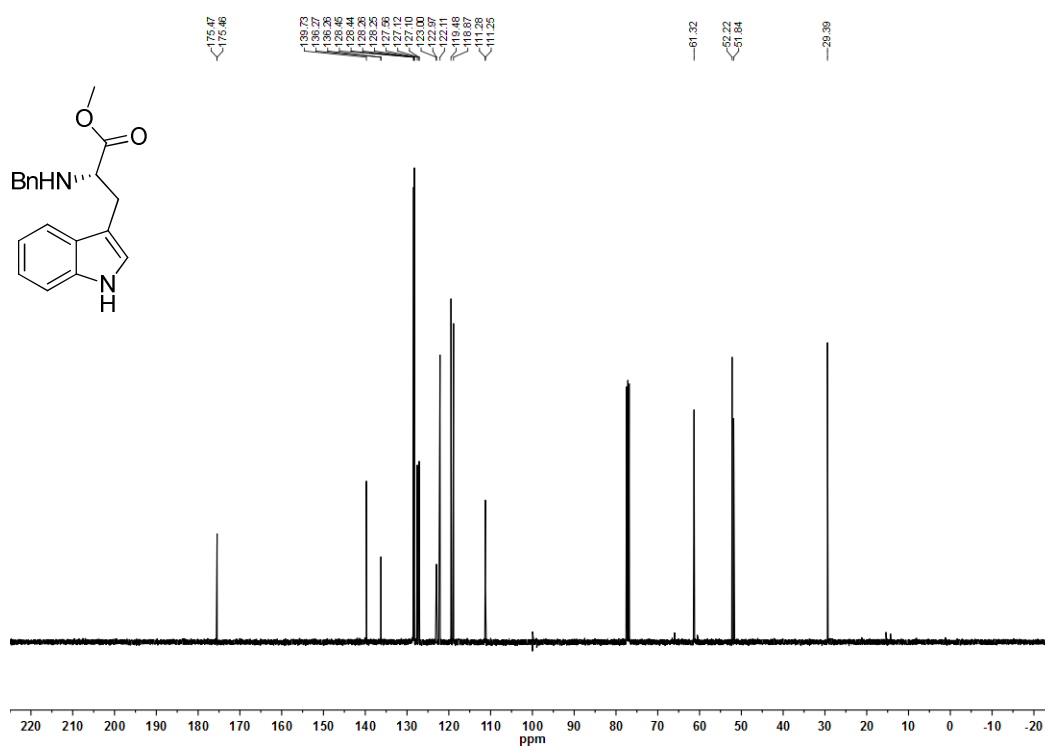
(1,3-Dibenzyl)-2-phenylbenzo[d]imidazolium bromide

Figure 15: ¹H NMR spectrum (400 MHz, CD₃CN).Figure 16: ¹³C NMR spectrum (101 MHz, CD₃CN).

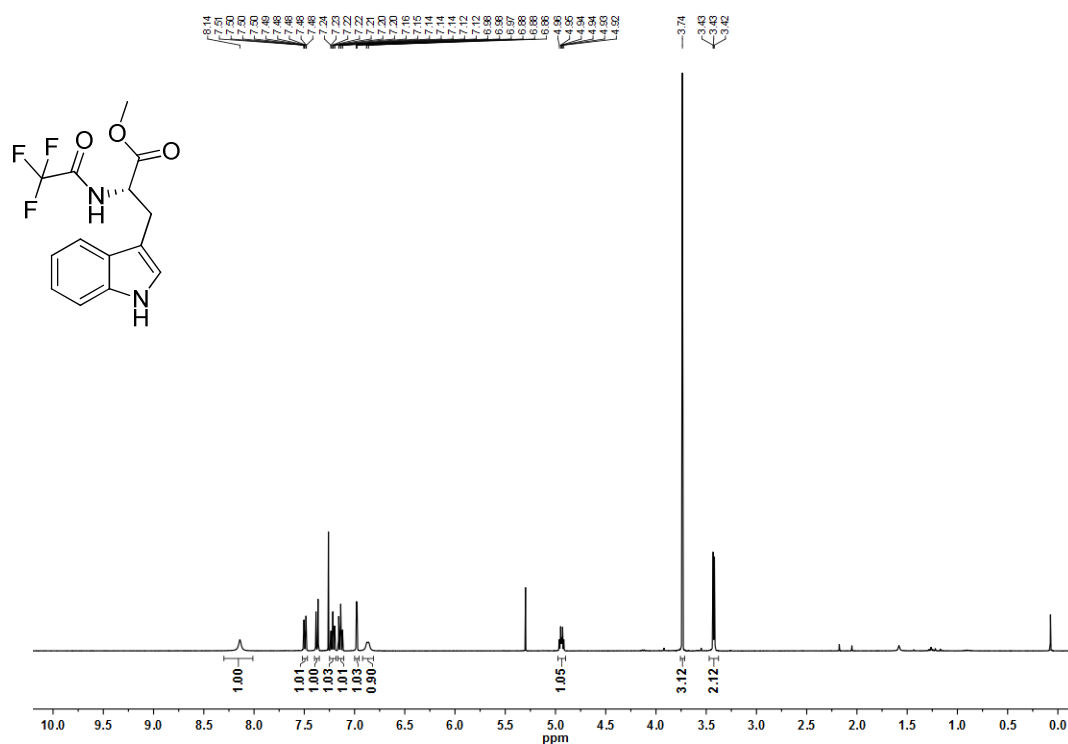
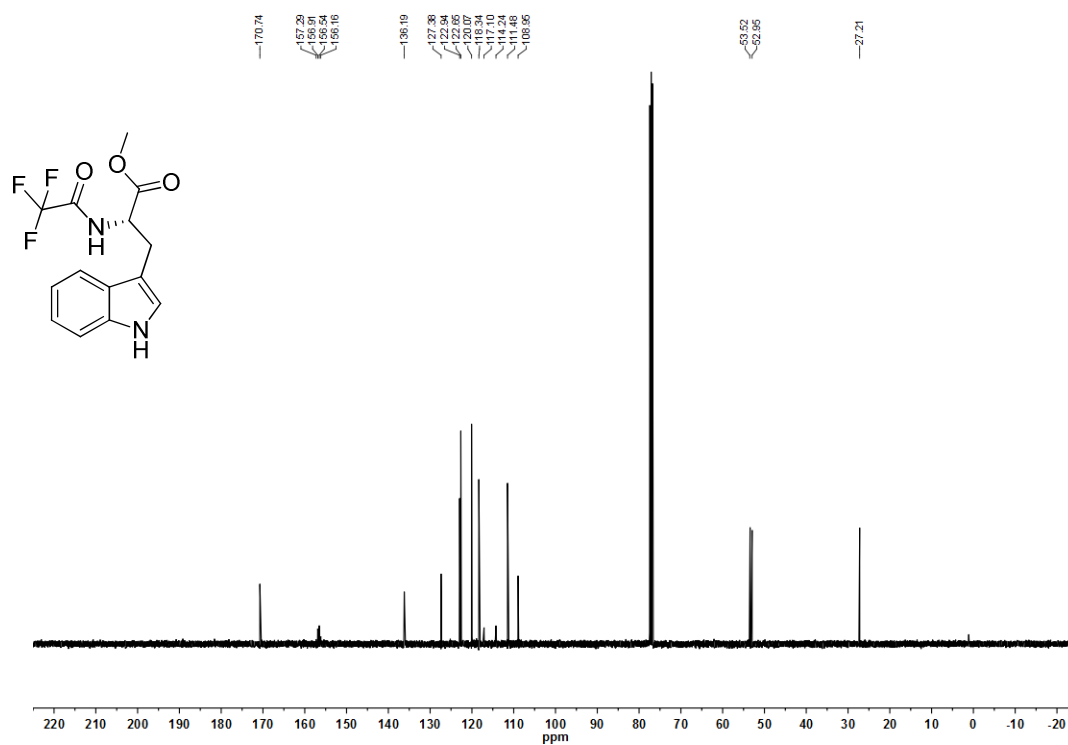
Methyl (2R)-2-amino-3-(1H-indol-3-yl)propionate hydrochloride

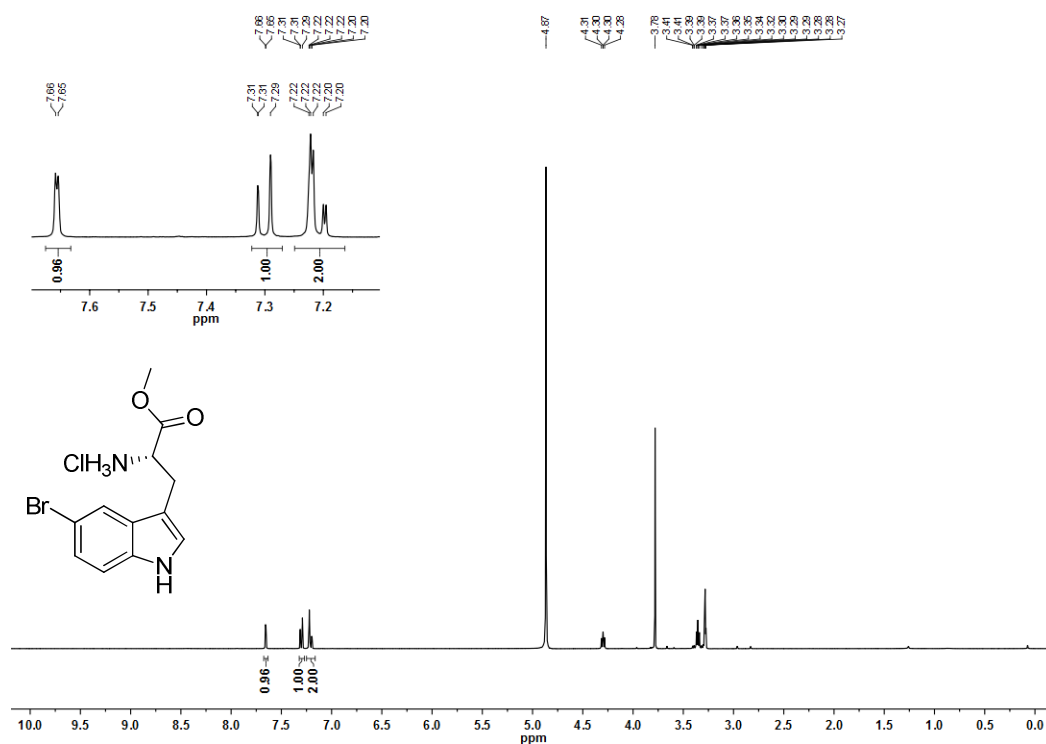
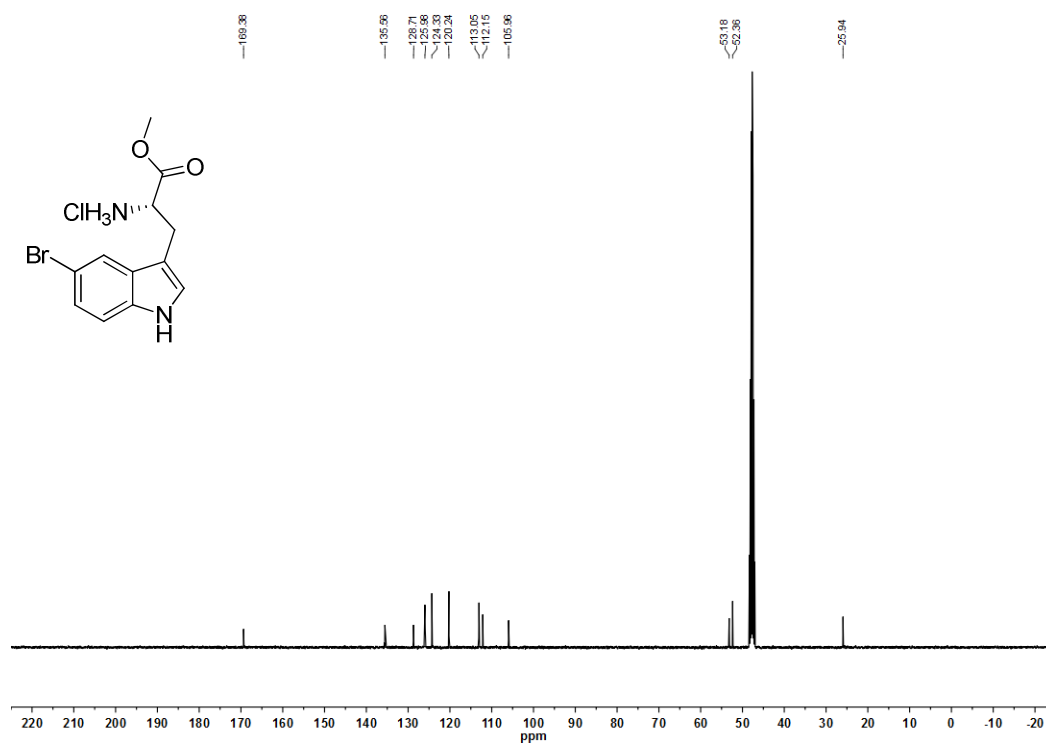
Figure 17: ¹H NMR spectrum (400 MHz, CD₃OD).Figure 18: ¹³C NMR spectrum (101 MHz, CD₃OD).

Methyl (2*R*)-2-acetylamino-3-(1*H*-indol-3-yl)propionateFigure 19: ¹H NMR spectrum (400 MHz, CDCl₃).Figure 20: ¹³C NMR spectrum (101 MHz, CDCl₃)

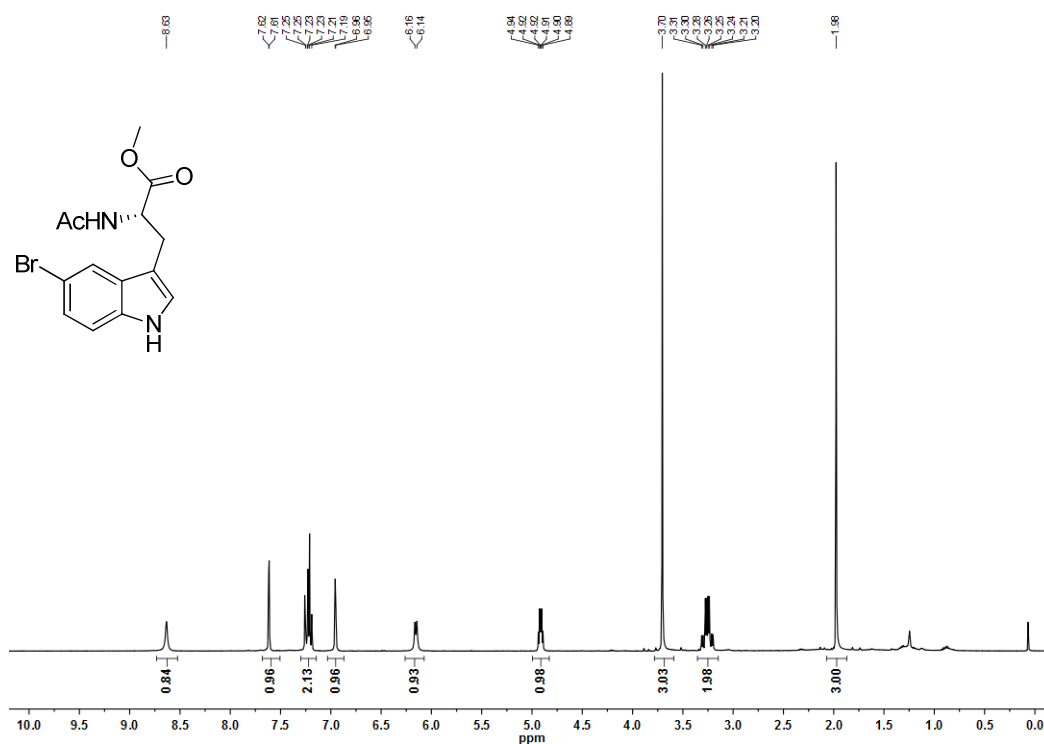
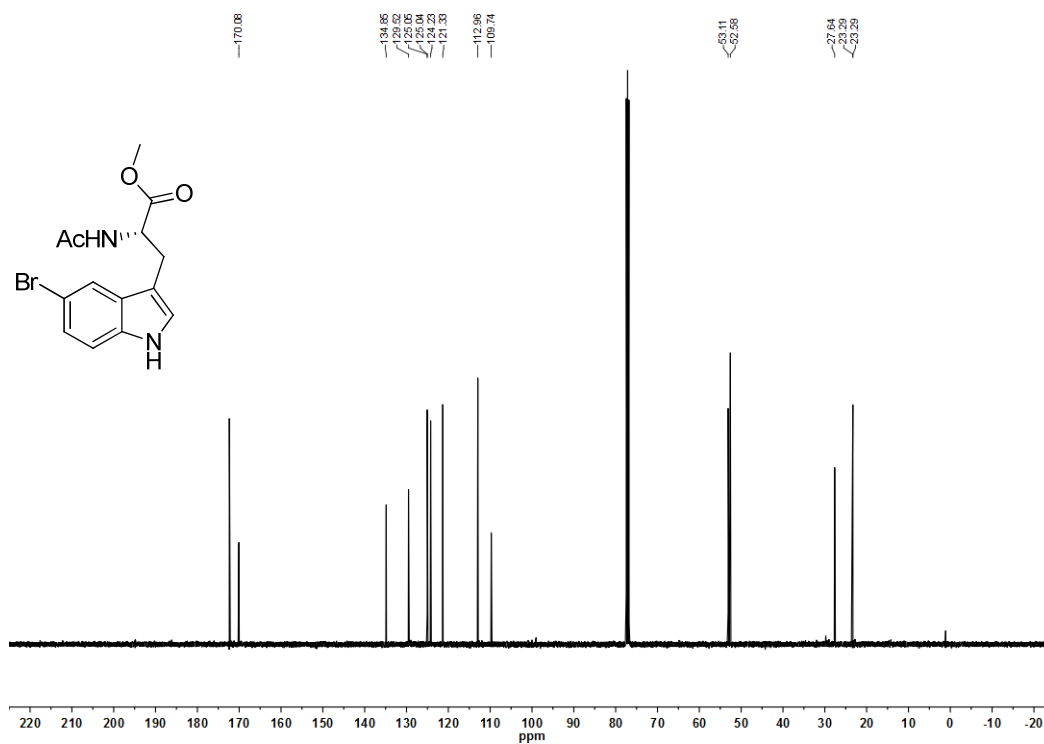
Methyl (2*R*)-2-benzylamino-3-(1*H*-indol-3-yl)propionateFigure 21: ^1H NMR spectrum (400 MHz, CDCl_3).Figure 22: ^{13}C NMR spectrum (101 MHz, CDCl_3).

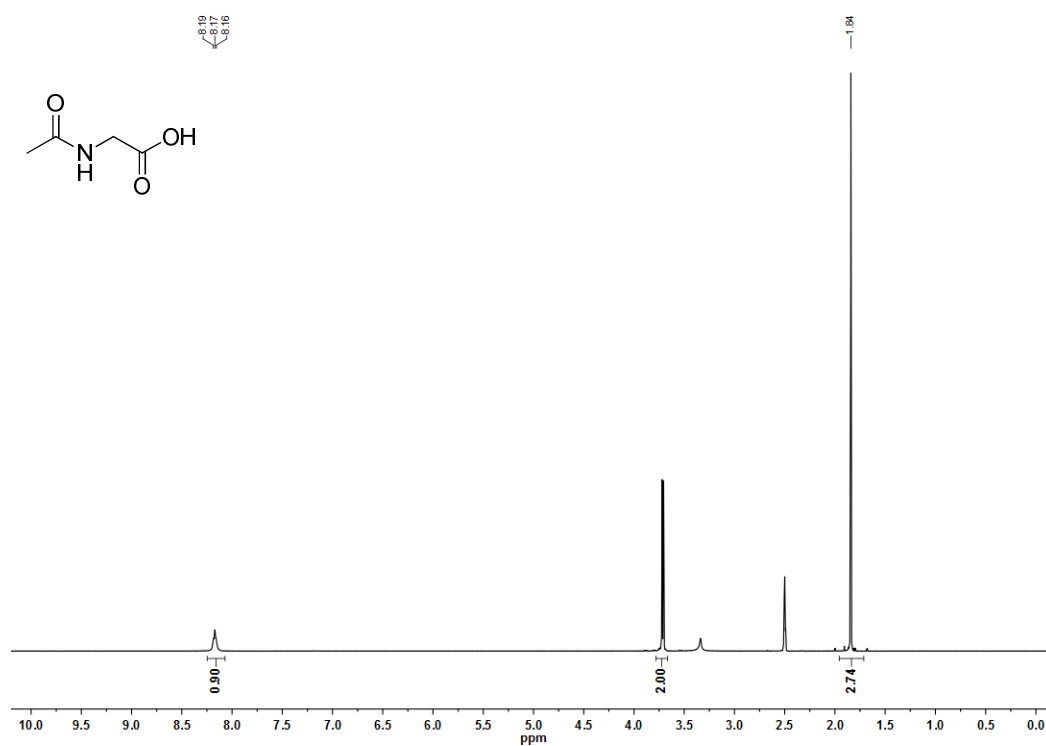
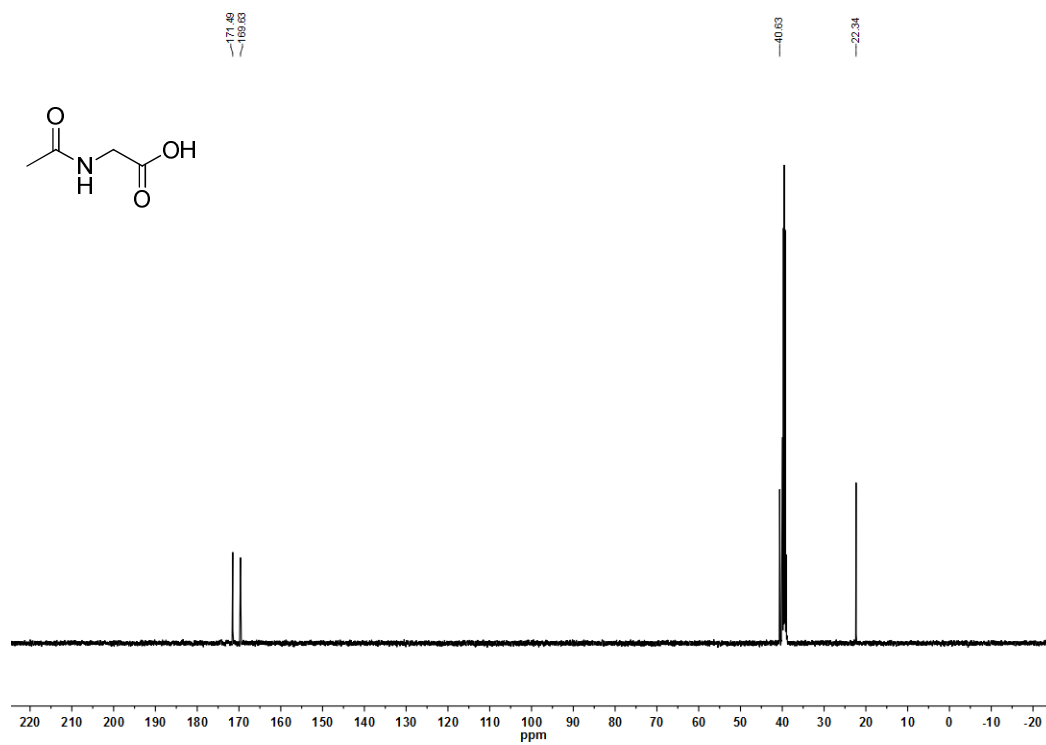
Methyl (2R)-2-(trifluoroacetyl)-3-(1H-indol-3-yl)propionate

Figure 23: ^1H NMR spectrum (400 MHz, CDCl_3).Figure 24: ^{13}C NMR spectrum (101 MHz, CDCl_3).

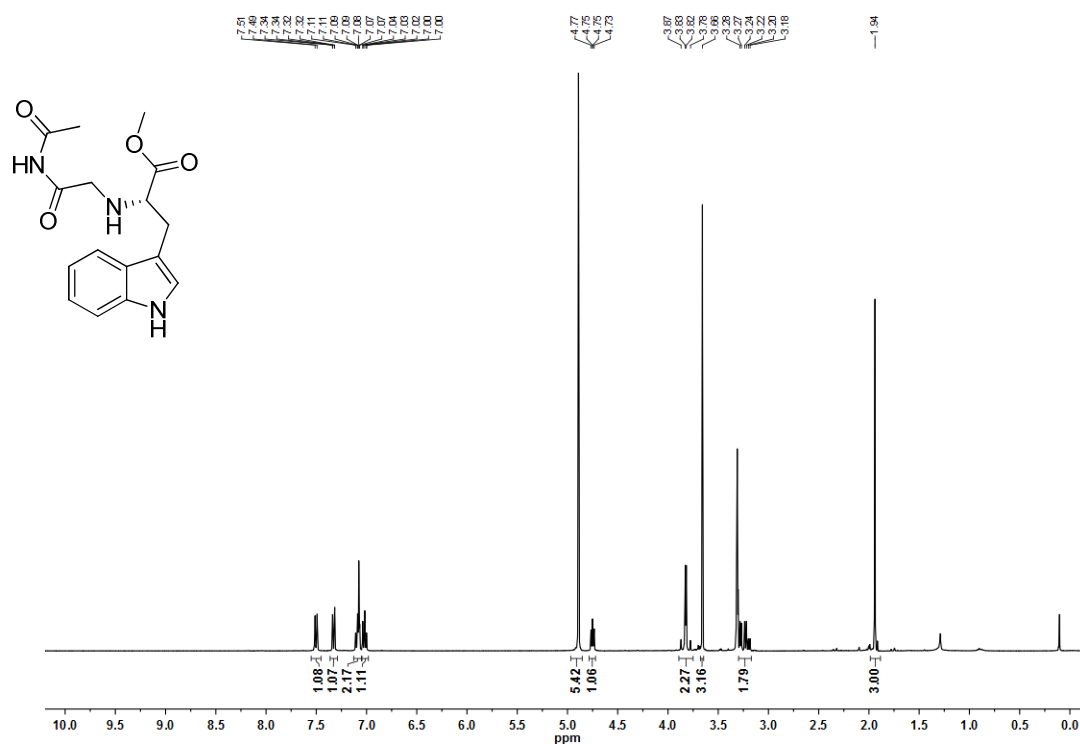
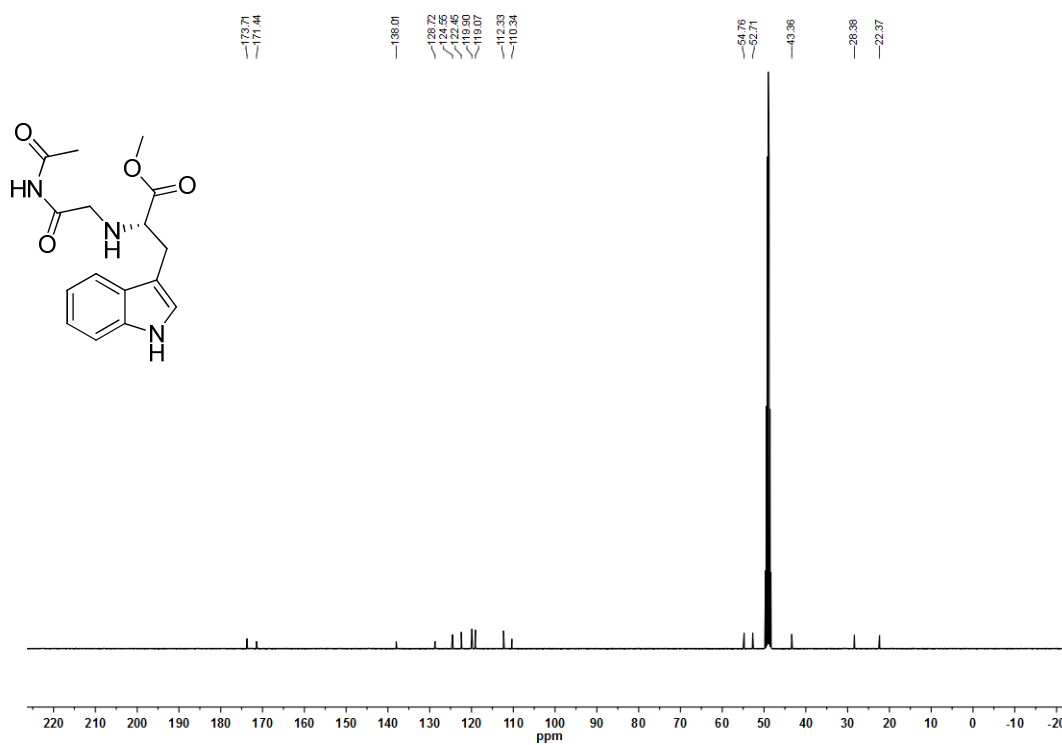
Methyl (2*R*)-2-amino-3-(1*H*-5-bromoindol-3-yl)propionateFigure 25: ¹H NMR spectrum (400 MHz, MeOD).Figure 26: ¹³C NMR spectrum (101 MHz, MeOD).

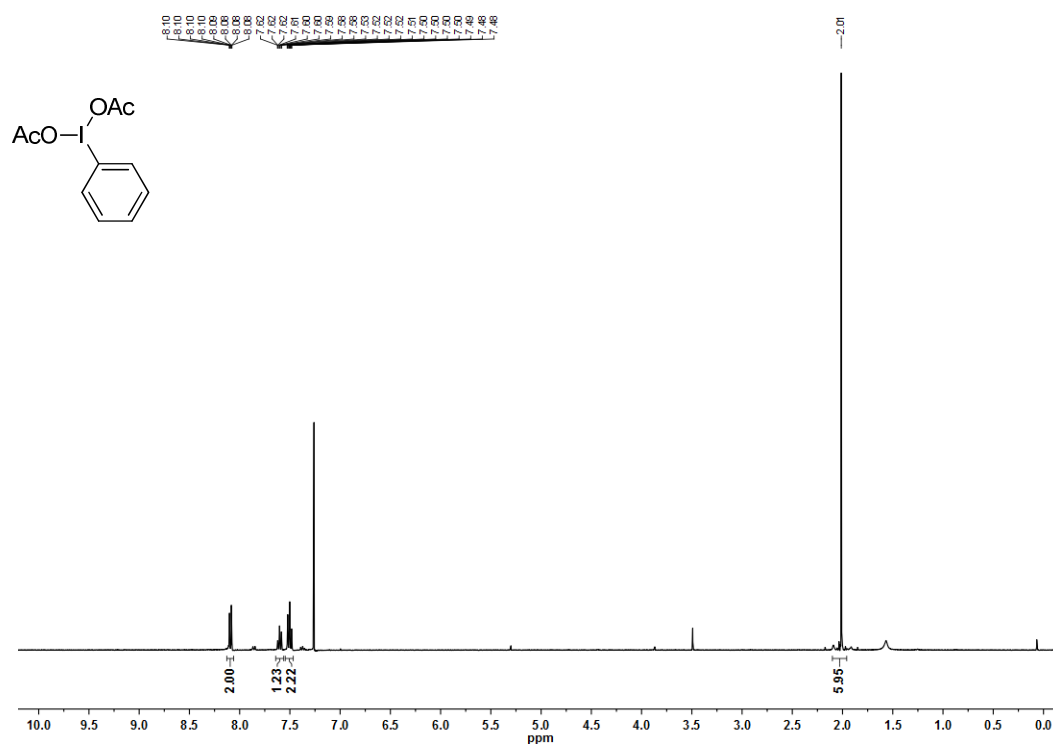
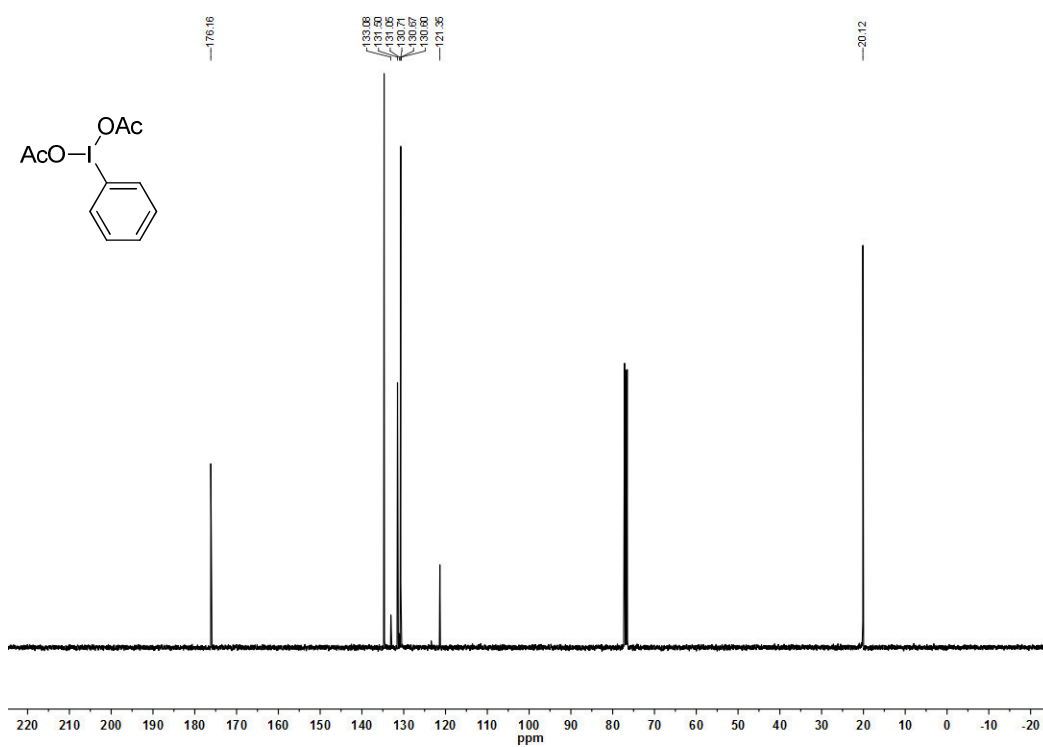
Methyl (2R)-2-acetyl-3-(1H-5-bromoindol-3-yl)propionate

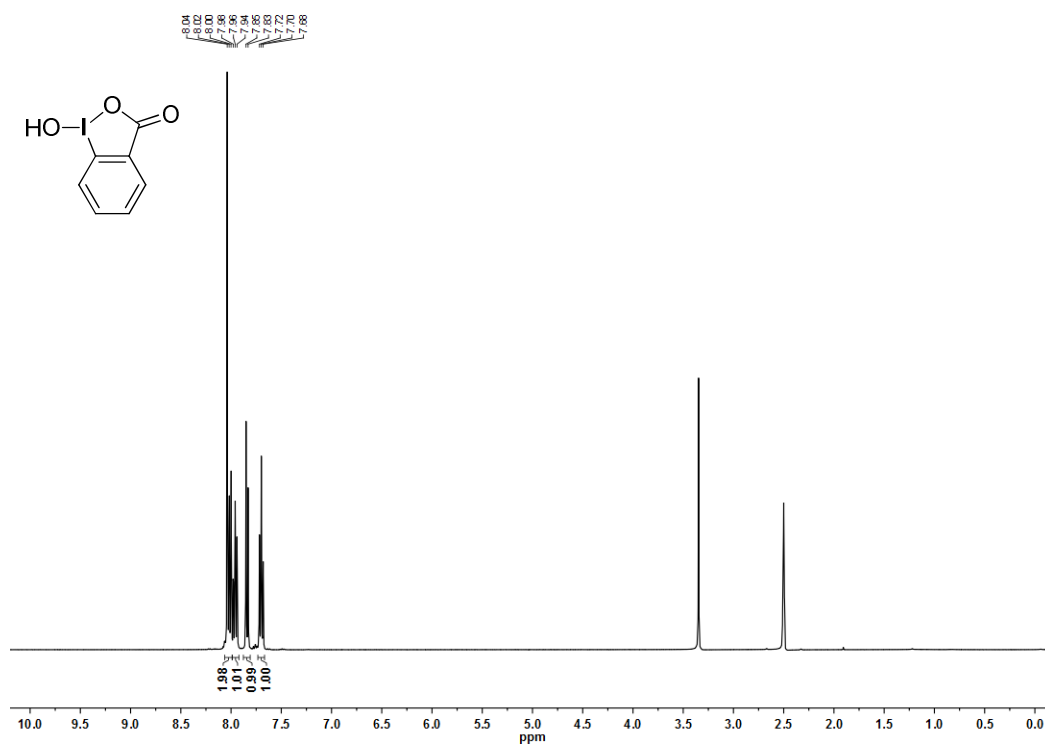
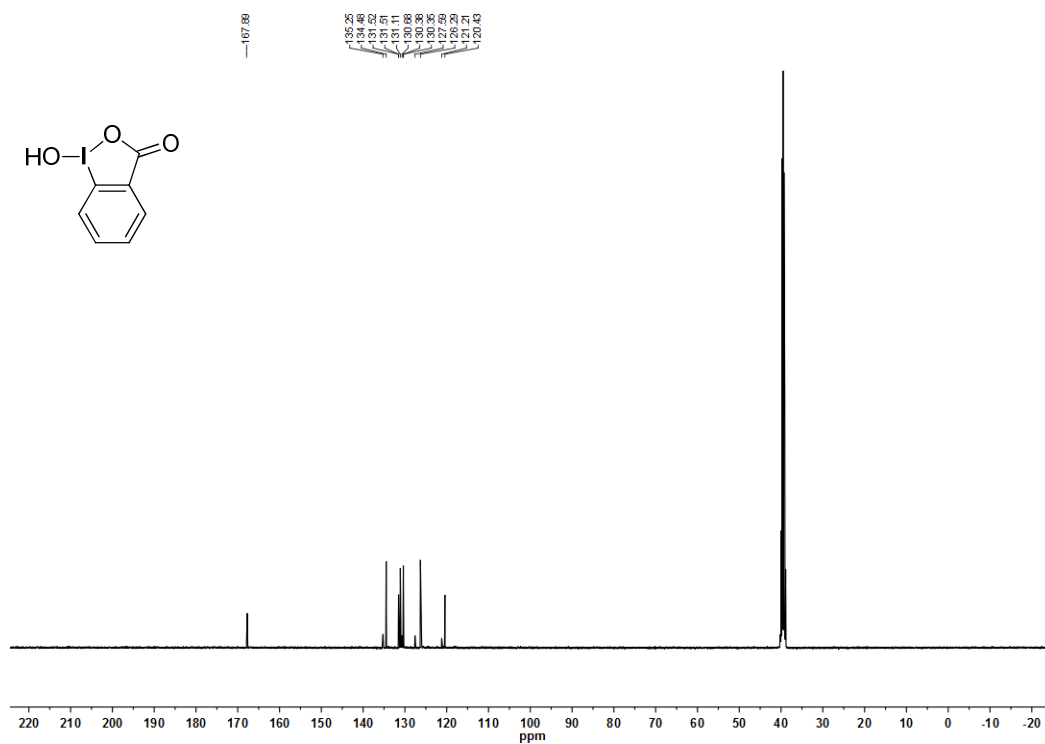
Figure 27: ¹H NMR spectrum (400 MHz, CDCl₃).Figure 28: ¹³C NMR spectrum (101 MHz, CDCl₃).

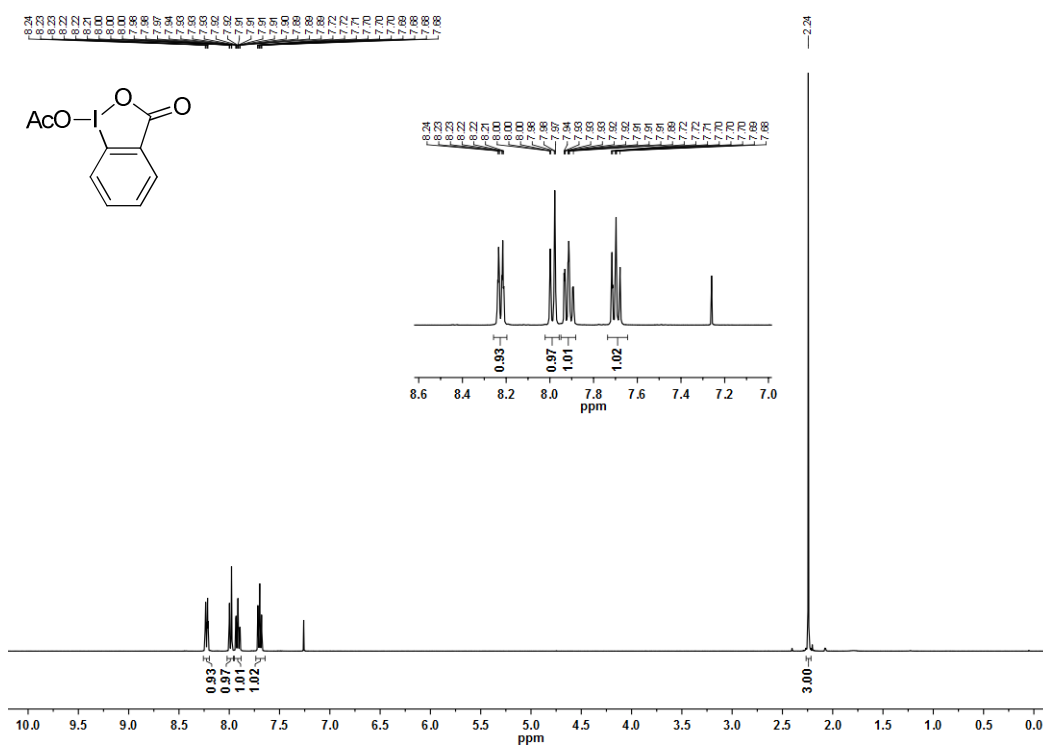
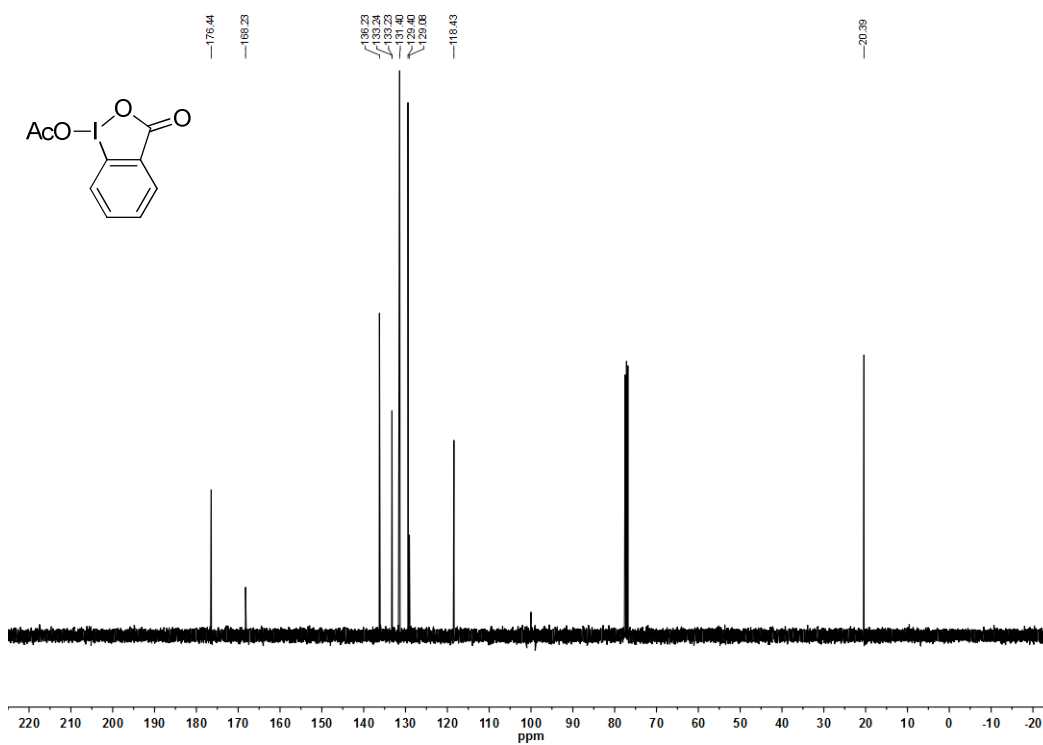
N-AcetylglycineFigure 29: ^1H NMR spectrum (400 MHz, MeOD).Figure 30: ^{13}C NMR spectrum (101 MHz, MeOD).

AcNGlyTrpOMe

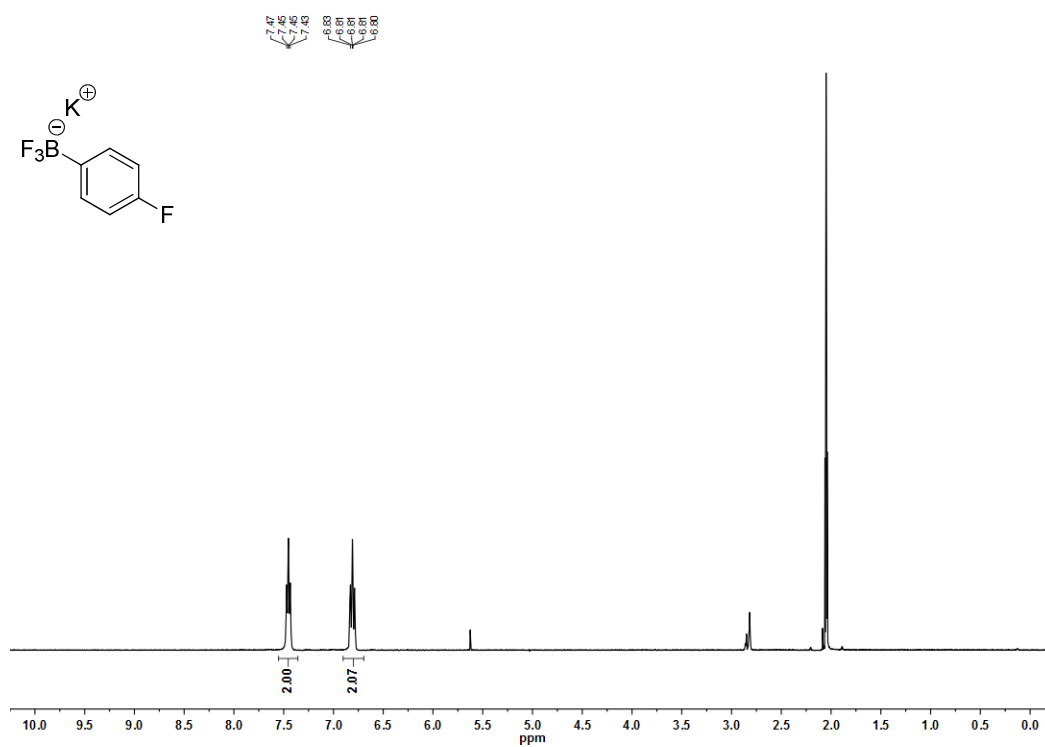
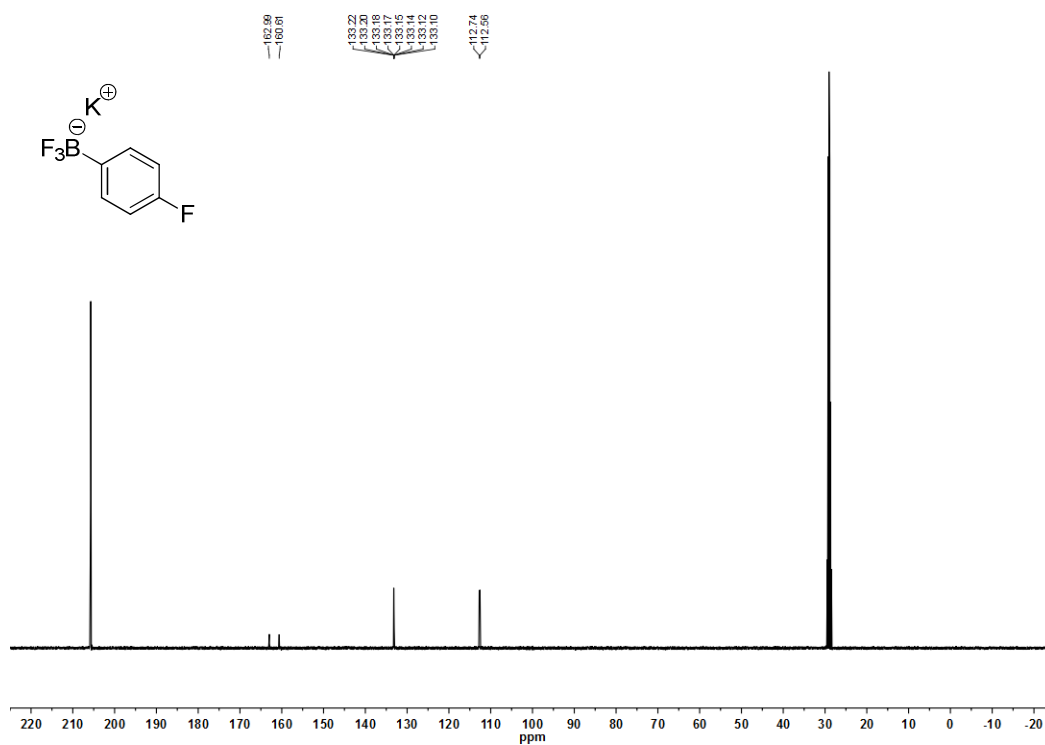
Figure 31: ¹H NMR spectrum (400 MHz, CD₃OD).Figure 32: ¹³C NMR spectrum (101 MHz, CD₃OD).

Bis(acetyloxy)phenyl- λ^3 -iodaneFigure 33: ^1H NMR spectrum (400 MHz, CDCl_3).Figure 34: ^{13}C NMR spectrum (101 MHz, CDCl_3).

1-Hydroxy-1*H*-1 λ^3 -benzo[*d*][1,2]iodoxol-3-oneFigure 35: ^1H NMR spectrum (400 MHz, $(\text{CD}_3)_2\text{SO}$).Figure 36: ^{13}C NMR spectrum (101 MHz, $(\text{CD}_3)_2\text{SO}$).

1-Acetyl-1*H*-1 λ^3 -benzo[*d*][1,2]iodoxol-3-oneFigure 37: $^1\text{H NMR}$ spectrum (400 MHz, CDCl_3).Figure 38: $^{13}\text{C NMR}$ spectrum (101 MHz, CDCl_3).

Potassium 4-fluorophenylborontrifluoride

Figure 39: ^1H NMR spectrum (400 MHz, $(\text{CD}_3)_2\text{CO}$).Figure 40: ^{13}C NMR spectrum (101 MHz, $(\text{CD}_3)_2\text{CO}$).

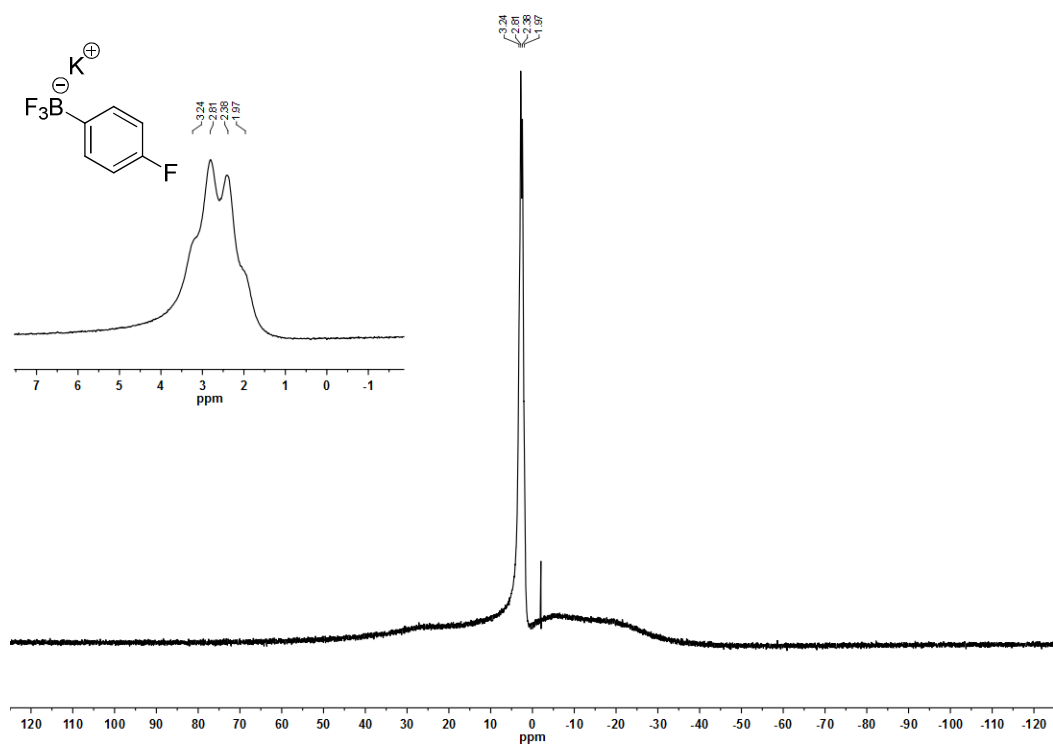


Figure 41: ^{11}B NMR spectrum (218 MHz, $(\text{CD}_3)_2\text{CO}$).

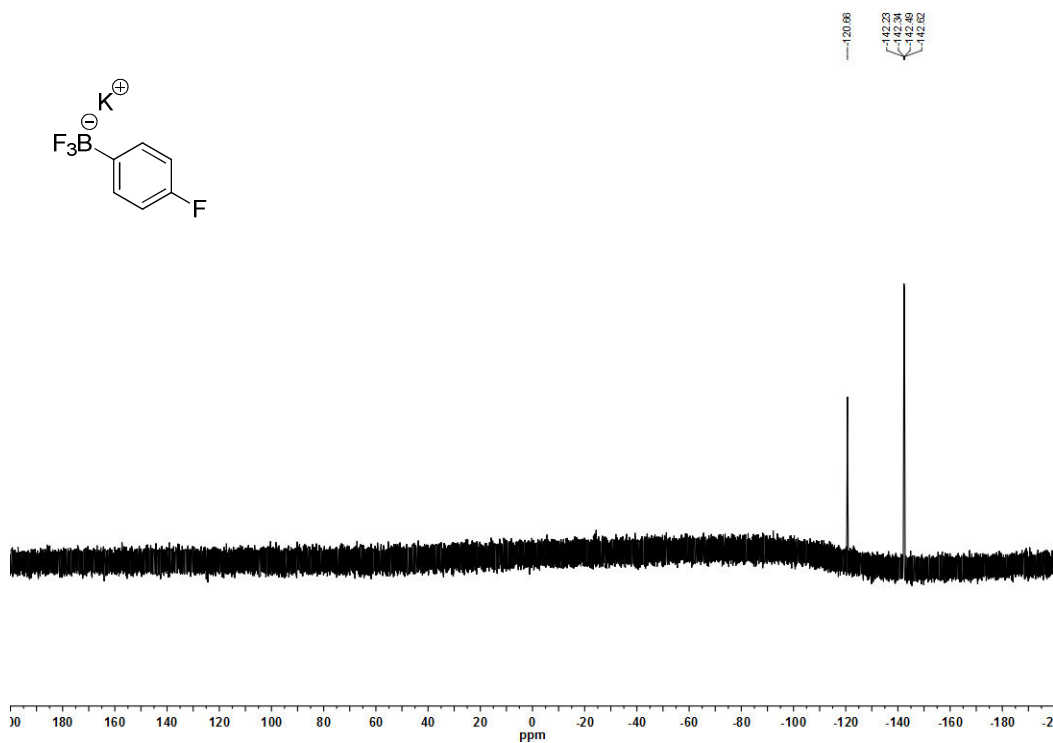
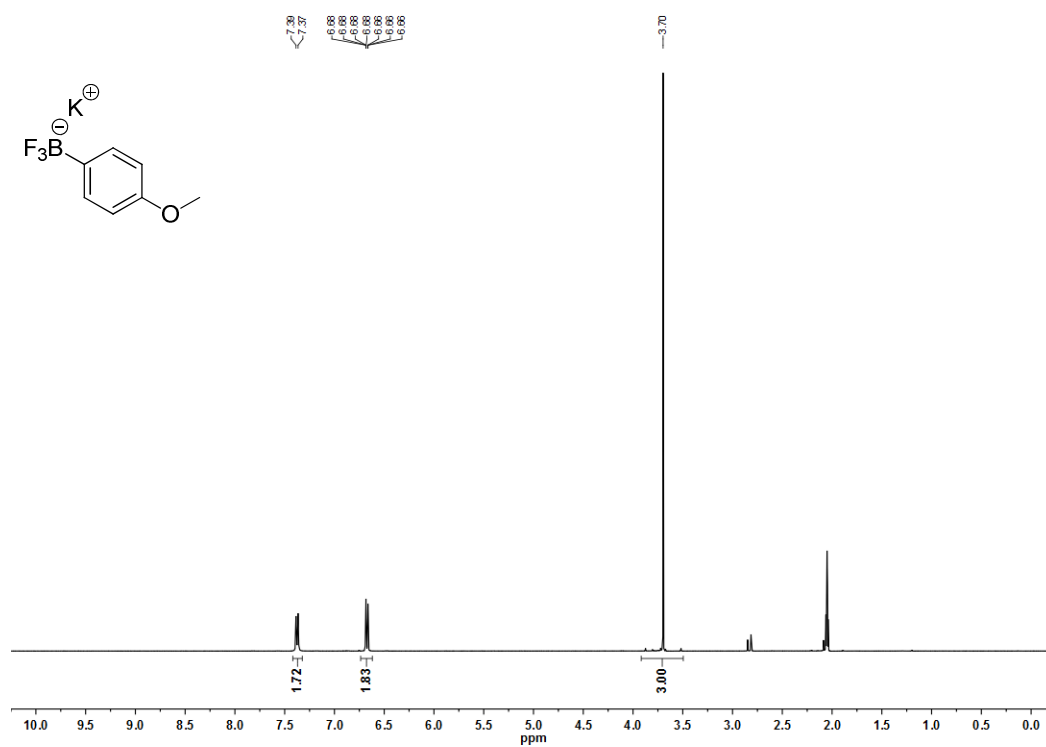
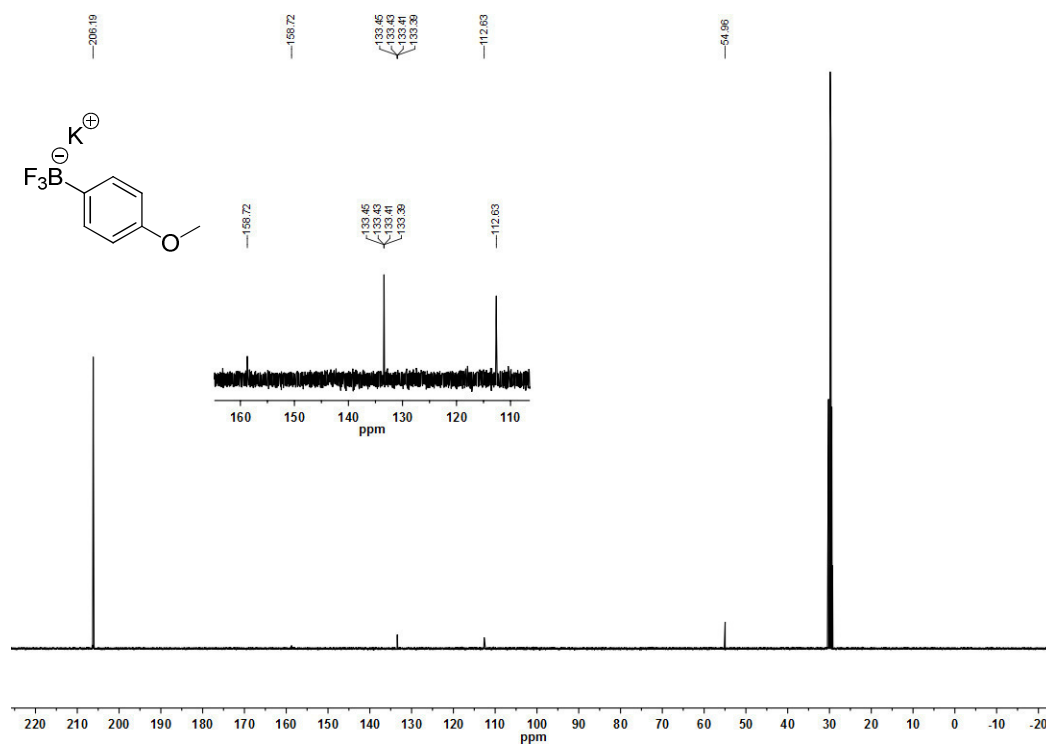


Figure 42: ^{19}F NMR spectrum (376 MHz, $(\text{CD}_3)_2\text{CO}$).

Potassium 4-methoxyphenylborontrifluoride

Figure 43: ^1H NMR spectrum (400 MHz, $(\text{CD}_3)_2\text{CO}$).Figure 44: ^{13}C NMR spectrum (101 MHz, $(\text{CD}_3)_2\text{CO}$).

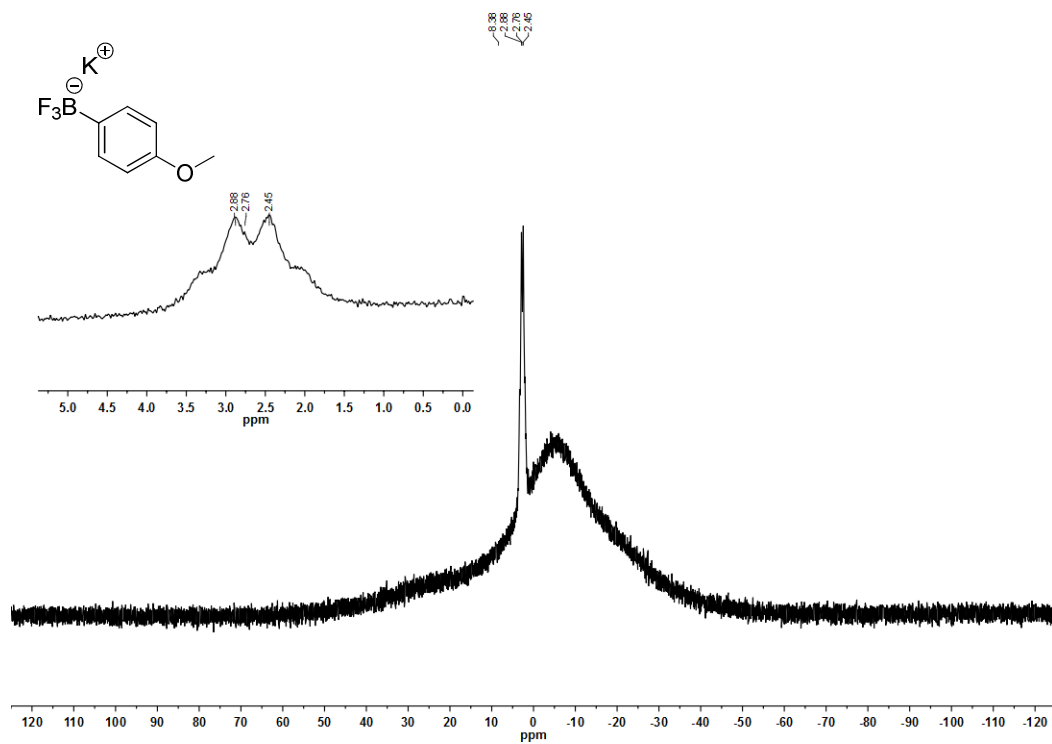


Figure 45: ^{11}B NMR spectrum (218 MHz, $(\text{CD}_3)_2\text{CO}$).

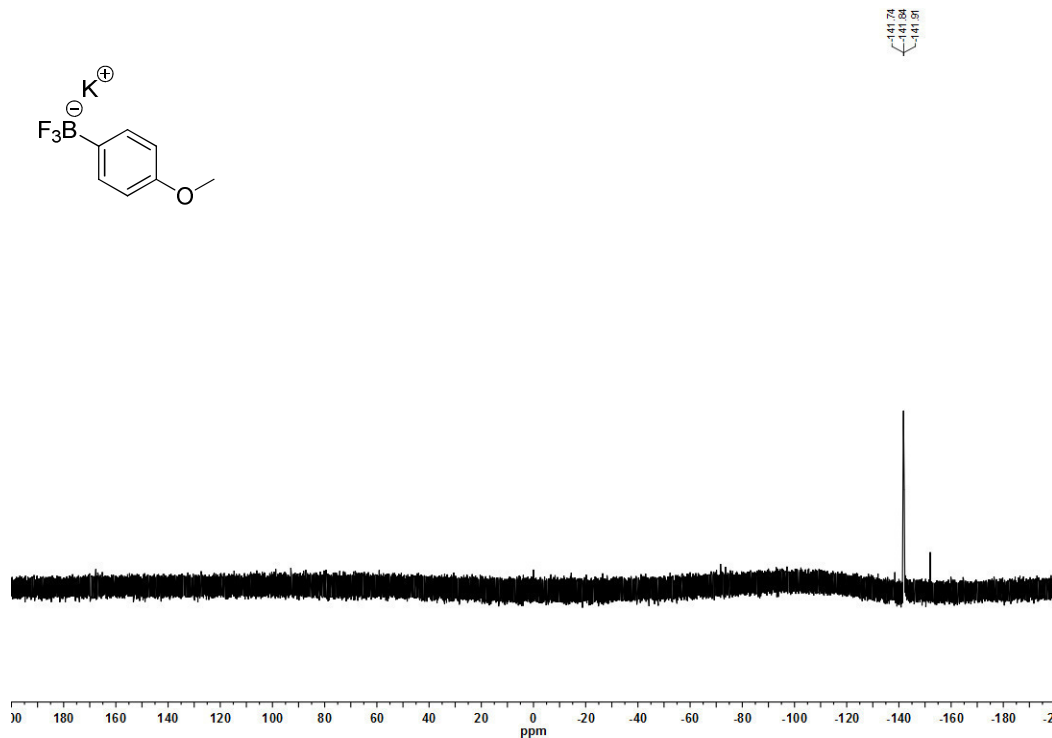
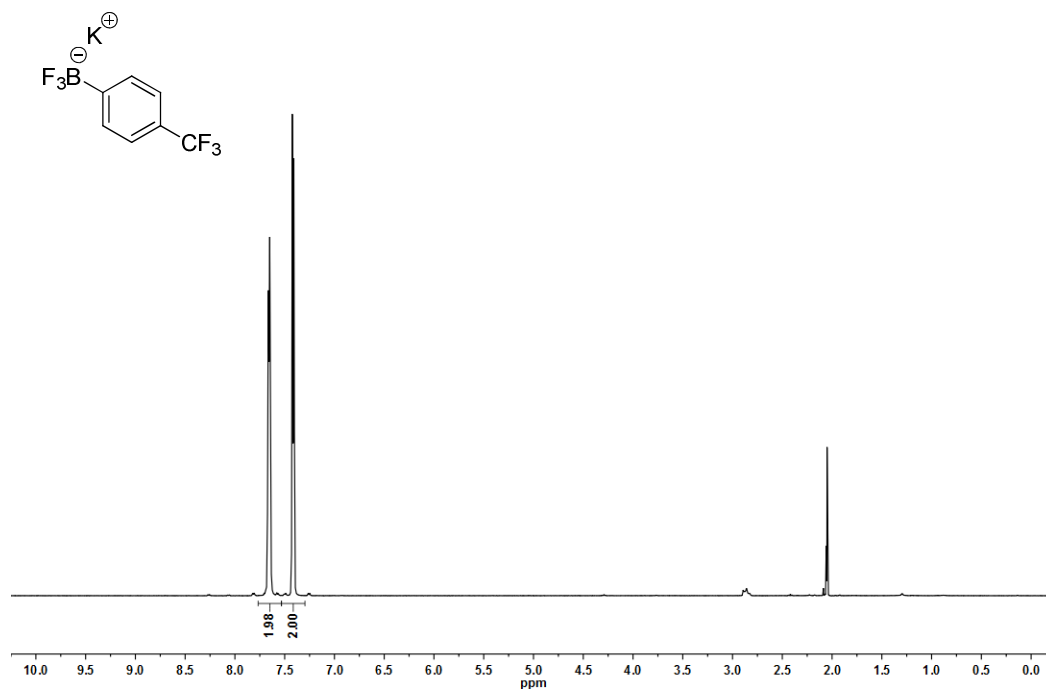
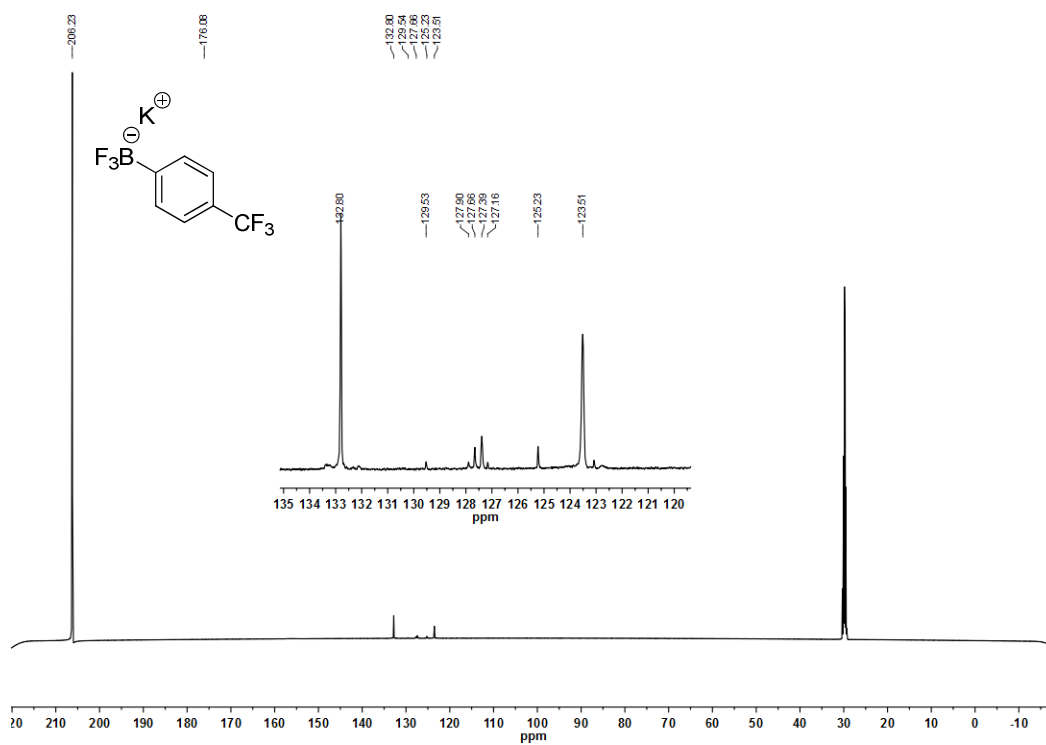


Figure 46: ^{19}F NMR spectrum (376 MHz, $(\text{CD}_3)_2\text{CO}$).

Potassium 4-(trifluoromethyl)phenylborontrifluoride

Figure 47: ^1H NMR spectrum (400 MHz, $(\text{CD}_3)_2\text{CO}$).Figure 48: ^{13}C NMR spectrum (101 MHz, $(\text{CD}_3)_2\text{CO}$).

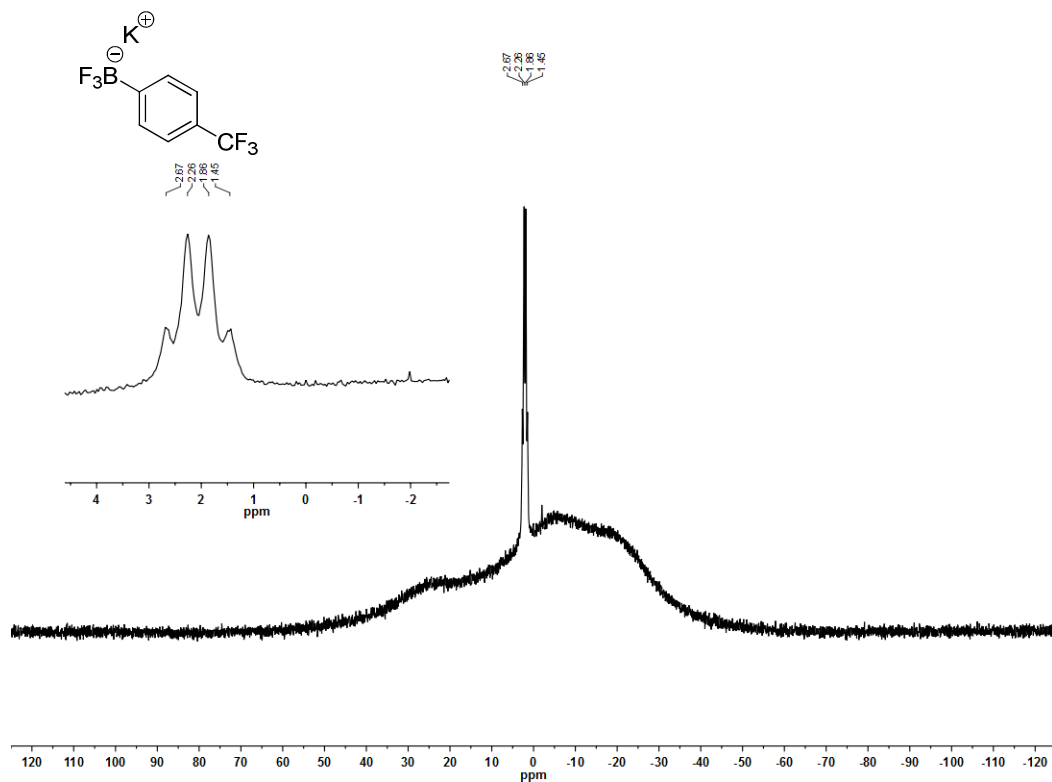


Figure 49: ^{11}B NMR spectrum (218 MHz, $(\text{CD}_3)_2\text{CO}$).

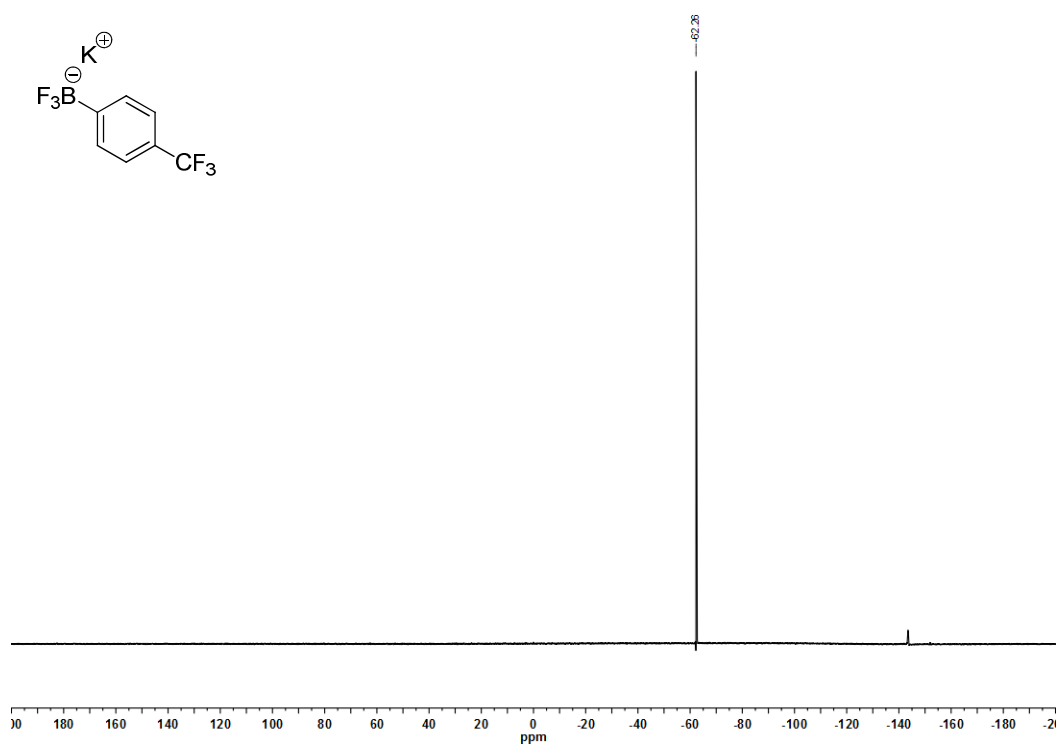


Figure 50: ^{19}F NMR spectrum (376 MHz, $(\text{CD}_3)_2\text{CO}$).

1,3-[di(2,4,6-trimethylphenyl)-4,5-dihydroimidazolylidene](η^3 -2-methylpropenyl)chloropalladium(II)

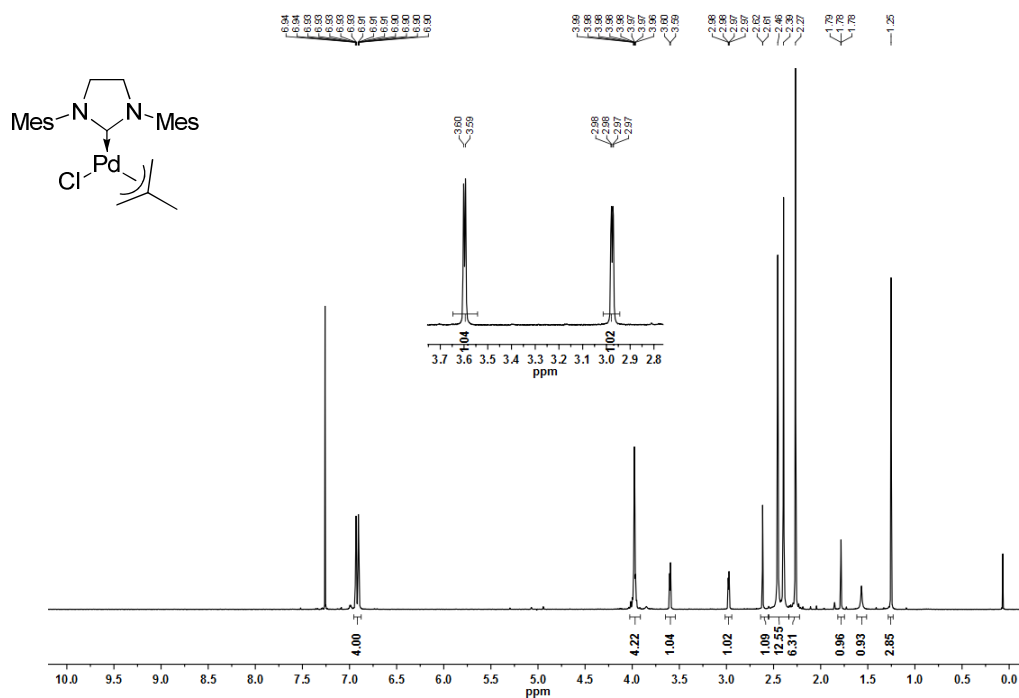


Figure 51: ^1H NMR spectrum (400 MHz, CDCl_3).

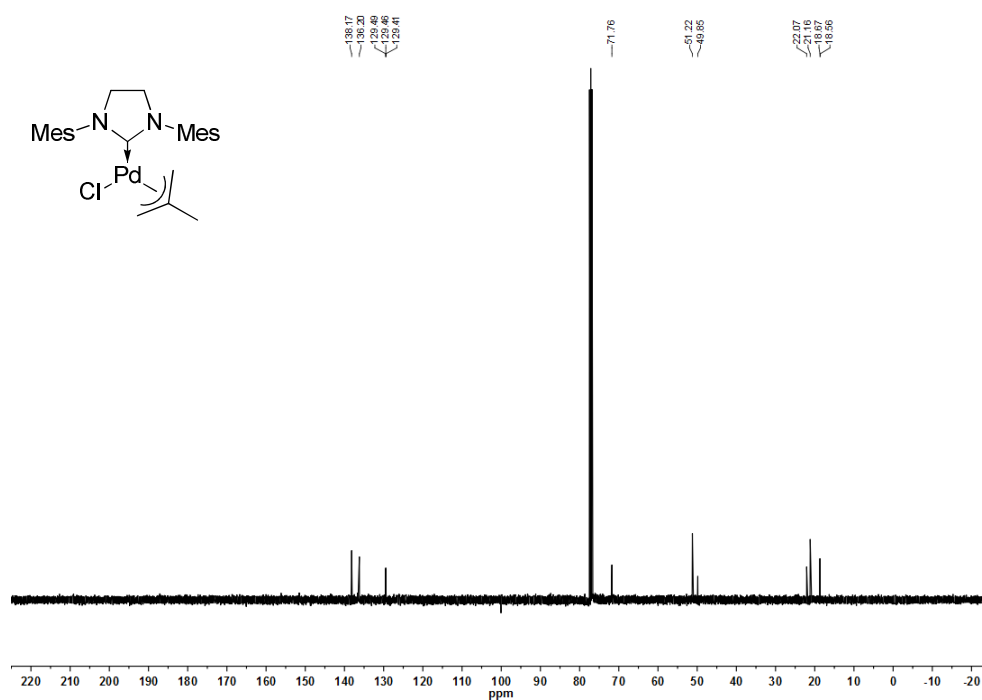


Figure 52: ^{13}C NMR spectrum (101 MHz, CDCl_3).

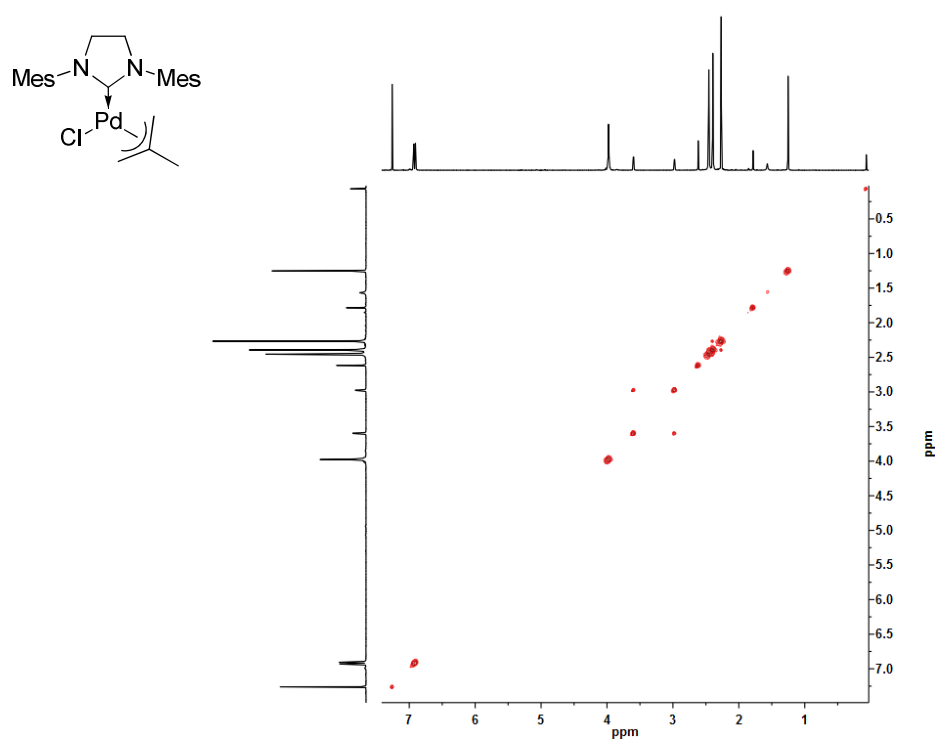


Figure 53: ^1H - ^1H COSY NMR spectrum (400 MHz, CDCl_3).

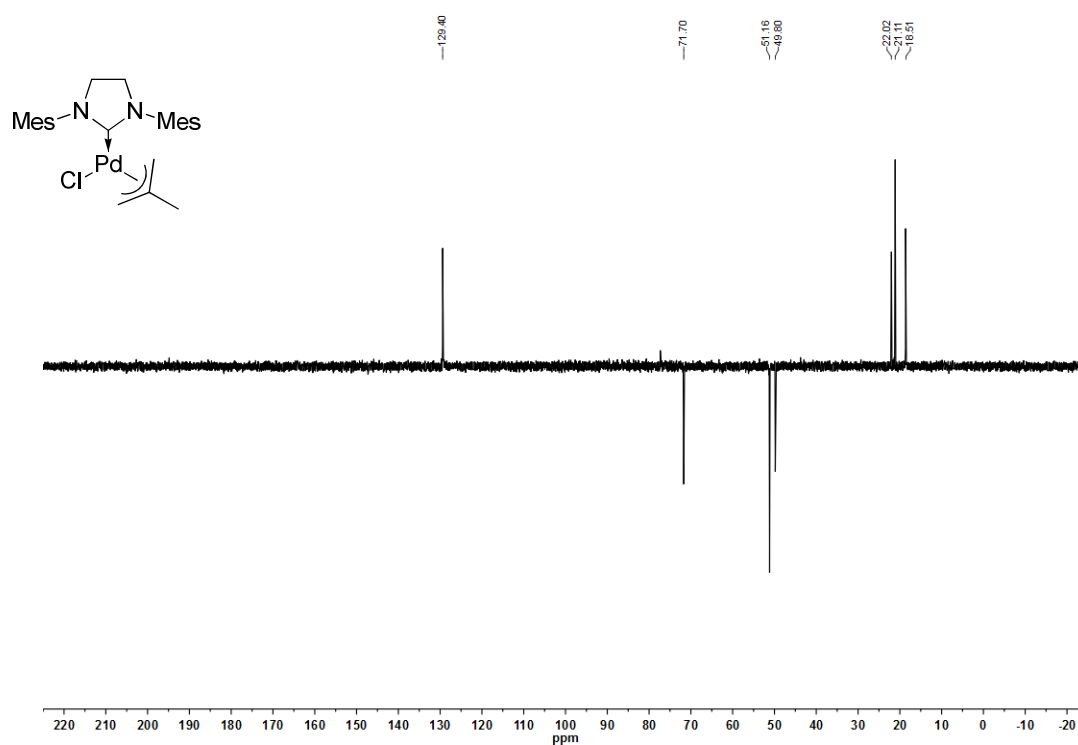


Figure 54: ^{13}C DEPT 135 NMR spectrum (101 MHz, CDCl_3).

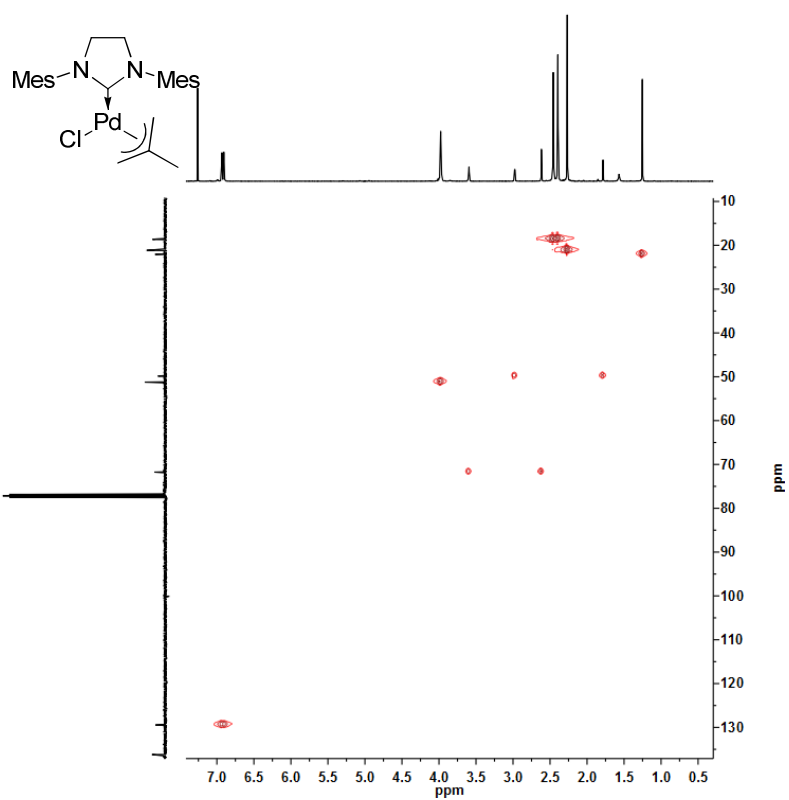


Figure 55: ^1H - ^{13}C HSQC NMR spectrum (400, 101 MHz, CDCl_3).

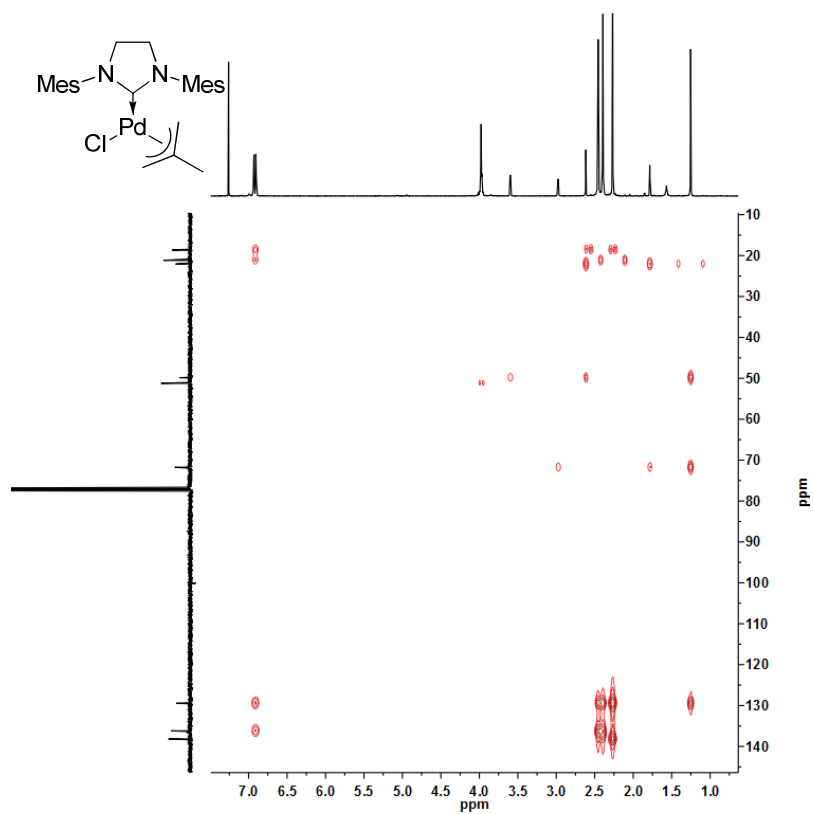


Figure 56: ^1H - ^{13}C HMBC NMR spectrum (400, 101 MHz, CDCl_3).

Trans-di- μ -chlorobis{[1,3-di(2,4,6-trimethylphenyl)-4,5-dihydroimidazolylidene]chloropalladium(II)}

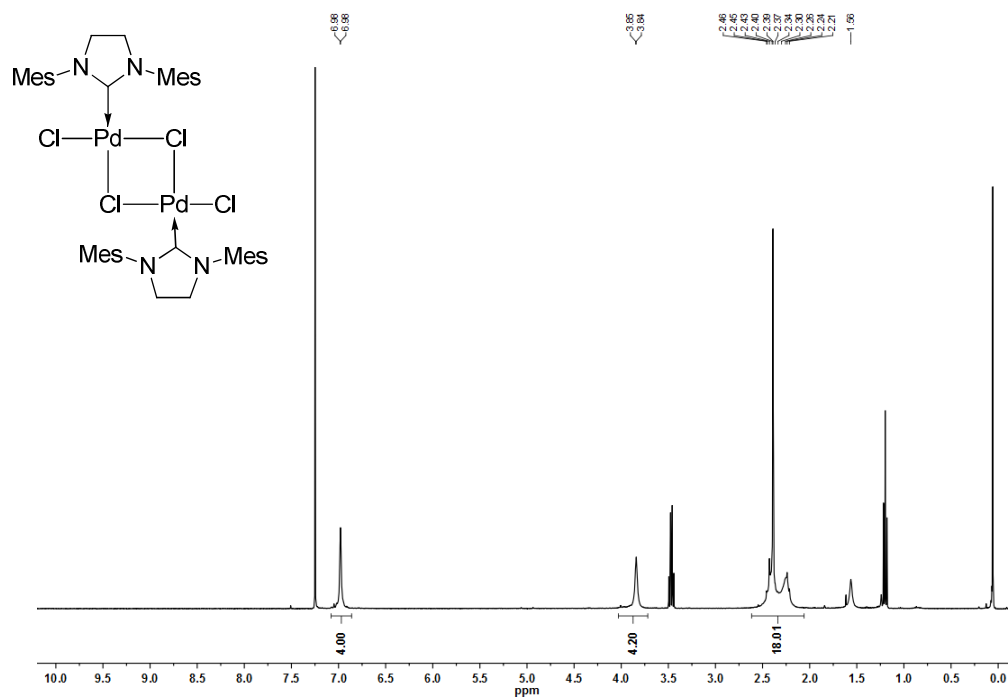


Figure 57: ¹H NMR spectrum (400 MHz, CDCl₃).

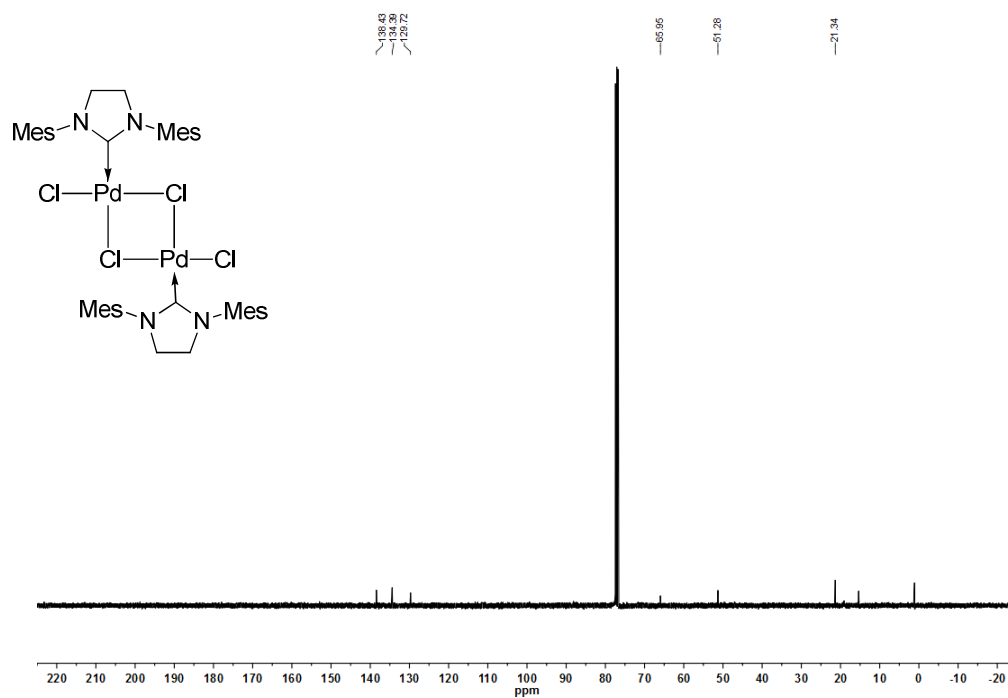


Figure 58: ¹³C NMR spectrum (101 MHz, CDCl₃).

[1,3-di(2,4,6-trimethylphenyl)-4,5-dihydroimidazolylidene]diacetateaquopalladium(II)

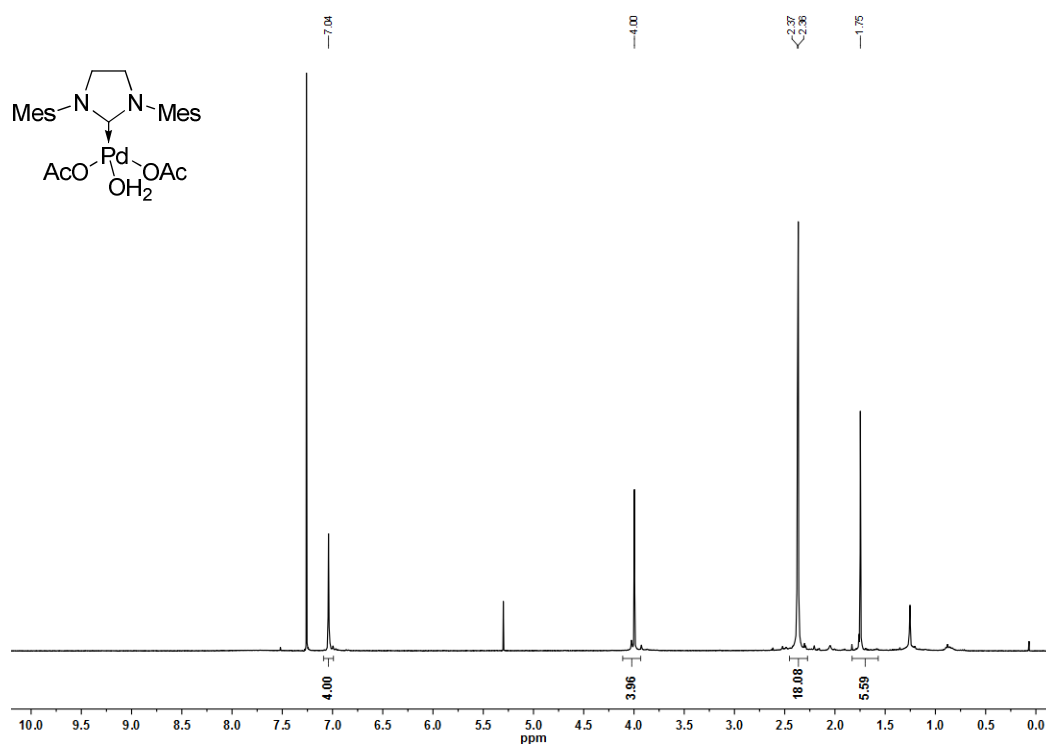


Figure 59: ^1H NMR spectrum (400 MHz, CDCl_3).

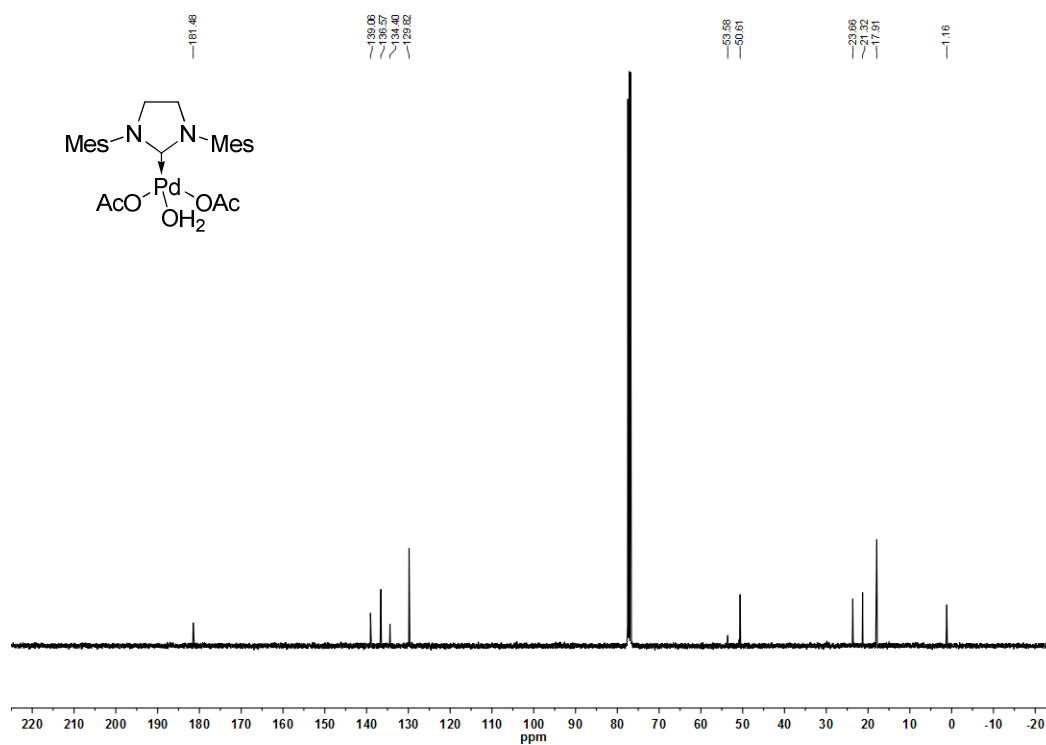
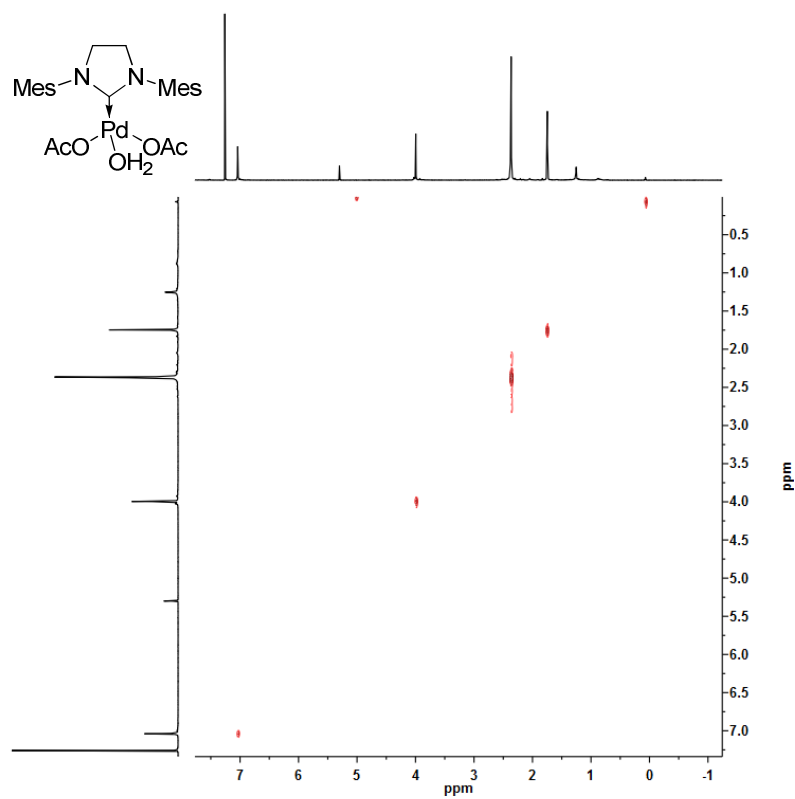
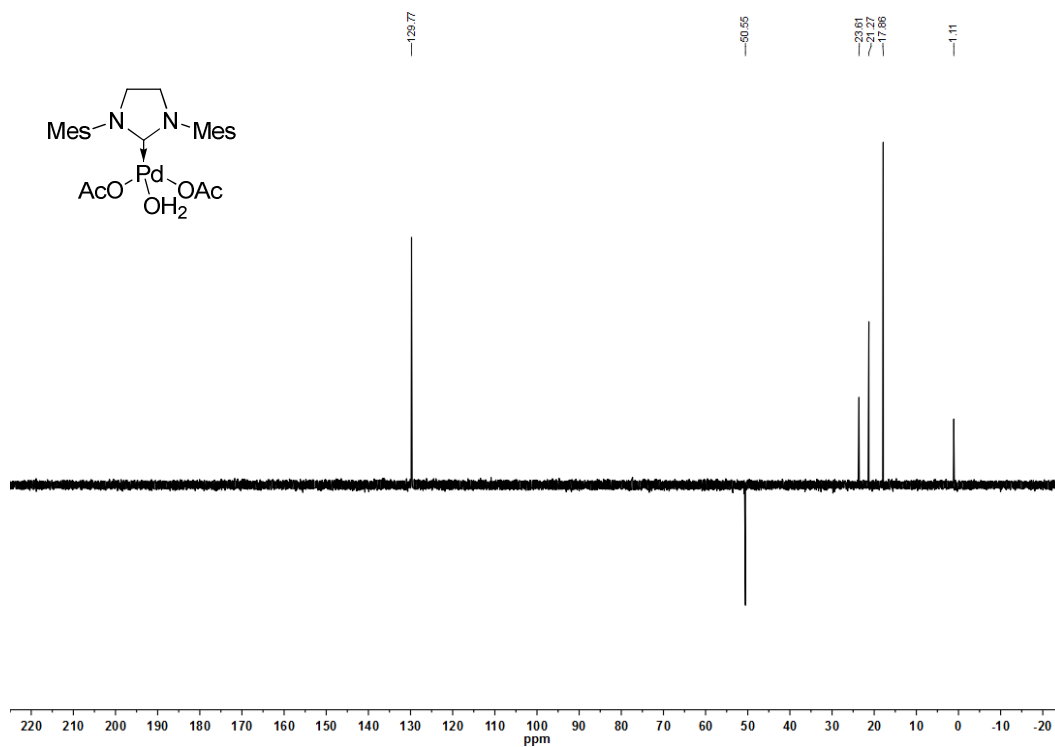


Figure 60: ^{13}C NMR spectrum (101 MHz, CDCl_3).

Figure 61: ^1H - ^1H COSY NMR spectrum (400 MHz, CDCl_3).Figure 62: ^{13}C DEPT 135 NMR spectrum (101 MHz, CDCl_3).

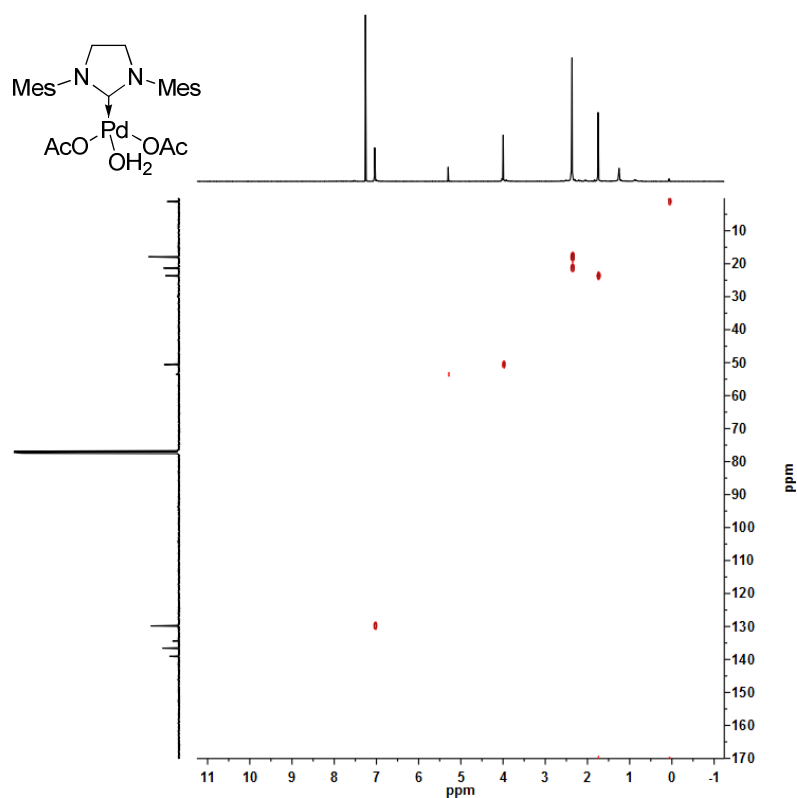


Figure 63: ^1H - ^{13}C HSQC NMR spectrum (400, 101 MHz, CDCl_3).

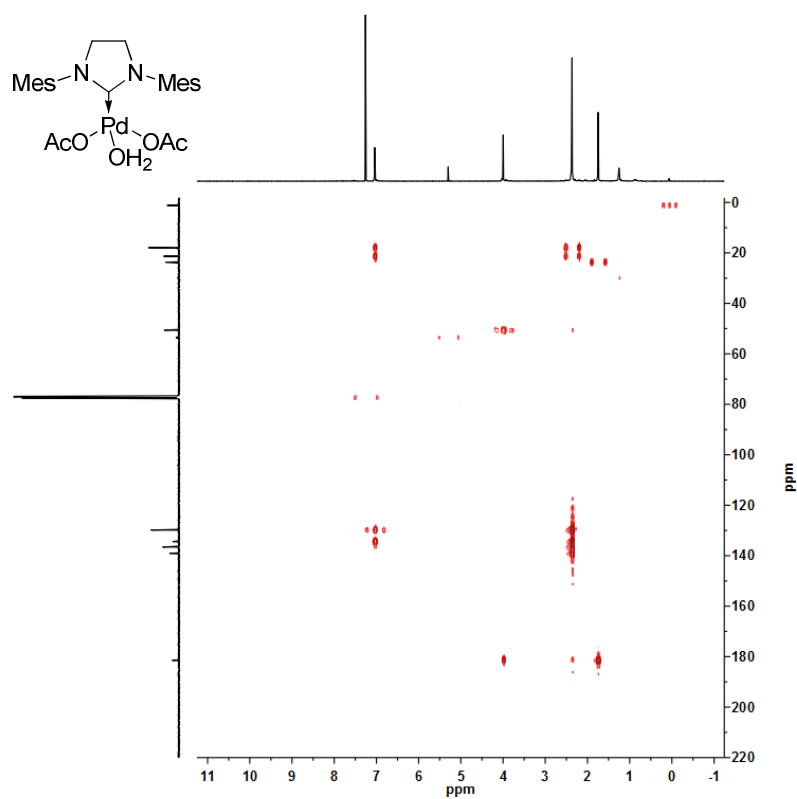
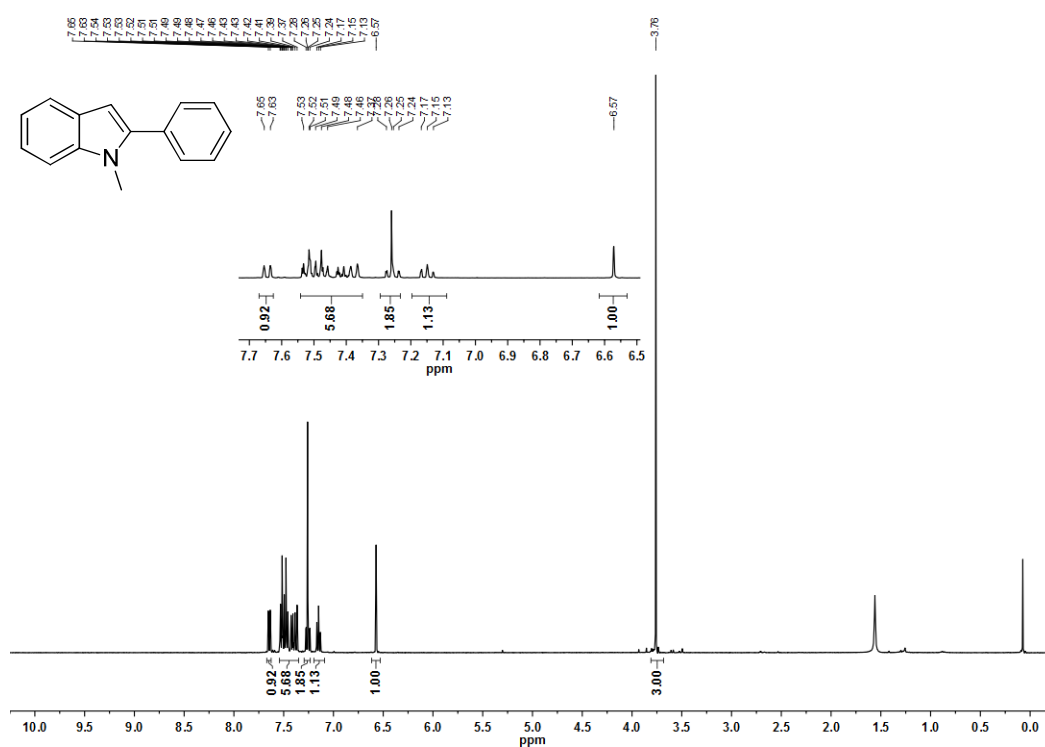
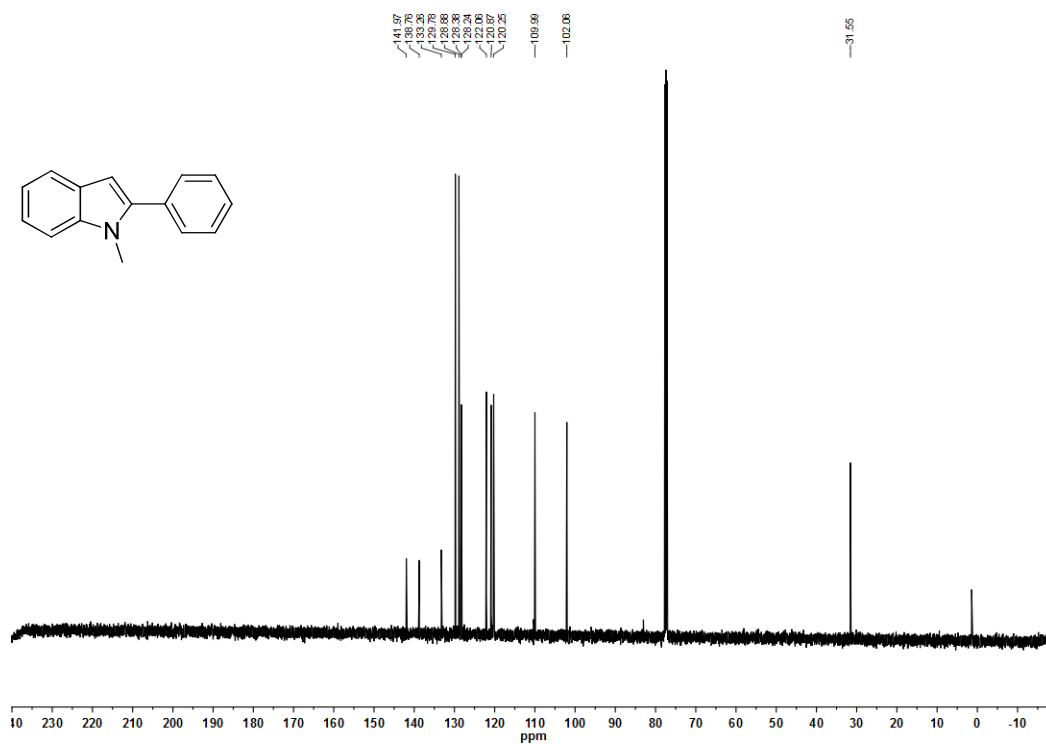


Figure 64: ^1H - ^{13}C HMBC NMR spectrum (400, 101 MHz, CDCl_3).

1-Methyl-2-phenylindole

Figure 65: ^1H NMR spectrum (400 MHz, CDCl_3).Figure 66: ^{13}C NMR spectrum (101 MHz, CDCl_3).

Methyl (2S)-2-acetyl-3-[2-phenyl-1H-indol-3-yl]propanoate

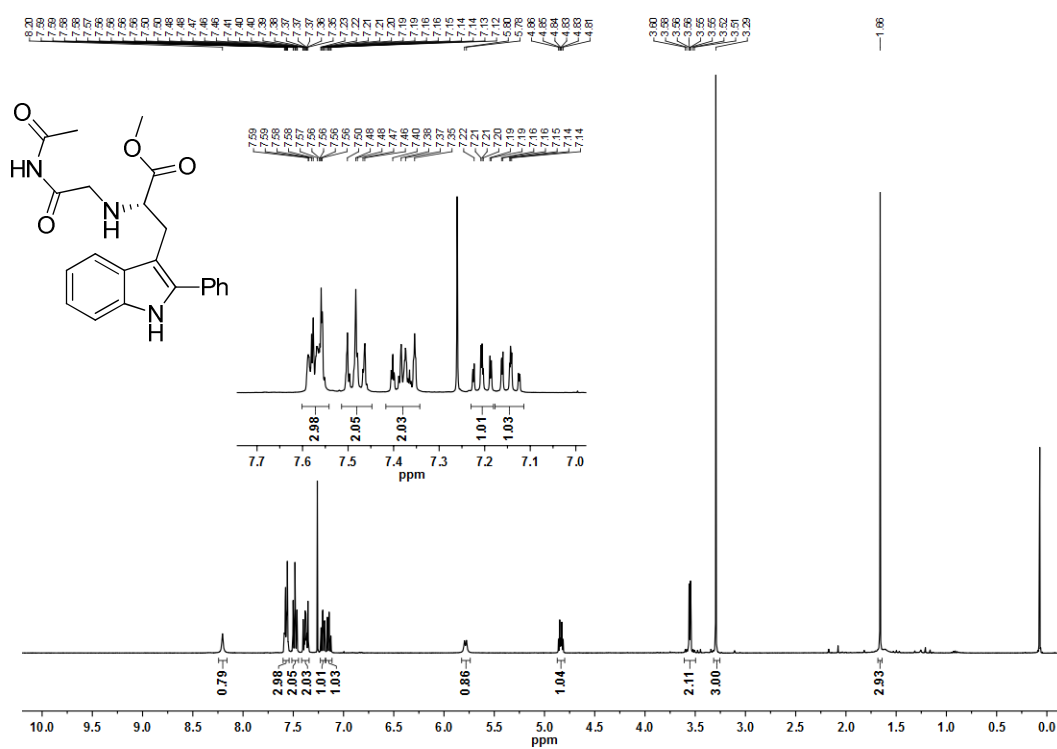
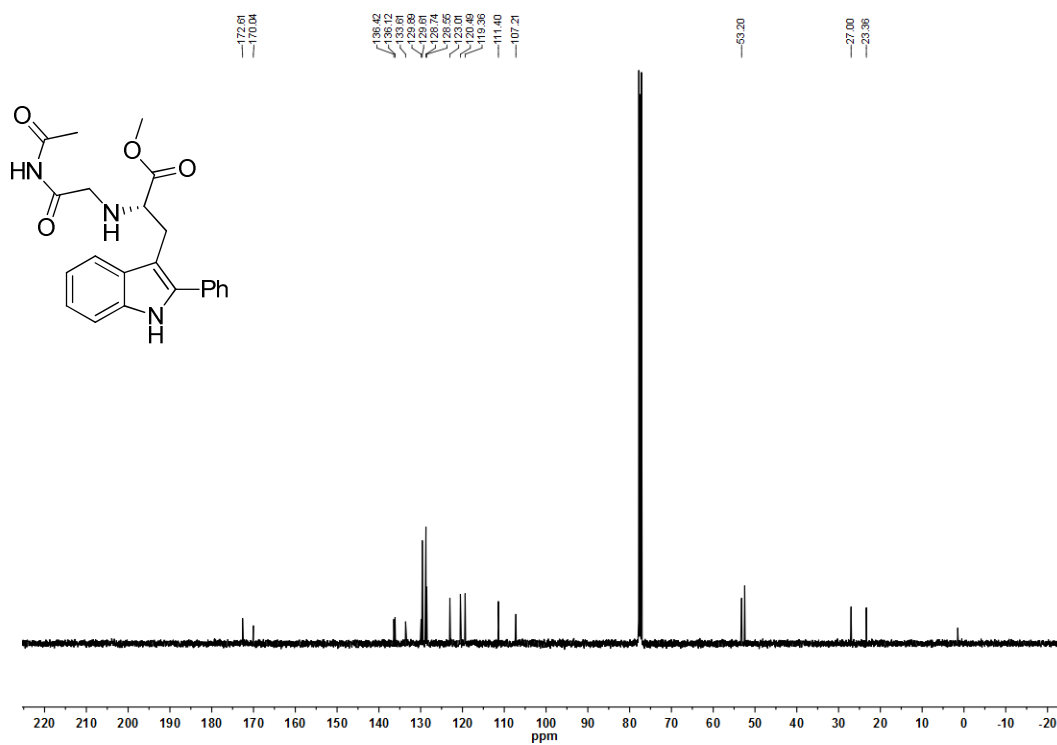
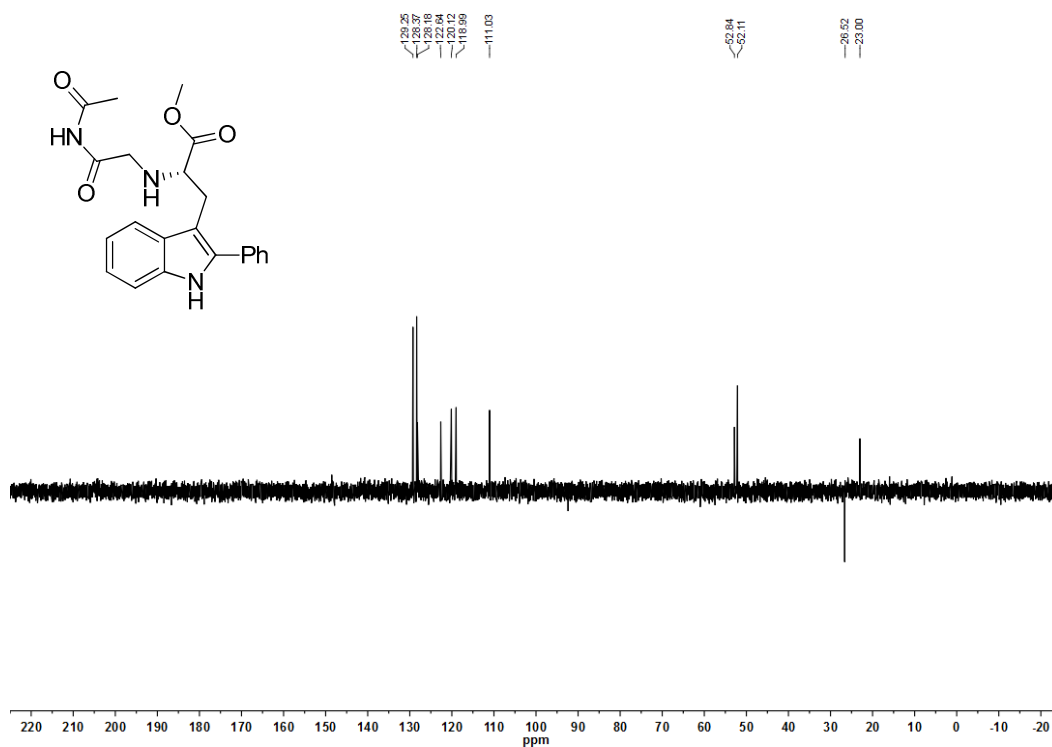
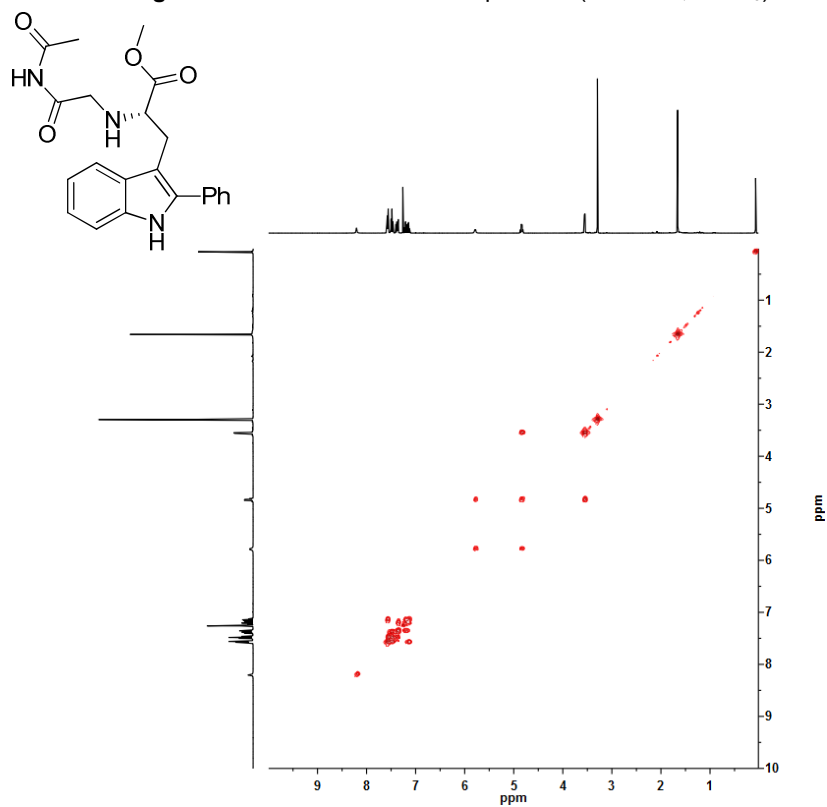
Figure 67: ¹H NMR spectrum (400 MHz, CDCl₃).

Figure 68: ^{13}C NMR spectrum (101 MHz, CDCl_3).Figure 69: ^{13}C NMR DEPT 135 spectrum (101 MHz, CDCl_3).Figure 70: ^1H - ^1H COSY NMR spectrum (400 MHz, CDCl_3).

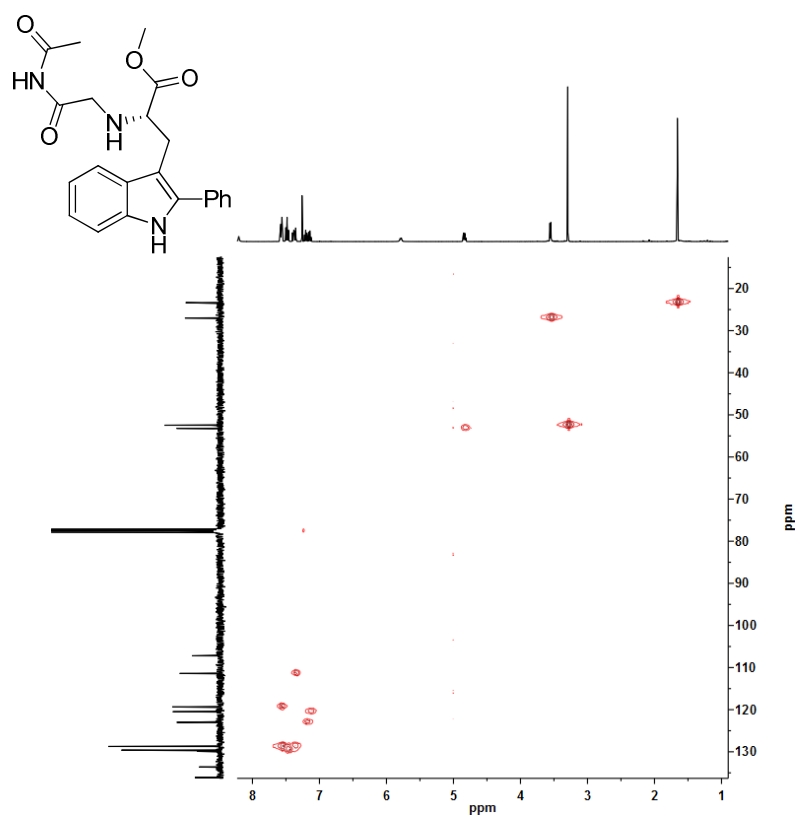


Figure 71: ^1H - ^{13}C HSQC NMR spectrum (400, 101 MHz, CDCl_3).

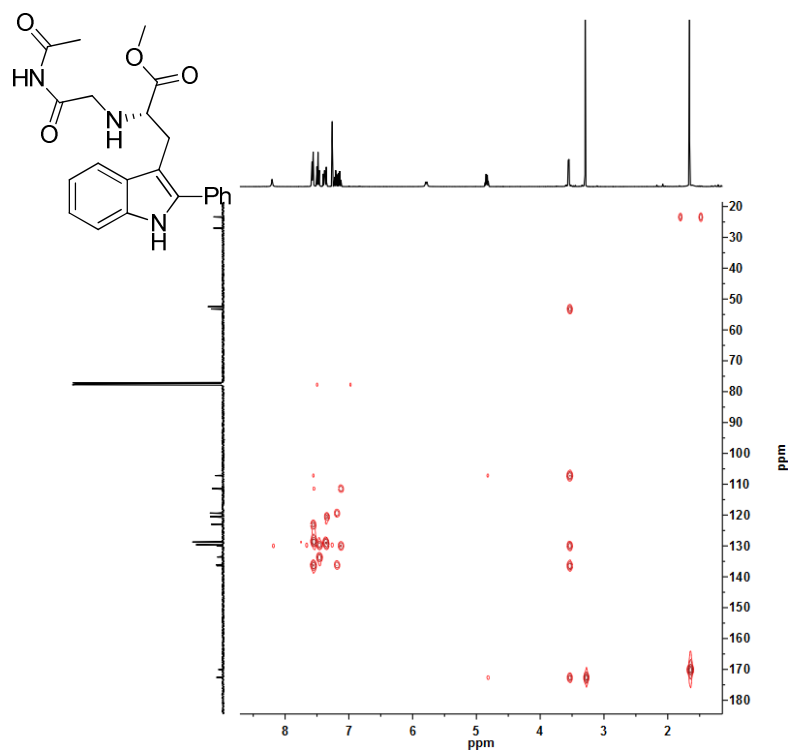
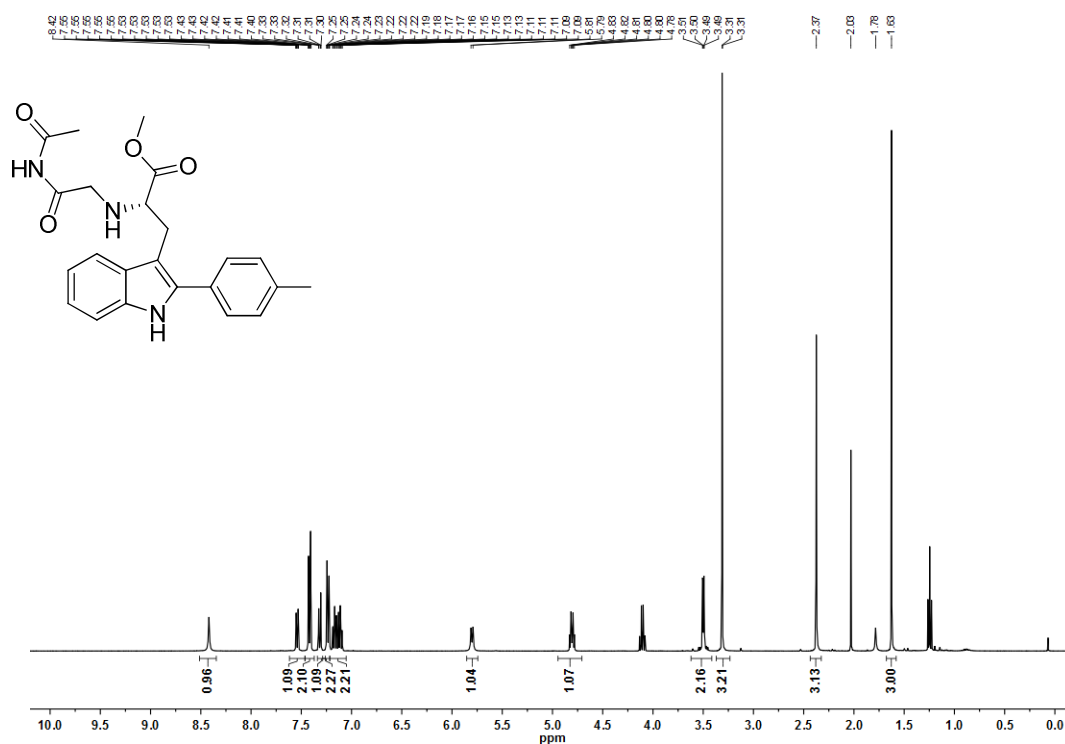
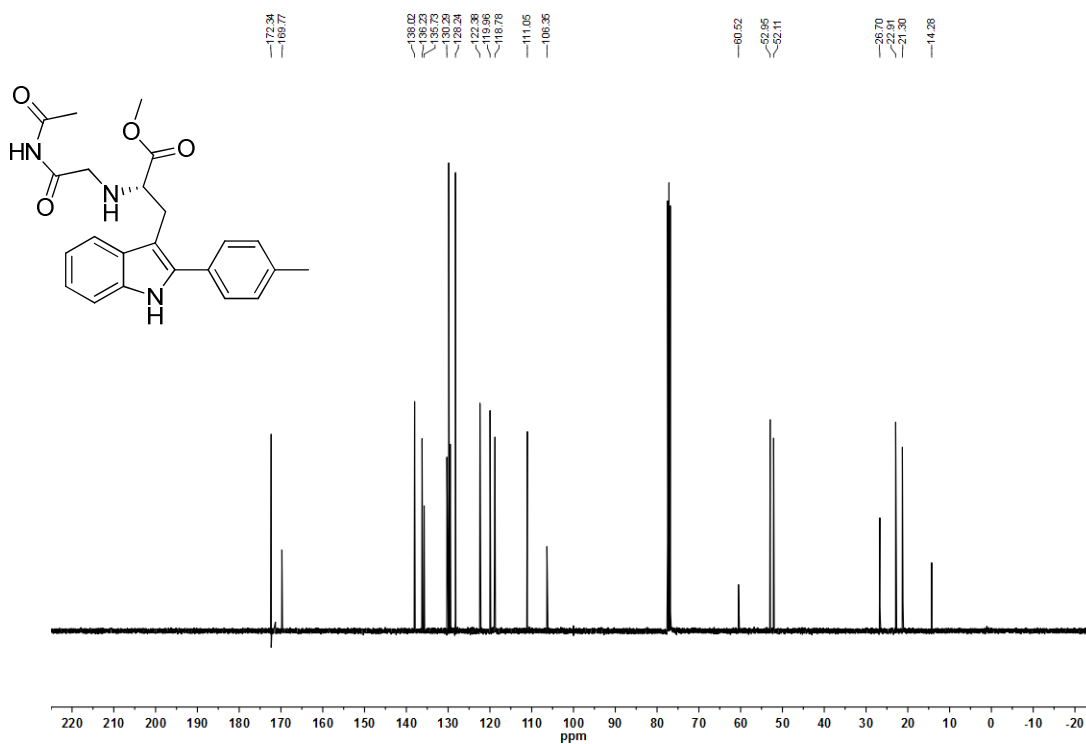
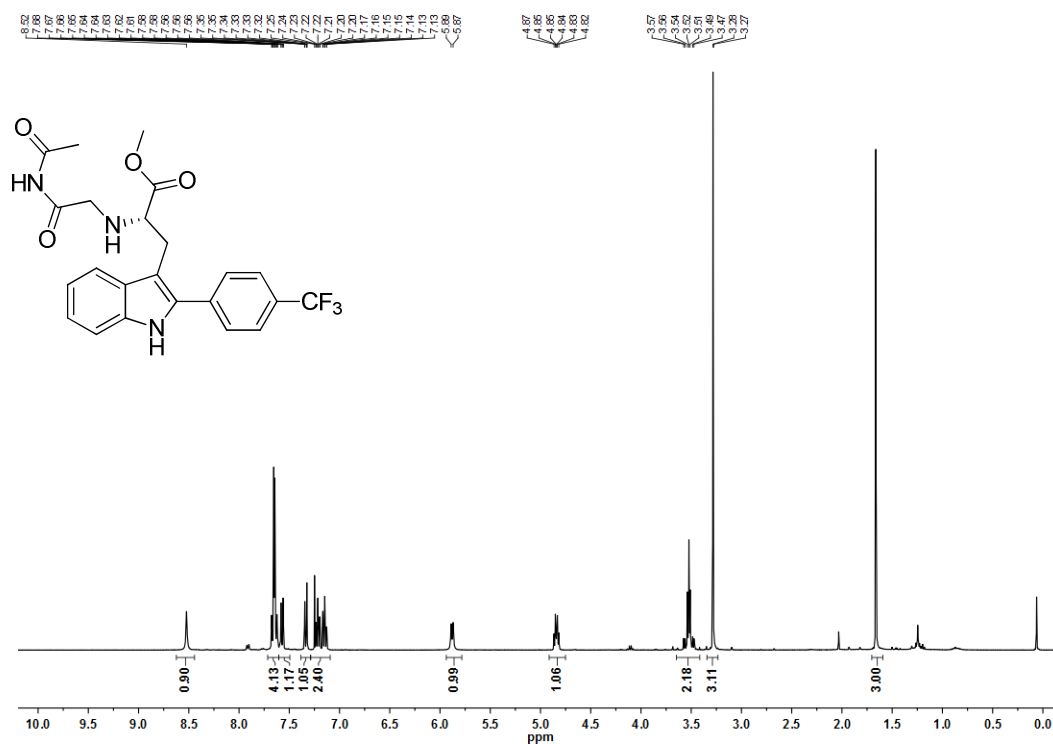
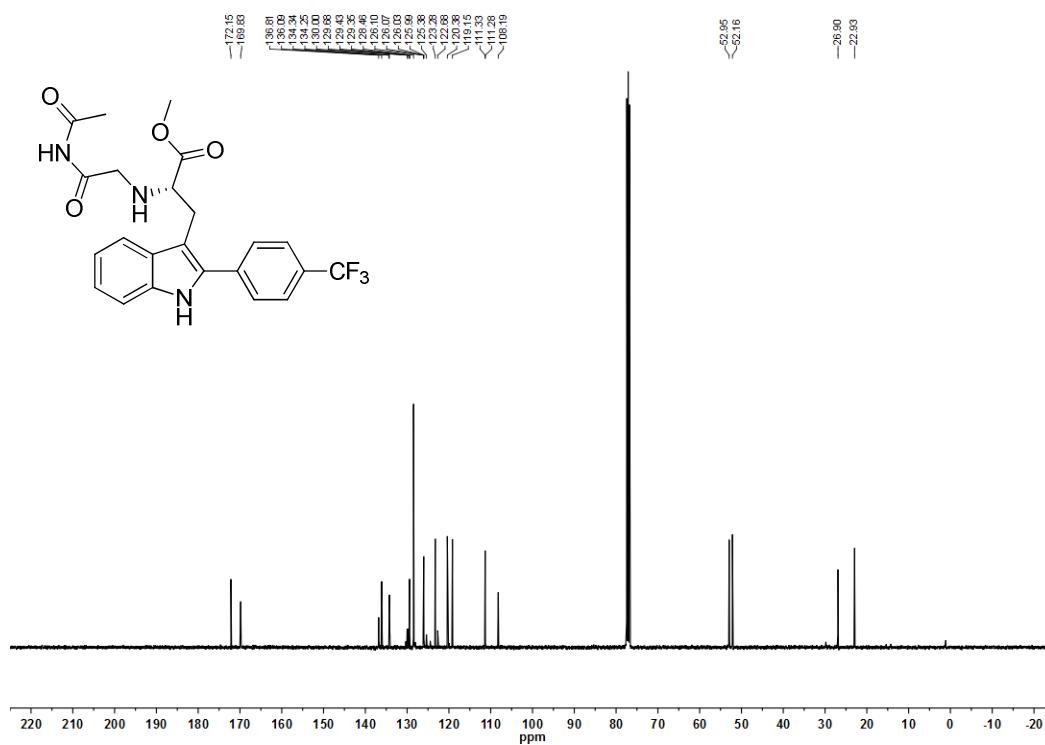


Figure 72: ^1H - ^{13}C HMBC NMR spectrum (400, 101 MHz, CDCl_3).

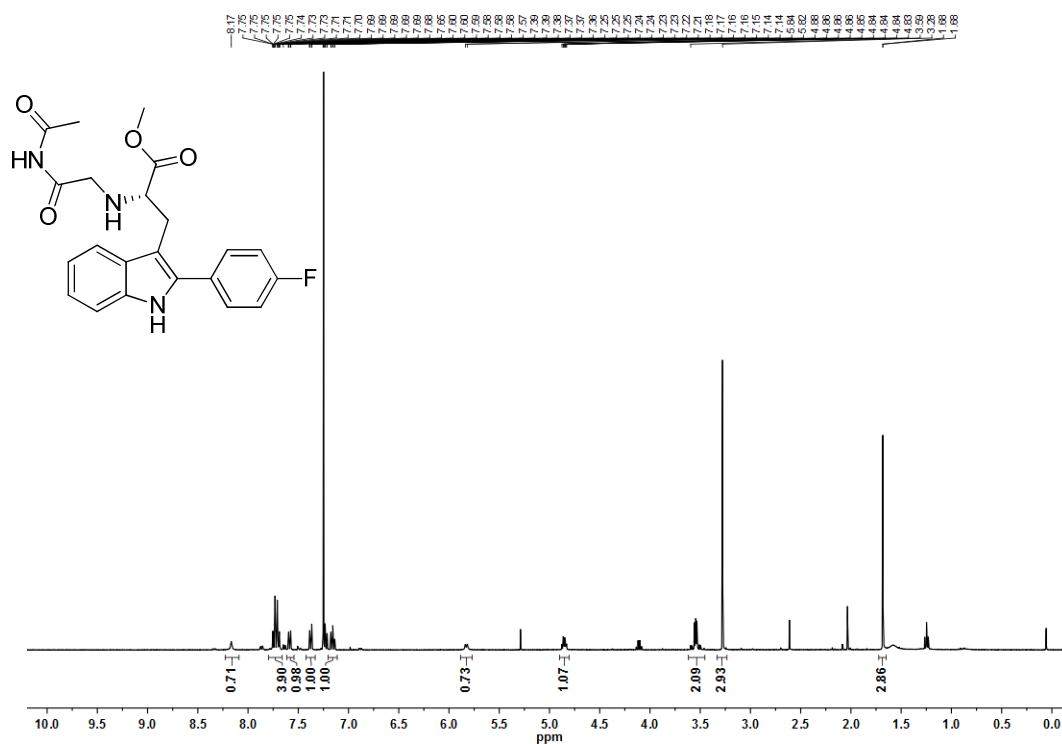
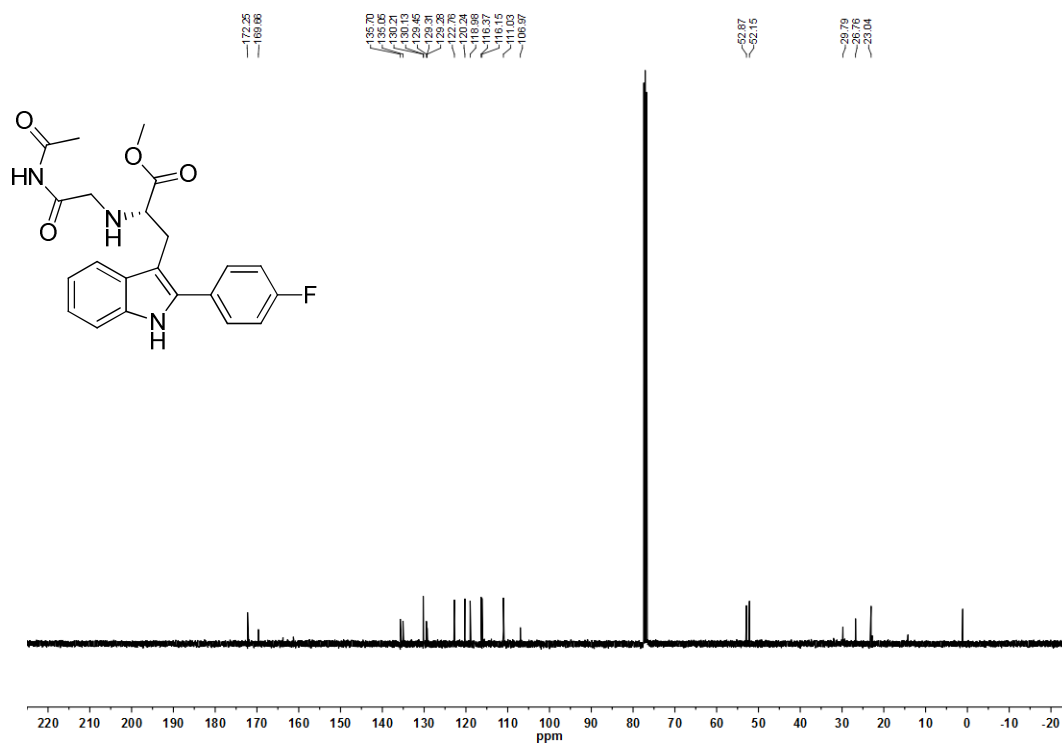
Methyl (2S)-2-acetyl-3-[2-(4-methylphenyl)-1H-indol-3-yl]propanoate

Figure 73: ¹H NMR spectrum (400 MHz, CDCl₃).Figure 74: ¹³C NMR spectrum (101 MHz, CDCl₃).

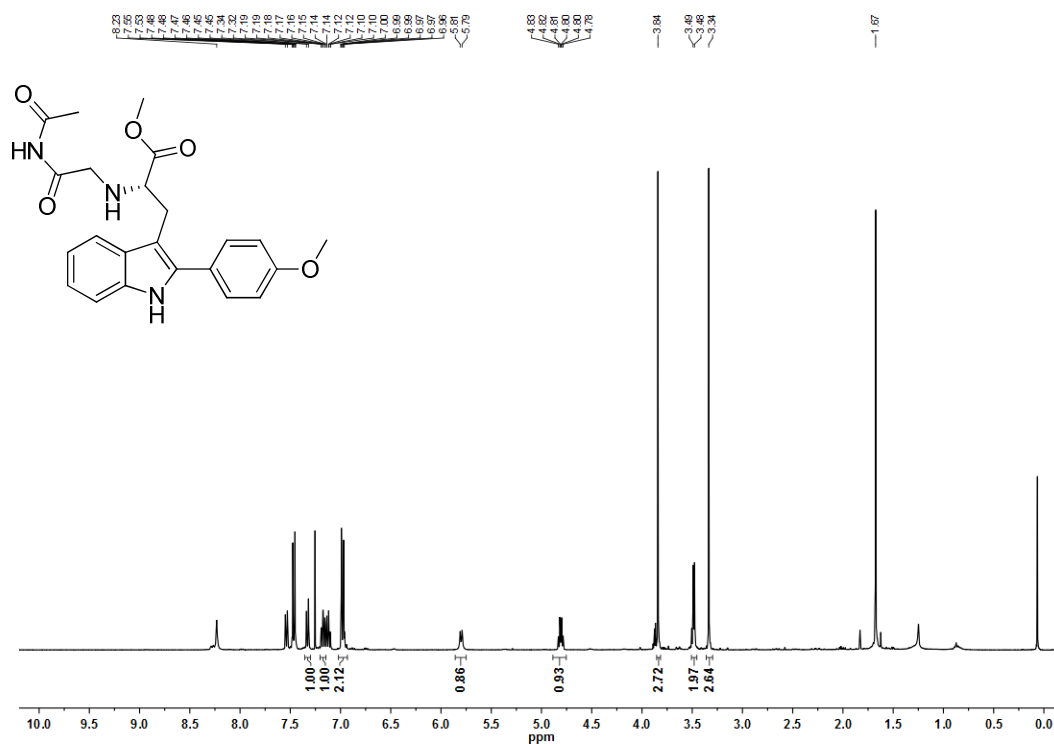
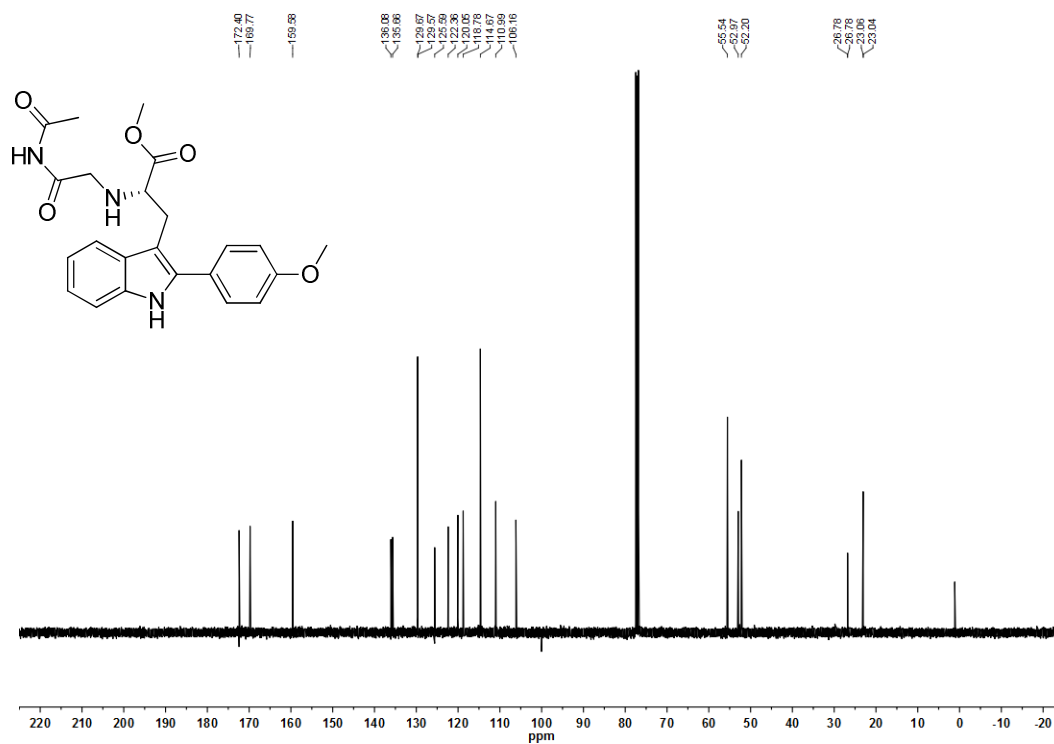
Methyl (2S)-2-acetyl-3-{2-[4-(trifluoromethyl)phenyl]-1H-indol-3-yl}propanoate

Figure 75: ¹H NMR spectrum (400 MHz, CDCl₃).Figure 76: ¹³C NMR spectrum (101 MHz, CDCl₃).

Methyl (2S)-2-amino-3-[2-(4-fluorophenyl)-1H-indol-3-yl]propanoate

Figure 77: ^1H NMR spectrum (400 MHz, CDCl_3).Figure 78: ^{13}C NMR spectrum (101 MHz, CDCl_3).

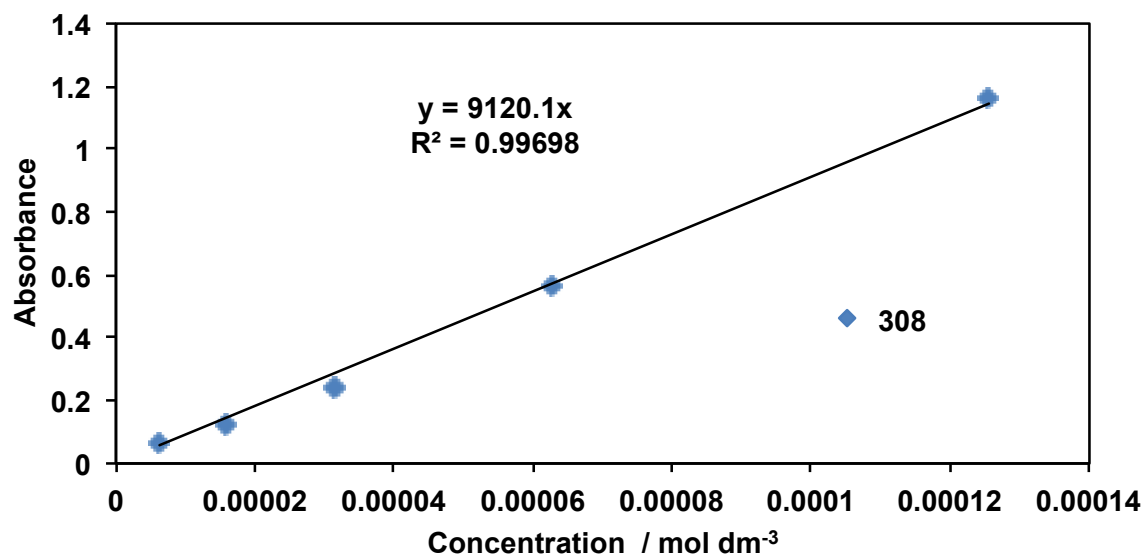
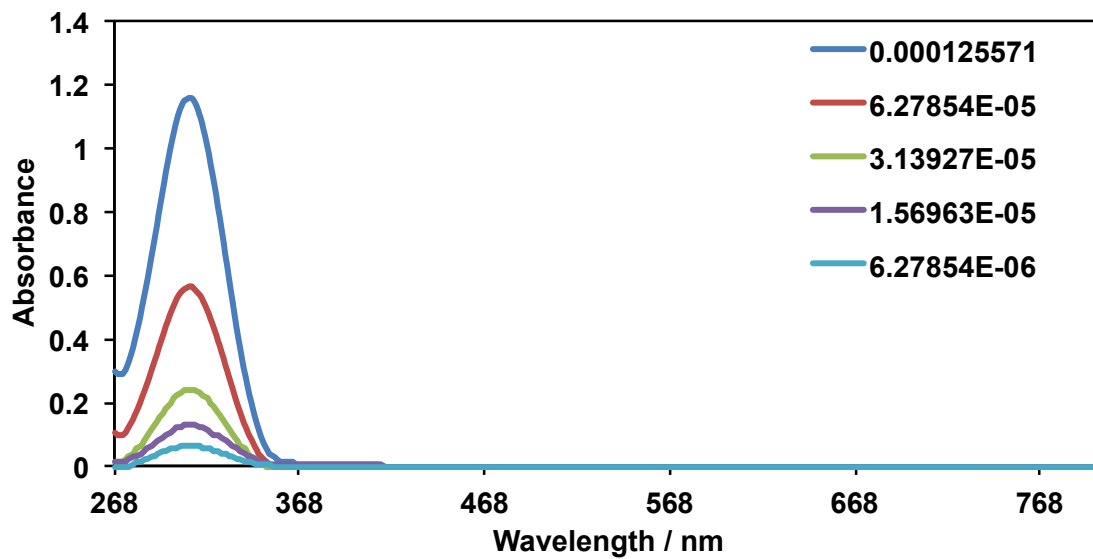
Methyl (2S)-2-amino-3-[2-(4-methoxyphenyl)-1H-indol-3-yl]propanoate

Figure 79: ¹H NMR spectrum (400 MHz, CDCl₃).Figure 80: ¹³C NMR spectrum (101 MHz, CDCl₃).

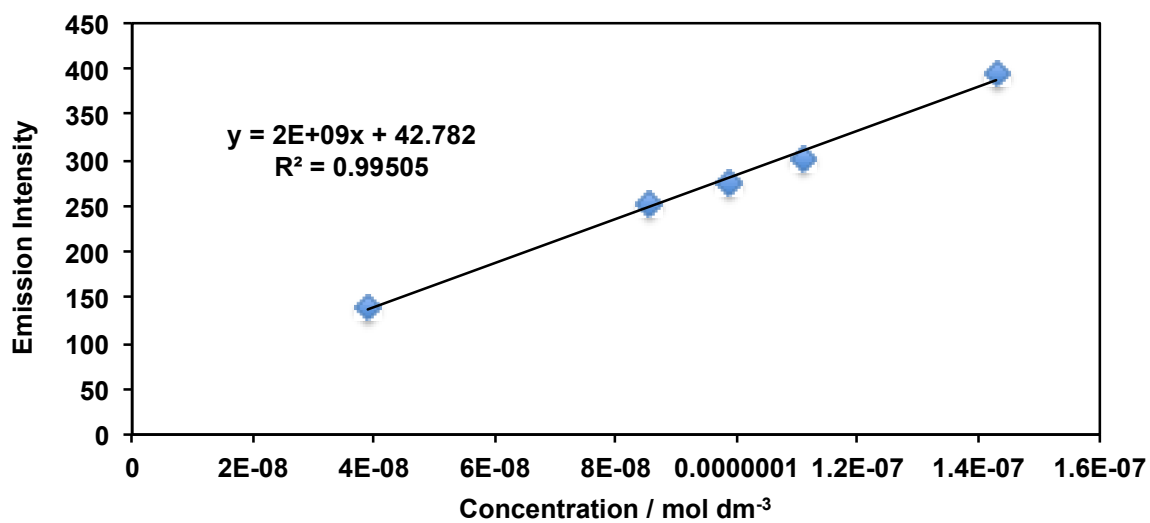
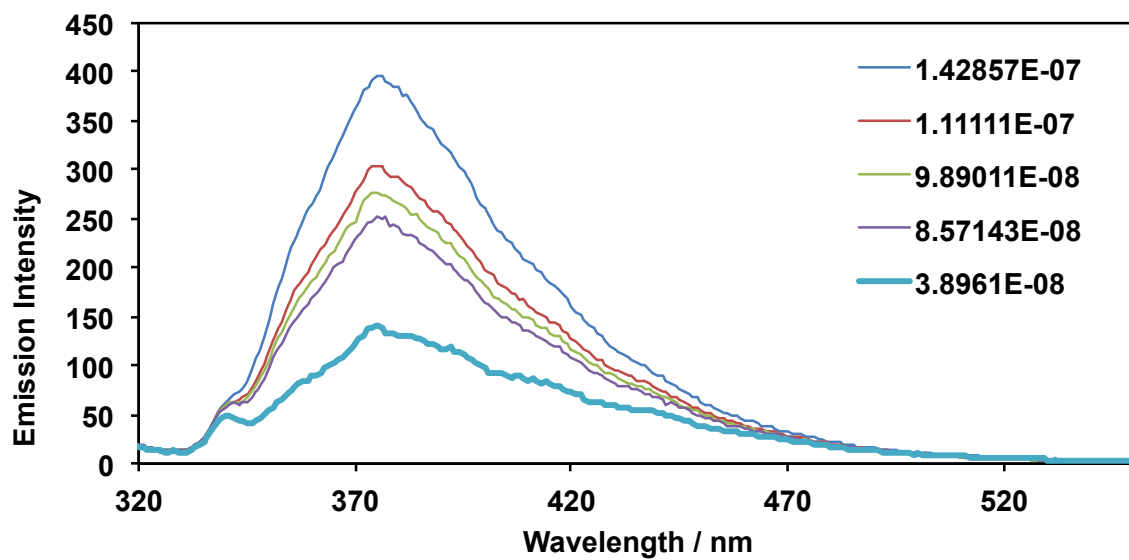
**APPENDIX B:
UV-VISIBLE AND FLUORESENCE DATA FOR 2-
ARYLTRYTOPHANS**

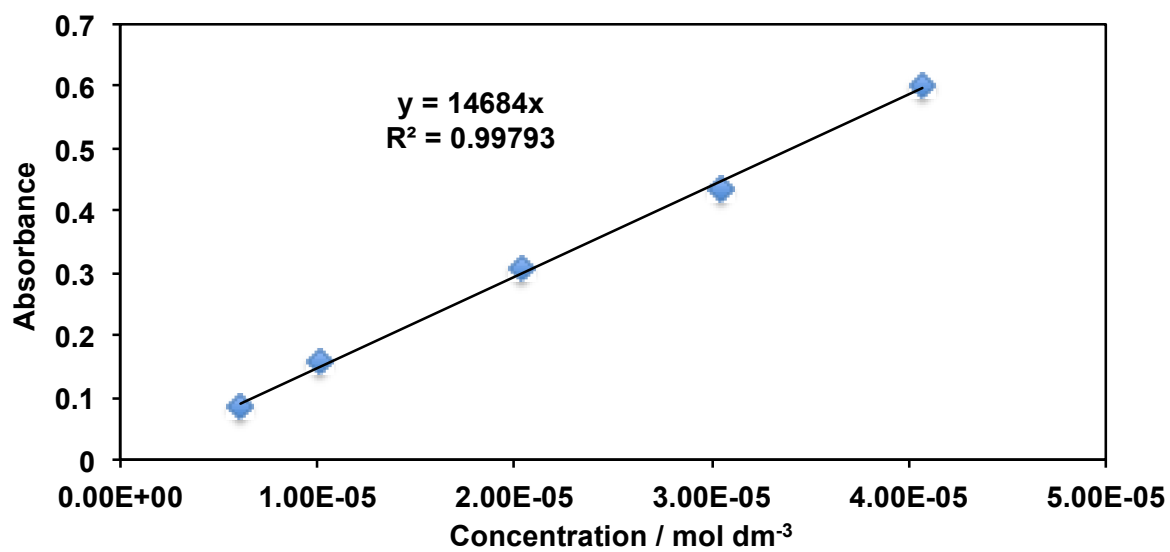
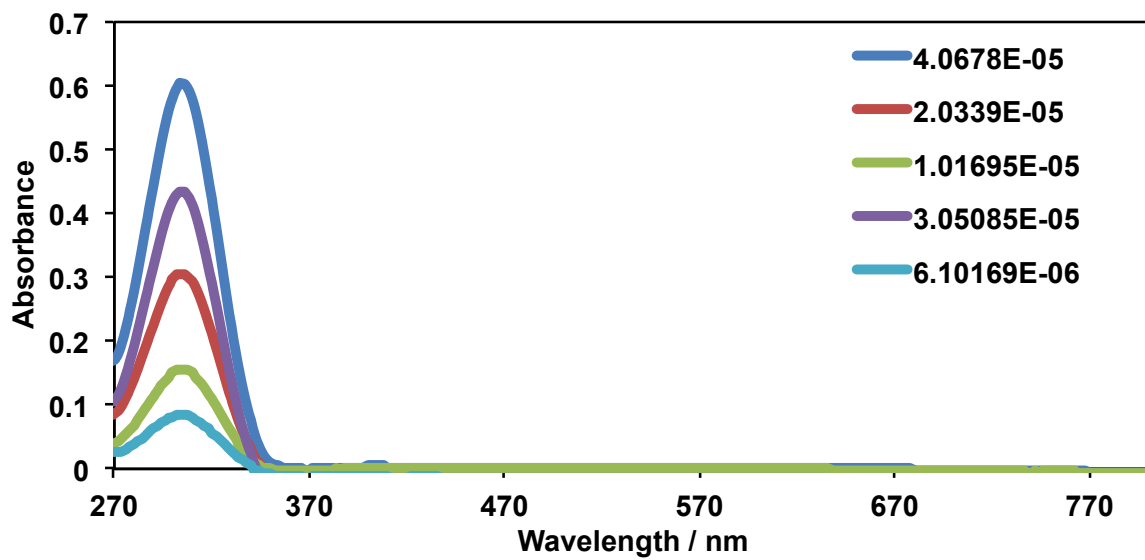
2-Phenyltryptophan

UV-Visible Spectroscopy

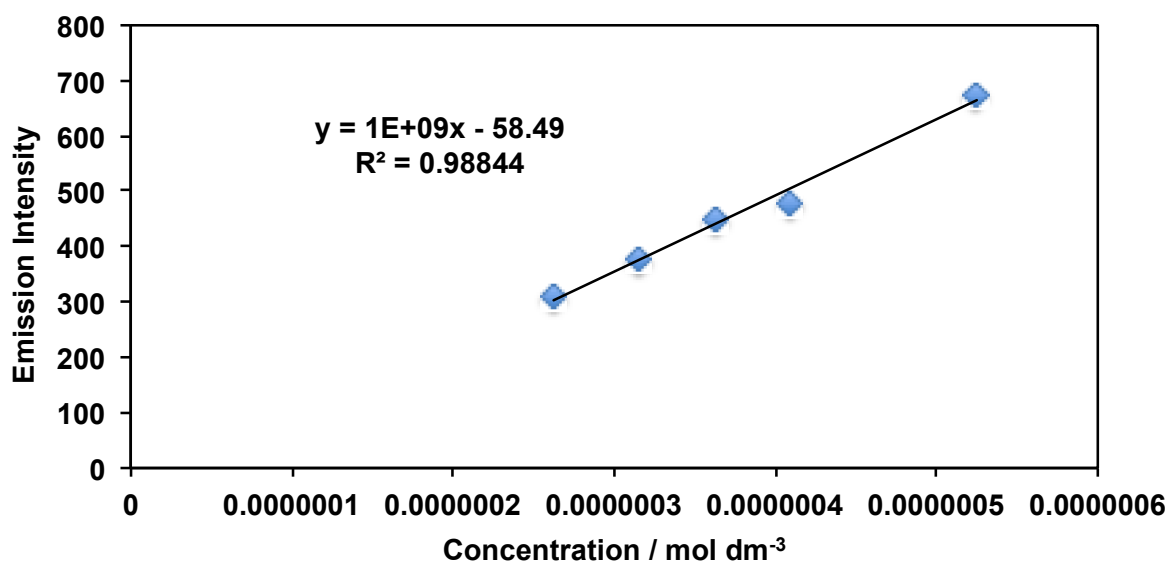
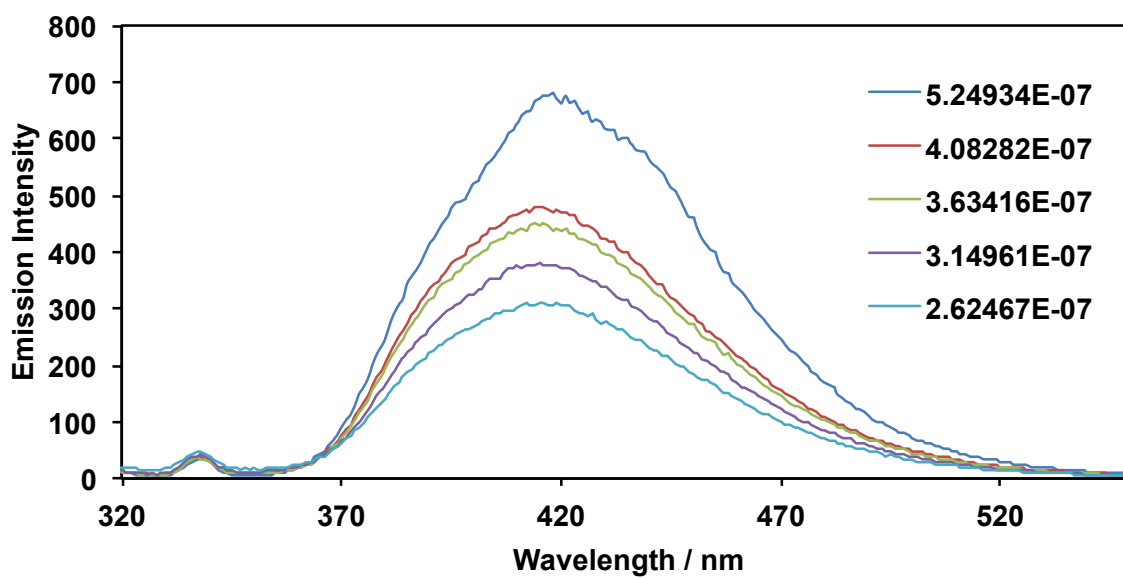


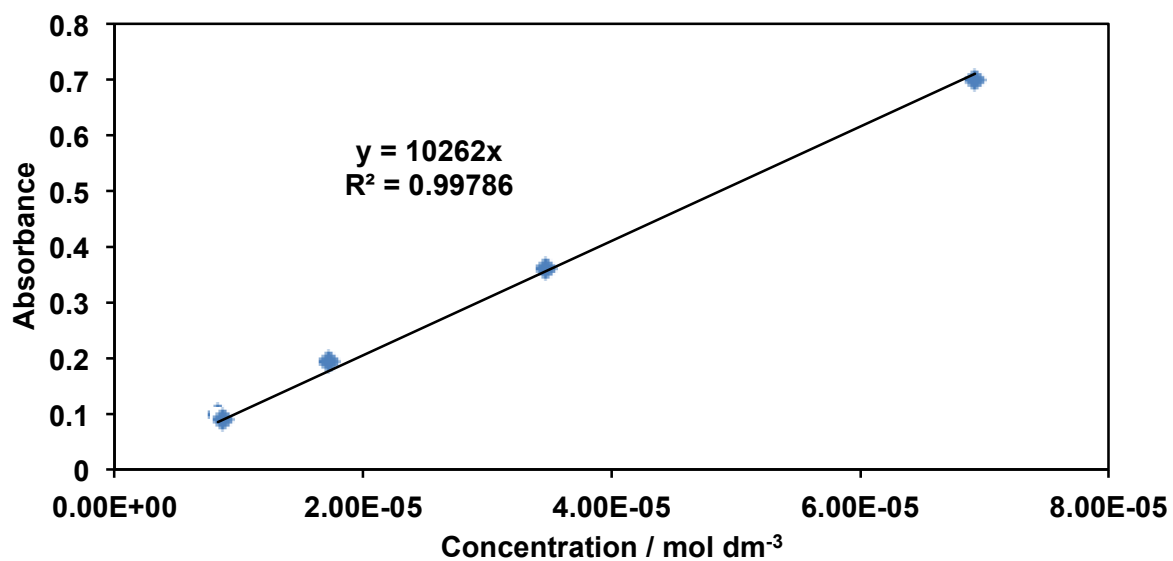
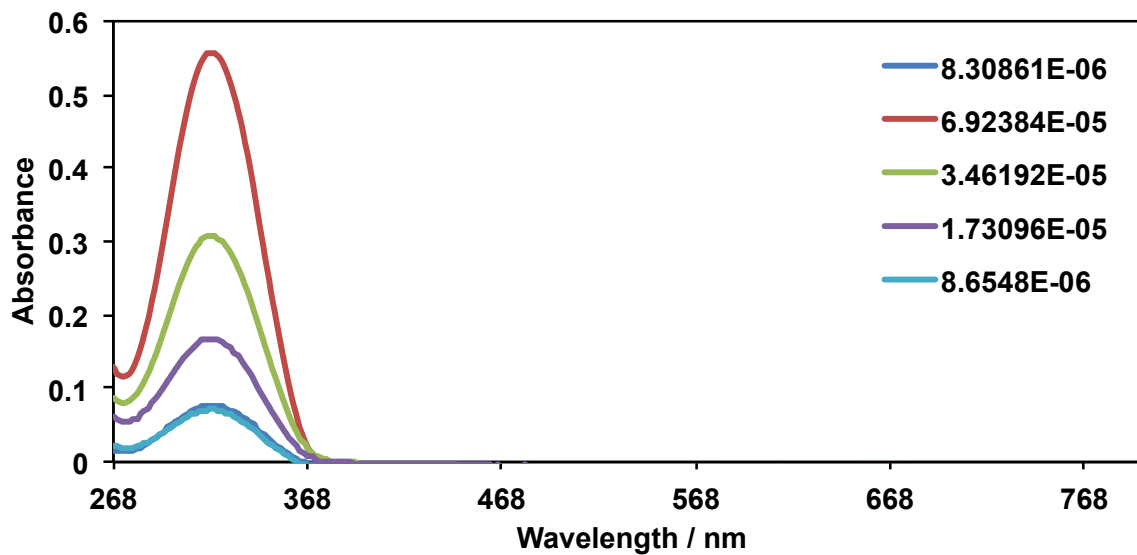
Fluorescence Spectroscopy



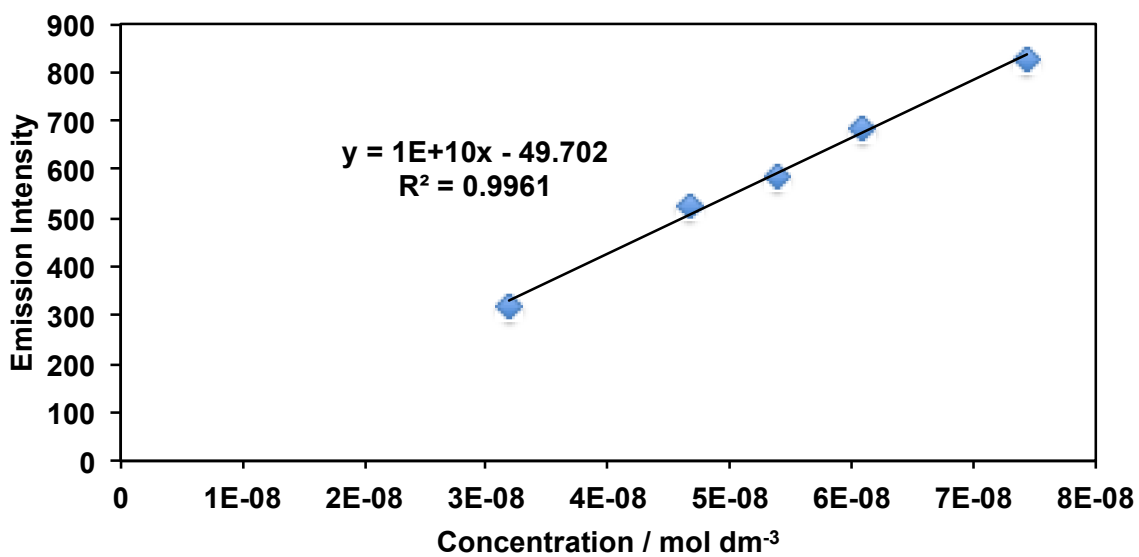
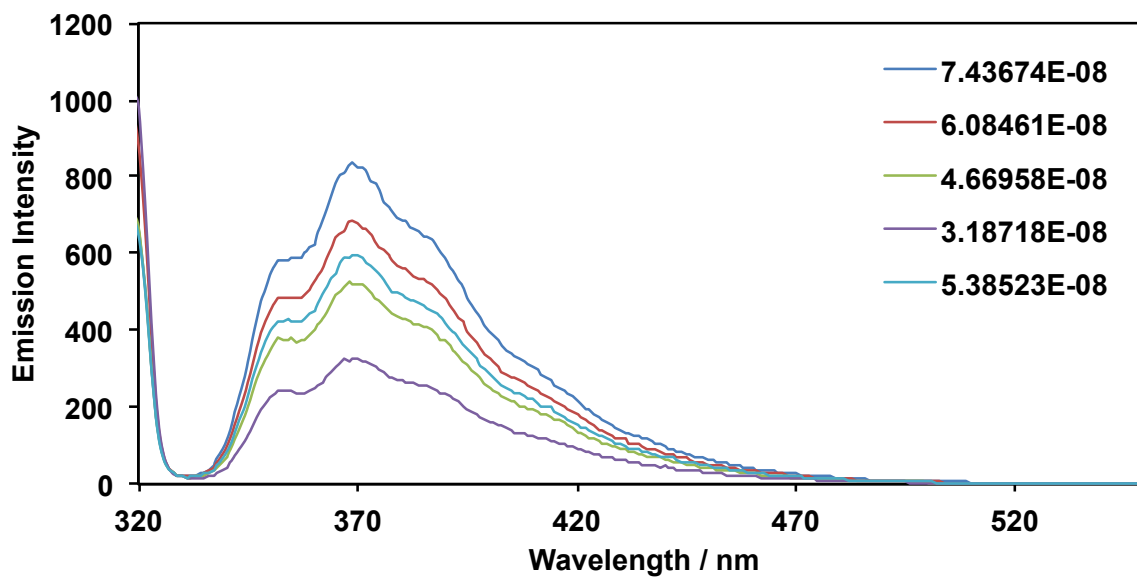
2-(4-Fluorophenyl)tryptophan*UV-Visible Spectroscopy*

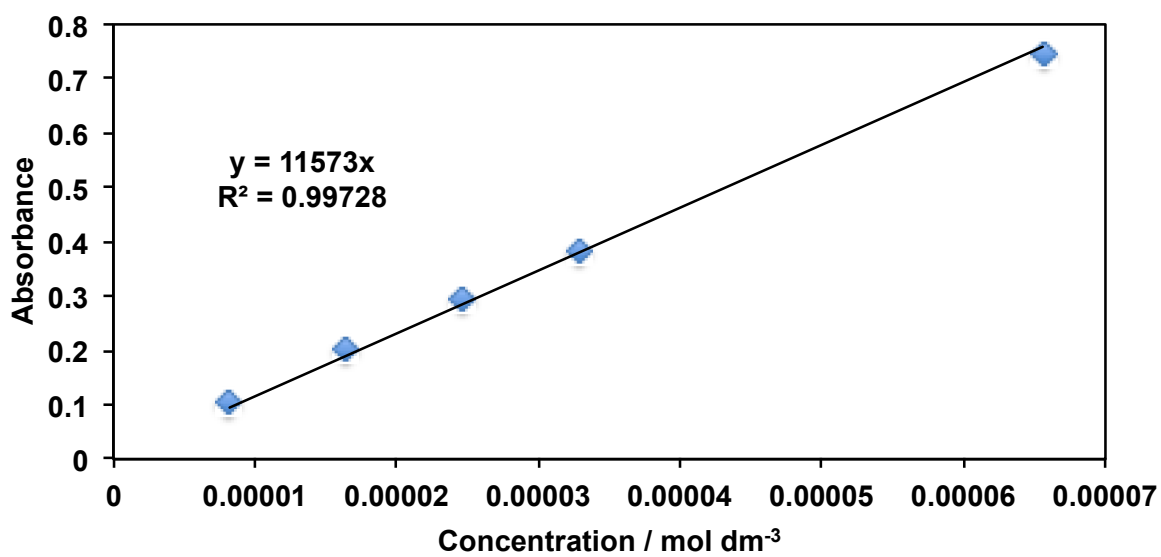
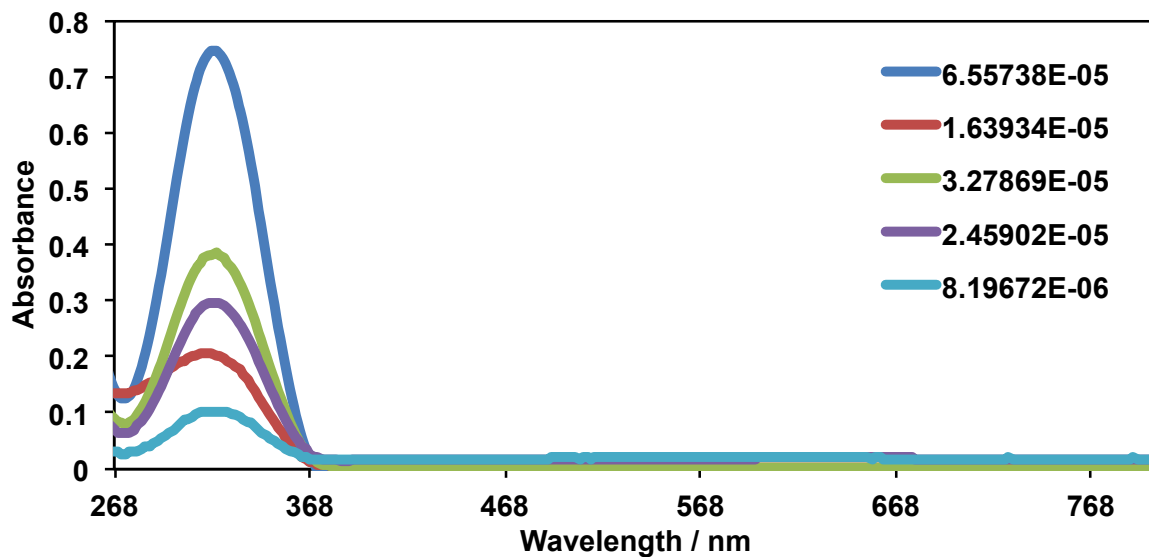
Fluorescence Spectroscopy



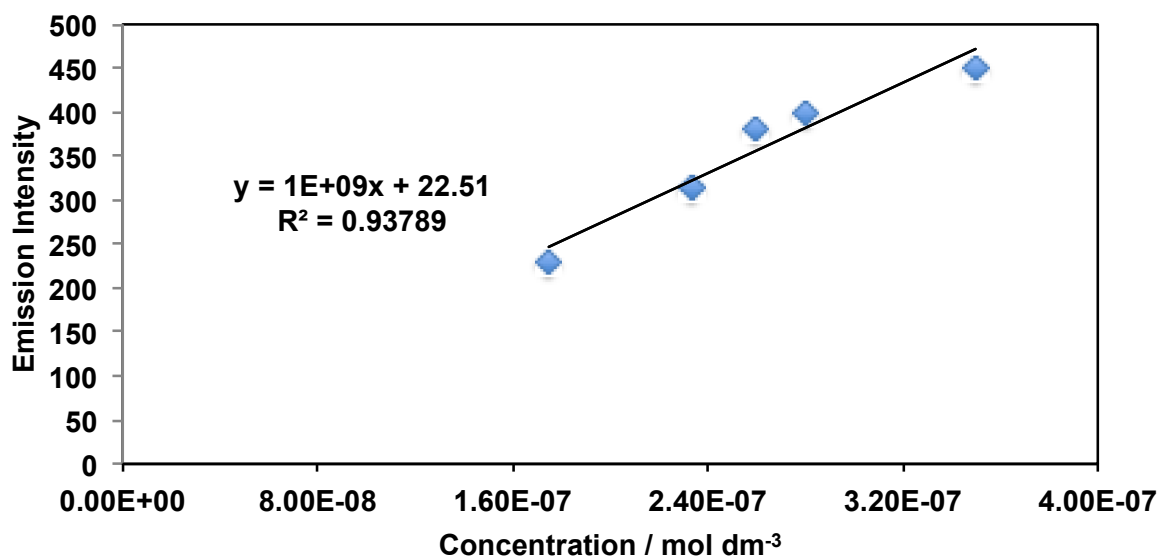
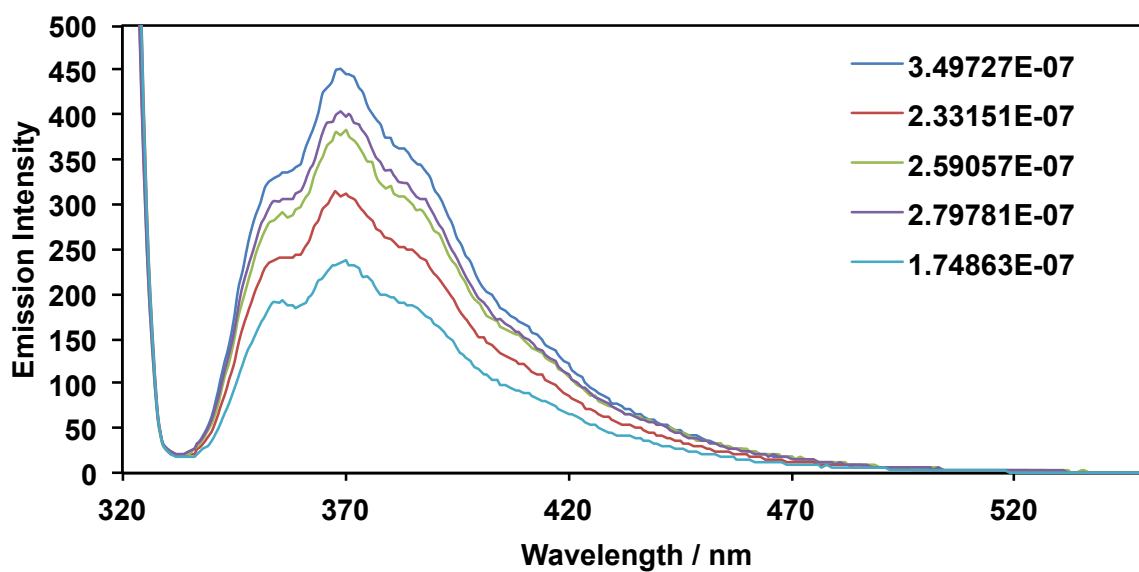
2-(4-(Trifluoromethyl)phenyl)tryptophan*UV-Visible Spectroscopy*

Fluorescence Spectroscopy



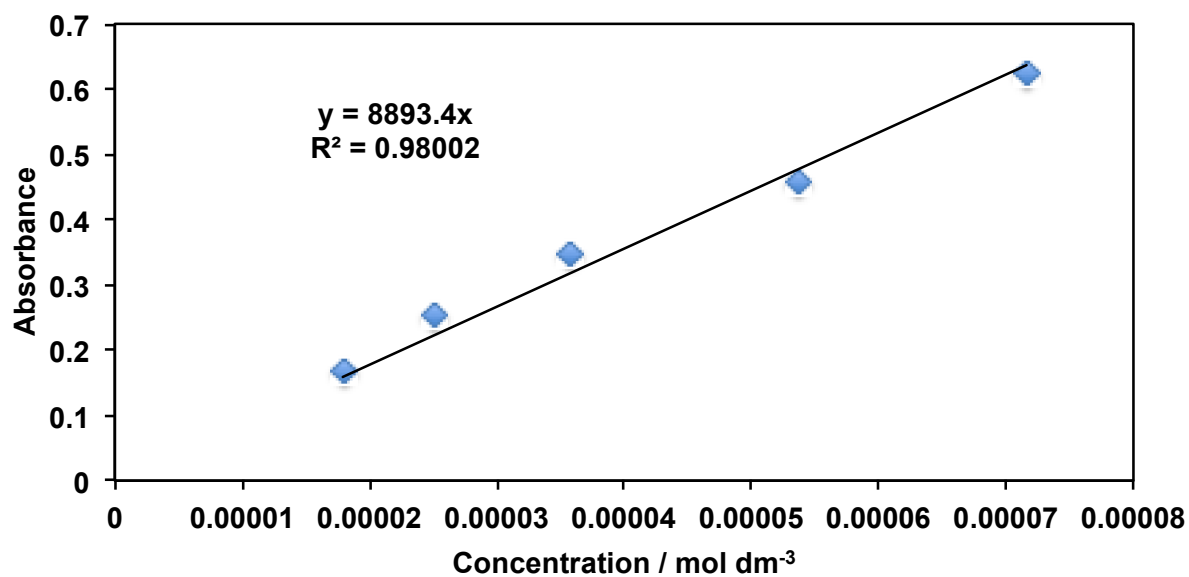
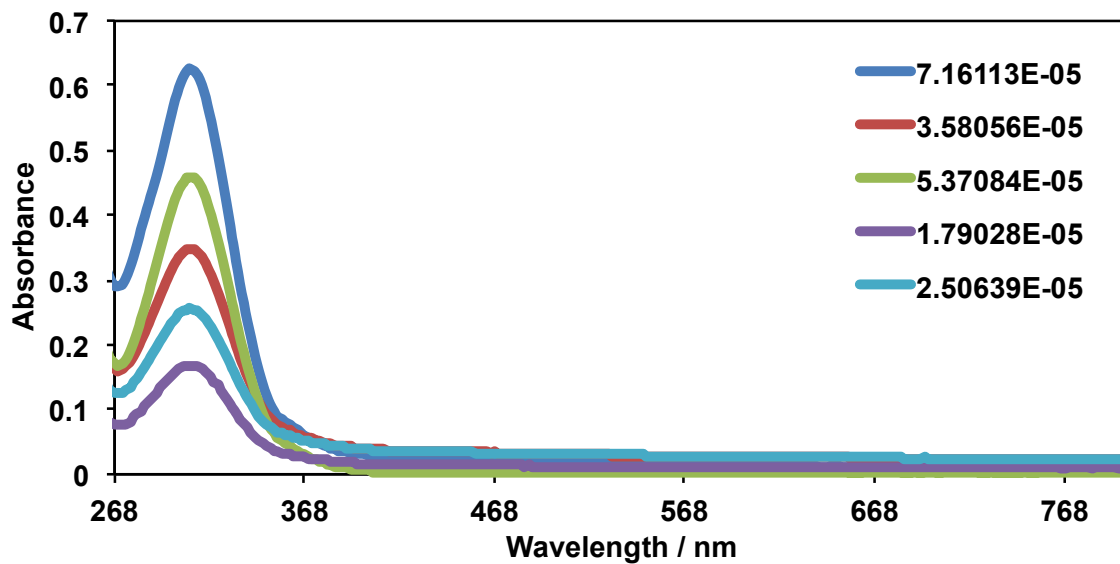
2-(4-Methoxyphenyl)tryptophan*UV-Visible Spectroscopy*

Fluorescence Spectroscopy

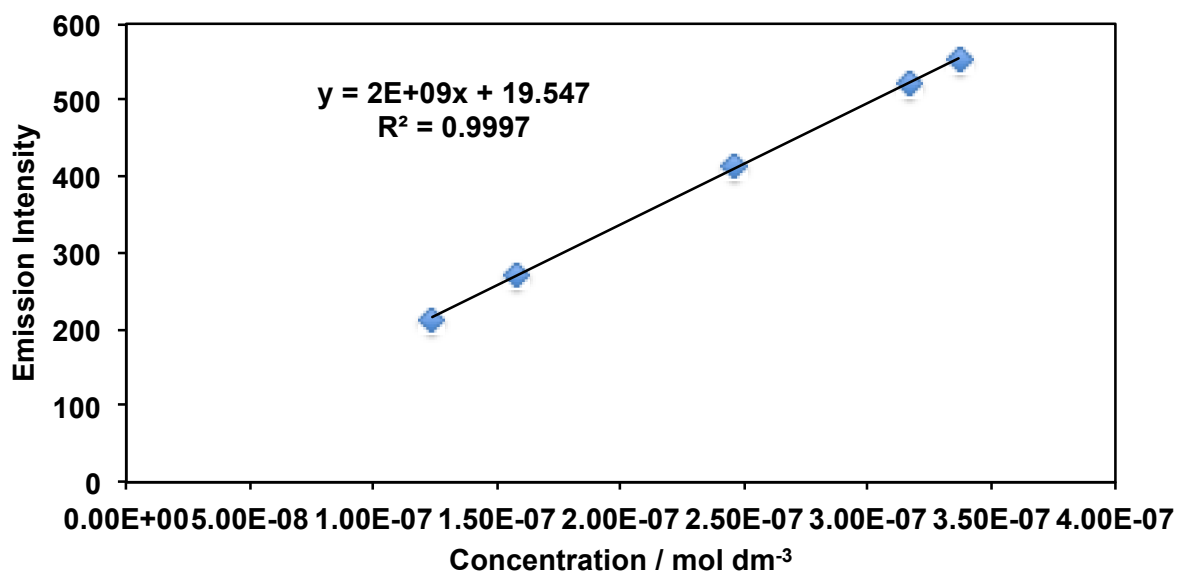
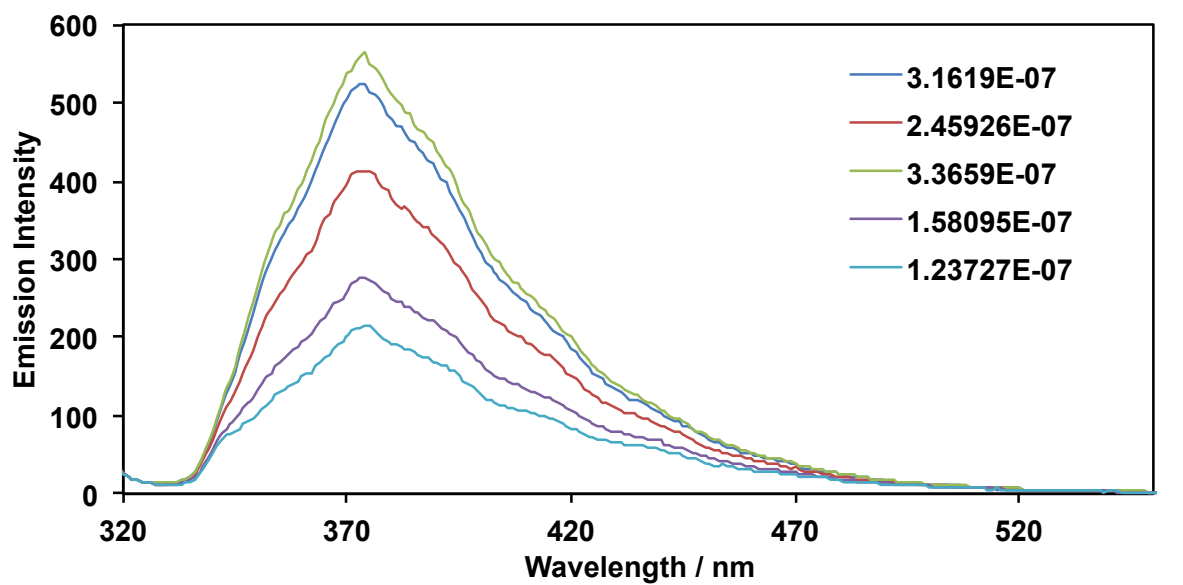


2-(4-Methylphenyl)tryptophan

UV-Visible Spectroscopy



Fluorescence Spectroscopy



APPENDIX C - Compopund 110

```

data_ijsf1115
_audit_creation_date      2011-09-13
_audit_creation_method
;
  olex2 1.1
  (compiled 2011.09.07 svn.r1971, GUI svn.r3853)
;
_publ_contact_author_address ?
_publ_contact_author_email  ?
_publ_contact_author_name   ?
_publ_contact_author_phone  ?
_chemical_name_common       ?
_chemical_name_systematic
;
?
;
_chemical_formula_moiety    'C42 H36 Br2 Cu2 N4'
_chemical_formula_sum       'C42 H36 Br2 Cu2 N4'
_chemical_formula_weight    883.65
_chemical_melting_point     ?
_chemical_oxdiff_formula    'C21 H18 Br1 Cu1 N2'
_chemical_oxdiff_usercomment 'Tom's BRML58'
loop_
  _atom_type_symbol
  _atom_type_description
  _atom_type_scatter_dispersion_real
  _atom_type_scatter_dispersion_imag
  _atom_type_scatter_source
  'C' 'C' 0.0033 0.0016 'International Tables Vol C Tables 4.2.6.8 and 6.1.1.4'
  'H' 'H' 0.0000 0.0000 'International Tables Vol C Tables 4.2.6.8 and 6.1.1.4'
  'N' 'N' 0.0061 0.0033 'International Tables Vol C Tables 4.2.6.8 and 6.1.1.4'
  'Cu' 'Cu' 0.3201 1.2651 'International Tables Vol C Tables 4.2.6.8 and 6.1.1.4'
  'Br' 'Br' -0.2901 2.4595
  'International Tables Vol C Tables 4.2.6.8 and 6.1.1.4'

_space_group_crystal_system 'triclinic'
_space_group_IT_number      2
_space_group_name_H-M_alt   'P -1'
_space_group_name_Hall      '-P 1'
loop_
  _space_group_symop_id
  _space_group_symop_operation_xyz
  1 'x, y, z'
  2 '-x, -y, -z'

_cell_length_a              9.4581(6)
_cell_length_b              9.5482(7)
_cell_length_c              11.2949(10)
_cell_angle_alpha           69.206(7)
_cell_angle_beta            82.837(6)
_cell_angle_gamma           69.262(6)
_cell_volume                891.80(12)
_cell_formula_units_Z       1
_cell_measurement_reflns_used 3571
_cell_measurement_temperature 110.00(10)
_cell_measurement_theta_max  31.2520
_cell_measurement_theta_min  2.9964
_exptl_absorpt_coefficient_mu 3.470
_exptl_absorpt_correction_T_max 0.827
_exptl_absorpt_correction_T_min 0.579
_exptl_absorpt_correction_type analytical
_exptl_absorpt_process_details
;
CrysAlisPro, Agilent Technologies,
Version 1.171.35.15 (release 03-08-2011 CrysAlis171 .NET)
(compiled Aug  3 2011,13:03:54)

```


CIF File - 110

Analytical numeric absorption correction using a multifaceted crystal
model based on expressions derived by R.C. Clark & J.S.

Reid.

(Clark, R. C. & Reid, J. S. (1995). Acta Cryst. A51, 887-897)

```

;
_exptl_crystal_colour      'dull ? colourless'
_exptl_crystal_colour_lustre      dull
_exptl_crystal_colour_modifier    ?
_exptl_crystal_colour_primary     colourless
_exptl_crystal_density_diffn      1.645
_exptl_crystal_density_meas       ?
_exptl_crystal_density_method     'not measured'
_exptl_crystal_description        needle
_exptl_crystal_F_000              444
_exptl_crystal_size_max            0.217
_exptl_crystal_size_mid            0.1108
_exptl_crystal_size_min           0.0626
_exptl_special_details
;
?
;
_diffn_reflns_av_R_equivalents    0.0285
_diffn_reflns_av_unetI/netI      0.0541
_diffn_reflns_limit_h_max         13
_diffn_reflns_limit_h_min         -11
_diffn_reflns_limit_k_max         13
_diffn_reflns_limit_k_min         -13
_diffn_reflns_limit_l_max         15
_diffn_reflns_limit_l_min         -15
_diffn_reflns_number              8485
_diffn_reflns_theta_full          29.07
_diffn_reflns_theta_max           31.32
_diffn_reflns_theta_min           3.00
_diffn_ambient_temperature        110.00(10)
_diffn_detector_area_resol_mean   16.1450
_diffn_measured_fraction_theta_full 0.9956
_diffn_measured_fraction_theta_max 0.887
_diffn_measurement_details
;
#_ type_ start_ end_ width_ exp.time_
  1 omega  -35.00  9.00  1.0000  20.0000
omega_    theta_    kappa_    phi_    frames
-        -23.1156  -84.0000  -133.0000  44

#_ type_ start_ end_ width_ exp.time_
  2 omega  -20.00  67.00  1.0000  20.0000
omega_    theta_    kappa_    phi_    frames
-        24.6781  -99.0000   0.0000  87

#_ type_ start_ end_ width_ exp.time_
  3 omega   60.00 101.00  1.0000  20.0000
omega_    theta_    kappa_    phi_    frames
-        24.6781 -178.0000 -180.0000  41

#_ type_ start_ end_ width_ exp.time_
  4 omega   4.00  89.00  1.0000  20.0000
omega_    theta_    kappa_    phi_    frames
-        24.6781  57.0000 -150.0000  85

#_ type_ start_ end_ width_ exp.time_
  5 omega  -46.00  97.00  1.0000  20.0000
omega_    theta_    kappa_    phi_    frames
-        24.6781  0.0000  0.0000  143
;
_diffn_measurement_device_type     'SuperNova, single source at offset), Eos'
_diffn_measurement_method          '\w scans'
_diffn_orient_matrix_UB_11         0.0773826000
_diffn_orient_matrix_UB_12        -0.0281660000

```

CIF File - 110

```

_diffrn_orient_matrix_UB_13      0.0168238000
_diffrn_orient_matrix_UB_21      0.0207234000
_diffrn_orient_matrix_UB_22     -0.0171925000
_diffrn_orient_matrix_UB_23     -0.0571610000
_diffrn_orient_matrix_UB_31      0.0035803000
_diffrn_orient_matrix_UB_32      0.0775774000
_diffrn_orient_matrix_UB_33     -0.0310147000
_diffrn_radiation_monochromator   mirror
_diffrn_radiation_type           'Mo K\alpha'
_diffrn_radiation_wavelength     0.7107
_diffrn_source                    'SuperNova (Mo) X-ray Source'
_diffrn_standards_decay_%        ?
_diffrn_standards_interval_count ?
_diffrn_standards_interval_time  ?
_diffrn_standards_number        ?
_reflns_number_gt                4252
_reflns_number_total             5176
_reflns_odcompleteness_completeness 99.56
_reflns_odcompleteness_iscentric 1
_reflns_odcompleteness_theta     29.07
_reflns_threshold_expression     >2sigma(I)
_computing_cell_refinement
;
CrysAlisPro, Agilent Technologies,
Version 1.171.35.15 (release 03-08-2011 CrysAlis171 .NET)
(compiled Aug  3 2011,13:03:54)
;
_computing_data_collection
;
CrysAlisPro, Agilent Technologies,
Version 1.171.35.15 (release 03-08-2011 CrysAlis171 .NET)
(compiled Aug  3 2011,13:03:54)
;
_computing_data_reduction
;
CrysAlisPro, Agilent Technologies,
Version 1.171.35.15 (release 03-08-2011 CrysAlis171 .NET)
(compiled Aug  3 2011,13:03:54)
;
_computing_molecular_graphics
;
O. V. Dolomanov, L. J. Bourhis, R. J. Gildea, J. A. K. Howard and H. Puschmann,
OLEX2: a complete structure solution, refinement and analysis program.
J. Appl. Cryst. (2009). 42, 339-341.
;
_computing_publication_material
;
O. V. Dolomanov, L. J. Bourhis, R. J. Gildea, J. A. K. Howard and H. Puschmann,
OLEX2: a complete structure solution, refinement and analysis program.
J. Appl. Cryst. (2009). 42, 339-341.
;
_computing_structure_refinement
;
XL, G.M. Sheldrick, Acta Cryst.
(2008). A64, 112-122
;
_computing_structure_solution
;
XS, G.M. Sheldrick, Acta Cryst.
(2008). A64, 112-122
;
_refine_diff_density_max          1.177
_refine_diff_density_min         -0.757
_refine_diff_density_rms         0.110
_refine_ls_extinction_coef       ?
_refine_ls_extinction_method     none
_refine_ls_goodness_of_fit_ref   1.045
_refine_ls_hydrogen_treatment    constr

```

CIF File - 110

```

_refine_ls_matrix_type          full
_refine_ls_number_parameters    226
_refine_ls_number_reflns       5176
_refine_ls_number_restraints    0
_refine_ls_R_factor_all        0.0539
_refine_ls_R_factor_gt         0.0406
_refine_ls_restrained_s_all     1.045
_refine_ls_shift/su_max        0.001
_refine_ls_shift/su_mean       0.000
_refine_ls_structure_factor_coef Fsqd
_refine_ls_weighting_details
'calc w=1/[\s^2^(Fo^2)+0.0335P]^2+0.6919P] where P=(Fo^2+2Fc^2)/3'
_refine_ls_weighting_scheme     calc
_refine_ls_wR_factor_gt        0.0877
_refine_ls_wR_factor_ref       0.0953
_refine_special_details
;

```

Refinement of F^2 against ALL reflections. The weighted R-factor wR and goodness of fit S are based on F^2 , conventional R-factors R are based on F, with F set to zero for negative F^2 . The threshold expression of $F^2 > 2\sigma(F^2)$ is used only for calculating R-factors(gt) etc. and is not relevant to the choice of reflections for refinement. R-factors based on F^2 are statistically about twice as large as those based on F, and R-factors based on ALL data will be even larger.

```

;
_atom_sites_solution_hydrogens  geom
_atom_sites_solution_primary    direct
_atom_sites_solution_secondary  difmap

```

```
loop_
```

```

_atom_site_label
_atom_site_type_symbol
_atom_site_fract_x
_atom_site_fract_y
_atom_site_fract_z
_atom_site_U_iso_or_equiv
_atom_site_adp_type
_atom_site_occupancy
_atom_site_symmetry_multiplicity
_atom_site_calc_flag
_atom_site_refinement_flags
_atom_site_disorder_assembly
_atom_site_disorder_group

```

```

Br1 Br 0.88769(3) 0.86509(3) 0.01639(3) 0.02247(8) Uani 1 1 d . . .
C1 C 0.6870(3) 1.2503(3) 0.1094(3) 0.0140(5) Uani 1 1 d . . .
C2 C 0.4412(3) 1.3572(3) 0.1612(2) 0.0133(5) Uani 1 1 d . . .
C3 C 0.2877(3) 1.3886(3) 0.1890(3) 0.0161(5) Uani 1 1 d . . .
H3 H 0.2377 1.3207 0.1884 0.019 Uiso 1 1 calc R . .
C4 C 0.2135(3) 1.5265(3) 0.2176(3) 0.0192(5) Uani 1 1 d . . .
H4 H 0.1109 1.5521 0.2365 0.023 Uiso 1 1 calc R . .
C5 C 0.2898(3) 1.6282(3) 0.2186(3) 0.0197(5) Uani 1 1 d . . .
H5 H 0.2360 1.7201 0.2376 0.024 Uiso 1 1 calc R . .
C6 C 0.4429(3) 1.5958(3) 0.1921(3) 0.0169(5) Uani 1 1 d . . .
H6 H 0.4934 1.6628 0.1936 0.020 Uiso 1 1 calc R . .
C7 C 0.5172(3) 1.4573(3) 0.1629(2) 0.0134(5) Uani 1 1 d . . .
C8 C 0.5152(3) 1.0960(3) 0.1240(3) 0.0158(5) Uani 1 1 d . . .
H8A H 0.5947 1.0403 0.0775 0.019 Uiso 1 1 calc R . .
H8B H 0.4207 1.1325 0.0793 0.019 Uiso 1 1 calc R . .
C9 C 0.5040(3) 0.9826(3) 0.2558(2) 0.0133(5) Uani 1 1 d . . .
C10 C 0.6192(3) 0.9276(3) 0.3441(3) 0.0197(5) Uani 1 1 d . . .
H10 H 0.7031 0.9608 0.3221 0.024 Uiso 1 1 calc R . .
C12 C 0.4855(4) 0.7714(3) 0.4976(3) 0.0233(6) Uani 1 1 d . . .
H12 H 0.4800 0.6999 0.5779 0.028 Uiso 1 1 calc R . .
C13 C 0.6086(3) 0.8234(3) 0.4646(3) 0.0227(6) Uani 1 1 d . . .
H13 H 0.6848 0.7884 0.5235 0.027 Uiso 1 1 calc R . .
C14 C 0.3712(3) 0.8257(3) 0.4114(3) 0.0240(6) Uani 1 1 d . . .
H14 H 0.2883 0.7909 0.4335 0.029 Uiso 1 1 calc R . .
C15 C 0.3794(3) 0.9328(3) 0.2908(3) 0.0188(5) Uani 1 1 d . . .
H15 H 0.3007 0.9710 0.2336 0.023 Uiso 1 1 calc R . .

```

CIF File - 110

```

C16 C 0.7913(3) 1.4465(3) 0.1303(3) 0.0160(5) Uani 1 1 d . . .
H16A H 0.7545 1.5617 0.0968 0.019 Uiso 1 1 calc R . .
H16B H 0.8706 1.4086 0.0746 0.019 Uiso 1 1 calc R . .
C17 C 0.8564(3) 1.3922(3) 0.2618(3) 0.0159(5) Uani 1 1 d . . .
C18 C 0.9635(3) 1.2420(3) 0.3103(3) 0.0196(5) Uani 1 1 d . . .
H18 H 0.9950 1.1750 0.2622 0.023 Uiso 1 1 calc R . .
C19 C 1.0236(3) 1.1918(3) 0.4304(3) 0.0217(6) Uani 1 1 d . . .
H19 H 1.0965 1.0919 0.4617 0.026 Uiso 1 1 calc R . .
C20 C 0.9757(3) 1.2895(4) 0.5039(3) 0.0218(6) Uani 1 1 d . . .
H20 H 1.0151 1.2552 0.5846 0.026 Uiso 1 1 calc R . .
C21 C 0.8684(3) 1.4388(3) 0.4559(3) 0.0212(6) Uani 1 1 d . . .
H21 H 0.8357 1.5048 0.5048 0.025 Uiso 1 1 calc R . .
C22 C 0.8094(3) 1.4905(3) 0.3354(3) 0.0186(5) Uani 1 1 d . . .
H22 H 0.7381 1.5913 0.3037 0.022 Uiso 1 1 calc R . .
Cu1 Cu 0.86386(4) 1.11836(4) 0.04996(3) 0.01957(9) Uani 1 1 d . . .
N1 N 0.5474(2) 1.2331(2) 0.1279(2) 0.0135(4) Uani 1 1 d . . .
N2 N 0.6671(2) 1.3875(2) 0.1316(2) 0.0132(4) Uani 1 1 d . . .

```

loop_

```

_atom_site_aniso_label
_atom_site_aniso_U_11
_atom_site_aniso_U_22
_atom_site_aniso_U_33
_atom_site_aniso_U_23
_atom_site_aniso_U_13
_atom_site_aniso_U_12
Br1 0.01446(13) 0.02129(14) 0.03516(18) -0.01419(12) 0.00375(11) -0.00652(10)
C1 0.0136(11) 0.0148(11) 0.0148(12) -0.0048(10) 0.0003(9) -0.0063(9)
C2 0.0139(11) 0.0149(11) 0.0097(11) -0.0018(9) -0.0004(9) -0.0055(9)
C3 0.0137(12) 0.0193(12) 0.0145(13) -0.0033(10) 0.0021(9) -0.0076(10)
C4 0.0142(12) 0.0237(13) 0.0161(13) -0.0051(11) 0.0019(10) -0.0042(10)
C5 0.0214(13) 0.0180(12) 0.0161(14) -0.0053(10) 0.0012(11) -0.0031(11)
C6 0.0206(13) 0.0152(12) 0.0148(13) -0.0044(10) 0.0010(10) -0.0071(10)
C7 0.0125(11) 0.0151(11) 0.0113(12) -0.0024(9) 0.0004(9) -0.0049(9)
C8 0.0163(12) 0.0184(12) 0.0156(13) -0.0066(10) -0.0001(10) -0.0081(10)
C9 0.0142(11) 0.0113(11) 0.0154(13) -0.0060(9) 0.0013(9) -0.0044(9)
C10 0.0164(12) 0.0191(12) 0.0226(15) -0.0038(11) -0.0025(11) -0.0071(10)
C12 0.0341(16) 0.0171(13) 0.0174(14) -0.0020(11) 0.0034(12) -0.0119(12)
C13 0.0237(14) 0.0200(13) 0.0205(15) -0.0023(11) -0.0051(11) -0.0053(11)
C14 0.0249(14) 0.0263(14) 0.0255(16) -0.0069(12) 0.0064(12) -0.0179(12)
C15 0.0176(12) 0.0191(13) 0.0216(14) -0.0054(11) -0.0002(10) -0.0098(11)
C16 0.0151(12) 0.0187(12) 0.0164(13) -0.0048(10) 0.0021(10) -0.0099(10)
C17 0.0150(12) 0.0180(12) 0.0179(13) -0.0058(10) 0.0018(10) -0.0101(10)
C18 0.0156(12) 0.0197(13) 0.0259(15) -0.0096(11) 0.0023(11) -0.0076(10)
C19 0.0159(12) 0.0201(13) 0.0274(16) -0.0048(11) -0.0029(11) -0.0063(11)
C20 0.0195(13) 0.0304(15) 0.0187(14) -0.0049(12) -0.0009(11) -0.0152(12)
C21 0.0208(13) 0.0271(14) 0.0224(15) -0.0120(12) 0.0015(11) -0.0125(12)
C22 0.0171(12) 0.0190(12) 0.0228(14) -0.0073(11) 0.0001(10) -0.0096(10)
Cu1 0.01534(16) 0.02226(18) 0.02025(19) -0.00870(14) 0.00149(13) -0.00418(13)
N1 0.0152(10) 0.0129(9) 0.0131(11) -0.0026(8) 0.0008(8) -0.0076(8)
N2 0.0131(10) 0.0134(10) 0.0135(11) -0.0032(8) 0.0009(8) -0.0064(8)

```

_geom_special_details

```

;
All esds (except the esd in the dihedral angle between two l.s. planes)
are estimated using the full covariance matrix. The cell esds are taken
into account individually in the estimation of esds in distances, angles
and torsion angles; correlations between esds in cell parameters are only
used when they are defined by crystal symmetry. An approximate (isotropic)
treatment of cell esds is used for estimating esds involving l.s. planes.
;

```

loop_

```

_geom_bond_atom_site_label_1
_geom_bond_atom_site_label_2
_geom_bond_distance
_geom_bond_site_symmetry_2
_geom_bond_publ_flag
Br1 Cu1 2.5073(5) . ?

```

Br1 Cu1 2.4183(5) 2_775 ?
 C1 Cu1 1.914(3) . ?
 C1 N1 1.369(3) . ?
 C1 N2 1.365(3) . ?
 C2 C3 1.393(3) . ?
 C2 C7 1.390(3) . ?
 C2 N1 1.391(3) . ?
 C3 H3 0.9300 . ?
 C3 C4 1.385(4) . ?
 C4 H4 0.9300 . ?
 C4 C5 1.404(4) . ?
 C5 H5 0.9300 . ?
 C5 C6 1.387(4) . ?
 C6 H6 0.9300 . ?
 C6 C7 1.394(4) . ?
 C7 N2 1.398(3) . ?
 C8 H8A 0.9700 . ?
 C8 H8B 0.9700 . ?
 C8 C9 1.516(4) . ?
 C8 N1 1.461(3) . ?
 C9 C10 1.396(4) . ?
 C9 C15 1.386(4) . ?
 C10 H10 0.9300 . ?
 C10 C13 1.389(4) . ?
 C12 H12 0.9300 . ?
 C12 C13 1.382(4) . ?
 C12 C14 1.376(4) . ?
 C13 H13 0.9300 . ?
 C14 H14 0.9300 . ?
 C14 C15 1.396(4) . ?
 C15 H15 0.9300 . ?
 C16 H16A 0.9700 . ?
 C16 H16B 0.9700 . ?
 C16 C17 1.520(4) . ?
 C16 N2 1.467(3) . ?
 C17 C18 1.392(4) . ?
 C17 C22 1.391(4) . ?
 C18 H18 0.9300 . ?
 C18 C19 1.389(4) . ?
 C19 H19 0.9300 . ?
 C19 C20 1.386(4) . ?
 C20 H20 0.9300 . ?
 C20 C21 1.385(4) . ?
 C21 H21 0.9300 . ?
 C21 C22 1.387(4) . ?
 C22 H22 0.9300 . ?
 Cu1 Br1 2.4183(5) 2_775 ?

loop_

_geom_angle_atom_site_label_1
 _geom_angle_atom_site_label_2
 _geom_angle_atom_site_label_3
 _geom_angle
 _geom_angle_site_symmetry_1
 _geom_angle_site_symmetry_3
 _geom_angle_publ_flag
 Cu1 Br1 Cu1 79.757(15) 2_775 . ?
 N1 C1 Cu1 126.29(18) . . ?
 N2 C1 Cu1 128.60(19) . . ?
 N2 C1 N1 104.9(2) . . ?
 C7 C2 C3 122.2(2) . . ?
 C7 C2 N1 106.4(2) . . ?
 N1 C2 C3 131.4(2) . . ?
 C2 C3 H3 121.8 . . ?
 C4 C3 C2 116.4(2) . . ?
 C4 C3 H3 121.8 . . ?
 C3 C4 H4 119.3 . . ?
 C3 C4 C5 121.5(3) . . ?

C5 C4 H4 119.3 . . ?
C4 C5 H5 119.0 . . ?
C6 C5 C4 121.9(3) . . ?
C6 C5 H5 119.0 . . ?
C5 C6 H6 121.8 . . ?
C5 C6 C7 116.5(2) . . ?
C7 C6 H6 121.8 . . ?
C2 C7 C6 121.5(2) . . ?
C2 C7 N2 105.9(2) . . ?
C6 C7 N2 132.6(2) . . ?
H8A C8 H8B 107.9 . . ?
C9 C8 H8A 109.3 . . ?
C9 C8 H8B 109.3 . . ?
N1 C8 H8A 109.3 . . ?
N1 C8 H8B 109.3 . . ?
N1 C8 C9 111.7(2) . . ?
C10 C9 C8 120.3(2) . . ?
C15 C9 C8 120.6(2) . . ?
C15 C9 C10 119.0(2) . . ?
C9 C10 H10 120.0 . . ?
C13 C10 C9 120.1(3) . . ?
C13 C10 H10 120.0 . . ?
C13 C12 H12 120.1 . . ?
C14 C12 H12 120.1 . . ?
C14 C12 C13 119.8(3) . . ?
C10 C13 H13 119.8 . . ?
C12 C13 C10 120.5(3) . . ?
C12 C13 H13 119.8 . . ?
C12 C14 H14 119.9 . . ?
C12 C14 C15 120.2(3) . . ?
C15 C14 H14 119.9 . . ?
C9 C15 C14 120.4(3) . . ?
C9 C15 H15 119.8 . . ?
C14 C15 H15 119.8 . . ?
H16A C16 H16B 107.9 . . ?
C17 C16 H16A 109.2 . . ?
C17 C16 H16B 109.2 . . ?
N2 C16 H16A 109.2 . . ?
N2 C16 H16B 109.2 . . ?
N2 C16 C17 111.9(2) . . ?
C18 C17 C16 119.9(2) . . ?
C22 C17 C16 120.9(2) . . ?
C22 C17 C18 119.2(3) . . ?
C17 C18 H18 119.9 . . ?
C19 C18 C17 120.2(3) . . ?
C19 C18 H18 119.9 . . ?
C18 C19 H19 119.8 . . ?
C20 C19 C18 120.4(3) . . ?
C20 C19 H19 119.8 . . ?
C19 C20 H20 120.3 . . ?
C21 C20 C19 119.4(3) . . ?
C21 C20 H20 120.3 . . ?
C20 C21 H21 119.8 . . ?
C20 C21 C22 120.5(3) . . ?
C22 C21 H21 119.8 . . ?
C17 C22 H22 119.8 . . ?
C21 C22 C17 120.3(3) . . ?
C21 C22 H22 119.8 . . ?
Br1 Cu1 Br1 100.242(15) 2_775 . ?
C1 Cu1 Br1 134.16(8) . 2_775 ?
C1 Cu1 Br1 125.58(8) . . ?
C1 N1 C2 111.3(2) . . ?
C1 N1 C8 124.8(2) . . ?
C2 N1 C8 123.7(2) . . ?
C1 N2 C7 111.4(2) . . ?
C1 N2 C16 123.3(2) . . ?
C7 N2 C16 125.1(2) . . ?

```

loop_
  _geom_torsion_atom_site_label_1
  _geom_torsion_atom_site_label_2
  _geom_torsion_atom_site_label_3
  _geom_torsion_atom_site_label_4
  _geom_torsion
  _geom_torsion_site_symmetry_1
  _geom_torsion_site_symmetry_2
  _geom_torsion_site_symmetry_3
  _geom_torsion_site_symmetry_4
  _geom_torsion_publ_flag
C2 C3 C4 C5 -0.2(4) . . . . ?
C2 C7 N2 C1 0.7(3) . . . . ?
C2 C7 N2 C16 -175.6(2) . . . . ?
C3 C2 C7 C6 -0.3(4) . . . . ?
C3 C2 C7 N2 179.5(2) . . . . ?
C3 C2 N1 C1 -179.8(3) . . . . ?
C3 C2 N1 C8 -4.6(4) . . . . ?
C3 C4 C5 C6 -0.5(4) . . . . ?
C4 C5 C6 C7 0.7(4) . . . . ?
C5 C6 C7 C2 -0.3(4) . . . . ?
C5 C6 C7 N2 179.9(3) . . . . ?
C6 C7 N2 C1 -179.5(3) . . . . ?
C6 C7 N2 C16 4.3(4) . . . . ?
C7 C2 C3 C4 0.6(4) . . . . ?
C7 C2 N1 C1 0.4(3) . . . . ?
C7 C2 N1 C8 175.6(2) . . . . ?
C8 C9 C10 C13 -179.8(3) . . . . ?
C8 C9 C15 C14 178.6(3) . . . . ?
C9 C8 N1 C1 100.5(3) . . . . ?
C9 C8 N1 C2 -74.1(3) . . . . ?
C9 C10 C13 C12 1.0(4) . . . . ?
C10 C9 C15 C14 -1.8(4) . . . . ?
C12 C14 C15 C9 1.5(4) . . . . ?
C13 C12 C14 C15 0.1(5) . . . . ?
C14 C12 C13 C10 -1.3(5) . . . . ?
C15 C9 C10 C13 0.6(4) . . . . ?
C16 C17 C18 C19 179.9(2) . . . . ?
C16 C17 C22 C21 179.2(2) . . . . ?
C17 C16 N2 C1 -93.7(3) . . . . ?
C17 C16 N2 C7 82.2(3) . . . . ?
C17 C18 C19 C20 1.1(4) . . . . ?
C18 C17 C22 C21 -0.3(4) . . . . ?
C18 C19 C20 C21 -0.8(4) . . . . ?
C19 C20 C21 C22 -0.1(4) . . . . ?
C20 C21 C22 C17 0.6(4) . . . . ?
C22 C17 C18 C19 -0.6(4) . . . . ?
Cu1 Br1 Cu1 Br1 -0.001(1) 2_775 . . 2_775 ?
Cu1 Br1 Cu1 C1 178.90(10) 2_775 . . . ?
Cu1 C1 N1 C2 -174.84(18) . . . . ?
Cu1 C1 N1 C8 10.0(4) . . . . ?
Cu1 C1 N2 C7 174.26(19) . . . . ?
Cu1 C1 N2 C16 -9.4(4) . . . . ?
N1 C1 Cu1 Br1 170.94(17) . . . 2_775 ?
N1 C1 Cu1 Br1 -7.6(3) . . . . ?
N1 C1 N2 C7 -0.4(3) . . . . ?
N1 C1 N2 C16 175.9(2) . . . . ?
N1 C2 C3 C4 -179.2(3) . . . . ?
N1 C2 C7 C6 179.5(2) . . . . ?
N1 C2 C7 N2 -0.6(3) . . . . ?
N1 C8 C9 C10 -51.6(3) . . . . ?
N1 C8 C9 C15 128.0(3) . . . . ?
N2 C1 Cu1 Br1 178.86(19) . . . . ?
N2 C1 Cu1 Br1 -2.6(3) . . . 2_775 ?
N2 C1 N1 C2 0.0(3) . . . . ?
N2 C1 N1 C8 -175.2(2) . . . . ?
N2 C16 C17 C18 82.8(3) . . . . ?
N2 C16 C17 C22 -96.6(3) . . . . ?

```

```
loop_
  _exptl_crystal_face_index_h
  _exptl_crystal_face_index_k
  _exptl_crystal_face_index_l
  _exptl_crystal_face_perp_dist
  _exptl_oxdiff_crystal_face_indexfrac_h
  _exptl_oxdiff_crystal_face_indexfrac_k
  _exptl_oxdiff_crystal_face_indexfrac_l
  _exptl_oxdiff_crystal_face_x
  _exptl_oxdiff_crystal_face_y
  _exptl_oxdiff_crystal_face_z
0 0 1 0.0378 0.0000 0.0000 1.0000 0.0168 -0.0572 -0.0310
0 0 -1 0.0378 -0.0000 -0.0000 -1.0000 -0.0168 0.0572 0.0310
1 1 1 0.0955 1.0000 1.0000 1.0000 0.0660 -0.0536 0.0501
-1 -1 -1 0.0955 -1.0000 -1.0000 -1.0000 -0.0660 0.0536 -0.0501
0 -1 0 0.0535 -0.0000 -1.0000 -0.0000 0.0282 0.0172 -0.0776
0 1 0 0.0535 0.0000 1.0000 0.0000 -0.0282 -0.0172 0.0776
-2 -1 1 0.0942 -2.0000 -1.0000 1.0000 -0.1098 -0.0814 -0.1158
2 1 -1 0.0942 2.0000 1.0000 -1.0000 0.1098 0.0814 0.1158
0 -1 -2 0.0313 -0.0000 -1.0000 -2.0000 -0.0055 0.1315 -0.0155
0 1 2 0.0313 0.0000 1.0000 2.0000 0.0055 -0.1315 0.0155
1 -1 0 0.0582 1.0000 -1.0000 -0.0000 0.1055 0.0379 -0.0740
-2 2 -1 0.0452 -2.0000 2.0000 -1.0000 -0.2279 -0.0187 0.1790
```


APPENDIX C - Compound 113

```

data_ijsf1118
_audit_creation_date          2011-10-06
_audit_creation_method
;
  Olex2 1.1
  (compiled 2011.09.07 svn.r1971, GUI svn.r3853)
;
_publ_contact_author_address  ?
_publ_contact_author_email    ?
_publ_contact_author_name     ''
_publ_contact_author_phone    ?
_chemical_name_common         ?
_chemical_name_systematic
;
?
;
_chemical_formula_moiety      'Br, C21 H19 N2, H2 O'
_chemical_formula_sum         'C21 H21 Br N2 O'
_chemical_formula_weight      397.31
_chemical_melting_point       ?
_chemical_oxdiff_formula      'C21 H19 Br3 N2'
_chemical_oxdiff_usercomment  'Toms pale pink block'
loop_
  _atom_type_symbol
  _atom_type_description
  _atom_type_scat_dispersion_real
  _atom_type_scat_dispersion_imag
  _atom_type_scat_source
'C' 'C' 0.0033 0.0016 'International Tables Vol C Tables
4.2.6.8 and 6.1.1.4'
'H' 'H' 0.0000 0.0000 'International Tables Vol C Tables
4.2.6.8 and 6.1.1.4'
'Br' 'Br' -0.2901 2.4595
'International Tables Vol C Tables 4.2.6.8 and 6.1.1.4'
'N' 'N' 0.0061 0.0033 'International Tables Vol C Tables
4.2.6.8 and 6.1.1.4'
'O' 'O' 0.0106 0.0060 'International Tables Vol C Tables
4.2.6.8 and 6.1.1.4'

_space_group_crystal_system   'triclinic'
_space_group_IT_number        2
_space_group_name_H-M_alt     'P -1'
_space_group_name_Hall        '-P 1'
loop_
  _space_group_symop_id
  _space_group_symop_operation_xyz
1 'x, y, z'
2 '-x, -y, -z'

_cell_length_a                9.3864(4)
_cell_length_b                9.9323(4)
_cell_length_c                11.3331(6)
_cell_angle_alpha             69.308(4)
_cell_angle_beta              80.860(4)
_cell_angle_gamma             69.207(4)

```

```

_cell_volume 923.36(7)
_cell_formula_units_Z 2
_cell_measurement_reflns_used 4358
_cell_measurement_temperature 110(2)
_cell_measurement_theta_max 31.9829
_cell_measurement_theta_min 2.9524
_exptl_absorpt_coefficient_mu 2.237
_exptl_absorpt_correction_T_max 0.440
_exptl_absorpt_correction_T_min 0.301
_exptl_absorpt_correction_type analytical
_exptl_absorpt_process_details
;
CrysAlisPro, Agilent Technologies,
Version 1.171.35.15 (release 03-08-2011 CrysAlis171 .NET)
(compiled Aug 3 2011,13:03:54)
Analytical numeric absorption correction using a multifaceted
crystal
model based on expressions derived by R.C.
Clark & J.S. Reid.
(Clark, R. C. & Reid, J. S. (1995). Acta Cryst. A51, 887-897)
;
_exptl_crystal_colour 'pinkish colourless'
_exptl_crystal_colour_modifier pinkish
_exptl_crystal_colour_primary colourless
_exptl_crystal_density_diffn 1.429
_exptl_crystal_density_meas ?
_exptl_crystal_density_method 'not measured'
_exptl_crystal_description block
_exptl_crystal_F_000 408
_exptl_crystal_size_max 0.1712
_exptl_crystal_size_mid 0.1642
_exptl_crystal_size_min 0.1105
_exptl_special_details
;
?
;
_diffn_reflns_av_R_equivalents 0.0204
_diffn_reflns_av_unetI/netI 0.0410
_diffn_reflns_limit_h_max 13
_diffn_reflns_limit_h_min -14
_diffn_reflns_limit_k_max 12
_diffn_reflns_limit_k_min -14
_diffn_reflns_limit_l_max 16
_diffn_reflns_limit_l_min -16
_diffn_reflns_number 8860
_diffn_reflns_theta_full 25.00
_diffn_reflns_theta_max 32.06
_diffn_reflns_theta_min 2.96
_diffn_ambient_temperature 110.0
_diffn_detector_area_resol_mean 16.1450
_diffn_measured_fraction_theta_full 0.998
_diffn_measured_fraction_theta_max 0.893
_diffn_measurement_details
;
# type start end width exp.time
1 omega 6.00 95.00 1.0000 24.0000
omega theta kappa phi frames

```

```

-      26.5735   57.0000  -90.0000  89

#  type_  start_  end_    width_  exp.time_
  2  omega_ -44.00  57.00   1.0000   24.0000
omega_  theta_  kappa_  phi_    frames
-      26.5735  -77.0000  -60.0000  101

#  type_  start_  end_    width_  exp.time_
  3  omega_ -36.00  54.00   1.0000   24.0000
omega_  theta_  kappa_  phi_    frames
-      26.5735  -77.0000   30.0000  90

#  type_  start_  end_    width_  exp.time_
  4  omega_  -3.00  97.00   1.0000   24.0000
omega_  theta_  kappa_  phi_    frames
-      26.5735   77.0000  150.0000  100

;
_diffraction_measurement_device_type      'SuperNova, Single source at
offset), Eos'
_diffraction_measurement_method           '\w scans'
_diffraction_orient_matrix_UB_11         0.0133329000
_diffraction_orient_matrix_UB_12        -0.0737616000
_diffraction_orient_matrix_UB_13         0.0449156000
_diffraction_orient_matrix_UB_21         0.0115947000
_diffraction_orient_matrix_UB_22         0.0270980000
_diffraction_orient_matrix_UB_23         0.0466279000
_diffraction_orient_matrix_UB_31        -0.0789367000
_diffraction_orient_matrix_UB_32         0.0182731000
_diffraction_orient_matrix_UB_33         0.0170567000
_diffraction_radiation_monochromator      mirror
_diffraction_radiation_type               'Mo K\alpha'
_diffraction_radiation_wavelength         0.7107
_diffraction_source                       'SuperNova (Mo) X-ray
Source'
_diffraction_standards_decay_%            ?
_diffraction_standards_interval_count     ?
_diffraction_standards_interval_time      ?
_diffraction_standards_number             ?
_reflections_number_gt                     4995
_reflections_number_total                  5751
_reflections_odcompleteness_completeness  99.13
_reflections_odcompleteness_iscentric     1
_reflections_odcompleteness_theta         30.01
_reflections_threshold_expression         >2sigma(I)
_computing_cell_refinement

;
CrysAlisPro, Agilent Technologies,
Version 1.171.35.15 (release 03-08-2011 CrysAlis171 .NET)
(compiled Aug  3 2011,13:03:54)
;
_computing_data_collection

;
CrysAlisPro, Agilent Technologies,
Version 1.171.35.15 (release 03-08-2011 CrysAlis171 .NET)
(compiled Aug  3 2011,13:03:54)
;
_computing_data_reduction

```

```

;
CrysAlisPro, Agilent Technologies,
Version 1.171.35.15 (release 03-08-2011 CrysAlis171 .NET)
(compiled Aug  3 2011,13:03:54)
;
_computing_molecular_graphics
;
O. V. Dolomanov, L. J. Bourhis, R. J. Gildea, J. A. K. Howard
and H. Puschmann,
OLEX2: a complete structure solution, refinement and analysis
program.
J. Appl. Cryst. (2009). 42, 339-341.
;
_computing_publication_material
;
O. V. Dolomanov, L. J. Bourhis, R. J. Gildea, J. A. K. Howard
and H. Puschmann,
OLEX2: a complete structure solution, refinement and analysis
program.
J. Appl. Cryst. (2009). 42, 339-341.
;
_computing_structure_refinement
;
XL, G.M. Sheldrick, Acta Cryst.
(2008). A64, 112-122
;
_computing_structure_solution
;
olex2.solve (L.J. Bourhis, O.V. Dolomanov, R.J. Gildea, J.A.K.
Howard,
H. Puschmann, in preparation, 2011)
;
_refine_diff_density_max          1.301
_refine_diff_density_min         -0.484
_refine_diff_density_rms         0.085
_refine_ls_extinction_coef       ?
_refine_ls_extinction_method     none
_refine_ls_goodness_of_fit_ref   1.045
_refine_ls_hydrogen_treatment    constr
_refine_ls_matrix_type           full
_refine_ls_number_parameters     226
_refine_ls_number_reflns        5751
_refine_ls_number_restraints     0
_refine_ls_R_factor_all          0.0482
_refine_ls_R_factor_gt           0.0392
_refine_ls_restrained_S_all      1.045
_refine_ls_shift/su_max          0.000
_refine_ls_shift/su_mean         0.000
_refine_ls_structure_factor_coef  Fsqd
_refine_ls_weighting_details
'calc w=1/[\s^2^(Fo^2^)+(0.0429P)^2^+0.6465P] where P=(Fo^2^+
2Fc^2^)/3'
_refine_ls_weighting_scheme       calc
_refine_ls_wR_factor_gt          0.0929
_refine_ls_wR_factor_ref         0.0978
_refine_special_details
;

```

H1, H1a and H1b were located in the difference map and their coordinates and isotropic displacement parameters restrained to ride on their connecting atom.

Refinement of F^2 against ALL reflections. The weighted R-factor wR and goodness of fit S are based on F^2 , conventional R-factors R are based on F , with F set to zero for negative F^2 . The threshold expression of $F^2 > 2\sigma(F^2)$ is used only for calculating R-factors (gt) etc. and is not relevant to the choice of reflections for refinement. R-factors based on F^2 are statistically about twice as large as those based on F , and R-factors based on ALL data will be even larger.

```

;
_atom_sites_solution_hydrogens      geom
_atom_sites_solution_primary         direct
_atom_sites_solution_secondary       difmap
loop_
  _atom_site_label
  _atom_site_type_symbol
  _atom_site_fract_x
  _atom_site_fract_y
  _atom_site_fract_z
  _atom_site_U_iso_or_equiv
  _atom_site_adp_type
  _atom_site_occupancy
  _atom_site_symmetry_multiplicity
  _atom_site_calc_flag
  _atom_site_refinement_flags
  _atom_site_disorder_assembly
  _atom_site_disorder_group
Br1 Br 0.35478(2) 0.30959(2) 0.51256(2) 0.02423(7) Uani 1 1 d
. . .
C2 C 0.0271(2) 0.9467(2) 0.66228(16) 0.0142(3) Uani 1 1 d . .
.
C3 C -0.0504(2) 1.0838(2) 0.68490(18) 0.0187(4) Uani 1 1 d .
.
H3 H 0.0008 1.1507 0.6854 0.022 Uiso 1 1 calc R . .
C4 C -0.2074(2) 1.1175(2) 0.7068(2) 0.0226(4) Uani 1 1 d . .
.
H4 H -0.2651 1.2097 0.7232 0.027 Uiso 1 1 calc R . .
C5 C -0.2830(2) 1.0184(3) 0.7051(2) 0.0226(4) Uani 1 1 d . .
.
H5 H -0.3904 1.0461 0.7201 0.027 Uiso 1 1 calc R . .
C6 C -0.2065(2) 0.8826(2) 0.68253(18) 0.0187(4) Uani 1 1 d .
.
H6 H -0.2581 0.8164 0.6811 0.022 Uiso 1 1 calc R . .
C7 C -0.0486(2) 0.8479(2) 0.66184(17) 0.0146(3) Uani 1 1 d .
.
C8 C 0.0375(2) 0.5883(2) 0.62933(19) 0.0190(4) Uani 1 1 d . .

```

```

.
H8A H 0.1261 0.5342 0.5844 0.023 Uiso 1 1 calc R . .
H8B H -0.0539 0.6207 0.5802 0.023 Uiso 1 1 calc R . .
C9 C 0.0163(2) 0.4806(2) 0.75854(19) 0.0175(3) Uani 1 1 d . .
.
C10 C -0.1114(3) 0.4335(3) 0.7868(2) 0.0260(4) Uani 1 1 d . .
.
H10 H -0.1872 0.4722 0.7261 0.031 Uiso 1 1 calc R . .
C11 C -0.1283(3) 0.3295(3) 0.9043(2) 0.0327(5) Uani 1 1 d . .
.
H11 H -0.2153 0.2967 0.9231 0.039 Uiso 1 1 calc R . .
C12 C -0.0192(3) 0.2738(3) 0.9935(2) 0.0296(5) Uani 1 1 d . .
.
H12 H -0.0309 0.2025 1.0733 0.035 Uiso 1 1 calc R . .
C13 C 0.1072(3) 0.3220(3) 0.9666(2) 0.0268(4) Uani 1 1 d . .
.
H13 H 0.1813 0.2851 1.0284 0.032 Uiso 1 1 calc R . .
C14 C 0.1257(2) 0.4242(2) 0.8492(2) 0.0223(4) Uani 1 1 d . .
.
H14 H 0.2134 0.4559 0.8306 0.027 Uiso 1 1 calc R . .
C15 C 0.3085(2) 0.9331(2) 0.63691(19) 0.0191(4) Uani 1 1 d .
.
H15A H 0.2743 1.0454 0.6007 0.023 Uiso 1 1 calc R . .
H15B H 0.3941 0.8917 0.5827 0.023 Uiso 1 1 calc R . .
C16 C 0.3629(2) 0.8859(2) 0.76866(18) 0.0172(3) Uani 1 1 d .
.
C17 C 0.4640(2) 0.7406(2) 0.8213(2) 0.0217(4) Uani 1 1 d . .
.
H17 H 0.4972 0.6711 0.7749 0.026 Uiso 1 1 calc R . .
C18 C 0.5164(2) 0.6969(3) 0.9420(2) 0.0240(4) Uani 1 1 d . .
.
H18 H 0.5857 0.5978 0.9776 0.029 Uiso 1 1 calc R . .
C19 C 0.4676(2) 0.7977(3) 1.0100(2) 0.0238(4) Uani 1 1 d . .
.
H19 H 0.5037 0.7680 1.0921 0.029 Uiso 1 1 calc R . .
C20 C 0.3663(2) 0.9418(3) 0.9584(2) 0.0237(4) Uani 1 1 d . .
.
H20 H 0.3317 1.0103 1.0057 0.028 Uiso 1 1 calc R . .
C21 C 0.3147(2) 0.9868(2) 0.8376(2) 0.0207(4) Uani 1 1 d . .
.
H21 H 0.2466 1.0865 0.8020 0.025 Uiso 1 1 calc R . .
N1 N 0.18130(17) 0.87743(18) 0.63776(15) 0.0151(3) Uani 1 1 d
.
N2 N 0.06234(18) 0.72409(18) 0.63593(15) 0.0155(3) Uani 1 1 d
.
C1 C 0.1971(2) 0.7455(2) 0.62298(18) 0.0170(3) Uani 1 1 d . .
.
H1 H 0.2877 0.6803 0.6086 0.020 Uiso 1 1 d R . .
O1 O 0.48452(19) 0.44528(19) 0.68588(14) 0.0288(3) Uani 1 1 d
.
H1A H 0.4648 0.3973 0.6680 0.035 Uiso 1 1 d R . .
H1B H 0.5357 0.4765 0.6728 0.035 Uiso 1 1 d R . .

```

```

loop_
  _atom_site_aniso_label
  _atom_site_aniso_U_11
  _atom_site_aniso_U_22

```

```

_atom_site_aniso_U_33
_atom_site_aniso_U_23
_atom_site_aniso_U_13
_atom_site_aniso_U_12
Br1 0.02397(11) 0.02083(11) 0.02819(12) -0.00962(8) -0.00177
(8) -0.00555(8)
C2 0.0131(7) 0.0149(8) 0.0122(7) -0.0027(6) -0.0007(6) -
0.0033(6)
C3 0.0207(9) 0.0153(8) 0.0182(9) -0.0046(7) -0.0021(7) -
0.0038(7)
C4 0.0203(9) 0.0206(9) 0.0224(9) -0.0100(8) 0.0000(8) 0.0014
(8)
C5 0.0149(8) 0.0274(10) 0.0215(9) -0.0076(8) 0.0002(7) -
0.0027(8)
C6 0.0156(8) 0.0236(9) 0.0160(8) -0.0050(7) 0.0000(7) -0.0069
(7)
C7 0.0147(8) 0.0138(8) 0.0130(8) -0.0025(6) -0.0020(6) -
0.0030(7)
C8 0.0227(9) 0.0152(8) 0.0212(9) -0.0070(7) -0.0032(7) -
0.0063(7)
C9 0.0184(8) 0.0138(8) 0.0209(9) -0.0075(7) 0.0006(7) -0.0047
(7)
C10 0.0237(10) 0.0260(11) 0.0307(11) -0.0066(9) -0.0037(8) -
0.0123(9)
C11 0.0304(11) 0.0354(13) 0.0369(13) -0.0083(10) 0.0057(10) -
0.0223(11)
C12 0.0393(13) 0.0254(11) 0.0228(10) -0.0034(9) 0.0051(9) -
0.0160(10)
C13 0.0289(11) 0.0254(11) 0.0222(10) -0.0037(8) -0.0038(8) -
0.0072(9)
C14 0.0189(9) 0.0221(10) 0.0239(10) -0.0038(8) -0.0023(8) -
0.0072(8)
C15 0.0163(8) 0.0235(9) 0.0201(9) -0.0062(7) 0.0003(7) -
0.0106(7)
C16 0.0139(8) 0.0207(9) 0.0189(9) -0.0064(7) 0.0012(7) -
0.0085(7)
C17 0.0192(9) 0.0211(9) 0.0256(10) -0.0086(8) -0.0012(8) -
0.0063(8)
C18 0.0208(9) 0.0227(10) 0.0264(10) -0.0035(8) -0.0050(8) -
0.0073(8)
C19 0.0219(9) 0.0304(11) 0.0217(9) -0.0055(8) -0.0024(8) -
0.0136(9)
C20 0.0231(9) 0.0293(11) 0.0254(10) -0.0140(9) 0.0014(8) -
0.0121(9)
C21 0.0180(8) 0.0206(9) 0.0246(10) -0.0083(8) -0.0009(7) -
0.0066(7)
N1 0.0123(7) 0.0160(7) 0.0161(7) -0.0051(6) 0.0002(5) -0.0039
(6)
N2 0.0161(7) 0.0133(7) 0.0162(7) -0.0044(6) -0.0007(6) -
0.0042(6)
C1 0.0147(8) 0.0173(9) 0.0183(8) -0.0075(7) -0.0004(7) -
0.0025(7)
O1 0.0300(8) 0.0245(8) 0.0237(8) -0.0083(6) -0.0004(6) 0.0012
(7)

```

```

_geom_special_details
;

```

All esds (except the esd in the dihedral angle between two l.s. planes) are estimated using the full covariance matrix. The cell esds are taken into account individually in the estimation of esds in distances, angles and torsion angles; correlations between esds in cell parameters are only used when they are defined by crystal symmetry. An approximate (isotropic) treatment of cell esds is used for estimating esds involving l.s. planes.

```

;
loop_
  _geom_bond_atom_site_label_1
  _geom_bond_atom_site_label_2
  _geom_bond_distance
  _geom_bond_site_symmetry_2
  _geom_bond_publ_flag
C2 C3 1.391(3) . ?
C2 C7 1.403(2) . ?
C2 N1 1.395(2) . ?
C3 H3 0.9500 . ?
C3 C4 1.392(3) . ?
C4 H4 0.9500 . ?
C4 C5 1.410(3) . ?
C5 H5 0.9500 . ?
C5 C6 1.377(3) . ?
C6 H6 0.9500 . ?
C6 C7 1.398(3) . ?
C7 N2 1.390(2) . ?
C8 H8A 0.9900 . ?
C8 H8B 0.9900 . ?
C8 C9 1.510(3) . ?
C8 N2 1.476(2) . ?
C9 C10 1.388(3) . ?
C9 C14 1.395(3) . ?
C10 H10 0.9500 . ?
C10 C11 1.393(3) . ?
C11 H11 0.9500 . ?
C11 C12 1.382(3) . ?
C12 H12 0.9500 . ?
C12 C13 1.383(3) . ?
C13 H13 0.9500 . ?
C13 C14 1.389(3) . ?
C14 H14 0.9500 . ?
C15 H15A 0.9900 . ?
C15 H15B 0.9900 . ?
C15 C16 1.513(3) . ?
C15 N1 1.481(2) . ?
C16 C17 1.392(3) . ?
C16 C21 1.392(3) . ?
C17 H17 0.9500 . ?
C17 C18 1.395(3) . ?
C18 H18 0.9500 . ?
C18 C19 1.383(3) . ?
C19 H19 0.9500 . ?

```


C19 C20 1.384(3) . ?
C20 H20 0.9500 . ?
C20 C21 1.390(3) . ?
C21 H21 0.9500 . ?
N1 C1 1.333(2) . ?
N2 C1 1.333(2) . ?
C1 H1 0.8993 . ?
O1 H1A 0.6675 . ?
O1 H1B 0.6324 . ?

loop_

_geom_angle_atom_site_label_1
_geom_angle_atom_site_label_2
_geom_angle_atom_site_label_3
_geom_angle
_geom_angle_site_symmetry_1
_geom_angle_site_symmetry_3
_geom_angle_publ_flag
C3 C2 C7 121.89(17) . . ?
C3 C2 N1 131.66(17) . . ?
N1 C2 C7 106.45(16) . . ?
C2 C3 H3 121.9 . . ?
C2 C3 C4 116.17(18) . . ?
C4 C3 H3 121.9 . . ?
C3 C4 H4 119.2 . . ?
C3 C4 C5 121.66(19) . . ?
C5 C4 H4 119.2 . . ?
C4 C5 H5 118.9 . . ?
C6 C5 C4 122.27(18) . . ?
C6 C5 H5 118.9 . . ?
C5 C6 H6 121.9 . . ?
C5 C6 C7 116.12(18) . . ?
C7 C6 H6 121.9 . . ?
C6 C7 C2 121.88(18) . . ?
N2 C7 C2 106.46(15) . . ?
N2 C7 C6 131.65(17) . . ?
H8A C8 H8B 107.9 . . ?
C9 C8 H8A 109.2 . . ?
C9 C8 H8B 109.2 . . ?
N2 C8 H8A 109.2 . . ?
N2 C8 H8B 109.2 . . ?
N2 C8 C9 112.20(16) . . ?
C10 C9 C8 119.90(18) . . ?
C10 C9 C14 119.35(19) . . ?
C14 C9 C8 120.73(17) . . ?
C9 C10 H10 120.0 . . ?
C9 C10 C11 120.0(2) . . ?
C11 C10 H10 120.0 . . ?
C10 C11 H11 119.8 . . ?
C12 C11 C10 120.3(2) . . ?
C12 C11 H11 119.8 . . ?
C11 C12 H12 120.0 . . ?
C11 C12 C13 119.9(2) . . ?
C13 C12 H12 120.0 . . ?
C12 C13 H13 120.0 . . ?
C12 C13 C14 120.1(2) . . ?
C14 C13 H13 120.0 . . ?

C9 C14 H14 119.9 . . ?
 C13 C14 C9 120.29(19) . . ?
 C13 C14 H14 119.9 . . ?
 H15A C15 H15B 108.0 . . ?
 C16 C15 H15A 109.4 . . ?
 C16 C15 H15B 109.4 . . ?
 N1 C15 H15A 109.4 . . ?
 N1 C15 H15B 109.4 . . ?
 N1 C15 C16 111.31(15) . . ?
 C17 C16 C15 119.75(18) . . ?
 C21 C16 C15 120.80(18) . . ?
 C21 C16 C17 119.45(19) . . ?
 C16 C17 H17 119.9 . . ?
 C16 C17 C18 120.1(2) . . ?
 C18 C17 H17 119.9 . . ?
 C17 C18 H18 120.0 . . ?
 C19 C18 C17 120.0(2) . . ?
 C19 C18 H18 120.0 . . ?
 C18 C19 H19 120.0 . . ?
 C18 C19 C20 120.0(2) . . ?
 C20 C19 H19 120.0 . . ?
 C19 C20 H20 119.8 . . ?
 C19 C20 C21 120.3(2) . . ?
 C21 C20 H20 119.8 . . ?
 C16 C21 H21 120.0 . . ?
 C20 C21 C16 120.07(19) . . ?
 C20 C21 H21 120.0 . . ?
 C2 N1 C15 126.74(16) . . ?
 C1 N1 C2 108.11(15) . . ?
 C1 N1 C15 125.02(16) . . ?
 C7 N2 C8 126.22(16) . . ?
 C1 N2 C7 108.35(15) . . ?
 C1 N2 C8 125.38(17) . . ?
 N1 C1 N2 110.62(17) . . ?
 N1 C1 H1 123.4 . . ?
 N2 C1 H1 125.9 . . ?
 H1A O1 H1B 138.7 . . ?

loop_

_geom_torsion_atom_site_label_1
 _geom_torsion_atom_site_label_2
 _geom_torsion_atom_site_label_3
 _geom_torsion_atom_site_label_4
 _geom_torsion
 _geom_torsion_site_symmetry_1
 _geom_torsion_site_symmetry_2
 _geom_torsion_site_symmetry_3
 _geom_torsion_site_symmetry_4
 _geom_torsion_publ_flag
 C2 C3 C4 C5 -0.4(3) ?
 C2 C7 N2 C8 178.18(16) ?
 C2 C7 N2 C1 0.7(2) ?
 C2 N1 C1 N2 0.2(2) ?
 C3 C2 C7 C6 0.8(3) ?
 C3 C2 C7 N2 179.76(17) ?
 C3 C2 N1 C15 3.9(3) ?
 C3 C2 N1 C1 179.9(2) ?

C3 C4 C5 C6 0.3(3) ?
 C4 C5 C6 C7 0.3(3) ?
 C5 C6 C7 C2 -0.9(3) ?
 C5 C6 C7 N2 -179.51(19) ?
 C6 C7 N2 C8 -3.0(3) ?
 C6 C7 N2 C1 179.49(19) ?
 C7 C2 C3 C4 -0.2(3) ?
 C7 C2 N1 C15 -175.73(17) ?
 C7 C2 N1 C1 0.2(2) ?
 C7 N2 C1 N1 -0.6(2) ?
 C8 C9 C10 C11 177.5(2) ?
 C8 C9 C14 C13 -178.2(2) ?
 C8 N2 C1 N1 -178.07(16) ?
 C9 C8 N2 C7 -76.2(2) ?
 C9 C8 N2 C1 100.8(2) ?
 C9 C10 C11 C12 0.6(4) ?
 C10 C9 C14 C13 0.0(3) ?
 C10 C11 C12 C13 0.3(4) ?
 C11 C12 C13 C14 -1.1(4) ?
 C12 C13 C14 C9 0.9(3) ?
 C14 C9 C10 C11 -0.8(3) ?
 C15 C16 C17 C18 179.10(18) ?
 C15 C16 C21 C20 -179.78(17) ?
 C15 N1 C1 N2 176.26(16) ?
 C16 C15 N1 C2 83.7(2) ?
 C16 C15 N1 C1 -91.6(2) ?
 C16 C17 C18 C19 0.3(3) ?
 C17 C16 C21 C20 -0.6(3) ?
 C17 C18 C19 C20 0.2(3) ?
 C18 C19 C20 C21 -0.9(3) ?
 C19 C20 C21 C16 1.1(3) ?
 C21 C16 C17 C18 -0.1(3) ?
 N1 C2 C3 C4 -179.73(19) ?
 N1 C2 C7 C6 -179.50(16) ?
 N1 C2 C7 N2 -0.57(19) ?
 N1 C15 C16 C17 81.9(2) ?
 N1 C15 C16 C21 -99.0(2) ?
 N2 C8 C9 C10 126.3(2) ?
 N2 C8 C9 C14 -55.4(2) ?

loop_

_exptl_crystal_face_index_h
 _exptl_crystal_face_index_k
 _exptl_crystal_face_index_l
 _exptl_crystal_face_perp_dist
 _exptl_oxdiff_crystal_face_indexfrac_h
 _exptl_oxdiff_crystal_face_indexfrac_k
 _exptl_oxdiff_crystal_face_indexfrac_l
 _exptl_oxdiff_crystal_face_x
 _exptl_oxdiff_crystal_face_y
 _exptl_oxdiff_crystal_face_z
 -12 -1 3 0.0444 -12.0139 -1.0157 2.9796 0.0486 -0.0279 0.9806
 12 2 -2 0.0807 12.0134 2.0160 -1.9799 -0.0775 0.1016 -0.9452
 -2 -14 -8 0.0485 -1.9993 -14.0090 -8.0029 0.6472 -0.7760 -
 0.2347
 5 14 8 0.1131 5.0023 14.0124 8.0074 -0.6072 0.8111 -0.0022
 1 3 -14 0.1054 1.0107 3.0087 -13.9890 -0.8368 -0.5590 -0.2634

-3 -3 13 0.0463 -3.0120 -3.0106 12.9865 0.7652 0.4890 0.4043
-12 1 -4 0.0506 -12.0089 0.9884 -4.0155 -0.4134 -0.2997
0.8975
12 0 0 0.0604 12.0118 0.0138 0.0182 0.1600 0.1405 -0.9476
-10 -10 -10 0.0521 -10.0051 -10.0146 -10.0125 0.1556 -0.8542
0.4360

APPENDIX C - Compound 222

```

data_ijsf1201
_audit_creation_date          2012-04-24
_audit_creation_method
;
  Olex2 1.1
  (compiled 2011.11.01 svn.r2039, GUI svn.r3906)
;
_publ_contact_author_address  ?
_publ_contact_author_email    ?
_publ_contact_author_name     ' '
_publ_contact_author_phone    ?
_chemical_name_common         ?
_chemical_name_systematic
;
?
;
_chemical_formula_moiety      'C21 H19 F3 N2 O3'
_chemical_formula_sum         'C21 H19 F3 N2 O3'
_chemical_formula_weight      404.38
_chemical_absolute_configuration unk
_chemical_melting_point       ?
_chemical_oxdiff_formula      'C21 H19 F3 N2 O3'
_chemical_oxdiff_usercomment  'Toms TJW/5/143/450/1'
loop_
  _atom_type_symbol
  _atom_type_description
  _atom_type_scat_dispersion_real
  _atom_type_scat_dispersion_imag
  _atom_type_scat_source
'C' 'C' 0.0033 0.0016 'International Tables Vol C Tables
4.2.6.8 and 6.1.1.4'
'H' 'H' 0.0000 0.0000 'International Tables Vol C Tables
4.2.6.8 and 6.1.1.4'
'N' 'N' 0.0061 0.0033 'International Tables Vol C Tables
4.2.6.8 and 6.1.1.4'
'O' 'O' 0.0106 0.0060 'International Tables Vol C Tables
4.2.6.8 and 6.1.1.4'
'F' 'F' 0.0171 0.0103 'International Tables Vol C Tables
4.2.6.8 and 6.1.1.4'

  _space_group_crystal_system  'monoclinic'
  _space_group_IT_number       4
  _space_group_name_H-M_alt    'P 1 21 1'
  _space_group_name_Hall       'P 2yb'
loop_
  _space_group_symop_id
  _space_group_symop_operation_xyz
1 'x, y, z'
2 '-x, y+1/2, -z'

_cell_length_a                 8.7492 (3)
_cell_length_b                 9.0043 (3)
_cell_length_c                 24.1842 (7)
_cell_angle_alpha              90.00
_cell_angle_beta               98.900 (3)

```

```

_cell_angle_gamma          90.00
_cell_volume               1882.30(10)
_cell_formula_units_Z     4
_cell_measurement_reflns_used 5381
_cell_measurement_temperature 110.00(10)
_cell_measurement_theta_max 27.8109
_cell_measurement_theta_min 3.1089
_exptl_absorpt_coefficient_mu 0.116
_exptl_absorpt_correction_T_max 0.996
_exptl_absorpt_correction_T_min 0.963
_exptl_absorpt_correction_type analytical
_exptl_absorpt_process_details
;
CrysAlisPro, Agilent Technologies,
Version 1.171.35.21 (release 20-01-2012 CrysAlis171 .NET)
(compiled Jan 23 2012,18:06:46)
Analytical numeric absorption correction using a multifaceted
crystal
                                model based on expressions derived by R.C.
Clark & J.S. Reid.
(Clark, R. C. & Reid, J. S. (1995). Acta Cryst. A51, 887-897)
;
_exptl_crystal_colour      'clear colourless'
_exptl_crystal_colour_lustre clear
_exptl_crystal_colour_modifier .
_exptl_crystal_colour_primary colourless
_exptl_crystal_density_diffn 1.427
_exptl_crystal_density_meas ?
_exptl_crystal_density_method 'not measured'
_exptl_crystal_description needle
_exptl_crystal_F_000      840
_exptl_crystal_size_max   0.3796
_exptl_crystal_size_mid   0.1807
_exptl_crystal_size_min   0.0328
_exptl_special_details
;
?
;
_diffn_reflns_av_R_equivalents 0.0306
_diffn_reflns_av_unetI/netI 0.0489
_diffn_reflns_limit_h_max 11
_diffn_reflns_limit_h_min -11
_diffn_reflns_limit_k_max 11
_diffn_reflns_limit_k_min -11
_diffn_reflns_limit_l_max 31
_diffn_reflns_limit_l_min -31
_diffn_reflns_number 14377
_diffn_reflns_theta_full 27.87
_diffn_reflns_theta_max 27.87
_diffn_reflns_theta_min 3.12
_diffn_ambient_temperature 110.00(10)
_diffn_detector_area_resol_mean 16.1450
_diffn_measured_fraction_theta_full 0.996
_diffn_measured_fraction_theta_max 0.996
_diffn_measurement_details
;
# __ type __ start __ end __ width __ exp.time __

```

```

1 omega   -97.00  -61.00   1.0000   70.0000
omega_____ theta_____ kappa_____ phi_____ frames
-          -21.7365 -178.0000  60.0000  36

```

```

# type_ start_ end_ width_ exp.time_
 2 omega -78.00 -51.00  1.0000  70.0000
omega_____ theta_____ kappa_____ phi_____ frames
-          -21.7365 -178.0000 -120.0000 27

```

```

# type_ start_ end_ width_ exp.time_
 3 omega -30.00  96.00  1.0000  70.0000
omega_____ theta_____ kappa_____ phi_____ frames
-           22.8303    0.0000 -150.0000 126

```

```

# type_ start_ end_ width_ exp.time_
 4 omega  35.00  77.00  1.0000  70.0000
omega_____ theta_____ kappa_____ phi_____ frames
-           22.8303 -141.0000  -29.0000 42

```

```

# type_ start_ end_ width_ exp.time_
 5 omega -43.00   9.00  1.0000  70.0000
omega_____ theta_____ kappa_____ phi_____ frames
-          -21.7365  57.0000  90.0000 52

```

```

# type_ start_ end_ width_ exp.time_
 6 omega -92.00   8.00  1.0000  70.0000
omega_____ theta_____ kappa_____ phi_____ frames
-          -21.7365 -77.0000  -30.0000 100

```

```

;
_diffraction_measurement_device_type 'SuperNova, Single source at
offset), Eos'
_diffraction_measurement_method '\w scans'
_diffraction_orient_matrix_UB_11 -0.0097380000
_diffraction_orient_matrix_UB_12 0.0026536000
_diffraction_orient_matrix_UB_13 -0.0296944000
_diffraction_orient_matrix_UB_21 -0.0294622000
_diffraction_orient_matrix_UB_22 0.0732094000
_diffraction_orient_matrix_UB_23 0.0005393000
_diffraction_orient_matrix_UB_31 0.0759031000
_diffraction_orient_matrix_UB_32 0.0287956000
_diffraction_orient_matrix_UB_33 0.0013631000
_diffraction_radiation_monochromator mirror
_diffraction_radiation_type 'Mo K\alpha'
_diffraction_radiation_wavelength 0.7107
_diffraction_source 'SuperNova (Mo) X-ray
Source'
_diffraction_standards_decay_% ?
_diffraction_standards_interval_count ?
_diffraction_standards_interval_time ?
_diffraction_standards_number ?
_reflections_number_gt 7201
_reflections_number_total 8188
_reflections_odcompleteness_completeness 99.65
_reflections_odcompleteness_iscentric 1
_reflections_odcompleteness_theta 27.82
_reflections_threshold_expression >2sigma(I)
_computing_cell_refinement

```

```

;
CrysAlisPro, Agilent Technologies,
Version 1.171.35.21 (release 20-01-2012 CrysAlis171 .NET)
(compiled Jan 23 2012,18:06:46)
;
_computing_data_collection
;
CrysAlisPro, Agilent Technologies,
Version 1.171.35.21 (release 20-01-2012 CrysAlis171 .NET)
(compiled Jan 23 2012,18:06:46)
;
_computing_data_reduction
;
CrysAlisPro, Agilent Technologies,
Version 1.171.35.21 (release 20-01-2012 CrysAlis171 .NET)
(compiled Jan 23 2012,18:06:46)
;
_computing_molecular_graphics
;
O. V. Dolomanov, L. J. Bourhis, R. J. Gildea, J. A. K. Howard
and H. Puschmann,
OLEX2: a complete structure solution, refinement and analysis
program.
J. Appl. Cryst. (2009). 42, 339-341.
;
_computing_publication_material
;
O. V. Dolomanov, L. J. Bourhis, R. J. Gildea, J. A. K. Howard
and H. Puschmann,
OLEX2: a complete structure solution, refinement and analysis
program.
J. Appl. Cryst. (2009). 42, 339-341.
;
_computing_structure_refinement
;
XL, G.M. Sheldrick, Acta Cryst.
(2008). A64, 112-122
;
_computing_structure_solution
;
XS, G.M. Sheldrick, Acta Cryst.
(2008). A64, 112-122
;
_refine_diff_density_max          0.262
_refine_diff_density_min         -0.294
_refine_diff_density_rms         0.049
_refine_ls_abs_structure_details  'Flack H D (1983), Acta
Cryst. A39, 876-881'
_refine_ls_abs_structure_Flack    -0.4(6)
_refine_ls_extinction_coef        ?
_refine_ls_extinction_method      none
_refine_ls_goodness_of_fit_ref    1.064
_refine_ls_hydrogen_treatment     mixed
_refine_ls_matrix_type            full
_refine_ls_number_parameters      535
_refine_ls_number_reflns         8188
_refine_ls_number_restraints      1

```



```

_refine_ls_R_factor_all          0.0572
_refine_ls_R_factor_gt          0.0480
_refine_ls_restrained_S_all     1.063
_refine_ls_shift/su_max         0.000
_refine_ls_shift/su_mean        0.000
_refine_ls_structure_factor_coef Fsqd
_refine_ls_weighting_details
'calc w=1/[\s^2^(Fo^2^)+(0.0442P)^2^+0.5706P] where P=(Fo^2^+
2Fc^2^)/3'
_refine_ls_weighting_scheme      calc
_refine_ls_wR_factor_gt         0.1077
_refine_ls_wR_factor_ref        0.1135
_refine_special_details
;
Refinement of F^2^ against ALL reflections. The weighted R-
factor wR and
goodness of fit S are based on F^2^, conventional R-factors R
are based
on F, with F set to zero for negative F^2^. The threshold
expression of
F^2^ > 2sigma(F^2^) is used only for calculating R-factors
(gt) etc. and is
not relevant to the choice of reflections for refinement. R-
factors based
on F^2^ are statistically about twice as large as those based
on F, and R-
factors based on ALL data will be even larger.
;
_atom_sites_solution_hydrogens  geom
_atom_sites_solution_primary    direct
_atom_sites_solution_secondary  difmap
loop_
  _atom_site_label
  _atom_site_type_symbol
  _atom_site_fract_x
  _atom_site_fract_y
  _atom_site_fract_z
  _atom_site_U_iso_or_equiv
  _atom_site_adp_type
  _atom_site_occupancy
  _atom_site_symmetry_multiplicity
  _atom_site_calc_flag
  _atom_site_refinement_flags
  _atom_site_disorder_assembly
  _atom_site_disorder_group
C1 C 0.1628(2) 0.3711(3) 0.53527(10) 0.0220(5) Uani 1 1 d . .
.
C2 C 0.0627(2) 0.2876(3) 0.48914(9) 0.0201(5) Uani 1 1 d . .
.
H2 H -0.0385 0.2700 0.5006 0.024 Uiso 1 1 calc R . .
C3 C 0.1362(3) 0.1356(3) 0.47892(9) 0.0196(5) Uani 1 1 d . .
.
H3A H 0.1630 0.0850 0.5145 0.023 Uiso 1 1 calc R . .
H3B H 0.0602 0.0753 0.4555 0.023 Uiso 1 1 calc R . .
C4 C 0.2785(2) 0.1482(3) 0.45141(9) 0.0184(5) Uani 1 1 d . .
.
C5 C 0.2724(2) 0.1561(3) 0.39190(9) 0.0188(5) Uani 1 1 d . .

```

.
 C6 C 0.1541(3) 0.1410(3) 0.34624(9) 0.0226(5) Uani 1 1 d . .
 .
 H6 H 0.0526 0.1247 0.3518 0.027 Uiso 1 1 calc R . .
 C7 C 0.1908(3) 0.1508(3) 0.29254(10) 0.0259(5) Uani 1 1 d . .
 .
 H7 H 0.1132 0.1394 0.2619 0.031 Uiso 1 1 calc R . .
 C8 C 0.3425(3) 0.1774(3) 0.28374(10) 0.0271(6) Uani 1 1 d . .
 .
 H8 H 0.3633 0.1850 0.2473 0.032 Uiso 1 1 calc R . .
 C9 C 0.4620(3) 0.1926(3) 0.32778(9) 0.0247(5) Uani 1 1 d . .
 .
 H9 H 0.5630 0.2097 0.3218 0.030 Uiso 1 1 calc R . .
 C10 C 0.4251(2) 0.1814(3) 0.38186(9) 0.0191(5) Uani 1 1 d . .
 .
 C11 C 0.4308(2) 0.1676(3) 0.47499(9) 0.0173(4) Uani 1 1 d . .
 .
 C12 C 0.5091(2) 0.1706(3) 0.53346(9) 0.0179(4) Uani 1 1 d . .
 .
 C13 C 0.6321(3) 0.2683(3) 0.54958(9) 0.0229(5) Uani 1 1 d . .
 .
 H13 H 0.6633 0.3318 0.5231 0.028 Uiso 1 1 calc R . .
 C14 C 0.7079(3) 0.2723(3) 0.60389(10) 0.0239(5) Uani 1 1 d .
 .
 H14 H 0.7889 0.3386 0.6139 0.029 Uiso 1 1 calc R . .
 C15 C 0.6635(3) 0.1775(3) 0.64369(9) 0.0222(5) Uani 1 1 d . .
 .
 C16 C 0.5426(3) 0.0775(3) 0.62865(9) 0.0241(5) Uani 1 1 d . .
 .
 H16 H 0.5127 0.0138 0.6553 0.029 Uiso 1 1 calc R . .
 C17 C 0.4673(3) 0.0733(3) 0.57391(9) 0.0226(5) Uani 1 1 d . .
 .
 H17 H 0.3880 0.0052 0.5638 0.027 Uiso 1 1 calc R . .
 C18 C 0.2592(3) 0.3801(4) 0.63124(11) 0.0378(7) Uani 1 1 d .
 .
 H18A H 0.3648 0.3762 0.6249 0.057 Uiso 1 1 calc R . .
 H18B H 0.2498 0.3291 0.6654 0.057 Uiso 1 1 calc R . .
 H18C H 0.2284 0.4818 0.6340 0.057 Uiso 1 1 calc R . .
 C19 C -0.0834(3) 0.3729(3) 0.40043(10) 0.0226(5) Uani 1 1 d .
 .
 C20 C -0.0845(3) 0.4746(3) 0.35091(10) 0.0310(6) Uani 1 1 d .
 .
 H20A H -0.0148 0.5559 0.3611 0.047 Uiso 1 1 calc R . .
 H20B H -0.1872 0.5122 0.3395 0.047 Uiso 1 1 calc R . .
 H20C H -0.0521 0.4205 0.3205 0.047 Uiso 1 1 calc R . .
 C21 C 0.7388(3) 0.1876(3) 0.70357(10) 0.0283(6) Uani 1 1 d .
 .
 F1 F 0.88076(17) 0.2472(2) 0.70945(6) 0.0412(4) Uani 1 1 d .
 .
 F2 F 0.65734(19) 0.2721(2) 0.73441(6) 0.0450(5) Uani 1 1 d .
 .
 F3 F 0.7543(2) 0.0553(2) 0.72878(7) 0.0469(5) Uani 1 1 d . .
 .
 N1 N 0.0412(2) 0.3807(2) 0.44009(8) 0.0200(4) Uani 1 1 d . .
 .
 H1 H 0.1119 0.4445 0.4361 0.024 Uiso 1 1 calc R . .
 N2 N 0.5184(2) 0.1904(2) 0.43276(7) 0.0186(4) Uani 1 1 d . .

.
 H2A H 0.620(3) 0.198(3) 0.4372(10) 0.019(6) Uiso 1 1 d . . .
 O1 O 0.1605(2) 0.3092(2) 0.58499(7) 0.0308(4) Uani 1 1 d . . .
 .
 O2 O 0.23705(19) 0.4804(2) 0.52751(7) 0.0303(4) Uani 1 1 d .
 .
 O3 O -0.19022(18) 0.2872(3) 0.40432(7) 0.0339(5) Uani 1 1 d .
 .
 C22 C 0.1505(2) 0.7248(3) 0.02831(9) 0.0197(5) Uani 1 1 d . .
 .
 C23 C 0.0497(2) 0.6447(3) -0.01873(9) 0.0203(5) Uani 1 1 d .
 .
 H23 H -0.0530 0.6311 -0.0081 0.024 Uiso 1 1 calc R . .
 C24 C 0.1167(2) 0.4893(3) -0.02893(9) 0.0205(5) Uani 1 1 d .
 .
 H24A H 0.1369 0.4367 0.0064 0.025 Uiso 1 1 calc R . .
 H24B H 0.0396 0.4334 -0.0536 0.025 Uiso 1 1 calc R . .
 C25 C 0.2637(2) 0.4947(3) -0.05416(9) 0.0173(4) Uani 1 1 d .
 .
 C26 C 0.2669(2) 0.4937(3) -0.11332(9) 0.0183(4) Uani 1 1 d .
 .
 C27 C 0.1535(3) 0.4778(3) -0.16087(9) 0.0214(5) Uani 1 1 d .
 .
 H27 H 0.0493 0.4720 -0.1573 0.026 Uiso 1 1 calc R . .
 C28 C 0.1994(3) 0.4709(3) -0.21307(10) 0.0243(5) Uani 1 1 d .
 .
 H28 H 0.1252 0.4587 -0.2447 0.029 Uiso 1 1 calc R . .
 C29 C 0.3566(3) 0.4819(3) -0.21907(10) 0.0244(5) Uani 1 1 d .
 .
 H29 H 0.3844 0.4771 -0.2546 0.029 Uiso 1 1 calc R . .
 C30 C 0.4699(3) 0.4997(3) -0.17332(9) 0.0214(5) Uani 1 1 d .
 .
 H30 H 0.5735 0.5079 -0.1774 0.026 Uiso 1 1 calc R . .
 C31 C 0.4238(2) 0.5052(3) -0.12056(9) 0.0180(5) Uani 1 1 d .
 .
 C32 C 0.4141(2) 0.5068(3) -0.02808(9) 0.0178(5) Uani 1 1 d .
 .
 C33 C 0.4830(2) 0.5069(3) 0.03150(9) 0.0178(5) Uani 1 1 d . .
 .
 C34 C 0.6000(3) 0.6056(3) 0.05213(10) 0.0236(5) Uani 1 1 d .
 .
 H34 H 0.6335 0.6750 0.0281 0.028 Uiso 1 1 calc R . .
 C35 C 0.6678(3) 0.6025(3) 0.10798(10) 0.0263(5) Uani 1 1 d .
 .
 H35 H 0.7457 0.6696 0.1213 0.032 Uiso 1 1 calc R . .
 C36 C 0.6187(3) 0.4987(3) 0.14376(9) 0.0242(5) Uani 1 1 d . .
 .
 C37 C 0.5028(3) 0.3987(3) 0.12434(10) 0.0235(5) Uani 1 1 d .
 .
 H37 H 0.4704 0.3293 0.1486 0.028 Uiso 1 1 calc R . .
 C38 C 0.4347(3) 0.4024(3) 0.06833(9) 0.0214(5) Uani 1 1 d . .
 .
 H38 H 0.3567 0.3352 0.0552 0.026 Uiso 1 1 calc R . .
 C39 C 0.2413(3) 0.7287(3) 0.12502(10) 0.0336(6) Uani 1 1 d .
 .
 H39A H 0.2277 0.6775 0.1587 0.050 Uiso 1 1 calc R . .
 H39B H 0.2123 0.8310 0.1278 0.050 Uiso 1 1 calc R . .

```

H39C H 0.3477 0.7228 0.1199 0.050 Uiso 1 1 calc R . .
C40 C -0.0848(3) 0.7312(3) -0.10948(10) 0.0228(5) Uani 1 1 d
. . .
C41 C -0.0779(3) 0.8393(3) -0.15650(10) 0.0316(6) Uani 1 1 d
. . .
H41A H -0.0343 0.9314 -0.1415 0.047 Uiso 1 1 calc R . .
H41B H -0.1805 0.8565 -0.1761 0.047 Uiso 1 1 calc R . .
H41C H -0.0146 0.7989 -0.1819 0.047 Uiso 1 1 calc R . .
C42 C 0.6867(3) 0.4952(3) 0.20451(10) 0.0316(6) Uani 1 1 d .
. .
F4 F 0.8198(2) 0.5696(2) 0.21585(7) 0.0550(5) Uani 1 1 d . .
.
F5 F 0.5953(2) 0.5546(4) 0.23679(7) 0.0842(9) Uani 1 1 d . .
.
F6 F 0.7218(3) 0.3589(2) 0.22285(8) 0.0643(6) Uani 1 1 d . .
.
N3 N 0.0344(2) 0.7404(2) -0.06716(8) 0.0213(4) Uani 1 1 d . .
.
H3 H 0.1046 0.8063 -0.0691 0.026 Uiso 1 1 calc R . .
N4 N 0.5103(2) 0.5180(2) -0.06845(8) 0.0180(4) Uani 1 1 d . .
.
H4 H 0.608(3) 0.514(3) -0.0604(9) 0.010(6) Uiso 1 1 d . . .
O4 O 0.1443(2) 0.6603(2) 0.07756(6) 0.0275(4) Uani 1 1 d . .
.
O5 O 0.22726(18) 0.8335(2) 0.02171(7) 0.0258(4) Uani 1 1 d .
. .
O6 O -0.19056(19) 0.6421(2) -0.10921(7) 0.0305(4) Uani 1 1 d
. . .

```

loop_

```

  _atom_site_aniso_label
  _atom_site_aniso_U_11
  _atom_site_aniso_U_22
  _atom_site_aniso_U_33
  _atom_site_aniso_U_23
  _atom_site_aniso_U_13
  _atom_site_aniso_U_12
C1 0.0175(10) 0.0241(13) 0.0251(12) -0.0022(10) 0.0052(9)
0.0029(10)
C2 0.0162(10) 0.0244(13) 0.0207(10) -0.0005(10) 0.0061(8) -
0.0020(9)
C3 0.0192(10) 0.0199(13) 0.0200(10) 0.0009(9) 0.0040(8) -
0.0033(9)
C4 0.0197(11) 0.0163(12) 0.0195(10) -0.0002(9) 0.0040(8) -
0.0012(9)
C5 0.0207(11) 0.0151(12) 0.0209(11) -0.0015(9) 0.0042(8)
0.0011(9)
C6 0.0217(11) 0.0230(13) 0.0225(11) -0.0021(10) 0.0020(9) -
0.0001(10)
C7 0.0273(12) 0.0290(15) 0.0194(11) -0.0030(10) -0.0025(9)
0.0027(11)
C8 0.0346(13) 0.0299(15) 0.0183(11) -0.0015(10) 0.0092(10)
0.0035(11)
C9 0.0237(11) 0.0284(14) 0.0232(11) -0.0011(10) 0.0079(9)
0.0054(10)
C10 0.0208(11) 0.0164(12) 0.0203(11) -0.0003(9) 0.0039(9)
0.0028(9)

```

C11 0.0193(10) 0.0136(11) 0.0201(10) 0.0006(9) 0.0065(8)
 0.0003(9)
 C12 0.0173(10) 0.0164(12) 0.0199(10) -0.0005(9) 0.0031(8)
 0.0020(9)
 C13 0.0249(11) 0.0199(13) 0.0238(12) 0.0055(10) 0.0033(9) -
 0.0020(10)
 C14 0.0252(11) 0.0193(13) 0.0252(12) -0.0010(10) -0.0029(9) -
 0.0048(10)
 C15 0.0266(12) 0.0190(12) 0.0201(11) 0.0000(10) 0.0011(9)
 0.0040(10)
 C16 0.0291(12) 0.0224(14) 0.0214(11) 0.0036(10) 0.0061(9)
 0.0000(10)
 C17 0.0243(11) 0.0201(13) 0.0235(12) 0.0012(10) 0.0039(9) -
 0.0034(10)
 C18 0.0466(16) 0.0383(18) 0.0250(13) -0.0106(12) -0.0055(11)
 0.0026(14)
 C19 0.0193(11) 0.0270(14) 0.0230(11) -0.0027(10) 0.0080(9)
 0.0028(10)
 C20 0.0329(13) 0.0351(16) 0.0256(12) 0.0040(12) 0.0061(10)
 0.0035(12)
 C21 0.0326(13) 0.0266(15) 0.0239(12) 0.0013(11) -0.0011(10)
 0.0063(12)
 F1 0.0352(8) 0.0549(12) 0.0295(8) -0.0036(8) -0.0072(6) -
 0.0062(9)
 F2 0.0519(10) 0.0575(13) 0.0254(8) -0.0109(8) 0.0055(7)
 0.0143(9)
 F3 0.0698(12) 0.0348(11) 0.0296(8) 0.0098(8) -0.0133(8) -
 0.0008(9)
 N1 0.0165(9) 0.0215(11) 0.0226(10) 0.0016(8) 0.0049(7) -
 0.0024(8)
 N2 0.0162(9) 0.0227(11) 0.0172(9) 0.0016(8) 0.0036(7) 0.0009
 (8)
 O1 0.0363(10) 0.0349(12) 0.0200(8) -0.0031(8) 0.0011(7) -
 0.0024(8)
 O2 0.0285(9) 0.0280(11) 0.0344(9) -0.0061(8) 0.0047(7) -
 0.0075(8)
 O3 0.0189(8) 0.0506(13) 0.0317(9) 0.0076(9) 0.0028(7) -0.0080
 (8)
 C22 0.0175(10) 0.0180(12) 0.0243(11) -0.0033(9) 0.0054(9)
 0.0030(9)
 C23 0.0179(10) 0.0224(13) 0.0216(11) -0.0026(10) 0.0063(9) -
 0.0004(9)
 C24 0.0195(10) 0.0210(13) 0.0218(11) -0.0037(10) 0.0062(8) -
 0.0059(10)
 C25 0.0201(10) 0.0126(11) 0.0197(10) -0.0019(9) 0.0049(8) -
 0.0008(9)
 C26 0.0194(10) 0.0152(12) 0.0206(11) -0.0019(9) 0.0044(8)
 0.0018(9)
 C27 0.0191(11) 0.0203(13) 0.0245(11) -0.0021(10) 0.0023(9) -
 0.0006(10)
 C28 0.0259(12) 0.0271(14) 0.0183(11) -0.0037(10) -0.0017(9)
 0.0019(11)
 C29 0.0282(12) 0.0287(14) 0.0167(11) -0.0009(10) 0.0045(9)
 0.0027(11)
 C30 0.0208(11) 0.0231(13) 0.0213(11) 0.0005(10) 0.0067(8)
 0.0007(10)
 C31 0.0182(10) 0.0165(12) 0.0193(10) 0.0003(9) 0.0032(8)

0.0011(9)
 C32 0.0187(10) 0.0151(12) 0.0207(11) 0.0013(9) 0.0063(8)
 0.0012(9)
 C33 0.0206(10) 0.0149(12) 0.0177(10) -0.0006(9) 0.0024(8)
 0.0045(9)
 C34 0.0268(12) 0.0183(13) 0.0253(12) 0.0048(10) 0.0023(9) -
 0.0015(10)
 C35 0.0275(12) 0.0228(14) 0.0266(12) 0.0000(10) -0.0024(10) -
 0.0034(11)
 C36 0.0295(12) 0.0237(14) 0.0185(11) -0.0004(10) 0.0005(9)
 0.0070(11)
 C37 0.0298(12) 0.0209(13) 0.0209(11) 0.0026(10) 0.0069(9)
 0.0001(10)
 C38 0.0275(12) 0.0178(13) 0.0197(11) -0.0009(9) 0.0059(9) -
 0.0006(10)
 C39 0.0420(15) 0.0351(17) 0.0210(12) -0.0053(11) -0.0037(10)
 -0.0008(13)
 C40 0.0201(11) 0.0235(14) 0.0252(11) -0.0061(10) 0.0053(9)
 0.0052(10)
 C41 0.0363(14) 0.0306(16) 0.0264(13) -0.0014(11) 0.0005(10)
 0.0002(12)
 C42 0.0369(14) 0.0352(17) 0.0214(12) 0.0015(12) 0.0000(10)
 0.0039(13)
 F4 0.0626(12) 0.0658(15) 0.0300(9) 0.0053(9) -0.0138(8) -
 0.0197(11)
 F5 0.0674(13) 0.162(3) 0.0225(9) -0.0155(12) 0.0045(8) 0.0471
 (15)
 F6 0.1032(16) 0.0395(12) 0.0381(10) 0.0153(9) -0.0268(10) -
 0.0047(12)
 N3 0.0170(9) 0.0240(12) 0.0232(9) -0.0006(8) 0.0037(7) -
 0.0028(8)
 N4 0.0143(9) 0.0206(11) 0.0193(9) 0.0003(8) 0.0033(7) -0.0003
 (8)
 O4 0.0327(9) 0.0284(10) 0.0208(8) -0.0023(7) 0.0021(7) -
 0.0031(8)
 O5 0.0217(8) 0.0274(10) 0.0285(9) -0.0052(7) 0.0044(7) -
 0.0045(7)
 O6 0.0200(8) 0.0336(11) 0.0370(10) -0.0028(9) 0.0019(7) -
 0.0033(8)

`_geom_special_details`

`;`

All esds (except the esd in the dihedral angle between two
 l.s. planes)
 are estimated using the full covariance matrix. The cell
 esds are taken
 into account individually in the estimation of esds in
 distances, angles
 and torsion angles; correlations between esds in cell
 parameters are only
 used when they are defined by crystal symmetry. An
 approximate (isotropic)
 treatment of cell esds is used for estimating esds involving
 l.s. planes.

`;`

`loop_`
`_geom_bond_atom_site_label_1`

```

_geom_bond_atom_site_label_2
_geom_bond_distance
_geom_bond_site_symmetry_2
_geom_bond_publ_flag
C1 C2 1.508(3) . ?
C1 O1 1.329(3) . ?
C1 O2 1.210(3) . ?
C2 H2 0.9800 . ?
C2 C3 1.548(3) . ?
C2 N1 1.441(3) . ?
C3 H3A 0.9700 . ?
C3 H3B 0.9700 . ?
C3 C4 1.505(3) . ?
C4 C5 1.434(3) . ?
C4 C11 1.377(3) . ?
C5 C6 1.398(3) . ?
C5 C10 1.413(3) . ?
C6 H6 0.9300 . ?
C6 C7 1.388(3) . ?
C7 H7 0.9300 . ?
C7 C8 1.397(3) . ?
C8 H8 0.9300 . ?
C8 C9 1.379(3) . ?
C9 H9 0.9300 . ?
C9 C10 1.398(3) . ?
C10 N2 1.370(3) . ?
C11 C12 1.473(3) . ?
C11 N2 1.384(2) . ?
C12 C13 1.397(3) . ?
C12 C17 1.403(3) . ?
C13 H13 0.9300 . ?
C13 C14 1.377(3) . ?
C14 H14 0.9300 . ?
C14 C15 1.386(3) . ?
C15 C16 1.393(3) . ?
C15 C21 1.498(3) . ?
C16 H16 0.9300 . ?
C16 C17 1.385(3) . ?
C17 H17 0.9300 . ?
C18 H18A 0.9600 . ?
C18 H18B 0.9600 . ?
C18 H18C 0.9600 . ?
C18 O1 1.451(3) . ?
C19 C20 1.507(3) . ?
C19 N1 1.338(3) . ?
C19 O3 1.226(3) . ?
C20 H20A 0.9600 . ?
C20 H20B 0.9600 . ?
C20 H20C 0.9600 . ?
C21 F1 1.340(3) . ?
C21 F2 1.345(3) . ?
C21 F3 1.335(3) . ?
N1 H1 0.8600 . ?
N2 H2A 0.88(2) . ?
C22 C23 1.511(3) . ?
C22 O4 1.334(3) . ?
C22 O5 1.211(3) . ?

```

C23 H23 0.9800 . ?
 C23 C24 1.551(3) . ?
 C23 N3 1.444(3) . ?
 C24 H24A 0.9700 . ?
 C24 H24B 0.9700 . ?
 C24 C25 1.507(3) . ?
 C25 C26 1.436(3) . ?
 C25 C32 1.373(3) . ?
 C26 C27 1.405(3) . ?
 C26 C31 1.414(3) . ?
 C27 H27 0.9300 . ?
 C27 C28 1.384(3) . ?
 C28 H28 0.9300 . ?
 C28 C29 1.409(3) . ?
 C29 H29 0.9300 . ?
 C29 C30 1.376(3) . ?
 C30 H30 0.9300 . ?
 C30 C31 1.397(3) . ?
 C31 N4 1.371(3) . ?
 C32 C33 1.473(3) . ?
 C32 N4 1.388(3) . ?
 C33 C34 1.389(3) . ?
 C33 C38 1.404(3) . ?
 C34 H34 0.9300 . ?
 C34 C35 1.389(3) . ?
 C35 H35 0.9300 . ?
 C35 C36 1.386(3) . ?
 C36 C37 1.383(3) . ?
 C36 C42 1.498(3) . ?
 C37 H37 0.9300 . ?
 C37 C38 1.393(3) . ?
 C38 H38 0.9300 . ?
 C39 H39A 0.9600 . ?
 C39 H39B 0.9600 . ?
 C39 H39C 0.9600 . ?
 C39 O4 1.454(3) . ?
 C40 C41 1.505(4) . ?
 C40 N3 1.346(3) . ?
 C40 O6 1.225(3) . ?
 C41 H41A 0.9600 . ?
 C41 H41B 0.9600 . ?
 C41 H41C 0.9600 . ?
 C42 F4 1.334(3) . ?
 C42 F5 1.315(3) . ?
 C42 F6 1.325(4) . ?
 N3 H3 0.8600 . ?
 N4 H4 0.85(2) . ?

loop_
 _geom_angle_atom_site_label_1
 _geom_angle_atom_site_label_2
 _geom_angle_atom_site_label_3
 _geom_angle
 _geom_angle_site_symmetry_1
 _geom_angle_site_symmetry_3
 _geom_angle_publ_flag
 O1 C1 C2 111.8(2) . . ?

O2 C1 C2 123.7(2) . . ?
O2 C1 O1 124.4(2) . . ?
C1 C2 H2 108.5 . . ?
C1 C2 C3 110.54(19) . . ?
C3 C2 H2 108.5 . . ?
N1 C2 C1 107.8(2) . . ?
N1 C2 H2 108.5 . . ?
N1 C2 C3 112.80(17) . . ?
C2 C3 H3A 108.9 . . ?
C2 C3 H3B 108.9 . . ?
H3A C3 H3B 107.7 . . ?
C4 C3 C2 113.39(19) . . ?
C4 C3 H3A 108.9 . . ?
C4 C3 H3B 108.9 . . ?
C5 C4 C3 122.9(2) . . ?
C11 C4 C3 129.8(2) . . ?
C11 C4 C5 107.03(18) . . ?
C6 C5 C4 134.1(2) . . ?
C6 C5 C10 118.95(19) . . ?
C10 C5 C4 106.93(19) . . ?
C5 C6 H6 120.6 . . ?
C7 C6 C5 118.8(2) . . ?
C7 C6 H6 120.6 . . ?
C6 C7 H7 119.5 . . ?
C6 C7 C8 121.1(2) . . ?
C8 C7 H7 119.5 . . ?
C7 C8 H8 119.2 . . ?
C9 C8 C7 121.6(2) . . ?
C9 C8 H8 119.2 . . ?
C8 C9 H9 121.4 . . ?
C8 C9 C10 117.2(2) . . ?
C10 C9 H9 121.4 . . ?
C9 C10 C5 122.3(2) . . ?
N2 C10 C5 107.61(18) . . ?
N2 C10 C9 130.1(2) . . ?
C4 C11 C12 132.57(19) . . ?
C4 C11 N2 108.91(18) . . ?
N2 C11 C12 118.50(19) . . ?
C13 C12 C11 120.2(2) . . ?
C13 C12 C17 118.1(2) . . ?
C17 C12 C11 121.7(2) . . ?
C12 C13 H13 119.4 . . ?
C14 C13 C12 121.3(2) . . ?
C14 C13 H13 119.4 . . ?
C13 C14 H14 120.0 . . ?
C13 C14 C15 120.0(2) . . ?
C15 C14 H14 120.0 . . ?
C14 C15 C16 120.0(2) . . ?
C14 C15 C21 120.3(2) . . ?
C16 C15 C21 119.6(2) . . ?
C15 C16 H16 120.1 . . ?
C17 C16 C15 119.8(2) . . ?
C17 C16 H16 120.1 . . ?
C12 C17 H17 119.6 . . ?
C16 C17 C12 120.8(2) . . ?
C16 C17 H17 119.6 . . ?
H18A C18 H18B 109.5 . . ?

H18A C18 H18C 109.5 . . ?
H18B C18 H18C 109.5 . . ?
O1 C18 H18A 109.5 . . ?
O1 C18 H18B 109.5 . . ?
O1 C18 H18C 109.5 . . ?
N1 C19 C20 116.2(2) . . ?
O3 C19 C20 122.2(2) . . ?
O3 C19 N1 121.6(2) . . ?
C19 C20 H20A 109.5 . . ?
C19 C20 H20B 109.5 . . ?
C19 C20 H20C 109.5 . . ?
H20A C20 H20B 109.5 . . ?
H20A C20 H20C 109.5 . . ?
H20B C20 H20C 109.5 . . ?
F1 C21 C15 112.9(2) . . ?
F1 C21 F2 106.1(2) . . ?
F2 C21 C15 112.2(2) . . ?
F3 C21 C15 112.7(2) . . ?
F3 C21 F1 106.4(2) . . ?
F3 C21 F2 106.0(2) . . ?
C2 N1 H1 118.4 . . ?
C19 N1 C2 123.2(2) . . ?
C19 N1 H1 118.4 . . ?
C10 N2 C11 109.49(18) . . ?
C10 N2 H2A 124.2(15) . . ?
C11 N2 H2A 125.8(15) . . ?
C1 O1 C18 115.0(2) . . ?
O4 C22 C23 111.4(2) . . ?
O5 C22 C23 123.9(2) . . ?
O5 C22 O4 124.7(2) . . ?
C22 C23 H23 108.3 . . ?
C22 C23 C24 111.07(19) . . ?
C24 C23 H23 108.3 . . ?
N3 C23 C22 107.2(2) . . ?
N3 C23 H23 108.3 . . ?
N3 C23 C24 113.53(17) . . ?
C23 C24 H24A 108.8 . . ?
C23 C24 H24B 108.8 . . ?
H24A C24 H24B 107.7 . . ?
C25 C24 C23 113.74(19) . . ?
C25 C24 H24A 108.8 . . ?
C25 C24 H24B 108.8 . . ?
C26 C25 C24 123.59(19) . . ?
C32 C25 C24 129.34(19) . . ?
C32 C25 C26 107.03(17) . . ?
C27 C26 C25 134.09(19) . . ?
C27 C26 C31 118.84(19) . . ?
C31 C26 C25 106.99(19) . . ?
C26 C27 H27 120.6 . . ?
C28 C27 C26 118.9(2) . . ?
C28 C27 H27 120.6 . . ?
C27 C28 H28 119.5 . . ?
C27 C28 C29 121.1(2) . . ?
C29 C28 H28 119.5 . . ?
C28 C29 H29 119.4 . . ?
C30 C29 C28 121.2(2) . . ?
C30 C29 H29 119.4 . . ?

C29 C30 H30 121.1 . . ?
 C29 C30 C31 117.7(2) . . ?
 C31 C30 H30 121.1 . . ?
 C30 C31 C26 122.2(2) . . ?
 N4 C31 C26 107.50(18) . . ?
 N4 C31 C30 130.3(2) . . ?
 C25 C32 C33 131.84(19) . . ?
 C25 C32 N4 108.97(19) . . ?
 N4 C32 C33 119.17(19) . . ?
 C34 C33 C32 121.2(2) . . ?
 C34 C33 C38 118.6(2) . . ?
 C38 C33 C32 120.2(2) . . ?
 C33 C34 H34 119.5 . . ?
 C35 C34 C33 121.1(2) . . ?
 C35 C34 H34 119.5 . . ?
 C34 C35 H35 120.2 . . ?
 C36 C35 C34 119.6(2) . . ?
 C36 C35 H35 120.2 . . ?
 C35 C36 C42 120.8(2) . . ?
 C37 C36 C35 120.6(2) . . ?
 C37 C36 C42 118.6(2) . . ?
 C36 C37 H37 120.2 . . ?
 C36 C37 C38 119.7(2) . . ?
 C38 C37 H37 120.2 . . ?
 C33 C38 H38 119.8 . . ?
 C37 C38 C33 120.5(2) . . ?
 C37 C38 H38 119.8 . . ?
 H39A C39 H39B 109.5 . . ?
 H39A C39 H39C 109.5 . . ?
 H39B C39 H39C 109.5 . . ?
 O4 C39 H39A 109.5 . . ?
 O4 C39 H39B 109.5 . . ?
 O4 C39 H39C 109.5 . . ?
 N3 C40 C41 114.7(2) . . ?
 O6 C40 C41 123.1(2) . . ?
 O6 C40 N3 122.2(2) . . ?
 C40 C41 H41A 109.5 . . ?
 C40 C41 H41B 109.5 . . ?
 C40 C41 H41C 109.5 . . ?
 H41A C41 H41B 109.5 . . ?
 H41A C41 H41C 109.5 . . ?
 H41B C41 H41C 109.5 . . ?
 F4 C42 C36 113.1(2) . . ?
 F5 C42 C36 112.8(2) . . ?
 F5 C42 F4 105.4(3) . . ?
 F5 C42 F6 108.0(3) . . ?
 F6 C42 C36 112.6(2) . . ?
 F6 C42 F4 104.3(2) . . ?
 C23 N3 H3 118.5 . . ?
 C40 N3 C23 122.9(2) . . ?
 C40 N3 H3 118.5 . . ?
 C31 N4 C32 109.40(18) . . ?
 C31 N4 H4 126.9(15) . . ?
 C32 N4 H4 122.4(15) . . ?
 C22 O4 C39 114.9(2) . . ?

loop_

```

_geom_torsion_atom_site_label_1
_geom_torsion_atom_site_label_2
_geom_torsion_atom_site_label_3
_geom_torsion_atom_site_label_4
_geom_torsion
_geom_torsion_site_symmetry_1
_geom_torsion_site_symmetry_2
_geom_torsion_site_symmetry_3
_geom_torsion_site_symmetry_4
_geom_torsion_publ_flag
C1 C2 C3 C4 -71.3(2) . . . . ?
C1 C2 N1 C19 -152.2(2) . . . . ?
C2 C1 O1 C18 177.6(2) . . . . ?
C2 C3 C4 C5 -86.2(3) . . . . ?
C2 C3 C4 C11 87.3(3) . . . . ?
C3 C2 N1 C19 85.5(2) . . . . ?
C3 C4 C5 C6 -7.3(4) . . . . ?
C3 C4 C5 C10 174.5(2) . . . . ?
C3 C4 C11 C12 5.8(5) . . . . ?
C3 C4 C11 N2 -173.0(2) . . . . ?
C4 C5 C6 C7 -177.8(3) . . . . ?
C4 C5 C10 C9 178.9(2) . . . . ?
C4 C5 C10 N2 -0.8(3) . . . . ?
C4 C11 C12 C13 -143.1(3) . . . . ?
C4 C11 C12 C17 39.2(4) . . . . ?
C4 C11 N2 C10 -1.9(3) . . . . ?
C5 C4 C11 C12 -179.9(2) . . . . ?
C5 C4 C11 N2 1.3(3) . . . . ?
C5 C6 C7 C8 -0.9(4) . . . . ?
C5 C10 N2 C11 1.6(3) . . . . ?
C6 C5 C10 C9 0.3(4) . . . . ?
C6 C5 C10 N2 -179.4(2) . . . . ?
C6 C7 C8 C9 1.0(4) . . . . ?
C7 C8 C9 C10 -0.4(4) . . . . ?
C8 C9 C10 C5 -0.3(4) . . . . ?
C8 C9 C10 N2 179.4(3) . . . . ?
C9 C10 N2 C11 -178.0(3) . . . . ?
C10 C5 C6 C7 0.3(4) . . . . ?
C11 C4 C5 C6 178.0(3) . . . . ?
C11 C4 C5 C10 -0.3(3) . . . . ?
C11 C12 C13 C14 -179.5(2) . . . . ?
C11 C12 C17 C16 179.8(2) . . . . ?
C12 C11 N2 C10 179.2(2) . . . . ?
C12 C13 C14 C15 0.5(4) . . . . ?
C13 C12 C17 C16 2.1(3) . . . . ?
C13 C14 C15 C16 0.4(4) . . . . ?
C13 C14 C15 C21 -176.3(2) . . . . ?
C14 C15 C16 C17 0.0(4) . . . . ?
C14 C15 C21 F1 -24.4(3) . . . . ?
C14 C15 C21 F2 95.4(3) . . . . ?
C14 C15 C21 F3 -145.0(2) . . . . ?
C15 C16 C17 C12 -1.2(4) . . . . ?
C16 C15 C21 F1 159.0(2) . . . . ?
C16 C15 C21 F2 -81.2(3) . . . . ?
C16 C15 C21 F3 38.4(3) . . . . ?
C17 C12 C13 C14 -1.7(4) . . . . ?
C20 C19 N1 C2 -177.8(2) . . . . ?

```

C21 C15 C16 C17 176.6(2) ?
N1 C2 C3 C4 49.4(3) ?
N2 C11 C12 C13 35.6(3) ?
N2 C11 C12 C17 -142.1(2) ?
O1 C1 C2 C3 -70.4(2) ?
O1 C1 C2 N1 165.95(18) ?
O2 C1 C2 C3 109.0(3) ?
O2 C1 C2 N1 -14.7(3) ?
O2 C1 O1 C18 -1.7(3) ?
O3 C19 N1 C2 2.0(4) ?
C22 C23 C24 C25 -70.1(2) ?
C22 C23 N3 C40 -156.4(2) ?
C23 C22 O4 C39 178.6(2) ?
C23 C24 C25 C26 -90.6(3) ?
C23 C24 C25 C32 86.7(3) ?
C24 C23 N3 C40 80.6(2) ?
C24 C25 C26 C27 -5.3(4) ?
C24 C25 C26 C31 177.9(2) ?
C24 C25 C32 C33 5.4(4) ?
C24 C25 C32 N4 -175.8(2) ?
C25 C26 C27 C28 -175.1(3) ?
C25 C26 C31 C30 176.6(2) ?
C25 C26 C31 N4 -2.0(3) ?
C25 C32 C33 C34 -137.6(3) ?
C25 C32 C33 C38 44.7(4) ?
C25 C32 N4 C31 -3.2(3) ?
C26 C25 C32 C33 -177.0(2) ?
C26 C25 C32 N4 1.9(3) ?
C26 C27 C28 C29 -1.0(4) ?
C26 C31 N4 C32 3.2(3) ?
C27 C26 C31 C30 -0.7(4) ?
C27 C26 C31 N4 -179.4(2) ?
C27 C28 C29 C30 0.1(4) ?
C28 C29 C30 C31 0.6(4) ?
C29 C30 C31 C26 -0.3(4) ?
C29 C30 C31 N4 178.1(3) ?
C30 C31 N4 C32 -175.3(3) ?
C31 C26 C27 C28 1.3(4) ?
C32 C25 C26 C27 176.8(3) ?
C32 C25 C26 C31 0.1(3) ?
C32 C33 C34 C35 -178.1(2) ?
C32 C33 C38 C37 177.9(2) ?
C33 C32 N4 C31 175.8(2) ?
C33 C34 C35 C36 0.4(4) ?
C34 C33 C38 C37 0.2(3) ?
C34 C35 C36 C37 -0.2(4) ?
C34 C35 C36 C42 -178.4(2) ?
C35 C36 C37 C38 0.0(4) ?
C35 C36 C42 F4 -16.9(4) ?
C35 C36 C42 F5 102.7(3) ?
C35 C36 C42 F6 -134.8(3) ?
C36 C37 C38 C33 0.0(3) ?
C37 C36 C42 F4 164.8(2) ?
C37 C36 C42 F5 -75.6(3) ?
C37 C36 C42 F6 47.0(3) ?
C38 C33 C34 C35 -0.4(3) ?
C41 C40 N3 C23 -179.0(2) ?

C42 C36 C37 C38 178.2(2) ?
 N3 C23 C24 C25 50.8(3) ?
 N4 C32 C33 C34 43.6(3) ?
 N4 C32 C33 C38 -134.0(2) ?
 O4 C22 C23 C24 -68.8(2) ?
 O4 C22 C23 N3 166.62(17) ?
 O5 C22 C23 C24 110.9(2) ?
 O5 C22 C23 N3 -13.7(3) ?
 O5 C22 O4 C39 -1.1(3) ?
 O6 C40 N3 C23 1.4(3) ?

loop_
 _exptl_crystal_face_index_h
 _exptl_crystal_face_index_k
 _exptl_crystal_face_index_l
 _exptl_crystal_face_perp_dist
 _exptl_oxdiff_crystal_face_indexfrac_h
 _exptl_oxdiff_crystal_face_indexfrac_k
 _exptl_oxdiff_crystal_face_indexfrac_l
 _exptl_oxdiff_crystal_face_x
 _exptl_oxdiff_crystal_face_y
 _exptl_oxdiff_crystal_face_z
 0 0 -1 0.0164 -0.0000 -0.0000 -0.9999 0.0297 -0.0005 -0.0014
 0 0 1 0.0164 0.0000 0.0000 0.9999 -0.0297 0.0005 0.0014
 1 0 0 0.0867 1.0001 0.0001 -0.0001 -0.0097 -0.0295 0.0759
 -1 0 0 0.0867 -1.0001 -0.0001 0.0001 0.0097 0.0295 -0.0759
 0 -1 0 0.1938 0.0000 -1.0000 -0.0001 -0.0027 -0.0732 -0.0288
 0 1 0 0.1858 -0.0000 1.0000 0.0001 0.0027 0.0732 0.0288
 2 -1 0 0.1409 2.0001 -0.9999 -0.0003 -0.0221 -0.1321 0.1230

Appendix C - Compound 230

```

data_ijsf1202
_audit_creation_date          2012-04-13
_audit_creation_method
;
  Olex2 1.1
  (compiled 2011.11.01 svn.r2039, GUI svn.r3906)
;
_publ_contact_author_address  ?
_publ_contact_author_email    ?
_publ_contact_author_name     ' '
_publ_contact_author_phone    ?
_chemical_name_common         ?
_chemical_name_systematic
;
?
;
_chemical_formula_moiety      'C20 F N2 O3'
_chemical_formula_sum         'C20 H19 F N2 O3'
_chemical_formula_weight      354.37
_chemical_absolute_configuration unk
_chemical_melting_point       ?
_chemical_oxdiff_formula      'C20 H19 F1 N2 O3'
_chemical_oxdiff_usercomment  'Tom Williams
TJW/5/173/465/1'
loop_
  _atom_type_symbol
  _atom_type_description
  _atom_type_scatter_dispersion_real
  _atom_type_scatter_dispersion_imag
  _atom_type_scatter_source
  'C' 'C' 0.0033 0.0016 'International Tables Vol C Tables
4.2.6.8 and 6.1.1.4'
  'H' 'H' 0.0000 0.0000 'International Tables Vol C Tables
4.2.6.8 and 6.1.1.4'
  'F' 'F' 0.0171 0.0103 'International Tables Vol C Tables
4.2.6.8 and 6.1.1.4'
  'N' 'N' 0.0061 0.0033 'International Tables Vol C Tables
4.2.6.8 and 6.1.1.4'
  'O' 'O' 0.0106 0.0060 'International Tables Vol C Tables
4.2.6.8 and 6.1.1.4'

  _space_group_crystal_system  'trigonal'
  _space_group_IT_number       146
  _space_group_name_H-M_alt    'R 3'
  _space_group_name_Hall       'R 3'
loop_
  _space_group_symop_id
  _space_group_symop_operation_xyz
  1 'x, y, z'
  2 '-y, x-y, z'
  3 '-x+y, -x, z'
  4 'x+2/3, y+1/3, z+1/3'
  5 '-y+2/3, x-y+1/3, z+1/3'
  6 '-x+y+2/3, -x+1/3, z+1/3'
  7 'x+1/3, y+2/3, z+2/3'

```

8 '-y+1/3, x-y+2/3, z+2/3'
9 '-x+y+1/3, -x+2/3, z+2/3'

_cell_length_a 21.0404(11)
_cell_length_b 21.0404(11)
_cell_length_c 10.4652(7)
_cell_angle_alpha 90.00
_cell_angle_beta 90.00
_cell_angle_gamma 120.00
_cell_volume 4012.2(6)
_cell_formula_units_Z 9
_cell_measurement_reflns_used 3569
_cell_measurement_temperature 110.00(10)
_cell_measurement_theta_max 32.0836
_cell_measurement_theta_min 2.9596
_exptl_absorpt_coefficient_mu 0.096
_exptl_absorpt_correction_T_max 0.990
_exptl_absorpt_correction_T_min 0.986
_exptl_absorpt_correction_type analytical
_exptl_absorpt_process_details

;
CrysAlisPro, Agilent Technologies,
Version 1.171.35.19 (release 27-10-2011 CrysAlis171 .NET)
(compiled Oct 27 2011,15:02:11)
Analytical numeric absorption correction using a multifaceted
crystal

model based on expressions derived by R.C.
Clark & J.S. Reid.
(Clark, R. C. & Reid, J. S. (1995). Acta Cryst. A51, 887-897)

;
_exptl_crystal_colour 'clear colourless'
_exptl_crystal_colour_lustre clear
_exptl_crystal_colour_modifier .
_exptl_crystal_colour_primary colourless
_exptl_crystal_density_diffn 1.320
_exptl_crystal_density_meas ?
_exptl_crystal_density_method 'not measured'
_exptl_crystal_description irregular
_exptl_crystal_F_000 1674
_exptl_crystal_size_max 0.2168
_exptl_crystal_size_mid 0.1531
_exptl_crystal_size_min 0.1393
_exptl_special_details

;
?

;
_diffn_reflns_av_R_equivalents 0.0271
_diffn_reflns_av_unetI/netI 0.0498
_diffn_reflns_limit_h_max 31
_diffn_reflns_limit_h_min -23
_diffn_reflns_limit_k_max 23
_diffn_reflns_limit_k_min -31
_diffn_reflns_limit_l_max 15
_diffn_reflns_limit_l_min -15
_diffn_reflns_number 9531
_diffn_reflns_theta_full 30.01
_diffn_reflns_theta_max 32.16


```

_diffrn_reflms_theta_min          2.96
_diffrn_ambient_temperature      110.00(10)
_diffrn_detector_area_resol_mean 16.1450
_diffrn_measured_fraction_theta_full 0.999
_diffrn_measured_fraction_theta_max 0.920
_diffrn_measurement_details
;
#  type  start  end  width  exp.time
  1  omega  -69.00  48.00  1.0000  12.8400
omega  theta  kappa  phi  frames
-      -25.1672  19.0000  -30.0000  117

#  type  start  end  width  exp.time
  2  omega  -65.00 -35.00  1.0000  12.8400
omega  theta  kappa  phi  frames
-      -25.1672 -178.0000  -30.0000  30

#  type  start  end  width  exp.time
  3  omega  31.00  77.00  1.0000  12.8400
omega  theta  kappa  phi  frames
-      26.4172 -128.0000  -7.0000  46

#  type  start  end  width  exp.time
  4  omega  39.00 100.00  1.0000  12.8400
omega  theta  kappa  phi  frames
-      26.4172 -178.0000  -90.0000  61

#  type  start  end  width  exp.time
  5  omega  31.00  62.00  1.0000  12.8400
omega  theta  kappa  phi  frames
-      26.4172  56.0000  117.0000  31
;
_diffrn_measurement_device_type  'SuperNova, Single source at
offset), Eos'
_diffrn_measurement_method      '\w scans'
_diffrn_orient_matrix_UB_11     -0.0179086000
_diffrn_orient_matrix_UB_12     -0.0357576000
_diffrn_orient_matrix_UB_13     0.0267633000
_diffrn_orient_matrix_UB_21     -0.0296459000
_diffrn_orient_matrix_UB_22     -0.0103234000
_diffrn_orient_matrix_UB_23     -0.0430230000
_diffrn_orient_matrix_UB_31     0.0175359000
_diffrn_orient_matrix_UB_32     -0.0111921000
_diffrn_orient_matrix_UB_33     -0.0453332000
_diffrn_radiation_monochromator  mirror
_diffrn_radiation_type          'Mo K\alpha'
_diffrn_radiation_wavelength    0.7107
_diffrn_source                  'SuperNova (Mo) X-ray
Source'
_diffrn_standards_decay_%       ?
_diffrn_standards_interval_count ?
_diffrn_standards_interval_time ?
_diffrn_standards_number        ?
_reflms_number_gt               5157
_reflms_number_total            5613
_reflms_odcompleteness_completeness 99.89
_reflms_odcompleteness_iscentric 1

```

```

_reflns_odcompleteness_theta      30.01
_reflns_threshold_expression      >2sigma(I)
_computing_cell_refinement
;
CrysAlisPro, Agilent Technologies,
Version 1.171.35.19 (release 27-10-2011 CrysAlis171 .NET)
(compiled Oct 27 2011,15:02:11)
;
_computing_data_collection
;
CrysAlisPro, Agilent Technologies,
Version 1.171.35.19 (release 27-10-2011 CrysAlis171 .NET)
(compiled Oct 27 2011,15:02:11)
;
_computing_data_reduction
;
CrysAlisPro, Agilent Technologies,
Version 1.171.35.19 (release 27-10-2011 CrysAlis171 .NET)
(compiled Oct 27 2011,15:02:11)
;
_computing_molecular_graphics
;
O. V. Dolomanov, L. J. Bourhis, R. J. Gildea, J. A. K. Howard
and H. Puschmann,
OLEX2: a complete structure solution, refinement and analysis
program.
J. Appl. Cryst. (2009). 42, 339-341.
;
_computing_publication_material
;
O. V. Dolomanov, L. J. Bourhis, R. J. Gildea, J. A. K. Howard
and H. Puschmann,
OLEX2: a complete structure solution, refinement and analysis
program.
J. Appl. Cryst. (2009). 42, 339-341.
;
_computing_structure_refinement
;
XL, G.M. Sheldrick, Acta Cryst.
(2008). A64, 112-122
;
_computing_structure_solution
;
Palatinus, L. & Chapuis, G. (2007).
SUPERFLIP - a computer program for the solution of crystal
structures
by charge flipping in arbitrary dimensions.
J. Appl. Cryst. 40, 786-790.
;
_refine_diff_density_max          0.313
_refine_diff_density_min         -0.229
_refine_diff_density_rms         0.045
_refine_ls_extinction_coef       ?
_refine_ls_extinction_method     none
_refine_ls_goodness_of_fit_ref   1.036
_refine_ls_hydrogen_treatment   mixed
_refine_ls_matrix_type           full

```

```

_refine_ls_number_parameters      245
_refine_ls_number_reflns         5613
_refine_ls_number_restraints      1
_refine_ls_R_factor_all           0.0479
_refine_ls_R_factor_gt            0.0424
_refine_ls_restrained_S_all       1.036
_refine_ls_shift/su_max           0.000
_refine_ls_shift/su_mean          0.000
_refine_ls_structure_factor_coef   Fsqd
_refine_ls_weighting_details
'calc w=1/[\s^2^(Fo^2^)+(0.0412P)^2^+1.5669P] where P=(Fo^2^+
2Fc^2^)/3'
_refine_ls_weighting_scheme        calc
_refine_ls_wR_factor_gt           0.0946
_refine_ls_wR_factor_ref          0.0995
_refine_special_details
;

```

Refinement of F^2 against ALL reflections. The weighted R-factor wR and goodness of fit S are based on F^2 , conventional R-factors R are based on F, with F set to zero for negative F^2 . The threshold expression of $F^2 > 2\sigma(F^2)$ is used only for calculating R-factors (gt) etc. and is not relevant to the choice of reflections for refinement. R-factors based on F^2 are statistically about twice as large as those based on F, and R-factors based on ALL data will be even larger.

The hydrogens on the nitrogens were found by difference map.

```

;
_atom_sites_solution_hydrogens    geom
_atom_sites_solution_primary       iterative
_atom_sites_solution_secondary     difmap
loop_
  _atom_site_label
  _atom_site_type_symbol
  _atom_site_fract_x
  _atom_site_fract_y
  _atom_site_fract_z
  _atom_site_U_iso_or_equiv
  _atom_site_adp_type
  _atom_site_occupancy
  _atom_site_symmetry_multiplicity
  _atom_site_calc_flag
  _atom_site_refinement_flags
  _atom_site_disorder_assembly
  _atom_site_disorder_group
C1 C 0.54326(9) 0.29788(9) 0.51985(15) 0.0237(3) Uani 1 1 d .
. .
C2 C 0.52022(9) 0.34868(9) 0.52482(15) 0.0233(3) Uani 1 1 d .
. .
H2 H 0.5149 0.3667 0.6028 0.028 Uiso 1 1 calc R . .
C3 C 0.50511(8) 0.37238(9) 0.41058(14) 0.0196(3) Uani 1 1 d .
. .

```

H3 H 0.4891 0.4063 0.4120 0.024 Uiso 1 1 calc R . .
C4 C 0.51388(8) 0.34549(8) 0.29391(13) 0.0157(3) Uani 1 1 d .
. .
C5 C 0.53818(8) 0.29447(8) 0.29351(14) 0.0191(3) Uani 1 1 d .
. .
H5 H 0.5446 0.2767 0.2161 0.023 Uiso 1 1 calc R . .
C6 C 0.55282(9) 0.27007(9) 0.40693(16) 0.0229(3) Uani 1 1 d .
. .
H6 H 0.5686 0.2359 0.4067 0.027 Uiso 1 1 calc R . .
C7 C 0.49634(8) 0.36751(8) 0.17097(13) 0.0151(2) Uani 1 1 d .
. .
C8 C 0.51401(8) 0.43501(8) 0.12255(13) 0.0146(2) Uani 1 1 d .
. .
C9 C 0.55844(8) 0.50912(7) 0.18290(14) 0.0161(3) Uani 1 1 d .
. .
H9A H 0.5455 0.5056 0.2726 0.019 Uiso 1 1 calc R . .
H9B H 0.5458 0.5429 0.1428 0.019 Uiso 1 1 calc R . .
C10 C 0.64169(7) 0.54050(8) 0.17169(13) 0.0139(2) Uani 1 1 d
. . .
H10 H 0.6561 0.5114 0.2248 0.017 Uiso 1 1 calc R . .
C11 C 0.66116(8) 0.53645(8) 0.03302(13) 0.0153(3) Uani 1 1 d
. . .
C12 C 0.68382(11) 0.46603(11) -0.11590(16) 0.0309(4) Uani 1 1
d . . .
H12A H 0.6398 0.4503 -0.1647 0.046 Uiso 1 1 calc R . .
H12B H 0.6970 0.4285 -0.1176 0.046 Uiso 1 1 calc R . .
H12C H 0.7228 0.5103 -0.1522 0.046 Uiso 1 1 calc R . .
C13 C 0.75258(8) 0.65834(8) 0.20747(13) 0.0162(3) Uani 1 1 d
. . .
C14 C 0.78405(9) 0.73524(9) 0.25806(17) 0.0258(3) Uani 1 1 d
. . .
H14A H 0.8185 0.7433 0.3250 0.039 Uiso 1 1 calc R . .
H14B H 0.7452 0.7418 0.2912 0.039 Uiso 1 1 calc R . .
H14C H 0.8086 0.7697 0.1902 0.039 Uiso 1 1 calc R . .
C15 C 0.48395(8) 0.42278(8) -0.00434(13) 0.0154(3) Uani 1 1 d
. . .
C16 C 0.48216(8) 0.46893(8) -0.09995(15) 0.0187(3) Uani 1 1 d
. . .
H16 H 0.5061 0.5195 -0.0880 0.022 Uiso 1 1 calc R . .
C17 C 0.44428(9) 0.43801(9) -0.21186(15) 0.0219(3) Uani 1 1 d
. . .
H17 H 0.4429 0.4682 -0.2754 0.026 Uiso 1 1 calc R . .
C18 C 0.40778(9) 0.36167(9) -0.23109(15) 0.0220(3) Uani 1 1 d
. . .
H18 H 0.3818 0.3421 -0.3064 0.026 Uiso 1 1 calc R . .
C19 C 0.40995(8) 0.31516(9) -0.13967(15) 0.0211(3) Uani 1 1 d
. . .
H19 H 0.3867 0.2648 -0.1531 0.025 Uiso 1 1 calc R . .
C20 C 0.44815(8) 0.34650(8) -0.02694(14) 0.0165(3) Uani 1 1 d
. . .
F1 F 0.55774(7) 0.27429(7) 0.63125(9) 0.0371(3) Uani 1 1 d .
. . .
N1 N 0.67922(7) 0.61582(7) 0.21652(12) 0.0174(2) Uani 1 1 d .
. . .
H1 H 0.6540(13) 0.6359(13) 0.241(2) 0.039(6) Uiso 1 1 d . . .
N2 N 0.45744(7) 0.31386(7) 0.08007(12) 0.0179(2) Uani 1 1 d .
. . .

```

H2A H 0.4351(13) 0.2686(14) 0.093(2) 0.036(6) Uiso 1 1 d . .
.
O1 O 0.66376(6) 0.57685(6) -0.05103(10) 0.0198(2) Uani 1 1 d
. .
O2 O 0.67144(6) 0.47957(6) 0.01536(10) 0.0205(2) Uani 1 1 d .
. .
O3 O 0.79097(6) 0.63528(6) 0.16024(10) 0.0196(2) Uani 1 1 d .
. .

loop_
  _atom_site_aniso_label
  _atom_site_aniso_U_11
  _atom_site_aniso_U_22
  _atom_site_aniso_U_33
  _atom_site_aniso_U_23
  _atom_site_aniso_U_13
  _atom_site_aniso_U_12
C1 0.0238(8) 0.0237(8) 0.0176(6) 0.0079(6) 0.0016(6) 0.0075
(6)
C2 0.0235(8) 0.0262(8) 0.0161(6) 0.0013(6) 0.0049(6) 0.0095
(6)
C3 0.0186(7) 0.0193(7) 0.0205(6) 0.0010(5) 0.0040(5) 0.0092
(6)
C4 0.0140(6) 0.0127(6) 0.0171(6) 0.0018(5) 0.0007(5) 0.0042
(5)
C5 0.0216(7) 0.0163(6) 0.0174(6) -0.0010(5) -0.0006(5) 0.0079
(6)
C6 0.0261(8) 0.0184(7) 0.0249(7) 0.0035(6) -0.0013(6) 0.0117
(6)
C7 0.0134(6) 0.0151(6) 0.0151(6) -0.0008(5) 0.0007(5) 0.0058
(5)
C8 0.0129(6) 0.0143(6) 0.0159(6) -0.0011(5) 0.0006(5) 0.0063
(5)
C9 0.0151(6) 0.0130(6) 0.0190(6) -0.0014(5) 0.0014(5) 0.0060
(5)
C10 0.0138(6) 0.0130(6) 0.0157(6) -0.0014(5) 0.0003(5) 0.0073
(5)
C11 0.0135(6) 0.0134(6) 0.0167(6) -0.0021(5) 0.0000(5) 0.0050
(5)
C12 0.0442(11) 0.0346(9) 0.0200(7) -0.0044(7) 0.0067(7)
0.0243(9)
C13 0.0149(6) 0.0161(6) 0.0171(6) -0.0005(5) -0.0003(5)
0.0074(5)
C14 0.0184(7) 0.0182(7) 0.0362(9) -0.0081(6) -0.0005(6)
0.0057(6)
C15 0.0137(6) 0.0156(6) 0.0163(6) -0.0003(5) 0.0012(5) 0.0067
(5)
C16 0.0166(6) 0.0167(6) 0.0229(7) 0.0021(5) 0.0011(5) 0.0084
(6)
C17 0.0194(7) 0.0268(8) 0.0200(7) 0.0056(6) 0.0005(6) 0.0119
(6)
C18 0.0182(7) 0.0280(8) 0.0178(7) -0.0021(6) -0.0029(5)
0.0101(6)
C19 0.0192(7) 0.0194(7) 0.0218(7) -0.0029(6) -0.0033(6)
0.0074(6)
C20 0.0151(6) 0.0152(6) 0.0183(6) -0.0005(5) -0.0003(5)
0.0068(5)

```

```

F1 0.0498(7) 0.0456(7) 0.0197(5) 0.0118(5) 0.0005(5) 0.0268
(6)
N1 0.0136(5) 0.0147(6) 0.0236(6) -0.0054(5) 0.0011(5) 0.0068
(5)
N2 0.0187(6) 0.0121(6) 0.0193(6) -0.0016(5) -0.0032(5) 0.0050
(5)
O1 0.0206(5) 0.0171(5) 0.0196(5) 0.0029(4) 0.0010(4) 0.0079
(4)
O2 0.0281(6) 0.0215(5) 0.0168(5) -0.0020(4) 0.0027(4) 0.0160
(5)
O3 0.0161(5) 0.0202(5) 0.0240(5) -0.0031(4) 0.0006(4) 0.0101
(4)

```

`_geom_special_details`

;

All esds (except the esd in the dihedral angle between two l.s. planes) are estimated using the full covariance matrix. The cell esds are taken into account individually in the estimation of esds in distances, angles and torsion angles; correlations between esds in cell parameters are only used when they are defined by crystal symmetry. An approximate (isotropic) treatment of cell esds is used for estimating esds involving l.s. planes.

;

loop_

```

  _geom_bond_atom_site_label_1
  _geom_bond_atom_site_label_2
  _geom_bond_distance
  _geom_bond_site_symmetry_2
  _geom_bond_publ_flag

```

```

C1 C2 1.378(3) . ?
C1 C6 1.377(2) . ?
C1 F1 1.3600(18) . ?
C2 H2 0.9300 . ?
C2 C3 1.392(2) . ?
C3 H3 0.9300 . ?
C3 C4 1.396(2) . ?
C4 C5 1.401(2) . ?
C4 C7 1.4755(19) . ?
C5 H5 0.9300 . ?
C5 C6 1.388(2) . ?
C6 H6 0.9300 . ?
C7 C8 1.373(2) . ?
C7 N2 1.3876(18) . ?
C8 C9 1.4989(19) . ?
C8 C15 1.4377(19) . ?
C9 H9A 0.9700 . ?
C9 H9B 0.9700 . ?
C9 C10 1.5366(19) . ?
C10 H10 0.9800 . ?
C10 C11 1.5218(19) . ?
C10 N1 1.4503(18) . ?
C11 O1 1.2052(18) . ?

```

C11 O2 1.3312(18) . ?
 C12 H12A 0.9600 . ?
 C12 H12B 0.9600 . ?
 C12 H12C 0.9600 . ?
 C12 O2 1.4526(19) . ?
 C13 C14 1.505(2) . ?
 C13 N1 1.3458(19) . ?
 C13 O3 1.2345(17) . ?
 C14 H14A 0.9600 . ?
 C14 H14B 0.9600 . ?
 C14 H14C 0.9600 . ?
 C15 C16 1.408(2) . ?
 C15 C20 1.411(2) . ?
 C16 H16 0.9300 . ?
 C16 C17 1.383(2) . ?
 C17 H17 0.9300 . ?
 C17 C18 1.406(2) . ?
 C18 H18 0.9300 . ?
 C18 C19 1.386(2) . ?
 C19 H19 0.9300 . ?
 C19 C20 1.394(2) . ?
 C20 N2 1.3778(19) . ?
 N1 H1 0.87(2) . ?
 N2 H2A 0.84(3) . ?

loop_
 _geom_angle_atom_site_label_1
 _geom_angle_atom_site_label_2
 _geom_angle_atom_site_label_3
 _geom_angle
 _geom_angle_site_symmetry_1
 _geom_angle_site_symmetry_3
 _geom_angle_publ_flag
 C6 C1 C2 123.01(14) . . ?
 F1 C1 C2 118.73(15) . . ?
 F1 C1 C6 118.26(15) . . ?
 C1 C2 H2 120.7 . . ?
 C1 C2 C3 118.53(14) . . ?
 C3 C2 H2 120.7 . . ?
 C2 C3 H3 119.8 . . ?
 C2 C3 C4 120.38(15) . . ?
 C4 C3 H3 119.8 . . ?
 C3 C4 C5 119.07(13) . . ?
 C3 C4 C7 122.07(13) . . ?
 C5 C4 C7 118.84(13) . . ?
 C4 C5 H5 119.5 . . ?
 C6 C5 C4 120.97(14) . . ?
 C6 C5 H5 119.5 . . ?
 C1 C6 C5 118.04(15) . . ?
 C1 C6 H6 121.0 . . ?
 C5 C6 H6 121.0 . . ?
 C8 C7 C4 131.75(13) . . ?
 C8 C7 N2 109.46(12) . . ?
 N2 C7 C4 118.73(13) . . ?
 C7 C8 C9 128.77(13) . . ?
 C7 C8 C15 106.77(12) . . ?
 C15 C8 C9 124.41(13) . . ?

C8 C9 H9A 108.9 . . ?
C8 C9 H9B 108.9 . . ?
C8 C9 C10 113.51(11) . . ?
H9A C9 H9B 107.7 . . ?
C10 C9 H9A 108.9 . . ?
C10 C9 H9B 108.9 . . ?
C9 C10 H10 109.3 . . ?
C11 C10 C9 109.25(11) . . ?
C11 C10 H10 109.3 . . ?
N1 C10 C9 109.00(11) . . ?
N1 C10 H10 109.3 . . ?
N1 C10 C11 110.79(11) . . ?
O1 C11 C10 125.11(13) . . ?
O1 C11 O2 124.20(13) . . ?
O2 C11 C10 110.62(12) . . ?
H12A C12 H12B 109.5 . . ?
H12A C12 H12C 109.5 . . ?
H12B C12 H12C 109.5 . . ?
O2 C12 H12A 109.5 . . ?
O2 C12 H12B 109.5 . . ?
O2 C12 H12C 109.5 . . ?
N1 C13 C14 115.58(13) . . ?
O3 C13 C14 122.74(13) . . ?
O3 C13 N1 121.68(13) . . ?
C13 C14 H14A 109.5 . . ?
C13 C14 H14B 109.5 . . ?
C13 C14 H14C 109.5 . . ?
H14A C14 H14B 109.5 . . ?
H14A C14 H14C 109.5 . . ?
H14B C14 H14C 109.5 . . ?
C16 C15 C8 133.95(14) . . ?
C16 C15 C20 118.84(13) . . ?
C20 C15 C8 107.18(12) . . ?
C15 C16 H16 120.5 . . ?
C17 C16 C15 119.03(14) . . ?
C17 C16 H16 120.5 . . ?
C16 C17 H17 119.5 . . ?
C16 C17 C18 121.06(15) . . ?
C18 C17 H17 119.5 . . ?
C17 C18 H18 119.5 . . ?
C19 C18 C17 121.06(14) . . ?
C19 C18 H18 119.5 . . ?
C18 C19 H19 121.1 . . ?
C18 C19 C20 117.72(14) . . ?
C20 C19 H19 121.1 . . ?
C19 C20 C15 122.26(13) . . ?
N2 C20 C15 107.62(12) . . ?
N2 C20 C19 130.10(13) . . ?
C10 N1 H1 119.8(16) . . ?
C13 N1 C10 121.37(12) . . ?
C13 N1 H1 118.4(16) . . ?
C7 N2 H2A 125.4(15) . . ?
C20 N2 C7 108.94(12) . . ?
C20 N2 H2A 124.3(15) . . ?
C11 O2 C12 115.68(12) . . ?

loop_


```

_geom_hbond_atom_site_label_D
_geom_hbond_atom_site_label_H
_geom_hbond_atom_site_label_A
_geom_hbond_distance_DH
_geom_hbond_distance_HA
_geom_hbond_distance_DA
_geom_hbond_angle_DHA
_geom_hbond_site_symmetry_A
N1 H1 O1 0.87(2) 2.06(2) 2.9155(16) 170(2) 6_565

```

```

loop_
  _geom_torsion_atom_site_label_1
  _geom_torsion_atom_site_label_2
  _geom_torsion_atom_site_label_3
  _geom_torsion_atom_site_label_4
  _geom_torsion
  _geom_torsion_site_symmetry_1
  _geom_torsion_site_symmetry_2
  _geom_torsion_site_symmetry_3
  _geom_torsion_site_symmetry_4
  _geom_torsion_publ_flag
C1 C2 C3 C4 -0.6(2) . . . . ?
C2 C1 C6 C5 -0.2(2) . . . . ?
C2 C3 C4 C5 -0.1(2) . . . . ?
C2 C3 C4 C7 178.13(14) . . . . ?
C3 C4 C5 C6 0.6(2) . . . . ?
C3 C4 C7 C8 47.4(2) . . . . ?
C3 C4 C7 N2 -135.53(15) . . . . ?
C4 C5 C6 C1 -0.5(2) . . . . ?
C4 C7 C8 C9 0.3(3) . . . . ?
C4 C7 C8 C15 177.89(14) . . . . ?
C4 C7 N2 C20 -179.18(13) . . . . ?
C5 C4 C7 C8 -134.34(16) . . . . ?
C5 C4 C7 N2 42.70(19) . . . . ?
C6 C1 C2 C3 0.7(2) . . . . ?
C7 C4 C5 C6 -177.66(14) . . . . ?
C7 C8 C9 C10 80.64(18) . . . . ?
C7 C8 C15 C16 178.36(15) . . . . ?
C7 C8 C15 C20 0.43(16) . . . . ?
C8 C7 N2 C20 -1.52(16) . . . . ?
C8 C9 C10 C11 50.88(16) . . . . ?
C8 C9 C10 N1 172.07(11) . . . . ?
C8 C15 C16 C17 -176.53(15) . . . . ?
C8 C15 C20 C19 177.08(14) . . . . ?
C8 C15 C20 N2 -1.35(16) . . . . ?
C9 C8 C15 C16 -4.0(2) . . . . ?
C9 C8 C15 C20 178.12(13) . . . . ?
C9 C10 C11 O1 75.70(17) . . . . ?
C9 C10 C11 O2 -101.15(13) . . . . ?
C9 C10 N1 C13 -174.53(13) . . . . ?
C10 C11 O2 C12 174.64(13) . . . . ?
C11 C10 N1 C13 -54.29(17) . . . . ?
C14 C13 N1 C10 -179.88(13) . . . . ?
C15 C8 C9 C10 -96.52(16) . . . . ?
C15 C16 C17 C18 0.1(2) . . . . ?
C15 C20 N2 C7 1.77(16) . . . . ?
C16 C15 C20 C19 -1.2(2) . . . . ?

```

C16 C15 C20 N2 -179.65(13) ?
 C16 C17 C18 C19 -1.4(2) ?
 C17 C18 C19 C20 1.4(2) ?
 C18 C19 C20 C15 -0.1(2) ?
 C18 C19 C20 N2 177.96(15) ?
 C19 C20 N2 C7 -176.50(15) ?
 C20 C15 C16 C17 1.2(2) ?
 F1 C1 C2 C3 -179.67(14) ?
 F1 C1 C6 C5 -179.82(14) ?
 N1 C10 C11 O1 -44.40(19) ?
 N1 C10 C11 O2 138.75(12) ?
 N2 C7 C8 C9 -176.90(13) ?
 N2 C7 C8 C15 0.65(16) ?
 O1 C11 O2 C12 -2.2(2) ?
 O3 C13 N1 C10 0.3(2) ?

loop_

_exptl_crystal_face_index_h
 _exptl_crystal_face_index_k
 _exptl_crystal_face_index_l
 _exptl_crystal_face_perp_dist
 _exptl_oxdiff_crystal_face_indexfrac_h
 _exptl_oxdiff_crystal_face_indexfrac_k
 _exptl_oxdiff_crystal_face_indexfrac_l
 _exptl_oxdiff_crystal_face_x
 _exptl_oxdiff_crystal_face_y
 _exptl_oxdiff_crystal_face_z
 -2 1 0 0.0998 -2.0000 0.9990 -0.0002 0.0001 0.0490 -0.0462
 2 -1 0 0.1128 2.0000 -0.9990 0.0002 -0.0001 -0.0490 0.0462
 0 0 1 0.0890 -0.0001 -0.0002 0.9992 0.0267 -0.0430 -0.0453
 0 0 -1 0.0736 0.0001 0.0002 -0.9992 -0.0267 0.0430 0.0453
 1 -1 -1 0.0662 0.9999 -0.9990 -0.9991 -0.0089 0.0237 0.0740
 -1 1 1 0.0732 -0.9999 0.9990 0.9991 0.0089 -0.0237 -0.0740
 -1 0 -1 0.0746 -1.0001 -0.0000 -0.9993 -0.0088 0.0726 0.0278
 1 0 1 0.0746 1.0001 0.0000 0.9993 0.0088 -0.0726 -0.0278
 1 -2 0 0.0574 0.9996 -1.9986 -0.0001 0.0536 -0.0090 0.0399
 -1 2 0 0.0854 -0.9996 1.9986 0.0001 -0.0536 0.0090 -0.0399
 -1 -1 0 0.0706 -1.0004 -0.9996 -0.0002 0.0537 0.0400 -0.0063
 1 1 0 0.0826 1.0004 0.9996 0.0002 -0.0537 -0.0400 0.0063